Joy Gopal Ghosh- 1998

U-Pb geochronology and structural geology across major shear zones of the Southern Granulite Terrain of India

and

Organic carbon isotope stratigraphy of the Gondwana coal basins of India:

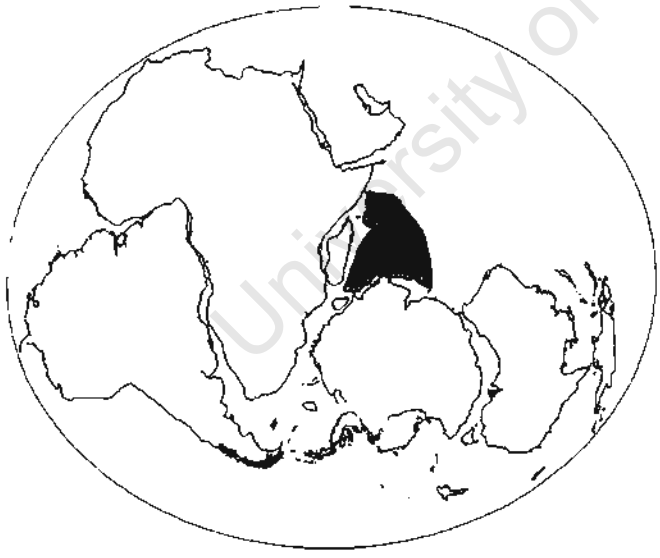

their implications for Gondwana studies.

Thesis presented for the degree of Doctor of Philosophy
in the Department of Geological Sciences
University of Cape Town

ABSTRACT

This thesis is divided into 2 parts. The first part (Chapters 1-5) concentrates on unravelling the Precambrian geological history of the high-grade poly-metamorphic and poly-deformed basement of southernmost India, using field geology and U-Pb geochronology. Because Peninsular India occupied a central position in Gondwana, this work bears on reconstruction models of central Gondwana between circa 600 Ma and 200 Ma. The second part of the thesis (Chapter 6) tests the use of organic carbon isotopes as a chemostratigraphic tool to correlate between the lower part of terrestrial Gondwana (Upper Carboniferous to Triassic) sequences in India. This work contributes to (i) intra-basinal and inter-basinal stratigraphic correlation and carbon isotope variations during the Permian-Triassic extinction event of Gondwana; and (ii) refines the inter-continental correlations of the Gondwana type sequences in India with those in South Africa and Madagascar.

This century much attention has been focused on the reconstruction of Gondwana, and as a result, the broad relative positions of different Gondwana fragments and their later dispersal histories is now well understood. Finer-scale reconstructions, based on modern geochronological and isotope studies integrated with field studies of continental rocks, are still needed to resolve the detailed kinematic histories of continental break-up and the evolution of continental lithosphere in general. Shear zones that cross the boundaries of continental fragments provide 'piercing points' in fitting the fragments back together. To realize this, the kinematics and the timing of major shear zones need to be determined. The first part of this thesis, therefore, primarily focuses on understanding the kinematics and geochronology of a number of subvertical continental scale shear zones in the Southern Granulite Terrain of India (SGT).

Peninsular India is a complex Precambrian terrain in which the Archean granite-greenstone basement of the Dharwar craton is flanked by high-grade metamorphic terrains of the SGT in the south and the Eastern Ghats in the east. These two high-grade terrains have suffered a Proterozoic polyphase history of deformation and charnockitization. The boundaries between the Dharwar craton and the two high-grade terrains intersect the eastern coast of India. Whether these high-grade terrains are parts of a single orogenic belt, however, remains an outstanding question. Also it is not known if the two high-grade terrains comprise remobilised Dharwar basement or not. A number of models propose that terrane boundaries exists (i.e., the SGT comprises a number of terranes) along some major shear zones/lineaments in the Peninsular India. However, these models are rarely backed up by field data and precise geochronology. To test these models, a number of corridors across major shear zones in the SGT were mapped in detail and 35 rock samples were collected and dated precisely using U-Pb geochronological techniques. The findings of this study are:
(i) Circa 2.5 Ga rocks of the Dharwar craton extend at least ~250 km into the SGT at least up

to a newly defined shear zone, the Karur-Kambam-Painavu-Trichur Shear Zone (KKPTSZ).
(ii) The KKPT Shear Zone is the best candidate for a terrane boundary in the SGT. High-grade equivalents of the Dharwar craton occur in the north of this shear zone and rocks of the Eastern Ghats extend to the south of this shear zone.
(iii) The SGT has experienced many magmatic and high-grade metamorphic and tectonic events spanning from Mid-Archean to Early Paleozoic. Events at circa 2.9 Ga, 2.5 Ga, 1.6 Ga, 1.0 Ga, 800 Ma, 720 Ma, 600 Ma, 570 Ma, 550 Ma and at 525 Ma are recorded from different part of the SGT using U/Pb zircon and monazite dating.
(iv) Two new major shear zones in the SGT have been proposed and the positions of two other shear zones have been re-defined. All these shear zones date between circa 600 Ma and circa 560 Ma. None of them, excepting the KKPTSZ, represents a terrane boundary.
(v) Charnockitization is not all of the same age. In the southern part of the SGT, it post-dates the shear zones, and has occurred between circa 550 Ma and 525 Ma. Much older ~2.5 Ga charnockitization occurs in the northern part of the SGT, but in places these rocks are also affected by the late Neoproterozoic - early Paleozoic charnockitization.
(vi) There is a marked similarity in the ages of charnockites, shear zones and other thermal events of southern India with those in Madagascar and Antarctica. The new data suggest that the KKPT Shear Zone in India is possibly continuous to the east with the boundary zone between the Napier Complex and the Rayner Complex in Antarctica, and to the west, with the Ranotsara Shear Zone in Madagascar.

The second part of this thesis examines the organic carbon isotope variations in terrestrial Gondwana sequences. To correctly understand the larger context of Gondwana evolution during its life span between about 500 Ma and 200 Ma, the terrestrial stratigraphic records preserved in the type localities, now separated as far as South Africa and India, need to be correlated with confidence. The plant and vertebrate fossil records cannot be correlated with sufficient resolution. Therefore, the use of organic carbon (C_{org}) isotopes as a high-resolution chemical stratigraphic tool is examined. More than 500 samples from different Gondwana sections in Peninsular India, Madagascar and South Africa, spanning ~ 100 million years of Middle to Late Paleozoic history, have been analysed for C_{org} isotope ratios (expressed as $\delta^{13}C_{org}$). A number of samples across the palynologically determined Permian-Triassic boundary came from different boreholes in India. The results of this pilot study demonstrate exciting new possibilities of using this technique for stratigraphic correlation between Gondwana basins. The findings of this study are:
(i) Sharp negative $\delta^{13}C_{org}$ spikes of >5-6‰ across the Permian-Triassic boundary are present in most but not all of the terrestrial Gondwana sections. The largest rapid $\delta^{13}C_{org}$ variation records a change of 19‰, between -18‰ to -37‰. Instead of single sharp negative spike commonly present at the Permian-Triassic boundary of marine carbonates, 2 or 3 sharp negative spikes, spanning a lithologic thickness of 40-60m, have been discovered across the

Permian-Triassic boundary in the terrestrial deposits of Gondwana of India.
(ii) In the Permian section of the type Gondwana sequences, a cyclic variation in the organic carbon isotope ratios is evident. These variations broadly correspond to established lithostratigraphic boundaries and/or well defined palynologic zones, suggesting that these patterns may be useful for high-resolution stratigraphic correlations.
(iii) Prelimanary inspection of the isotopic signatures suggests that the P-T boundary in Madagascar has been incorrectly placed.

In summary, both the radiogenic and light stable isotope studies of this thesis have improved correlation of both the basement and cover rocks between fragments of the former Gondwana supercontinent.

PREFACE AND ACKNOWLEDGEMENTS

At the end of 3½ years of continuous and hectic work for this thesis, I feel great pleasure in thanking all those who have helped and contributed towards completion of this thesis. I value all the help I have received from a large number of people to be as important as my own work.

Before starting this thesis, I worked with the Geological Survey of India (GSI) where I mapped and did field geology with some emphasis in structural geology. Analytical work and computing used to be fearsome things to me. But not anymore. I enjoy both analytical work and computing as much as I do fieldwork and mapping.

The idea of this thesis was initiated by Prof. Maarten de Wit soon after Gondwana-IX conference in India in 1994. I am not sure why he was interested in having an Indian student on his research team, but I guess he was convinced that the granulite terrain of southern India and Gondwana successions in the Peninsular India are exciting fields of research which needed to be addressed for our understanding of Gondwana. On Maarten's request, I was chosen by Dr. N. D. Mitra, retired Deputy Director General of GSI to work as part of Maarten's research group. My professor in India, Dr. D. Mukhopadhyay, and Dr. N. D. Mitra and Dr. S. K. Acharyya of GSI convinced me that I should accept Maarten's offer. I am thankful to them for their good advice. Many other colleagues in GSI helped to get the long period of leave required for this work. I am thankful to GSI and my colleagues there.

My wife Anjana agreed to let me come over to Cape Town alone for my studies in spite of the fact that she was half way through her pregnancy with our first child. She had a hope that she would be able to join me in a year or so. Unfortunately, she could only join me in Cape Town just two months before the completion of my thesis. For more than three years she silently suffered my absence from her and from our newly born daughter Srijoyee but went on encouraging me to complete my thesis. Her only satisfaction was her believe that my studies in Cape Town would be beneficial to me, my family and to my country. I am proud of my wife for her courage and encouragement. Once while I was on a field trip in India, she digitized three big maps for me. The compiled version of those maps appear as Fig. 1.3 in this thesis. My parents and my elder brothers took on the responsibility of maintaining my family during my absence. I could not have done this work without their support, and I have highest regards for them.

This thesis deals with two apparently unrelated topics: i) the tectonics of the southern granulite terrain of India and (ii) organic carbon isotope stratigraphy in Gondwana sequences. My initial work was on organic carbon isotope stratigraphy, a completely new topic for me, for which there is very little previous research. In the beginning, this work progressed in a

dampening mood, not knowing at all whether carbon isotope ratios are worth testing as a stratigraphic tool. Prof. de Wit encouraged me with one or two references per day and at times telling philosophically that science is all about trying new things and getting ready for the unexpected. However, only after my initial set of analyses, could I understand the meaning of this. It became clear to me that carbon isotope study had exciting potential for stratigraphic analyses. Since then I have gained much interest in understanding organic carbon isotope ratios in the rock record. With good analytical facilities at the University of Cape Town, I analyzed more than 500 samples for organic carbon isotopes. Thanks goes to Ernest, a chemical laboratory assistant, for quickly supplying labware whenever needed. The results of my analyses were very exciting. However, to calibrate carbon isotope ratios as a stratigraphic tool, it needed to be integrated with palynology and geochronology. Both of these studies were my handicaps.

After spending about 6 months with carbon isotope analyses, I became interested in the problem of tight reconstruction of Gondwana. There is no denying that tight reconstruction of Gondwana cannot be done without high quality geochronological work and its integration with field work. A great opportunity came to me when Prof. Sam Bowring of the Massachusetts Institute of Technology (MIT) offered to let me work in his laboratory for U/Pb zircon dating of some Indian Granulites. I could not think of anything better than getting trained for U/Pb zircon geochronology at Prof. Sam Bowring's laboratory, and my stay at MIT changed the course of this thesis. All the changes were to my liking, first, because it gave me a chance to learn the U-Pb geochronological techniques and, second, because it allowed me to do field work in an Archean-Proterozoic high-grade terrain in India, with scope to do some structural work, my basic training. I stayed at the MIT for five months. It is not an easy task for someone who has never worked in a chemistry laboratory (other than what was needed to pass examinations) to work in a clean laboratory for high-precision zircon geochronology. However, Sam and all his laboratory associates, Dave Hawkins, Drew Coleman and Kathy Davidek used all their tricks, both strict and lenient, to make me qualified to work in a clean lab. I am thankful to all of them for their help, consideration and patience with my many mistakes while leaning the technique. Sam arranged a breather during my stay at MIT, which will always be a great memory-- a two-week field-trip to the Nevada desert with Prof. Clarke Burchfiel of MIT and also a sight-seeing trip to the Grand Canyon.

Coming back to the University of Cape Town (UCT), I came across another surprising opportunity. Dr. Robert (Bob) Zartman joined the UCT after retirement from the US Geological Survey and took up the responsibility of setting up a U-Pb zircon dating facility at the Department of Geological Sciences. I immediately joined Bob in setting up a zircon dating laboratory. Setting up a high-precision zircon dating laboratory is an extremely painful exercise, full of frustrations. Bob went through all the pains and frustrations of setting up a lab

even though he was towards the end of his active professional life. I feel very proud to be associated with him and sharing his pains and frustrations. Had it not been for a caring person like Bob with teaching instinct, I would not have continued working in the lab. Bob was available anytime, early in the morning to late at night. And if he was not in the lab or at his office, I could call him anytime, and he would be ready with a solution. Ruth, Bob's wife, supported our unscheduled odd working hours in the lab and often brought food so that we could survive. After ~1½ years of undergoing pains, frustrations and disappointments, we could produce good analytical results comparable to some of the best labs in the world. Both Bob and myself were in good smiles. We received invaluable assistance from some people at UCT and from outside. Shireen Govender and Judy Green, our laboratory officers, provided us whatever help they could. Outside UCT, Prof. Sam Bowring of MIT, his student Mark Schmitz, post-doctoral fellow Mark Martin were always available by e-mail to help us with suggestions and often gave us some invaluable clean reagents. All of this support contributed to our success in setting up the clean lab for zircon dating at UCT.

My association with Bob has been a very good learning exercise for me. We enjoyed long hours of discussions on many topic of geochemistry, isotope geology and the history of their developments. I treasure those discussions with Bob.

I had two field trips to India and one to Madagascar. In India, my parent organisation, GSI, gave me full logistical support. Two geologists from GSI, Mr. K. Duraisamy of the Tamil Nadu Circle and Mr. K. Raghunath Pillay of the Kerala Circle, accompanied me during my field trips to Tamil Nadu and Kerala respectively. I am thankful to both of them for assisting me in my fieldwork in some difficult areas. Mr. K. Raghunath Pillay, especially, accompanied me in numerous field traverses and always participated in discussions which helped me to iron-out many confusions in the field. His enthusiasm for fieldwork always encouraged me. Bernd Müller of the Rand African University accompanied me during my fieldwork in Madagascar. I enjoyed that trip very much. I am thankful to Bernd for his assistance.

At UCT, many friends have helped me in many ways. Be it sharing tidbits of computing skills, giving advice and suggestions, looking at the details of analyses and diagrams, giving me a lift to my home after long hours of work, my friends at UCT were always available. A very friendly and helpful atmosphere for work helped to ease my tensions over the work or personal matters. A few times I almost had decided to quit my studies because of personal reasons. But friends like Jesse Dann and Moctar Doucoure at the Centre of Interactive Graphical Computing (CIGC, where my office was located) would not let me do that. Their affection for me and their persuasive power were so great that I remained at UCT, at times against my own will. Now both of them are happy to see that I have completed my thesis, and I appreciate the interest they took in me.

Maarten, my principle supervisor for this thesis, has been very inspiring to me all through. He gave me the best available opportunities for my work. Every now and then he would put on my desk a couple of references, not necessarily related to my work, with a tag like, 'Joy, you may find this interesting'. He trusted and cared for me and also ensured that I did not get frustrated and my work never got stuck. He always tried to impress upon me how important it is to look at things both in detail and in broad perspective. He had to undergo the unpleasant task of correcting my English in several versions of the manuscript of this thesis. Maarten deserves my sincere thanks for all his care and for providing me with great opportunities. And finally, I thank Maarten for sponsoring my wife's and daughter's travel expenses towards the end of my stay at Cape Town.

Financial support for this thesis came from a FRD (Foundation Research Development, South Africa) Grant Holder Bursary held by Professor Maarten de Wit. I thank FRD for generously supporting my thesis work. Professor Sam Bowring of the MIT sponsored my stay at MIT and all the expenses for geochronological work carried out at the MIT. I also thank him for both his financial support and numerous other help he gave to me.

TABLE OF CONTENT

FIGURE CAPTIONS

FIGURES IN APPENDICES:

TABLE CAPTIONS

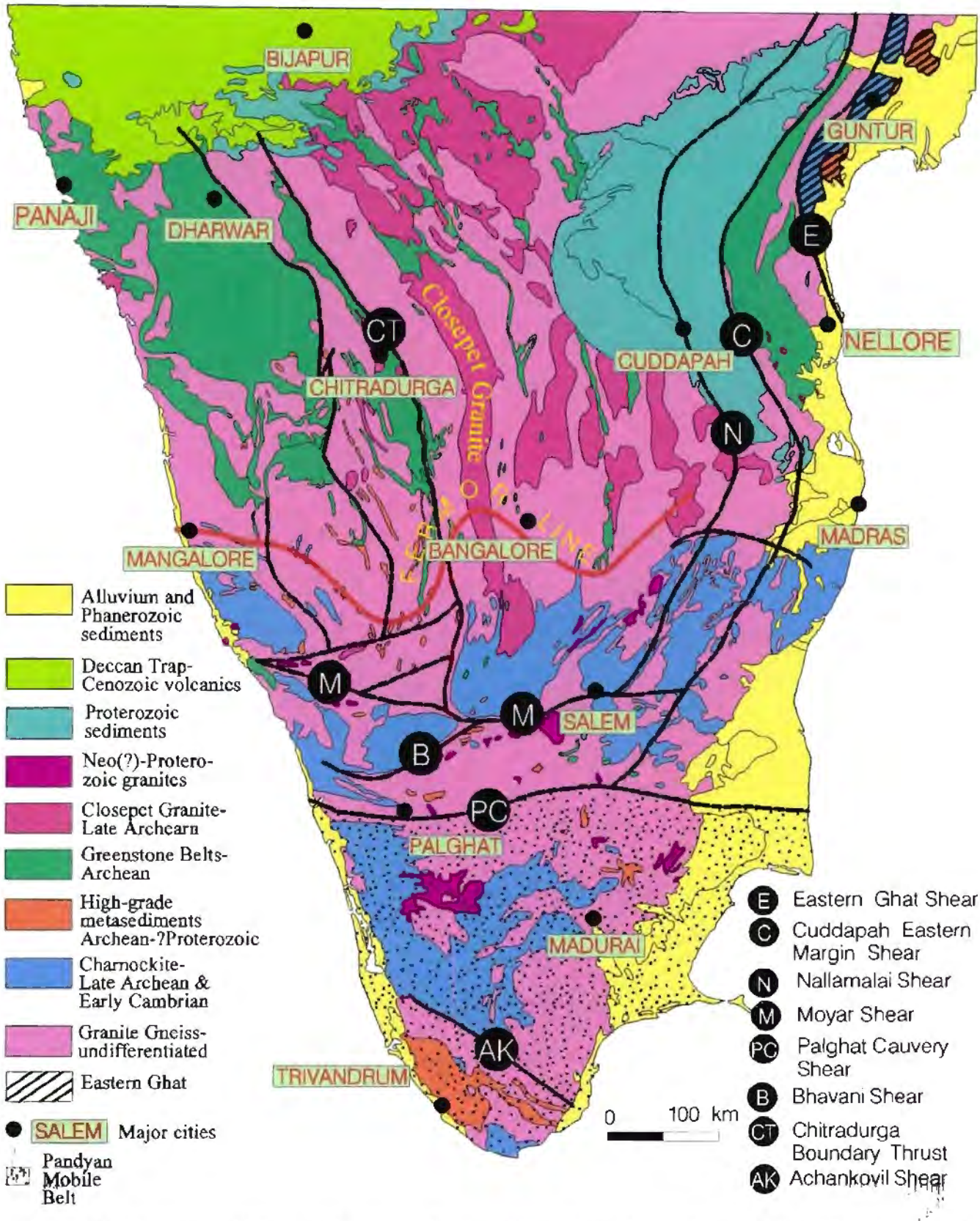

Fig. 1.2. Geological Map of Southern Indian Shield (modified from GSI, 1994). Location of major shear zones is based mainly on the interpretation of satellite imagery.

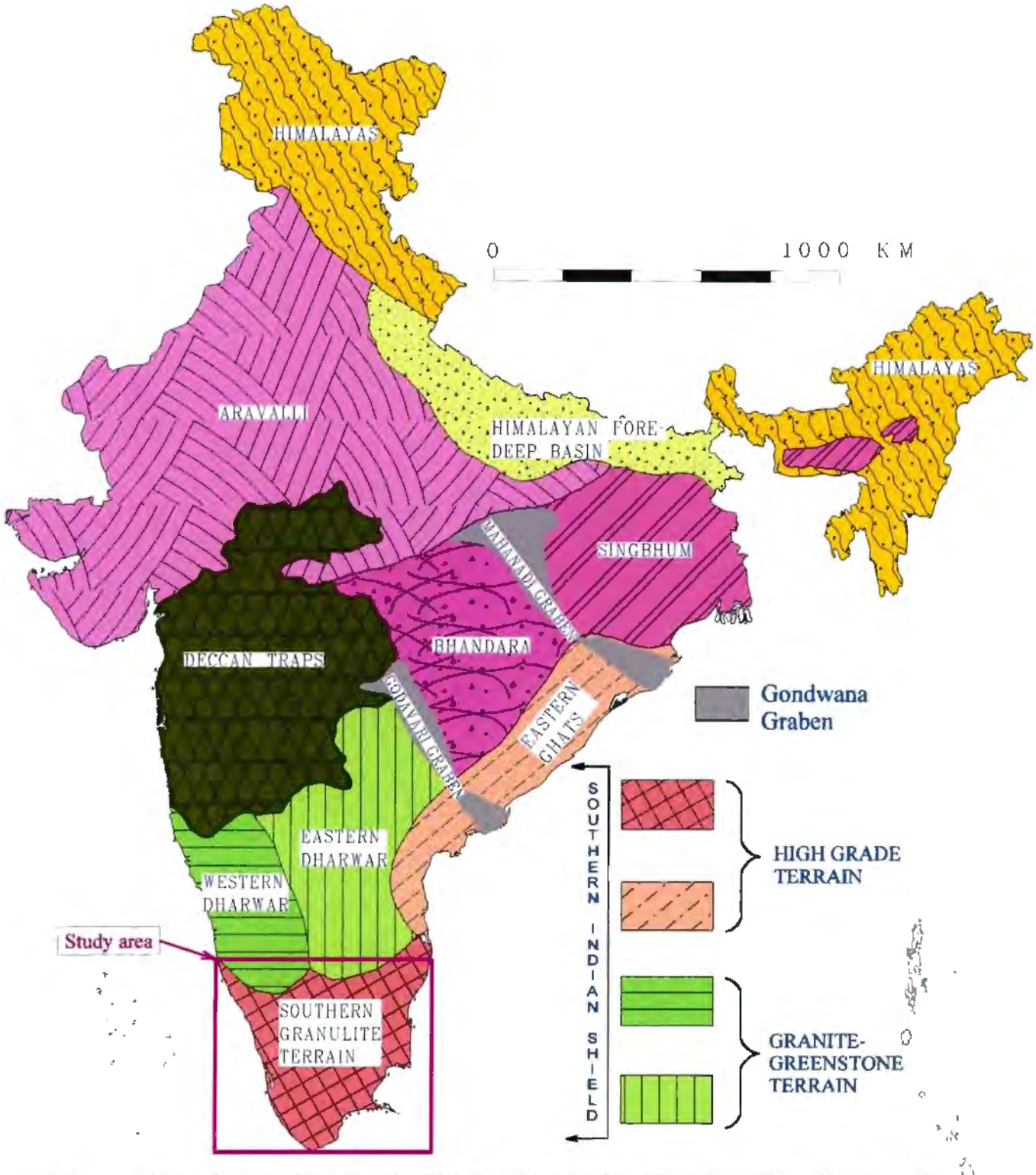

Fig. 1.1. Tectonic domains of India. The Southern Indian Shield consists of high-grade terrains (the Eastern Ghats and the Southern Granulite Terrain) and granite-greenstone belts (the Dharwar Craton). The Dharwar craton is subdivided into two blocks, the Eastern Dharwar and the Western Dharwar (see text for explanation).

Chapter-1: Introduction to the geology of Southern India

1.1. Overview of a tectonic problem

India can be divided into a number of crustal sub-domains (Fig. 1.1) bounded in the north by the Himalayan tectonic domain, and in the south by the Southern Granulite Terrain (SGT). This thesis focuses predominantly on the geologic evolution of the Southern Indian Shield (SIS), which exposes various Archaean to Early Proterozoic rock associations (Fig. 1.2). Broadly, the northern part of this shield is dominated by rocks of granite-greenstone association (Eastern and Western Dharwar cratons) whilst the eastern and southern parts are dominated by high-grade metasediments and charnockites (the Eastern Ghats and the SGT). This broad spatial differentiation in the distribution of the rocks of different metamorphic grade has been used as a key element in a number of different hypotheses bearing on the tectonic evolution of the SIS. A geological map of the SIS compiled and modified mainly after the geological maps of the Indian states of Kerala, Tamil Nadu, Pondichery and Karnataka (GSI, 1981, 1995a, 1995b) is given in Fig. 1.3.

The relatively low grade rocks of the granite-greenstone association in the north of the SIS form part of the Dharwar craton, while the southern and eastern sectors of the SIS are represented by high-grade lithologic assemblages of the SGT and the Eastern Ghats, respectively Each of these litho-tectonic regions vary in their relative proportions of rock types, their geochronology, metamorphic history and geophysical makeup. On the basis of these variations, attempts have been made by various workers to delineate boundaries between these principal regions and to understand their mutual relationships. One of the earliest attempts was by Fermor (1936), who divided the Peninsular India into a charnockitic terrain in the south and east, and a non-charnockitic terrain in the north. The rocks of the charnockitic terrain retain evidence of intense ductile deformation and high grade of metamorphism, and

was considered a mobile belt adjacent to the non-charnockitic terrain, the Dharwar craton. Fermor considered that the boundary between these two provinces represents a fundamental litho-tectonic boundary along which there must have been considerable vertical movement. This boundary became known as the 'Fermor line' (Figs. 1.2, 1.4). However, from the 1950s onward studies on the charnockites, all along the Fermor line made it clear that charnockites south of the Fermor line represent metasomatic alteration products of a variety of precursor litho-units which are also present north of the Fermor line (Pichamuthu, 1965; Subrahmanyam, 1967). Thus, the significance of the Fermor line as a fundamental litho-tectonic boundary came to be questioned and subsequent models proposed continuity of Dharwar craton across the Fermor line into the SGT (Pascoe, 1950; Pichamuthu, 1965). In these models, the SGT represents either vertically uplifted parts of the Dharwar craton, or the exposure of the core of a northerly plunging regional anticlinorium of the Dharwar craton.

During the last 15 years, there has been another major reformulation of the tectonic models of the Peninsular India, based primarily on the recognition of trans-continental shear zones along major physiographic lineaments (Fig. 1.5) recognised using satellite imagery (Drury and Holt, 1980). These shear zones include (i) the Moyar and the Bhavani Shear Zones, (ii) the Palghat-Cauvery Shear Zone and (iii) the Achankovil Shear Zone (Fig.1.5). The identification of these major shear zones, and variations of metamorphic P-T estimates (Drury et al. 1984) as well as Nd-model ages (Harris et al. 1994) across the Palghat-Cauvery Lineament, have largely influenced recent tectonic interpretations of the Peninsular India. In these models, the Palghat-Cauvery Lineament, a pronounced physiographically low area in the SIS (Fig. 1.5), has been interpreted by various workers as a major lithospheric boundary variously interpreted as: (i) a dextral transcurrent shear belt (Drury and Holt, 1980); (ii) a collapsed marginal basin (Drury et al. 1984); (iii) a cryptic collisional suture zone (Gopalakrishnan et al. 1990); (iv) a

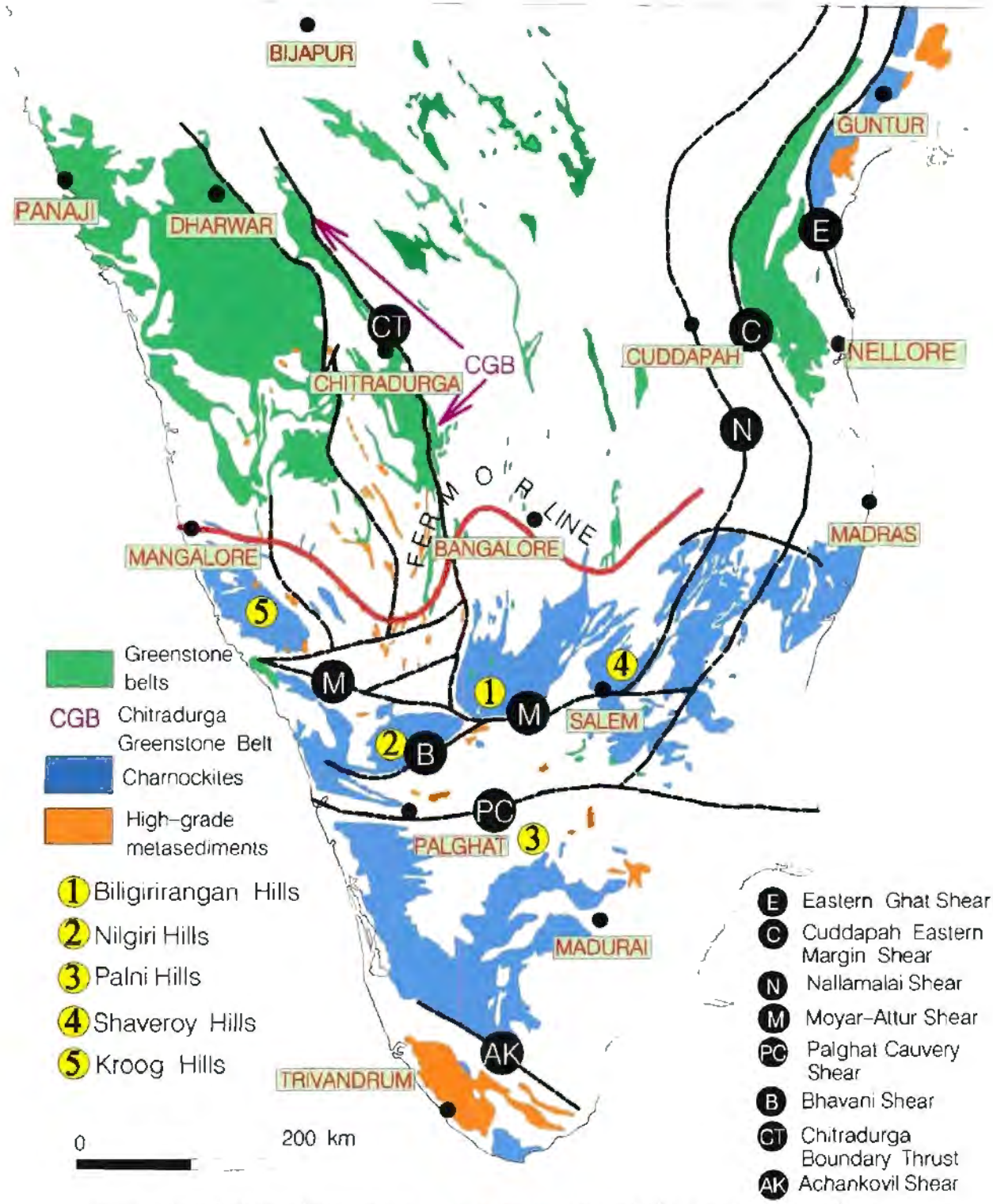

Fig. 1.4. Distribution of greenstone belts, charnockites and high-grade meta-sediments in the Southern Indian Shield (after GSI, 1994). The boundary between the dominantly charnockitic terrain and the granite-greenstone terrain is known as the 'Fermor Line'.

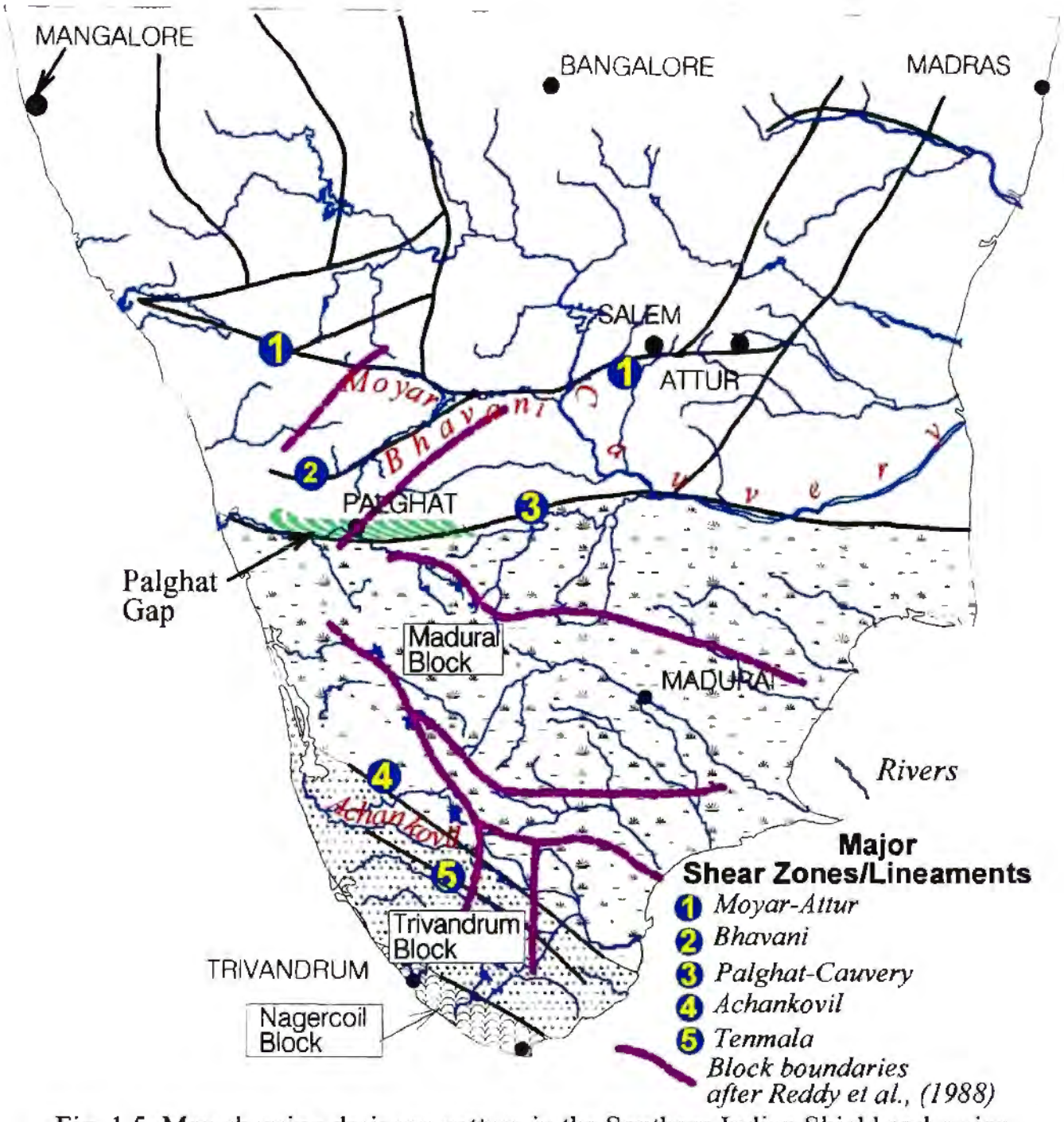

Fig. 1.5. Map showing drainage pattern in the Southern Indian Shield and major lineaments and previously interpreted (Drury et al.1984; GSI, 1994) shear zones. Note that these shear zones are aligned sub-parallel to major rivers present in the area. The Palghat Gap (green strippled area) is a corridor of negative topography bounded on either side by positive topography of chanockite massifs. Harris et al., (1994) classified the Southern Granulite Terrain (SGT) into three tectonic blocks, the Madurai Block, the Trivandrum Block and the Nagercoil Block along major lineaments. Similarly, Reddy et al. (1988) subdivided the SGT into seven blocks based on their interpretation of magnetic anomalies. Note that block boundaries defined by Harris et al. (1994) and Reddy et al. (1988) do not coincide.

prominent terrane[1] boundary with its continuation in the suspected terrane boundary between the Archaean Napier Complex and Proterozoic Rayner Complex of East Antarctica (Harris et al..1994); and (v) a prominent west-directed thrust belt (Chetty and Bhaskar Rao, 1996). Various geophysical constraints, for example, gravity (Mishra, 1988, 1992), magnetic (Reddy, 1988) and teleseismic (Rai et al. 1993; Ramesh, 1992) data have been used to support tectonic models involving the Palghat-Cauvery Lineament as a major crustal boundary. However, other interpretations of geophysical data highlight the absence of any geophysical break between the Dharwar craton and the Southern Granulite Terrain and infer that the granulites are exposed in the south because of northward tilting of the SIS (Hari Narayan and Subramhaniam, 1986).

To date, all these models are seriously impaired by absence of good field and geochronological data; some of the existing structural investigations across the Palghat-Cauvery Lineament, have cast doubt on large scale shearing along the Palghat-Cauvery Lineament, and thus question its status as a terrane boundary (Gopalakrishnan, 1981; Nair and Nair, 1980; Naha et al. 1996). The publication of new geologic maps at a scale of 1:500,000 (GSI, 1995a, b.) covering of whole of the SGT area and its contact with the Dharwar craton (Fig. 1.3) also highlights many hitherto unknown geological features on a scale beyond the small-scale geological maps generally used to support tectonic models. The most conspicuous feature of these new geologic maps is the near-absence of any large-scale tectonic lineaments along the zones previously interpreted as major shear zones on the basis of satellite data interpretation (i.e., Drury et al. 1984; GSI, 1994). This apparent difference between the geological maps and the satellite-based maps requires a re-evaluation of the structures and tectonic models of Peninsular India. A major question to be addressed in such re-evaluations is whether or not the

[1] The term terrane has a specific meaning in geology. According to Howell (1989), 'the term *terrane* describes a particular geologic body. ... A tectono-stratigraphic terrane has both structural (tectonic) and stratigraphic criteria- a fault bounded package of strata that is genetically unrelated to the adjoining stratigraphic packages - generically distinct from the other tectono-stratigraphic terranes and this is allochthonous with respect to surrounding terranes. ... *Terrain* with this spelling refers to topographic or physiographic features, as in a mountainous terrain, ...'

major shear zones interpreted on the basis of the satellite-imagery data actually exist. If they do exist, then what is the nature and the timing of movement along these large scale shear zones; and what do these shear zones tell us about the tectonic evolution of Peninsular India? Does any one of these shear zones represents a terrane boundary *sensu stricto* (cf. Howell, 1989)? If the shear zones are not terrane boundaries, what is their tectonic significance? Linked to these questions is the origin of geophysical anomalies commonly interpreted to extend along and across the Palghat-Cauvery Lineament (Fig. 1.3; GSI, 1994). Finally, can these major lineaments/shear zones be used with confidence in various models of reconstruction of Gondwana, in which these shear zones are linked with apparently similar shear zones on other continental fragments such as East Africa, Sri Lanka and East Antarctica (de Wit et al. 1995, 1998)?

In this thesis a number of corridors across several of the previously-inferred shear zones have been mapped to unravel the structural history within these lineaments. Field data were supplemented by U-Pb single-crystal zircon and monazite dating of a number of geologically well-constrained samples from different regions in several of these corridors. These new data have been used to re-evaluate tectonic models of the Peninsular India.

1.2. Introduction to the geology of the Southern Indian Shield (SIS)

1.2.1. Geological framework of the SIS

The southern Indian shield comprises essentially three geological provinces. These are the Eastern Ghats, the Dharwar craton and the SGT (Fig.1.1). A 20-35 km wide zone of transition between the Dharwar craton and the Southern Granulite Terrain, where amphibolitic rocks of the Dharwar craton transform to granulitic rocks of the SGT is known as the Transition Zone. The characteristics of these geological provinces are summarized in Table 1.1.

Table 1.1. Summary of geological features of principal tectonic units of the SIS.

	Dharwar craton		Southern Granulite Terrain	Eastern Ghats
	Western	Eastern		
Rock types	Granite-greenstone association; greenstone belts with substantial clastic sediments. These belts cover >15% of the area	Granite-greenstone association; greenstone belts have only subordinate elastic sediments. These belts cover <5% of the area	Charnockite, migmatite, paragneisses and metasediments.	Charnockite, migmatite, paragneisses and metasediments.
Structural trends	WNW-ESE to N-S; broad E-W trending warps	N-S to NNE-SSW	NE-SW to NW-SE through E-W; tight regional folds are common.	NE-SW
Metamor-phism	Greenschist to amphibolite facies with localy granulite facies	Low pressure-high temperature type	Mainly granulite grade	Mainly granulite grade
Geochro-nology	3.4 Ga-2.5 Ga; limited Neoproterozoic granitic activity is common in the south.	Dominated by ~2.5 Ga old gneisses. Sporadic Neoproterozoic granitic activity is common.	No reliable data for basement age are available. Neoproterozoic granitic activity and metamorphism are common.	Limited data indicate Archaean basement. Mesoproterozoic-Neoproterozoic granitic activity is widespread.

The eastern part of the Indian shield is bordered by a prominent NE-SW trending, elevated physiographic region (400 to 4000 metres) known as Eastern Ghats. The Eastern Ghats is mainly underlain by strongly deformed high-grade rocks, charnockite and khondalite (quartz-garnet-sillimanite-biotite±graphite±cordierite gneiss), intruded by a number of anorthositic massifs and alkaline plutons. The Eastern Ghats stretches from the Mahanadi (Gondwana) "graben" in the north almost to Nellore in the south, where the belt is covered by younger sediments (Figs. 1.1, 1.2). A central portion of the Eastern Ghats is cut by the Godavari rift basin (Fig.1.1).

To the west of the Eastern Ghats is the Dharwar craton of the Indian Peninsula Physiographically the Dharwar craton is represented by an undulating rolling topography, with an elevation range between 500m to 800m and an average elevation of ~600m. The Dharwar

craton comprises of a vast terrain of granitic gneiss (>200,000 km^2) with supracrustal belts of different lithological associations at various grades of metamorphism. The northern extension of the Dharwar craton is covered by the ~60-65 Ma Deccan flood basalts and Mesoproterozoic sedimentary basins. The Dharwar craton has been subdivided into the Eastern Dharwar and Western Dharwar blocks on the basis of contrasting litho-tectonic features (Swami Nath et al. 1976). The southern margin of the Dharwar craton is marked by a transitional boundary (spanning over ~30 km) into the Southern Granulite Terrain (SGT)[2].

The Southern Granulitic Terrain (SGT) is a topographically rugged terrain (600m to 2700m). It is essentially composed of high-grade rocks, charnockite and khondalite with associated amphibolite facies granitic gneiss and supracrustals. Charnockite generally occupies the higher terrain whilst associated granitic gneisses occur at lower elevations.

The tectonic relationships amongst these three geological provinces in the Peninsular India and their contact relationships are important in understanding the geological evolution of the SIS. A review of our present understanding of these geological provinces is given below.

1.2.2. The Eastern Ghat Granulite Belt

The Eastern Ghat Granulite Belt (Fig. 1.6; EGGB) comprises essentially high-grade metamorphic, polyphase-deformed rocks (Ramakrishnan et al. 1998). These include charnockite (orthopyroxene-bearing quartzo-felspathic gneiss), leptynite (garnet-perthite-

[2] Traditionally, the term Southern Granulite Terrain (SGT) is restricted to the area south of the granite-greenstone terrain of the Dharwar craton (see for example, see Fig.1 in Subrahmanyam, 1983). More recently, the term is often confined in a tectonic sense to a block (terrane) of the SGT to the south of the Palghat Cauvery Shear Zone which has a distinct lithological assemblages and thermal history as well as geophysical signatures (see for example, Santosh, 1996). The important distinction in this definition of the Southern Granulite Terrain (SGT) is the recognition of Neoproterozoic to Early Paleozoic charnockitization, in contrast to the Late Archean charnockitization of the Dharwar craton. The subdivision of the Southern Indian Shield into two separate terranes is based on limited data. In this thesis, for example, it will be shown that Neoproterozoic charnockitization and thermal events are present as least as far north as the Moyar-Attur Shear Zone. For this reason, the traditional description of the term Southern Granulite Terrain, i.e., a terrain dominated by granulite facies rocks and occurring south of the granite-greenstone terrain of the Dharwar craton is retained in this thesis (e.g., Fig.1.1).

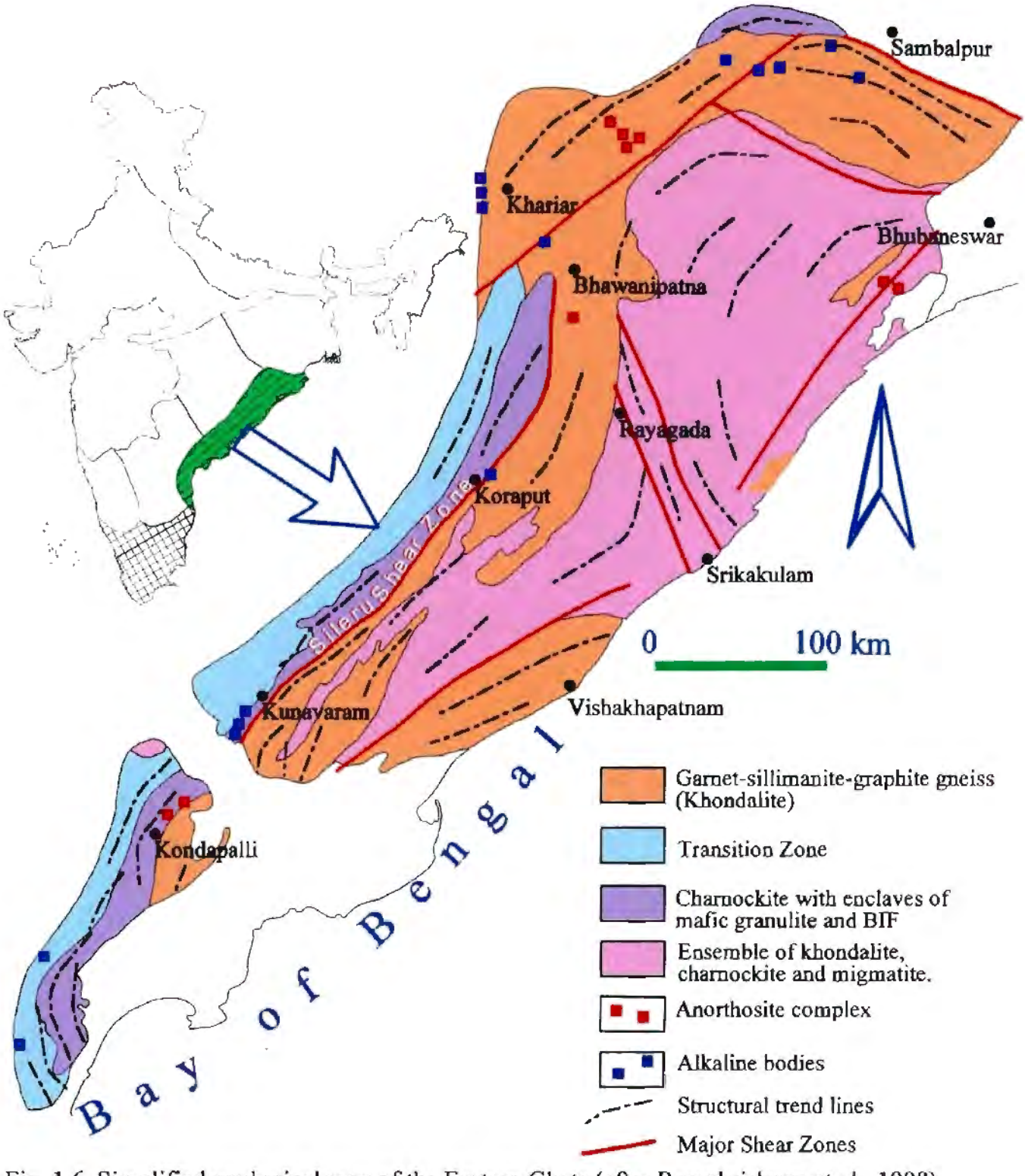

Fig. 1.6. Simplified geological map of the Eastern Ghats (after Ramakrishnan et al., 1998). Note that the Eastern Ghats is dominated by khondalite and associated paragneiss. The Sileru Shear Zone separates two contrasting lithological assemblages. The northwestern part is dominated by charnockite, basic granulite and BIF while the southeastern part is dominated by khondalite, migmatite with minor charnockite.

quartz ± plagioclase gneiss), mafic granulite (orthopyroxene-clinopyroxene-garnet ± plagioclase) and khondalite (quartz-garnet-sillimanite-biotite±graphite±cordierite gneiss). Structurally the area represents a complicated metamorphic terrain transected by a number of anastomosing regional shears (Chetty, 1995). The overall gneissic fabric of the Eastern Ghats is NE-SW, subparallel to the regional trend of the EGGB. A NE-SW trending major shear zone, the Sileru Shear Zone (Fig. 1.6) separates the EGGB into two distinct lithological provinces (Ramakrishnan et al., 1998). The western part is dominated by charnockite, basic granulite and BIF while the eastern part is dominated by khondalite, migmatite and minor charnockite.

Available geochronological data from the Eastern Ghats are mostly Rb-Sr and Sm-Nd whole rock isochrons or model ages. In many areas these ages are not well integrated with tectonic and metamorphic events. Shaw et al. (1997) have compiled available geochronological data from the Eastern Ghats. A few available Archaean ages from different parts of the Eastern Ghats indicate the antiquity of at least some of the Eastern Ghat rocks (Perraju et al. 1979; Paul et al. 1990). Available data suggest more than one period of high grade metamorphism. A 2.6 Ga metamorphic event is suggested by Perraju et al. (1979; whole rock Rb-Sr isochron) and by Vinogradov et al. (1964; U-Pb zircon age). Granulitic rocks of the EGGB have been sheared and subsequently migmatized and intruded by alkaline and anorthositic plutons. A few of the anorthosite massifs have been dated as between 1200 and 1400 Ma (Rb-Sr whole rock isochron; Sarkar et al. 1981). This implies the presence of a pre-1400 Ma granulitic event in Eastern Ghats. Subsequent metamorphic events at ~1.0 Ga, 800 Ma and 500-550 Ma have been recorded a number of workers (Shaw et al. 1997 and references therein). Some of these important events are summarized in Table 1.2.

Table 1.2: Summary of available geochronological data from the Eastern Ghats.

Age	Rock type/ Method	Location	Reference
~3025 Ma	Khondalite; Rb-Sr model age	Puri, Kashipatnam	Perraju et al. 1979
~2.9 Ga	Charnockite; Sm-Nd model age	Visakhapatnam	Paul et al. 1990
~2430 Ma	Khondalite; Rb-Sr model age	Kashipatnam	Perraju et al. 1979
~1400 to ~1200 Ma	Rb-Sr whole rock isochron of anorthosite	Chilka Lake	Sarkar et al. 1981
985±5 Ma	Charnockite; U-Pb monazite	Phulbani	Paul et al. 1990
~1088 Ma	Charnockite; U-Pb zircon	Angul	Aftalion et al. 1988
~1.0 Ga	U-Pb xenotime	Anakapalle and Vishakha-pattanam.	Grew and Manton, 1986
800-850 Ma	Rb-Sr and Sm-Nd mineral isochron of charnockite and pelite	Vishakhapatnam	Shaw et al. 1997
~600 Ma	K-Ar biotite		Aswathanaraya na, 1964
~550 Ma	Rb-Sr and Sm-Nd mineral isochron of pelites	Vishakhapatnam	Shaw et al. 1997

The boundary between the Eastern Ghats and the Dharwar craton is tectonic and generally modelled as a suture zone, mainly on the basis of a steep gravity gradient (Subrahmanyam, 1983) which is believed to represent more than 5 km vertical displacement (Kalia and Tewari, 1982 , referenced in Rogers, 1986). However, there is almost no field validation of this suture contact. Crookshank (1938) proposed that the contact between the granulite facies rocks of the Eastern Ghats and the amphibolite facies rocks of the Dharwar craton is gradational implying that both of them are parts of a single terrane.

1.2.3. The Dharwar Craton

1.2.3.1. Introduction

The principal rocks of the Dharwar craton are Early- to Late-Archaean TTG (tonalitic-trondhjemitic-granodioritic) gneisses of different ages (3.4 Ga to 2.9 Ga), collectively known as the Peninsular Gneiss, interspersed with Archaean supracrustal belts (greenstone belts) containing continental and oceanic-like volcano-sedimentary rocks, all intruded by Late Archaean (~2.5 Ga) calc-alkaline- to K-rich- granitic intrusives (Radhakrishna and Naqvi, 1986). The Dharwar craton is divided into eastern and western cratonic blocks (known as Eastern Dharwar and Western Dharwar, respectively) along the N-S trending ~2.5 Ga old Closepet Granite batholith (Swami Nath et al. 1976; Fig. 1.2). A deep Seismic Sounding (DSS) survey has identified two deep steeply dipping faults bounding the crustal blocks beneath the Closepet Granite (Kalia et al. 1979) . An alternative boundary has been identified along the eastern margin of the Chitradurga Schist Belt (CBT, the Chitradurga Boundary Thrust; Fig. 1.4; Drury et al. 1984) on the basis of Landsat imagery interpretation. A prominent lineament passes CBT. Southward, this lineament can be traced within gneisses, and further south defines the western flank of Biligirirangan granulite massif (Fig. 1.4). This lineament is reflected as a strong gravity gradient along the eastern margin of the Chitradurga Schist Belt (Fig. 1.4) as well as strong air-borne total magnetic intensity profiles (Hari Narain and Subrahmanyam, 1986) and as deep faults in DSS (Deep Seismic Sounding) profiles (Kalia et al. 1979). It is interpreted as an east dipping thrust along which deeper levels of Eastern Dharwar were emplaced across the western tectonic block. The Eastern Dharwar contains an abundance of K-rich granites (~2.5 Ga) with scattered occurrences of volcano-sedimentary supracrustal belts which, according to Drury et al. (1983), represent a deeper crustal level than that of the Western Dharwar. Important differences between the Eastern Dharwar and the Western Dharwar are given in Table 1.3.

Table 1.3 Important characteristics of Western and Eastern Dharwar.

	Western Dharwar	Eastern Dharwar
Areal Extent (Rogers and Giral, 1997)	6,500,000 km^2	375,000,000 km^2
Supracrustal Belts: Distribution and abundance	Supracrustal belts cover ~15% of the area	Supracrustal belts cover <5% of the area
Lithologies	Clastic sediments dominate supracrustal belts	Mafic volcanic rocks along with oceanic-like sediments dominate the supracrustal belts
Metamorphism	Medium pressure metamorphism is common	Low pressure metamorphism is common
Paleoproterozoic reactivation	Sparse	Very common

1.2.3.2. The Western Dharwar

The Western Dharwar is mainly composed of Archaean TTG (tonalite-trondhjemite-granodiorite) gneiss within which occur numerous scattered linear and irregular high-grade and low-grade supracrustal belts and younger granitoids. The relationship between these different litho-tectonic units is controversial (Srinivasan and Naqvi, 1990; Ventaka Dasu et al. 1991; Rogers and Giral , 1997; Pichamuthu, 1982; Pichamuthu and Srinivasan, 1983, 1984; and Naha, 1987; Mukhopadhyay, 1986). Amongst the supracrustals, the high-grade and low-grade supracrustal belts have been classified into two different lithostratigraphic units: the older Sargur Group and the younger Dharwar Supergroup (Swami Nath et al. 1976; Radhakrishna and Vasudev, 1977). The basis of this classification has been lithologic-association, metamorphic and structural discordance and presence of a regional angular unconformity between the Sargur and Dharwar Group, marked by presence of a distinct quartz-pebble conglomerate at the contact (Ramakrishnan and Viswanatha, 1987). The Sargur Group is composed mainly of high-grade supracrustals including serpentinised komatiite, high grade pelite, fuchsitic quartzite and minor layered barite. These rocks are mainly restricted in

the southern part of the Dharwar craton. The Dharwar Supergroup consists of low- to medium-grade supracrustals and are common in the northern part of the Dharwar craton. Based on lithological association, the Dharwar Supergroup has been classified into a lower Bababudan Group and an upper Chitradurga Group. The lithologic-assemblage of the Bababudan Group consists of vesicular basalt, quartzite, pelitic schist, phyllite alternating with subordinate felsic volcanics, ultramafic rocks and BIF. The upper Chitradurga Group is dominated by quartzite, marble, pelitic schist, phyllite and BIF, with subordinate polymict conglomerate, pillow basalt, rhyolite and manganiferous sediments. Within the Dharwar greenstone belts, in general, metamorphic grade commonly increases towards their margins (Mukhopadhyay, 1986 and references therein). Belts containing high-grade rocks have also been reported from many widely separated regions in central and northern part of Dharwar craton (Mukhopadhyay, 1986 and references therein). These high-grade supracrustals are often included within the Sargur Group. However, it is not certain whether these spatially separated high-grade supracrustals constitute a single litho-stratigraphic unit or if they represent high-grade equivalents of low- to medium-grade rocks of different greenstone belts.

1.2.3.3. The Eastern Dharwar

The Eastern Dharwar comprises mainly younger granites with subordinate TTG (tonalite-trondhjemite-granodiorite) gneiss. Supracrustal belts are much less abundant than in the Western Dharwar, and are smaller and narrower (Figs. 1.3,1.4). They occur as long N-S trending linear belts. These lithologic assemblage of the supracrustal belts also differs from that of the Western Dharwar. The Eastern Dharwar supracrustal belts contain mainly volcanic assemblages of pillow basalts, rhyolite, pyroclastics and associated polymict conglomerate, phyllite, and BIF with subordinate quartzite, marble and pelite. Similar to the Western Dharwar, both high-grade and low-grade supracrustals are present in the Eastern Dharwar. Supracrustals of this block exhibit low-pressure metamorphism in contrast to the medium-pressure metamorphism of the Western Dharwar. Radhakrishna (1983) hypothesized that the

supracrustals of the Eastern Dharwar belong to an older greenstone cycle than those in the Western Dharwar, because their lithologic assemblagesuggest that they were formed prior to the large-scale intrusion of TTG (~3 Ga), while the supracrustals of the Western Dharwar postdate these TTG. However, others maintain that available structural data suggest coeval development of the supracrustals in both blocks and that the two blocks represent exposures of different levels of Archaean crust (Mukhopadhyay, 1986).

1.2.3.4. The Transition Zone

The boundary zone across which rocks of Dharwar craton change from low- to medium-grade to high grade and charnockitic rocks in the south is known as the Transition Zone (Ramienger et al. 1978). The width of the Transition Zone varies between 20 to 35 kilometres (Condie and Allen, 1984). South of the Transition Zone is the Southern Granulite Terrain (SGT). The SGT is occupied by vast expanse of massif charnockites in the Nilgiri Hills, Biligirirangan Hill, Sheveroy Hills and in the Madras area (Fig. 1.4, 1.7).

The tectonic nature of the boundary between the Dharwar craton and the granulitic terrain in the south (Southern Granulite Terrane, SGT) remains unclear. Fermor (1936) first suggested that the boundary between the charnockitic province in the south and the non-charnockitic province in the north ('Fermor line') is a fundamental litho-tectonic boundary. The charnockitic region of the SGT was traditionally considered as a mobile belt surrounding the Dharwar craton. Subsequently, however, areas showing incipient charnockitization, indicating metasomatic transformation of the granitic rocks of the Dharwar craton, were reported from all along the 'Fermor line' (Pichamuthu, 1965, Subramaniam, 1967). Gradual increase in paleopressure from 5-6 kbar north to 8-10 kbar in the south (Gopalakrishna et al. 1986) and metamorphic grade from the Dharwar craton to the SGT in the south were documented across the Transition Zone, whilst some structural and lithologic elements were traced continuously across the amphibolite facies-granulite facies boundary along the southern margin of the

Dharwar craton (Hansen et al. 1984; Mukhopadhyay, 1986). Similarly, gravity and magnetic trends continue across the Fermor line without any major deflections. The charnockitic massifs along the southern edge of the amphibolite facies rocks of the Dharwar craton are also part of the Dharwar craton. These observations undermine the nature of the 'Fermor line' as a simple tectonic boundary. Ramakrishnan and Swami Nath (1981) had suggested that the boundary between the Dharwar craton and the mobile belt in the south (which SGT is believed to represent) should be placed either along the Bhavani lineament or the Achankovil Lineament. Harris et al. (1994) suggested that the northern boundary of the SGT can be placed along the Palghat-Cauvery lineament and that charnockites north of the lineament including the Transition Zone should be considered as part of the Dharwar craton.

1.2.3.5. Charnockitization in the Transition Zone

Charnockites are abundant in the Transition Zone. Within the Transition Zone, gneissic rocks of the Dharwar craton and mafic enclaves in them have apparently been converted into charnockites and mafic granulite, respectively. The transitional relationship between charnockites and granite gneiss has been described by many in detail (Pichamuthu, 1960; Ramiengar et al. 1978, Janardhan et al. 1979, 1982; Friend, 1985). Charnockite in the Transition Zone occurs in irregular patches or along ductile shear zones cutting across the gneissic foliation. The earlier foliation is generally obliterated within the charnockite, although ghost relics of foliation can commonly be traced through the converted part (Chapter 2, Fig. 2.8; 2.9). This can be shown both on outcrop scale (Chapter 2) and regional scale (Drury and Holt, 1980). These relationships have led to the interpretation that charnockite formation is a metasomatic process (Newton et al. 1980)

Janardhan et al. (1979, 1982) first described the mechanism by which the conversion of amphibolite facies rocks into charnockitic rocks could have occurred during prograde metamorphism and fluid activity. This process is believed to involve the dehydration of

amphibolite facies rocks during their equilibration with an invading CO_2-rich volatile phase introduced from an undetermined deep source. The CO_2-rich solutions are believed to have driven off H_2O-bearing solutions from the rocks which, in turn, caused K-metasomatism and partial melting. More recently, hypersaline brine has been considered the most important charnockitizing fluid (Newton et al. 1998).

The possibility of more than one charnockitization event in the Dharwar craton was first suggested by Pichamuthu (1953, 1960), who classified charnockites into two groups: an earlier group formed by regional metamorphism of pre-existing Peninsular Gneiss and Dharwar schist, known as massive- or highland-charnockite; and (ii) a later group of charnockite formed by widespread metasomatism of Peninsular Gneiss This later variety is also known as incipient type or the 'low-land charnockite-type'. This two-fold classification of charnockites has received wide acceptance, although neither their genetic nor their chronologic distinctions have been verified. It may be instead that incipient types progressively give way to massive types of charnockite (Ramienger et al. 1978, Friend, 1985). In this model, during charnockitization, channelized fluid flow causes incipient charnockitization; with time, the fluid impregnates the entire rock, which leads to complete conversion of the rock into massive charnockite (Friend, 1985). This model is consistent with my own observation that incipient charnockites are common in the foot-hills of large massive charnockites (Chapter 3) Thus it may be that for both incipient charnockites of the Transition Zone and the massive charnockites south of the Transition Zone, the process of charnockitization has taken place *in situ*, under essentially static conditions, postdating major processes of formation of gneissic fabric of the terrain.

1.3. Structure and Tectonics of the Southern Indian Shield

1.3.1. Structure of the Dharwar craton

The dominant structural trend of the supracrustal belts of the Dharwar craton in the north is NNW-SSE which swings to N-S in the south. Trends of the supracrustals of the Western Dharwar are more variable. For example, the Bababudan belt in the northern part shows dominant E-W trends. According to Drury and Holt (1980), the NNW-SSE trend of the supracrustal belts reflects the trend of shear belts into which preexisting structures have been rotated. From Landsat satellite imagery studies, Drury and Holt (1980) identified a number of NNW-SSE to N-S trending shear zones. The existence of many of these shear zones is, however, not supported by field data (Mukhopadhyay, 1986). Parallelism of the linear supracrustal belts and the consistent structural pattern over a wide region does, however, suggest a regionally consistent stress pattern.

1.3.2. Structure of the Southern Granulitic Terrain (SGT)

1.3.2.1. Distribution of lithological units

The area south of the Transition Zone is known as the Southern Granulite Terrain (SGT). It is dominated by a number of large charnockitic massifs that occupy generally elevated topography. Some of the prominent charnockitic massifs include: the Biligirirangan Hills, the Nilgiri Hills, the Sheveroy Hills of the Salem area, the Anaimalai Hills, the Palni Hills, the Cardamom Hills and the Nagercoil Massif (Fig. 1.7). These charnockitic massifs comprise massive charnockite and enderbite with mafic granulite and high grade metasedimentary enclaves. The massive charnockites are non-foliated rocks in which there is no trace of an earlier planar penetrative fabric of the protolith. The protoliths of massive charnockites include both para- and ortho-gneisses. The charnockitic massifs are surrounded by granitic gneiss

(both ortho- and para- gneisses) and non-charnockitized supracrustals of amphibolite to granulite facies, which include khondalite, calc-silicate rocks, quartzite, and amphibolite (Fig. 1.3). The supracrustals occur generally at low elevations. Around many of the charnockite massifs, over widely scattered areas, evidence of incipient charnockitization showing prograde relationships are present. Most the of the contact regions between the charnockitic massifs and amphibolite facies gneisses in the southern granulitic terrain have been described as gradational (e.g., Narayanaswamy and Lakshmi, 1967, near Tinnevelly; Saravanan and Ramanathan, 1973, near Salem; Holt and Wightman, 1983, on the eastern side of the Kodaikanal Massif). Thus, around each of the isolated charnockitic massif in SGT, there exists a local transition zone varying from few 100s metres to few km in width, similar to the Transition Zone south of the Dharwar craton.

1.3.2.2. Major lineaments of the SGT

The southern boundary of the Dharwar craton is marked by a number of Charnockite massifs. These are, from west to East, the Kroog Massif, the Biligirirangan Hill Massif and the Saveroy Hill Massif (Figs. 1.4, 1.7). To the south of these charnockitic massifs there is a ca.100 km wide E-W trending belt which, with some exceptions, lacks the high topographic expression of the charnockitic massifs to the north. To the south of this belt, a number of charnockitic massifs give rise to elevated topography (Anaimalai Hills Massif, Palni Hills Massif, Cardamom Hills Massif, Fig. 1.7). The southern boundary of the topographic low region extends from Palghat in the west to Tiruchirapally in the east, and is known as the Palghat-Cauvery Lineament (PCL). The northern boundary is along the Moyar river in the western part through a prominent valley in the eastern part passing through Salem and Attur (Fig. 1.5) and is known as the Moyar-Attur lineament (MAL). Between the northern and southern bounding lineaments there are a number of smaller lineaments, either sub-parallel to or at a low angle to the bounding lineaments. These lineaments also mark boundaries of a few charnockite massifs (*e.g.*, the Nilgiri Hill Massif in the west and the Kollimalai Hill Massif in

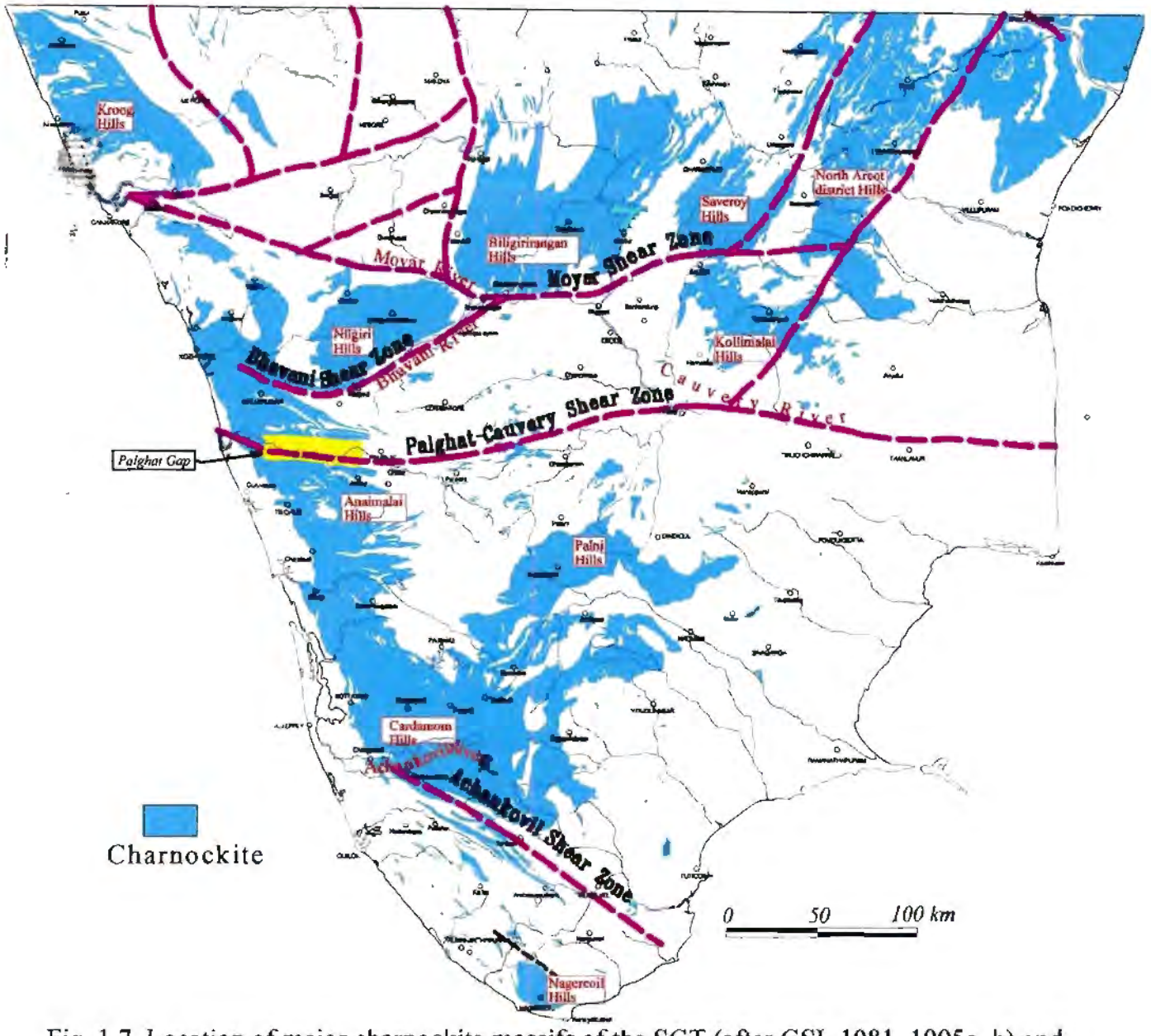

Fig. 1.7. Location of major charnockite massifs of the SGT (after GSI, 1981, 1995a, b) and previously interpreted shears (Drury and Holt, 1980; GSI, 1994). Note that shear zones are mostly located along major rivers and along boundaries of major charnockite massifs.

the east). The E-W trending region of low topography bounded by the MAL in the north and the PCL in the south has long been recognized by many workers. The best expression of this physiographic contrast is in the western part of the PCL near Palghat, where it is known as the Palghat Gap (Fig. 1.7). Different interpretations have been given for the origin of the Palghat Gap, including tectonic (Reddy et al. 1988, Thara and Soman, 1993), fluvial erosion (Jacob and Narayanaswamy, 1954), marine erosion (Arogyaswamy, 1962), crustal-upwarp and related development of fractures (Subrahmanian and Muralledharan, 1985), post Jurassic uplift of blocks on either side of the physiographic lineament (Vaidyanadhan, 1977) and escarpment slopes.

Another prominent lineament, the Achankovil lineament, occurs further south (Fig. 1.6 and 1.7). It demarcates a boundary between massive charnockite of the Cardamom Hills and the granitic gneiss-metasediments dominated Kerala Khondalite Belt (also known as the Trivandrum Block; Fig. 1.7). This lineament trends NW-SE from just south of Kottayam in the west to Tirunelveli in the south. In the west, part this lineament follows the trend of the Achankovil River (Fig. 1.7) and from there become asympotic to the west coast of India.

1.3.2.3. Shear zones in the SGT

The SGT has been interpreted to comprise a number of tectonic blocks (Reddy et al. 1988; Harris et al. 1994). The model of Harris et al. (1994) is an integrated interpretation of the satellite imagery interpretation of Drury and Holt (1980), and Nd-model age data (n=56) from both the SGT and the Dharwar craton. Based on geological arguments, Harris et al. (1994) distinguish three tectonic blocks within the SGT. These are: the Madurai Block, the Trivandrum Block and the Nagercoil Block (Fig. 1.5).

The block boundaries of Reddy et al. (1988) were interpreted on the basis of low-pass filtered magnetic anomaly data. They argued that the SGT is composed of a mosaic of at least seven

different blocks and that the block boundaries mark zones of considerable vertical and/or horizontal movement. However, the block boundaries interpreted by Reddy et al. (1988) and by Harris et al. (1994) do not coincide (Fig. 1.5).

Although precise block boundaries of various models differ, it is generally agreed that the block boundaries are marked by major shear zones that follow major topographic lineaments (Fig. 1.7). For example, the tectonic blocks of Harris et al. (1984) are bounded by three major shear zones: the Moyar Shear Zone (MSZ), the Bhavani Shear Zone (BSZ), the Palghat-Cauvery Shear Zone (PCSZ) and the Achankovil Shear Zone (ASZ) of which the PSZ is considered to mark a major terrane boundary in the SGT. The basis of the identification of these shear zones has remained mainly the interpretation of satellite imagery data (Drury and Holt, 1980; GSI, 1994; Chetty, 1996). The presence of sharp changes in the trends of various lithologic units as observed in satellite imagery data influenced the identification of the shear zones. However, on the ground, these trends of lithologic units, interpreted from satellite imagery, do not always reflect the tectonic fabric of an area. Field validation of the major shear zones based on satellite imagery is lacking; those few field-based investigations available have cast doubt on the interpretation of the satellite imagery interpretations (Naha and Srinivasan, 1996, Nair and Nair, 1980; Gopalakrishnan, 1981 for the PCSZ; and Radhakrishna et al. 1990 for the ASZ).

One of the main factors that influenced the development of major topographic lineaments in the SGT is the competance difference between charnockites and their non-charnockitized protoliths. The boundaries between these different rock types are metasomatic boundaries which often transect litho-stratigraphic boundaries and shear zones. The newly-published geological maps of SGT (GSI, 1995 a,b; Fig. 1.3) highlight this relationship. In a number of places on these maps, quartzite and calc-silicate bands transect the charnockite-granite gneiss boundaries. For example, near Rajampalayam in the Madurai Block, the charnockite-gneiss boundary transects quartzite bands (Fig. 1.3). Because these shear zones are crucial in

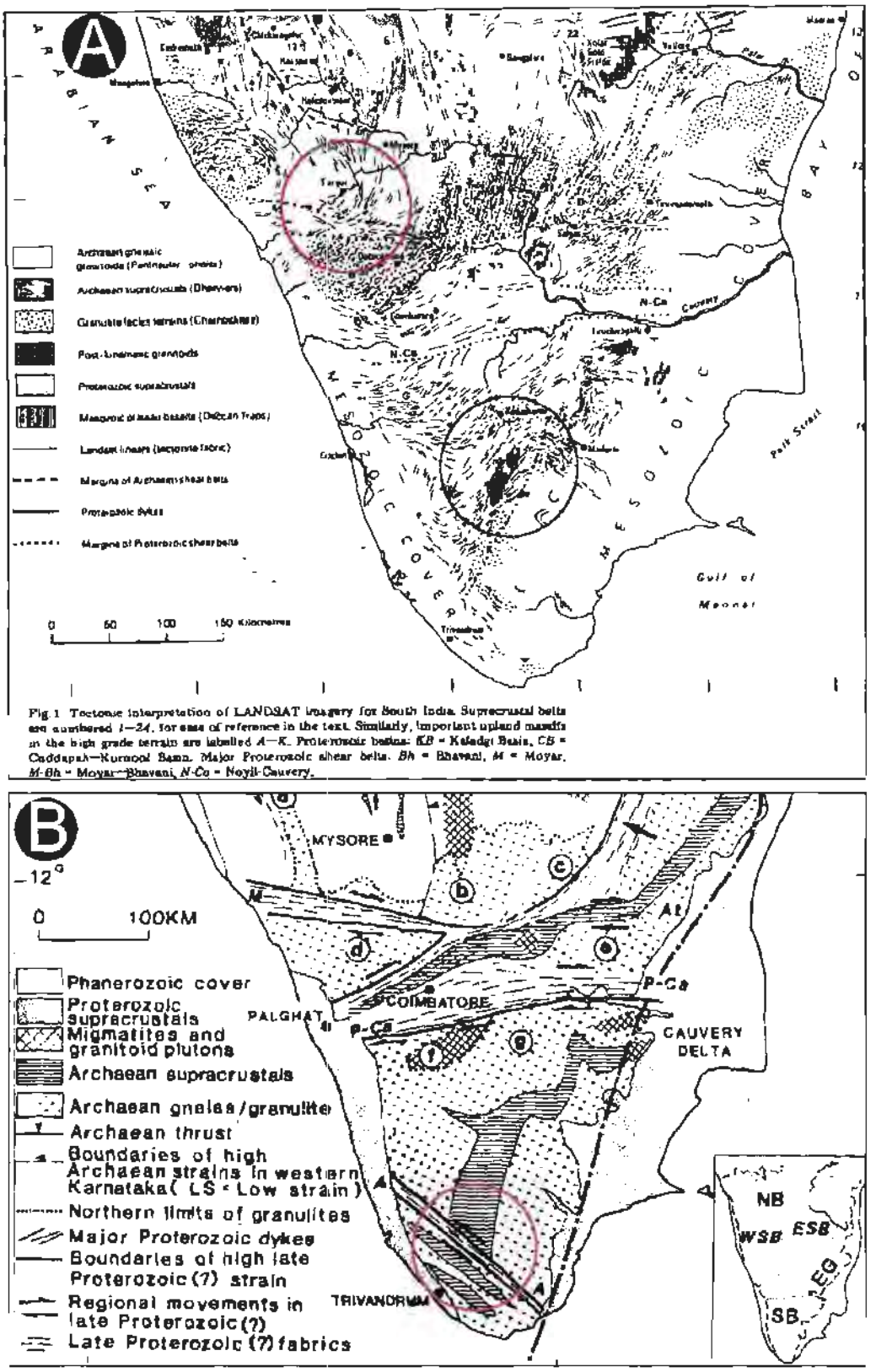

Fig. 1.8. Tectonic fabric map and its interpretation of the South Indian Shield (SIS) by Drury and Holt (1980) and Drury et al. (1984). A. Landsat Imagery interpretation of the SIS (Drury and Holt, 1980). Note: (i) south of Sargur (marked by pink circle) curvilinear tectonic grain cuts across the Moyar Shear zone and (ii) a discordance in the structural grains exists between the areas northwest and southeast of Kodaikanal (marked by blue circle). B. Tectonic interpretation of structural fabric of the SIS (Drury et al., 1984). Note that a sharp discordance in the structural trend has been interpreted across the Achankovil Shear Zone (marked by red circle). This discordance is not evident in the Landsat imagery interpretation (see map A).

understanding the tectonic framework of the SGT, the status of understanding of these shear zones is described below in some detail.

1.3.2.4. Description of the major shear zones in the Southern Granulite Terrain

A Landsat imagery study by Drury and Holt (1980) recognised three major subvertical shear zones with dominant strike-slip movement in Southern Indian Granulite Terrain (see Fig. 1.8). These are:

(1) **The Moyar and Bhavani Shear Zone** (MSZ and BSZ)

(2) **The Palghat-Cauvery Shear Zone** (PCSZ) and

(3) **The Achankovil Shear Zone** (ASZ)

1.3.2.4.1. Moyar, Bhavani and Palghat-Cauvery shear zones

The MSZ, the BSZ and the PCSZ were considered by Drury and Holt (1980) to be part of a complex anastomosing shear system with broadly E-W trend bound in the north by the Moyar Shear Zone (MSZ) along the Moyar-Attur Lineament (MAL), and in the south by the PCSZ along the Palghat-Cauvery Lineament (PCL). There are a number of smaller shear zones within this shear system, either subparallel or at low to moderate angle to the two major boundary shears. These smaller shear zones mark boundaries of some prominent charnockitic massifs within the PCSZ; for example, Kollimalai Hills Massif in the east and the Nilgiri Hills Massif in the west (Fig. 1.7 & 1.8). The most prominent of these smaller shear zones is the NE-SW trending Bhavani Shear Zone (BSZ), which marks the southeastern boundary of the Nilgiri Hills Massif.

Drury and Holt (1980), through study of satellite imagery, noted that in the western part of the MAL, across the E-W trending Moyar valley, the regional strike swings from roughly N-S through NE-SW to roughly E-W in the valley itself; then south of the valley, the regional strike reverts back to NE-SW in the Nilgiri Hills. Based on this observation, they proposed that the MAL represents a major dextral shear zone that follows the Moyar valley in the west, to the Attur valley in the east, passing through the Bhavani and Salem areas (Fig. 1.7 & 1.8). They interpreted this shear zone as being nearly 20 km wide. They further assumed that the Nilgiri Hill Massif (south of the MAL), and the Biligirirangan Hill Massif (north of the MAL), were originally adjacent to each other, and subsequently displaced by at least 70 km of dextral strike-slip movement along the MSZ. They also noted the presence of new planar and linear fabrics, extensive augen gneiss and retrogression of high grade rocks along the MSZ. The BSZ marks the southeastern limit of Nilgiri Hill Massif. The trend of this shear is sub-parallel to the strike of lithological units on both sides of it. Drury et. al. (1984) also assumed dextral strike-slip movement along this shear zone (Fig. 1.8). It was thought by them that the MSZ and the BSZ merge near Satyamangalam (Fig. 1.7) and from there they continue as one shear zone upto Salem. Further east, the shear zone bends to the NE and merges with the shears along the eastern boundary of the Cuddapah basin where they have affected Neoproterozoic rocks. On this basis, Drury et al. (1984) interpreted both the MSZ and the BSZ to be Neoproterozoic.

The southern boundary of the shear system is defined by a prominent E-W trending shear zone, the Palghat-Cauvery Shear Zone, broadly along the Noyil and Cauvery Rivers (Fig. 1.5). The PCSZ is not evident in the Landsat imagery data, as it is concealed for most of its length by recent alluvium. Drury et al. (1984) noted that there is no structural evidence in field for this shear zone. However, they placed the southern limit of PCSZ along the northern flank of the Anaimalai and Palni Hills charnockitic massifs (Fig. 1.7, 1.8). The overall delineation of this shear zone was accepted by many later workers (e.g., GSI, 1994; Chetty, 1996). Chetty (1996) cited gravity and aeromagnetic anomaly maps in support of the existence of this shear zone, but neither gravity nor aeromagnetic maps show any well defined lineament along this

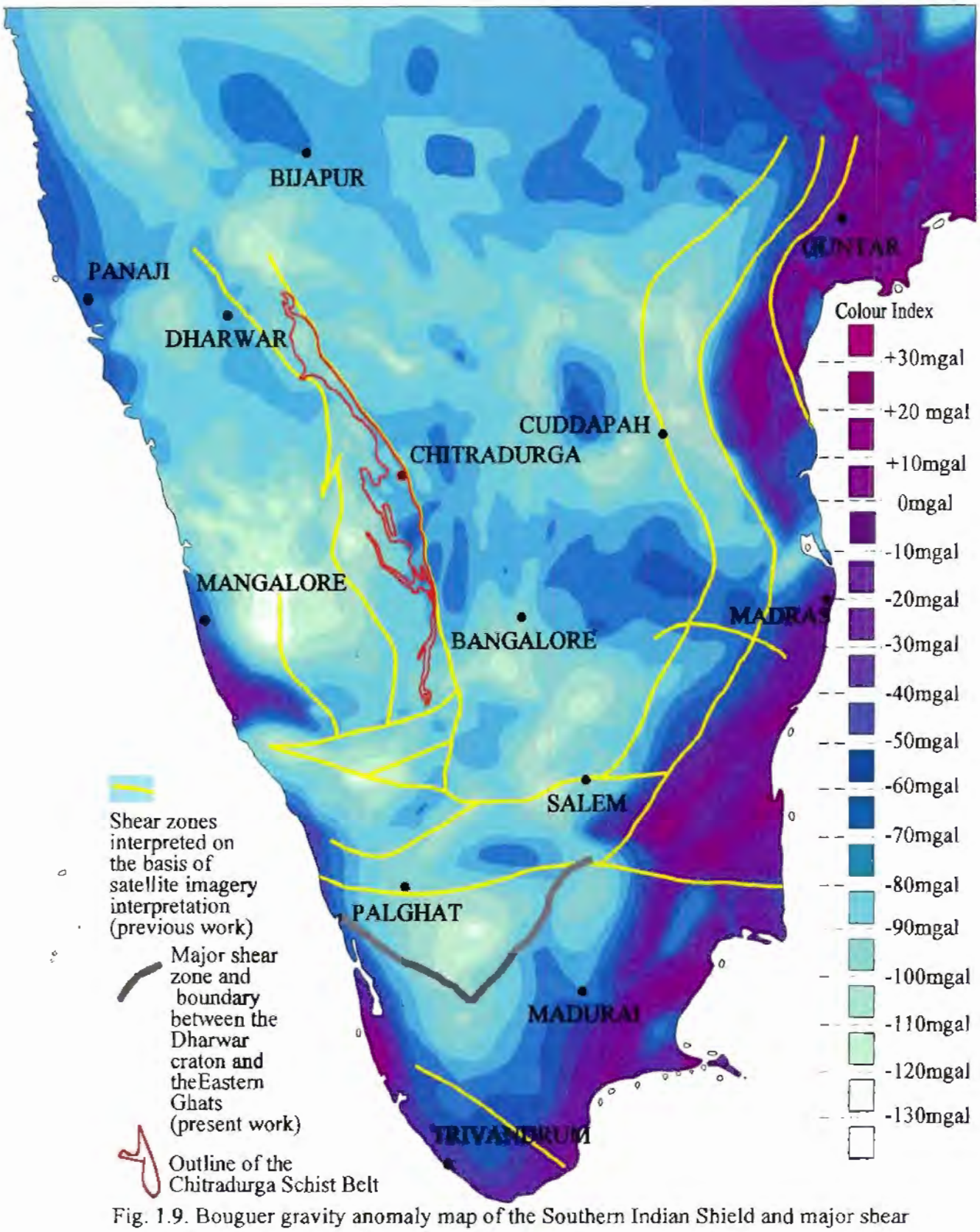

Fig. 1.9. Bouguer gravity anomaly map of the Southern Indian Shield and major shear zones. Note that the Chitradurga Schist Belt broadly coincides with a strong gradient. Sources: Bouguer gravity anomaly, N.G.R.I., 1978; Shear zones and outline of the Chitradurga Schist Belt, Geological Survey of India, 1994.

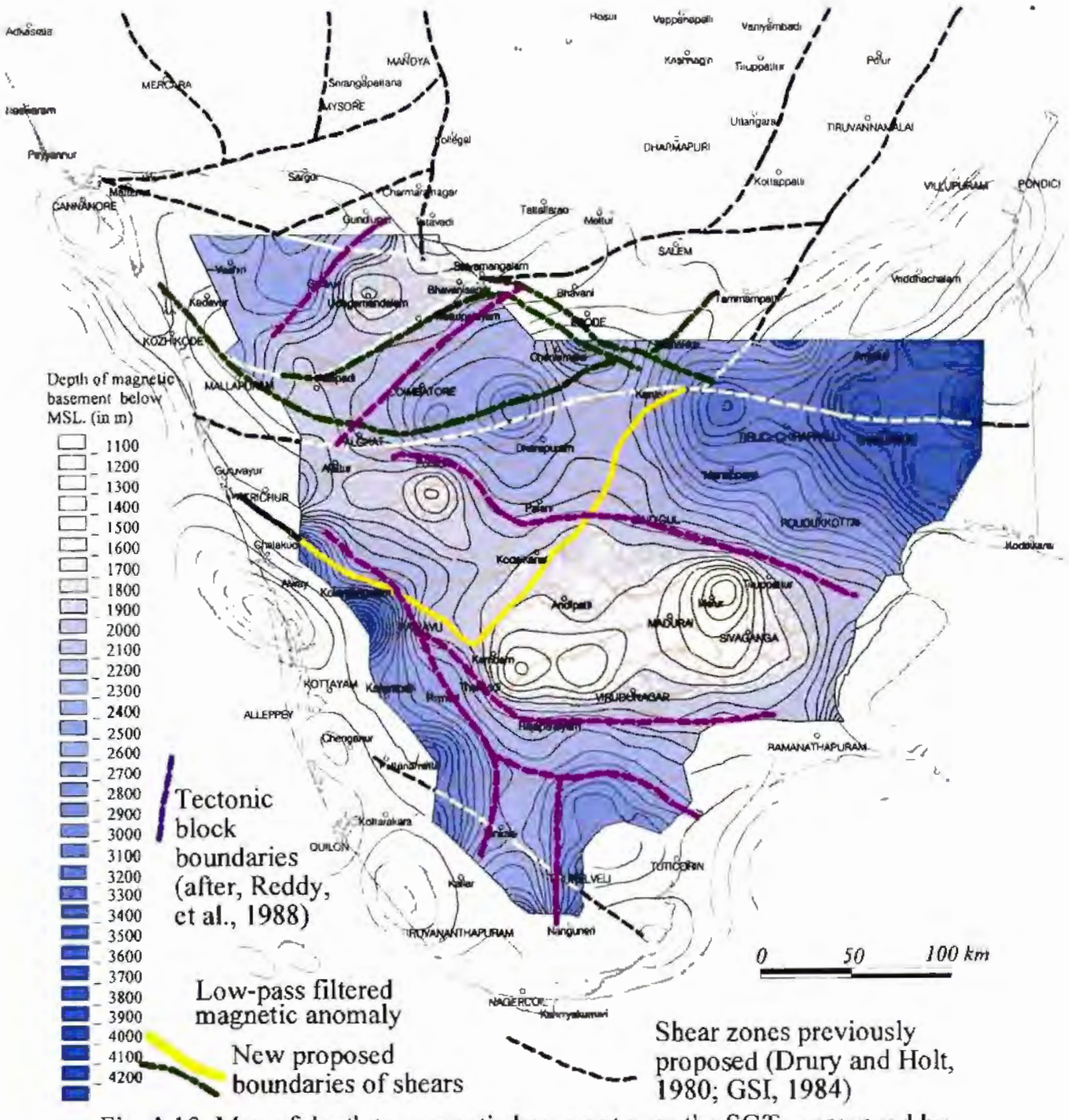

Fig. 1.10. Map of depth to magnetic basement over the SGT superposed by contours of low-pass filtered anomaly and boundaries of tectonic blocks (after Reddy et al., 1988). The magnetic basement was assumed to reflect a horizon marking change of magnetisation and hence composion of rocks. The low-pass filtered anomaly shows the trend of variation in the magnetisation in the lower crust or Moho. Note that the PCSZ and the ASZ both cut across a number of lows and highs in the magnetic basement.

shear zone (Fig. 1.9 & 1.10). Ramakrishnan (1993) opined that the Palghat-Cauvery Shear Zone marks the southern boundary of the Dharwar craton, and he named the area south of this shear zone the Pandyan Mobile Belt (Fig. 1.2).

1.3.2.4.2. The Achankovil Shear Zone

The Achankovil Shear Zone (ASZ) was identified along the Achankovil Lineament (Fig. 1.5) primarily on the basis of assumed differences in the strikes of the lithological units on both sides of the lineament (Drury et al. 1984). From satellite imagery study it was interpreted that the structural trends of lithological units in the northeastern part of the Achankovil Lineament is NNE-SSW, and that this trend abuts against the lineament. On the other hand, in the area south of the lineament, the structures are NW-SE, subparallel to the lineament. The ASZ was interpreted to have a dominantly sinistral strike-slip movement (Drury et al. 1984). Radhakrishna et al. (1990), on the other hand, pointed out that at least some of the lithological units can be traced across the Achankovil Lineament. This is also clear on the recent 1:500,000 scale geological map of the area (GSI 1995a,b), which depicts a gradational change in the litho-tectonic strike across the lineament (Fig. 1.3), possibly related to folding. This negates presence of substantial strike slip movement along this shear zone.

Another shear zone, the Tenmala Shear Zone, grazing the southern boundary of the Achankovil Lineament and south of the ASZ, has been identified by some workers (Chacko et al. 1987; GSI, 1995b; Sacks et al. 1997). This shear zone is about 3-4 km wide. Sacks et al. (1997) proposed that the Tenmala Shear Zone is a major shear zone with dominantly dextral strike-slip movement. However, others maintain that the Achankovil and the Tenmala shear zones have dominantly sinistral strike-slip movement (Rajesh et al. 1998).

1.3.2.5. Discussion

Since Drury et al. (1980) first proposed the presence of major trans-continental shear zones in the SGT, these have been widely accepted by majority of workers in the Southern Indian Shield; and these shear zones have been widely applied as a structural framework for many subsequent tectonic model of the SGT and for Gondwana reconstructions (Kriegsman, 1993; Windley and Razakamanana, 1996). These shear zones have been hypothesized as representing terrane boundaries and/or suture zones by various workers (e.g., ASZ, Srikantappa, 1984; MSZ, Srikantappa 1993; PCZ, Harris et al. 1994).

In much of the above quoted literature, field validation of the structural model proposed by Drury et al. (1980) is generally lacking. However, some investigators (e.g., Nair and Nair, 1980, Gopalakrishna; 1981 and Naha and Srinivasan, 1996) of the PCSZ have cast doubt on the presence of the major shear system proposed by Drury et al. (1980). Gopalakrishnan (1981), for example, mentions that structural trends of the Precambrian rocks from the northeastern part of the Anaimalai Hills into the Palghat Gap (Fig. 1.6) are continuous. Nair and Nair (1980) noted that the general structural style of the Palghat area is dominated by NE-SW to NNE-SSW trending isoclinal folds, which in many cases are coaxially refolded. There is no evidence of intense shearing in the western part of the Palghat lineament (Gopalakrishnan, 1981; Nair and Nair, 1980; Naha and Srinivasan, 1996). Naha and Srinivasan (1996) observed that there is no major difference in the structural style from north of the Moyar lineament to south of Palghat lineament. Recently published geological maps of the area at a scale of 1:500,000 (GSI, 1995) corroborate these observations: these maps do not depict any major shear zone along the Palghat-Cauvery Lineament.

1.4. Geophysics of the Southern Indian Shield

1.4.1. Magnetic data

The sub-surface map of the magnetic basement of the SGT reveals a block structure of the SGT in which the depth to the basement varies from -1100m to -4000m below mean sea level (Fig. 1.10). Seven block boundaries were recognized by (Reddy et al. 1988; Figs. 1.5, 1.10). The majority of these block boundaries display NW-SE or NE-SW trends, at a high angle to the E-W trending Palghat-Cauvery Lineament. Low-pass filtering processing on the magnetic data reveals that some of the block boundaries identified in the magnetic basement map may extend to deeper crustal levels. The anomaly trends in the magnetic maps and those in the low-pass filtered map do not correspond unequivocally (Fig. 1.10) although good coherence between these two types of magnetic anomaly maps has been suggested by Reddy et al. (1988) and has been used as a support for the block structures of the SGT. The Palghat-Cauvery Lineament zone is not reflected in either the magnetic basement map or the low-pass filtered anomaly map. On the magnetic basement map, two conical depressions separated by a NNE-SSW trending high in the central part may outline this area (Fig. 1.10). The lineament is also at a high angle with other prominent anomaly trends evident on the low-pass filtered anomaly map.

1.4.2. Gravity Data

1.4.2.1. Dharwar craton

The gravity field over the Peninsular India maintains a general north-easterly trend along the east coast and a north-westerly trend along the western coast (Fig. 1.9). In the central part, across the Dharwar craton, the gravity field is mainly negative, varying between -60 and -120 mgal and is characterised by several highs and lows (Fig. 1.9). The 'highs' (-60 to -80 mgal) in most cases are associated with greenstone belts, while the 'lows' (-90 to -130 mgal) often occur over granitic bodies. Gravity modelling of the greenstone belts and associated granites

suggests that they are bounded by steeply dipping faults (Subrahmaniyam and Verma, 1982). It also shows that Chitradurga belt has a deep narrow trough of at least 8-10 km thickness in the central part (Hari Narain and Subrahmanyam, 1986), consistent with the interpretations of sutures between the eastern and the western blocks.

1.4.2.2. Southern Granulitic Terrain (SGT)

The SGT is characterized by a strong negative gravity fields (-50 to -120 mgal) with a sharp negative anomaly in the interior of the region. This overall negative gravity field signature has been explained by the effect of regional gravity compensation of the elevated charnockitic massifs of the Nilgiri, Palni, Cardamom and other Hills having long roots (Subrahmanyam, 1983). However, within the charnockite massifs there are considerable variations over in gravity signatures. Within the charnockitic terrain, gravity highs are associated with mafic granulites and gravity lows are observed over felsic charnockites. Neither the Transition Zone nor the major satellite interpretation based shear zones are associated with any sharp gradients on the Bouguer anomaly map (Hari Narain and Subrahmanyam, 1986).

1.4.2.3. Eastern Ghat Granulite Belt (EGGB)

The gravity field of this belt ranges from -50 mgal to +40 mgal. Such an elevated gravity field compared to that of the Dharwar craton, in spite of the higher topographic elevations of the EGGB, suggests either a basic difference in the lithologic associations or a difference in the crust/mantle depths. Or it could be due to a difference in the depth of compensation. In detail, there are several narrow anomaly belts that run for hundreds of km along the length of the Eastern Ghats terrain. A number of the gravity highs have been explained by the presence of partly exposed and unexposed gabbro bodies (Verma, 1985, p. 84) whilst subparallel negative gravity anomalies have been interpreted in terms of emplacement of granitic and charnockitic bodies.

The gravity gradient across the boundary of the Eastern Ghats and the Dharwar craton is very steep, which was interpretated as a sharp tectonic contact (Hari Narain and Subrahmanyam, 1986).

1.4.3. Seismic data

3-D seismic tomography studies (Rai et al. 1992, 1993) reveal that the crust beneath the southern granulitic belt is thicker by 2-4 km and displays lower velocity than that underlying the Dharwar craton. The estimated crustal thickness below the Dharwar craton is around 33 - 34 km, while the estimated thickness below the SGT is around 35 - 37 km (Ramesh et al. 1992). A low velocity zone of the SGT extends from 35 km up to 200 km in the upper mantle while the mantle underneath the Dharwar craton is of high velocity. The velocity break, which is gradational, between the two terrains may be placed along lat. 12°30'N, which roughly coincides with the boundary between the charnockitic and non-charnockitic province (Fermor Line). The low velocity, thickened crust and the low velocity upper mantle below the granulitic terrain have been interpreted as due to Precambrian continent-continent collision during which subduction of the Dharwar plate occurred southwards beneath an "ancient continent" (Rai et al. 1993). This model supports the hypothesis that the Fermor line may represent a fundamental tectonic boundary (e.g. Fermor, 1936). This model, however, cannot explain the higher heat flow observed in the granulitic terrain compared to the adjacent gneissic terrain. Within the granulitic terrain, the area adjacent to the Palghat-Cauvery Lineament is underlain by higher velocity crust, which was hypothesised to be due to underplated mafic material (Rai et al. 1993). But, as mentioned in the section 1.4.2.2, the area does not show a gravity high which is expected if there is underplating mafic material along the Palghat Cauvery Lineament.

1.4.4. Palaeomagnetism

Available palaeomagnetic data from the Dharwar craton and the SGT were compiled by Radhakrishna and Joseph (1993). Both terrains have similar pole positions and Apparent Polar Wandering Paths (APWP) after ~2.0 Ga, implying that the Dharwar and the SGT had been in approximately their present positions relative to one another since then. This is in contrast to the hypothesis Drury et al. (1984) that there has been substantial displacement and even convergence among different crustal blocks along ductile shears in the SGT.

1.5. Geochronological Framework of Southern Indian shield

1.5.1. Overview

Available geochronological data from the Southern Indian Shield are meagre. A compilation of available geochronological data up to 1986 is given on the Isotopic Age Map of India, published by the Gelogical Survey of India (1988). The majority of the data consist of Rb-Sr or Sm-Nd whole rock data. However, in recent years some new U-Pb zircon age data from different areas have become available. These data allow some constraints on the various magmatic and metamorphic events. A compilation of representative age data highlighting various geological events is summarized in Table 1.4 and in Fig. 1.11

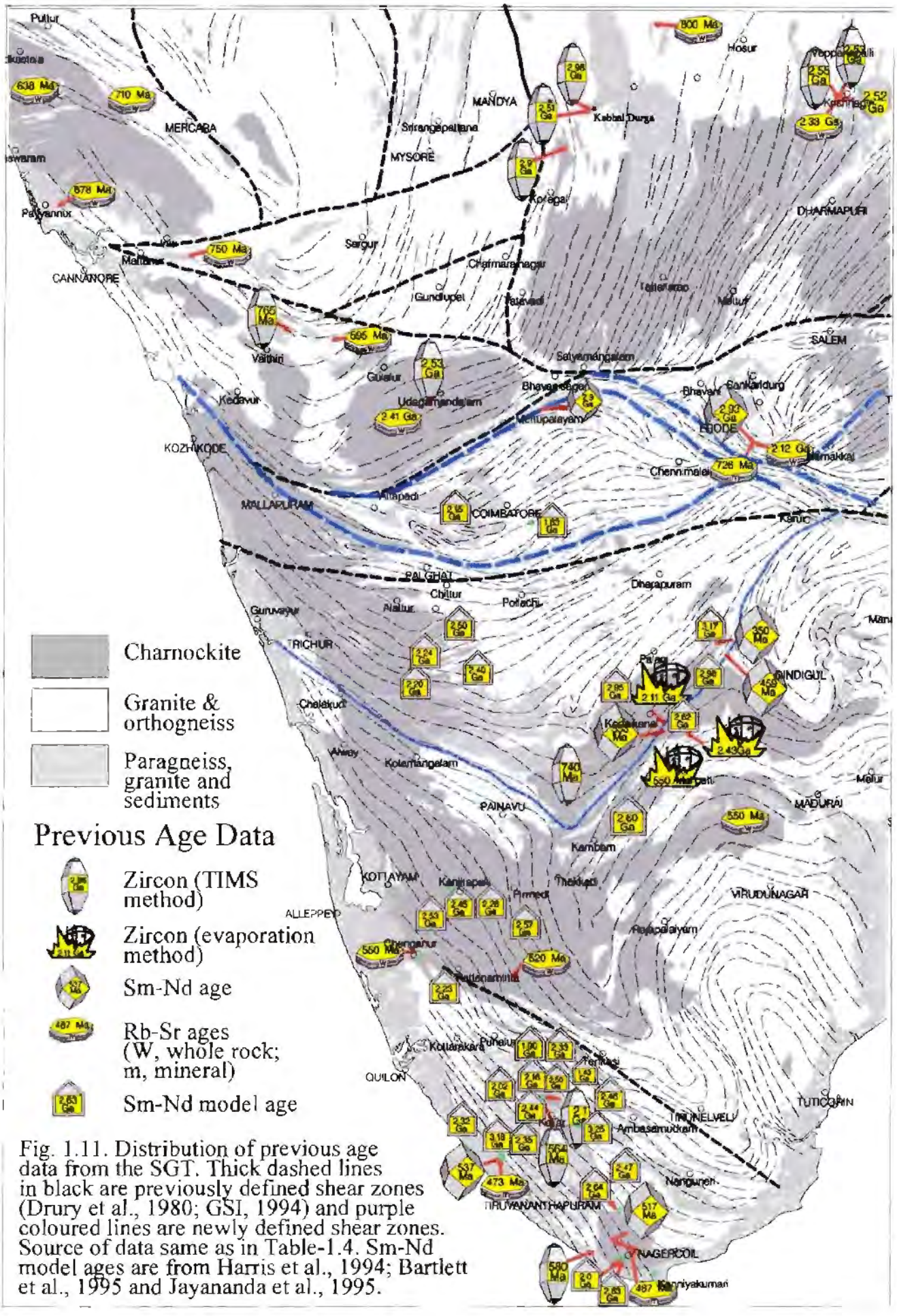

Fig. 1.11. Distribution of previous age data from the SGT. Thick dashed lines in black are previously defined shear zones (Drury et al., 1980; GSI, 1994) and purple coloured lines are newly defined shear zones. Source of data same as in Table-1.4. Sm-Nd model ages are from Harris et al., 1994; Bartlett et al., 1995 and Jayananda et al., 1995.

Table 1.4. Geochronology of magmatic and metamorphic events from different parts of the southern Indian shield:

Age range	Dharwar Craton		Transition Zone	SGT
	West	East		
~3.4 Ga 3.6-3.1 Ga	(a). Rb-Sr whole-rock isochron (Beckinsale et al. 1980) and Pb-Pb isochron age of feldspar (Meen et al. 1992) from Peninsular gneiss. (b). SHRIMP ages of zircons (Nutman et al. 1992) and Nd-model age (Taylor et al. 1988) of meta-sediments of the Sargur Group.		~3.4 Ga U-Pb concordia upper intercept of zircons (Buhl, 1987; Peucat et al. (in prep.) cited by Jayananda et al. 1996)	
3.3-3.1 Ga	(a). 3.3-3.2 Ga ($^{206}Pb/^{207}Pb$ age by single zircon evaporation technique [Peucat et al. 1993]; Rb-Sr whole rock isochron of granite gneiss [Bhaskar Rao et al. 1991]) (b). 3.3 Ga U-Pb SHRIMP age of zircons from felsic volcanics [Peucat et al. 1995]. (c). 3.0-2.9 Ga (Rb-Sr whole rock isochron age of granite gneiss [Monrad, 1983; Stroh et al. 1983] and Sm-Nd whole rock isochron age [Drury, 1983] and Rb-Sr whole rock isochron age [Bhaskar Rao et al. 1992 and 1996] of mafic volcanics).		~2.9 Ga U-Pb zircon (SHRIMP) dating [Friend and Nutman, 1992] and zircon evaporation age [Mahabaleswar et al 1995]	
2.7-2.5 Ga	(a). 2.7-2.5 Ga (Rb-Sr whole rock isochron age [Bhaskar Rao et al. 1992]; Pb-isotope whole rock isochron [Taylor et al 1984] and single zircon SHRIMP age [Nutman et al. 1996] of felsic volcanics in Dharwar Supergroup. (b). ~2.6 Ga U-Pb zircon age [Vinagradov et al. 1964]; ~2.5 Sm-Nd whole rock isochron [Bernard-Griffiths et al. 1987] of Madras Chamockite.	(a). ~2.7 Ga (Sm-nd whole rock isochron age [Balakrishnana et al. 1990] of mafic volcanics. (b). ~2.5 Ga single and sphene age from granite gneiss (Krogstad et al. 1991)	~2.5 Ga single zircon and monazite ages from chamockites and gneisses (Peucat et al. 1989, 1993; Jayananada et al. 1995 and Mahabaleswar et al. 1995)	~2.5 Ga (U-Pb concordia upper intercepts of zircons [Buhl.,1987]; zircon evaporation age [Peucat et al. quoted by Jayananda et al. 1996]
2.5-2.1 Ga		~2.4 Ga $^{40}Ar/^{39}Ar$ age of muscovite (W. D. Sharp as cited by Krograd et al. 1991).	(a). ~2.3 Ga and ~2.1 Ga Rb-Sr biotite-whole rock age (Peucat et al. 1993) (b). Rb-Sr biotite age in granite gneiss within MSZ [Peucat et al. cited by Jayananda et al. 1996)	~2.4 Ga zircon evaporation age of granite gneiss [Bartlett et al. 1995] and ~2.1 Ga zircon evaporation age of Chamockite [Jayananda et al. 1995]
~1.8 Ga			$^{40}Ar/^{39}Ar$ age of biotite from khondalite in KKB [Kelley et al. 1997]	
800-850 Ma		K-Ar and Rb-Sr whole rock age of alkaline dykes (Anil Kumar et al. 1989; Radhakrishna and Joseph, 1993)		
800-600 Ma	Rb-Sr whole rock isochron of alkaline granites (Nair and Vidyadharan, 1982; Nair et al. 1985; Santosh et al. 1989			Sm-Nd mineral isochron of mafic granulite from Sittampudi complex (Bhaskar Rao et al. 1996]
~600-500 Ma				Kr-Ar whole rock age of granite (Soman et al. 1983); U-Pb monazite age and Sm-Nd mineral isochron in chamockite (Buhl., 1987; Choudhary et al. 1992; Unnikrishnan-Warrior et al. 1995; 1997) Re-Os dating of molybdenite in chamockite (Santosh et al. 1994)

1.5.2. Protolith ages

1.5.2.1. The Dharwar Craton

Recently geochronological data on some areas of the Dharwar craton and Southern Granulitic Terrain have been compiled by Jayananda and Peucat (1996). Protolith ages, determined by U-Pb zircon and Rb-Sr whole rock methods, of the Peninsular Gneiss date at ca 3.3-3.4 Ga and 2.9-3.1 Ga. Many intermediate ages are common, and the Peninsular Gneiss can be regarded to span an evolutionary continuum from ~3.4 Ga and ~3.0 Ga. Field classification of the supracrustals into age groups and their relationship with various phases of the Peninsular Gneiss is unresolved. However, detrital zircons from supracrustals of the Holenarashipur and Banavara belts have yielded U-Pb zircon ages between 3.58 Ga and 3.13 Ga (Nutman et al. 1992). Peucat et al. (1995) reported U-Pb zircon ages of 3298 ± 7 Ma from a meta-rhyolite layer in 'Dharwar type' supracrustal of the Holenarashipur belt. These data suggest that at least some of the supracrustals are Early Archaean in age, similar to the surrounding gneisses.

Younger ages have been recorded from some other supracrustal belts. Notable are a Sm-Nd whole rock isochron age of 3.03 ± 0.23 Ga from mafic volcanics of the Bababudan belt (Drury, 1983); a 2.614 ± 8 Ma SHRIMP age of zircons from felsic volcanics in the Shimoga belt (Nutman et al. 1996); and 2.658 ± 14 Ma to 2.691 ± 18 Ma SHRIMP ages of zircons from the Sandur belt in the northern part of the craton. In the Eastern Dharwar mafic volcanics of the Kolar Schist Belt yield an Sm-Nd whole rock isochron age of 2732 ± 155 Ma (Balakrishnan et al. 1990).

Thus both the supracrustals and the surrounding gneiss of the Dharwar craton have an Early to Late Archaean range of formation ages.

Early Archaean TTG gneisses (>3.0 Ga) have mostly been recorded from central and northern part of the Western Dharwar craton. In the eastern and southern part of the craton there are

records of extensive 2.6-2.5 Ga crustal magmatism. Gneisses from the Kolar-Bangalore area in the southeast, from the Salem-Krishnagiri-Gundlupet area in the southern part and from the Nilgiri Hills area in the southwestern part all have recorded extensive 2.6-2.5 Ga granitic intrusion followed by charnockitization (Krogstad et al. 1991; Peucat et al. 1989; Jayananda et al. 1995b).

1.5.2.2. The Southern Granulite Terrain

Geochronological information south of the Palghat-Cauvery Lineament is more limited. Single crystal zircon ages have been obtained (using the zircon evaporation technique) on a meta-granite and a charnockite, yielding 2436 ± 4 Ma and 2115 ± 8 Ma, respectively (Bartlett et al. 1995; Jayananda et al. 1995). The zircon evaporation technique yields ^{206}Pb-^{207}Pb ages which are reliable only if the zircons are concordant and simple; any discordance yields a falsely lower age. Thus, these ages can be taken to indicate ~2.5 Ga or older protoliths south of the Palghat-Cauvery lineament. However to date, there is no confirmation of rocks older than ~2.5 Ga south of the lineament. Further south, in the Kerala Khondalite Belt, no reliable protolith ages are available.

1.5.3. Ages of metamorphism and other tectono-thermal events

1.5.3.1. Dharwar craton: Archaean to Paleoproterozoic

In the Dharwar craton, the Sargur Group is demonstrably polymetamorphic. The first metamorphism, which was of upper amphibolite to granulite facies, has been dated at about 3.1 to 3.0 Ga (see Mukhopadhyay, 1986 for review). Charnockitization within and north of the Transition Zone has been well constrained to have occurred at around 2.5 Ga by U-Pb allanite, monazite and zircon dating of charnockites (Buhl et. al., 1983; Grew and Manton, 1984; Friend and Nutman, 1992; Mahabaleswar, 1995). More than one event of

metamorphism has been recognised in outcrop as well as on a regional scale (Mahabaleswar and Peucat, 1988). But delineation of domains of different metamorphic events has not yet been attempted. Until such time when different metamorphic events can be distinguished on a geochronological basis and their domains delineated, a broad generalisation that the metamorphic grade increases towards south may not have any tectono-thermal meaning.

Dating of biotite from charnockites in the Transition Zone by Rb-Sr method has yielded ages ranging 2.4 Ga to 2.2 Ga (Buhl, 1987; Peucat et al. 1993). Because the closure temperature of biotite is <350°C, it is generally taken that the area remained undisturbed from 2.2 Ga onward.

1.5.3.2. Dharwar craton: Neoproterozoic thermal events

Some newly available U-Pb dating of granitiods from different parts of Dharwar craton have concordia lower intercept ages between 500-800 Ma. For example, Rogers et. al. (1995) report a U-Pb concordia from the Arsikere Granite of the Dharwar craton in which zircon and allanite grains define an upper intercept of ~2.62 Ga and a lower intercept of 442 ± 54 Ma. This may indicate a significant Pb-loss event during the Early Paleozoic.

Nutman et al. (1996) dated a number of granitoid bodies (U-Pb on zircon using the SHRIMP method) from the central and northern parts of the Dharwar craton. Many of these results yield well-defined lower concordia intercepts between ~500 Ma and ~800 Ma. Although near-surface leaching of Pb may also cause concordia lower intercepts (Mezger and Krogstad, 1997), the possibility of a Neoproterozoic thermal event cannot be excluded. In fact, Neoproterozoic magmatic and metamorphic events are well documented in the eastern part of the Dharwar craton. Here, for example, whole-rock biotite ages (Rb-Sr and K-Ar; Aswathanarayana, 1964), fission track ages of apatite and zircon from the Nellore Schist Belt and elsewhere in the east of Dharwar craton (Nagpaul and Mehta, 1975; Prasad et al. 1979)

have documented magmatic and metamorphic event between ~440 and ~700 Ma. In the southeast of the Krishnagiri area (i.e., in the southeastern part of Eastern Dharwar craton) a number of alkaline bodies have Rb-Sr whole-rock ages between ~700 Ma and ~800 Ma (see Anil Kumar et al. 1996 for review). An isotopic age map of India published by GSI (1986) also reveals a few Neoproterozoic K-Ar and Pb-Pb whole rock ages from the Dharwar craton north of the Moyar-Attur Lineament. Nutman et al. (1996) believe that the scatter in many published Rb-Sr mineral and whole rock 'errorchrons' from the Western Dharwar craton could be the result of Neoproterozoic resetting.

There are also a number of Neoproterozoic alkaline granite bodies in the western part of the Dharwar craton, north of the Moyar lineament (see review by Santosh et al. 1989). Although it may be argued that such Neoproterozoic alkaline bodies represent anorogenic emplacement, and may not represent a regional tectono-thermal event, they overlap in age with thermal events in the southern granulite belt (see below).

1.5.3.3. The Southern Granulite Terrain: The Madurai Block

Neoproterozoic thermal events have been revealed in the area between the KKB and the PCL (known as the Madurai Block) through circa 560 Ma zircon evaporation ages from charnockites of the Kodaikanal and Gangurapatti area (Bartlett et al. 1995; Jayananda et al. 1995), and by Rb-Sr mineral isochrons between ~760 Ma and ~550 Ma of a number of granitic bodies (Santosh et al. 1989). However, geochronologic information from this area is sparse and there are no reliable age data from non-charnockitized terrains of the Madurai Block. Therefore, whether the Neoproterozoic thermal event was pervasive throughout the Madurai block, especially in its eastern part, is not known at present.

1.5.3.4. The Southern Granulite Terrain: the Kerala Khondalite Belt

In the Kerala Khondalite Belt, a Neoproterozoic granulite facies metamorphic event at ~550-520 Ma has been well-documented from Sm-Nd mineral isochrons obtained on charnockite, khondalite and cordierite gneiss (Choudhary et al. 1992; Unnikrishnan-Warrior et al. 1995; Jayananda et al. 1996). A number of alkali granite plutons also record this Neoproterozoic granulite facies event. Sm-Nd and Rb-Sr whole rock and mineral isochrons illustrate that these isotopic systems were completely reset during this Neoproterozoic granulite facies event (Choudhary et al. 1992, Santosh et al. 1992; Unnikrishnan-Warrier et al. 1995, 1997). An U-Pb monazite age (~550 Ma) from patchy charnockites of the Kerala Khondalite Belt also record this Neoproterozoic thermal event (Buhl., 1987). Rb-Sr whole rock-biotite isochrons from charnockites and khondalites have yielded ages that range between ~470 Ma and ~480 Ma (Buhl., 1987; Unnikrishnan-Warrior, 1995) which suggests that the terrain passed through the biotite blocking temperature of ~350°C around that time. Recently, Ar-Ar dating of biotite in the matrix of khondalite and as inclusions within garnet have yielded ~455 Ma and ~1.8 Ga ages (Kelly et al. 1997). The ~455 Ma age has been interpreted as the age of cooling of the rock below ~350°C; the ~1.8 Ga age has been interpreted as the age of garnet growth during a previous high-grade metamorphism and was not reset by Neoproterzoic event because of protective cover of garnet.

1.5.4. Discussion

Presently available data suggest that the Dharwar craton is made up of ~3.0 Ga and older TTG gneisses and greenstone belts. In the Transition Zone and further south in the Nilgiri Hills Massif, the protolith ages are ~2.5 Ga. Further south in the Kodaikanal area there are indications of continuation of this ~2.5 Ga old protolith. However, precise age information is lacking.

There are at least two well-documented charnockitization/high-grade metamorphic events in the SIS. One is at ~2.5 Ga, which is well recorded in the Transition Zone; the other is ~550 Ma, which is well-documented in the Kerala Khondalite Belt and in the Nagercoil Block. This implies that different parts of the Southern Indian Shield have been affected by charnockitization separated in time by ~2000 Ma. A ~2.9 Ga charnockitization event has also been suspected in the Transition Zone, but this has not been confirmed (Mahabaleswar and Peucat, 1988).

Many workers have highlighted the abundance of Neoproterozoic Rb-Sr (whole rock or mineral reset) ages south of the Palghat-Cauvery Lineament in contrast to their absence north of the Palghat-Cauvery Lineament. This has prompted the suggestion that this lineament marks the boundary between two (allochthonous) terranes with contrasting tectonothermal histories (Harris and Santosh, 1993; Harris et al. 1994). The question as to why it is that Rb-Sr systematics in biotite from the charnockites of the Transition Zone were not reset during Neoproterozoic time, however, remains unanswered. A possible explanation may be that although biotite generally releases its Sr above about 350°C or higher (Dodson, 1979) and thus resets the Rb-Sr radiometric clock in it, at such temperature other minerals surrounding the biotite may not able to accept the released Sr, particularly in dry environments containing charnockite.

The Neoproterozoic thermal event was clearly more intense in the southern part than in the Dharwar craton. Rogers et al. (1995) pointed out that the Dharwar craton had suffered a major tectonic-magmatic event at ~3.0-3.1 Ga. This, they hypothesized, depleted the lower crust of its significant incompatible heat-producing elements.

1.6. Summary of Tectonic Framework of the Southern Indian Shield

There have been a number of tectonic models of the evolution of Peninsular India. Fermor (1936) believed that high grade terrains of the Eastern Ghats and the SGT represent mobile belts to the Dharwar craton (Fig. 1.12a), and that there has been considerable vertical movement between the craton and these mobile belts. With the discovery of gradual variation in metamorphic grade across the charnockite non-charnockite terrains, the Dharwar craton was thought to extend beyond this Transition Zone into the SGT. Pichamuthu (1965) postulated a northward plunging anticlinorium for the rocks of the Southern Indian Shield, so that the deeper portions are now exposed in the south. Important assumptions in such simplistic tectonic interpretations have been that: (i) all the charnockitic rocks in the SGT represent higher grade metamorphic equivalents of the greenstone to amphibolite facies rocks in the north, and formed at deeper levels of the crust, and (ii) the higher grade rocks in the south and the lower grade rocks in the north are products of the same metamorphic event. The common occurrence of incipient charnockites in unmetamorphosed granites (Nathan et al. 1994) and along brittle fractures in them (Chapter 2) it is likely that in many places charnockites also have formed at a higher level in the crust than where amphibolitic rocks are generally stable. Thus, the assumption in (i) above is not always true. Again, the presence of more than one generation of charnockite in the SIS have been demonstrated by well constrained geochronological data (Grew and Manton, 1984; Choudhary et al. 1992). So the assumption (ii) is also not correct.

It is now generally accepted that charnockites of the SGT have formed during at least two different charnockitization events, at ~2.5 Ga and the other ~550 Ma (Peucat et al. 1993; Choudhary et al. 1992; Unnikrishnan-Warrier et al. 1995). The ~2.5 Ga event occurs in the northern part of the SGT while the ~550 Ma event is more prevalent in the southern part of the SGT. Therefore, neither of these charnockitization events affected the entire SGT. In fact, the SGT includes large mappable regions of amphibolite facies rocks with widespread

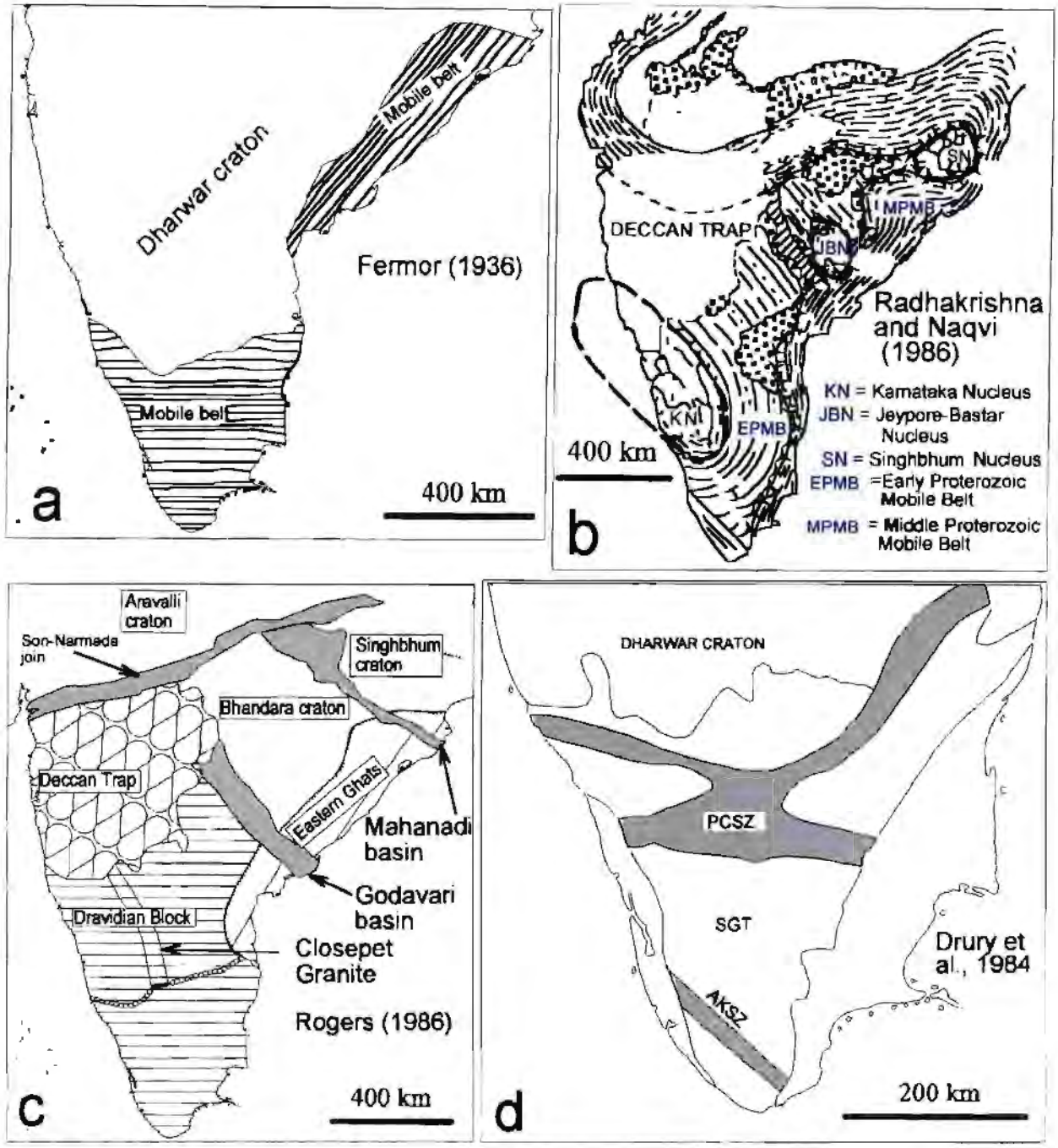

Fig. 1.12. Simplified maps of southern India showing major models referred in text.

a. Fermor (1936) considered that the Eastern Ghats and the Southern Granulite Terrain are mobile belts flanking the Dharwar craton. He hypothesized considerable vertical movement along the contact between these two terrains. b. Radhakrishna and Naqvi (1986) considered that the entire Peninsular sheild are made up of three relics of Archaean nucleii (KN, JBN and SN) surrounded by distinct Early Proterozoic and Middle Proterozoic mobile belts (EPMB and MPMB).

c. Rogers (1986) considered that Peninsular India is a mosaic of five tectonic blocks superated by 'joins'. These 'joins' are either thrust planes (e.g., the Eastern Ghats-Bhandara contact) or rift valleys (e.g., the Bhandara- Dravidian Block). He considered that the Dharwar craton and the Southern Granulite Terrain form a single tectonic block which he named as the Dravidian Block.

d. Drury et al., (1984) considered that the peninsular sheild is madeup of a number of anastomosing trans-continental shears. One of these shears (the Palghat Cauvery Shear Zone, PCSZ) was later interpreted as a terrane boundary marking a suture zone between the Dharwar craton and the SGT (Harris et al. 1993).

occurrence of only incipient charnockites.

Because more than one regional metamorphic event and charnockitization has occurred in the Southern Indian Shield, it is difficult to test a hypothesis that holds that the charnockitic terrain is merely a deeply eroded equivalent of a non-charnockitic part in the north. This is because the extent and intensity of each metamorphic event are not known. In fact, the pattern of distribution of high grade rocks in the Dharwar craton shows that although there is a dominance of higher grade rocks in its southern part than the northern part, no single boundary can be drawn that differentiates its higher-grade rocks from its lower-grade rocks. Amphibolite facies supracrustals and gneisses occur in abundance within the SGT. Although there are some hypotheses inferring that the amphibolite facies supracrustals within the SGT are retrogressed products of granulite facies rocks (Khan and Janardhan, 1989), prograde relationships observed from a number of locations spread over the SGT (Chapter 2 & 3) indicate that gneisses are precursors to charnockite and not the other way round. The irregular and isolated distribution of the high grade metamorphic rocks in the southern Indian shield are more likely to be the result of polymetamorphism and polydeformational events, perhaps causing dismemberment of early metamorphic assemblages with variable metamorphic/deformational intensities. The simplistic model of Pichamuthu (1965) and others, that the SGT represents a deeper level of a northerly plunging anticlinorium does not adequately explain the existing structural and paleopressure data

Radhakrishna and Naqvi (1986) proposed that the bulk of the Indian Shield was cratonised prior to 2600 Ma and was subsequently remobilised, leaving only three surviving early Archaean nucleii. These Archaean nuclei are: the Karnataka nucleus (KN), the Jeypore-Bastar nucleus (JBN), and the Singhbhum nucleus (SN) (Fig. 1.12b). Areas around these nucleii were remobilised along two belts (the EPMB, Early Proterozoic mobile belt and the MPMB, Middle Proterozoic mobile belt).

Rogers (1986) divided the Indian Shield into five distinct crustal areas, the Bhandara, Singhbhum and Aravalli cratons, the Eastern Ghat and the Dharwar-Granulite terrains (Fig. 1.12c). These crustal areas are separated by a number of "joins" representing both thrusts (for example, the Eastern Ghat-Dharwar join) or rifts zones (for example, the Dharwar-Bhandara join along Godavari rift). The granulitic terrain of southern India and the Dharwar craton was considered as part of a single crustal block, which Rogers named the Dravidian Block.

Presently the model of Drury et al. (1984), which advocates that the SIS is composed of two terranes, the northern and the southern terranes, separated along the Palghat-Cauvery Shear Zone (PCSZ; Fig. 1.12c) has received wide acceptance. Table 1.5 summarizes arguments in favour of the sub-division of the SIS into two separate terranes. However, these arguments need substantiation and can be counterbalanced, as is summarized in the discussion column in Table 1.5.

Table 1.5 Criteria for subdivision of the Southern Indian Shield into two geological terranes

Feature	Northern Terrane	Southern Terrane	References	Discussion and counter arguments
Shear zones	Major shear system (Palghat-Cauvery Shear Zone) exist along the boundary between the northern block and the southern block.		Drury et al. 1984	Field data (Nair and Nair, 1980; Naha and Srinivasan, , 1996 and present work) question the presence of a major trans-continental shear zone along the PCSZ.
Litholo-gical assem-blages	a. Mafic and ultramafic volcanics are common.	a. Mafic and ultramafic volcanics are sparse	Drury et al. 1984	The spatial variation in the abundances of various lithological assemblages are not abrupt across the PCSZ; rather there is a gradual decrease in the abundances of mafic volcanics and BIFs from the Dharwar craton to the SGT.
	b. BIFs are common while calc-silicates are sparse	b. BIFs are sparse and calc-silicates are common	Prasad et al. 1982	
Struc-tures	a. Dominated by N-S striking shear belts	a. N-S striking shear belts are lacking	Drury et al. 1984	Field data do not support existence of many of the N-S trending shears in the Dharwar (Mukhopadhyay, 1986) or presence of structural discordance between the Dharwar and the SGT (Naha and Srinivasan, 1996; present work). The basement-cover relationship in the SGT has not been worked out in the field so a comparison between the SGT and the Dharwar on this basis cannot be done.
	b. Dominant structural trend is N-S	b. Structural trends are highly variable.	Drury et al. 1984	
	c. Supracrustal belts have autochthonous relations with gneiss	c. Supracrustals are interfolded and inter-thrusted with sheets of granulites	Drury et al. 1984	
Metamo r-phism	Mainly greenschist to amphibolite grade of metamorphism	Mainly granulite facies metamorphism	Drury et al. 1984	Although in general the SGT is represented by high-grade rocks and the Dharwar craton is dominated by greenschist and amphibolite facies rocks, in detail, their distribution is heterogenious. High-grade rocks occur in many isolated places in the Dharwar craton (Mukhopadhyay, 1986). Both SGT and the Dharwar craton are polymetamorphic so overall difference in the metamorphic grade cannot be taken as evidence for two separate terranes until these metamorphic events are dated.
Nd model age data	Nd model age range is between 3.4 and 2.4 Ga	Nd model age (corrected for a depletion event at 550 Ma) range is between 2.7 and 1.3 Ga	Harris et al. 1994	There is an overlap of 300 Ma in the Nd-model ages reported by Harris et al. (1994). Subsequently, ~3.1 Ga Nd-model ages have been reported from the Madurai Block (Jayananda et al. 1995), narrowing down the difference in Nd-model ages between the Dharwar craton and the SGT. Somewhat younger model ages in the SGT could be the result of Nd-fractionation during a number of post-Archean thermal events in the SGT.
Biotite-whole rock Rb-Sr age data	Ranges between 2.0 Ga and 2.2 Ga	Available data from the KKB indicate ~480 Ma age.	Peucat et al. 1989; Choudhary et al. 1992; Unnikrishna n -Warrior et al. 1997	Rb-Sr whole rock-biotite ages give the time since rocks pass below ~350°C. SGT has suffered a number of Neoproterozoic to Early Paleozoic magmatism and charnockitization, which explains ~480Ma Rb-Sr biotite-whole rock ages. Neoproterozoic magmatism has also been recorded from north of the Moyar Shear Zone (Table 1.4). However, the preservation of the ~2.0 Ga biotite Rb-Sr ages in the charnockites of the Transition zone is not well understood. It is possible that because of the dry nature of charnockites, Rb/Sr element mobilisation during the Late Neoproterozoic was retarded in the ~2.5 Ga old charnockites.

To conclude, models invoking juxtaposition of two different terranes in the make up of the Southern Indian Shield along the Palghat lineament are based on limited and questionable data First, the very existence of the crustal-scale shear zone along the Palghat Cauvery Lineament is in doubt; second, there is no break in the metamorphism across this lineament; and finally, the significance of Nd-model age in a multiply deformed and metamorphosed terrain is uncertain (because of known mobility of Sm and Nd in respose to medium to high-grade thermal events)[3]. Rb-Sr whole rock-biotite ages, however, do show a difference between the SGT and the Dharwar craton. But, because of paucity of such data, it is not known whether such difference is across any of the major lineaments or it is just a reflection of spatial variation any thermal event. It is necessary, therefore, to further explore the cause of such variation between the SGT and the Dharwar craton. Other tectonic models for the southern Indian shield may be equally viable (Fig 1.12). Some of these are variants of the model proposed by Harris et al. (1994).

Within this general framework, a study of field relations across the major lineaments in southern Indian shield viz., Moyar, Bhavani, Palghat-Cauvery and Achankovil lineaments was undertaken before commencing with new geochronological studies. Because the distribution of the charnockites, and the timing of charnockitization vis-a-vis deformation have influenced

---

[3] The calculation of Sm-Nd model ages of crustal rocks assumes close system behaviour of Sm and Nd in a rock (which, in turn, means constant of Sm/Nd ratios) subsequent to mantle extraction of the crustal rock (de Paolo, 1988). This requires that garnet or any other minerals (like monazite and apatite in acidic rock) with significant affinity of Sm (Sm decays to Nd) have not participated in any crustal processes such as intra-crustal differentiation, metasomatism, crustal melting and weathering. Recent work has demonstrated that Sm and Nd in crustal rocks may undergo significant fractionation in response to various metasomatic processes in different metamorphic environments (Gruau et al. 1996 and references therein). If Sm and Nd are fractionated during such crustal processes, Sm/Nd ratios are disturbed and model ages are partially reset. In addition, in a polymetamorphic high-grade terrains, multiple overgrowth and inclusions of minerals with high Sm-Nd content are common in both garnet and monazite. These can significantly alter the Sm/Nd distributions in these rocks. Fractionation and mobility of Sm-Nd during Neoproterozoic-Paleozoic charnockitization in the SGT has been demonstrated by Choudhary et al. (1992). It is possible, therefore, that Sm-Nd budget in various rocks was fractionated during the many thermal events in the SGT. Only in the case of juvenile magmatic rocks and their single-stage metamorphic derivatives, can a primary model age (i.e., age of extrction of the rock from mantle) be confidently calculated. Since several assumptions concerning the isotopic composition and evolution of the upper mantle must be made (e.g., mantle homogeneity), the model ages are only crude approximation of geological events and may have errors up to several hundreds million years more particularly in terrains that are subjected to repeated tectonothermal processes in the crust (Arndt and Goldstein, 1987).

the many available tectonic models, unravelling the study of field relations of charnockites was one of the main aims of the present study. This work was then followed by U-Pb single crystal zircon and monazite dating, using both conventional TIMS (Thermal Ionisation Mass Spectrometry) and SHRIMP (Sensitive High-Resolution Ion Micro Probe) technique on samples collected from well constrained field relations. This geochronological work supplements presently available age information from the SGT to better constrain the distribution of protolith ages of different magmatic events across the major lineaments; and to identify different deformation and charnockitization events. Data obtained during this study on the SGT have been used to construct a new tectonic model for the SGT The data are then compared with similar available data from southern Madagascar, and a model for possible India-Madagascar reconstruction is proposed

Chapter-2: Charnockites of the Southern Indian Shield

2.1: Introduction

2.1.1. Historical background and the charnockite problem

Holland (1900) introduced the term charnockite for a dark greasy-grey-coloured rock from the Madras area in India, having quartz, microcline, plagioclase, hypersthene and garnet as major minerals, and accessory iron oxides, zircon, and biotite. Previously this rock was mapped as "syenitoid granite". Holland thought the rock to be igneous in origin and applied the term 'Charnockite Series' to a group of rocks with hypersthene and granulitic texture, varying in composition from silicic to pyroxenite, all of which he believed to be genetically related. Holland believed that the terms "Charnockite" and "Charnockite Series" need never become a burden to petrographical nomenclature. However, since then, the term charnockite has been embroiled in controversary.

The charnockite debates have revolved around the nomenclature of charnockite, the origin of its distinctive colour, and above all its petrogenesis (Stillwell, 1918; Vredenburg, 1919; Ghosh, 1941; Rama Rao, 1945; Pichamuthu, 1953, 1961; Howie, R. A., 1954; Subramaniam, 1959, 1967; Janardhan et al. 1979; Friend, 1981; Condie et al. 1982; Janardhan et al. 1982; Condie and Allen, 1984; Hansen et al. 1987). Controversary about charnockite nomenclature centres on whether the term should be used only for rocks with silicic composition, or whether it should be extended to include rocks of broader chemical composition. Terms like acidic-charnockite, intermediate-charnockite and mafic-charnockite were frequently used, with the assumption that the charnockitic "series" has a similar genetic relationship as do the granite "series". Whether charnockites are magmatic or metasomatic or both also remained a core problem. An excellent review of the charnockite debate before the mid-70s can be found in Bhattacharyya (1977).

Field mapping of charnockites is especially challenging. Irrespective of their modal composition, charnockites are dark greasy greyish-green coarse grained rock with a granulitic texture. The main constituent minerals are quartz and feldspar, with variable amounts of orthopyroxene, garnet, opaque minerals and in some cases hornblende, biotite. In charnockite, all these minerals, including quartz and feldspar are dark in colour[4]. Uniformity in the colour and texture of charnockites in spite of differences in various modal proportions of different minerals makes it very difficult to identify different varieties of charnockites in field for example, to classify them as charnockite (K-rich) or other varieties like enderbite (Na-rich) etc. Thus, mapping contacts between charnockite, charno-enderbite and enderbite, depends almost entirely on follow-up petrography.

The southern part of the Southern Indian Shield is dominated by high-grade rocks, of which charnockite is the most common (~40% by area; Fig. 1.7) and much work on the origin of charnockite was initiated in India. In recent years there has been remarkable progress in understanding processes of charnockitization and particularly the recognition that these rocks may have a metasomatic origin. Such work has focussed on the characterisation of fluids involved in lower crustal processes mainly through application of geochemistry and high-quality stable isotope geochemistry. However, there are a number of unresolved problems regarding charnockites that have bearing in understanding the tectonics of the SGT. These are:

(i) Is there more than one episode of charnockitization; and how would this be recognised?

---

[4]. The dark colour of charnockite (not all charnockites are dark coloured) is mainly due to the dark colour of its most predominant minerals, quartz, feldspar and iron oxides. In thin sections numerous thin bluish and green veins, derived from chloritic alteration of margins of orthopyroxene and other ferromagnesian minerals, can be observed along cracks of feldspar and quartz along with dust-like opaque impurities, which cause dark colours of quartz and feldspars in charnockite (Howie, 1964, 1967; Bhattacharyya, 1966). Dark coloured charnockite bleaches upon treatment with warm HCl (Howie, 1964; 1967). It is observed in many quarry sections that the weathered shell of charnockite resembles normal light-coloured granite. Bleaching of charnockite also occurs upon prolonged exposures of the drill holes where explosives are used for quarrying. The oily appearance and bluish-grey colour of charnockite has been suggested to have been caused by the diffraction effect of coarse exsolution perthite blebs and scapolite veins in quartz (Bhattacharyya, 1966; Ray, 1972).

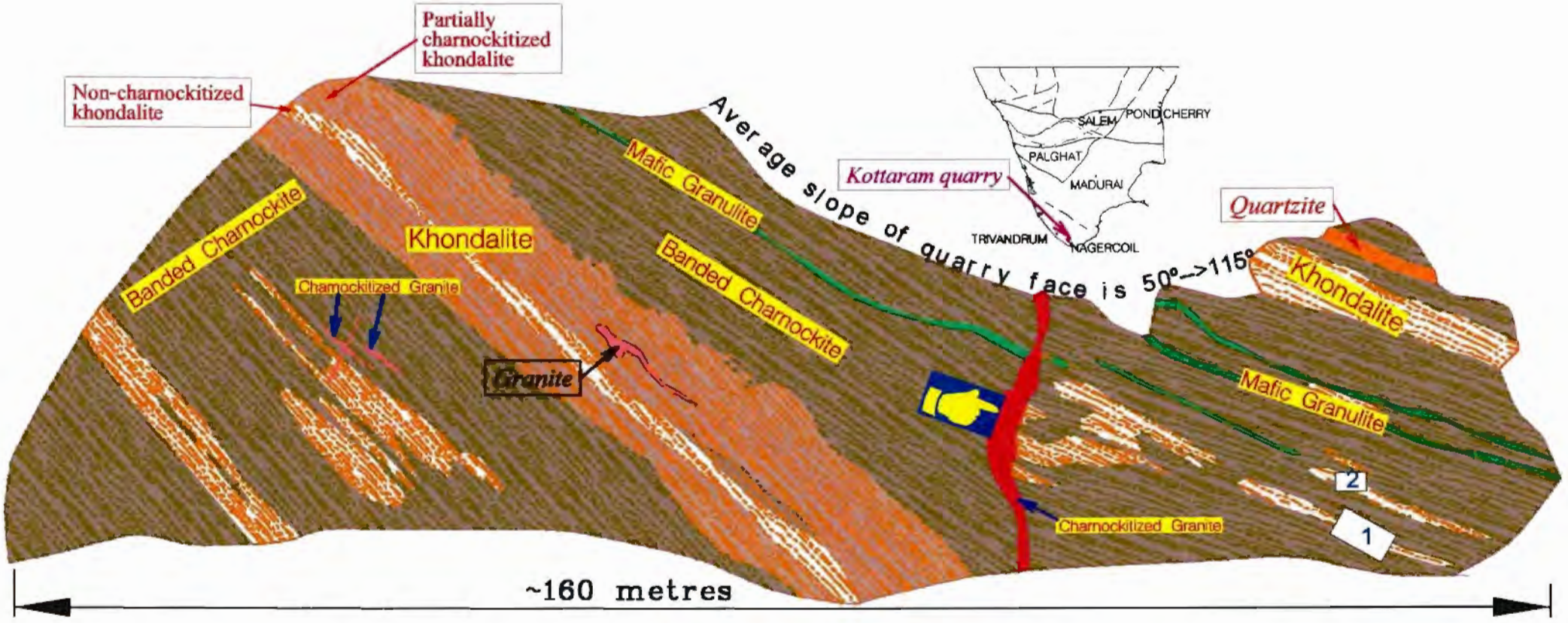

Fig. 2.1. Sketch map of the Kottaram quarry face showing continuity and parallelism of gneissosity in charnockitized and non-charnockitized parts of quartz-biotite-garnet gneiss. The quarry face dips 50°-->115°. = sample location for zircon geochronology. Zircons from the massive charnockitized granite dike have a core age of ~2.0 Ga and rim age of ~575 Ma. Rectangular boxes 1 and 2 are positions of field phatos showing continuity of gneissosity across the charnockite-khondalite gneiss boundary (Fig. 2.2).

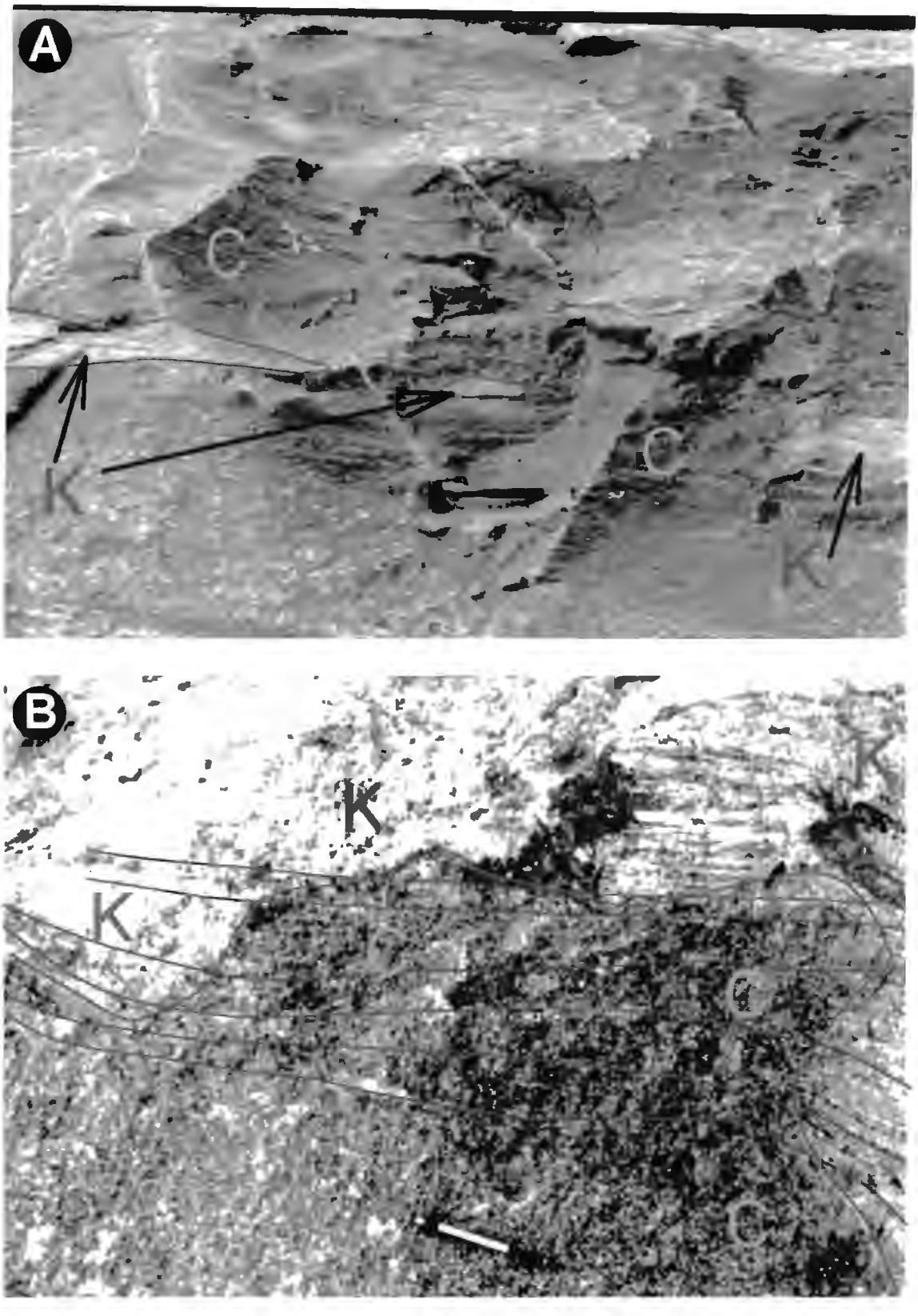

Fig. 2.2 . Continuity of the gneissic banding across the charnockite (C) khondalite (K) boundary. A and B corresponds to positions 1 and 2, marked in Fig. 2.1. Location, Kottaram quarry, ~ 5 km north of Kannyakumari.

(ii) Do some charnockites, such as the Cardamom Hill charnockite and the Nagercoil Hill charnockite massifs, represent magmatic charnockites, as interpreted by Farquhar et al. (1991), Chacko et al. (1996); and Santosh (1996)? Or were all charnockites in southern India formed during secondary processes, such as during fluid infiltration.

(iii) Is there a relationship between the timing of charnockitization and/or charnockite emplacement with tectonism, and/or granitic igneous activity?

In this chapter, I will explore some of these questions further.

There are three main hypotheses for the origin of charnockite:
(i) magmatic (Holland, 1900; Howie, 1954; Kilpatrick and Ellis, 1992 and references therein).
(ii) metamorphic (Vredenburg, 1919; Stillwell, 1918; Ghosh, 1941) and
(iii) metasomatic (Pichamuthu, 1953; Friend, 1981; Janardhan et al. 1982; Newton and Hansen, 1983; Stahle et al. 1987).
Another, hybrid model, holds that both magmatic and metasomatic processes were involved, whereby metasomatic alteration is linked to magmatic charnockite intrusion, much like autometamorphism associated with late stages of the crystallization of granites (Ravindra Kumar and Chacko, 1986)

The granulitic texture of charnockites do not provide a clear cut petrographic answer as to whether or not the rocks result from crystallization from a magma under high P-T conditions (available P-T data indicate charnockite formed at pressure between 5 to 9 kbar and temperature >650°C), or they represent metamorphic rocks with textures developed at high P-T conditions in the solid state. There have been a number of field observations which argue for an intrusive origin of charnockites (some of them are mentioned in Pichamuthu, 1953; others include Bohlender et al. 1992; Santosh et al. 1996). However, the exposures mentioned in

Santosh et al. (1996) have been re-examined in this work and it was found that the intrusive relationships described by them are a misinterpretation (section 2.12).

2.1.2. Charnockitization: dehydration metasomatism[5] of rocks

With increasing discovery of occurences where incipient charnockite formation has been proposed to have taken place, ('charnockite in the making', Pichamuthu, 1960) from various parts of southern India, the term charnockitization came to be used to infer a process of transformation of granitic rocks into charnockitic rocks (Pichamuthu, 1960). The modal compositions of the orthopyroxene-bearing granulitic rocks largely depend on the modal compositions of the precursor rocks. Thus, in general, a tonalitic rock transforms to enderbite and granite transforms to charnockite. In some cases, this process of transformation accompanies replacement of plagioclase by alkali feldspar so that a tonalitic (Na-feldspar bearing) rock may get transformed into charno-enderbite or charnockite (Touret, 1996). In a poly-deformed terrain, such as in the SGT, precursor mafic and acidic rocks occur inter-layered on a scale which varies from hand-specimen scale to map scale. Upon metasomatic transformation, the acidic portion becomes charnockite (or enderbite) while the mafic portion transforms to mafic granulite. It is now well recognised that the process of transformation is a metasomatic process which necessarily includes a process of dehydration of the rock (Newton et al. 1986; Stahle et al. 1987; Touret, 1995).

The most obvious changes that accompany charnockitization through metasomatism are (i) recrystallization of minerals and consequent destruction of any planar and linear penetrative fabrics that are present in the rock and (ii) transformation of pale coloured minerals (for example, quartz and feldspar) into dark coloured minerals. These changes commonly make it

---

[5] I have used the term metasomatism and metamorphism in their classical sense, i.e., metasomatism is a process of replacement of minerals by different ones within a rock by the action of externally-derived percolating fluids. Metamorphism on the other hand is a process of changing mineralogical and structural constitution of the rock as a result of changing physicochemical environment, notably, pressure and temperature (Dictionary of the physical sciences, Oxford University Press, New York, 1987).

difficult to identify the precursor rocks of the charnockites. However, gneissose layering or bedding of precursor rocks can often be recognised, both in hand-specimen and outcrop scales, within the charnockitized part, as 'ghost' layering (Fig. 2.1, 2.2). Careful observation of 'ghost' layering in the rock, and comparison with associated non-charnockitized portions and recognition of the minerals that are not affected by charnockitization, often help in identifying the precursor rocks of charnockites.

The near absence of hydrous mineral phases in charnockite suggests anhydrous condition during granulite facies conditions. Granulite metamorphism typically occurs with $a_{H_2O} \leq 0.4$ (Newton, 1986). Fluid-absent metamorphism for the origin of charnockite has thus been suggested by some workers (Lamb and Valley, 1984; Harley, 1989). However, recognition of abundant of high-density CO_2-bearing fluid inclusions in charnockites and high CO_2/H_2O ratios in fluid inclusions of charnockites has further supported the model of a 'carbonic metamorphism' whereby extensive influx of the rock with CO_2 on regional scale drives off the H_2O in the host rocks, and this causes, in turn, causes transformation of amphibolite facies rocks to charnockites (Newton et al. 1980). Carbonic metamorphism has been the most popular hypothesis for the origin of the charnockites of the SGT for more than a decade and half. Some workers have since proposed, however, that the abundance of CO_2-rich inclusions in charnockites does not represent fluids trapped during peak of metasomatism, but instead, fluids trapped during retrogression (Lamb et al. 1987; Sterner and Bodnar, 1989). The following possible explanations, based on field and experimental data, for the high CO_2/H_2O ratio in fluid inclusions of charnockites were compiled by Santosh et al. (1991).

(i) Removal of H_2O during late plastic deformation of crystals (Hollister, 1988; Buick and Holland, 1991).

(ii) Preferential removal of H_2O by granitic partial melts (cf., Fyfe, 1973; Burton and O'Nions, 1990). However, the absence of granitic melts associated with the majority of patchy

charnockites on outcrop scale does not support that dehydration occured by removal of granitic partial melts, unless all granitic melts have been removed to higher level. Experimental data, moreover, indicate that CO_2 might readily dissolve in silicate melts during partial melting of phlogopite-bearing rocks (Haggerty, 1990). Therefore, removal of granitic melts alone cannot explain the dominance of CO_2-rich inclusions, unless such melting occurs only in the biotite stability field.

(iii) Influx of CO_2 from external sources (Hoefs and Touret, 1975; Dunai et al. 1992; Dunai and Touret, 1993; Santosh and Wada, 1993). This hypothesis suffers from difficulty in identifying a deep source for CO_2. However, most of these models assume a mantle origin or a decarbonation reaction in the lower crust involving limestones/marbles (Janardhan et al. 1982; Hansen et al. 1984, 1987). Lack of oxygen and carbon isotope homogenization in some charnockites is one of the main difficulties with this hypothesis (Hoernes et al. 1994) although charnockites of the SGT show both low and near-uniform values of $\delta^{18}O$ in individual minerals of charnockites (Jiang et al. 1988).

(iv) Influx of internally buffered CO_2 (Stahle, et al. 1987; Hansen et al. 1987; Raith et al. 1989).

A major objection to the carbonic metamorphism model has been the lack of isotopic homogenisation, which should have occurred if pervasive influx of CO_2-rich fluid causes charnockitization. Also, low solubilities of silicate constituents in CO_2 , and the low wetting ability of such fluids, inhibiting infiltration, do not support CO_2 as an important fluid for granulite metasomatism. In recent years it has been convincingly shown that the isotopic compositions of CO_2 fluid inclusions in charnockites retain their pre-charnockitization "memory" (Vry and Brown, 1991; Hoernes et al. 1994; Touret, 1995). An alternative explanation, which proposes the importance of hypersaline brine as the most important granulite facies fluid, has recently been stressed by a number of workers (Touret, 1995;

Newton et al. 1998). Hypersaline brine solutions are also common in fluid inclusions in charnockites. It is argued by Newton et al. (1998) that brine better explains complex trace element patterns in charnockites.

2.1.3. Charnockite and regional high-grade metamorphism

Charnockites are generally limited to high-grade granulitic terrains, and the essential presence of opx and granulitic texture justifies charnockite as a granulite. However, although broadly confined within high-grade terrains, charnockites also occur as small patches within amphibolite facies rocks or in upper-crustal granites that have apparently not suffered granulite-grade metamorphism (Nathan, 1994; Newton, 1995). It was observed during the present study that charnockitization may be restricted to large (10s of metres to 100s of metres) brittle fractures within granite or other host rocks (Figs. 2.5A, B and 2.10), which have developed at upper crustal levels. Broad confinement of charnockites to high-grade metamorphic terrains suggests that high-grade metamorphic conditions are a pre-requisite for triggering charnockitization, but some of the actual transformation process might occur at upper crustal levels where host rocks are not metamorphosed and large brittle fractures can form along which fluids might penetrate (Figs., 2.5, 2.10; Nathan et al. 1994).

There are two opposing views regarding the relationship of charnockitization and regional metamorphism. One view (Janardhan et al. 1982; Newton, 1986; Hansen et al. 1987) is that charnockite forms in zones of infiltration of syn-metamorphic fluids derived from a deep crustal or mantle reservoir. The other view (Stahle et al. 1987; Baur and Kroner, 1987; Raith et al. 1988, 1989) is that charnockites represent late, structurally-controlled dehydration processes following granulite metamorphism.

2.2. Previous works on charnockites of the SGT

2.2.1. Nature and origin of charnockite in the SGT

In the SGT, charnockites of the Transition Zone, in the Nilgiri Hill Massif and in the KKB are believed to be derived either from ortho-gneiss or para-gneiss protoliths, through metasomatism (Janardhan et al 1979, 1982; Friend, 1981, 1985; Stahle et al. 1987, Raith et al. 1989; Srikantappa et al. 1992; Srikantappa et al. 1985; Ravindra-Kumar and Chacko, 1986; Yoshida and Santosh, 1987; Raith and Srikantappa, 1993; Friend, 1995). The precise mechanism of transformation of pre-existing rocks into charnockites, however, remains elusive.

Although it is generally agreed that majority of the charnockites of the SGT are metasomatic in origin, some workers believe that magmatic charnockite exists in the charnockitic massifs of the Cardamom Hills and the Nagercoil area (Farquher and Chacko, 1991; Chacko et al, 1996; Santosh, 1996). Support for magmatic charnockite comes mainly from geochemical arguments (mainly stable isotopic work; e.g., Farquhar and Chacko, 1991). Other indirect evidences cited for a magmatic origin for the charnockites of the Cardamom Hill massif and the Nagercoil Massif, (situated north and south of the KKB respectively) are:

(i) Calculation of temperature estimates from the Kerala Khondalite Belt (KKB) using the Al-based geothermobarometer (regarded as less susceptible to retrograde resetting; Chacko et al. 1996), yield results between ~700°C and ~880°C for rocks in the central part of the KKB, while in the marginal part of the KKB, close to the contacts of the Cardamom Hill and the Nagercoil Massif, higher temperatures were obtained (between ~820°C and ~1070°C; Chacko et al. 1996). On the basis of this large difference in the temperature estimates, Chacko et al. (1996) suggested that both the Cardamom Hill Massif north of KKB and the Nagercoil Massif south of KKB represent magmatic charnockites (C-type magma, after Kilpatrick and Ellis,

1992).

(ii) Charnockites of the Kottaram quarry within the Nagercoil Massif contain rotated blocks of metasediments and pyroxene granulite, and their whole-rock $\delta^{18}O$ values across khondalite blocks within charnockite gneiss reveal an increasingly magmatic signature (lower $\delta^{18}O$ value) away from the khondalite enclaves (Santosh, 1996). Also, possible melt (glass) fractions in fluid inclusions in feldspars were identified (Santosh, 1996). Finally, Sm-Nd and Rb-Sr mineral isochrons of the charnockite gneiss from this quarry define ages of 517 ± 26 Ma and 484 ± 15 Ma, respectively (Unnikrishnan-Warrior et al. 1995). These dates have been interpreted as representing the timing of magmatic charnockite emplacement in the Nagercoil block. Similar to the rocks of the Kottaram quarry, charnockites of the entire Nagercoil Massif were then inferred to be magmatic in origin.

The idea of the existence of magmatic charnockite in the charnockite massifs in the SGT is sometimes influenced by the generally held believe that charnockitic massifs are represented by charnockite of near uniform composition (Ravindra Kumar, 1996). Unequivocal field evidence supporting magmatic charnockites from the SGT is absent.

These interpretations on the origin of charnockites have profoundly influenced tectonic modelling of SGT. One of the principal criteria for dividing SGT into three tectonic blocks (the Madurai block, the Trivandrum Block and the Nagercoil Block, Santosh, 1996; see also Chapter 1) has been that both the Nagercoil Massif and the Cardamom Hills Massif represent magmatic charnockites, while the charnockites of the Trivandrum Block represent metasomatic charnockites.

In the SGT, two first-order field observations are crucial with respect to the origin of charnockites: (i) 'patchy charnockites' are common within amphibolite facies country rocks. These charnockite patches, at various stages of development, are suggestive of replacement of

pre-existing rocks. These observations have fuelled the hypothesis of secondary replacement of various rocks to charnockite. (ii) Close temporal (but not necessarily spatial) relationship between charnockitization and granitic activity has been recorded. Two well-documented charnockite-forming events, one at ~2.5 Ga in the Transition Zone and the other in the Kerala Khondalite Belt at around ~530 Ma (Table 3.1) are both broadly associated with widespread granitic activity that either just precede or overlap with charnockitization. Experimental works indicate that in fluid-absent granulite metamorphism, substantial (up to ~50%) granitic melt generation is possible if the temperature of granulite metamorphism exceeds ~850°C (Vielzeuf et al 1990).

Mapping of the charnockitic terrains of southern India has largely been influenced by a non-genetic definition of charnockite as a dark greasy-grey green coloured rock with granulitic texture and composition varying from alkali granite to tonalite, and which commonly contains orthopyroxene. Often this non-genetic descriptive definition has been given a stratigraphic status for example, 'charnockite series' (Narayanaswami, 1975). This makes charnockite more resistant to weathering compared to other rocks such as granite gneiss. Vast areas of SGT north of the Achankovil Lineament have been mapped as part of charnockite Series although they include many non-charnockitized khondalite and other gneissic rocks.

2.2.2. Age of charnockitization in the SGT

It has been suggested that a ~ 3.0 Ga charnockite event occurred in the transition zone and in the Madras area in the northeastern part of the SGT (Mahabaleswar and Peucat, 1988 and Unnikrishnan-Warrior et al. 1997, respectively). In the transition zone this is based on a Rb-Sr errorchron (Table 6.1) whilst in the Madras area it is based on a ~3.0 Ga Sm-Nd garnet mineral isochron age. The latter yields an abnormally large negative ϵ_{Nd} value[6] at ~3 0 Ga

[6] ϵ_{Nd} is defined as below, where CHUR is the acronym for Chondritic Uniform Reservoir.

$$\epsilon_{Nd} = \left[\frac{\left(^{143}Nd/^{144}Nd\right)_{sample} - \left(^{143}Nd/^{144}Nd\right)_{CHUR}}{\left(^{143}Nd/^{144}Nd\right)_{CHUR}} \right] \times 10000$$

(Unnikrishnan-Warrior et al. 1995b). Since garnet commonly contains small inclusions of rutile and monazite, the ~3.0 Ga Sm-Nd isochron data given by Unnikrishnan-Warrior (1995b) needs to be critically assessed, particularly because a ~2.5 Ga Sm-Nd whole rock isochron from a number of nearby samples has also been reported from the Madras area (Bernard-Griffith et al. 1987). Thus, although ~3.0 Ga charnockitization event may be present, this remains to be proven beyond doubt. Table 2.1 summarizes the presently available isotopic age information on the charnockites of southern India.

Table 2.1: Age data for charnockites of the SGT : previous work (see Fig.1.11 for location)

Charnockiti-zation age	Location/rock type	Method/procedure	Reference	Interpreted as
~2.97 Ga	Kabbal Durga quarry, charnockite	U-Pb SHRIMP on zircons	Friend and Nutman, 1982	Protolith age
	Sivasamudram area, west of Krishnagiri; charnockite	U-Pb zircon evaporation age	Mahabaleswar et al. 1995	Protolith age
~2.9 Ga errorchron	~100 km south of Bangalore; within the transition zone	Rb-Sr whole rock errorchron.	Mahabaleswar and Peucat, 1988	Charnockitization
	Madras area; eastern part of Dharwar craton; charnockite	Sm-Nd garnet-whole rock isochron	Unnikrishnan-Warrior et al. 1995	Charnockitization
2440±155 Ma	Biligirirangan Hills; charnockite	Sm-Nd whole rock isochron	Peucat et al. 1989	Charnockitization
~2.5 Ga	Kabbal Durga quarry; Transition Zone; charnockite and intruding granite.	U/Pb zircon	Friend and Nutman , 1992	Charnockitization
	Krishnagiri Area, Transition Zone; charnockite	$^{207}Pb/^{206}Pb$ age of monazite	Mahabaleswar et al. 1995	Charnockitization
~2.53 Ga	Kabbal Durga; transition zone; charnockite	U-Pb dating on allanite	Grew and Manton, 1984.	Charnockitization
2555±140 Ma	Madras area; composite isochron of charnockite, granite and mafic granulite	Sm-Nd whole rock isochron on 4 genetically unrelated rocks	Bernard-Griffith et al. 1987	Protolith/ Charnockitization
~2.0 Ga	Ponmudi quarry, KKB; charnockite.	Upper intercept of U-Pb discordia on zircons.	Buhl.,1987	Protolith age of detrital zircon
1.5-1.2 Ga	KKB; cordierite- bearing charnockite	Sm-Nd model ages	Harris et al. 1994; Bartlett et al. 1995	Mixed protolith age
~550 Ma	Ponmudi quarry, KKB; charnockite	Sm-Nd garnet-WR age	Choudhary et al. 1992	Charnockitization
	Kodaikanal area, Madurai Block; charnockite	U-Pb zircon evaporation age	Jayananda et al. 1995; Bartlett et al. 1995	
539 ± 20 Ma	Nellikala quarry, KKB; charnockite	Sm-Nd mineral isochron.	Santosh et al. 1992	Charnockitization
517 ± 26 Ma	Kottaram quarry, Nagercoil Block; charnockite	Sm-Nd mineral isochron.	Unnikrishnan et al. 1995	Charnockitization
484 ± 15 Ma	Kottaram quarry, Nagercoil Block; charnockite	Rb-Sr mineral isochron	Unnikrishnan et al. 1995	Thermal event after charnockite formation
458 ± 8 Ma	Ponmudi quarry, KKB; charnockite	Rb-Sr biotite-plagioclase pair	Choudhary et al. 1992	Thermal event after charnockite formation

Evidence for ~2.5 Ga charnockitization event in the Transition Zone (Table 2.1) has been well documented by U-Pb dating of monazite and allanite in charnockites (Peucat et al. 1989; Grew and Manton, 1984), since the closure temperature of these minerals are similar to that of temperature of charnockitization, and also by U-Pb zircon dating of charnockitized granite and

granite cutting across charnockite (Friend and Nutman, 1992).

Circa ~550-520 Ma charnockitization event is also well documented in the Kerala Khondalite Belt by U-Pb monazite dating (Buhl, 1987) and a Sm-Nd mineral isochron (Unnikrishnan et al. 1995; Santosh et al. 1987). In the Madurai Block, north of the Kerala Khondalite Belt, a ~550 Ma regional metamorphism event has been suggested on the basis of Rb-Sr whole-rock isochron dating of granite gneiss (Hansen et al. 1985). Recently, Bartlett et al. (1995) and Jayananda et al. (1995) have interpreted ~550 Ma peaks in their evaporation analyses on zircons from charnockite and granite gneiss samples from the Kodaikanal area (Madurai Block) as the age of charnockitization in the area. This suggests the possible presence of ~550 Ma charnockitization events in the Madurai block. Work with more precise techniques like U-Pb TIMS or SHRIMP on single minerals or their parts is now needed to confirm this.

In summary, at least two periods of charnockitization have been recorded in the SGT; ca. 2.5 Ga and ca. 550 Ma. Charnockitization was widespread throughout the Transition Zone at ca. 2.5 Ga, but the southern extent of this ~2.5 Ga event is not known. This is because of the lack of high-quality geochronological data, and because of the difficulty in identifying isotopic memories of an earlier granulitic event in an area that has suffered younger granulitic metamorphism. The ~550 Ma charnockitization event has been well documented in the Kerala Khondalite Belt by Sm-Nd mineral isochron (Choudhary et al. 1992). In the present work it has been shown that this charnockitization event extends at least as far north as the Moyar Lineament.

2.3. Nature and origin of charnockite in the SGT: New field observations and geochronology

2.3.1. Field observations bearing on the origin of charnockite in the SGT

During the present work more than 150 quarry sections in different parts of Southern Indian granulite terrain were studied. Many of them display excellent relationships between charnockite/enderbite and their host/protolith non-charnockite rocks. Both in the Transition Zone and in the Kerala Khondalite Belt, there are numerous exposures of incipient charnockites ("patchy charnockite") in which various stages of transformation of the protolith into charnockite can be observed (Fig. 2.3). Such incipient charnockite provides strong evidence for the metasomatic origin of charnockites[7]. Charnockites of the Nagercoil Block and of the Madurai Block, which are dominated by charnockite massifs are, however, considered by some workers as magmatic in origin (see section 2.2.1). In the following section my field observations in these two blocks are summarized, which indicate that charnockites of these two blocks are also metasomatic in origin.

[7] There are, however, some divergent views regarding the origin of the incipient charnockite patches (Sen and Bhattacharyya, 1993; Bhattacharyya et al. 1993). These authors believe that in many cases, the charnockite patches represent pre-existing charnockite xenoliths (in magmatic rocks) or structurally dismembered clots within highly deformed meta-sediments. They argue that the commonly observed continuation of the planar fabric of the host rocks into the charnockite patches as ghost layering are results of later deformation and that in many cases charnockite patches and host rocks have sharp boundaries. However this view seems unlikely because of (i) well-documented transitions between the incipient charnockite patches and the host rocks (Figs. 2.2, 2.3, 2.4), (ii) lack of internal planar fabric within the charnockites that is often present in the host rocks; in many cases gneissosity layering within host rocks can be traced continuously into the charnockite patches as 'ghost' layering and (iii) the age of the youngest granite affected by charnockitization and the age of the granite intruding the charnockite clearly demonstrate charnockitization to be younger than the planar fabric present in metasedimentary host rocks (Fig. 2.5; 2.6; Chapter 4 for relevant geochronology). Apparent sharp boundaries are observed in the present work between the charnockite and the granite host rocks (Fig. 2.4a, 2.5a). Protoliths of these charnockites are xenoliths of granite gneiss or khondalite.

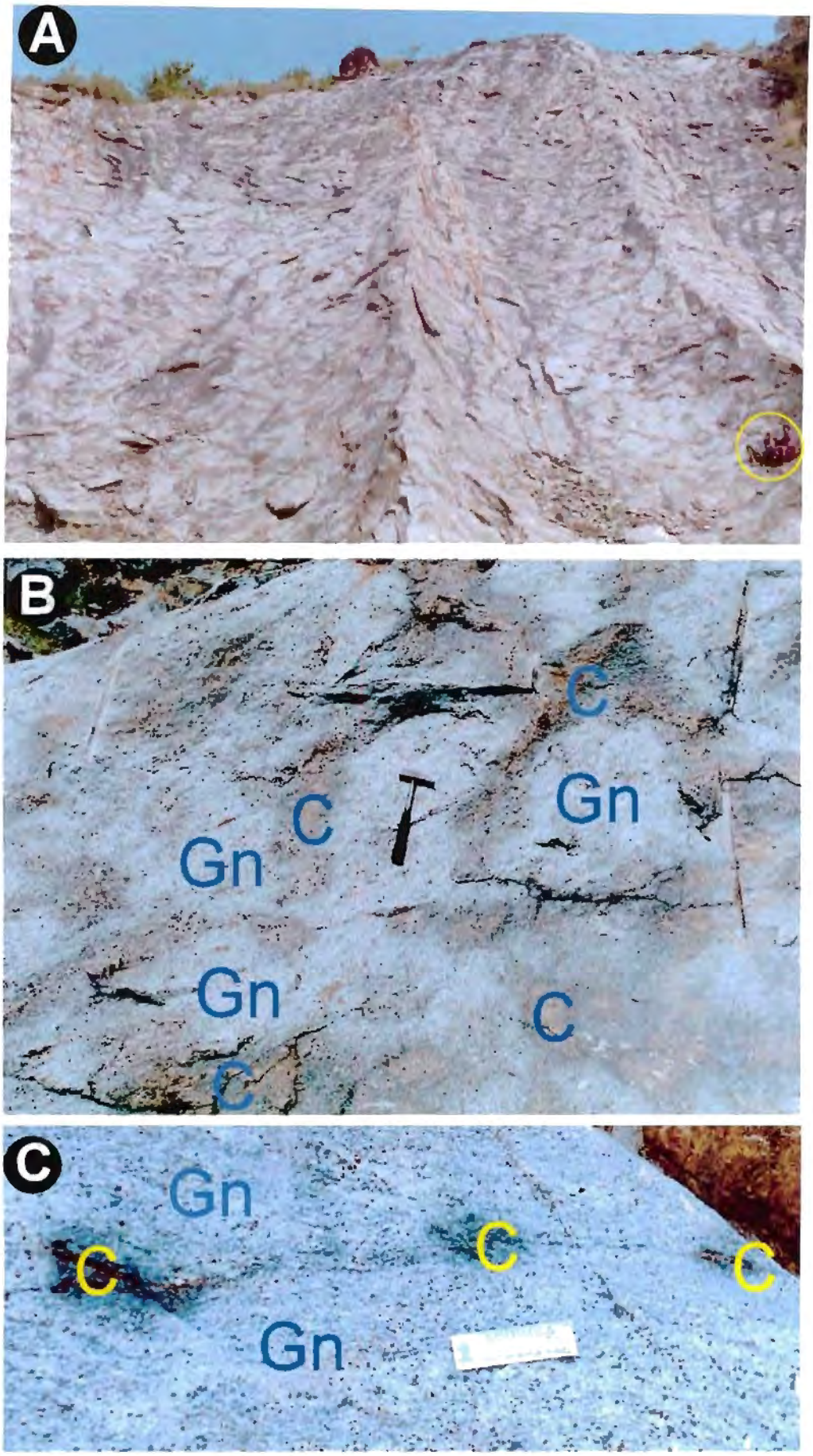

Fig. 2.3. Patchy charnockite (C) within garnet-biotite gneiss (Gn) in the Kerala Khondalite Belt. Location, Kottavattam quarry, ~4km south of Ilampally, Kerala. A. Irregular distribution of charnockite (dark) on the quarry face. Note: people for scale). B. Close-up view showing that charnockite-gneiss boundary is gradational. C. Charnockite patches developed irregularly along a biotite-rich layer within granite gneiss (Gn). Scale is 15 cm long.

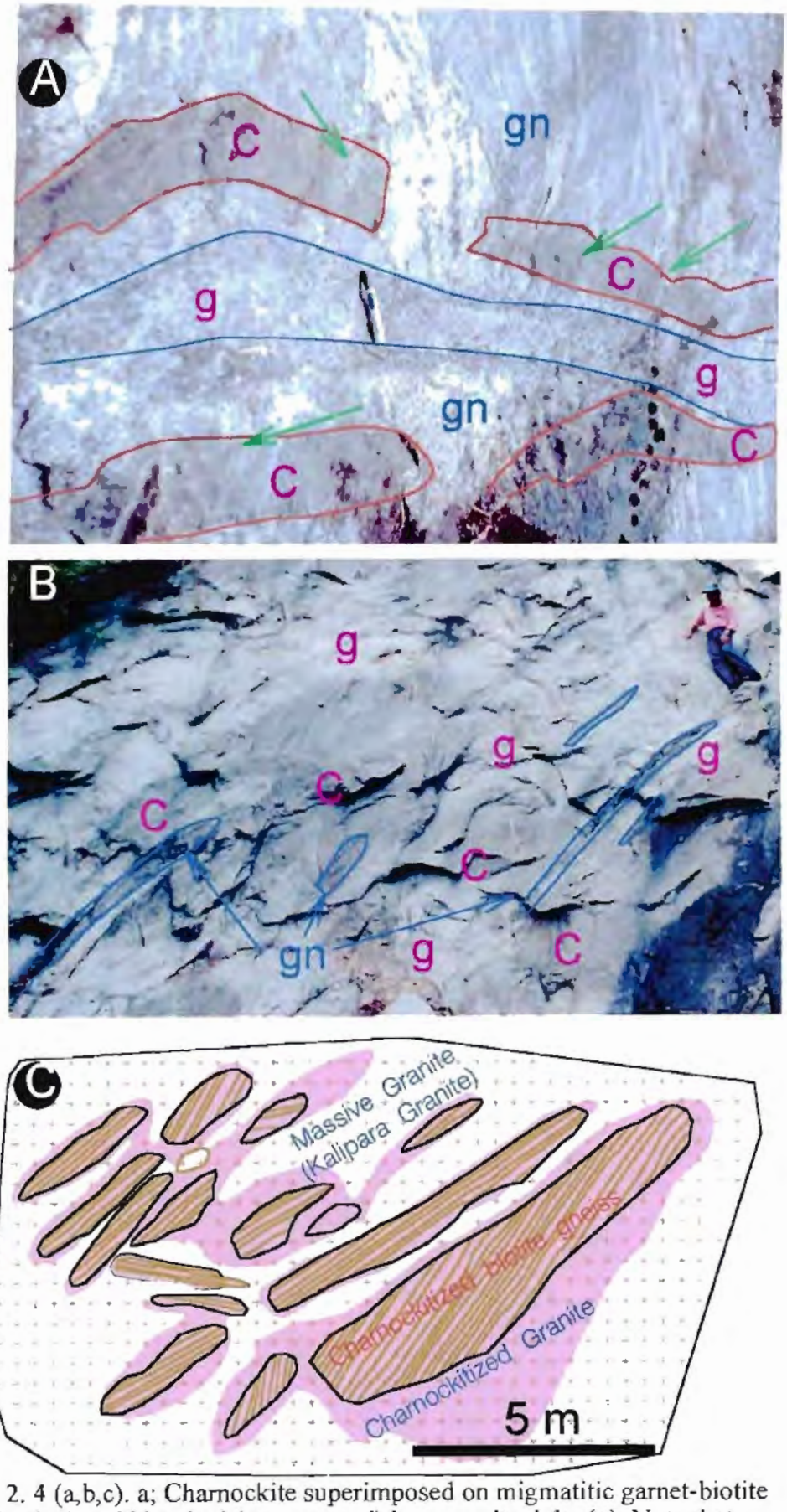

Fig. 2. 4 (a,b,c). a; Charnockite superimposed on migmatitic garnet-biotite gneiss (gn) and bleached (retrogressed) by a granite dyke (g). Note that leucosomes (green arrow) in migmatite are also charnockitized. Location, ~2km east of Kalanjhur, Achankovil Lineament, (location 316 in Fig. 3.61). b,c; Charnockite superimposed on Kalipara Granite (g) and granite gneiss (gn) xenoliths within it. Note that charnockite granite (g) and granite gneiss (gn) boundary transgresses gneiss and granite boundary. Location Kalipara quarry, PPP Corridor (location 318 in Fig. 3.61).

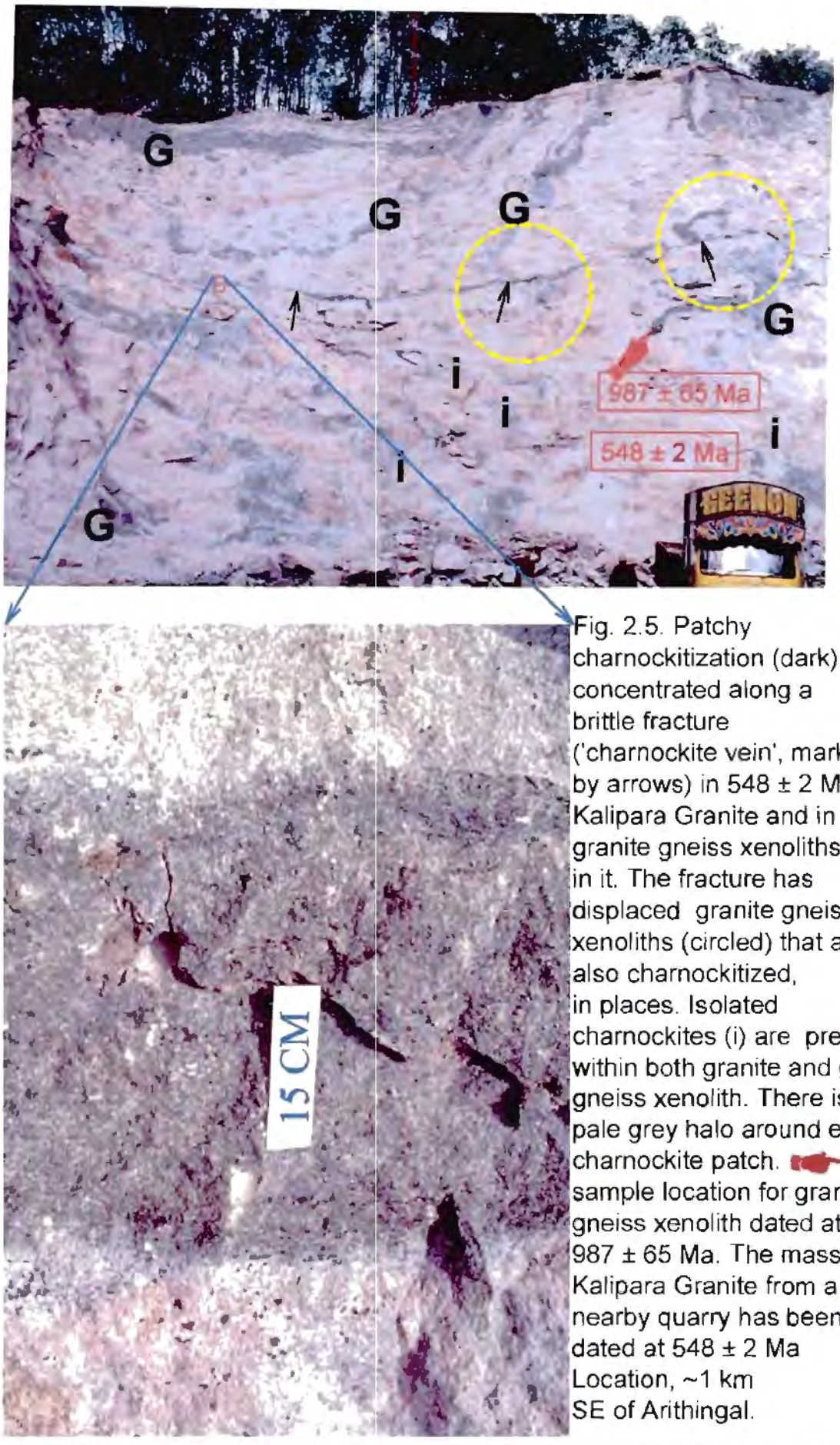

Fig. 2.5. Patchy charnockitization (dark) concentrated along a brittle fracture ('charnockite vein', marked by arrows) in 548 ± 2 Ma Kalipara Granite and in granite gneiss xenoliths (G) in it. The fracture has displaced granite gneiss xenoliths (circled) that are also charnockitized, in places. Isolated charnockites (i) are present within both granite and granite gneiss xenolith. There is a pale grey halo around each charnockite patch. ☚, sample location for granite gneiss xenolith dated at 987 ± 65 Ma. The massive Kalipara Granite from a nearby quarry has been dated at 548 ± 2 Ma Location, ~1 km SE of Arithingal.

B. A close-up of a portion of the 'charnockite vein' (red rectangle in A). Note that charnockite-granite boundary is gradational (pale grey) over 5-10 cm.

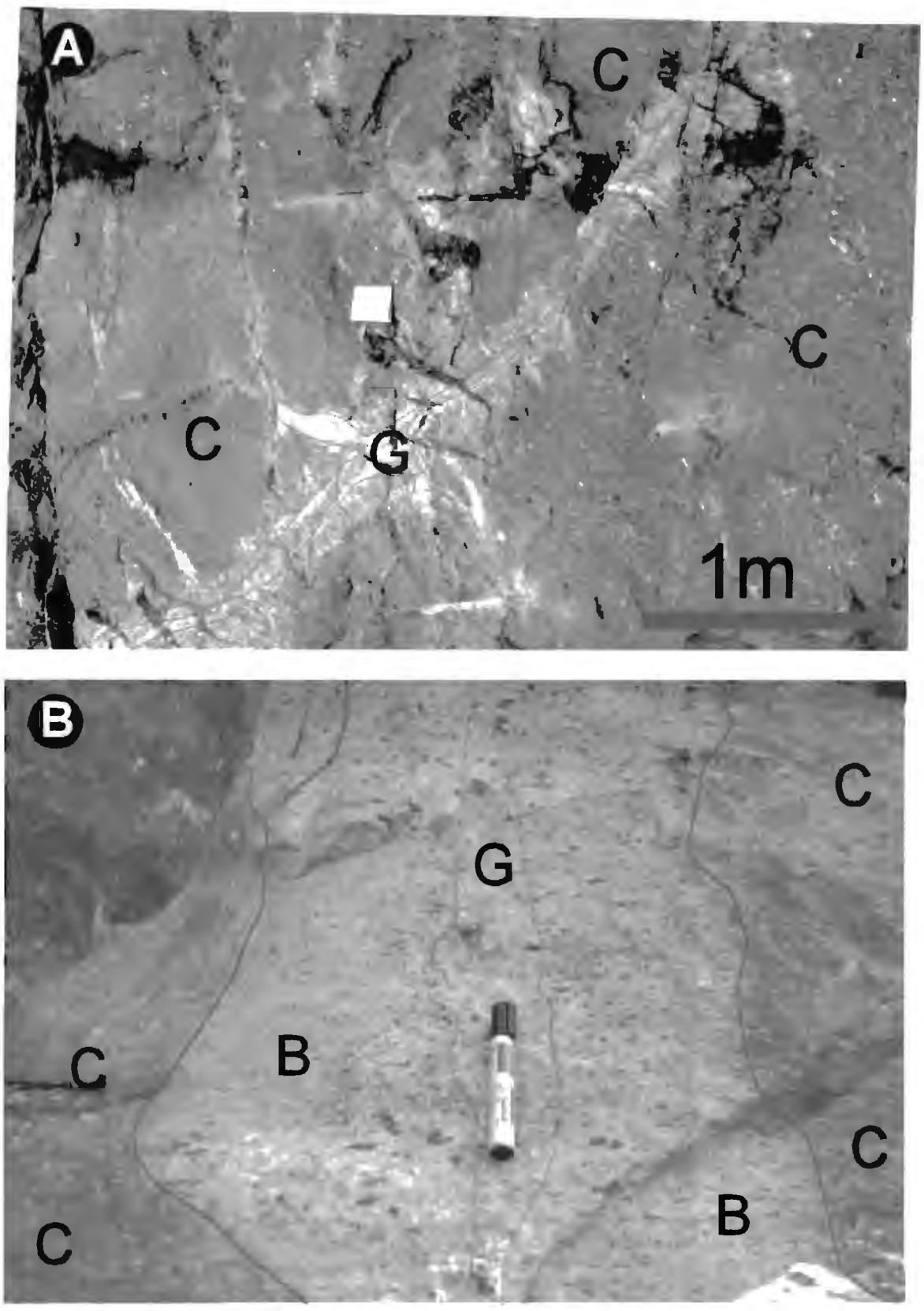

Fig. 2.6. Regrogression of charnockite around pegmatitic granite veins (G) Thin section study shows that in the bleached part (B), orthopyroxene of chanockite (C) is replaced by biotite and quartz. This granite has been dated at 526 ± 2 Ma in the area from two nearby quarries (Chapter-4). Location: A, Malayampuzha quarry, ~ 3 km NE of Pathanamthitta (Fig. 3.61). B. Chamber quarry, 11 km NNE of Pathanapuram (Fig. 3.61).

2.3.1.2. Nagercoil Block

Detailed mapping (1:1000 scale) of part of the Kottaram quarry in the Nagercoil Block (~5 kms north of Kannyakumari, within the Nagercoil Block, Fig. 2.1) was carried out to study the relationship between charnockite and khondalite. The Kottaram quarry comprises charnockite-gneiss with enclaves of mafic granulite, quartzite and garnet-cordierite-sillimanite-biotite gneiss (khondalite). The quarry has been studied by a number of workers (Unnikrishnan - Warrior et al. 1995; Santosh, 1996) who interpreted the charnockite gneiss to be magmatic in origin.

Detailed mapping of this quarry face (Fig. 2.1) reveals that no crosscutting relationship between the charnockite gneiss and metasedimentary enclaves is present. Contacts are always gradational, and the layering in the khondalite gneisses can be traced continuously as "ghost" layering into the charnockite gneiss across their contacts (Fig. 2.1). Veins and dykes of undeformed (massive) charnockite in the quarry cut across both the charnockite gneiss and khondalite enclaves (Fig. 2.1; 2.2). At places such dykes are partially charnockitized. Therefore, the massive charnockite veins are interpreted as charnockitized granite dykes.

These observations contradict observations made by Santosh (1996) that khondalite enclaves in the quarry merely represent rotated blocks of gneiss. The continuity of gneissic fabric across the khondalite gneiss and the charnockite gneiss in which the gnessic fabric is recrystallized and also gradational boundaries across charnockite and khondalite indicate that charnockite gneiss in the quarry is charnockitized khondalite. The later veins and dykes of unfoliated charnockite which intrude charnockite gneiss are charnockitized granite. Zircons from one such late charnockitized dyke has a complicated core-rim structure. The core age is ~2.1 Ga and the rim age is ~570 Ma (sample S-361; Chapter 4). This places the minimum age of this dyke at ~570 Ma. Since a Sm-Nd mineral isochron of charnockite gneiss of this quarry gives an age of 517 ± 26 Ma, the charnockite gneiss from this quarry could not have been magmatic

and emplaced at that age because they are cut by the ~570 Ma dyke. These observations undermine the use of $\delta^{18}O$ values of *whole rock* samples as a reliable indicator of magmatic origin the charnockite gneiss.

A terrane boundary between the Trivandrum and the Nagercoil blocks was proposed by Harris and Santosh (1993) and Santosh (1996) because, in their opinion, the Nagercoil Block contains magmatic charnockite and the Trivandrum Block contains metasomatic charnockite. My work questions the basis for this tectonic interpretation because the charnockites of the Nagercoil Block are probably not magmatic in origin.

2.3.1.3. Cardamom Hills

In a number of places in the southern part of the Cardamom Hill massif, charnockite includes significant amounts of charnockitized khondalite, garnet biotite gneiss and cordierite gneiss. Although charnockites are more abundant here than in the Kerala Khondalite Belt, non-charnockitized khondalite, garnet-biotite gneiss also occur in many places (Fig. 2.7 a,b). Gneissose layering and foliations in these rocks can be traced continuously into charnockite patches where they are retained as 'ghost' layering (Fig. 2.8b). Nowhere do the contacts between the such charnockite and non-charnockitized rocks reveal intrusive relationships. Many subparallel intercalated quartzite and calc-silicate layers in the massif suggest that much of the charnockite has a metasedimentary protolith (Fig. 1.3, 2.8). In the Rajampalayam area, east of the Cardamom Hill Massif, quartzite layers can be traced from the non-charnockitized granite gneiss into charnockites (Fig. 1.3). This suggests that the charnockite-granite gneiss boundary is a metasomatic boundary rather than a magmatic boundary.

My field observations (see also Chapter 3) thus suggest that charnockites in both the Nagercoil Massif and the Cardamom Hills Massif are products of dehydration metasomatism of preexisting rocks, predominantly khondalite and paragneisses, and are not magmatic

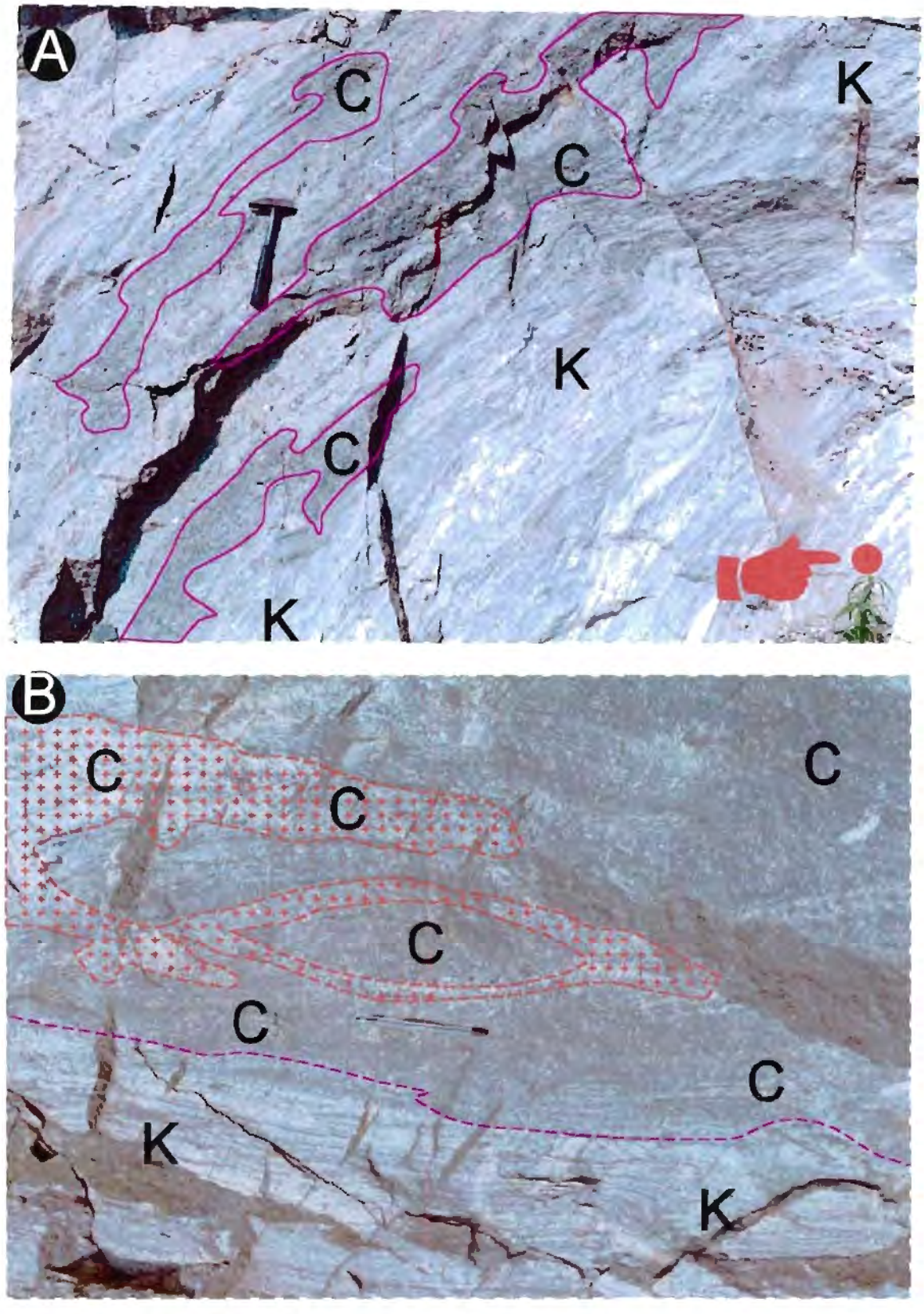

Fig. 2.7. Patchy charnockites within khondalite in the Cardamom Hills. Location, ~8km NNW of Pattanamitta (Figs. 3.61; 4.1).

A. Patchy charnockites (C) cross-cut the gneissic foliation in khondalite (K). = sample location for U-Pb monazite dating (524 ± 1 Ma).

B. Charnockitized Kalipara Granite (age ~550 Ma; patterned areas) cross-cutting layering in khondalite (K) which is also partially charnockitized.

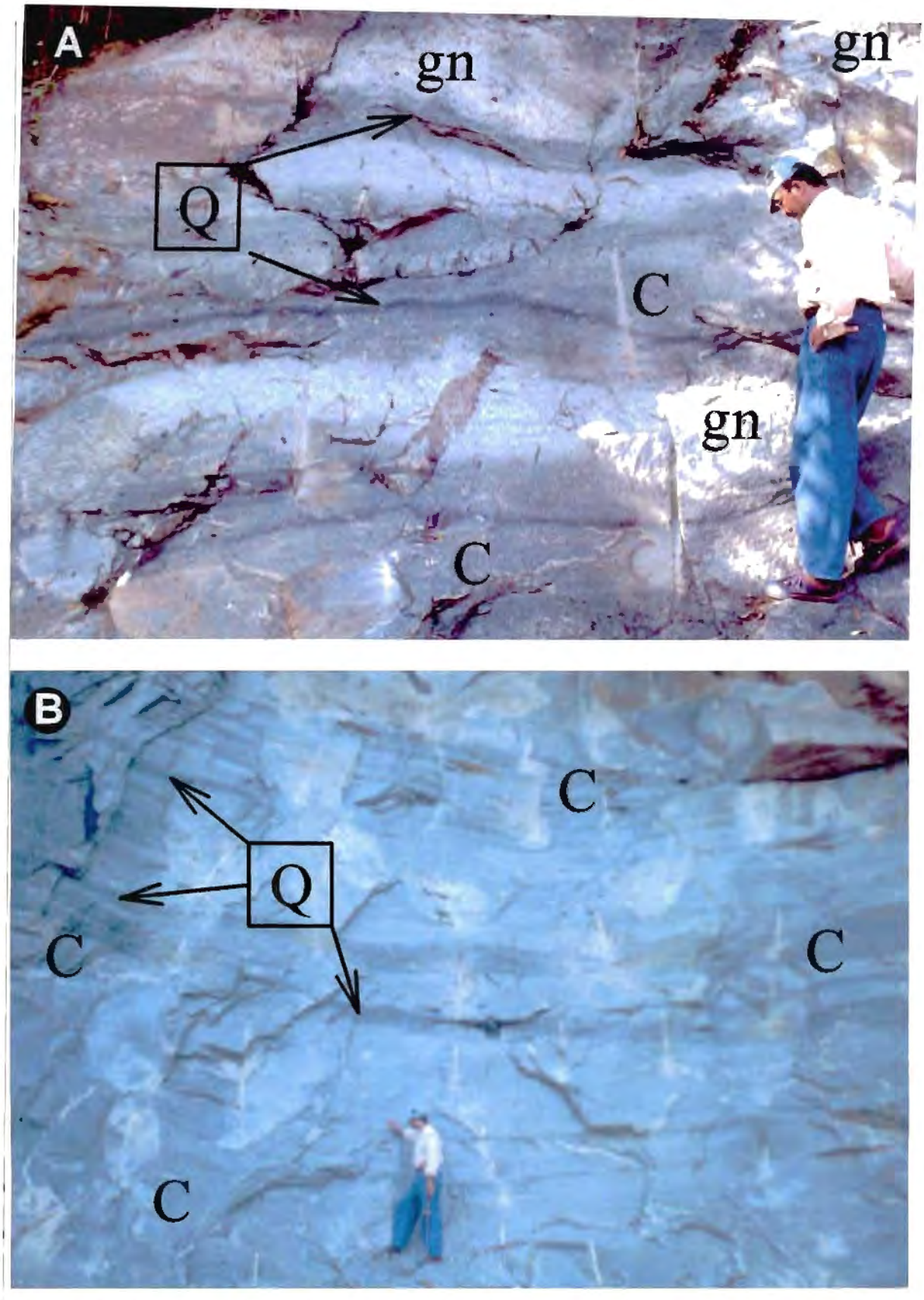

Fig. 2.8. Charnockite (C) superimposed on layered garnet-biotite gneiss (gn) interlayered with quartzite layers (Q) which are also charnockitized. Location, A. 2km north of Murinjikallu (north of the Achankovil Lineament; 326 on Fig. 3.61). B, 5km north of Mekkazhuvur, (south of the Achankovil Lineament; 352 on Fig. 3.61).

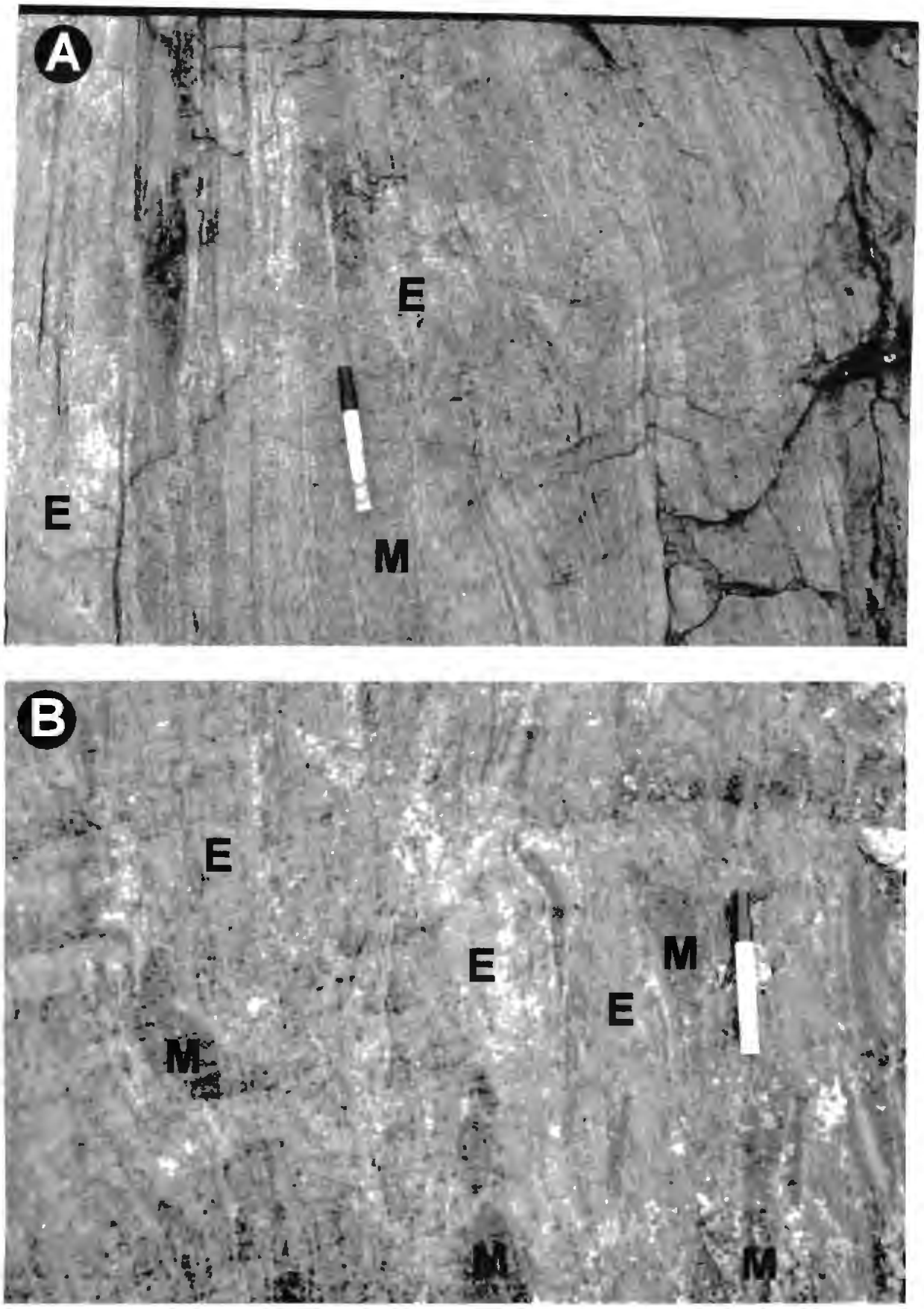

Fig. 2.9. Charnockitization of migmatitic rock in Namakkal area, Corridor-I
A. Interlayered mafic granulite (M) and Enderbite (E).
B. Mafic granulite (M) occurring as patches within enderbite (E)
Location, southern slope of the Nainarmalai Hill (Fig. 3.13).

charnockite. The difference between the charnockites of the Kerala Khondalite Belt vis-a-vis the charnockite massifs of the Cardamom Hills and the Nagercoil Hills thus lies in their degree of charnockitization and not in their genesis: the Nagercoil Massif and the Cardamom Hills Massif are both more intensely charnockitized rocks than the rocks of the Kerala Khondalite Belt. The protolith assemblages of all these three terrains are, however, similar. This implies that the division of the SGT into tectonic blocks such as the Madurai block, Trivandrum block and the Nagercoil block on the basis of spatial distribution of charnockites may be erroneous. This proposition will be explored further throughout this thesis.

2.3.1.4. Summary of other field observations on charnockitization in SGT

The following summarizes my field observations on charnockites of the SGT.

(i) Rocks affected by charnockitization include a wide compositional range: granitic gneiss, massive granite, khondalite, amphibolite, migmatite etc (Fig. 2.9). In one exposure along the southern slope of the Nainar Malai Hill north east of Namakkal (Corridor-I; Chapter-3), charnockitization is superimposed (as deduced from presence of patchy charnockites in quarry section) on a migmatite formed by subparallel intercalation of tonalite gneiss and amphibolite at their contact region (Fig. 2.9). Tonalite which had an original composition of quartz+plagioclase+biotite/hornblende is converted to enderbite and orginal amphibolite which had the composition of hornblende+plagioclase+quartz is converted to mafic granulite. This confirms that the end product of charnockitization depends on the pre-exiting rock type.

(ii) Charnockitization involves reconstitution of the mineralogy and recrystallization of the rock. When complete, this process destroys original planar penetrative fabrics in the rocks.

(iii) Patchy charnockitization is preferentially localised along pre-existing anisotropy within the protolith rocks, though at places charnockitization is simply patchy without any structural

control Structures such as lithologic contacts, fracture planes, schistosity, shear planes etc. (Fig.2.3, 2.5, 2.10) are often preferentially charnockitized. In many outcrops various stages of charnockitization can be observed. With progressive charnockitization, more massive parts of various lithologic units are also transformed and in many places protoliths are completely charnockitized.

(iv) The original relationships amongst various lithologic units are not affected by charnockitization. For example, an intrusive relationship between khondalite and massive granite (Kalipara Granite, descriped in Chapter-3) is unaffected by later charnockitization (Fig. 2.7b). A charnockitized quartz-biotite gneiss or khondalite preserves the gneissose layering in them, although the original mineralogy and remnant planar penetrative fabric has been progressively transformed depending on the intensity of the charnockitization process. Charnockitized massive granite lacks any layering. Thus, although a charnockitized granitic gneiss and charnockitized massive granite have similar mineralogy and appearance, presence or absence of layering in them may allow broad characterization of their protolith. It is, however, generally not possible to characterize the original mineralogy of the rocks because charnockitization transforms original mineralogy into a near uniform mineralogy of opx-plag-kf-quartz. Where charnockitization is less pervasive, relics of original mineralogy can be observed, which may help broad characterization of the protolith. Mesoscopic field relations like intrusive contacts, inter-layering of contrasting lithologies (e.g., garnet-biotite gneiss and quartzite) may be recognized even in most intensely charnockitzed areas.

(v) Charnockitization first affects rocks along pre-existing brittle fractures. Two localities where this feature has been studied are (a) a quarry section about 1 km east of Arithingal and (b) another quarry section at Maveli Para, 20 km west of Patanamthitta.

(a) *Arithingal quarry*: This quarry exposes mainly pinkish-white to greyish-white massive coarse-grained granite (Kalipara Granite) with numerous large

Fig. 2.10. Charnockitization along brittle fractures ('charnockite veins') in khondalite (K). Location, Maveli Para, 11 km WSW of Pattanamitta (Fig. 3.61).

A. Charnockitized brittle fractures (F) on quarry face (marked by yellow arrows). Note person in the lower left part for scale.

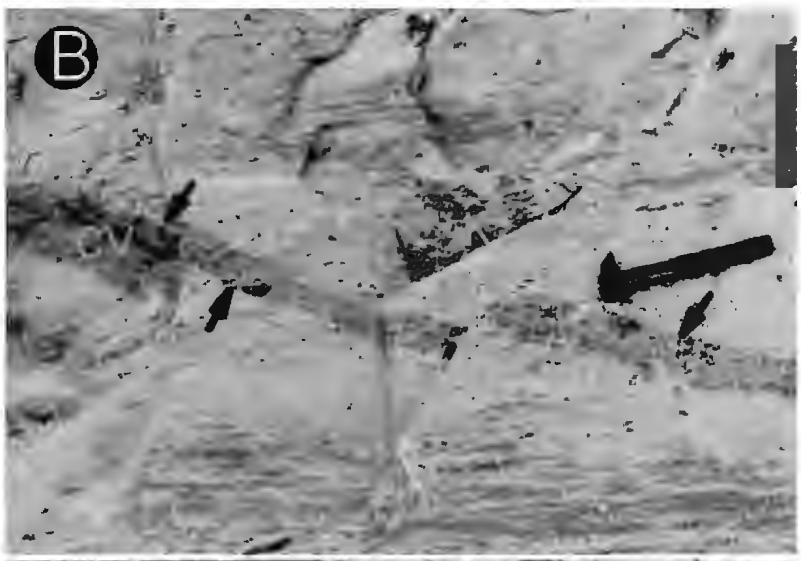

B. Close-up of one of the 'charnockite veins' (CV). Note that the gneissic foliation in the khondalite (K) can be traced across the 'charnockite vein' (marked by arrow).

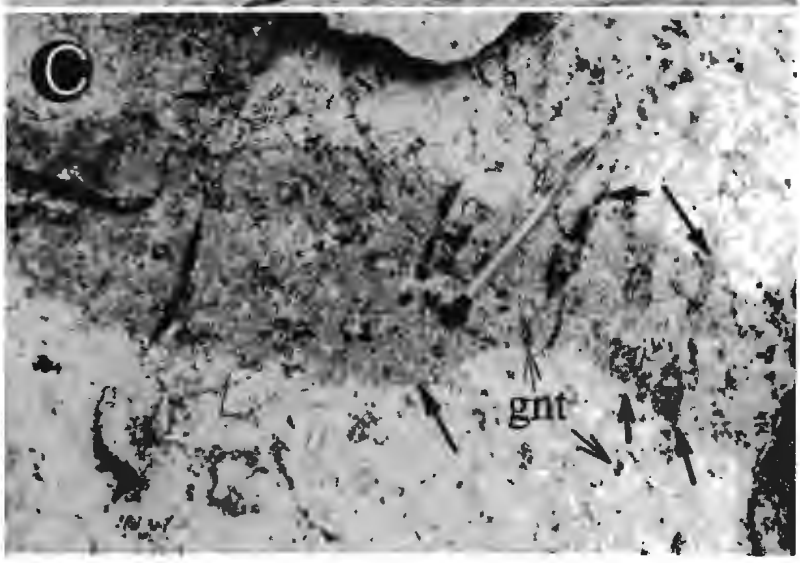

C. Close-up of another 'charnockite vein' showing that garnet stingers (gnt) extend across the veins (marked by arrows).

(up to 10s of metres long) xenoliths of granite gneiss and quartzite. Brittle fault planes in the quarry face cut across some of the quartzite and quartz-biotite schist xenoliths with displacements up to a metre or more. One fault could be traced for more than 60 metre on the quarry face (Fig. 2.5a). Along the entire length of this fracture, the massive granite has been charnockitised on both margins over a width of about 25-35 cm. In the charnockitised parts the host rock has turned into greasy green colour with a halo of about 20 cm where the granite is blueish-grey in colour. The boundary between the charnockitised portion and the non-charnockitised portion is gradational over about 5 cm.

(b) *Maveli para quarry*: This is a quarry of khondalite located in the western part of the PPT corridor in the Kerala Khondalite Belt within the Achankovil Lineament. There are many N-S trending fractures within the quarry face which are charnockitized (Fig. 2.10). These fractures are at a low oblique angle with the gneissosity. In places garnet stingers of khondalite can be traced across the charnockite-khondalite boundary.

2.3.1.5. Inferences from field observations

The following inferences can be drawn from the above summarized observations:

(i) The localization of charnockite patches in exposures showing patchy charnockites along planes of mechanical weakness, such as brittle fracture, shear planes, gneissosity planes rich in flaky minerals suggest that the charnockitization is probably caused by passage of some fluid (either CO_2-rich fluid and/or brine) along available zones of weakness.

(ii) The fluid responsible for charnockitization affects almost all rock types through which it passes. The resulting mineral composition of the rock largely depends on the precursor rock

type. But the physical appearance of charnockites with varying modal composition are similar due to uniform granulitic texture and dark greasy grey-colour of the rock.

(iii) There is no field evidence for the presence of magmatic charnockite in the studied area. On the other hand, the common presence of metasedimentary rocks, like khondalite, points again to a secondary process. While in theory, magmatic charnockite may exist, the observations from southern India do not provide unequivocal demonstration of igneous contact relationships or igneous textures.

(iv) A superficial similarity may be drawn between the processes of charnockitization and lateritization in that both these processes may pervasively affect the precursor rocks irrespective of their composition and involve bulk geochemical changes. Both these processes progressively destroy internal fabrics of the precursor rocks and transform the rocks into near uniform rock types, often quite different from their precursor rock types in texture. In the transitional areas, gradations between the transformed rocks and the precursor rocks remain preserved.

Mapping in charnockite terrain:

The common use of the term charnockite for mapping purpose excludes distinction of its relative proportion of alkali feldspar and plagioclase (because these are difficult to identify in field) and includes any quartzo-felsdpathic rock type affected by the process of charnockitization. A mapping strategy in charnockitic terrain might best aim at identifying the precursor rock type by studying the ghost fabric in them and by their relationship with non-charnockitized parts. Using this approach, in the present work, precursor rocks of vast areas in the southern part of the Cardamom Hills charnockite massif have been identified as khondalite and garnet biotite gneiss.

2.3.2. New Results: geochronology

During this study, field work, and geochronology on samples from different parts of the SGT were carried out with an aim to better constrain the charnockitization events. Although the analyses are documented in detail in chapters 3 and 4, the following results that have bearing on charnockitization are also summarized below:

1. In the Namakkal area, (Corridor I, Fig. 3.14), monazites from a charnockitized tonalite were analysed. The most concordant (within 1% of the concordia) crystal has a $^{207}Pb/^{206}Pb$ age of 2507 ± 5 Ma (Chapter 4; sample S-130M). I interpret this as the minimum age of charnockitization because monazite is likely to record peak granulite facies metamorphic conditions (Mezger, 1990). If this is correct, then the circa 2.5 Ga charnockitization, which was previously documented in the Transition zone (Friend and Nutman, 1992; Peucat et al. 1993), extends at least as far south as the Namakkal area.

2. Zircons from neosomes of migmatites, which are abundant south of Namakkal, were dated at 603 ± 14 Ma. The neosomes are tightly folded and charnockitization is superposed across these folds (Chapter 3; Fig. 3.38). Thus evidence of both Early Proterozoic and Neoproterozoic charnockitization are present in the Namakkal area of Corridor-I.

3. U/Pb SHRIMP analyses on monazites from granite gneiss in the Bhavani area, within the Moyar lineament (Corridor-II), have yielded two clusters of ages, one at ~2.52 Ga and the other at ~612 ± 10 Ma (sample S-273; Chapter-4). Since monazite is likely to record peak granulite facies metamorphic conditions (Mezger, 1990), I interpret the ~612 ± 10 Ma age as the age of high-grade metamorphism. The ~2.52 Ga age represents either the age of the Late Archean metamorphism or the protolith age of the granite gneiss.

4. In the Palghat area (Corridor-IV), charnockitization is superposed on a granite dated at 568

± 2 Ma (Fig. 2.11; S-404B; Table 5.1). A different population of zircons with very low Th/U ratio (<0.1) in this rock gave a concordant age of 524 ± 2 Ma. This age is interpreted as late growth of zircon possibly due to circulation of hydrothermal fluid through these rocks.

5. In the eastern part of the SGT, in the Palayam area (Corridor-I), a 791 ± 17 Ma high grade metamorphic event has been identified by U-Pb monazite dating of khondalite (Sample S-259m; Chapter-5; Fig. 4.1).

6. In the western part of Palayam area, zircons from a banded charnockite have an upper intercept age of 804 ± 31 ma and a lower intercept age of 473 ± 83 Ma. The lower intercept age constrains minimum age of charnockitization or a younger event.

7. In the Kerala Khondalite Belt, a charnockitization event has been dated in the present investigation by U-Pb analysis on zircon from the youngest granite that is charnockitized (548 ± 2 Ma), and the granite which has retrogressed (Fig. 2.6) the charnockites (526 ± 2 Ma) respectively (sample nos. S-318A and S-318b; Chapter 4). Thus the charnockitization event in the Kerala Khondalite Belt can be bracketed between these two ages. This age constraint of charnockitization is in agreement with previous Sm-Nd mineral isochron ages from the area (Table 6.1; Santosh et al. 1992; Unnikrishnan-Warriror, 1997 and Choudhary et al. 1992).

8. In the southern part of the Cardamom Hill, north of the Achankovil lineament, monazite from the non-charnockitized portion of khondalite within a charnockite massif (Fig. 2.7a) was dated in the present work at 524 ± 2 Ma (Chapter-4, Sample, s-355). This age is interpreted as either the age of charnockitization or a period of cooling following peak of charnockitization event in the area.

From the above results it can be said that Late Archean (~2.5 Ga) charnockitization which has been documented by many workers in many places in the Transition Zone (Grew and Manton,

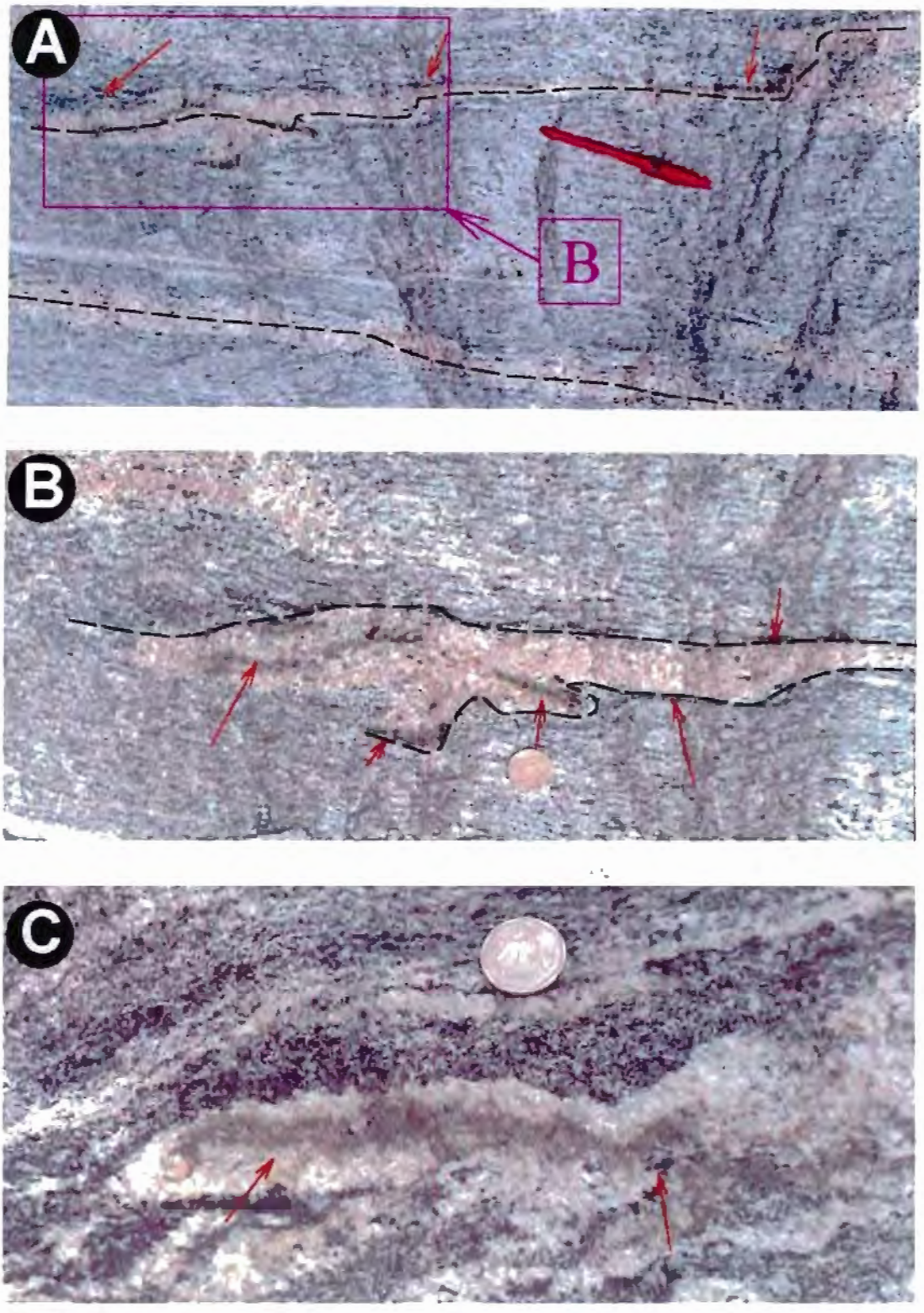

Fig. 2.11(a,b,c). Charnockite patches within unmetamorphosed massive granite veins within biotite gneiss. A, B, location southern slope of the Puzhikkunnumala Hill, Maruthamkad village, 20 kms NNW of Palghat.
A. Charnockite along the contact between granite gneiss and folded granite dykes. Red arrows show charnockite patches.
B. A close-up of part of A. Charnockite along both along the contact between type D granite and granite gneiss also within type D granite.
C. Charnockite entirely within massive granite. Red arrows show charnockite patches within granite. Location, 1 km SSW of Mundur, 12 km NW of Palghat.

1984; Friend and Nutman, 1992; Peucat et al. 1993), extended as far south as the Namakkal area of Corridor-I. Whether or not this charnockitization event extended further south, i.e., south of the Palghat lineament is not yet clear. Superimposition of Neoproterozoic high-grade metamorphism and granitic magmatism, which has been recorded as far north as the Moyar-Attur lineament, may have obliterated most chemical "memories" of any ~2.5 Ga charnockitization in the area south of the Palghat-Cauvery Lineament. Early Paleozoic charnockitization is very common in the area south of the Palghat-Cauvery Lineament but has been recorded as far north as the Moyar-Attur lineament. In the Kerala Khondalite Belt, this later charnockitization has been well constrainted to have occurred between 548± 2 Ma and 526 ± 2 Ma. The U/Pb monazite age of 524 ± 2 Ma from khondalite within charnockite gneiss in the Cardamom Hill possibly narrows down age of charnockitization to within few m.y.

2.4. Relationship between the charnockitization and the tectonism

During this study, the age of the charnockitization in the KKB has been constrained to have occurred after the emplacement of the Kalipara-type granite (548 ± 2 Ma). This is because widespread charnockitization has affected this granite, and which in turn has been intruded by later pegmatitic granite (526 ± 2 Ma) that has retrogressed (bleached) the charnockite. The Kalipara-type granite has been emplaced across the regional tectonic fabric of the Kerala Khondalite Belt, which is NW-SE (for example, in the Chenganoor area, Fig. 3.61). The Kalipara-type granite sheets are folded into outcrop-scale open to tight folds (Fig.3.63; Chapter 3). Thus although intrusion of the Kalipara-type granite likely to be syntectonic with the deformation expressed by the regional NW-SE tectonic fabric of the area, the deformation outlasted intrusion.

Elsewhere, in the Kottamangalam, Palghat and in the Namakkal areas, Neoproterozoic charnockitization has been superimposed on the syntectonic granites that have been dated at ~568±2 Ma, 600 ± 4 Ma, and 603 ± 14 Ma, respectively. Thus it can be concluded that

Neoproterozoic charnockitization post-dates Neoproterozoic tectonism in the SGT or is contemporaneous with the terminal phase of tectonism.

2.5. Conclusion

Use of the term charnockite has varied since the term was first introduced in 1900. Such variation in the use of the term has arisen mainly because of difficulty in applying of the charnockite as a useful field term for mapping. The term charnockite, refers to a rock with granulitic texture[8], with more than 66% of the feldspars as potash feldspar (orthoclase) in addition to the essential mineral orthopyroxene. Such a strict definition is difficult to apply in the field, because the texture and dark colour of the rock does not allow differentiation of the orthoclase- from the plagioclase-feldspar in the field. The process of charnockitization gives rise to rocks of different modal composition depending on the precursor rocks, which may vary significantly in a multiply deformed high-grade granitoid terrain. So, a strict use of the term charnockite is difficult to practise as a field-term. For example, in many parts of SGT, precursor rocks include an ensemble of khondalite, paragneisses, tonalite, granite, granite gneiss, quartzite and amphibolite. Upon charnockitization each of these rocks changes to "granulites" with various modal composition, but many such rocks do not contain the hypersthene essential for a strict definition of charnockite. Thus, a strict use of the term charnockite becomes unwieldy in the field. To circumvent such problem many people have used various qualifiers reflecting modal composition along with the term charnockite. For example, Pichamuthu (1969) proposed use of the term 'acidic charnockite', 'intermediate charnockite', 'mafic charnockite' etc.

---

[8] Although there is lot of controversy about the origin of charnockite, its granulitic texture is nearly universal. Charnockites, whether igneous or metamorphic, almost always have even-grained textures lacking preferred crystallographic orientation. Charnockites obviously lack the most distinctive feature of magmatic crystallization, such as, euhedral or subhedral feldspar, ophitic and sub-ophitic textures and preferred crystallographic orientation of such crystals. The dominance of metamorphic textures, however, does not eliminate the possibility of some earlier magmatic origin of these rocks. However, textural evidence for magmatic crystallization, even if found, may be related to local melting rather than widespread igneous activity. The evidence for magmatic or metamorphic origins of charnockites has to be found in field.

Vast areas of the SGT are underlain by charnockite/enderbite rocks which are products of charnockitization. The reported presence of magmatic charnockites in the Nagercoil Block and in the Cardamom Hills are not confirmed in the present study. Contacts between charnockitic rocks and their hosts show signatures of metasomatism and generally do not have any stratigraphic or tectonic significance. Two such periods of regional dehydration metasomatism have been recorded: the first at ~2.5 Ga and the second at ~525 Ma. Both these events were associated with and/or followed regional granitic activity and tectonism.

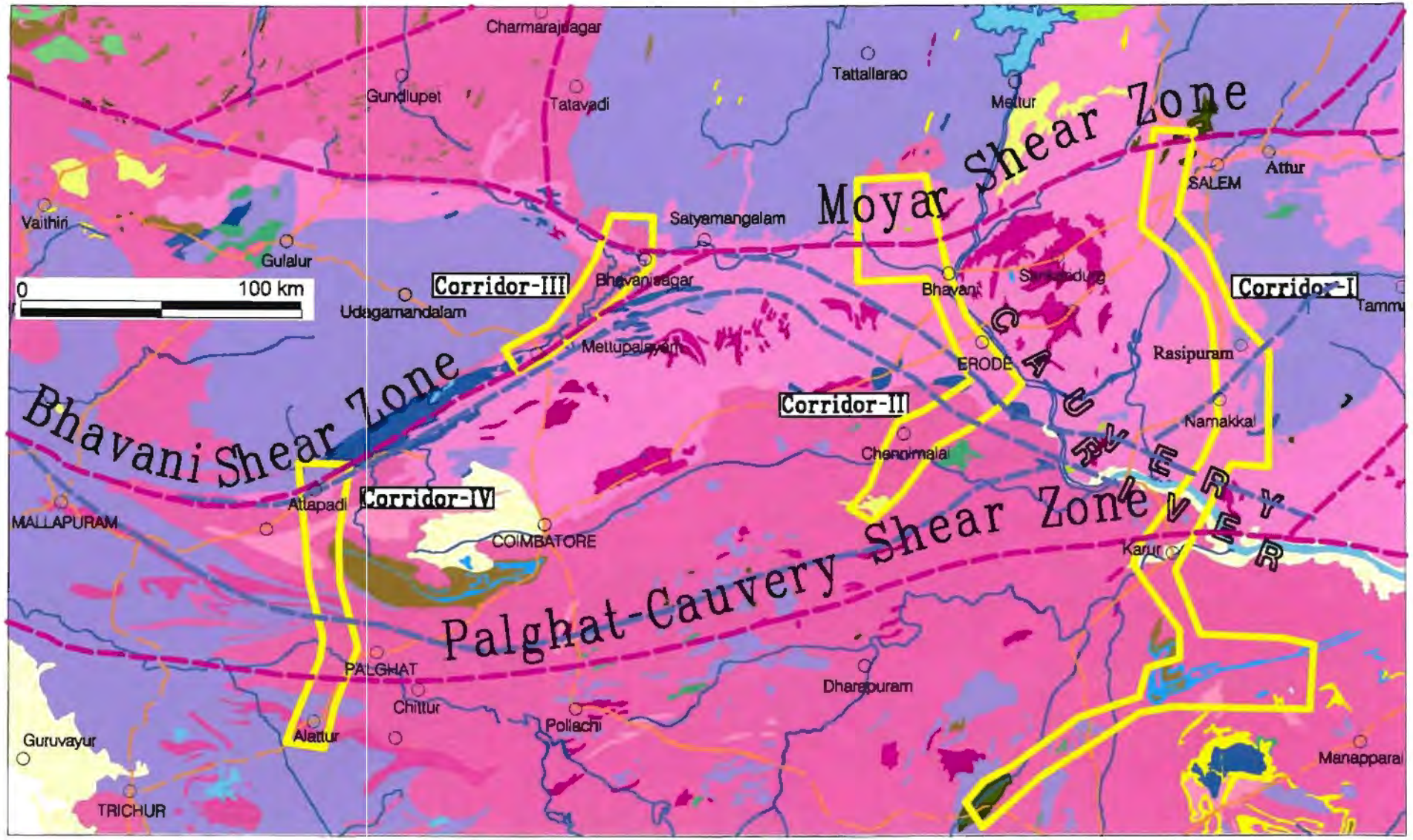

Fig. 3.1. Geological map of part of the Southern Indian Shield showing showing four corridors (I-IV) studied in the present investigation along with previously interpreted (in dashed magenta lines) and newly defined (in dashed white lines) shear zones. The legend for various lithological units is same as in Fig. 1.3.

Chapter-3: Geology of major shear zones of the SGT

3.1. The regional setting of major shear zones of SGT

Three trans-continental shear zones were first identified in the SGT by Drury and Holt (1980) using Landsat satellite imagery: (i) the Moyar and Bhavani shear zones (MSZ and BSZ) (ii) the Palghat-Cauvery Shear Zone (PCSZ) and (iii) the Achankovil Shear Zone (ASZ) (Fig.1.5). The broad existence and delineation of these shear zones were later confirmed by others (e.g., Ramakrishnan, 1993; GSI, 1994; Chetty, 1996), also on the basis of satellite imagery interpretation. The three shear zones mark the boundaries of a number of charnockite massifs in SGT (Figs. 1.7; 3.1). For example, the MSZ passes between the Sheveroy Hill, the Biligirirangan Hill and the Kroog Massif in the north, and the Kollimalai Massif and Nilgiri Massifs in the south. The BSZ cuts close to the southeastern boundary of the Nilgiri Hills Massif; and the PCSZ follows a physiographic low area in the western part, known as the 'Palghat Gap', surrounded on either side by elevated charnockite massifs (Fig. 1.7). Drury and Holt (1980) acknowledged that along its southern boundary, the PCSZ is not well defined. There, the shear zone follows the northern slope of Anaimalai and Palni Hills (Fig. 1.7). The GSI (1994) have defined this shear zone as passing through Palghat, Polachi, Karur and Tiruchiraplly (Fig.1.7). The PCSZ is variously considered as: (i) a craton-mobile belt boundary (the Dharwar craton in the north and the Pandian Mobile Belt in the south, Ramakrishnan, 1993 and GSI, 1994); (ii) a terrane boundary defining a suture between the Dharwar craton and the SGT (Harris et al. 1994;) and (iii) a tectonic block boundary (Dharwar craton in the north and the Madurai Block in the south, Santosh, 1996).

The ASZ has a NW-SE trend and follows the southwestern margin of the Cardamom Hill Massif. This shear zone marks the boundary between the charnockite-dominated Madurai Block and the high-grade metasediment-dominated Trivandrum Block (also known as the Kerala Khondalite Belt; Chacko et al. 1987). In the northwest, the Achankovil Shear Zone

follows the course of the Achankovil river. The GSI (1994) has identified yet another shear zone, the Tenmala Shear Zone, south of, but parallel to, the Achankovil Shear Zone.

The contacts between the of charnockitic terrains and non-charnockitic terrains are metasomatic in nature and often cross-cut the tectonic trends of the area. In places these margins define prominent lineaments on satellite images mainly due to differential weathering of charnockite and granitic gneisses. Such lineaments have been interpreted as shear zones, neglecting the tectonic fabric of the terrains (Drury and Holt, 1980, Drury et al. 1984; Chetty, 1996). Field validation of the existence of these shear zones is generally lacking. Indeed, the few available field studies (Nair and Nair, 1980, Gopalakrishna, 1981 and Naha and Srinivasan, 1996 across parts of the Palghat-Cauvery Shear Zone and Radhakrishna et al.1990 in the Achankovil Shear Zone) do not support the interpretation of the lineaments as trans-continental shear systems. For example, Nair and Nair (1980) and Gopalakrishnan (1981) mentioned that in the Palghat Gap area, the structural trends of the Precambrian gneisses are continuous from the north across the Palghat Gap region. Nair and Nair (1980) specifically stated that there is no apparent evidence of intense shearing in the western section of the Palghat-Cauvery Lineament. Similarly, Naha et al. (1996) demonstrated that there is no apparent change in the structural geometry from north of the Moyar Attur Lineament to the south of the Palghat-Cauvery Lineament. The recently published geological maps of the area on 1:500,000 (GSI, 1995a, b) also do not identify any major shear zone along the PCL.

The Achankovil Shear Zone (ASZ) in the southernmost part of the SGT is also regarded as a major tectonic boundary (Srikantappa et al. 1985; Santosh, 1996) and has been argued to separate boundaries between the two tectonic blocks in the SGT. (e.g., the northern Madurai Block and the southern Trivandrum Block, Harris and Santosh, 1993; Fig. 1.5).

To further test the possible existence of the inferred trans-continental shear zones and their nature as potential terrane boundaries, four selected corridors (Corridors I to IV; Fig. 3.1)

across the MSZ, BSZ and PCSZ, and another one across the ASZ (the PPP Corridor; Fig. 3.1, inset) were selected for structural studies and geochronology. It was envisaged that this approach would yield a better understanding of the geological evolution of the SGT area regionally, and that locally the relationship between the geology north and south of the PCSZ might be unravelled. Reconnaissance mapping involved a few wide traverses within the corridors to identify key areas which were later taken up for detailed structural mapping. U-Pb zircon, monazite, sphene and apatite geochronology on a number of samples collected from within these corridors were also carried out to establish the distribution of protolith ages for different magmatic rocks and the age(s) of high grade metamorphism across different parts of the SGT. The geology of these major shear zones are described in the following sections:

3.2. Geology of the Moyar, Bhavani and Palghat-Cauvery Shear Zones

3.2.1. Introduction

Four corridors (I-IV) covering the MSZ, the BSZ and the PCSZ were selected using available geological maps from the area so that these corridors cover key geologic elements, such as sharp changes in regional trends, and intersections of regional shear zones.

Corridor I. The Salem-Namakkal-Palayam corridor:

The northern extension of this corridor includes the Salem area covering the eastern extension of the Moyar Lineament (Fig. 3.1). The structural trend of rocks north of Salem area is NE-SW (extension of the Eastern Ghat trend (Fig. 1.3). This trend swings to nearly E-W around Salem and then reverts back to a NE-SW trend south of Salem (GSI, 1995a). In the central sector of the corridor, around Namakkal, the regional trend of various lithologies changes from NE-SW (extension of Eastern Ghats trend) in the north, to WNW-ESE in the south. South of Namakkal, the Cauvery valley is poorly exposed. Here the PCSZ has been inferred to pass beneath a thick alluvial

cover (Drury et al.1980; GSI, 1994). The southern sector of this corridor covers the Karur and the Palayam areas to the south of the PCSZ (Fig. 3.1). This area is also poorly exposed but appears dominated by charnockite, granite gneiss and high-grade metasediments. The area south of the PCSZ has been interpreted as a separate terrane from the Dharwar craton (Harris et al. 1994) and/or part of a mobile belt (the Pandian Mobile Belt; Fig. 1.2) flanking the Dharwar craton (Ramakrishnan, 1993; GSI, 1994).

Corridor II. The Bhavani-Erode-Chennimalai corridor:

The northern section part of this corridor passes through an extension of the Moyar Lineament in the Bhavani area (Fig. 3.1). The southern part of this corridor exposes broadly E-W trending litho-units defining the broad E-W trending shear system (the PCSZ as defined by Drury and Holt, 1980).

Corridor III. The Bhavani Sagar-Mettupalayam-Agali corridor:

This corridor extends from north of the Bhavanisagar to south of Mettupalayam (Fig. 3.1). The northern section of this corridor is across the MSZ, whilst the southern section of the corridor is along the BSZ.

Corridor IV: The Palghat Gap corridor:

This corridor crosses the Palghat Gap, an area of physiographic low between the Nilgiri Hills Massif charnockites in the north and the Anaimalai Hills Massif charnockites in the south. The Palghat lineament is best expressed in this area (Fig. 1.5).

3.2.2. Geology of Corridor I

Present investigations in this corridor were focused on three areas:

(i) The Salem area, which includes part of the Moyar Shear Zone.

(ii) The Namakkal area, which includes part of the area where the NE-SW trending structural fabric of the north changes to WNW-ESE trends in the south. This domain has been sub-divided into three sub-domains (I, II and III) on the basis of differences in their structural styles.

(iii) The Karur-Palayam domains, which represent an area south of the Palghat-Cauvery Lineament.

3.2.2.1. Geology of the Salem Area

3.2.2.1.1. Geological setting

The Moyar-Attur Lineament in this area is represented by a 2 to 5 km wide valley extending from Salem in the west to Attur in the east, a distance of about 100 km. This physiographically low area is bounded in the north by the charnockitic massifs of the Sheveroy Hills and of the North Arcot district and in the south by the charnockitic massifs of the Kollimalai and the Pachaimalai Hills (Fig. 1.7). Drury and Holt (1980) inferred that the MSZ has a strike-slip displacement of ~70 km and that it extends in the east up to the Attur area from where it swings to a NNE-SSW direction and then, further north, merges with the eastern extremity of the Cuddapah Shear System. Because the shear systems along the eastern boundary of the Cuddapah basin are of probable Neoproterozoic age, Drury and Holt (1980) assumed that the MSZ, and by extrapolation the entire PCSZ, are also of Neoproterozoic in age. Chetty (1996) noted sub-horizontal to low-plunging stretching lineations in the MSZ near Salem, lending support to the strike-slip model of Drury and Holt (1980). However, Palniswamy et al. (1990), who worked in the Attur valley area, demonstrated that the E-W trending MSZ, which passes through the Salem area, has only a limited strike-slip component and which, moreover, is superposed on NE-SW trending shear zones in the area. According to them, the MSZ does not swerve towards NE-SW to join the shear systems along the eastern boundary of the

Cuddapah basin The part of the MSZ between Salem and Attur is known as Salem-Attur Shear Zone (Palniswamy et al. 1990).

During the present study, an area of about 150 km^2, immediately west of Salem, was mapped along widely spaced traverses using the 1:50,000 scale topographic sheets (Fig.3.2). The regional strike of lithologic and tectonic fabric in the northern and southern sectors of the area is N-S to NNE-SSW while the tectonic fabric and lithologic units in the central part of the mapped area has a dominantly E-W strike (Fig. 3.2). The most prominent physiographic feature of the area is the Kanja Malai Hill, which is about 8 km long and 3 km wide and rises to about 700 m above ground level. This hill comprises inter-layered BIF and mafic granulite bands. Part of the eastern extension of this hill was also mapped at 1:25,000 scale (Fig. 3.3).

3.2.2.1.2. Lithology

The major lithologies of the Salem area are represented by tonalite gneiss, enderbite gneiss, amphibolite and mafic granulite, banded iron formation and associated metasediments, including quartzite, meta-greywacke and pelites

Granite gneiss is the most dominant rock type. It comprises quartz, plagioclase, hornblende and biotite with accessory phases of apatite, epidote, zircon and opaques. Gneissosity (S_1) is defined by alternation of indistinct quartzofelspathic layers and mafic mineral-rich layers. In places along the northern and southern flanks of the Kanja Malai Hill, granite gneiss is distinctly mylonitised (Fig. 3.4a-c). The mylonites are characterised by a well developed planar-fabric (S_2, s-tectonites). In thin section they are charactacterized alternation of ribbons of fine & coarse granulated layers. Flattened mafic-clots of variable size ranging from few centimetres to few metres, are aligned within the plane of gneissosity of the rock (Fig. 3.4c, 3.5a).

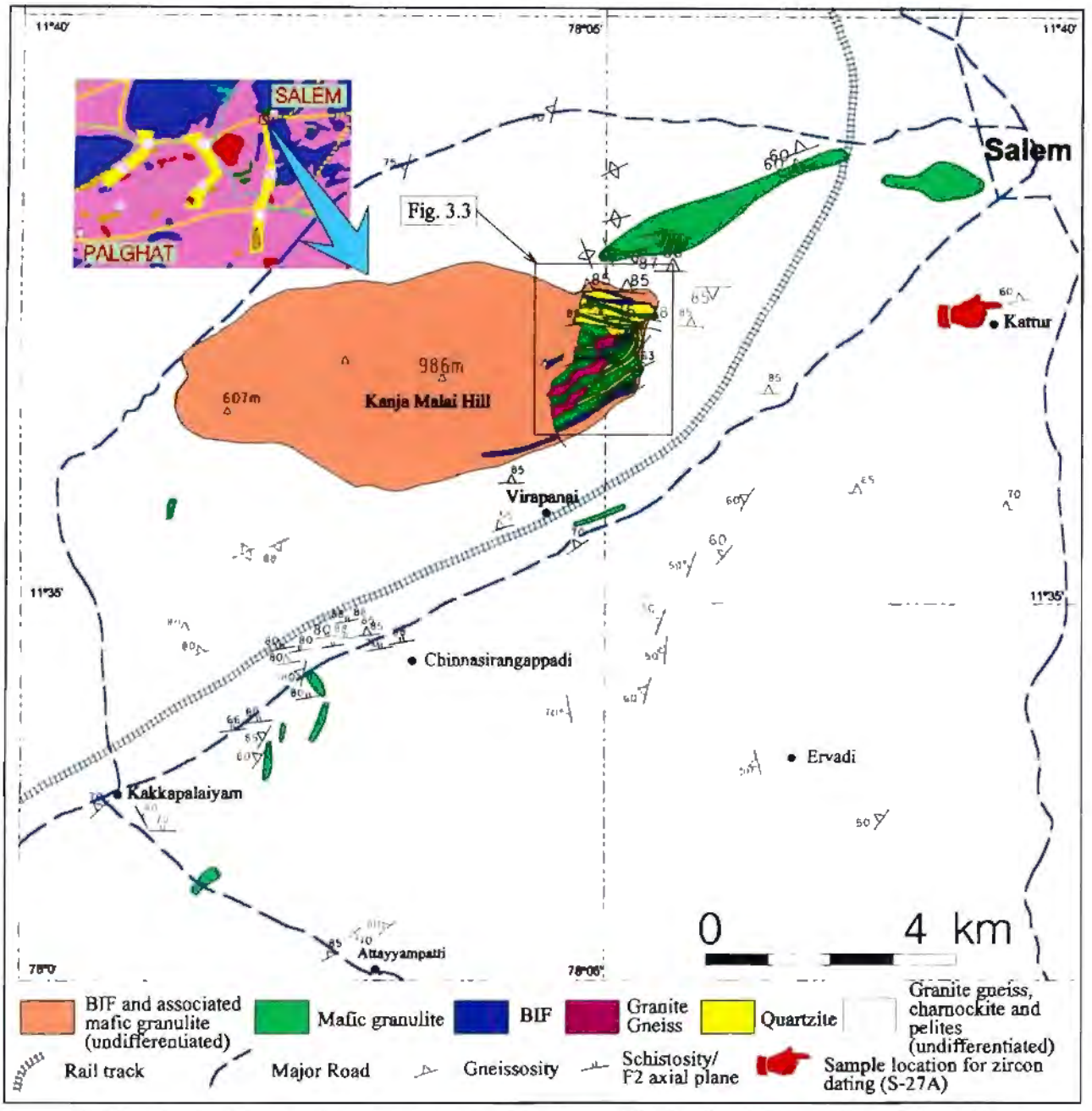

Fig. 3.2. Geological map of an area west of Salem, within the Moyar-Attur Shear Zone, mapped as part of this study. Inset shows position of the area within the Corridor-I.

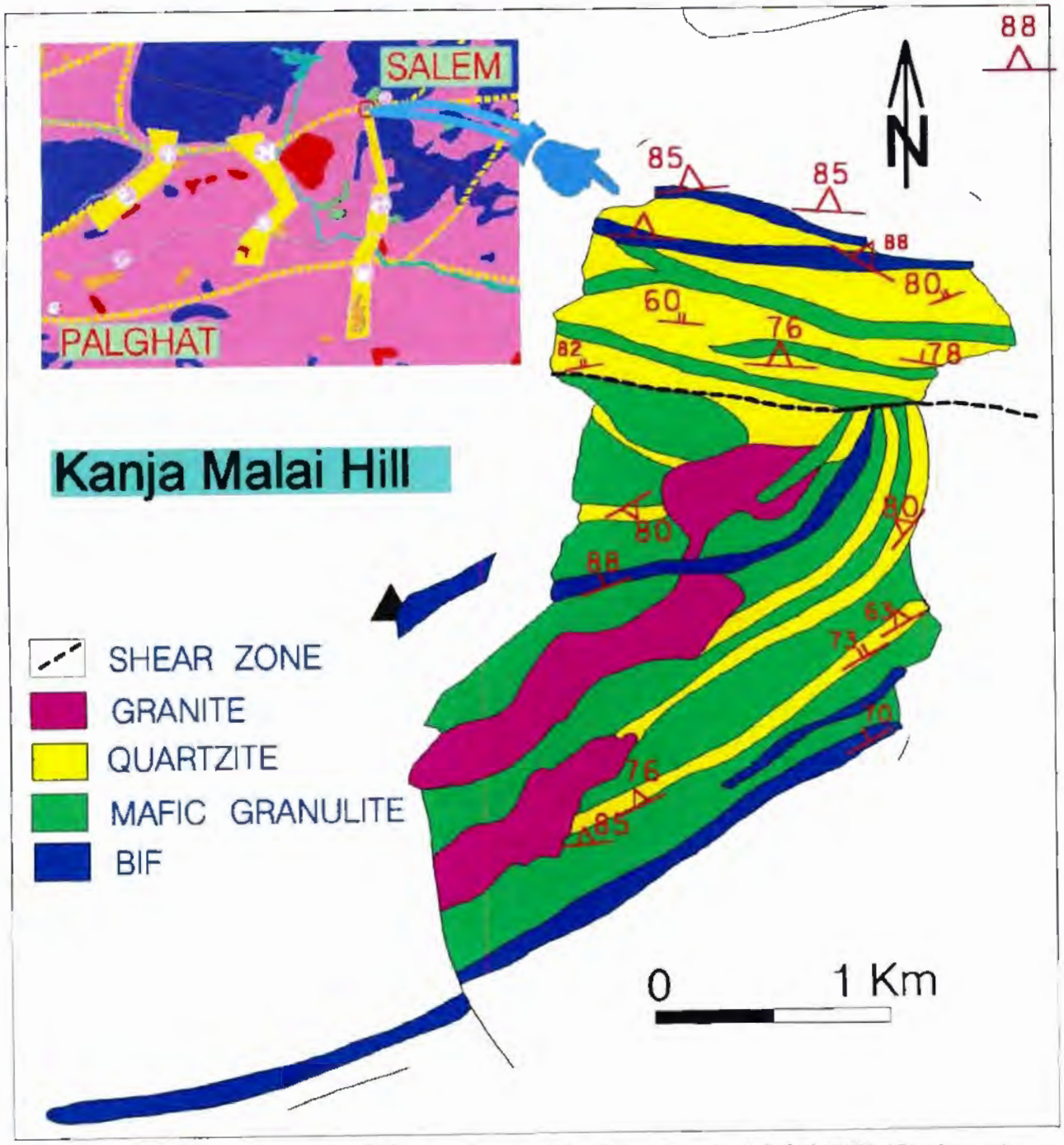

Fig. 3.3. Geological map of the eastern part of the Kanja Malai Hill (for location see Fig. 3.2). Note that in the northern part, a mafic granulite band bifurcate suggesting an intrusive origin for these rocks.

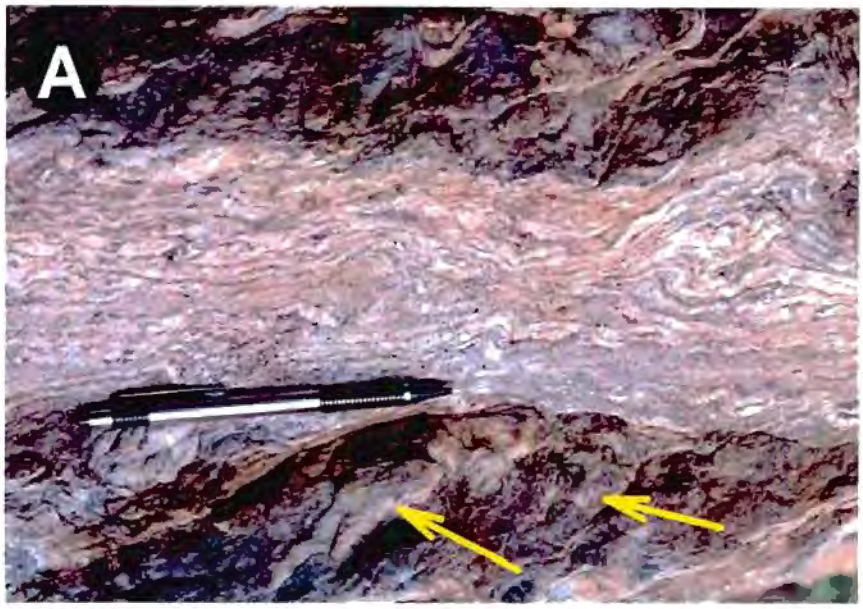

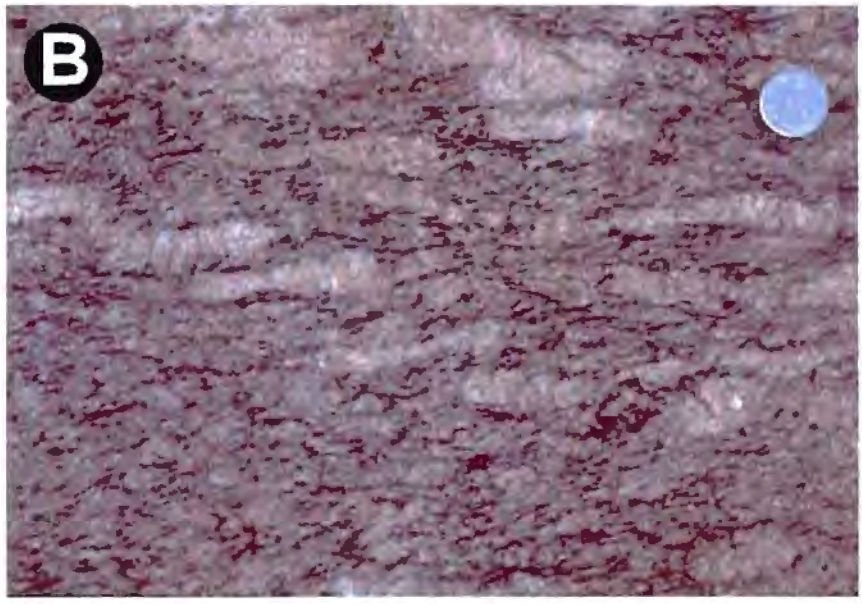

Fig. 3.4. Sheared granite gneiss within the Moyar-Attur Shear Zone.

a. Tight and isoclinal folds with sub-vertical to moderately east-dipping axes (marked by arrow) in the quartzose layers within granite gneiss. Location, eastern margin of Kanja-malai Hill, Salem.

b. Sheared quartz veins (pale) within granite gneiss surrounded by discrete shear planes. Location, 1km NNW of Virapandi Railway station, south of Kanjamalai Hill, Salem

c. Flatterned xenoliths of amphibolite within granite mylonite. Coin in the centre is ~1.5 cm diam. Location, 1km NNW of Virapandi Railway station, south of Kanja Malai Hill, Salem.

Fig.3.5a. Charnockite (dark grey patches, marked by blue arrows) superposed on E-W trending ductile shears (D_2) in grantie gneiss (lower half of the photograph). The charnockitized parts are completely recrystallized while the non-charnockitized parts retain ductile deformation fabric. Flattened mafic clots within the shear zone are marked by yellow arrow. Location, 1/2 km north of Kattur (Fig. 3.2).

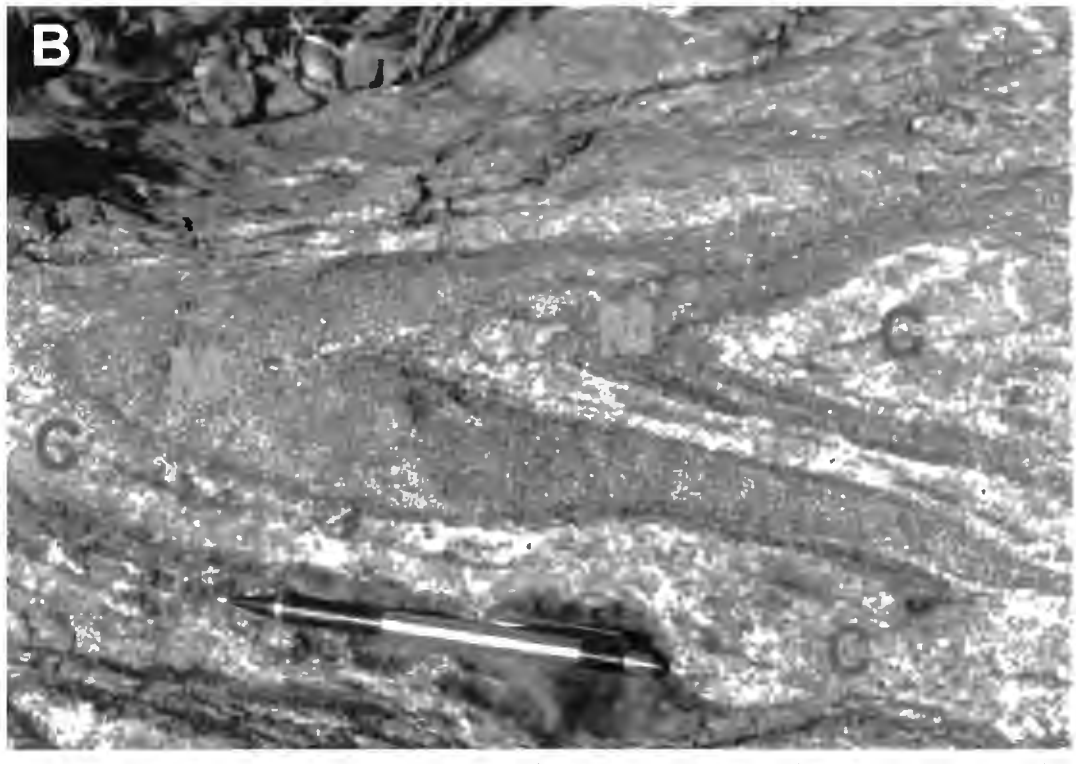

Fig.3.5b Tight fold in charnockite (C) and mafic granulite (M) layers. The rocks are recrystallized and do not have a penetrative axial planar fabric, suggesting that charnockitization is post-deformational. Location, ~1km west of Ervadi (Fig. 3.2).

In outcrop, the granite gneisses display intrusive relationships with the mafic granulite, BIF and associated metasediments. This is also evident from the map pattern of the part of the Kanja Malai Hill (Fig. 3.3).

The granite gneiss displays incipient (patchy) charnockitization (Fig. 3.5a). Charnockites are composed of quartz, plagioclase, orthopyroxene, biotite and hornblende with apatite, zircon and opaques as minor minerals. Charnockitization is clearly younger than the E-W trending ductile shear fabric (S_2). Where charnockitization is superimposed on the E-W trending mylonitic fabric (S_2) of the granite gneiss, S_2 is replaced by a granoblastic texture. However, in outcrop, the remnant mylonitic layering of the granite gneiss can be traced into the charnockitized portion as 'ghost' layering (Fig. 3.5a). In the charnockitic parts, prograde orthopyroxene occurs as rims around hornblende crystals. Khan and Janardhan (1989) mentioned extensive retrogression of charnockites to granite gneisses in the area, which they assumed to be related to shearing along the MSZ. However, this was not confirmed during the present study. Only limited retrogression affected the charnockites, as evidenced by small, patchy alteration of orthopyroxene into biotite and chlorite.

Enderbite gneiss is the most dominant rock type present in the northern and southern part of the area, where these rocks form isolated hills. Enderbite patches are common in the tonalite gneiss exposed in quarries at the foothills of the enderbite massifs, suggesting that these massifs are charnockitized tonalite gneiss. In places mafic enclaves are common within charnockitic massifs. These enclaves are flattened and are commonly isoclinally folded (Fig. 3.5b). Isoclinal folds lack any associated axial planar penetrative fabric. Presumably such fabric that may have been present has been destroyed by recrystallization associated with charnockitization. Presently both the charnockitic portions and the mafic enclaves have granoblastic texture.

Mafic granulite and amphibolite bands occur within tonalitic gneiss or are associated with BIF

and metasediments. Mafic granulite comprises diopsidic-clinopyroxene, hypersthene, plagioclase and garnet, with secondary hornblende and chlorite. Foliation in the mafic granulite is defined by alternating leucocratic (plagioclase-rich) and melanocratic (mafic mineral-rich) layers on a centimetre scale. A schistosity is also commonly developed in mafic granulites along discrete late shear zones (for example in the northern flank of the Kanjamalai Hill). Garnet (varying from few mm up to a dm across) is mainly present in the mafic melanocratic layers.

The relationship between the mafic granulites and the BIF and associated metasediments is not clear. Due to deformation in the area, both BIF and mafic granulite bands are sub-parallel and display sub-parallel planar fabrics. It is thus difficult to decide whether the mafic granulite bands originally were extrusive or intrusive igneous rocks. A few exposures in the eastern part of the Kanjamalai Hill display complex relationship at the contact between quartzite and mafic granulite. In one of the exposures both mafic granulite and quartzite are co-folded into tight to isoclinal folds (Fig. 3.6). Gneissosity in the mafic granulite and the bedding in the quartzite are all subparallel. Fold hinges in mafic granulites are cuspate (Fig. 3.6 a, b) and there is marked variation in the thickness of individual folded mafic granulite layers (Fig. 3.6 a, central part). These features suggest considerable contrast in viscosity between quartzite and mafic granulite during folding. Mafic granulite layers also show bifurcation within quartzite (Fig. 3.3, 3.6a,c) suggesting that they were intruded into quartzite prior to deformation. In a few places along the contact between the mafic granulite and the meta sediments, the quartzite contains clots (centimetre to decimeter size) of mafic minerals (Fig. 3.7). These clots are possibly the result of intrusion of mafic magma into quartzites along their contacts.

BIF and quartzite are common in the Kanja Malai Hill area, while pelites and psamites are common in the area south of Kanja Malai Hill between Kakkapalaiyam and Chinnasirangappadi (Fig. 3.2). BIFs in the Kanjamalai Hill area are mainly magnetite-bearing. Psammites comprises quartz, muscovite, epidote-zoisite, biotite with accessory zircons and

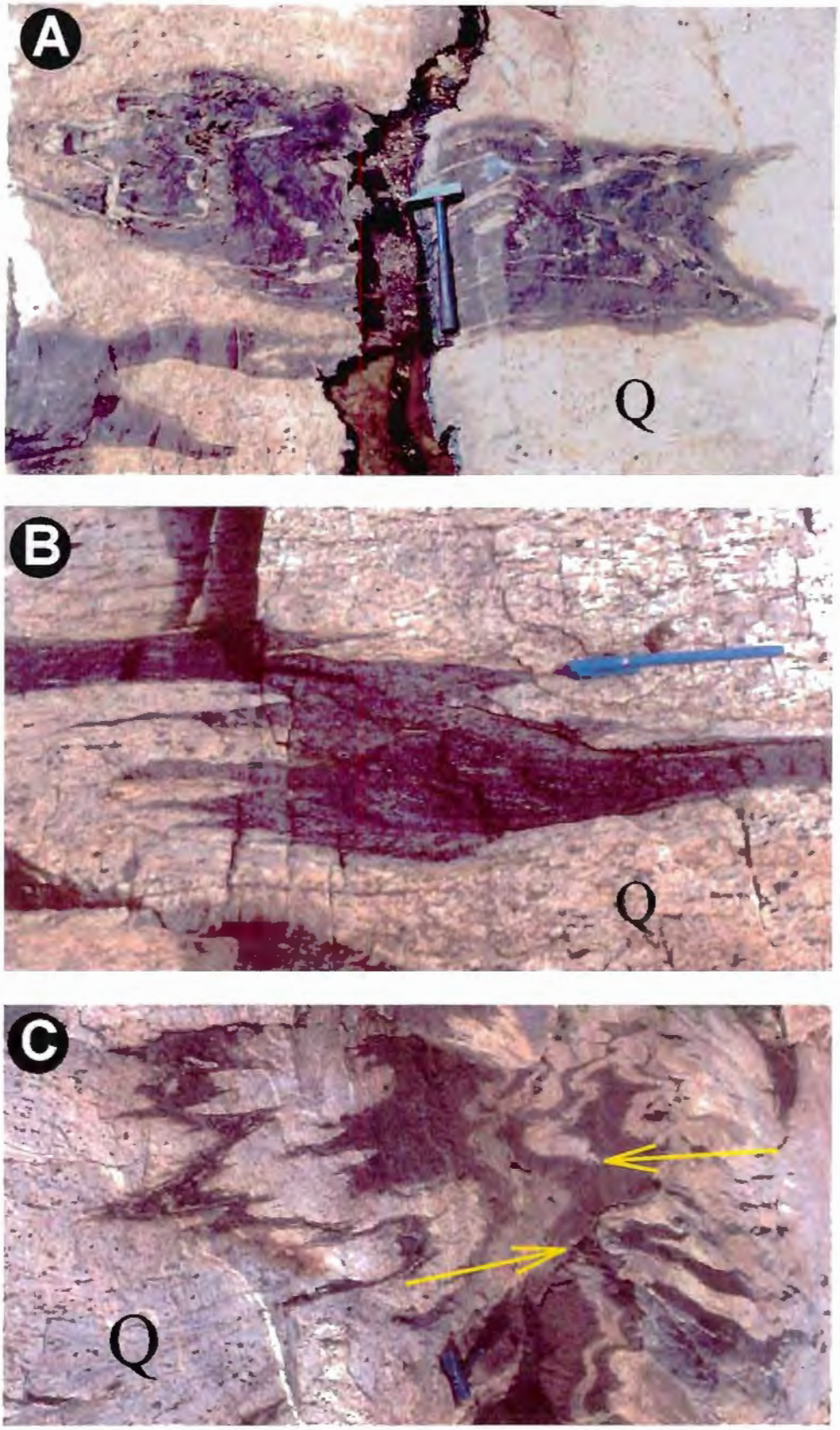

Fig.3.6 (a-c). Mafic granulite interbanded and folded within quartzite (Q). Fold hinges are mostly cuspate. Schistosity in the quartzite and the mafic granulite are subparallel (parallel to the blue pen in b). In places, mafic granulite bands bifurcate (marked by arrows in c), which suggests that the protolith of the mafic rocks may have been intrusive into the quartzite. Location, eastern slope of the Kanjamalai Hill, Salem (Fig. 3.3).

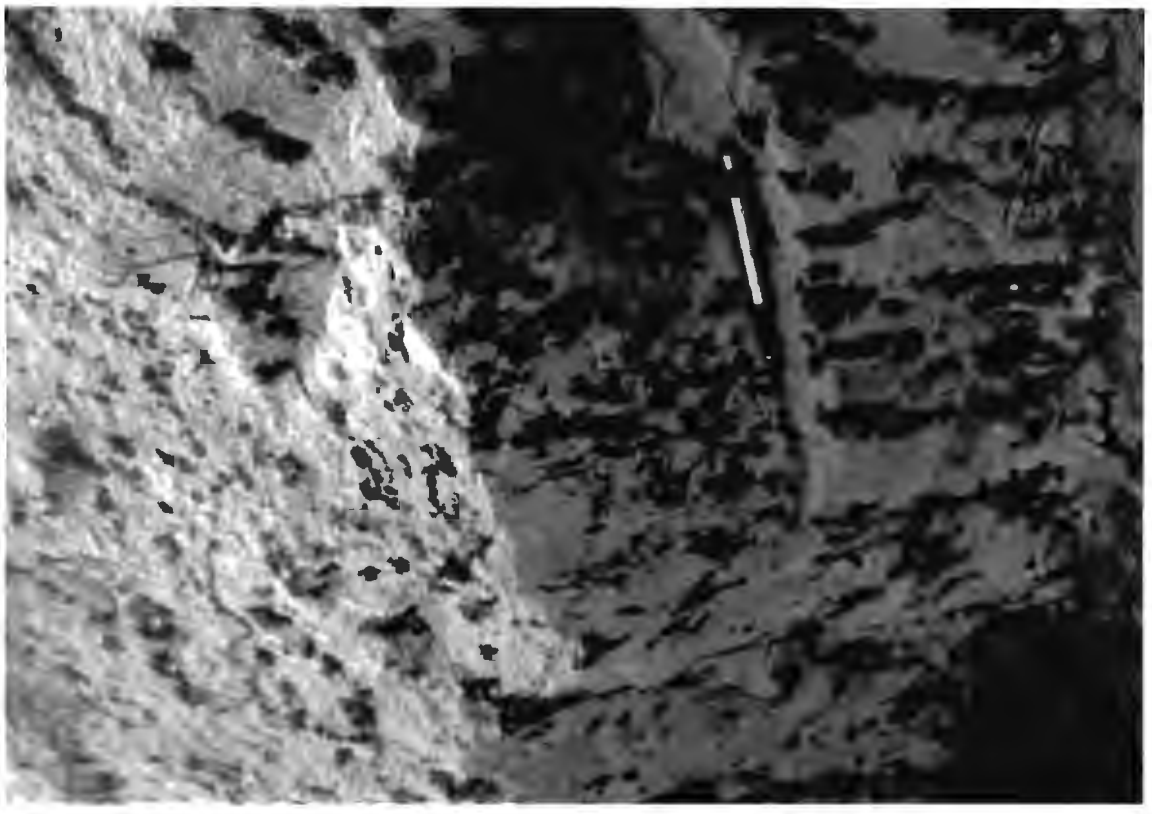

Fig. 3.7. Intimate mixing of mafic granulite clots and quartzite at the contact between a mafic granulite layer and a quartzite layer suggesting that the mafic granulites are intrusive into the quartzite. Location, southern slope of the Kanjiramalai Hill, Fig. 3.3.

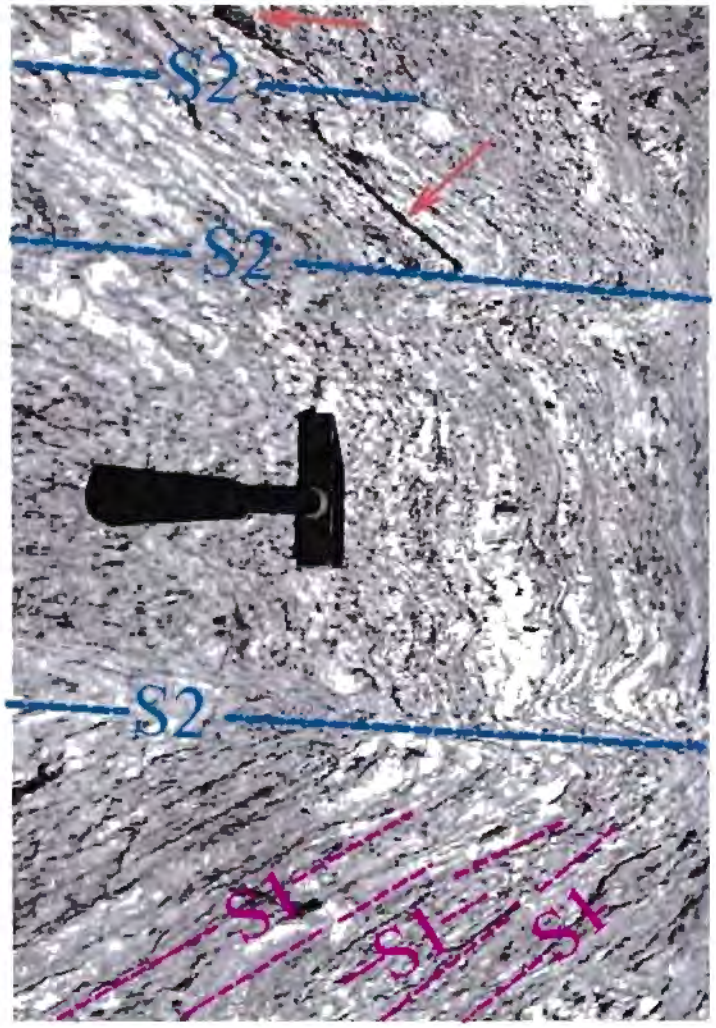

Fig. 3.8a. Fold in granite mylonite in Kanja Malai Hill. Rootless F_1 folds and flattened xenoliths along S_1 (arrow) may be preserved at places. However, E-W trending F_2 folds are the most commonly preserved folds.

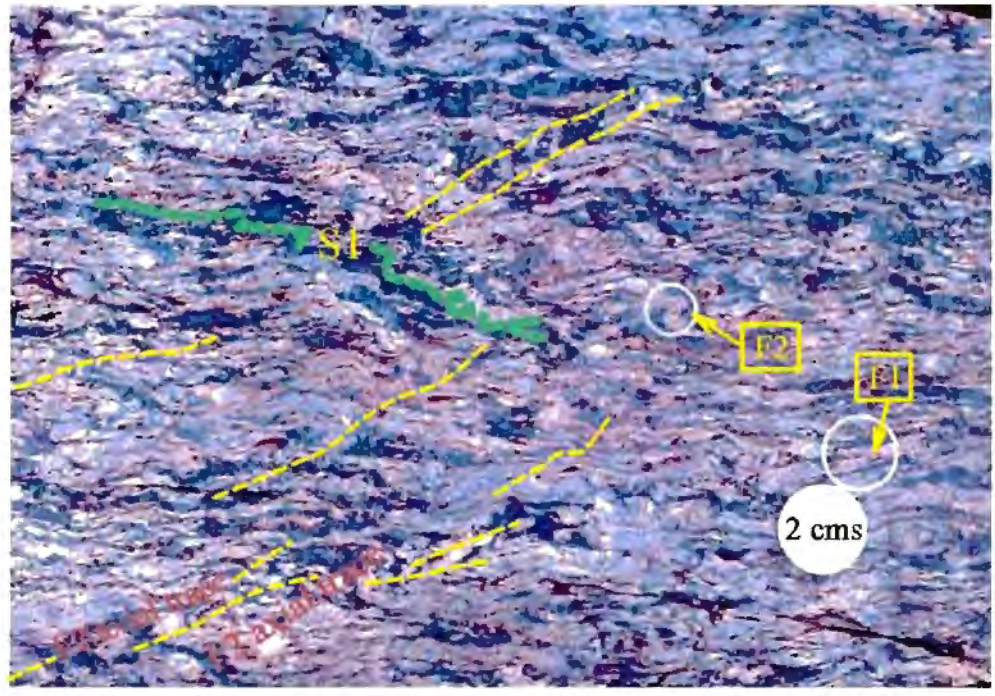

Fig. 3.8b. Small-scale D_1 folds in BIF layers in the Kanja Malai Hills. Original bedding is transposed by D_2 shearing. Rootless F_1 folds are preserved at places within the sheared BIF. Later open F_2 folds are, however, the most common type of fold present in the area. These F_2 folds are Z-shaped with steep sub-vertical axes.

opaque minerals. Pelitic rocks are composed of muscovite, biotite and quartz, with kyanite and staurolite. The presence of kyanite and staurolite together suggests a medium grade of metamorphic facies of these rocks. Close association of charnockite patches together with kyanite and staurolite bearing pelites suggest that charnockitization process in the area did not involve high grade regional metamorphism. Rather, charnockitization might have occurred in an essentially dry condition.

3.2.2.1.3. Structural geology

Both the northern and the southern sections of the area contain a N-S to NE-SW regional strike of the gneissosity whilst the central section has an E-W strike (Fig. 3.2). In the present area, a number of discrete E-W trending shear zones have been identified at the eastern end of the Kanja Malai Hill and south of it, one of which in the eastern part of the Kanja Malai Hill has a sinistral sense of movement (Fig. 3.3). South of the Kanjamalai Hill, some outcrops of granite and tonalite gneiss are mylonitized. Chevron to open E-W trending F_2 folds are common in these outcrops (Fig. 3.8a). Granite gneiss in the area is generally flattened (S_1). Quartzofelspathic layers and lenses surrounded by few millimetres to few centimetres spaced sigmoidal discrete shear planes are common in granite gneiss (Fig. 3.4b, c). In BIF, the original layering is transposed by a later E-W trending planar fabric (S_2) into rootless intrafolial folds. In most places original bedding and folds in the rock are obscured by transposition of a later (D_2) E-W trending flattening fabric (S_2; Fig. 3.8b). Minor folds are scarce in the BIF and mafic granulite of the Kanja Malai Hill. However, two periods of folding (deformation) can still be clearly recognized (D_1 and D_2). F_1-folds are represented by rootless folds bounded within S_1 shear planes in BIF. F_2-folds are represented by open - tight steep plunging 'Z' shaped folds which are superposed on both early F_1-folds and S_1. On a stereoplot, schistosity and axial planes of F_1 and F_2 all cluster around an orientation with ENE-WSW strike and a steep northwesterly dip (Fig. 3.9). Gneissosity however, displays a spread on a girdle reflecting variation in strike from E-W to N-S through NE-SW, with dips varying from

steep northwesterly to steep south-southeasterly. The variation in the strike of the gneissosity is explained by rotation into E-W trending shears in the central part of the area.

Lineations are uncommon in the BIF and quartzite. In a few places, micromullions are present in quartzite and granite mylonite. Mineral stretching lineation defined by stretched garnet are present in some exposures of mafic granulite. For example, northeast of Kanja Malai Hill, a vertical stretching lineation of garnet is well developed on the gneissic plane of mafic granulites (Fig. 3.10). In the granite gneiss lineation of long drawn-out subvertical mafic-rich clots are common on gneissosity planes. Lineations in BIF and granite gneiss are subparallel to the subvertical to moderately east-plunging 'Z' shaped F_2 fold axes (Fig. 3.9). These lineations in the mylonitized granite gneiss and in garnetiferous mafic granulites suggest subvertical movement along the studied shear zones. No evidence for horizontal lineations was observed.

The nature of transition between E-W strike of the central section of the area with the general N-S to ENE-WSW strike in the southern part of the area was studied in detail in the pelites exposed between Chinnasirangappadi and Kakkapalaiyam. Here the pelites have a general NE-SW strike. They are intruded by dense quartzofelspathic veins subparallel to the S_1 in the pelites. The veins are open to tightly folded (Fig. 3.11). These F_2 folds have E-W trending subvertical axial planes with subvertical to moderately easterly plunging fold axes. Such folds are mostly symmetrical ("M"-type). Occasionally, the relative displacement of quartzose layers by shear planes associated with the E-W trending folds indicates a sinistral sense of movement along minor shear planes (Fig. 3.11a).

In summary, rocks in the central section of the Salem area thus record flattening and shearing on subvertical planes with subvertical movements as indicated by occasional presence of subvertical stretching lineation. There is no evidence for significant strike-slip movement along these shears. E-W trending D_2 shears are superposed on regional NNE-SSW to NE-SW

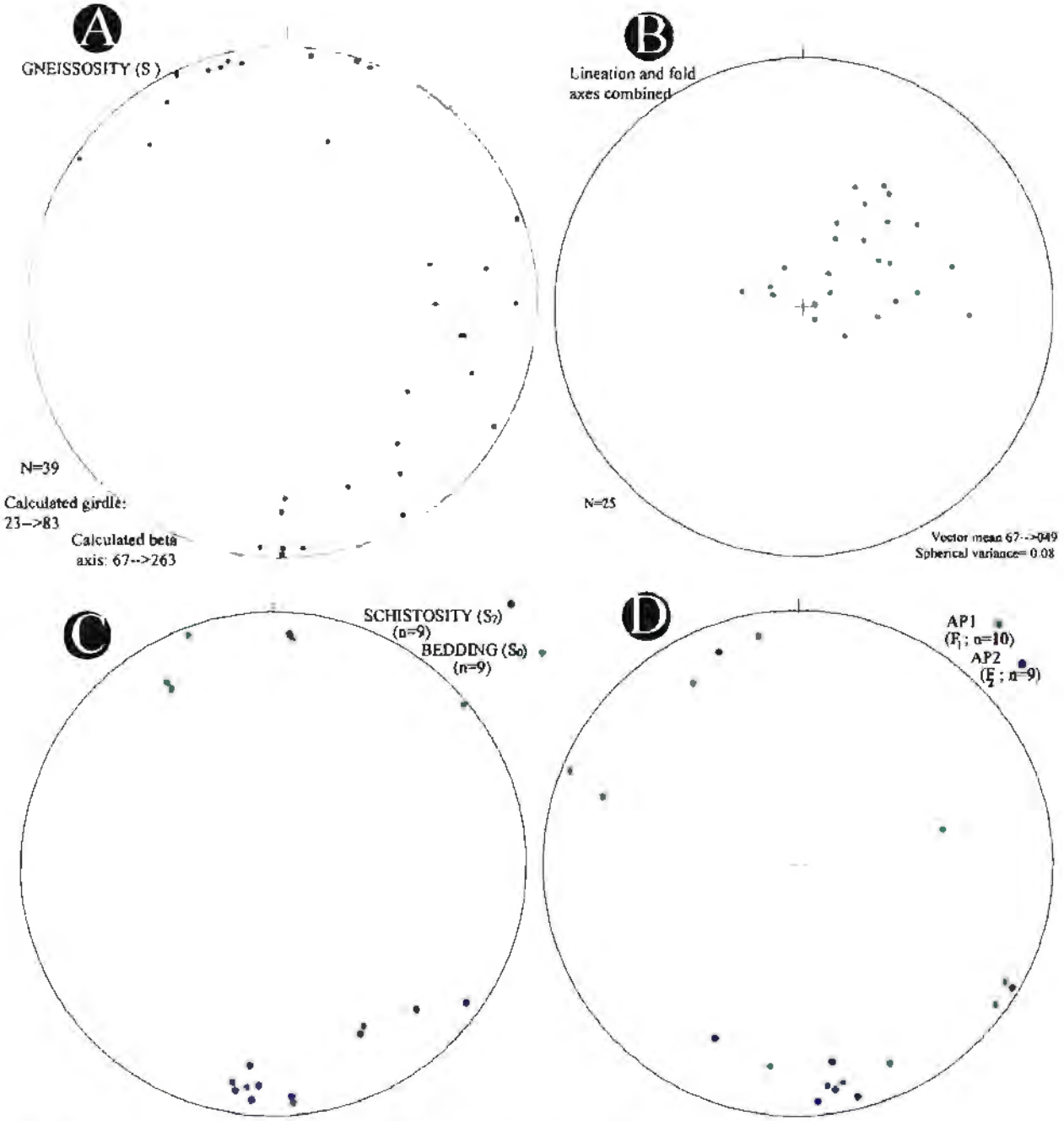

Fig. 3.9. Equal area plot of various structural elements in the Salem area.
A. Gneissosity (S_1); the spread in the gneissosity poles is due to the effect of superposed E-W trending D_2 shearing.
B. Linear elements show a concentration with a steep NE-dipping attitude (D_1 & D).
C. Poles to schistosity (S_2) and bedding (S_0).
D. Poles to axial planes of F_1 and F_2 folds all indicate steeply dipping ENE-WSW attitudes.

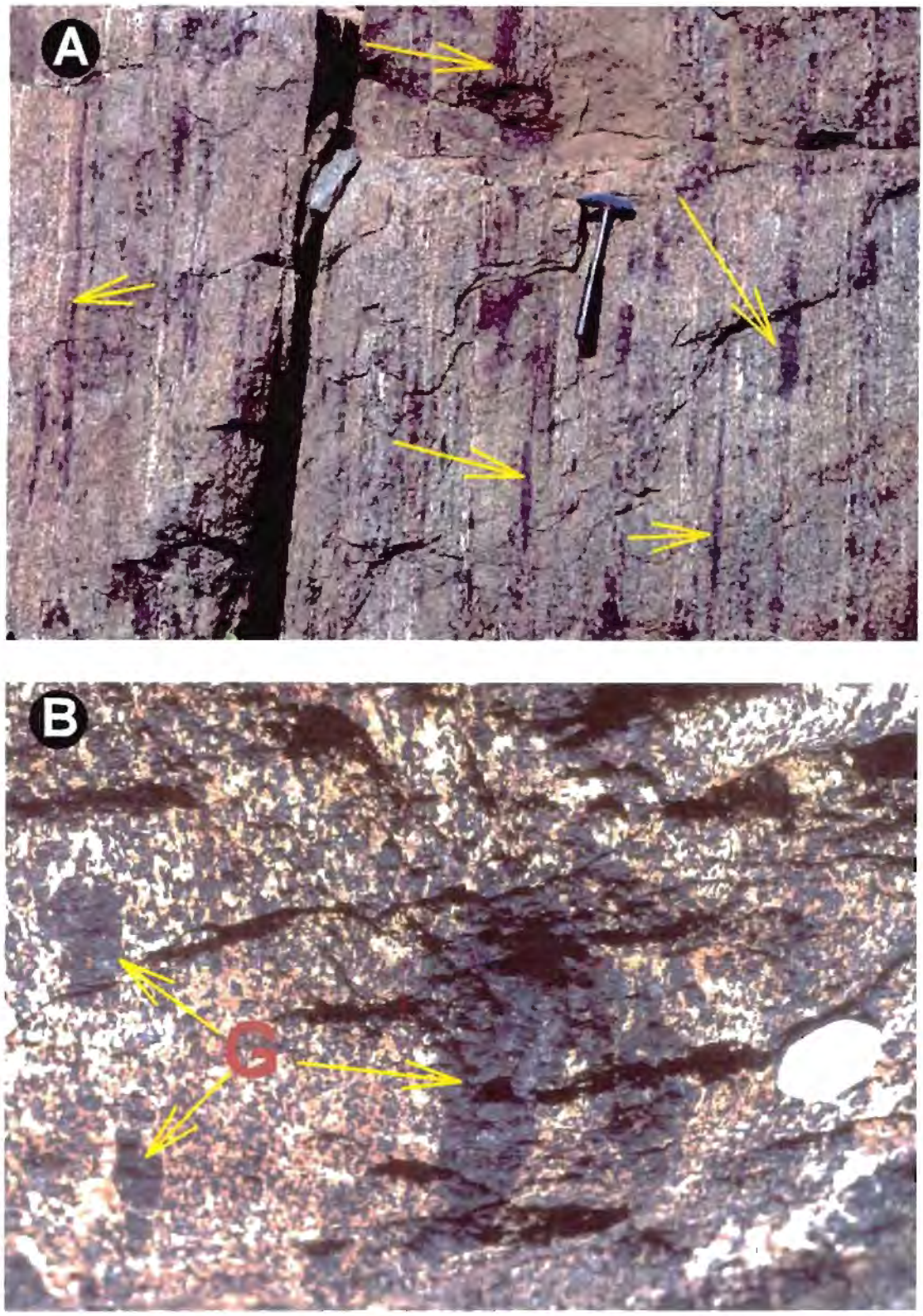

Fig. 3.10. Sub-vertical stretching lineation in mafic granulite. Location, noththeastern tip of the Kanjamalai Hill, 6 km west of Salem (Fig. 3.2).
a. Sub-vertical section, perpendicular to the gneissosity in which garnet megacrysts (marked by arrows) are stretched in down-dip direction.
b. Sub-horizontal surface; garnet megacrysts (G) are either equidimensional or show minor flatterning.

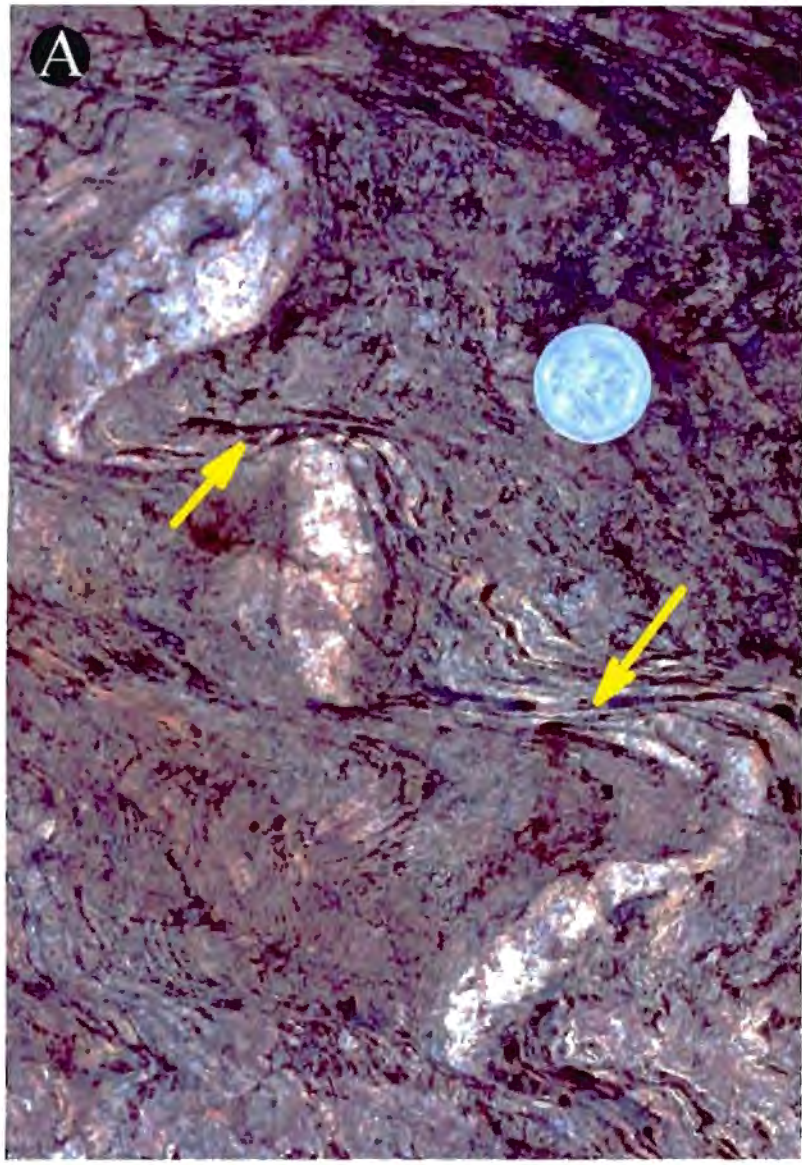

Fig. 3.11. E-W trending sinistral shear bands (D_2) (marked by yellow arrows) in metapelite with quartzo-feldspathic veins within the Moyar-Attur shear zone. White arrow head points to north. Location: 12 km southwest of Salem, south of National Highway 47 (see Fig. 3.2)

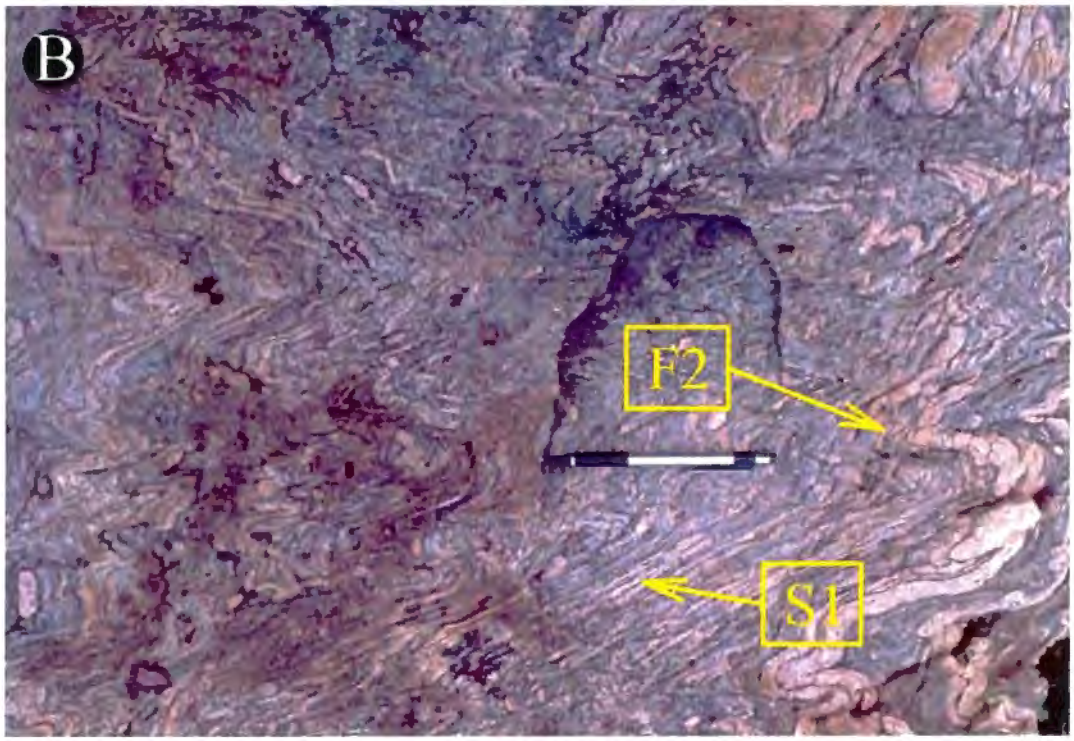

B. Near symmetrical (M-shaped) F_2 folds in pelitic rocks with the Moyar-Attur Shear Zone. Location, 13 km southwest of Salem, north of National Highway 47

striking tectonic fabric present in the rocks both to the northern and to the southern sections of the Salem area.

3.2.2.1.4. Conclusion

The oldest recognisable rocks of the area are the BIF and associated metasediments. Mafic granulites present in the area are probably intrusive sills into the BIF and associated metasediments. However, conclusive evidence is lean. A granite gneiss sample collected from a quarry in the Kattur area (Fig. 3.2) with incipient charnockitization (Fig. 3.5a) has an U-Pb zircon age of 2528 ± 2 Ma (Chapter 4). Granite gneiss in this area is intrusive into mafic granulites, BIF and associated metasediments. Therefore, granite gneiss in the area is of Archaean age. The E-W trending shears present in the central part of the area are subvertical in orientation and have both stretching and flattening components. Subvertical stretching lineations present at few places indicate subvertical tectonic transport during flattening. The shearing predate incipient charnockites patches present in the area because the incipient charnockites crosscut the tectonic fabric (Fig. 3.5a). There are no age data available for this charnockitization event. In the Krishnagiri area, about ~100 km north of the Salem area, Peucat et al. (1993) reported a ^{206}Pb-^{207}Pb monazite age of ~2507 Ma from charnockite. A U-Pb monazite age of 2507 ± 5 Ma from charnockite in the Namakkal area (about 60 km south of Salem) was obtained during this study; and is interpreted as the age of charnockitization (see Chapter-4). A Rb-Sr whole rock isochron from charnockite in the Salem area gives an age of 2476 ± 115 Ma age (Spooner and Fairbairn, 1970). Thus, assuming that charnockitization in Salem area is also about ~2.5 Ga, the N-S tectonic fabrics (S_1) and the E-W shear fabric (S_2) in the Salem area, which predates this charnockitization (Fig. 3.5a), are also Archaean in age. Again, Neoproterozoic-Ealy Paleozoic charnockitization which has been recorded in the Namakkal, Bhavani and Bhavanisagar areas where they are present along with Archean charnockites. The incipient charnockitization in the Salem area could also be Neoproterozoic in age. If so, then the E-W shear fabric (S_2) are also Neoproterozoic in age. S_1

is likely to be Archean in age as S_1 fabric in the Namakkal area is dated to be older than 2.5 Ga.

3.2.2.2. Geology of the Namakkal area

3.2.2.2.1. Geological setting

The Namakkal area falls within the eastern extremity of the PCSZ and is also underlain by granite gneiss, charnockite gneiss, BIF and associated metasediments. Rocks in the northern part of Namakkal have a consistent NE-SW strike (Fig. 3.1). This strike continues south of Namakkal where it takes on an E-W orientation along a number of NW-SE trending shear zones (GSI, 1995). Chetty and Bhaskar Rao (1996) interpreted this zone to represent a westerly-directed thrust. About 200 km^2 around Namakkal was mapped at 1:50,000 scale during the present study (Fig. 3.12; 3.13) complemented by detailed mapping on 1:25,000 scale in few key areas. The area of study extends from about 8 km south of Rasipuram in the north to about 5 km north of the Cauvery River in the south. The area further south is covered by alluvium of the Cauvery River system. The Palghat Shear Zone has been extrapolated to pass through this alluvium-covered area (Fig. 3.1).

3.2.2.2.2. Lithology

Similar to the Salem area, the major lithologic units of the Namakkal area are represented by granite gneiss, charnockitic gneiss, mafic granulite, BIF and associated metasediments. However, in the southern part of the area, south of Namakkal, there occur a number of massive granite intrusions. These younger granites have *intruded* subparallel to the planar fabrics of deformed older rocks, giving rise to extensive migmatites. Large tors of the younger granite occur in the southern part of the area. A sample of this granite yields U/Pb zircon age of ~600 Ma (Chapter 4).

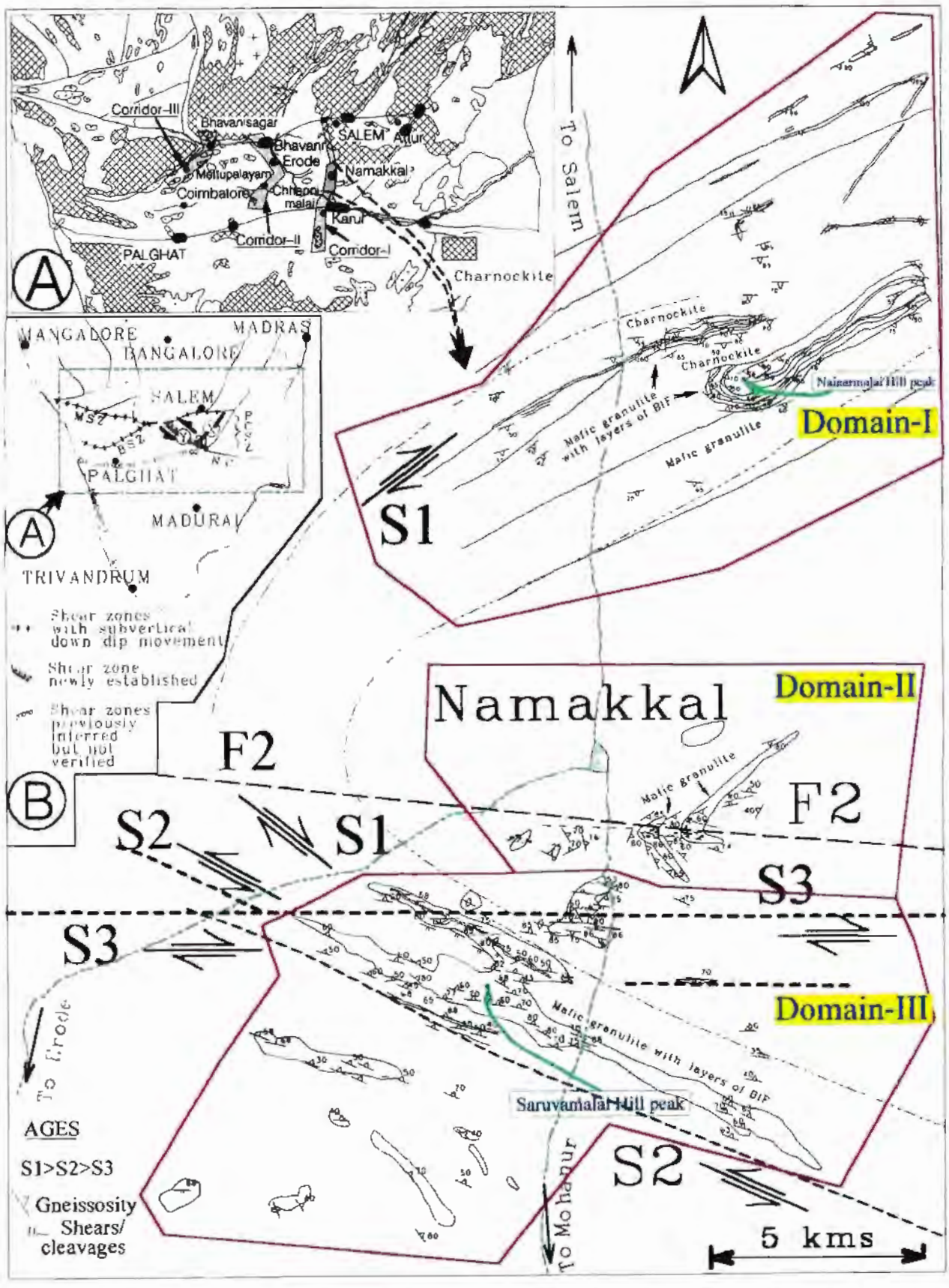

Fig. 3.12. Structural map of Namakkal area showing 3 domains referred in text.

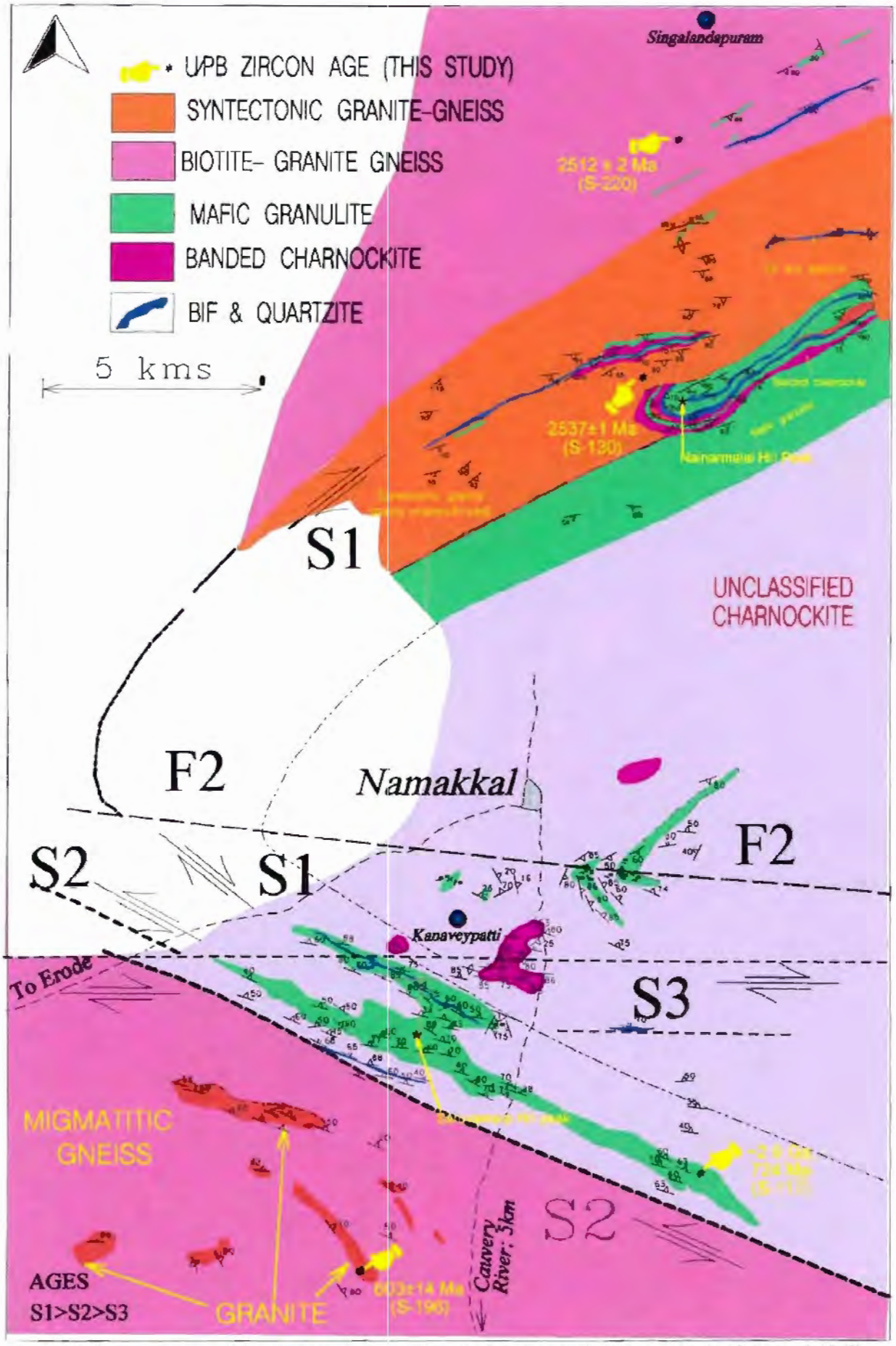

Fig. 3. 13. Geological map of the Namakkal area, corridor-I. Note that one BIF band near the Nainarmalai Hill peak is intruded by mafic granulite.

Tonalite and enderbite gneiss are spatially closely associated and commonly, transitions between these two rock types are marked by a zone of incipient charnockitization. The tonalite gneiss comprises plagioclase, quartz, hornblende and biotite; the enderbitic gneiss comprises quartz, plagioclase and hypersthene as major minerals. Secondary alteration of hypersthene to chlorite is common in enderbitic rocks.

Metasedimentary rocks are represented mainly by BIF and associated quartzite and metagreywacke. Rare calc-silicate rock exposures occur in the southern part of the area. The two most prominent hills in the area (Nainar Malai Hill [743m] in the northern part of the area and Saruva Malai Hill [436m] in the southern part of the area) are predominatly underlain by BIF and mafic granulite. Psammites associated with the BIF are partially charnockitized in many places. The best examples occur along the southern slope of the Nainar Malai Hill.

Mafic granulites are commonly gneissose and occur interlayered with BIF, quartzite and psammites. Mafic granulites are also present as large (km-scale) layers within granitic gneiss. Major minerals of the mafic granulites include plagioclase, clinopyroxene, orthopyroxene, garnet, quartz and secondary hornblende and chlorite. Foliation in the mafic granulites is defined by alternating layers rich in pyroxene and garnet, with layers rich in plagioclase. Within some large mappable units of mafic granulite apparent primary igneous layering is preserved. For example, layers rich in chromite and magnetite present along the southern slope of the Saruva Malai Hill are probably cumulates (Fig. 3.14). Mafic granulite in the area is intrusive into the BIF and associated metasediments. The geological map of Nainar Malai Hill illustrates this (Fig. 3.13); and on outcrop scale, exposures showing an intrusive relationship between the mafic granulite and quartzite are present in a quarry about 1 km NW of Pulavakkal along the southern slope of Nainar Malai Hill. The mafic granulites and BIF on the other hand have both been intruded by syntectonic granite gneiss present in the area. This is clearly visible just to the north of the Nainar Malai Hill and in numerous outcrops (Figs. 3.13, 3.15). This granite has

been dated at 2537 ± 1 Ma (Chapter 4). Thus, the BIF - mafic granulite rocks are Archean in age.

A few late gabbro and dolerite dykes are present in the northern part of the present area. They crosscut structural fabric of the older rocks but themselves are undeformed.

3.2.2.2.3. Structural Geology

Regional Structure

In this area, the general strike of the lithologic units and gneissosity are subparallel and vary from NE-SW in the north to WNW-ESE in the south, whilst in between the strike is E-W. This strike variation is due to a major E-W trending fold (F_2; named here the Namakkal Fold; Fig 3.12, 3.13). The northern limb of the F_2 fold occupies the Nainarmalai Hill and the southern limb occupies the Saruva Malai Hill (Fig. 3.12, 3.13). Both limbs of this F_2 fold preserve km-scale Z-shaped folds (F_1) without complimentary S-shaped folds; these Z-shaped folds are, therefore, interpreted as earlier folds (F_1). These F_1 folds are defined by folding of lithological contacts and gneissosity. The presence of Z-shaped folds along both limbs of the Namakkal fold without intervening S-shaped folds is interpreted to represent an early dextral shear zone (S_1) which was subsequently folded by the F_2 Namakkal fold. The southern limb of the Namakkal fold is highly deformed and is also affected by two later shearing events (S_2 and S_3). S_2 shearing is present in a zone along the southern limb of the Namakkal fold, while S_3 shearing crosscuts this southern limb (Fig. 3.12, 3.13).

The Namakkal area has been subdivided into three distinct structural domains (Fig. 3.12). Domain-I represents the northern limb of the Namakkal fold. It extends from Singalandapuram to just north of Namakkal. Domain-II represents the core of the Namakkal fold. It extends from about 3 km north of Namakkal to Kanaveypatti (about 4 km south of Namakkal).

Fig. 3.14. Primary layering in mafic granulite: Fine layering within the dark layer in the centre represents chromite-rich and chromite-poor layers. Layers rich in garnet and chromite and other opaque minerals (dark coloured, marked by arrow) also define primary layering. Pale coloured portions are feldspar-rich. Location, southern slope of the Saruva Malai Hill (Fig. 3.13), Namakkal, Corridor-I.

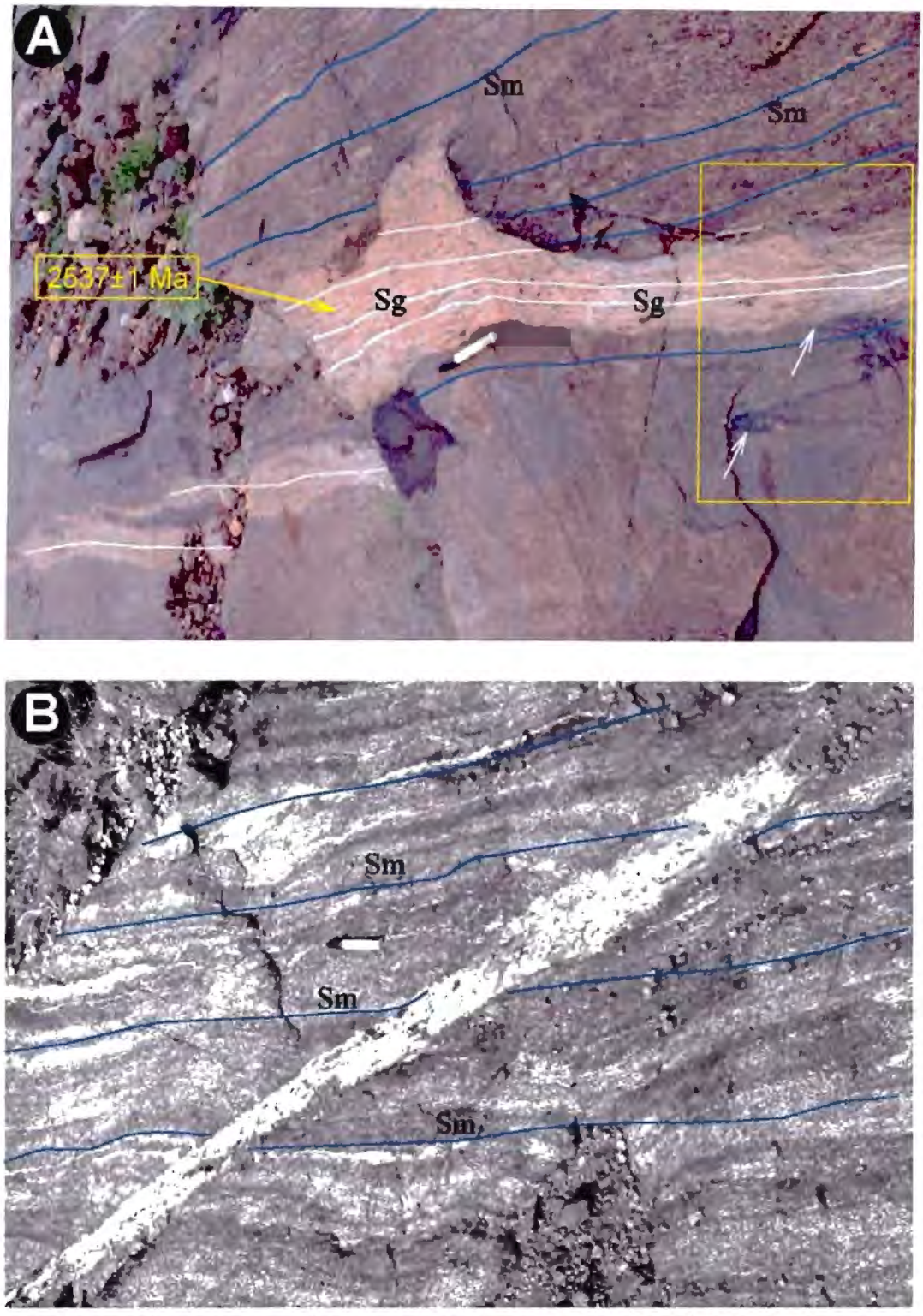

Fig. 3.15. Intrusion of syntectonic granite gneiss across the gneissosity (Sm) in mafic granulite. The granite gneiss in the Nainarmalai is dated at 2537±1 Ma.

A. Gneissosity in the mafic granulite (Sm) and schistosity in the syntectonic granite gneiss (Sg) are subparallel. Note that in the boxed area, the granite gneiss cuts across a limb of a fold defined by a garnet-rich layer (marked by white arrows) suggesting Sg (described regionally as S_4) is post Sm.

B. Dykelet of granite gneiss cross-cutting gneissosity in mafic granulite (Sm).

Locations: A, southern slope of Nainarmalai Hill;

B., northern slope of Saruva Malai Hill. (see Fig. 3.13).

Domain III covers the southern part of the Namakkal fold, extending from south of Kanaveypatti in the north to the Cauvery River. A summary of the main characteristics of these domains is given in Table 3.1

Table 3.1 Characteristics of three structural domains of Namakkal area.

	Domain I	Domain II	Domain III
Regional strike	NE-SW to ENE-WSW	ENE-WSW to NW-SE	NW-SE
Folding	Z-shaped F_1 fold	Open to tight F_2 fold	Z-shaped F_1 fold
Rock types	Tonalite, granite and their charnockitized	Same as in Domain- I	Same as in Domain I and II; in addition this domain has extensive migmatite and young granite
Shearing	S_1 shears related to D_1 deformation	S_1 and S_3 shears related to D_1 and D_3 shearing	S_2 and S_3 shears related to D_2 and D_3 shears

Domain I

The most prominent feature of this domain is the structure of the Nainar Malai Hill. Here, an ENE-WSW trending, 1-3 km thick inter-layered sequence of BIF, quartzite and mafic granulite can be traced for a length of about 10 km. The BIF and mafic granulites of the hill define a Z-shaped fold with a subvertical axis and axial plane. The gneissic fabric in mafic granulite is also folded and thus predates the folding. The northern limb is attenuated. An elongate granite sheet (~2 km wide) has intruded this fold along its shorter limb (Figs. 3.13, 3.16b) and has since been charnockitized. Zircons from this granite sheet was dated at 2537 ± 1 Ma (U-Pb zircon) which is interpreted as the protolith age of this charnockite body, whilst monazite from this sheet is gives an age of 2507 ± 5 Ma (Chapter 4). This later age is interpreted as the age the charnockitization. The granite sheet has a prominent gneissosity and

fracture cleavage subparallel to the axial plane of the folding. Numerous xenoliths of BIF and mafic granulite occur within this granite sheet. These xenoliths are highly flattened and are aligned subparallel with the gneissosity of the rocks (Fig. 3.16a). The contact between the BIF or mafic granulite with the granite is also highly deformed and dextrally sheared (Fig. 3.16b). I interpret these structure to indicate that the granite sheet is syntectonic. This implies that the suggested that NE-SW trending deformation fabric in the area is the result of circa 2.53 Ga deformation. Isoclinal folds and subvertical stretching lineation are common in BIF in the Nainar Malai Hill (Fig. 3.17) but fold interference is not common. All planar fabrics in this domain (S_0, S_1 and S_2) are steeply dipping and strike ENE-WSW. The dominant lineation (L_3) is also subvertical (Figs. 3.18).

Domain-II

This domain represents the core of the Namakkal fold, best depicted by two prominent mafic granulite bands (Fig. 3.13). Late discrete D_3 shears have transposed earlier S_1 and S_2 fabric of the rock (Fig. 3.19). Minor structures associated with D_3 have dextral sense of movement (Fig. 3.20). In places within the D_3 shear zones, rocks have been transformed into schists (Fig. 3.21). About 4 km SSW of Namakkal (west of Kanaveypatti village, see Fig. 3.13) a D_3 shear zone has completely transposed the BIF into a lineated rock plunging steeply to west (Fig. 3.22). Around Kanaveypatti, garnet-rich zones have been folded into rootless isoclinal folds within D_3 shears (Fig. 3.23). In these shear zones granite gneiss and mafic granulite are straightened into interlayered gneisses over lengths of up to 100 m (Fig. 3.24). Equal area plot of S_1 planes Domain-II show wide variation in attitude (Fig. 3.25), which is possibly the result of both F_2 folding and So shearing.

Domain-III

The best structures representative of this domain are exposed on Saruva Malai Hill.

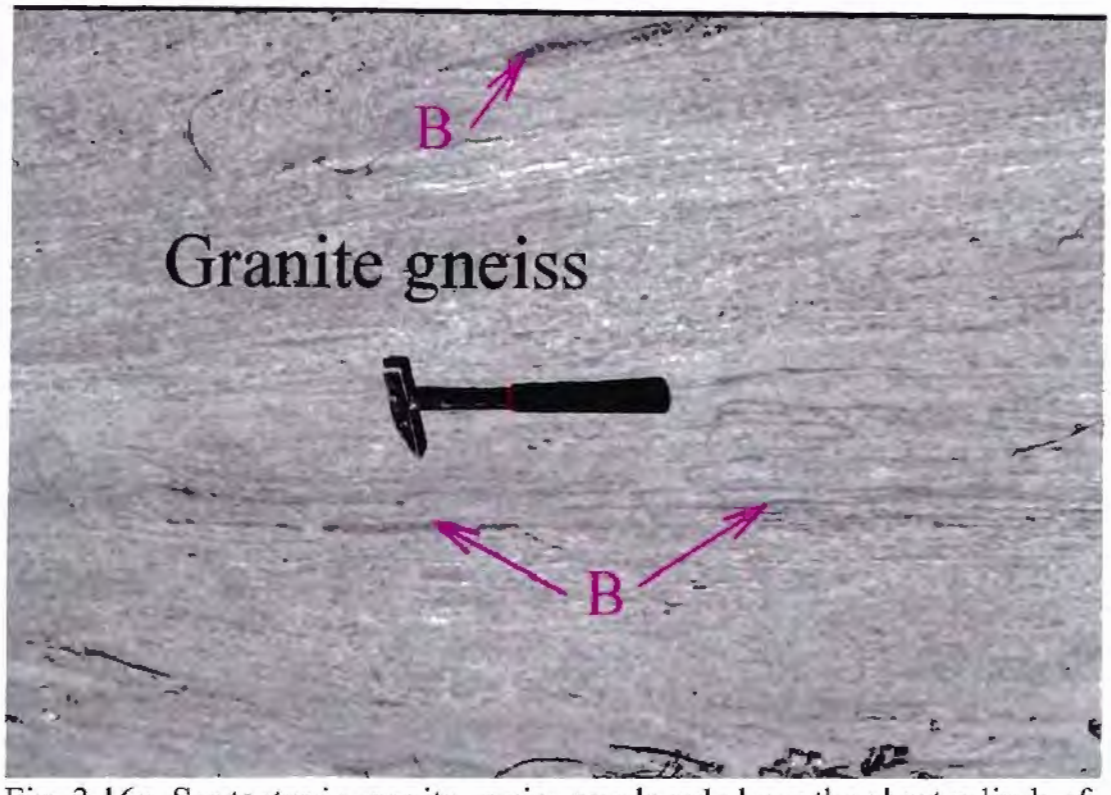

Fig. 3.16a. Syntectonic granite gneiss emplaced along the shorter limb of Z-shaped fold in the Nainarmalai Hill, Namakkal, Corridor I. Note that xenoliths of BIF (B) are flattened and aligned parallel to the gneissosity. Zircons from this granite gneiss has been dated at 2537 ± 1 Ma and monazites have an age of 2507 ± 5 Ma (Chapter 4).

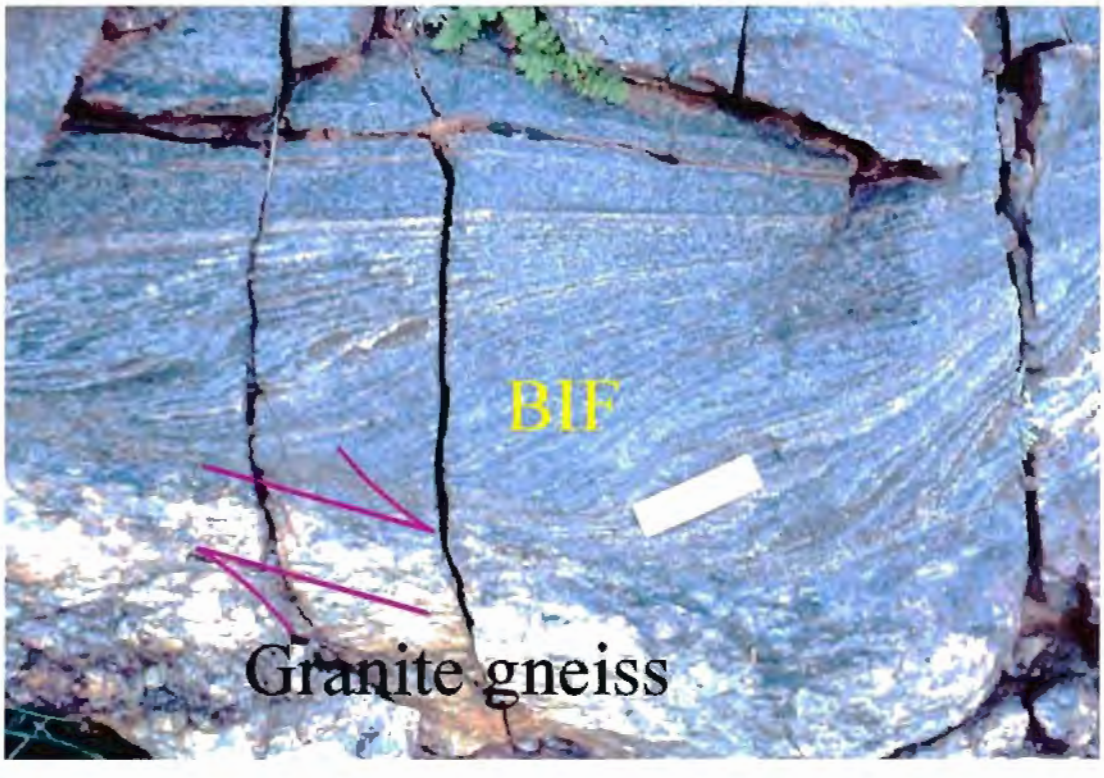

Fig. 3.16b. Dextrally sheared contact between the BIF and granite gneiss (arrows). Layers of BIF are dragged into parallelism at the contact. Location: ~1.5 km NW of the peak of the Nainarmalai Hill (Fig. 3.13)

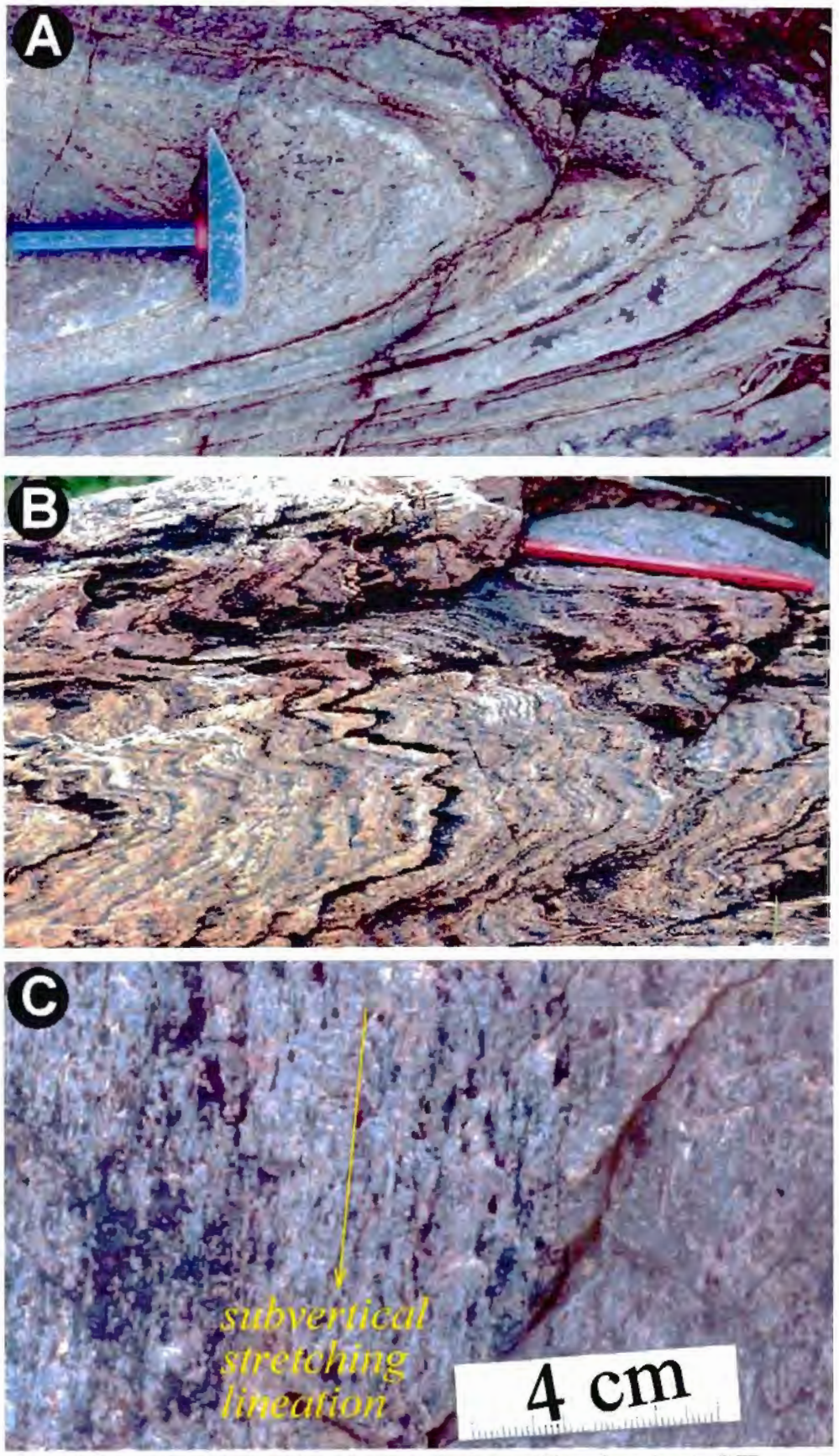

Fig. 3.17. Isoclinal folds (F_1) and subvertical stretching lineation in BIF.
A. Plan view; along the nothern limb of the F_1 at Nainarmalai Hill, Namakkal.
B. Plan view; along the southern limb of the F_1, Nainarmalai Hill, Namakkal.
C. Vertical section; stretching lineation, defined by subparallel alignment of iron-rich clots along bedding plane of BIF. Location, ~1.5 km SE of the Nainarmalai Hill peak, Namakkal (Fig. 3.13).

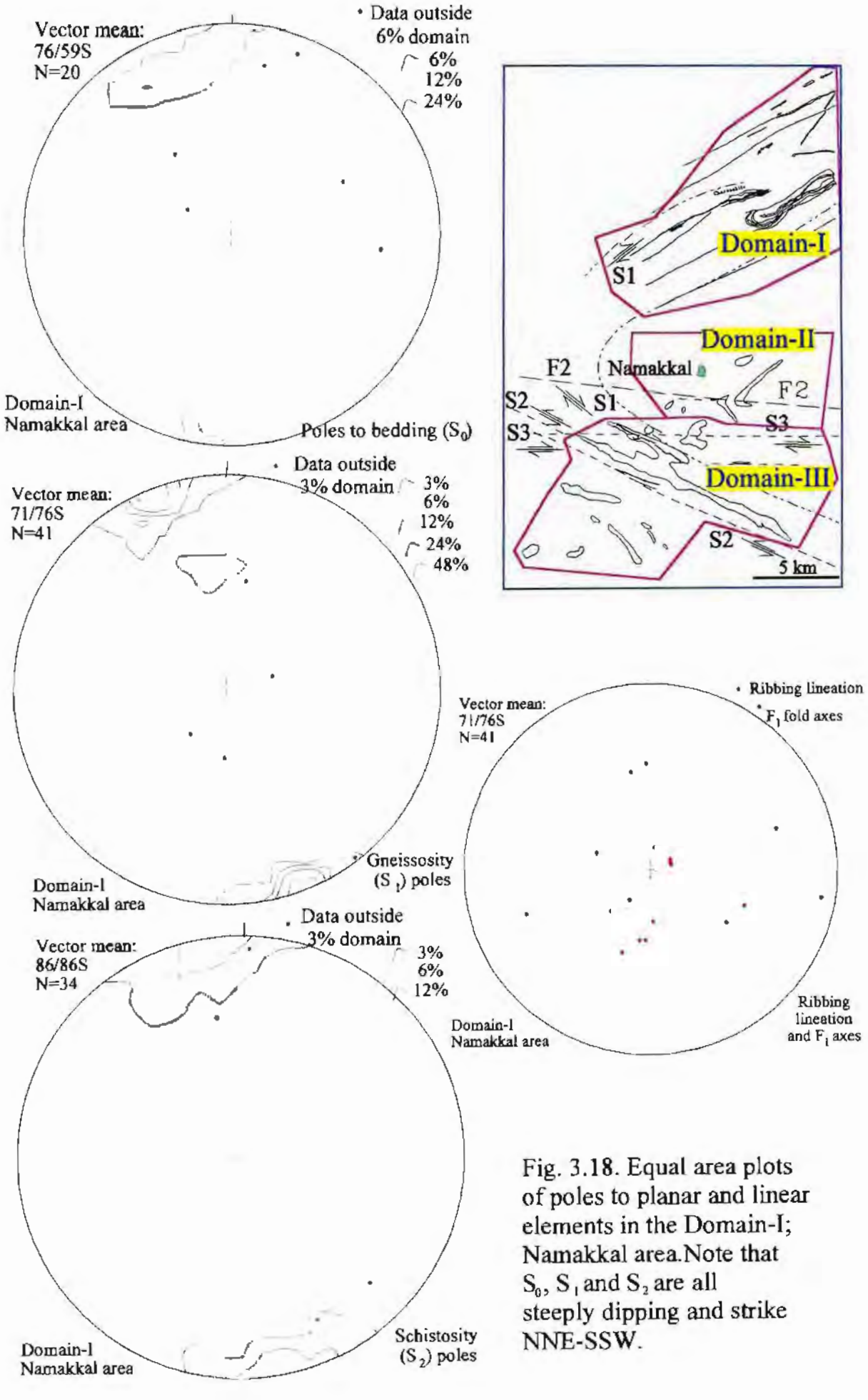

Fig. 3.18. Equal area plots of poles to planar and linear elements in the Domain-I; Namakkal area. Note that S_0, S_1 and S_2 are all steeply dipping and strike NNE-SSW.

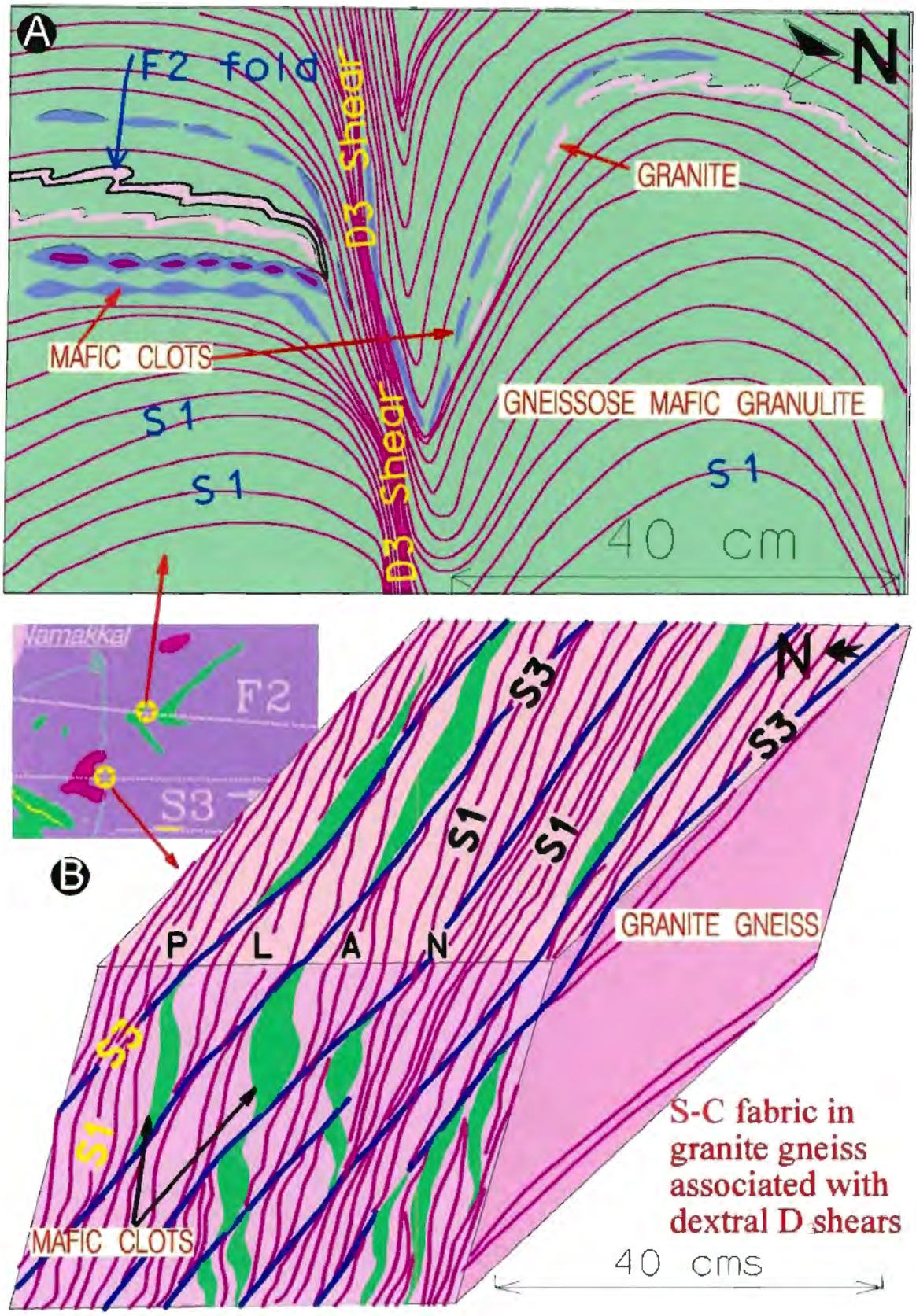

Fig. 3.19. Superimposition of D_3 shears on S_1 gneissosity in mafic granulite and granite gneiss
a, Location,~2 km SE of Namakkal on the top of a 309m high peak.
b, S-C fabric developed in granite gneiss due to superposition of dextral D_3 shears on S_1 gneissosity in granite gneiss, Location, ~3km south of Namakkal.
Inset map shows part of Fig. 3.13.

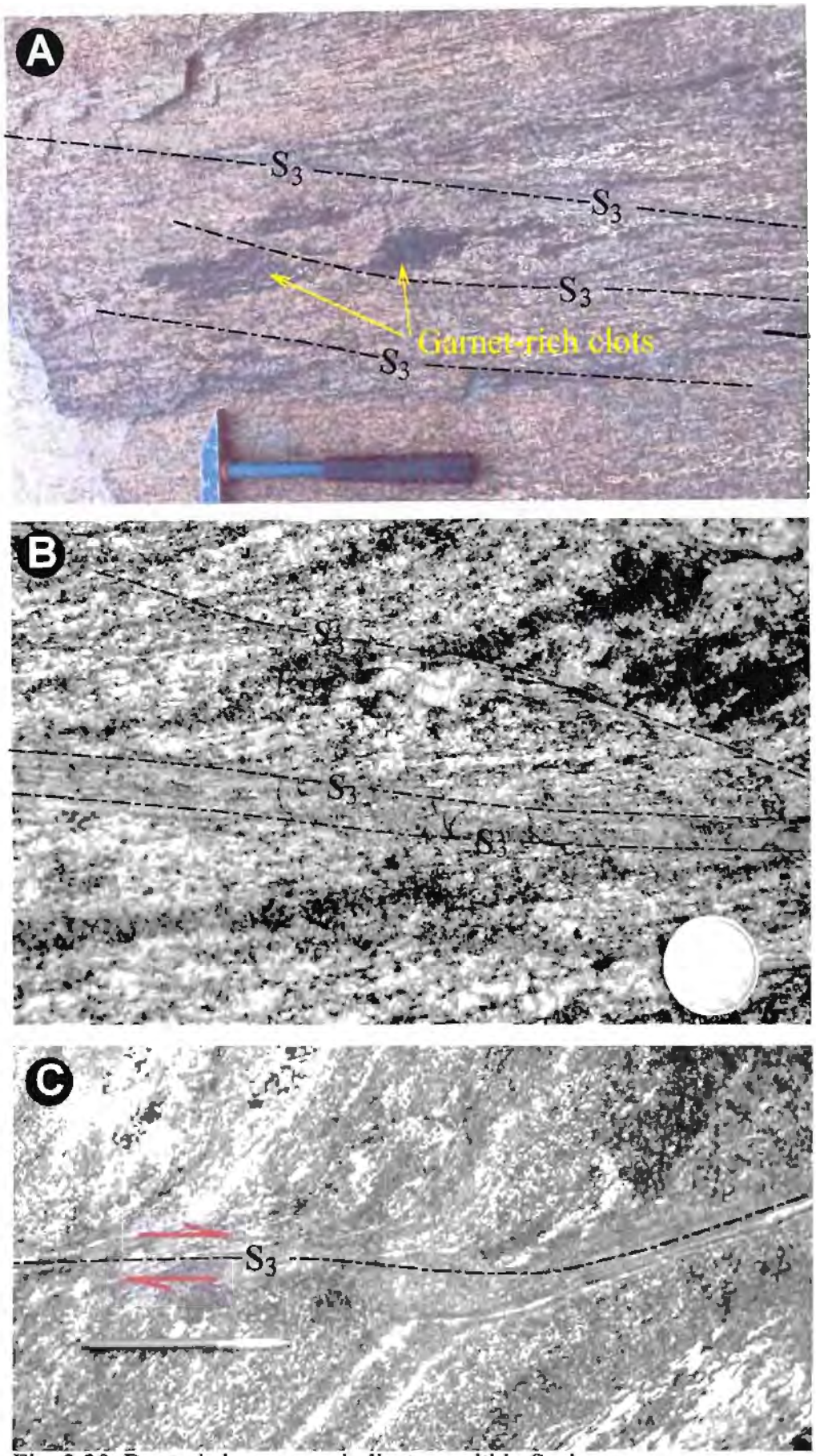

Fig. 3.20. Dextral shear sense indicators within S_3 shears.
a. Garnet-rich clots in tonalite gneiss displaced by S_3 shears.
b. Gneissose layering and S_3 shears in granite gneiss with asymptotic relationship.
c. Dextral sense of S_3 shearing in mafic granulite.
Locations, a & b, ~ 3km south of Namakkal; c, 1 km east of Kanaveypatti (Fig.3.13)

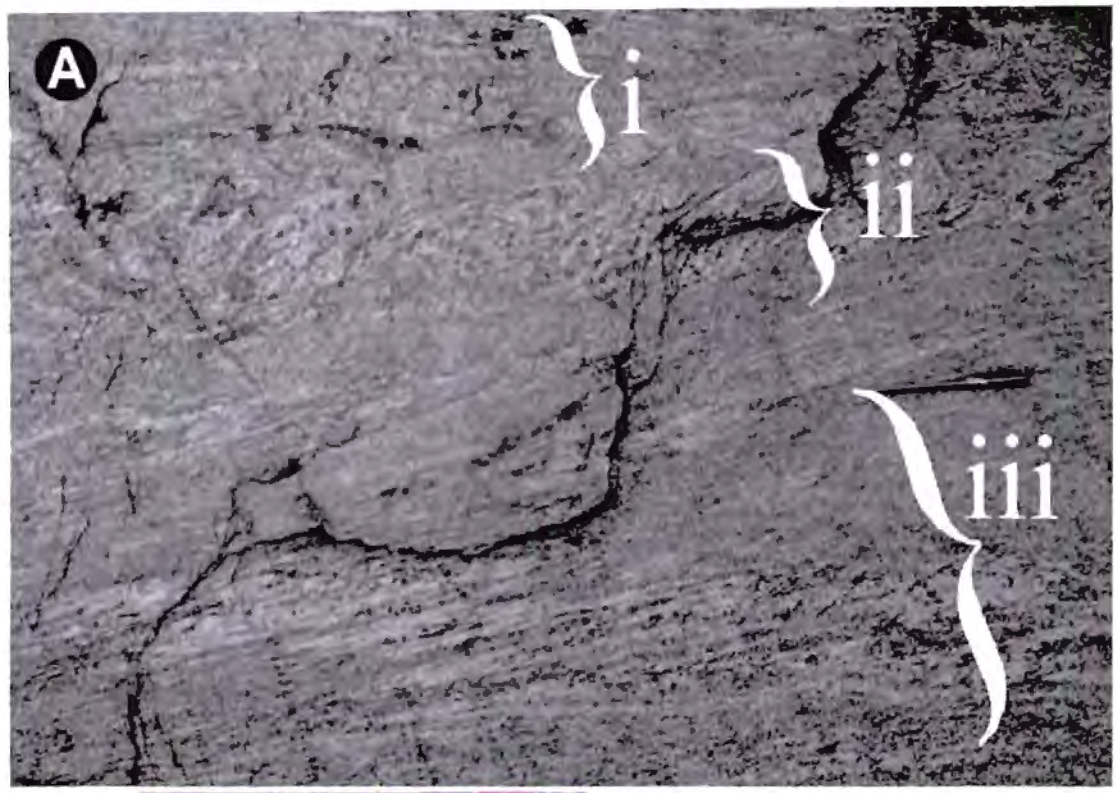

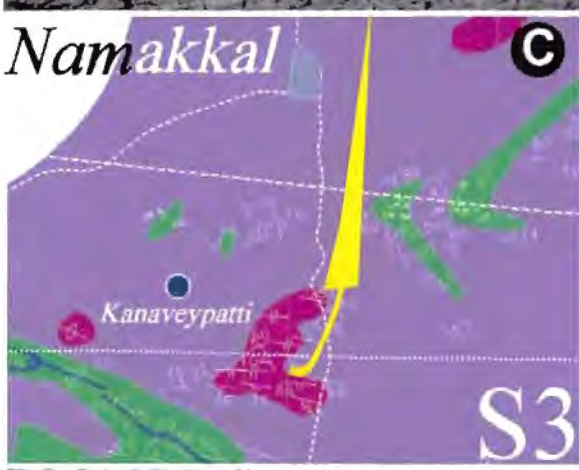

Fig. 3.21. Transformation of tonalite gneiss into schistose rock within D_3 shears. Location, ~3 km south of Namakkal (see inset c). a. Gradation of gneissose structure (zone-i) to schistose structure (zone-iii) through a zone where gneissosity is folded (zone-ii) in between shear planes. b. Enlarged part of photograph A. showing dismemberement of a vein quartz due to shearing.

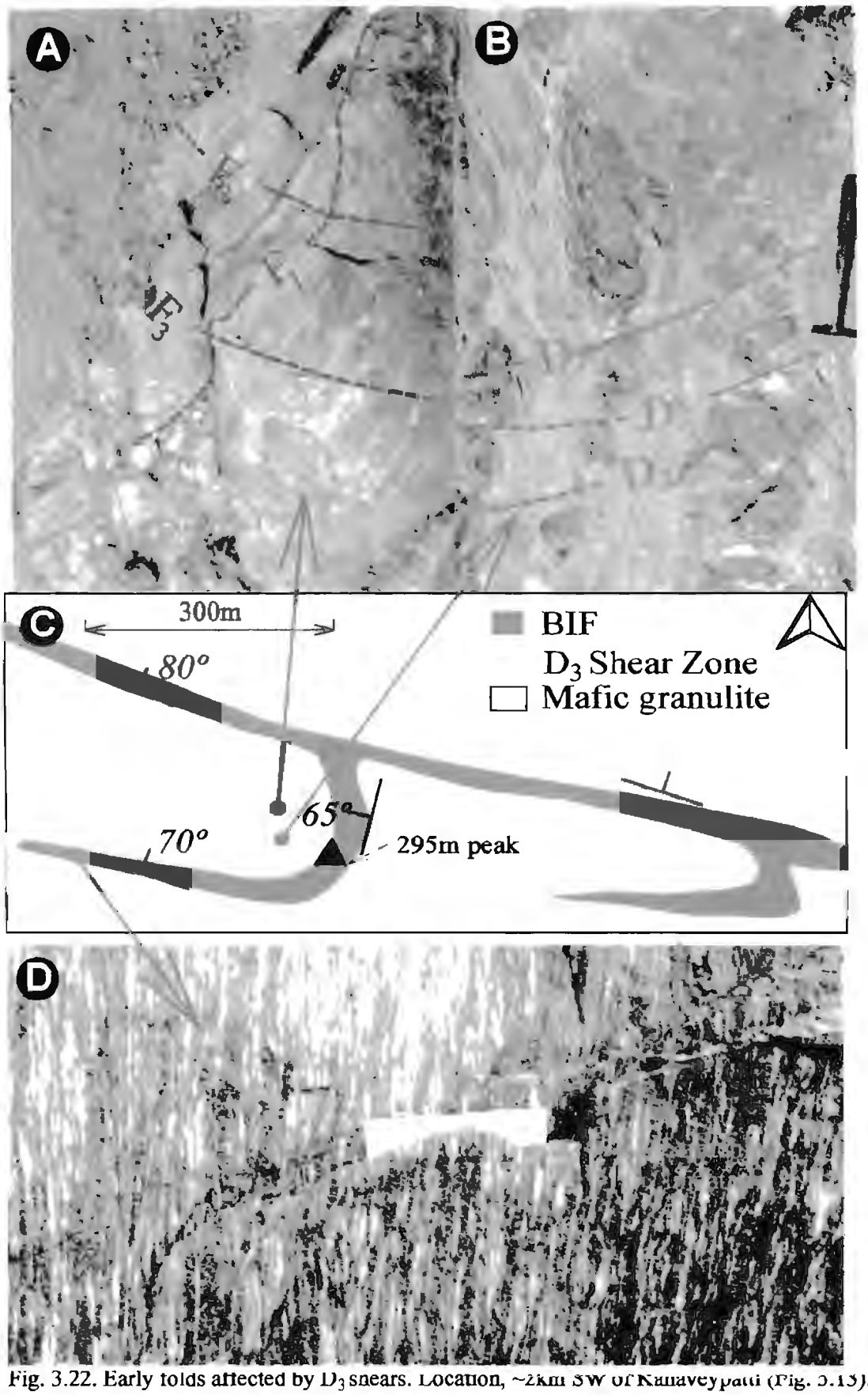

Fig. 3.22. Early folds affected by D_3 shears. Location, ~2km SW of Kallaveypatti (Fig. 3.15).
D_3 shear zones are marked by highly strained rocks.
a, In between two D_3 shear zones, F_1 fold in mafic granulite is folded by F_3 folds related to D_3 shears.
b, A layer of boudins in mafic granulite cut by D_3 shears.
c., Map pattern of a BIF band affected by D_3 shears.
d, subvertical stretching lineation in BIF within D_3 shear zone. In this rock lineation is the most dominant fabric.

Fig. 3.23. Rootless fold (F_1) in garnet-rich layers (G) in mafic granulite (M) within D_3 shear zone. Location, ~1.5 km east of Kanaveypatty, Namakkal area (Fig. 3.13).

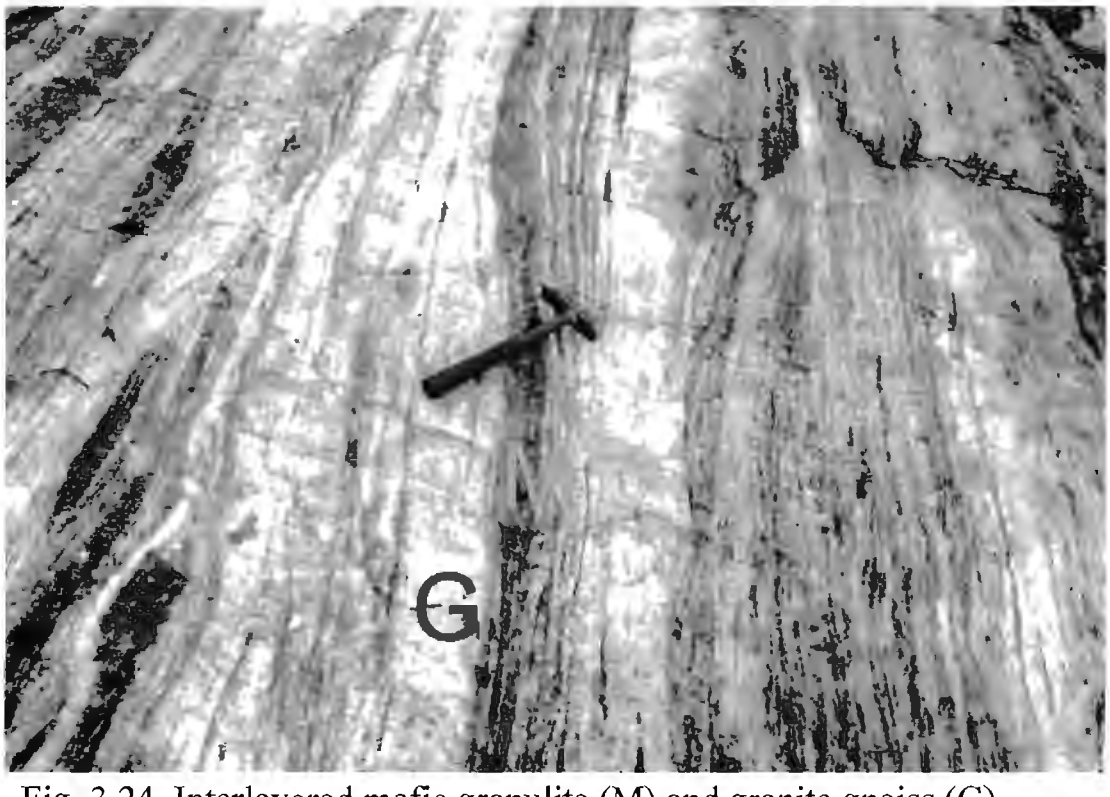

Fig. 3.24. Interlayered mafic granulite (M) and granite gneiss (G) within D_3 shear zone, ~1/2 km east of Kanaveypatti, Namakkal, Corridor-I (Fig. 3.13). These zones can be traced for over 100 metres.

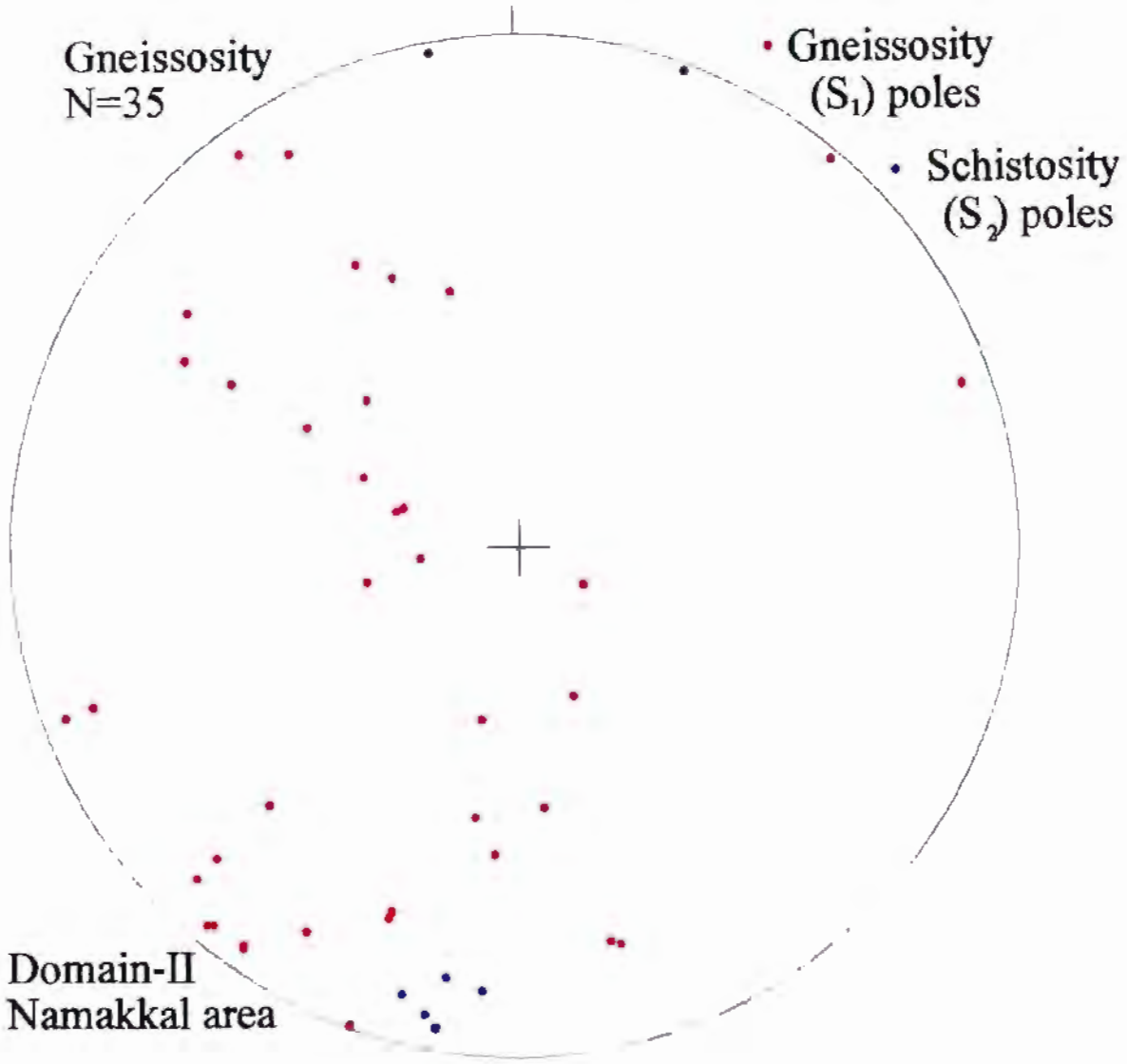

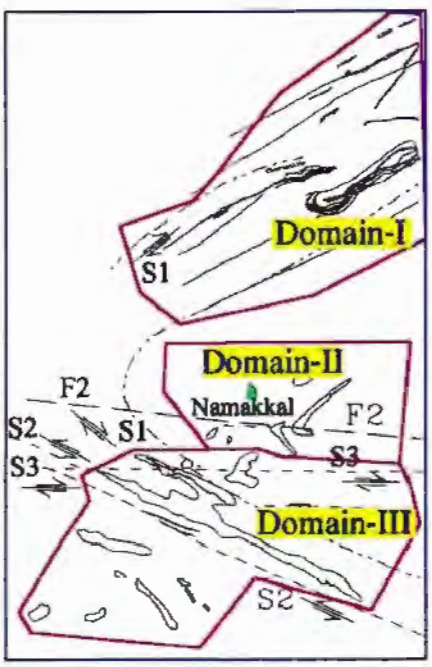

Fig. 3.25. Equal area plotting of poles to the gneissosity (S_1) and schistosity (S_2) in Domain-II, Namakkal.

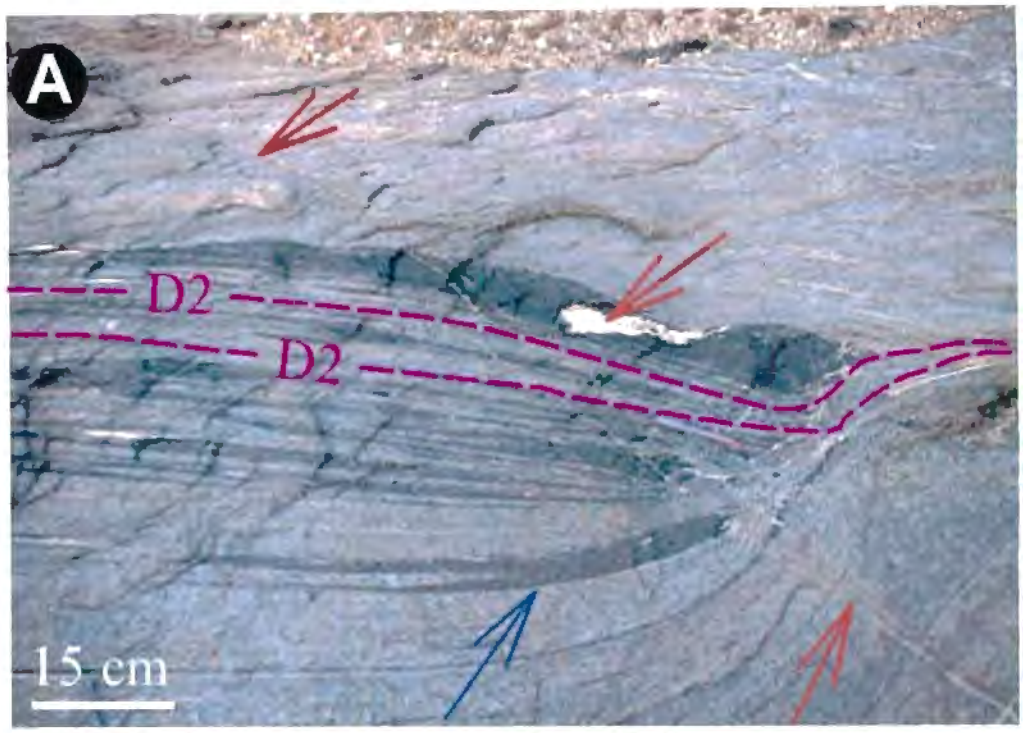

Fig. 3.26. Transposition of D_2 folds within granite gneiss by D_2 shears. Rootless F_1 folds (marked by blue arrow) are also bend by later D_3 shears. Pink granitic veins have intruded along the axial trace of late D_3 bends (marked by red arrows). This pink granite from a nearby exposure has been dated at 603±12 Ma. Location, ~1 km SW of Aniyapuram, ~2.5 km SE of the peak of the Saruvamalai Hill (Fig. 3.12) .

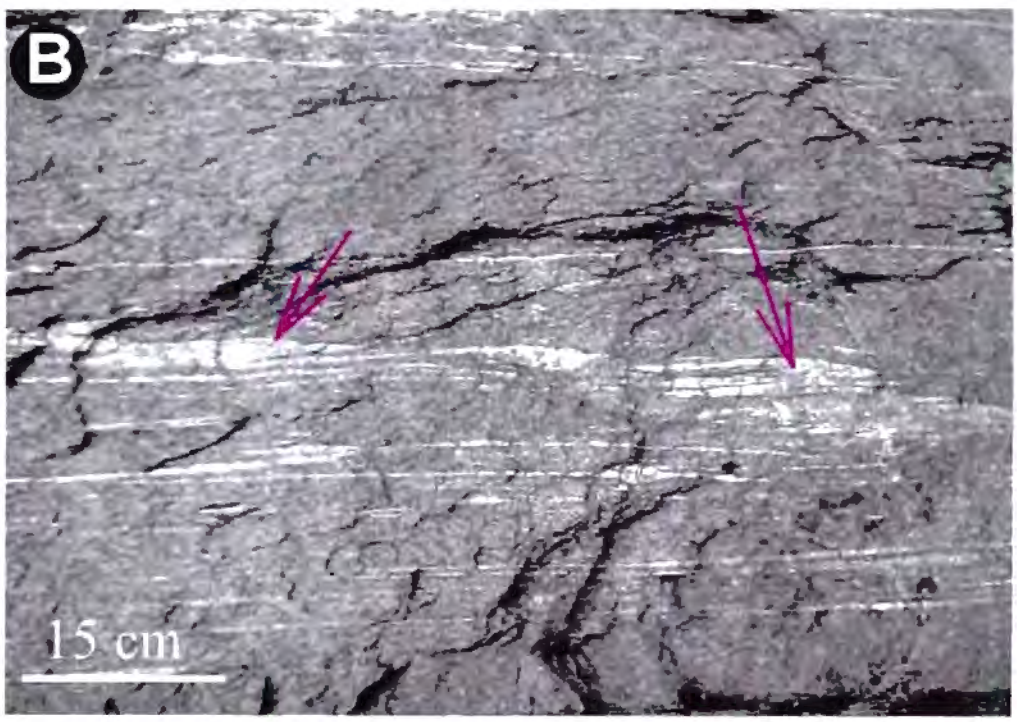

Fig. 3.27. Transposition of early gneissosity (S_1) by D_2 shears in mafic granulite. Both S_1 and D_2 are subparallel to the light coloured quartzo-feldspathic layers. Rootless fold hinges can be seen in leucocratic quartzo-feldspathic layers (marked by arrows). Location, same as the above figure.

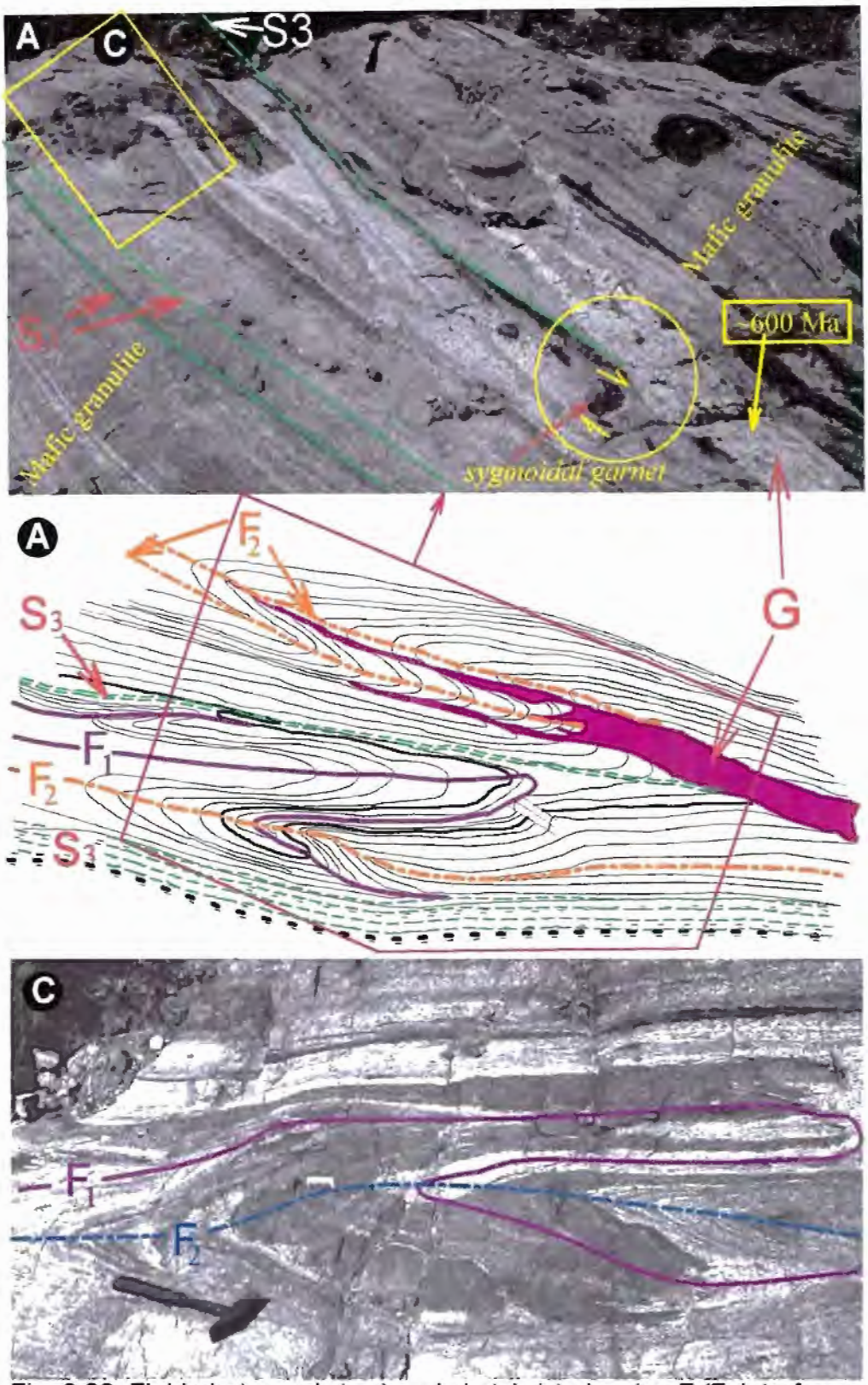

Fig. 3.28. Field photograph (a,c) and sketch (c) showing F_1 /F_2 interference folding (Type-2, Ramsay, 1967) and both cut by D_3 shears.
Location, ~1 km NW of Saruvamalai Hill peak, Namakkal area (Fig. 3.13). F_1 (axial planes of "Z-shaped" folds related to D_1 deformation) are deformed by F_2 (axial planes of "S-shaped" folds related to D_2 deformation). D_3 shears are present as discrete planes with clear dextral shear movement as revealed by sygmoidal garnet rich clots on S_3 planes (marked by yellow circle). Granite-pegmatoid dykes (G) intrude along S_2 and also cut across S_3 shear planes (circled). A similar nearby pegmatoid has been dated at 603 ± 14 Ma, indicating that S_3 is older than 600 Ma.

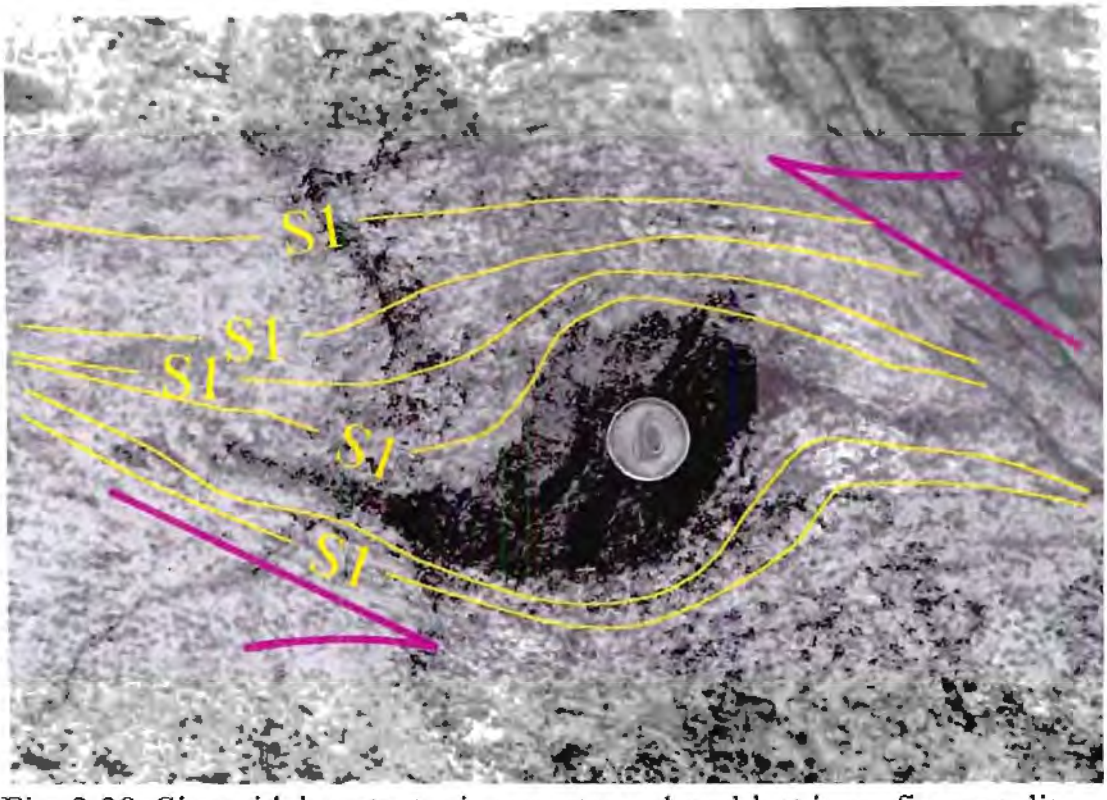

Fig. 3.29. Sigmoidal syntectonic garnet prophyroblast in mafic granulite within D_2 shear zone. Curvature of the gneissosity (S_1) planes suggests a sinistral sense of movement. Location, 3km NW of Saruvamalai peak, Namakkal, Corridor-I (Fig. 3.13).

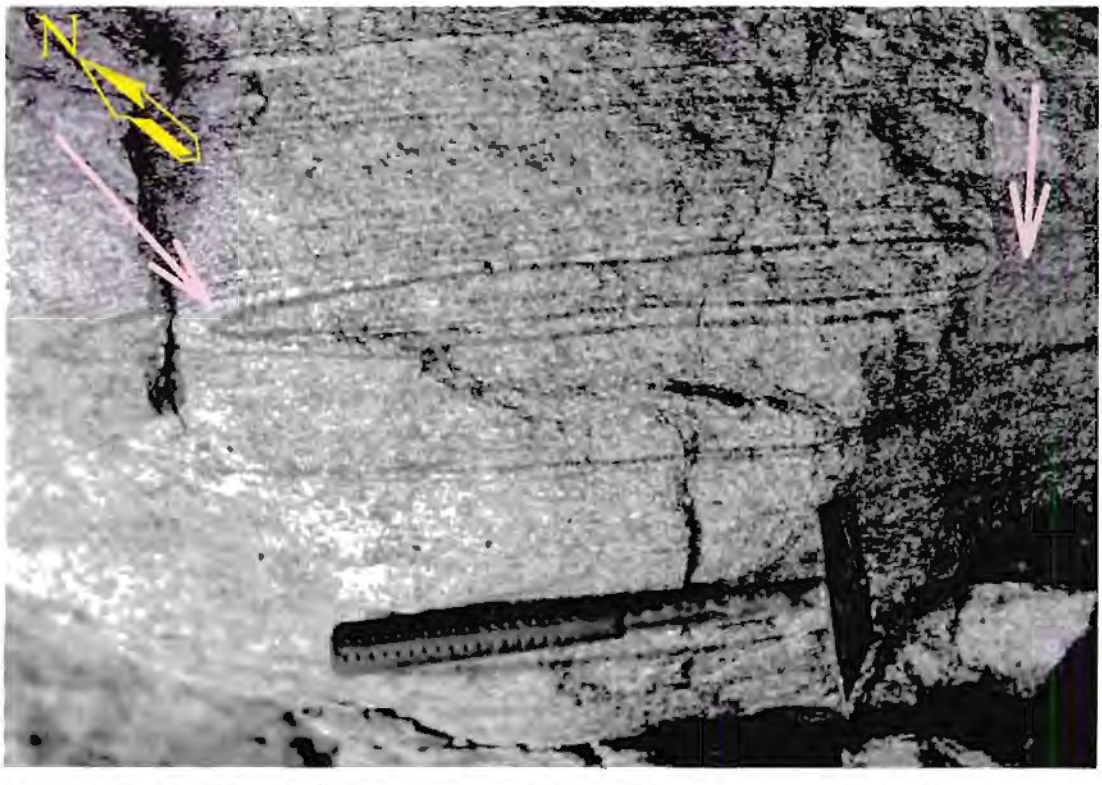

Fig. 3.30. F_2 Sheath fold developed in mafic granulite within D_2 shear zone. Hinges of the 'eyed' fold is marked by arrows. Transport direction perpendicular to the outcrop. Location: ~2km NW of Saruvamalai peak, Namakkal, Corridor-I (Fig. 3.13).

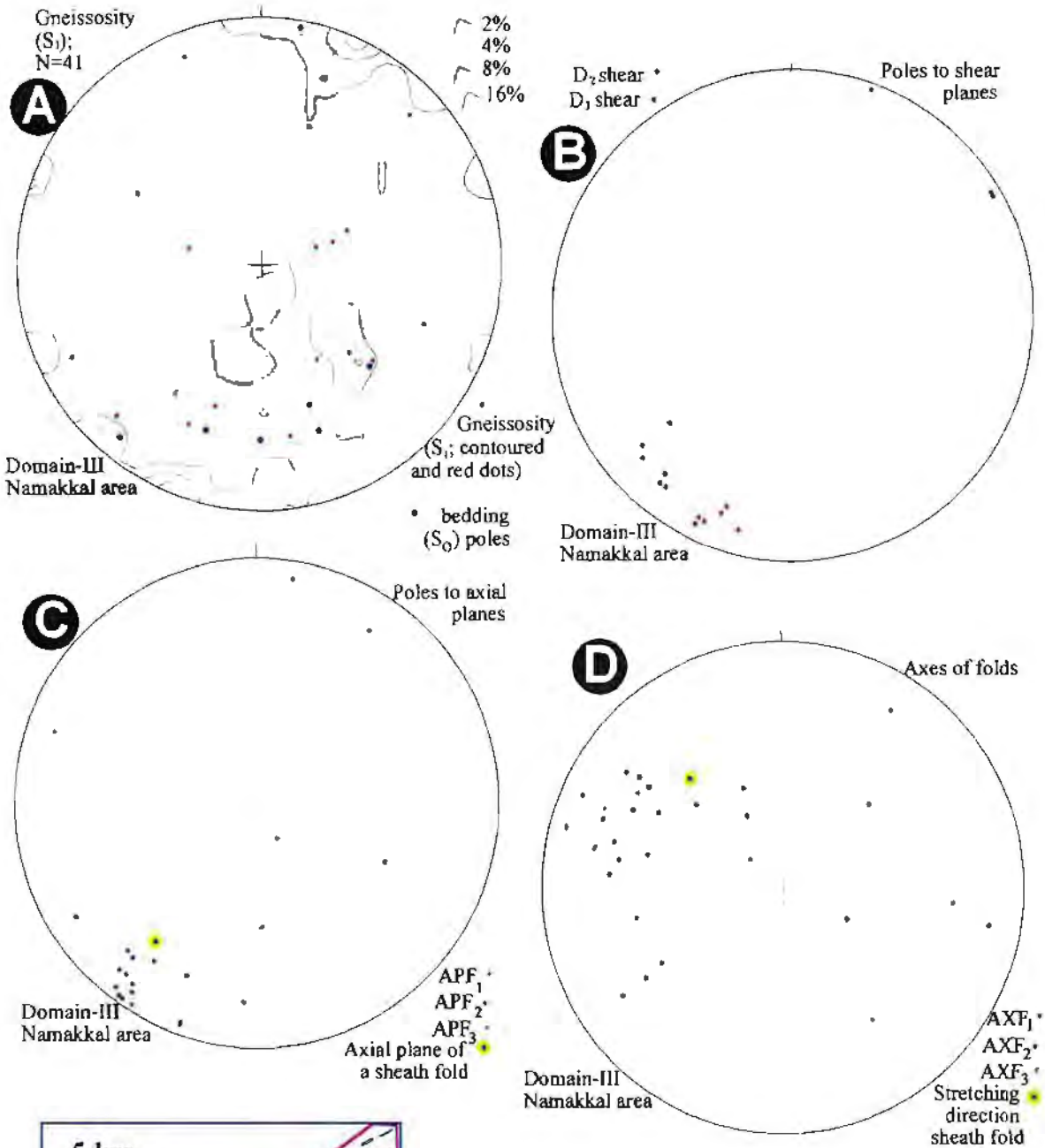

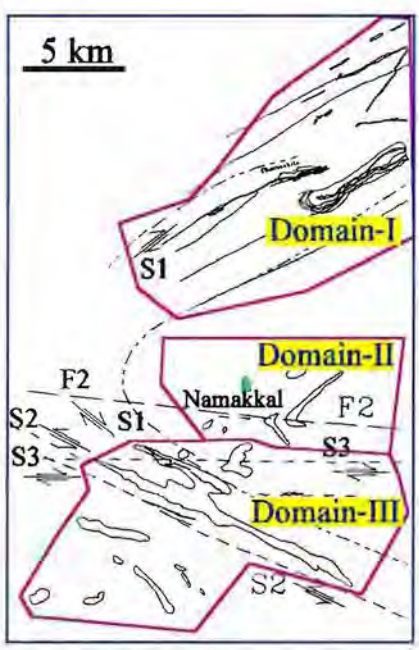

Fig. 3.31. Equal area plots of various structural element in the Domain-III, Namakkal area

A: poles to gneissosity and bedding

B: poles to D_2 and D_3 shear planes

C: poles to F_1,F_2 and F_3 fold axial planes

D: axes of F_1, F_2 and F_3 folds

Alternating bands of mafic granulite and a few thin BIF and quartzite layers (Fig. 3.13) depict a major Z-shaped fold. This fold is superposed by at least two events (D_2 and D_3) of shearing. D_2 shears have a predominantly sinistral sense of movement and are best exposed along the southern slope of the Saruva Malai Hill. Within D_2 shear zones, the early S_1 gneissic fabric and F_1 folds in mafic granulite and bedding of BIF and quartzite are completely transposed (Fig. 3.26; 3.27). 'S'-shaped F_2 folds associated with D_2 shears have been superimposed on 'Z'-shaped F_1 folds associated with D_1 shears. D_3 shears cut across all early structures (Fig. 3.28). Numerous shear sense indicators in the garnetiferous mafic granulite indicate sinistral sense of movement across the D_2 shears (Fig. 3.29). S_2 is sub-vertical and strikes WNW-ESE (Fig. 3.31). The stretching direction associated with sheath folds (Fig. 3.30) present within D_2 shear zones indicate shear transport direction to be moderately westerly dipping. The northern boundary of the D_2 shear can be traced along the southern slope of the Saruva Malai Hill. Its southern boundary is, not exposed. South of Saruva Malai Hill, the gneissosity of the mafic granulites are completely transposed parallel to D_2 shears along which there is a dense network of granitic veins subparallel to S_2 simulating a migmatitic structure. Because of the extensive impregnation by these granitic veins, the characteristics of the original rocks are obscured. Exposure south of the Saruva Malai Hill is poor.

D_3 shearing is represented only along some discrete zones varying from few cms to a few 100s of metres wide (Fig. 3.13). Numerous shear sense indicators indicate dextral sense of movement (Fig. 3.20). D_3 shear planes are subvertical and strike ESE-WNW (Fig. 3.31). F_3-axes are randomly oriented (Fig. 3.31). This is possibly due to pre-F_3 random orientation of the lithological units.

Summary and conclusion

The major Z-shaped F_1 folds, mapped in the Nainar Malai Hill in Domain-I do not have S-shaped counterpart in Domain III. Instead, a similar large dextral fold have been mapped in the

Saruva Malai Hill in Domain-III. I there fore interpret these two major mappable dextral folds in the area to be part of the same dextral shear system (S_1) which was later folded by E-W trending Namakkal fold (F_2).

The F_1 fold in the Nainar Malai Hill has ENE trending axial trace which, on regional scale, is continuous with the trend of the Eastern Ghats. Syn-tectonic granite with F_1 fold in the Nainar Malai Hill is dated at ~2.53 Ga. This may mean that the Eastern Ghat trends in the SGT are as old as Late Archaean.

Similar to the Salem area, the oldest recognisable lithologic units of the area are the BIF and associated metasediments, intruded by mafic granulites. Zircon from a mafic granulite body south of Namakkal (Fig. 3.14; sample S-117) has a near concordia spread between 2.9 and 3.0 Ga which is interpreted as possible the protolith age of these mafic granulites. If this is correct, then the BIF and associated sediments are at least ~3.0 Ga old. BIFs and mafic granulites have suffered intense deformation (D_1) in which flattening was a significant component. This deformation was contemporaneous with intrusion of voluminous granite, which was subsequently charnockitized in many places. Whether the biotite gneiss, the most dominant rock type occurring in between Salem and Namakkal areas, and the charnockitized granite and tonalite gneiss of the Namakkal area are part of the same rock suite could not be confidently established in field. However, both the biotite gneiss and the tonalite gneiss yield similar U/Pb zircon ages (~2.53 Ga, see Chapter-4) suggesting that the dominant granitic gneisses present in the area are intrusive into the BIF-mafic granulite association and do not represent basement to the metasediments. Thus it can be concluded that BIFs and mafic granulites represent older xenoliths of various sizes within a regional terrain of ~2.53 Ga old granitoids.

The entire region suffered at least two younger shearing events (D_2 and D_3) and younger granitic intrusions at ~600 Ma. D_2 shearing pre-dates 600 Ma, as D_2 shear planes are intruded by ~600 Ma granitic veins (Fig. 3.26). The age of D_3 shear could not be constrained by the

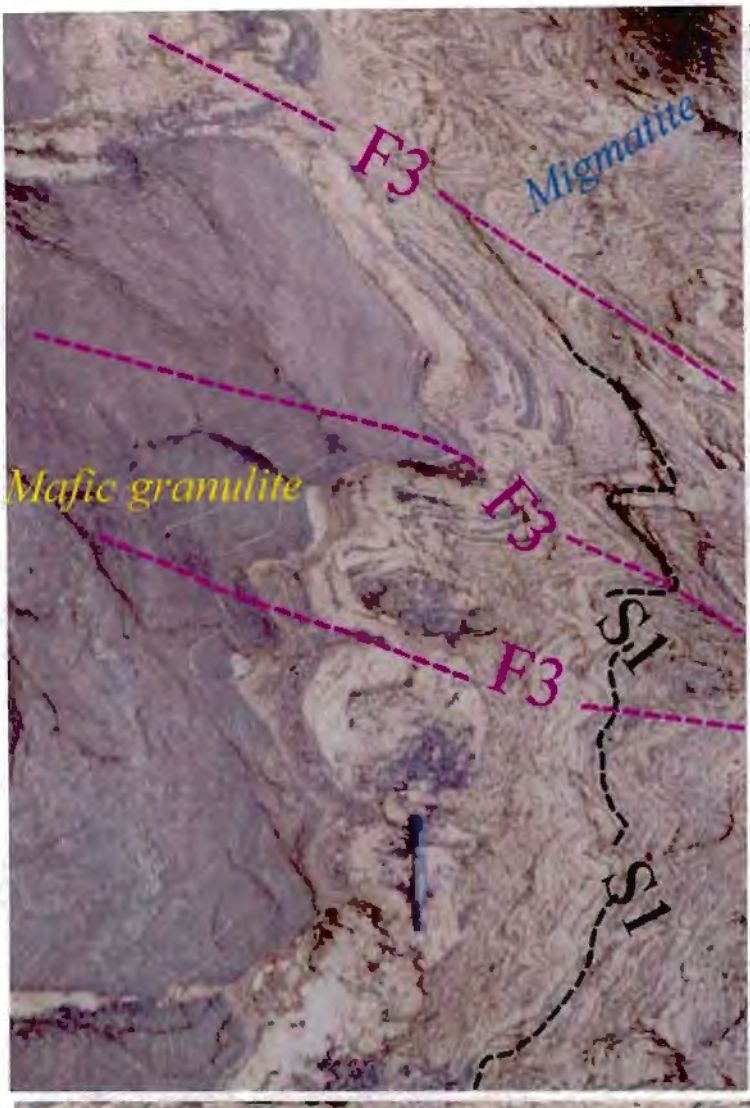

Fig. 3.32. Subparallel impregnation of granite veins within mafic granulite.The resultant rock is a migmatite The migmatites are deformed by E-W to ESE-WNW trending F_3 folds and D_3 shears. Location: Kutamparai, ~12 km south of Namakkal (S-196 in Fig. 3.13).

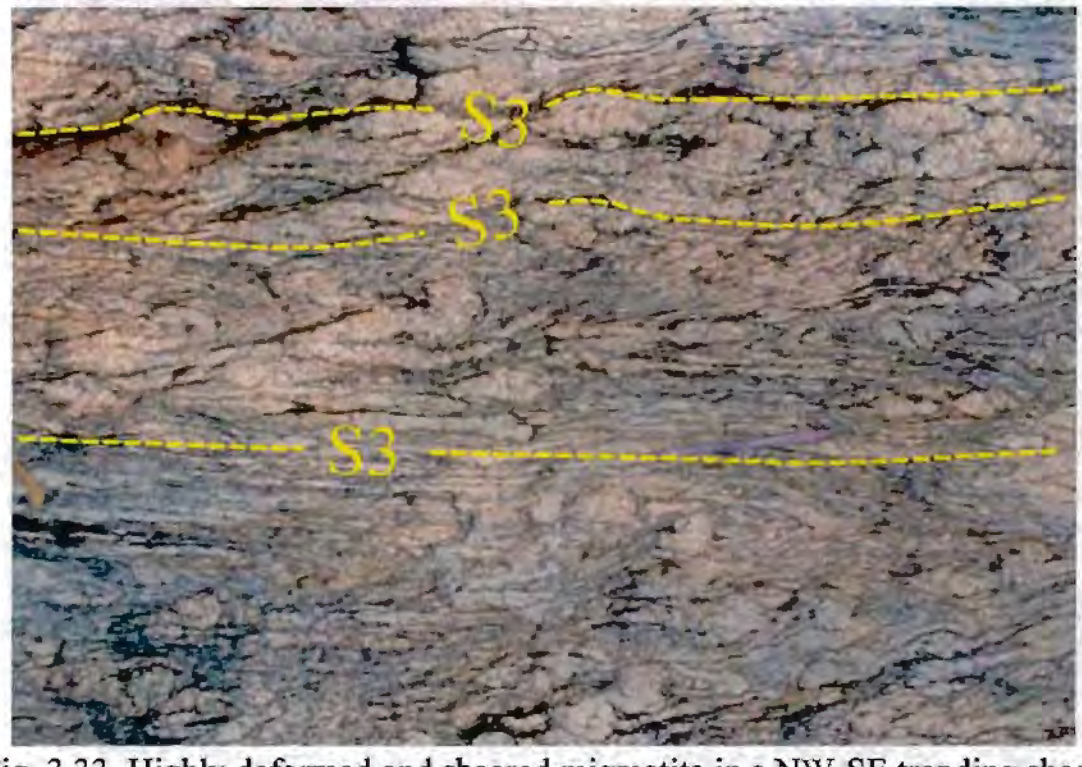

Fig. 3.33. Highly deformed and sheared migmatite in a NW-SE trending shear zone. Location: Peruma-palayam village, ~3 km WSW of Bhavani, Corridor-II.

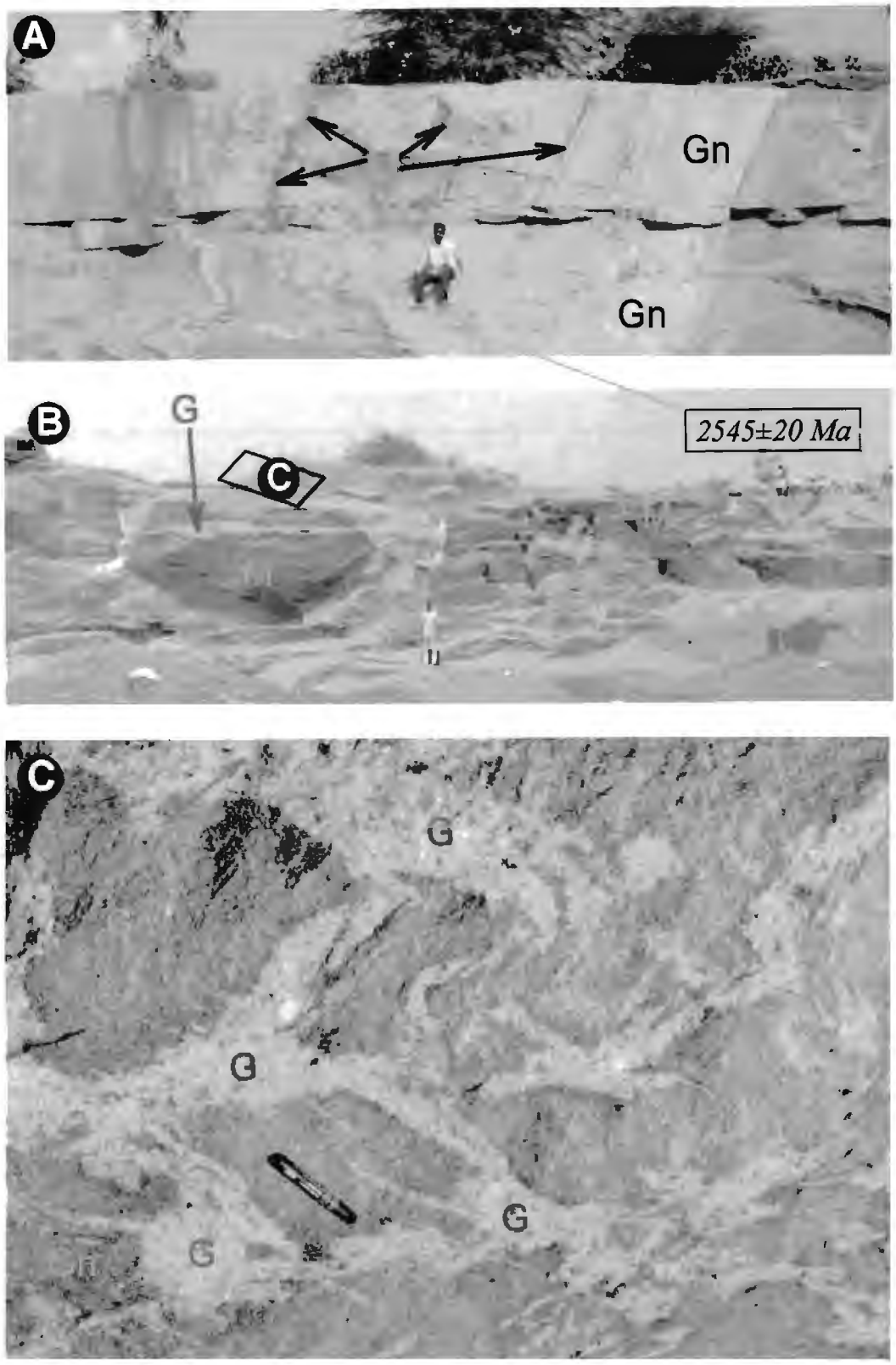

Fig. 3.34. Interrelationship between mafic granulite, granite gneiss and massive granite in the Karur area, south of the Palghat-Cauvery Lineament. Location, Ottaiyur quarry, ~5 southwest of Karur, Corridor-I.
A. Xenoliths of mafic granulite (M) within granite gneiss (Gn).
B. Mafic granulite (M) cross-cut by both granite gneiss (Gn) and massive granite sheet (G). ☛, sample location (S-326A) for zircon dating.
C. Plan view of granite sheet intruded along and across the foliation of granite gneiss and folded along with it.

present work. Granitic veins within gneissic rocks (migmatite) south of the Namakkal area are intensely folded (Fig. 3.32). Deformed migmatites are the predominant rock types along a NW-SE trending shear zone from south of Namakkal to south of Bhavani in Corridor-II (Fig. 3.33). These granitic veins in the Namakkal area have been dated in the present work to be ~600 Ma (Chapter-4). It is possible, therefore, that regionally these veins are pre- to syn-tectonic with respect to the D_3 shearing.

3.2.2.3. Geology of the Karur-Palayam area

3.2.2.3.1. Geological setting

The southern part of Namakkal, where the Palghat-Cauvery Lineament (PCL) follows the course of the Cauvery River, is poorly exposed. The Karur area to the south of the PCL (Fig. 3.1), is also poorly exposed as it is mostly covered by flood plains of the Cauvery River. Between Karur and Palayam which is ~30 km south of Karur, there are few tors and quarries in an otherwise alluvium covered area.

3.2.2.3.2. Lithology

The main lithologies of the Karur area are granite gneiss, enderbite gneiss, mafic granulite gneiss and massive coarse grained granite. The granite gneiss has an intrusive relationship with mafic granulite (Fig. 3.34). The coarse grained massive granite is intrusive into both the granite gneiss and the mafic granulite. Granite gneiss from a quarry in Ottayur village, about 6 km SW of Karur has yielded a 2545 ± 20 Ma age (U-Pb zircon age; chapter 4). Thus the mafic granulites are older and Archaean in age.

South of Karur, the Palayam area (Fig. 3 1) is dominated by metasedimentary rocks. The common metasedimentary rocks present in the area include khondalite schist (garnet-biotite-

sillimanite-graphite), calc-silicate, garnet-biotite gneiss and quartzite. Most of these rocks have been densely intruded by granitic veins subparallel to the schistosity (S_1). The original relationship between these metasedimentary rock types with the surrounding granite gneiss is not clear. On the southwestern slope of Vidya Malai Hill, about 20 km east of Palayam, khondalite and mafic granulite occur in close juxtaposition. Near the contact, numerous clasts of mafic granulite and folded BIF (Fig. 3.35) occur within the khondalite. The mafic granulite clasts are mostly ellipsoidal as well as rounded and are aligned subparallel to the schistosity of the host. The clasts of folded BIF are angular with sharp boundaries. This relationship suggests the presence of a possible unconformity between the mafic granulites and the metasediments. On the basis of this observation, therefore, metasediments of the Palayam area are probably younger than the Archaean BIF and mafic granulites present in the Karur and Namakkal area.

The majority of the detrital zircons from khondalite have yielded ages of ~2.5 Ga age (sample S-259Z; Chapter-4) placing an upper age limit to the deposition of the metasediments. Monazites from the khondalite of this area have a concordant U-Pb age of ~800 Ma (Chapter-4). This is interpreted as the time of granulite facies metamorphism of these rocks.

3.2.2.3.2. Structure

The general strike of the granite gneiss in the Karur-Palayam area is NE-SW contiguous with the strike of various lithologic units north of the Namakkal area. This NE-SW trend of lithologic units continues further south up to Palayam area. There are no E-W trending shears or planar fabrics in the area. This places doubt on the presence of an E-W trending shear zone along the Cauvery River as suggested by Drury and Holt (1980) and GSI (1994). South of Palayam, the structure is more complex as is evident from the highly contorted pattern of the quartzite bands south to the Palayam (Fig. 3.1). West of the Palayam area, calc-silicate and BIF bands define a major fold with a SW-NE trending axial trace. The axes of the dominant

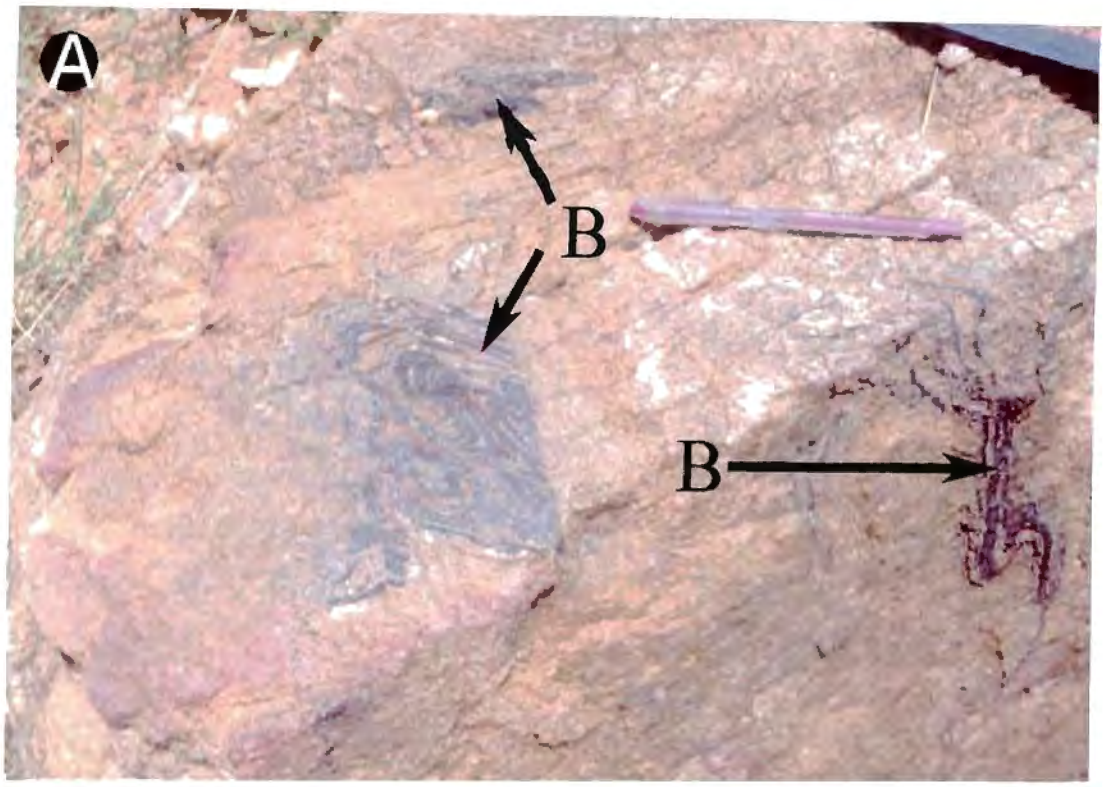

Fig. 3.35a. Folded BIF clasts (B) within khondalite gneiss. Location, western slope of the Valya Malai Hill, 16 km ESE of Palayam, Corridor-I. Monazites from this khondalite have yielded ~790 Ma age while zircons (detrital) are between ~2.0 Ga and ~2.5 Ga old.

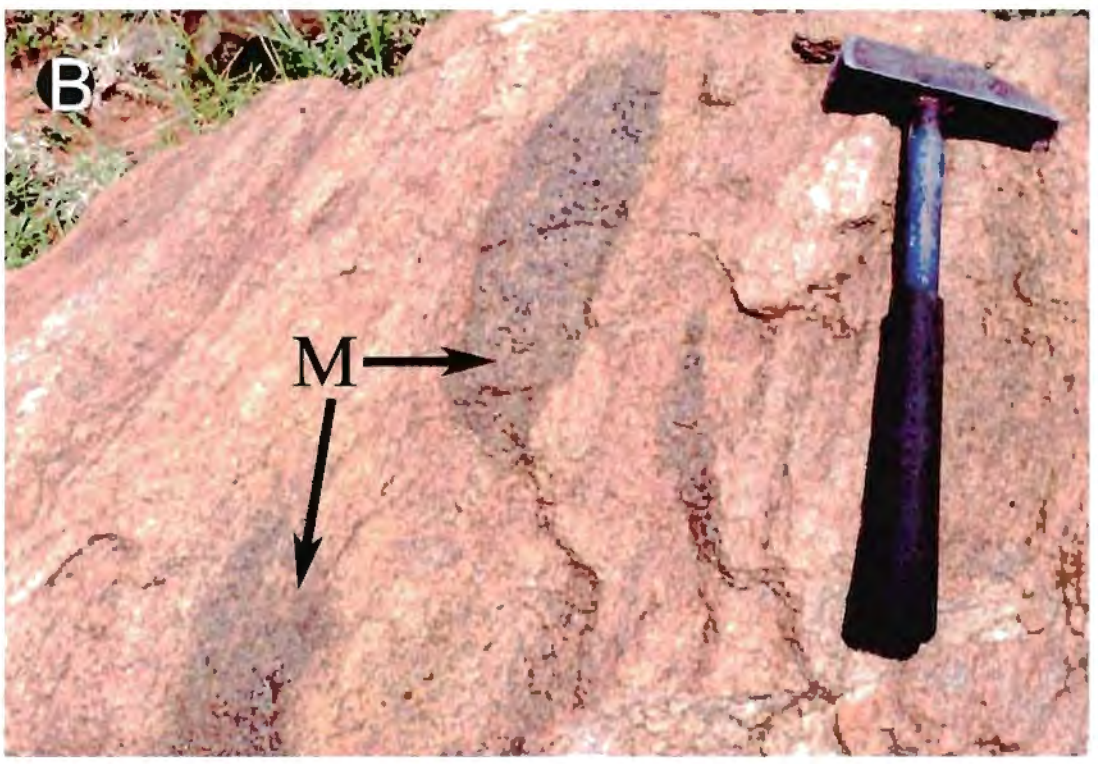

Fig. 3.35b. Deformed clasts of mafic granulite (M; now altered to amphibolite) within khondalite gneiss.
Location, ~700 m SSW of the peak of Valya Malai Hill, ~16 km ESE of Palayam, Corridor-I.

minor folds and prominent mineral lineations have a subvertical to steep easterly plunge.

The question of the structural continuity between the areas north of the Cauvery River and south of it was not resolved during the present investigation because of lack of exposures in the Cauvery valley. However, NE-SW regional strikes of the lithologic units north and south of the Cauvery River are similar.

3.2.2.3.4. Summary and conclusion

In the Karur area south of the PCL and the Namakkal area north of the PCL, the lithologic-associations and the ages of the granitic gneisses are similar. Regional structural trends are also continuous across the PCL. I interpret this to indicate continuity of the geology across the PCL. However, the areas east and south of Palayam differ in their lithologic association and metamorphism from the Karur and Namakkal areas. Although the broad structural trends in the Palayam area and the Namakkal area are similar, there are differences in the lithologic and structural in detail. The southern part of the Palayam area, for example, is affected by younger NNW-SSE trending folding. Khondalites which are the most dominant metasediments in the area south of Palayam, are younger than ~2.5 Ga whereas the metasediments encountered in the Namakkal and Salem area are older than ~2.5 Ga. It is thus possible, that in the southern part of the PCL there are two different geological assemblages. One, which is exposed in the Karur area and to the immediate west of it is the continuation of the Dharwar craton north of PCL. The other, exposed in the Palayam area and further south, represents a younger metasedimentary dominated geological assemblage. The boundary between these two terrains is interpreted to be a shear zone (the KKPT Shear Zone, discussed in Chapter-5).

3.2.3. Geology of Corridor-II

3.2.3.1. Introduction

Corridor II covers a N-S trending area from north of Bhavani (on the Moyar-Attur Lineament) in the north to Surya Malai Hill in the south (~10 km north of the Palghat-Cauvery Lineament (Fig. 3.1). The corridor was mapped across wide traverses. A part of the area, north of Bhavani, where three different regional structural trends converge (Fig.3.1), was mapped on 1.50,000 scale (Fig. 3.36). These three trends are:

(I) N-S to NNE-SSW trends of the Dharwar craton. The northern part of this corridor includes continuation of the charnockitic massif of Biligirirangan Hill which is considered a southern extremity of the Dharwar craton.

(ii) E-W trends of the Moyar Shear Zone.

(iii) NW-SE trends of the D_2 shear which continues from the south of Namakkal in Corridor I up to Bhavani following the Cauvery River.

The Bhavani area is poorly exposed. Rocks of this area are densely intruded by late massive granitic veins making it difficult to study the pre-migmatization structural elements of the lithologic units

3.2.3.2. Lithology

The principal lithologic units of the northern part of the corridor, the area north of Bhavani, include granite gneiss, enderbite gneiss, charnockite gneiss, fuchsite quartzite, and mafic granulite. Granite gneiss is made up of quartz, plagioclase, hornblende and opaque. The main

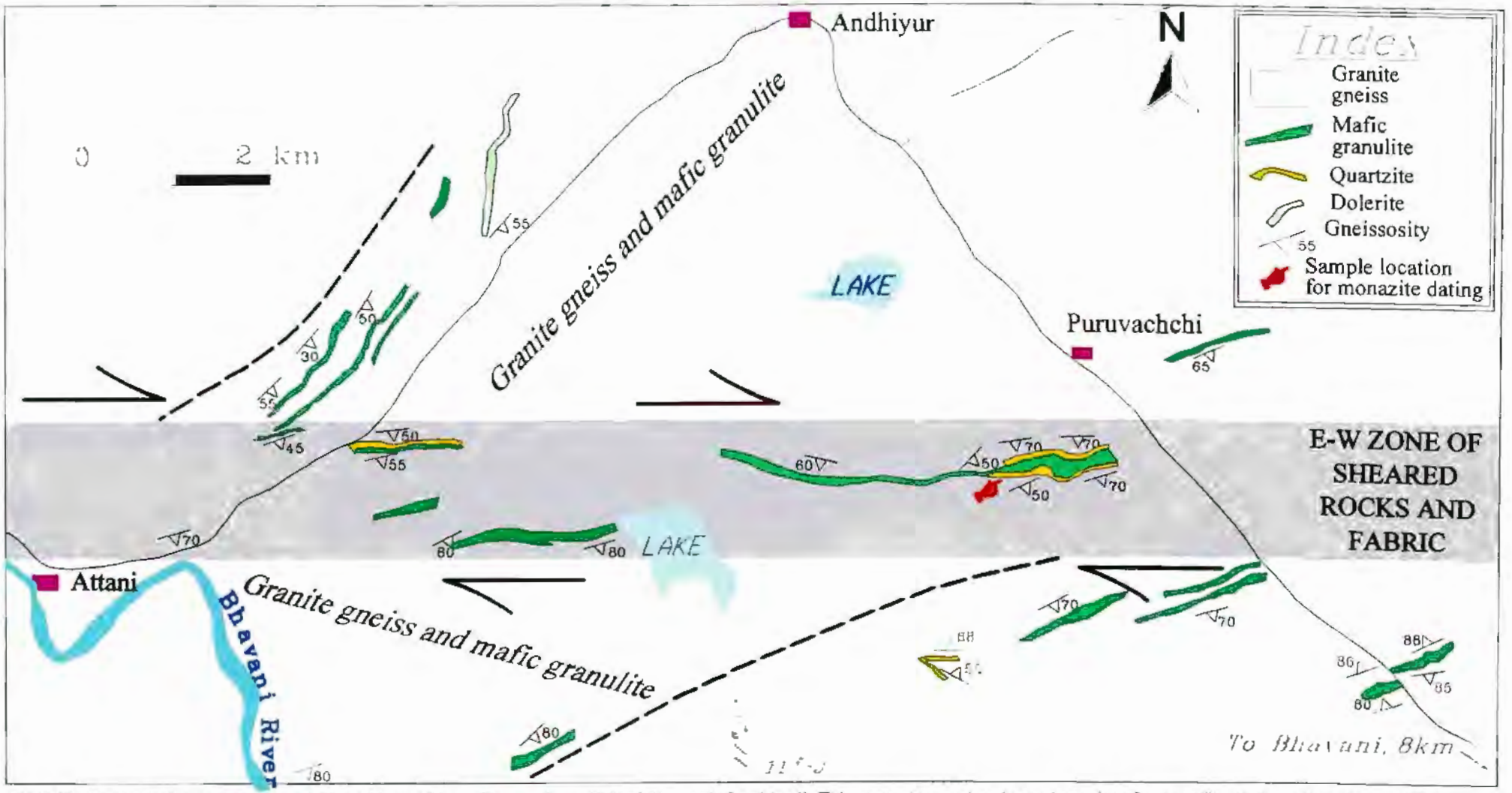

Fig.3.36. Geological map across part of the Moyar Shear Zone, ~8 km NW of Bhavani, Corridor-II. This map shows showing selected mafic granulite and quartzite layers. Their distribution suggests a dextral sense of movement along this shear zone. An intrusive relationship between the quartzite and mafic granulite can be observed in exposures ~2km south of Puruvachchi. Monazites from the quartzite have yielded two concordant ages at 612±9 Ma and 2522±10 Ma. Note that the mafic granulite band south of Puruvachchi intrudes quartzite band (near the hand symbol). Both these bands are presently subparallel to each other because of shearing.

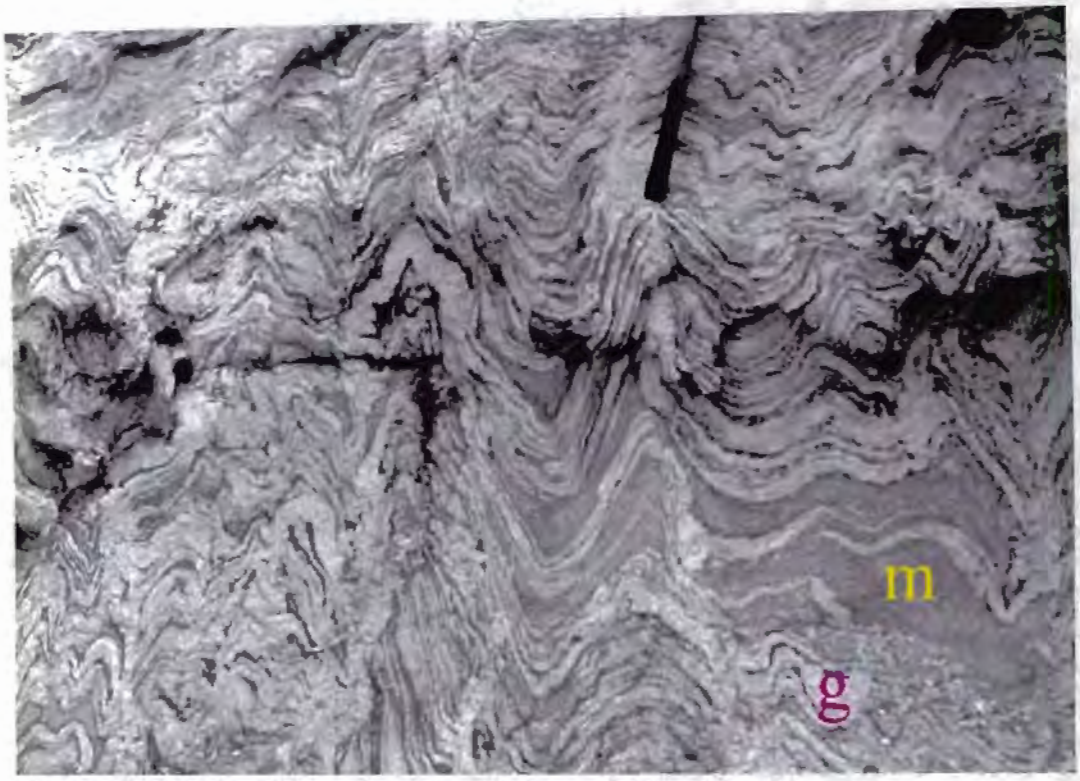

Fig. 3.37. Migmatites of south of Bhavani, Corridor-II. Subparallel dense intrusion of granitic veins (g) into schistose mafic granulite (m) has given rise to migmatite. Migmatite is intensely folded and sheared. Folds have NE-SW axial traces and sub-vertical axes. Similar leucosomes of migmatite has been dated in the Namakkal area of Corridor-I at ~603±14 Ma.

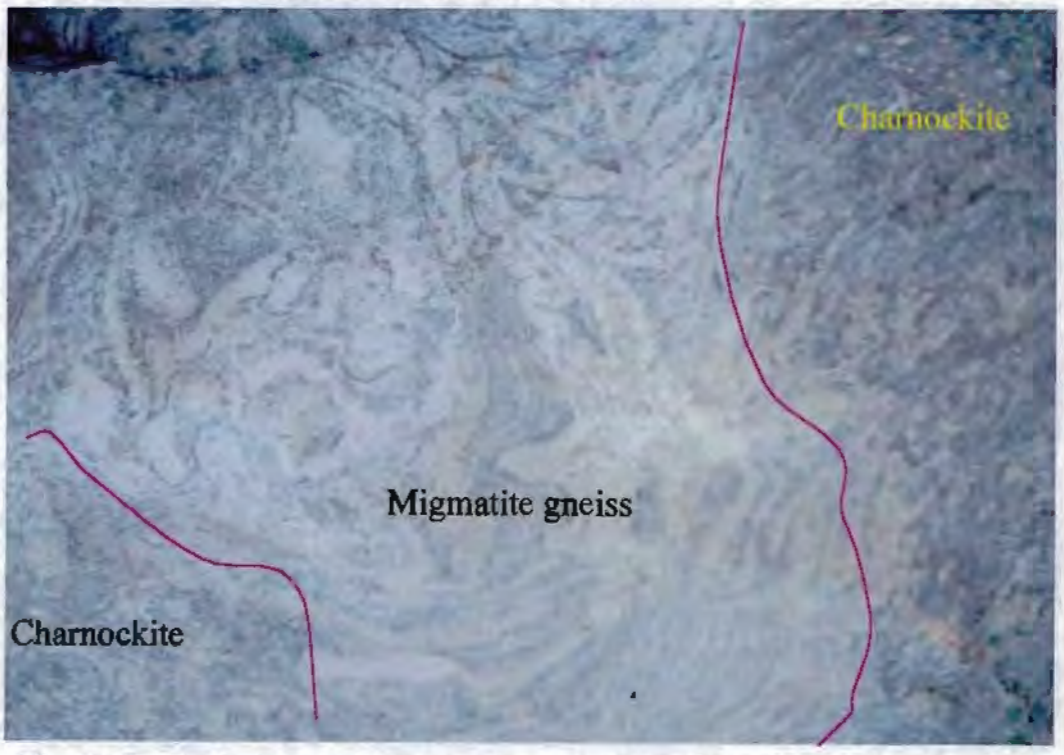

Fig. 3.38. Dark charnockite superimposed on migmatite gneiss. Note the boundary between the charnockite and the migmatite transgresses folds and gneissosity in the migmatite. Location, south of Perumapalayam, ~3 km WSW of Bhavani, Corridor-II.

mineral constituents of mafic granulite are hornblende, plagioclase, garnet, clinopyroxene and occasional orthopyroxene. The mafic granulite intrudes fuchsitic quartzite layers (Fig. 3.36). In the southern part of the Bhavani area all these rock types are profusely impregnated by massive coarse granitic leucosomes giving the rock a migmatitic appearance (Fig. 3.37). These migmatites are the most dominant rock type between Bhavani to south of Erode. Similar leucosomes of migmatite in the Namakkal have been dated at 603 ± 14 Ma (sample S-196A, Chapter 4). In places (for example, in the hills, 4 km SW of Bhavani) these migmatites are patchily charnockitzed (Fig. 3.38). In the southern part of this corridor, in the Chennimalai area, there are a number of BIF and calc-silicate bands intruded by massive coarse granite bodies.

3.2.3.3. Structure

The northern part of this corridor records a change in the strike of the lithologic units from the NNE-SSW trend in the Dharwar craton in the northern part, to a 2-3 km wide zone of E-W strike just north of the Bhavani (Fig. 3.1). This change in the strike is gradational over ~1km. Lineations in this area are scarce. All rocks within the E-W trending zone are mylonitised. The transition from NE-SW trending strike in the northern part of this area into E-W zone can be traced along near-continuous exposures in the western part of the area. Regional structural trends indicate that the E-W zone is possibly the continuation of the MASZ, which has been identified in the Bhavani Sagar area (Corridor-III) and in the Salem area (Corridor-I).

South of Bhavani, migmatitic gneisses show well developed E-W to ENE-WSW trending folds (Fig. 3.37) with steep easterly dipping axes. The area between Bhavani in the north and just south of Erode is represented by NW-SE strikes (Fig. 3.1), subparallel with the alignment of the Cauvery River. Here, mainly migmatitic gneisses strike parallel to the D_2 shearing identified in the Namakkal area. Further northwest this D_2 shear zone curves into an E-W orientation, subparallel to the alignment of the Bhavani River, and merges with the MSZ

southeast of Bhavanisagar. This D_2 shear zone is hence named as the Cauvery-Bhavani Shear Zone (CBSZ; Fig. 3.1).

In the southern part of the corridor, around Chennimalai and further south, the strike of the lithologic units changes from NW-SE in the northern part to E-W and ENE-WSW. The two most conspicuous structural features of this part of the corridor are the E-W trending BIF ridge of the Chennimalai Hill and the mafic granulites northeast of Sivamalai Hill. Minor folds of the Chennimalai Hill are dominated by E-W trending nearly upright folds with subhorizontal axes. There is no evidence of mylonitization in the BIFs or in associated mafic granulites and calc silicates. South of the Chennimalai Hill mafic granulite layers show variations in trend from NW-SE to NE-SW, due to open warps superimposed on a shallow to moderately dipping gneissosity.

3.2.3.4. Metamorphism/Charnockitization

Along this corridor two different types of charnockites have been recognized, which have formed at different times: (i) massive charnockite and (ii) patchy charnockite. Massive charnockites occur in the northern part of this corridor and represent a continuation of the charnockites in the Biligirirangan Hill. These charnockites were formed at ~2.5 Ga (U-Pb dating of monazite and allanite from charnockite; Mahabaleswar et al. 1995; Grew and Manton, 1984). During the present investigation, patchy charnockites have been recorded in migmatite gneiss south of the Bhavani. The migmatitic gneisses are folded and are charnockitized in small heterogeneous patches in many places (Fig. 3.38). Leucosomes of similar gneisses from the Namakkal area have been dated to be 604 ± 14 Ma (Chapter 4) indicating an additional chanockitization event in the Neoproterozoic. Nathan et al. (1991; 1994) also reported charnockitization within the Neoproterozoic Tiruchengodu granite massif, about 30 km to the east of Bhavani (Fig. 3.1). Thus charnockitization of two distinct ages, Late Archaean and Neoproterozoic, is present.

3.2.3.5. Geochronology

Monazites from a fuchsitic quartzite from in the E-W trending shear zone were dated using the SHRIMP (Chapter 4). Most of the monazites are concordant, giving an average U-Pb age of ca. 612 ± 6 Ma. However, a few grains record ages ~2.5 Ga. This indicates that the latest granulite facies metamorphism in the area was around 600 Ma. The ~2.5 Ga monazite age possibly represents an earlier high grade metamorphism, which has been recorded by previous workers ~100 km north of the present area. These ~2.5 Ga monazite is not likely to be inherited grains because the host rock (fuchsitic quartzite) is most likely older than ~2.5 Ga since elsewhere they are intruded by ~2.5 Ga old granite gneiss.

3.2.3.6. Geological Evolution of the Corridor-II and the Moyar Shear Zone

Fuchsitic quartzite, BIF and associated sediments are the oldest rocks present in the area. These were intruded by the mafic magma (now mafic granulite). The interrelationship between quartzite and associated metasediments and granite gneiss could not be established due to lack of sufficient suitable outcrops. By extrapolation from the Namakkal and Karur area (in Corridor-I), I assume that granite gneisses are intrusives into quartzite and mafic granulites. Younger massive coarse grained granites have intruded all the above. Similar relationships have also been recorded in the Biligirirangan Hills, ~100 km north of Bhavani.

The northern part of this corridor marks the intersection of three different structural trends: the N-S trending Archaean Dharwar trend, E-W trending Moyar Shear Zone of unknown age and the NW-SE trending D_2 (?and D_3) shear zone(s) of Neoproterozoic age, which continue from south of Namakkal area. The E-W trending Moyar Shear Zone has been superimposed on the Dharwar strike. The NW-SE D_2 trends swerves and become assympotic with the E-W trending Moyar Shear. The D_2 shear can thus be interpreted to be pre- to syn-Moyar (~600

Ma) shear. In the southern part of the corridor, in the Chnnimalai area, numerous folds in E-W striking BIF and calc-silicate layers probably represent the regional folding associated with this shear zone activity.

Extensive Neoproterozoic migmatization and shearing confirms extensive remobilisation of the northern part of this corridor at about 600 Ma.

3.2.4. Geology of the Corridor-III

3.2.4.1. Regional setting

This corridor covers the area of intersection between the Moyar and the Bhavani lineaments in the Bhavani Sagar area. Both lineaments are well developed in this corridor. The Moyar lineament has an E-W trend while the Bhavani lineament has an NE-SW trend. These two lineaments comprise mylonitised-schistose granitic gneiss and define northern and southeastern limits of the Nilgiri Hill charnockitic massif (Fig. 1.6). The corridor was studied along wide spaced traverses and detailed studies in some quarry sections. The area was previously mapped by Rajan and Sundara Moorthy (1992) and by Srinivansan et al. (1994). Their map was modified during the present study (Fig. 3.39).

3.2.4.2. Lithology

The principal lithologies of the area include tonalitic gneiss, mafic granulite, BIF and massive coarse grained granite. Mafic granulite intrudes BIF (Fig. 3.40). These are, in turn, intruded by the tonalite gneiss. Younger massive granite intrudes all rock types. This sequence of events occurs both to the north and to the south of the Moyar lineament. The northern part of the corridor is occupied by massive enderbite which is the continuation of the Biligirirangan Hill

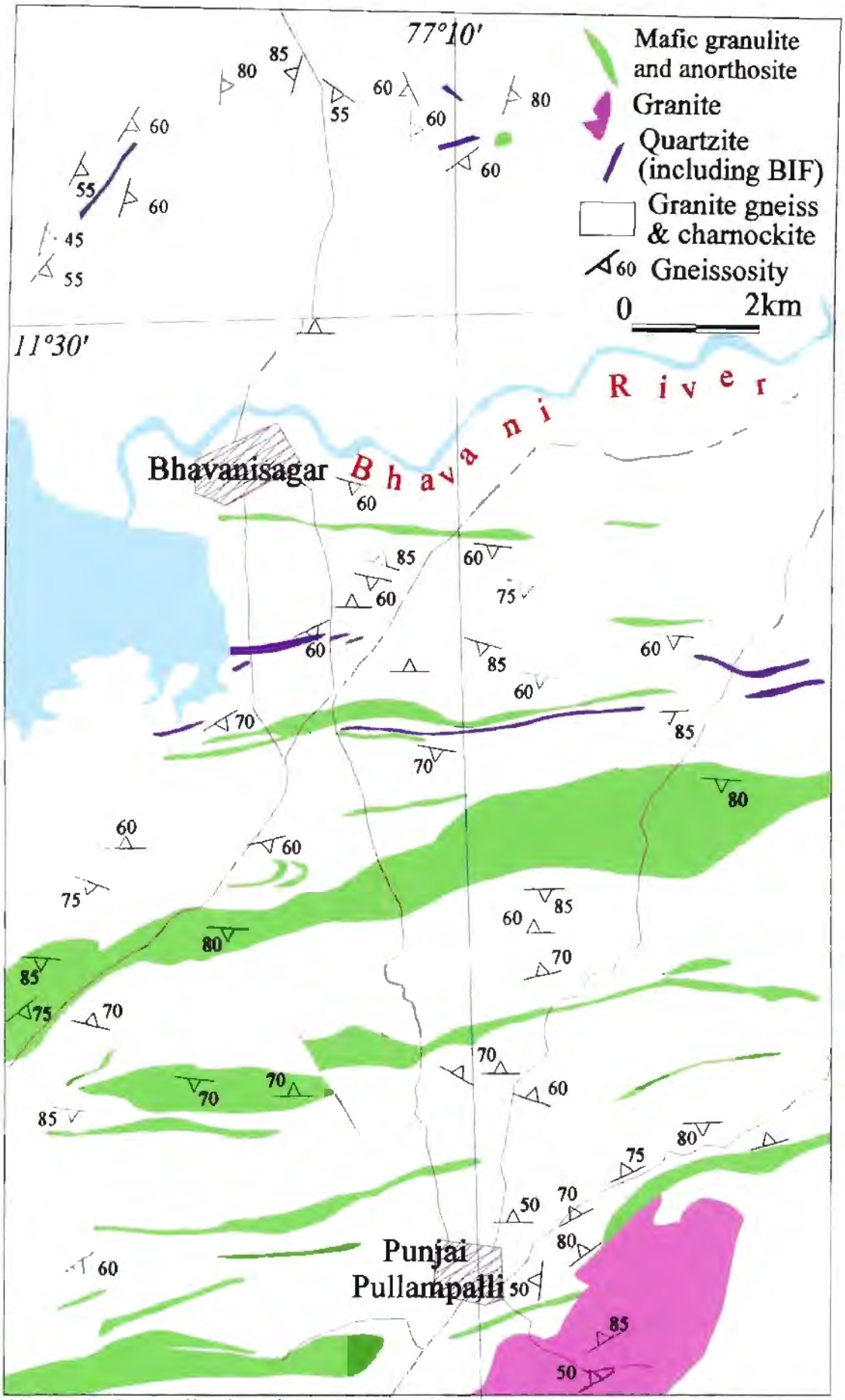

Fig. 3.39. Generalised geological map of the Bhavanisagar area, the area of intersection between the E-W trending Moyar lineament and ENE trending Bhavani lineament (modified after Rajan and Sundara Moorthy, 1992).

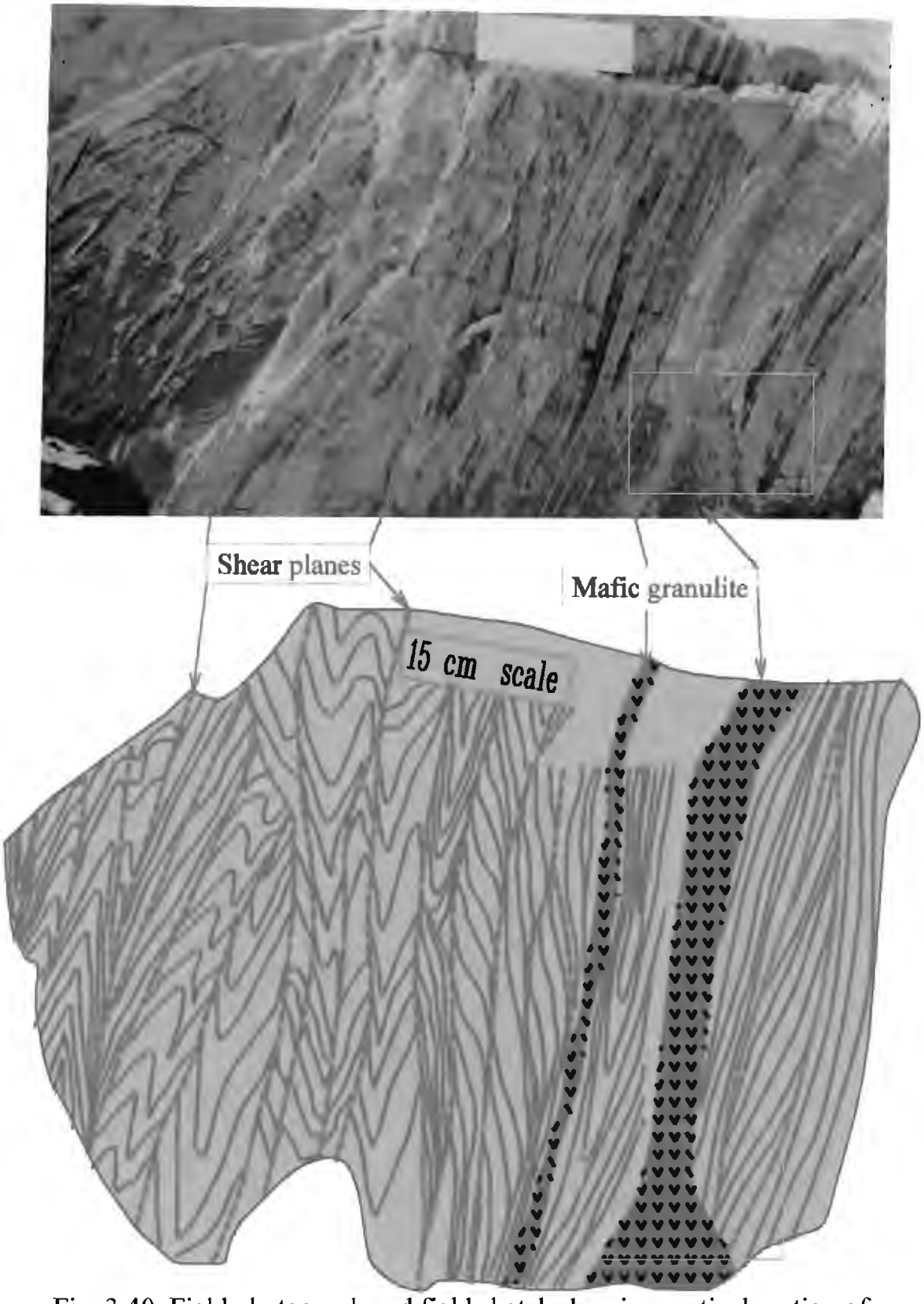

Fig. 3.40. Field photograph and field sketch showing vertical section of a sheared BIF intruded by mafic granulite dyke. The shear planes have sub-vertical dips and NE-SW trends. Note that mafic granulite cuts shear planes and foliation in BIF (marked by box). A nearby mafic granulite has been dated at ~2.9 Ga (Sm-Nd mineral isochron; Bhaskar Rao et al., 1996) which is similar to the U-Pb age of mafic granulite from the Namakkal area (Chapter 4). The shear fabric in BIF north of the Moyar Shear Zone is, therefore, older than ~2.9 Ga.

Fig.3.41a. Mylonite fabric in tonalite gneiss. Original gneissic fabric is transposed parallel to the ductile shear fabric. Rootless folds (F) defined by mafic-rich clots and layers are present in the mylonite. A granite (G) dyke intrudes the mylonite fabric. Vertical section. Trend of mylonitie fabric is NNE-SSW. Location ~3km south of Bhavani Sagar, Corridor-III

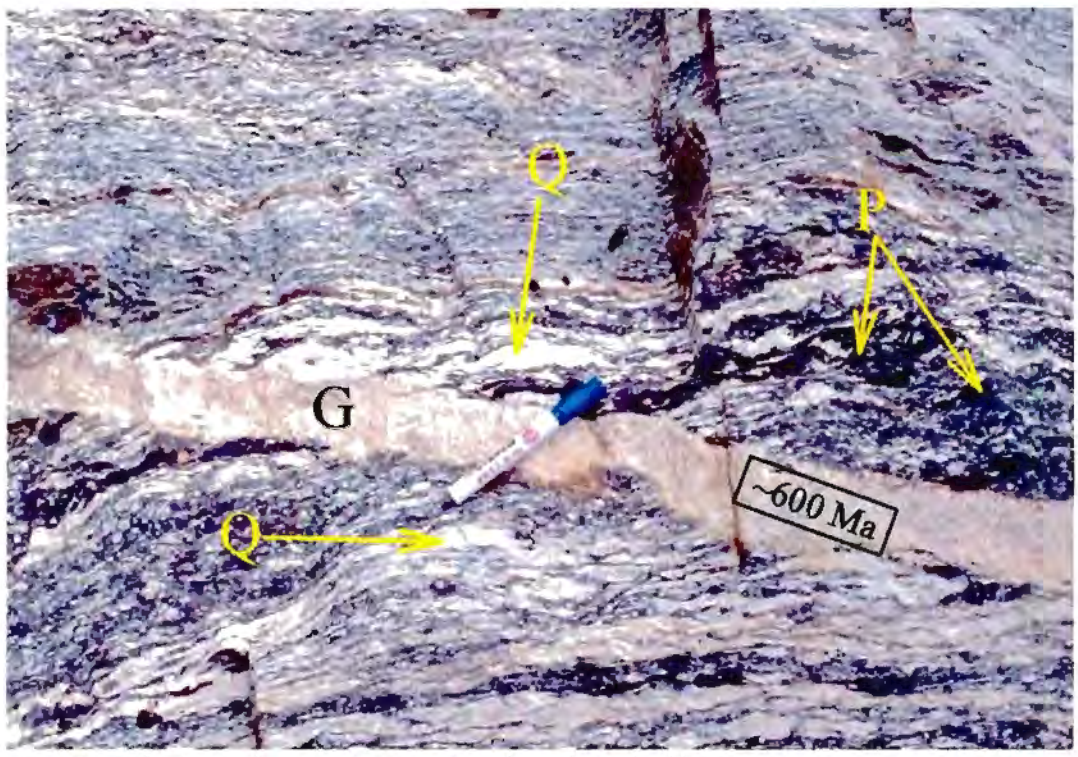

Fig. 3.41b. Late isotropic granite dykelets (~600 Ma) cutting across the mylonite fabric in granite gneiss within the Bhavani Shear Zone. Quartzo-feldspathic layers (Q) within biotite gneiss are finely granulated and are cut by psuedotachylite veins (P). Plan view. Trend of mylone fabric is E-W. Location: ~ 3 km south of Bhavanisagar.

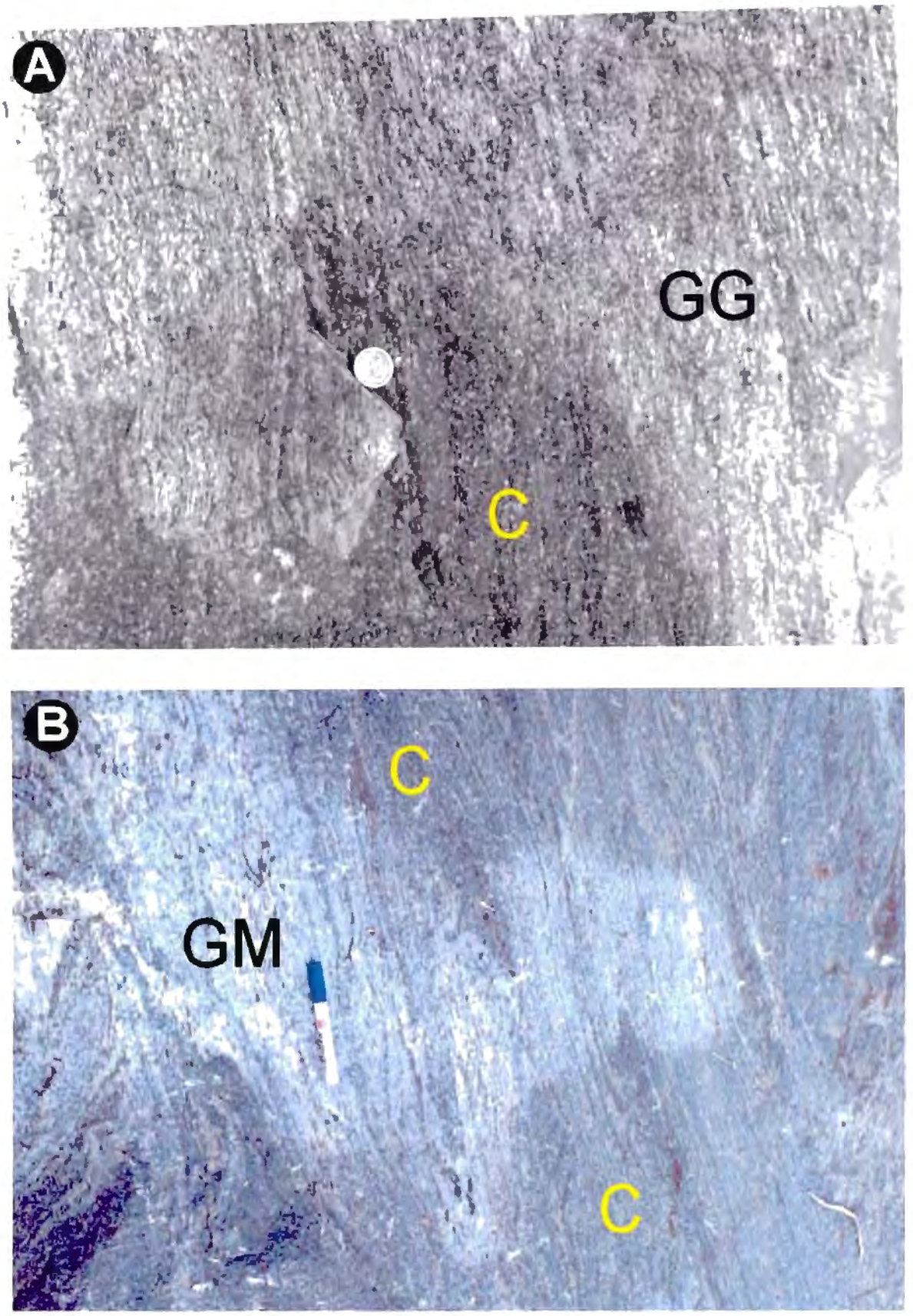

Fig. 3.42. Patchy charnockite (C; dark grey/blue) superimposed on granite gneiss (GG, upper photograph) and granitic mylonite (GM, lower photograph). Note the preservation of the layering and tectonic fabric across the charnockite-host rock boundary.
Location: A, ~3 km south of Bhananisagar; B, Gudiyar quarry, ~ 5 km east of Mettupalayam.

charnockite massif in the north (Fig. 3.1). They comprise plagioclase, orthopyroxene, garnet and hornblende. BIF and mafic granulite occur as xenoliths within enderbitic rocks. The principal lithology of the corridor is tonalite gneiss also with a number of isolated outcrops of mafic granulites, quartzite and BIFS. Tonalite gneiss is composed of plagioclase, quartz, hornblende, biotite and garnet. Gneissosity in many places has been transposed by a ductile mylonitic shear fabric (Fig. 3.41a). Patchy charnockites are present in the granite gneiss (Fig. 3.42). Within the charnockitized patches, the prominent fabric (S_2) present in the granitic gneiss has been recrystallized to a massive granulitic texture. Granite gneiss is intruded by coarse massive granite which is present as veins within granitic gneiss (Fig. 3.41). There are also a number of tors of massive granite in the area.

3.2.4.3. Structure

3.2.4.3.1. The Moyar Shear Zone

North of the Moyar Attur Lineament the general trend of the lithological units is NNE-SSW, with subvertical to steep easterly dips as a continuation of those in the Dharwar craton (Fig. 1.3). All the lithologic units in the area are highly deformed as evidenced by flattening of the mafic-rich clots and feldspar porphyroblasts in tonalite gneiss. There is well developed schistose fabric and augen structure in the tonalite-gneiss. In the enderbites the augen structure has been preserved but the schistose fabric has been recrystallized into coarse grained granoblastic texture. One NNE-SSW trending BIF band north of Moyar lineament shows development of shear lenses. Mafic granulite truncates these shear planes (Fig. 3.40). Mafic granulites in nearby areas has been dated at ~2.9 Ga (Nd-Sm whole rock isochron, Bhaskar Rao et al. 1996). Thus the NNE-SSW shear fabric north of the MSZ is older than 2.9 Ga.

The general strike of the lithologic units in the Moyar lineament is E-W and the general dip is

subvertical to steep to the south. The E-W trend of the lithologic units is restricted to a width of about 3-5 km centred on the Bhavanisagar. The zone of transition between the NE-SW strike in the north and the E-W strike of the Moyar lineament is covered by alluvials of Bhavani River. North of the Bhavani River, there are some exposures of E-W trending tonalite/granite gneiss in which cataclastic fabric and pseudotachylite veins are common (Fig. 3.43b). These may be related to late brittle shearing movement along the Moyar Shear Zone. Granite gneisses have discrete E-W trending ductile shear planes and mylonite zones (Fig. 3.43a). Bedding in one BIF layer, about 3 km south of Bhavanisagar (Fig. 3.39), has been totally transposed by this mylonitic fabric.

3.2.4.3.2. The Bhavani Shear Zone

South of Bhavanisagar, in the Bhavani lineament, the strike of different lithologic units reverts back to NE-SE to ENE-WSW similar to that area north of the Moyar Shear Zone. The rocks contain deformed mafic clots and quartzofelspathic ribbons. The original gneissosity in tonalite gneiss is transposed by ductile mylonite fabric in which rootless folds is preserved (Fig. 3.41a). In many places flattened mafic and quartzofelspathic clots commonly show down-dip elongation, suggesting stretching within the Bhavani Shear Zone. The granite gneiss contains well developed subvertical ribbing lineation (micro-mullions; Fig. 3.44). Schistosity planes in tonalite gneiss either wraps around or cut across garnet and feldspar porphyroblasts (Fig. 3.45; 3.46) suggesting that schistosity were developed after or during growth of garnet. Deformed granitic gneiss is commonly cut by discrete zones of brittle to brittle-ductile shears. Within these shears quartzose layers of the gneisses are granulated. Late coarse granite veins cut across brittle shears and at places these granite veins are also deformed (Fig. 3.41b; 3.47), indicating that these granite veins in the area are syntectonic with the brittle shearing deformation in the Moyar and Bhavani Shear Zones. Pseudotachylites are common within the brittle shears, and occur as subparallel or anastomosing veins and dykes enclosing the unaffected fragments of granite gneiss (Fig 3.48). Patchy charnockitization is common, and in

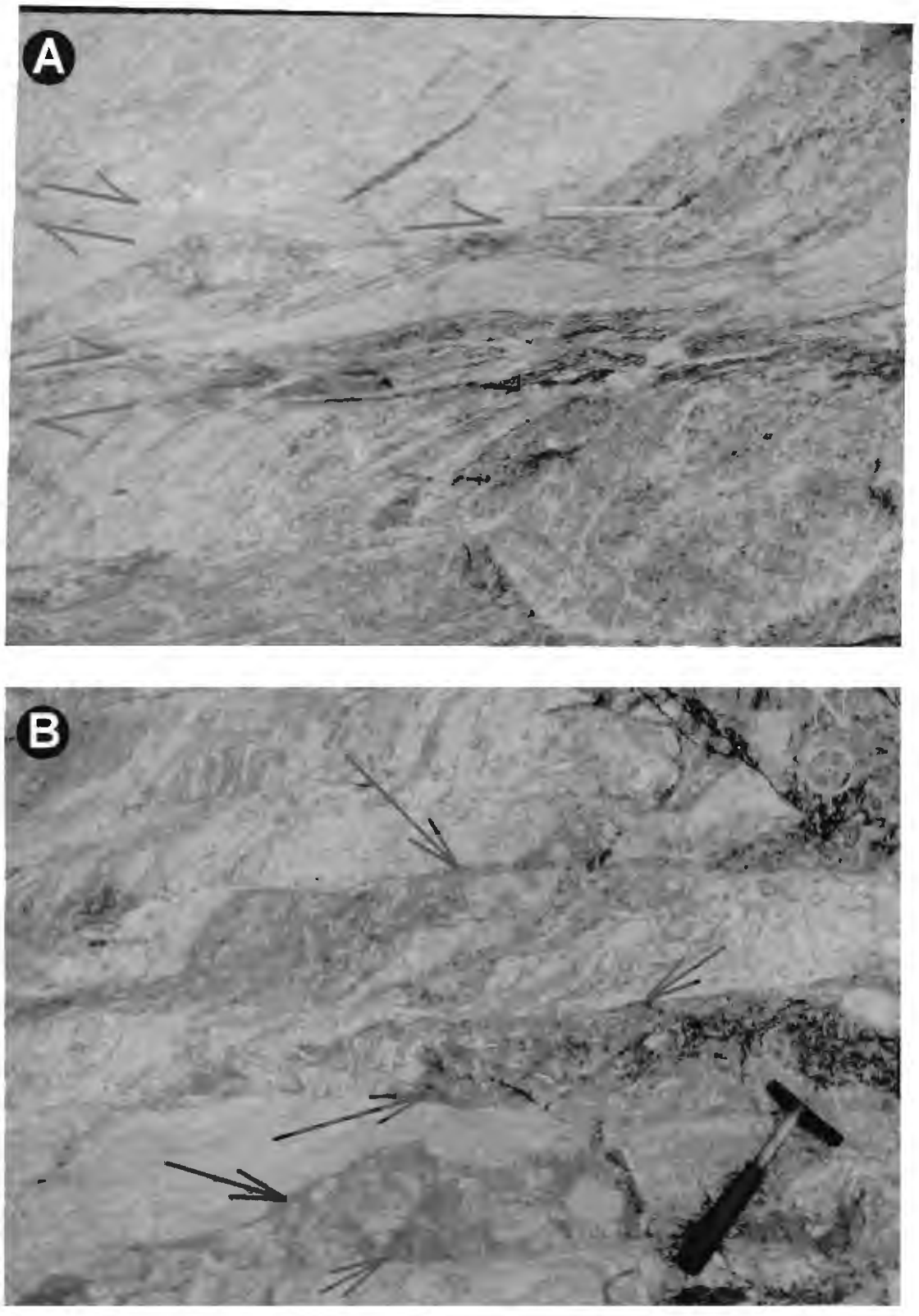

Fig. 3.43. Ductile and brittle-ductile shears in the Moyar Shear Zone. A. Tonalite gneiss show E-W trending ductile shear with dextral sense of movement. Plan view. Location: ~2 km SE of Bhavanisagar.

B. E-W trending brittle and brittle-ductile shears superimposed on foliated tonalite gneiss. Pseudotachylite veins are present along some brittle shears (marked by arrows). Location: ~2km north of Bhavanisagar; along the northern margin of the Moyar Shear Zone.

Fig. 3.44. Subvertical ribbing (micro-mullion) lineation in granite gneiss within the Bhavani Shear Zone. Pen for scale is ~15 cms long. Location: a quarry section in Gudiyar, ~5 km east of Mettupalayam., Corridor-III.

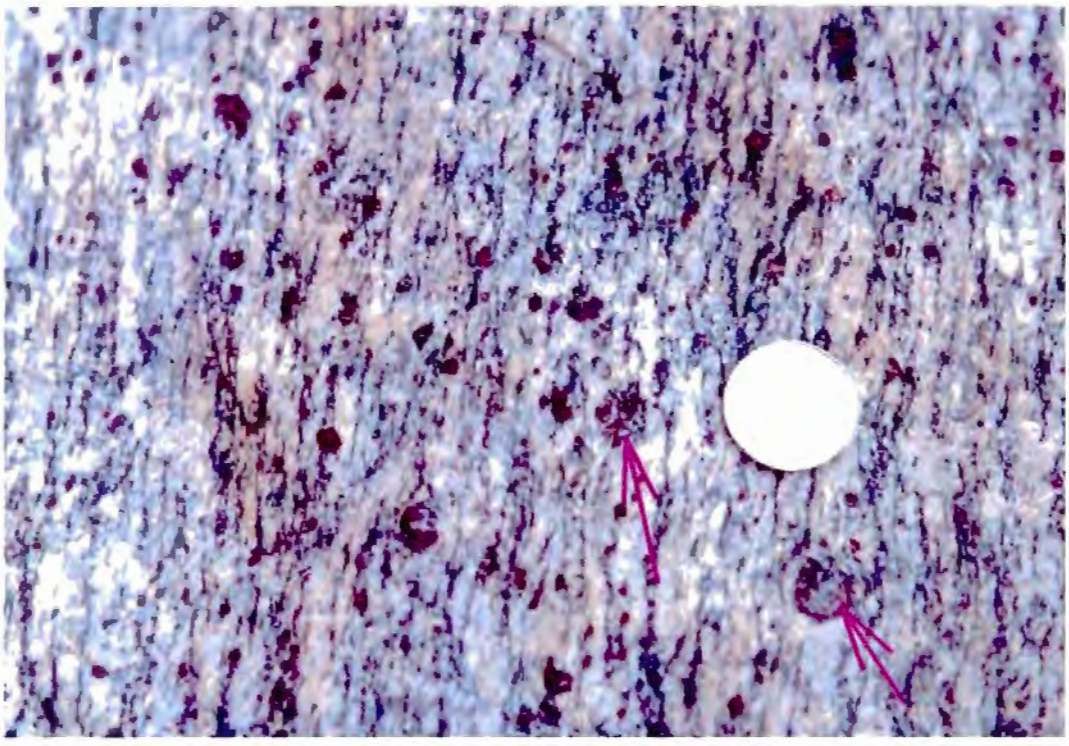

Fig. 3.45. Close-up of granite gneiss exposed in the Bhavani Shear Zone. Foliations in the gneiss wrap around (arrow at the bottom right) or cut across (arrow near the centre) the garnet porphyroblast, suggesting that the garnet porphyroblast could either be syn-tectonic to post-tectonic with respect to the development of schistosity (S_1). Location: ~5 km south of Bhavanisagar, Corridor-III.

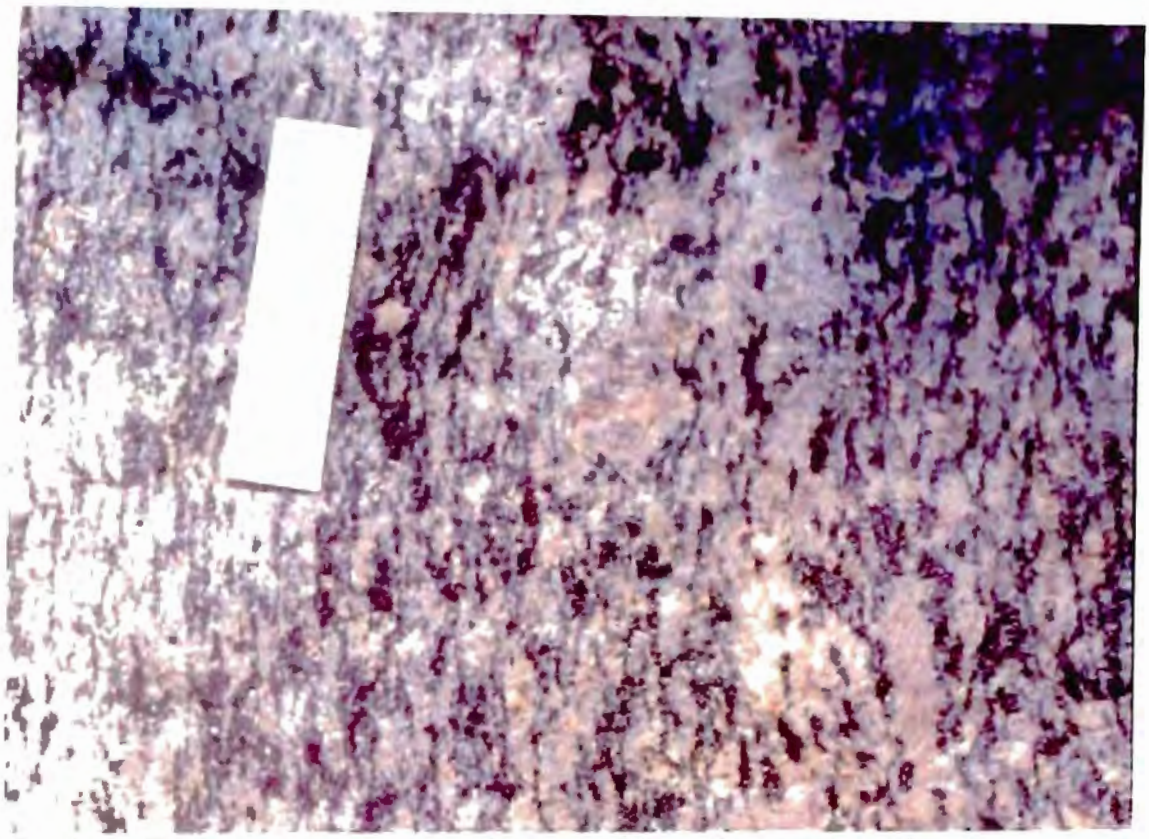

Fig.3.46.Tonalite gneiss in the Bhavani Shear Zone. Note that gneissosity wraps round a feldspar phenocryst in the centre. Location, Gudiyar quarry, ~5km east of Mettupalayam, Corridor-III

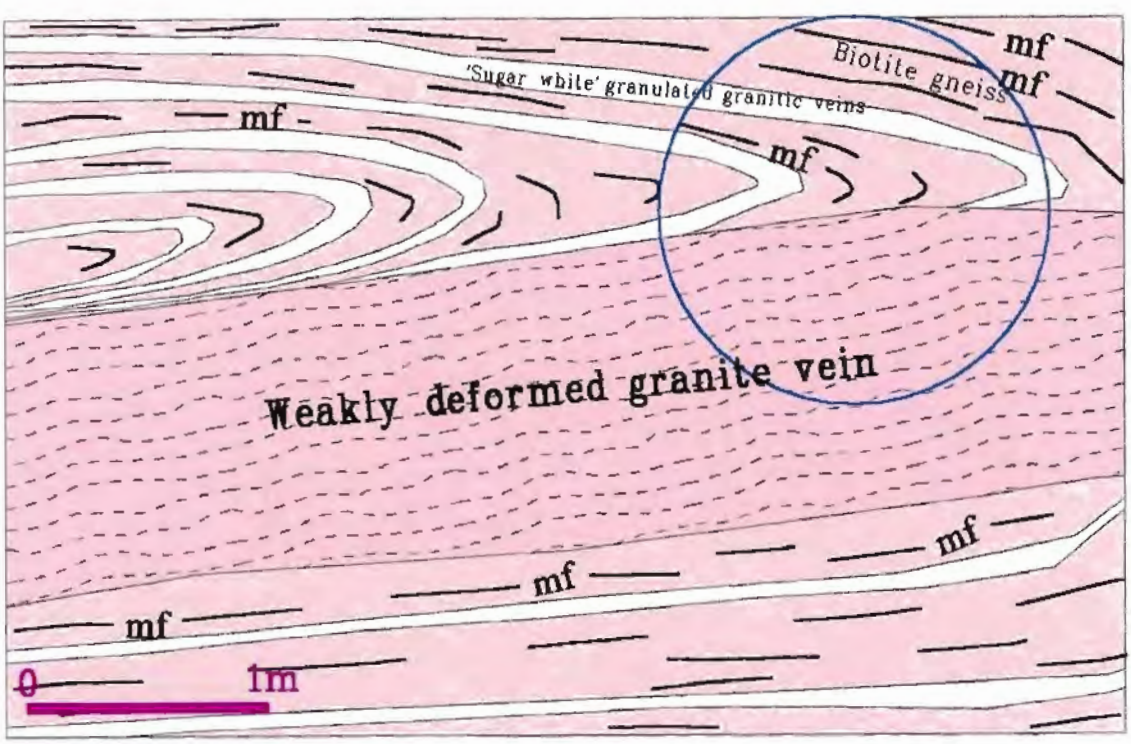

Fig.3.47. Granite dyke cutting across folded brittle-ductile mylonite fabric (D_2) within the MSZ (circled area). The granite dyke also has developed a weak schistosity parallel to the E-W trending brittle-ductile mylonitic fabric (mf). Location, ~2 km ESE of Bhavanisagar, Corridor-III.

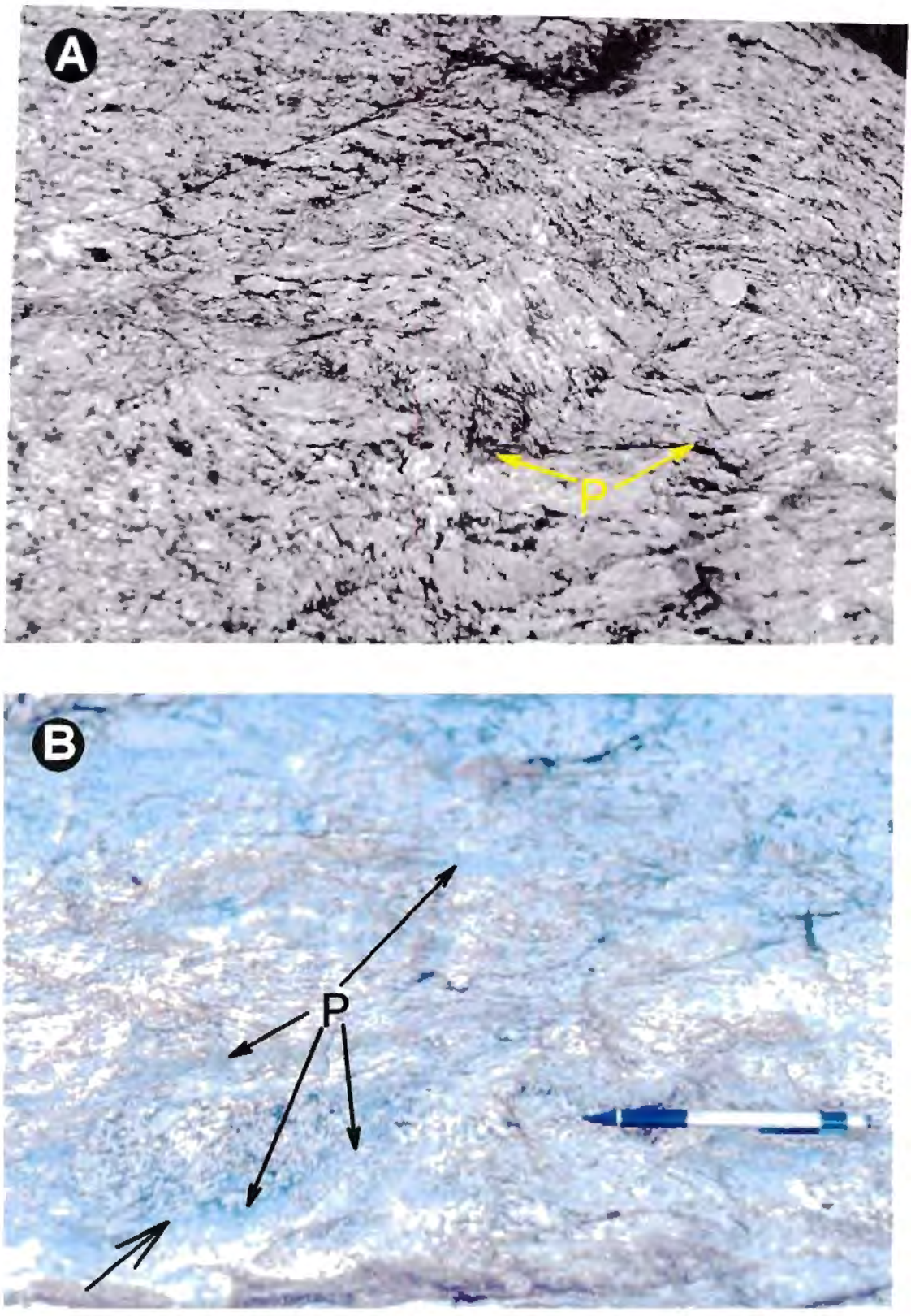

Fig. 3.48. Brittle and brittle-ductile shears in granite gneiss within the Bhavani Shear Zone. Location: a quarry section at Gudiyar, ~5 km east of Mettupalayam, Corridor-III

A. Anastomosing brittle fracture planes surrounding tonalite gneiss fragments. Thin psuedo-tachylite (P) veins cut across S_1 fabric in the gneiss. Coin for scale is of ~1.5 cm diameter.

B. Pseudotachylite veins (P) cuts tonalite gneiss. Location: a quarry section at Gudiyar, ~5 km east of Mettupalayam, Corridor-III.

such charnockitized patches, the original schistose fabric of the granite gneiss has been recrystallized into coarse granulitic texture although "ghost" layering commonly persists. .Garnet porphyroblasts present in the rock have grown across the schistose fabric in the granite gneiss, but in the brittle shear zones, these garnet porphyroblasts are also deformed.

A number rock types from the Bhavani Shear Zone have been dated during the present study (Chapter 4). Zircons from the granite gneiss and granitic mylonite have U/Pb ages of ~2.53 Ga, which are interpreted as the protolith age of the granite gneiss (Chapter-4). Zircons from the mafic granulite have a U/Pb age of ~2.48 Ga. However, field relations shows that mafic granulite is intruded by the granite gneiss. Also, mafic granulite from this corridor has been dated recently by the Sm-Nd whole rock method which yielded ~2.9 Ga age (Bhaskar Rao et al. 1996). The ~2.48 Ga age of zircons from the mafic granulite are thus interpreted as metamorphic, documenting a Late Archaean high grade metamorphism. Zircons from a crosscutting pegmatitic granite yielded an age of ~600 Ma, providing an approximate age of the syntectonic brittle to brittle ductile deformation in the Moyar Shear Zone.

3.2.4.4. Geological evolution in Corridor-III

Similar to Corridors I & II, the oldest lithologic types encountered in the area Corridor III are the BIF and other metasediments. These were intruded by mafic granulite, all of which were subsequently intruded by ~2.53 Ga old granite gneiss. The granitic gneisses are highly deformed. Charnockitization was superimposed on these deformed rocks. A ~2.5 Ma charnockitization event has previously been recorded in the Dharwar craton north of the present corridor by (Friend and Nutman, 1992; Grew and Manton, 1984; Peucat et al. 1993; Mahabaleswar et al. 1995). The ~2.48 Ga age of zircons from the mafic granulite in the present area is possibly related to the Late Archaean Paleoproterozoic charnockitization. It is, however, not clear whether more than one charnockitization event is present in the area, as has been recorded in Corridor II. The youngest magmatic activity is represented by ~600 Ma

coarse massive granite. In many places, these coarse granitic veins truncate the brittle to brittle-ductile shear fabric, but they themselves are also affected by shearing. This granite event is thus interpreted as syntectonic with the brittle to brittle-ductile shearing in the MASZ.

Granite gneisses both north and south of the MASZ are highly deformed. Zones of ductile shearing are common both north and south of Moyar shear zone. The NE-SW strike of the lithologic units north of the Moyar Shear Zone are the same as those to the south in the Bhavani Lineament. But along the MASZ, the strike is E-W. Both the Moyar and the Bhavani lineaments have well developed brittle to brittle-ductile shear zones. But the general continuity of the structural trend and rock types both north and south of the Moyar lineament suggests that the MASZ is not a fundamental terrane boundary.

3.2.5. Geology of the Corridor-IV

This corridor covers part of the Palghat Gap (Fig 1.7). The Palghat-Cauvery Lineament is best developed in this area. The general trend of the lithologic units in this corridor is E-W. The corridor was covered by wide traverses and studies of selected quarry sections.

The area is dominated by granite gneiss, coarse massive granite and mafic granulite. At least four different granitic events separated by deformational episodes can be recognized (Fig. 3.49). The earliest granitic rocks recognized in the area are homogeneous schistose biotite-rich tonalite-gneiss (type-A), is made up of plagioclase, biotite and quartz. This variety is intruded by gneissose hornblende-biotite-gneiss (type-B) which is the most dominant rock type in the area. The third granitoid rock type (type-C) is represented by thin, pale coloured medium-grained quartzofelspathic veins which have intruded subparallel to the gneissosity in type-B. In places the veins show cross-cutting relationship with both type-A and type-B (Fig. 4.49; 4.50). The veins are deformed and have developed internal planar fabric. The rock has isolated and subparallely aligned ellipsoidal mafic rich clots, which define a weak gneissosity. Similar rock

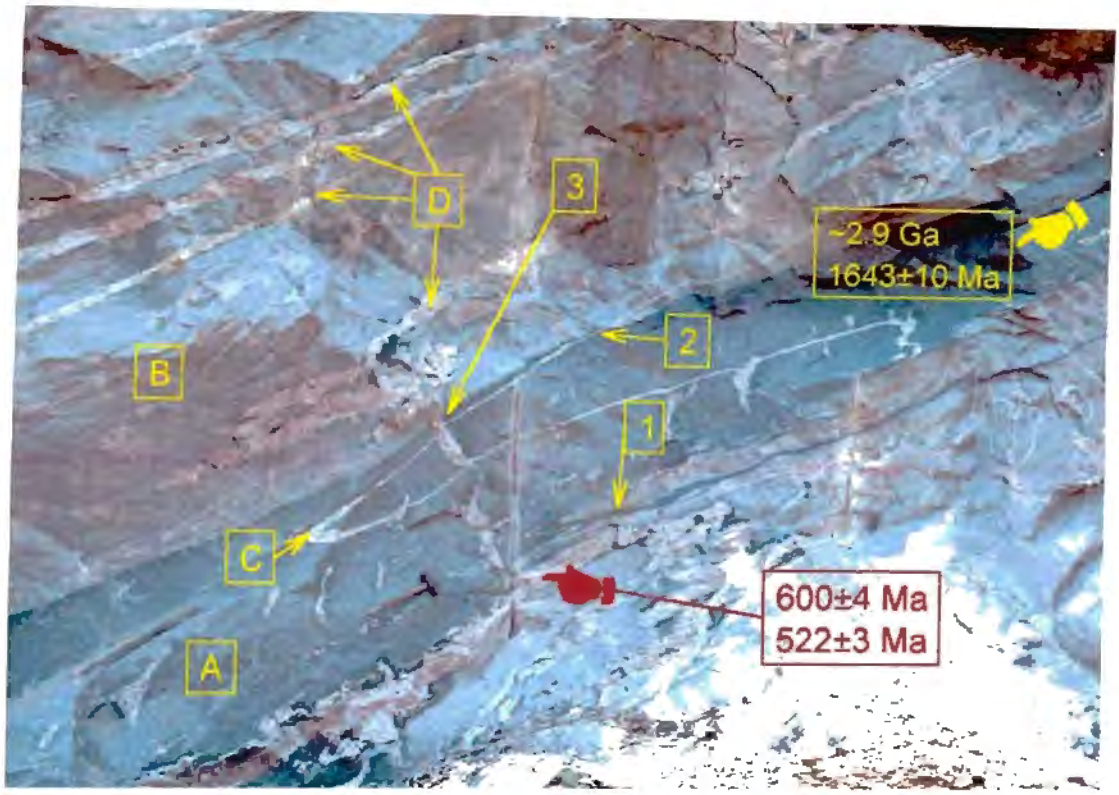

Fig. 3.49. Four types of granites (A,B,C and D) and their inter-relationships in a vertical quarry section in Maruthamkad village, ~30 km north of Palghat. Type A is intruded (1) by type B. Both are intruded (2) by type C. Type C is intruded (3) by type D. ☛, sample locations for U-Pb zircon dating of type A (S-404A) and type D (S-404B) granites. Zircons from both varieties contain multiple populations (see Chapter 4 for details).

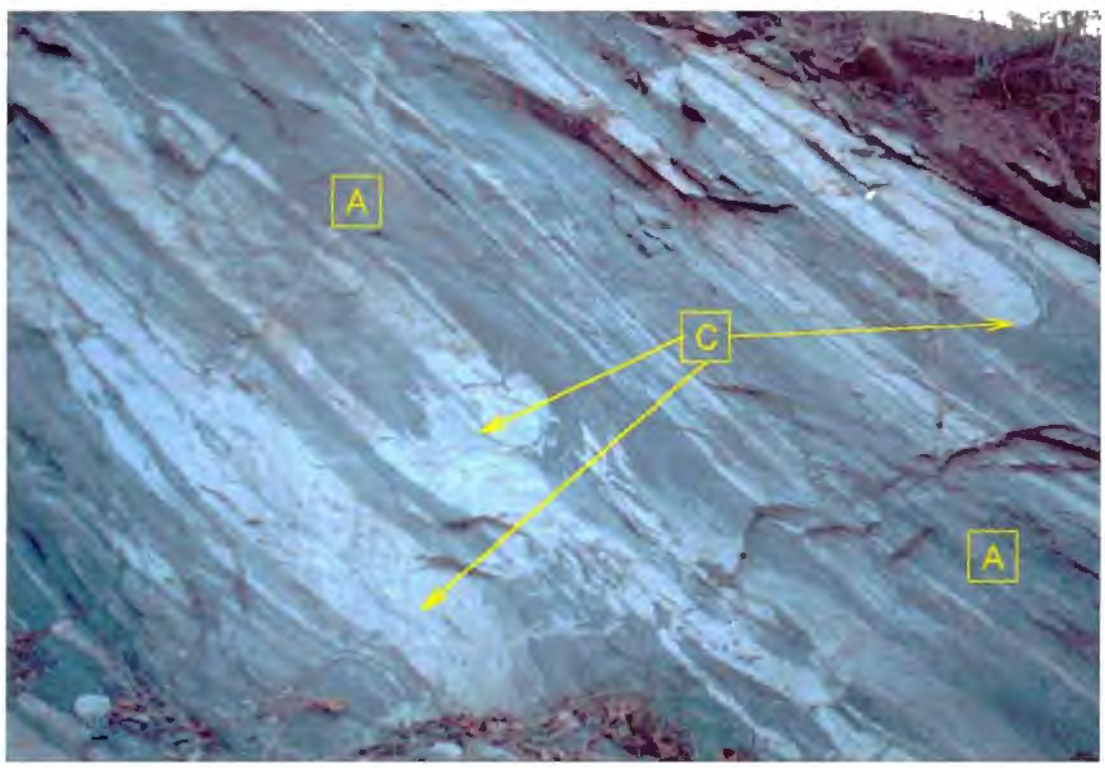

Fig. 3.50. Isoclinal folds in type C granites intruded into the type A granites. Location, Vayalur quarry, ~30 km east of Attapadi, Bhavani Shear Zone (Fig. 3.1).

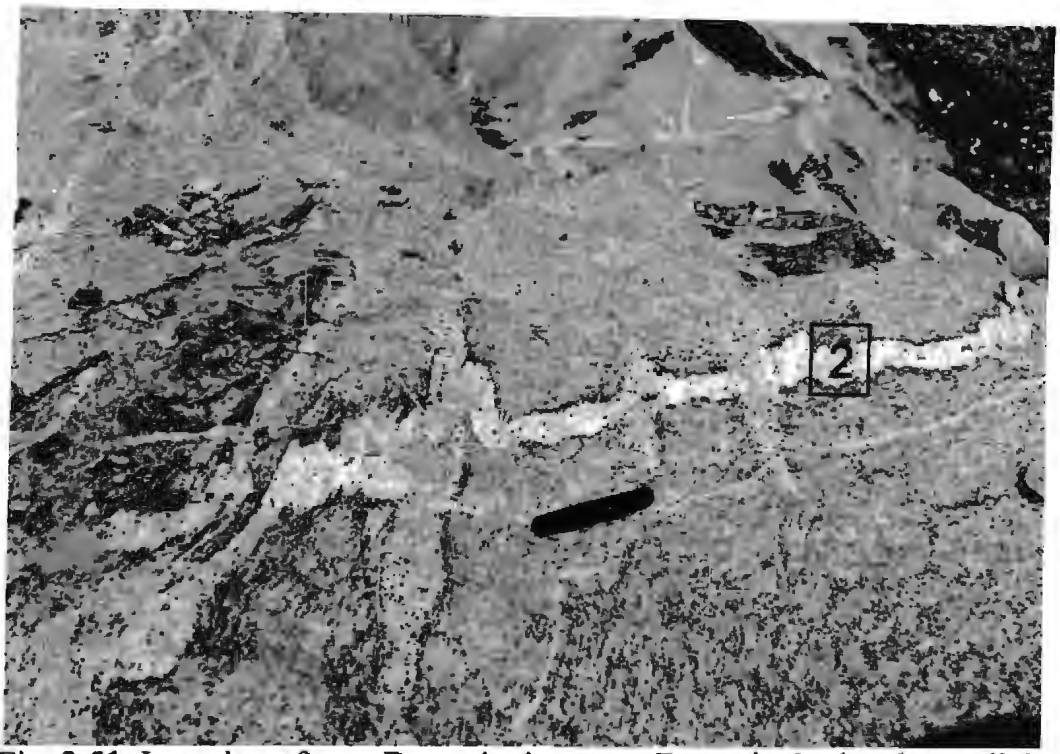

Fig. 3.51. Intrusion of type D granite into type B granite both sub-parallel (1) to the gneissosity and cutting across (2) it. Type D may include two separate phases (D_1 and D_2). But the boundary between these two varieties is not sharp. It is possible that the D_1 variety which is folded in places, were intruded late-syntectonically, while the D_2 variety may represent in situ partial melt product following D_1.
Location, Maruthamkad quarry,~30 km north of Palghat.

Fig. 3.52. Intrusion of type D granite into type A, subparallel to the gneissosity in type A, resulting in a composite multilayered rock. This multilayered rock has been affected by isoclinal folding (F) and shearing (S). Location, Nachchipilli quarry, ~ 20 km north of Palghat.

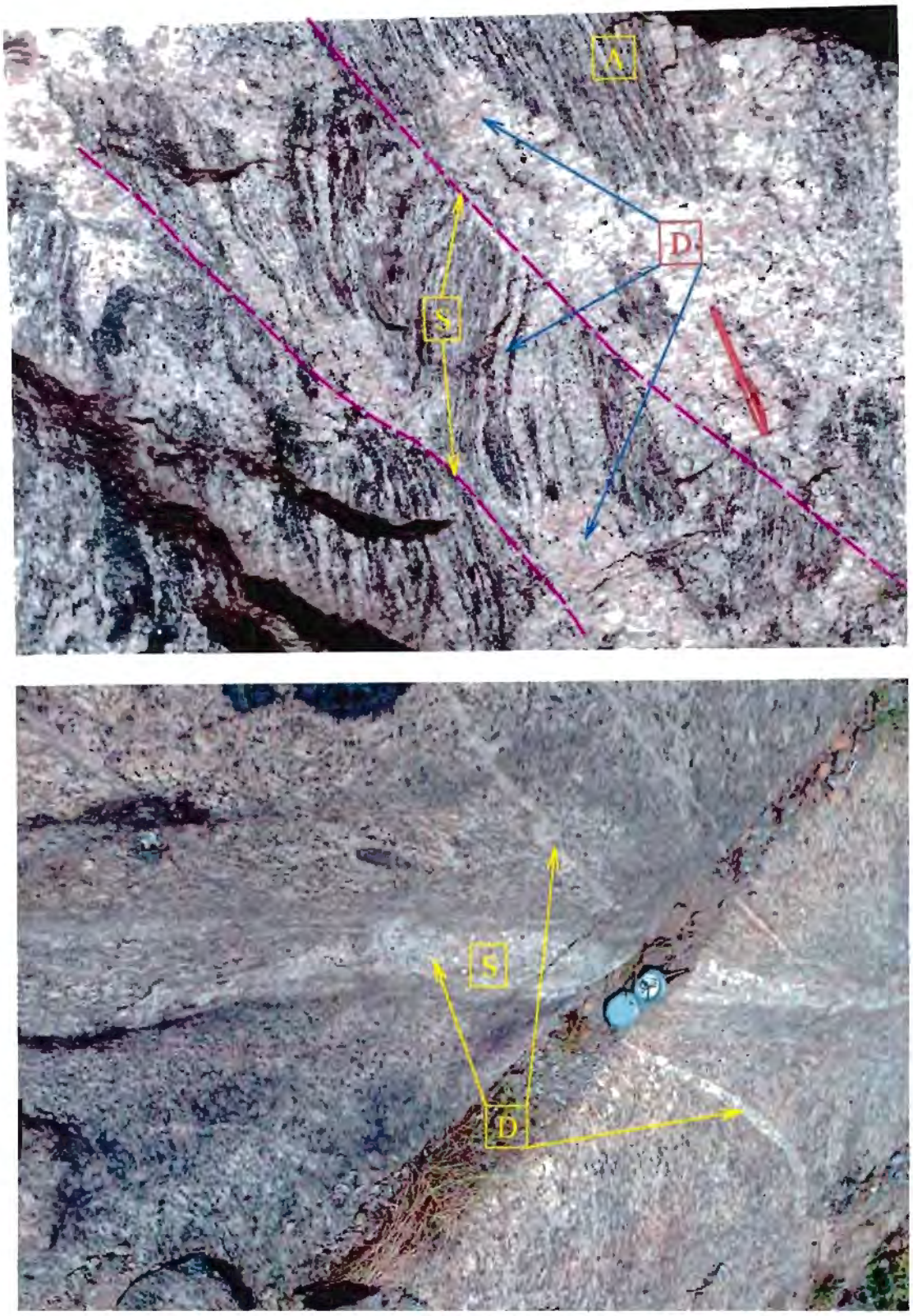

Fig. 3.53. Intrusion of type-D granite both along and across the gneissosity of types-A and -B granite gneisses. An ealier phase of type D has been sheared (S) along with host rocks but a younger phase intrudes the shear fabric. Thus type-D granite includes more than one phase and these phases overlaps with the shearing along the PCSZ. Shear planes (S) have a sinistral sense of movent.
Location, A., Mudur quarry, ~15 NW of Palghat. B., Vellapara quarry, ~20 km south of Palghat.

types form a ~50 km^2 batholithic body (known as the Sholiyur Granite; Fig. 4.50) north of the corridor. The youngest granitic rock is represented by coarse pink coloured massive granite (type-D). It cross-cuts foliation in both type-A and B. (Fig. 3.51). Subparallel dense intrusion by this variety into the type-A and B granitoids have commonly developed composite multi-layered rocks which in places are isoclinally folded and sheared in both sinistral and dextral simple shears (Fig. 3.52, dextral; 3.53, sinistral). In many places, type-D granite has crosscut simple shear planes in composite multi-layered rocks (Fig. 3.52; 3.53). Thus, type-D granite includes more than one generation of granites. The older phase (type-D_1) has been deformed and sheared (without development of planar penetrative fabric, while the younger phase (type-D_2) have apparently crosscut the shear fabric in D_1. However, both types D_1 and D_2 are coarse grained pink granites and nowhere has any sharp contact between these two types been observed. It is thus possible that intrusions of type-D granite overlapped with simple shear deformation in the rock in which younger phase intrude deformed earlier phases. All four types of granitoids, including type-D granite, show partial charnockitization at places (Fig. 2.5) indicating a phase of charnockitization that is younger than intrusion of the type-D granite. A younger phase of type-D granite has, in turn, intruded and retrogressed charnockites (Fig. 2.6).

Zircons from type-A granite gneiss and type-D (specifically type-D_1) granite have been dated in the present work using the SHRIMP and conventional IDTIMS respectively (Chapter 4). Type-A granite gneiss yielded two separate concordant population of zircons with igneous zoning in them. These two populations gave ages of ~2.9 Ga and 1643 ± 10 Ma, respectively (Fig. 3.49). While the ~2.9 Ga population is interpreted as the protolith age of type-A granite gneiss, the 1.65 Ga population represent another thermal event which may be related to intrusion of either type-B or type-C granites which have intruded type-A granite gneiss. Zircons from type-D granite have also yielded two distinct populations of zircon. One population, with a Th/U ratio of ~0.3 yielded near concordant age of 600 ± 4 Ma while the other population with Th/U ratio of ~.02 yielded a concordant 522 ± 3 Ma age (Fig. 3.49).

The magmatic crystallization age of the type-D granite is interpreted as ~600 Ma. The very low Th/U ratios in the younger population possibly represent their formation during later hydrothermal activity.

3.2.6. Synthesis of geological observations in Palghat-Cauvery, Moyar and Moyar Shear Zones

3.2.6.1. Lithostratigraphy

The areas covered in four corridors (I-IV) comprise a diverse variety of rock types. These include metasedimentary units, mafic granulite, granite gneiss and coarse massive granite intruded by late dolerite and gabbro. Metasedimentary assemblages are represented by BIF, quartzite (sometimes fuchsitic), calc-silicates, psamites and pelites. Calc-silicate rocks are mostly represented by diopsidic gneiss and marbles. The lithologic assemblages on either side of the Palghat-Cauvery Lineament are similar but their relative proportions differ. While calc-silicates and pelites are abundant in the southern part of the lineament, BIFs are more common in the area north of the lineament. This difference may simply be due to the original facies variations. Except for the area south of Palayam, the broad litho-stratigraphic relationship amongst various lithologic units in all the corridors are similar.

BIF and its associated metasediments are the oldest recognizable rock types of the area. They were deformed and later intruded by mafic granulites (Fig. 3.36). The age of the mafic granulite bodies is around 2.9 Ga to 3.0 Ga (Chapter 4 and Bhaskar Rao et al. 1996). Thus, the BIFs were deformed prior to ~2.9 Ga. Mafic granulites and BIFs were folded together and sheared at around 2.53 Ga, during large scale intrusion of tonalite. This tonalite has dismembered the early BIF and mafic granulites, which presently occur as isolated xenoliths at various scales. They must have been deformed prior to the intrusion of tonalitic gneiss. The granitic gneisses have, in turn, been intruded by a variety of younger granitic and mafic

intrusives. The most abundant variety is the pink coarse granite which has been dated in the Namakkal (Corridor-I), Mettupalayam (Corridor-III) and in Palghat (Corridor-IV) areas at about 600 Ma and in Palghat area at about 570 Ma. This variety is syntectonic with respect to an event of shearing deformation in the area. Two distinct phases of charnockitization are present in the area. One is Late Archaean (~2.5 Ga) and the other is Late Neoproterozoic (<~600 Ma) to Early Paleozoic.

South of Corridor I, in the Palayam area metasediments dominate. There, khondalite (quartz-muscovite-garnet-sillimanite-graphite schist) contains clasts of mafic granulite and folded BIF fragments suggesting that the khondalite may have an unconformable relationship with the mafic granulites and BIF, and thus probably represent younger metasediments. Two detrital zircons from khondalite yielded ~2.5 Ga ages, which supports this interpretation.

3.2.6.2. Structural geometry

The MASZ has been studied in the present investigation in three corridors (I, II and III). In all these corridors the shear zone was found be a E-W trending zone of 2-3 km wide with a subvertical planar shear fabric. Nowhere is there any evidence of large scale strike-slip movement. Instead, subvertical downdip stretching lineations are present in several places. Shear zone rocks display a high degree of flattening. This suggest that the MASZ had mainly subvertical movement with a significant pure shear component. Rocks on either side of the 2-3 km wide Moyar Shear Zone have broadly NNE-SSW to NE-SW trend.

The NW-SE trending CBSZ, identified during this study has a complex movement history. South of the Namakkal area both sinistral D_2 and dextral D_3 shears are present within this shear zone. Regionally, the tectonic fabric suggests an overall dextral movement along the CBSZ.

The BSZ has been investigated in Corridor-III. There, E-W to NE-SW trending subvertical ductile to brittle-ductile shears deform an earlier NE-SW striking gneisses. The width of the BSZ is not known.

Evidence for an E-W trending PCSZ was not observed either in Corridor I or Corridor II. If present, it could be below the alluvial sediments of the Cauvery River in these corridors. In Corridor I, both sides of the PCSZ have similar lithologic association, structural trends, and ages of dominant granite gneisses (~2.53). This suggests that even if an E-W trending shear zone is present underneath the alluvial sediments of the Cauvery River, the PCSZ is unlikely to be a major crustal shear zone, and less so a terrane boundary.

3.2.6.3. Geochronology

U-Pb geochronological studies carried out in the present work have revealed that ~2.5 Ga granitic rocks, known to exist in the Transition zone, continue further south across both MSZ and PCSZ. Granulite metamorphism at ~2.5 Ga has also been recorded in the Namakkal area, which is the southernmost extent of this Late Archeam-Early Proterozoic metamorphism known to date. Syntectonic and post-tectonic granites from the Namakkal area of Corridor-I, the Metttupalayam area of Corridor-III and Palghat area of Corridor IV have been dated at 603 ± 14, 601 ± 1 Ma and 600 ± 4 Ma. Monazite from the MSZ in Corridor-II have been dated at 612 ± 6 Ma. These ages suggests that the MSZ, the CBSZ, the BSZ and the PCSZ were formed or reactivated at ~600 Ma. A group of hydrothermal(?) zircons from a syntectonic granite from Palghat area of Corridor III have yielded an age of 522 ± 3 Ma which is possibly the final phase of movement along this shear zone.

3.3. Geology of the area between the PCSZ and the ASZ: The Madurai Block

3.3.1. Introduction

The area between the PCSZ and the ASZ is known as the Madurai Block (Harris and Santosh, 1994; Chapter 1; Fig. 1.7). The Madurai Block is the largest but least studied area of the SGT. Only a few recent studies on metamorphism (Sivasubramanian, 1991; Anand Mohan, 1996; Janardhan et al. 1997) and geochronology (Hansen et al. 1985; Jayananda et al. 1995; Bartlett et al. 1995, 1998) from selected localities exists.

The age relationship between the high grade metasediments of the Madurai Block and those of the high grade metasediments of the Sargur Group of the Dharwar craton is not known. There is no convincing record of Archaean basement from either the Madurai Block or the KKB south of it. Only Odom (1982) has recorded a U-Pb zircon age of ~2.9 Ga from a charnockite from the Trivandrum area. The continuity of this rock is, however, unknown. Two zircon evaporation ages from charnockites of the Kodaikanal area hint at the possible presence of granitic basement older than ~2.4 Ga (Jayananda et al. 1995; Bartlett et al. 1995; 1998). The entirety of the SGT might have been accreted to the Dharwar craton during a ~2.5 Ga event and the vast expanse of metasediments in the area might have been deposited on ~2.5 Ga basement. Available data have recorded Neoproterozoic migmatization and charnockitization event in the SGT (Santosh et al. 1989; Jayananda et al. 1995; Bartlett et al. 1995, 1998).

The Madurai Block has suffered polymetamorphism and has a very complex structural geometry. The distribution of the charnockites, granite gneiss and supracrustals in the Madurai Block is irregular. They define a broad regional trend suggestive of major NNW-SSE trending folds (Fig. 1.3). However, the satellite images of the Madurai Block have revealed N-S

structural trends (Drury and Holt, 1980), which broadly conform to the charnockite-granite gneiss contacts of the area.

A major discontinuity in the regional structure and lithological assemblage within the Madurai Block has been identified during the present investigation, which is interpreted as a major shear zone (the KKPT Shear Zone; Fig. 1.3). This discontinuity can be traced along a NE-SW trending zone broadly from south of Karur through south of Kodaikanal up to north of Kambam.. From there, this shear zone takes a turn towards NW and passes through north of Painavu up to the west coast of India, north of Trichur.

3.3.2. Rock types

The Madurai Block is dominated by amphibolite facies granitic para- and ortho-gneisses, high grade metasediments, and their charnockitized equivalents. Charnockitization is more extensive in the western part of the area, where the Kodaikanal and the Cardamom Hill ranges form a vast expanse of massive charnockite. Other than charnockite/enderbite and granitic gneisses, the Madurai Block has a high abundance of khondalite, calc-silicate gneiss, quartzite and mafic granulite. In addition there are a number of younger granitic bodies, which includes alkaline rocks. Two massive anorthosite bodies, namely the Oddhanchattram anorthosite and the Kadavur anorthosite occur in the northeastern part of this block (Janardhan and Wiebe 1985).

3.3.3. Structure

The distribution of quartzite, calc-silicate and mafic granulite layers define the distinct regional structural pattern of this block. These, along with trends of gneissosity in earlier published studies display the complex structural geometry of the terrain. A clear distinction can be made between structures north and south of the KKPT Shear Zone. South of the KKPT Shear Zone,

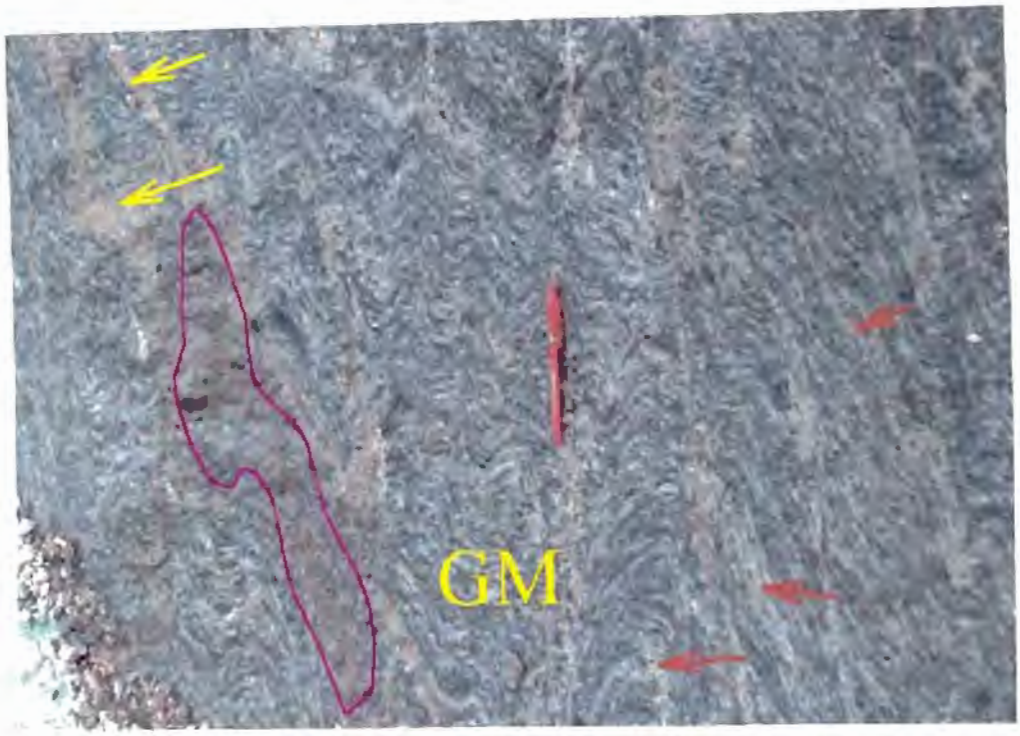

Fig.3.55. Crenulated granite mylonite (GM) in the KKPT Shear Zone, ~35 East of Kotamangalam. Granite veins of different generations, both folded with crenulation (red arrow) and cross-cutting the crenulation (yellow arrow) intrudes the mylonite. Granite and mylonite both are affected by patchy charnockitization (pink outline) within which the mylonitic fabric is no longer discernable. Location: Mamalakandu village, 35 km east of Kotamangalam.

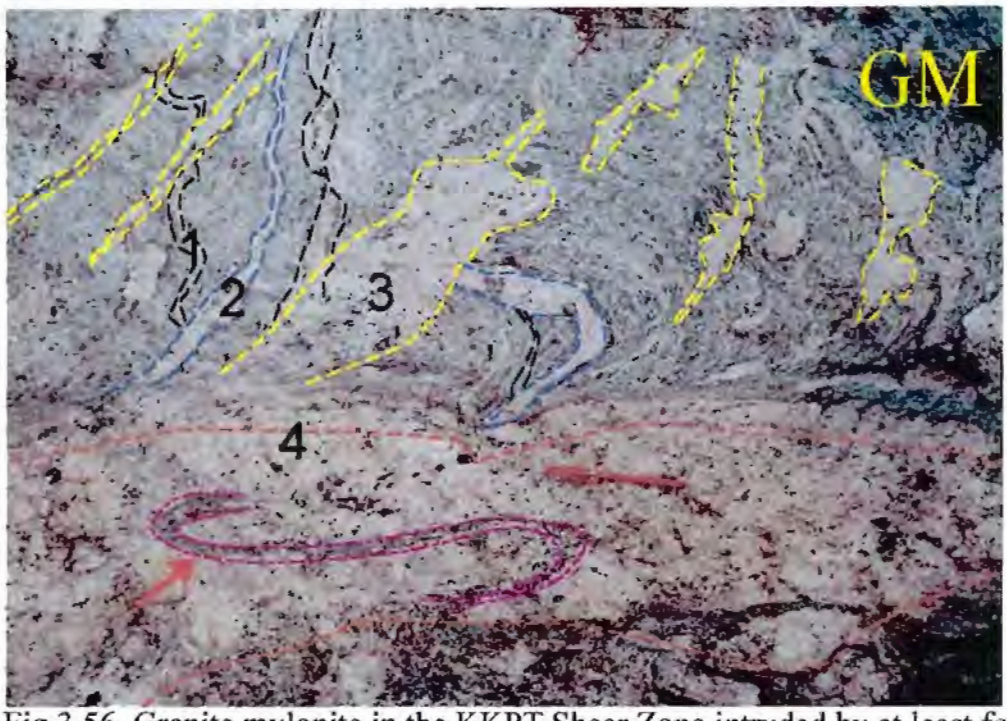

Fig.3.56. Granite mylonite in the KKPT Shear Zone intruded by at least four different granite phases (marked by different colors). Early shears (along Type 3 granites) have dextral sense of movement. A granite sample dated from a nearby area (S-415; Fig. 3.57) corresponds to type 1 or type 2 granite in this outcrop. Mafic clots within the youngest granite type (4) are folded (marked by red arrow). Location, Mamalakandu village, 35 km east of Kotamangalam.

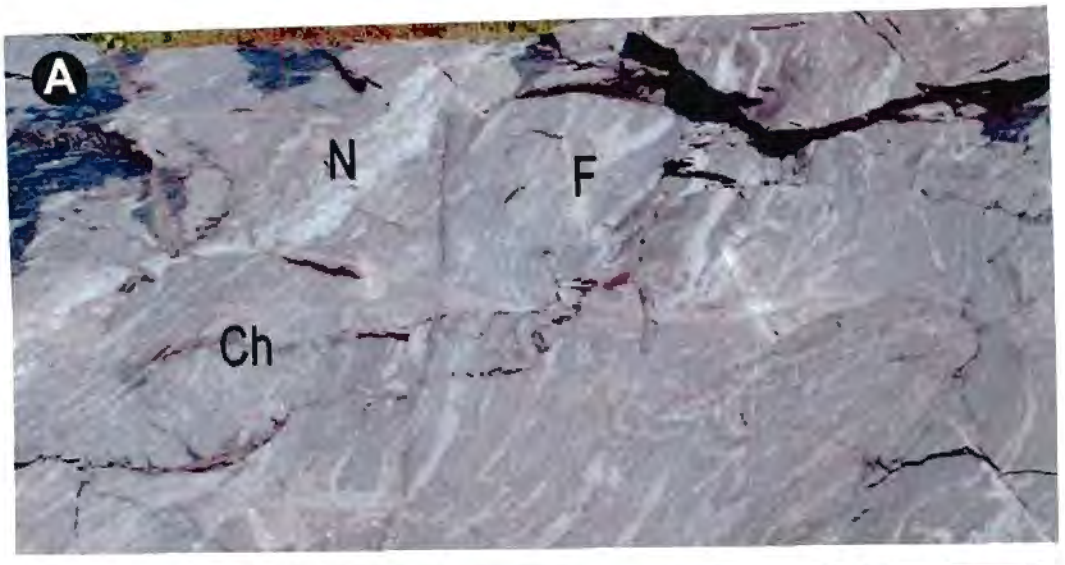

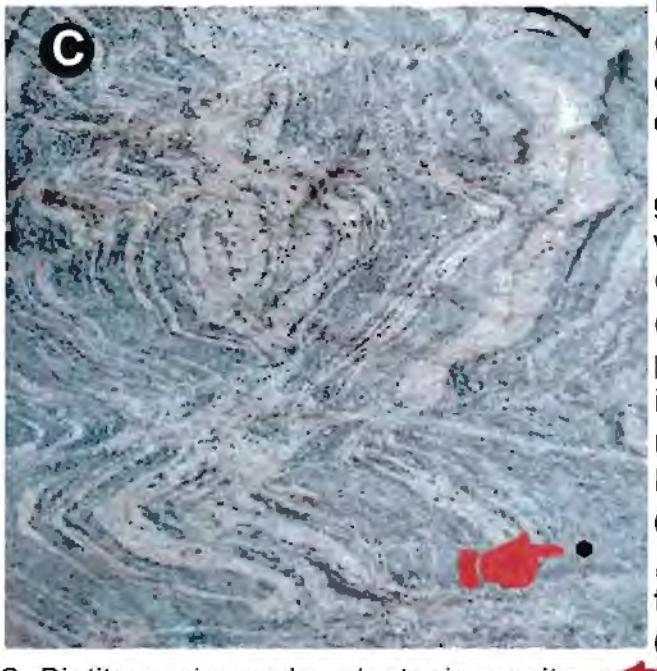

Fig.3.57.Biotite gneiss and (syntectonic) granites in a quarry near Tallakod, ~30 east of Kotamangalam.
A. Both biotite gneiss and granite are partially or wholly charnockitized (Ch). Granite occur as folded (F) or non-folded (N) veins, probably depending on their initial orientation viz a viz the regional strain orientation.
B. Partially charnockitized (Ch) folded granite vein. , sample (S-415) location for U-Pb geochronology. (age, 568 ± 2 Ma)
C. Biotite gneiss and syntectonic granite. , sample (S-416) location for U-Pb geochronology (age, 2511±17 Ma).

in the northeastern part, quartzite bands show complex refolding of early tight to isoclinal folds of variable trends by late tight NNW-SSE trending folds. The northern part of the KKPT Shear Zone comprises broad open folds that belong to the structures seen in the Dharwar craton. Because of this structural distinction and difference in the lithological association across the KKPT Shear Zone, it is possible that KKPT Shear Zone is a major shear zone separating two different types of terranes in the SGT. Three traverses were taken across this shear zone in the area east of Kotamangalam (Fig. 3.1). Granite gneiss within the shear zone is mylonitized and is intruded by granites of more than one generation (Fig. 3.55, 3.56). Mylonitic fabric has NW-SE strike and subvertical dips. Granite mylonite, biotite granite, and granites within the KKPT Shear Zone are charnockitized (Fig. 3.55). Within the charnockite patches, mylonites are recrystallized into massive charnockite (Fig. 3.55; 3.57A). Since most of the KKPT Shear Zone is underlain by charnockites, it is likely that the mylonites associated with the KKPT Shear Zone are converted to massive charnockites

3.3.4. Geochronology

A number of rock types from the Madurai Block have been dated in the present investigation. Granite gneiss from the Kotamangalam falling within the KKPT Shear Zone has been dated at 2511 ± 17 Ma, while a syntectonic granite has been dated at 568±2 Ma (Chapter 5). The Oddhanchatram anorthosite massif, which is NE-SW trending body and lies close to the KKPT Shear Zone, has also been dated at 563 ± 9 Ma (Chapter 4). These data suggest a major period of movement along the KKPT Shear Zone at about 560-570 Ma. Since patchy charnockites have been superposed on syntectonic granite, and have obliterated the mylonitic fabric along the KKPT Shear Zone, charnockitization is post-tectonic in nature and is younger than 560-570 Ma granites.

Monazite from a khondalite sample from eastern part of the Madurai Block has been dated at 791 ± 17 Ma which is interpreted as the age of the high-grade metamorphism in the area.

Zircons from a charnockite gneiss sample, also from eastern part of the Madurai Block, have been dated at 796 ± 1 Ma which interpreted as its protolith age. Thus ~790-800 Ma represents the latest high-grade metamorphism and a period of granitic magmatism in the eastern part of the Madurai Block.

3.3.5. Summary

The Madurai Block is dominated by paragneisses, metasediments and their charnockitized equivalent rocks. The ~2.5 Ga granitic gneiss, that continues from the southern part of the Dharwar craton that has been recorded to continue as far south as the PCSZ, also continues at least as far south as the Kotamangalam area. A major lithological and structural discontinuity exists in the Madurai Block along the the newly defined KKPT Shear Zone. The KKPT Shear Zone was formed or reactivated in a period between 560 and 570 Ma. The latest high-grade metamorphism and a period of granitic magmatism in the eastern part of the Madurai Block occurred between 790 and 800 Ma. This suggests that the ~550 Ma granulite metamorphism, which has been recorded in the Kerala Khondalite Belt, may not have affected the eastern part of the Madurai Block.

3.4. The Trivandrum Block and the Achankovil Shear Zone

3.4.1. Introduction

The southern margin of the Madurai Block is placed along the NW-SE trending Achankovil Lineament, which marks the southern margin of the Cardamom Hill charnockite massif (Fig. 1.6). The area south of the Achankovil Lineament is dominated by khondalite and related metasedimentary rocks and is popularly known as the Kerala Khondalite Belt (KKB), which Harris and Santosh (1993) named as the Trivandrum Block following their interpretation that the Achankovil Lineament marks a tectonic boundary between two blocks. The Trivandrum

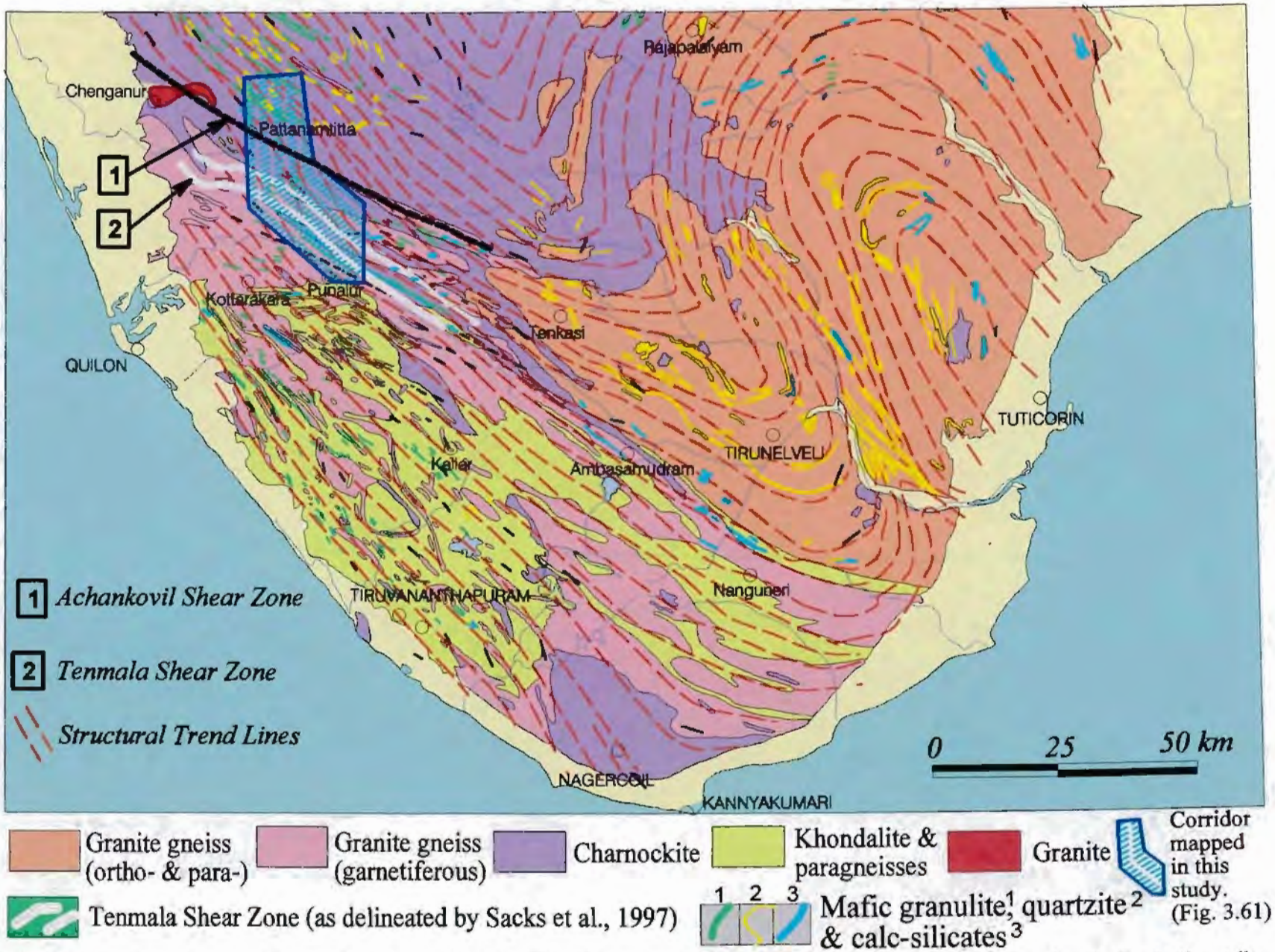

Fig.3.60. Geological map of the southern tip of the Indian Peninsula (modified after GSI, 1995) showing regional variation in the strike of various lithological units across the Achankovil Lineament. The studied PPP Corridor is outlined in blue line.

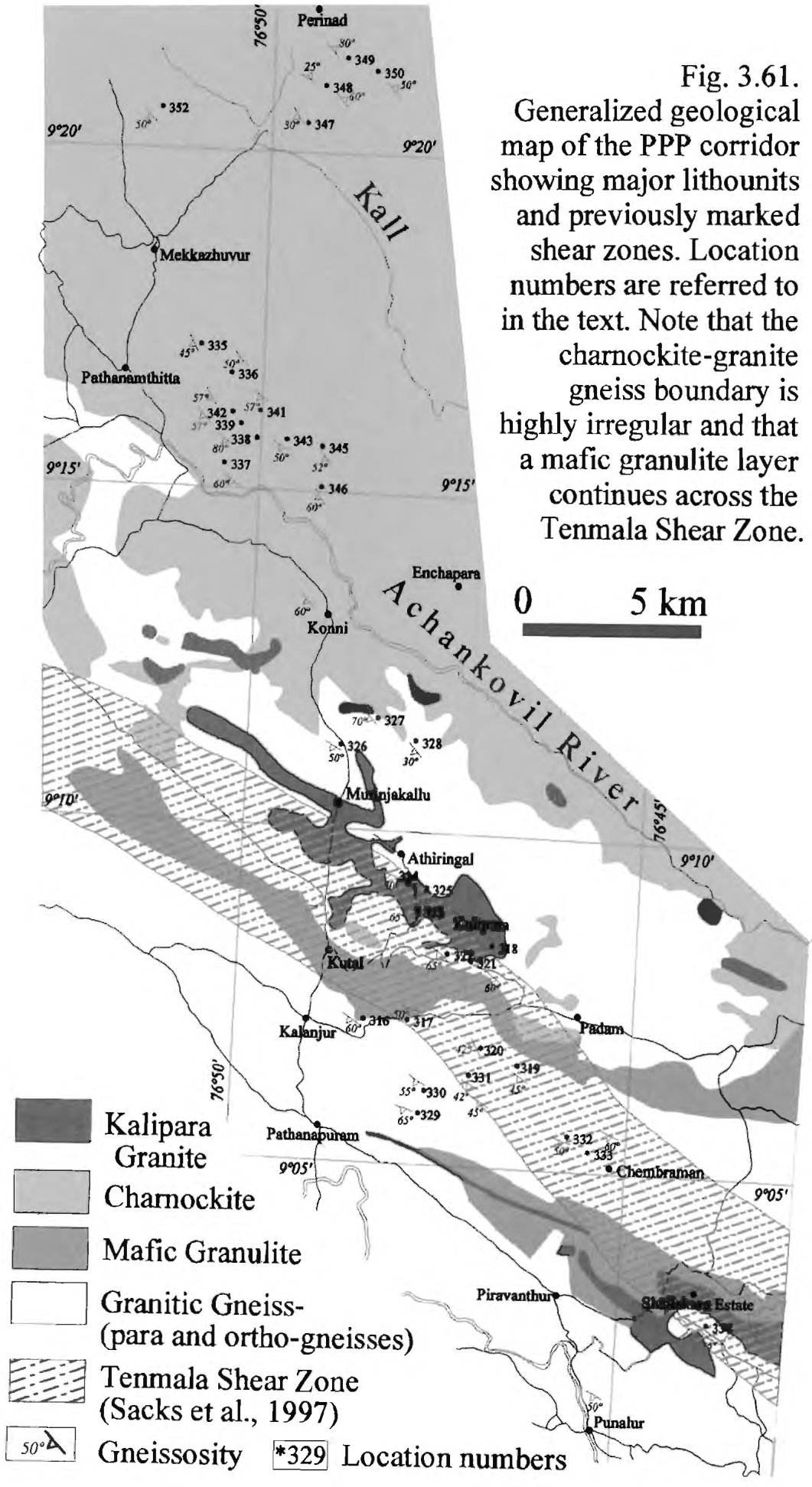

Fig. 3.61. Generalized geological map of the PPP corridor showing major lithounits and previously marked shear zones. Location numbers are referred to in the text. Note that the charnockite-granite gneiss boundary is highly irregular and that a mafic granulite layer continues across the Tenmala Shear Zone.

Block has been interpreted as having NW-SE structural trend as against N-S trend of the Madurai Block (Drury and Holt, 1980). The discordance in the imagery-interpreted structural trends between the Madurai Block and the Trivandrum Block has been explained by hypothesizing a major shear zone (the Achankovil Shear Zone, ASZ) with significant sinistral strike-slip movement along the Achankovil lineament. The Achankovil Lineament is prominent in the northwestern part along the southern edge of the Cardamom Hills charnockite massif. In the southeast, the lineament is not well developed However, the Achankovil Shear Zone has been hypothesized to have extended right up to the southeastern coast of the Peninsula. Since proposed, there has been very little structural work on this shear zone. Limited available field observations by Sinha Roy et al. (1984) and Radhakrishna et al. (1990) have questioned the presence of a shear zone along the Achankovil Lineament. Recently Sacks et al. (1997) have proposed an alternate position for a major shear zone with dextral strike-slip movement along the Tenmala Lineament, which marks the southern margin of the Achankovil shear zone. This shear zone is known as the Tenmala Shear Zone (Chacko et al. 1987; Ramakrishnan, 1993; GSI, 1995).

3.4.2. Geology of the Perinad-Pattanamitta-Punalur (PPP) corridor

3.4.2.1. Introduction

During the present study a ~10 km wide NW-SE trending corridor across the Achankovil and Tenmala lineaments covering parts of KKB and Cardamom Hill charnockite massif has been mapped on scale 1:50,000 (Fig. 3.60). The corridor passes through Perinad in the north, Pattanamitta in the centre and Punalur in the south (Fig. 3.61; henceforth referred as PPP Corridor). The southern part of PPP corridor falls within the KKB, while the northern part of it falls within the Cardamam Hills charnockite massif. A number of quarry sections in the area were studied in detail with the aim to understanding nature of the charnockite-granite gneiss transition and to examine the inferred shear zones. One aim was to understand the sequence of

geological events in SGT, and especially any possible contrast in the evolutionary history between the Kerala Khondalite Belt and the Cardamom Hill Massif. U-Pb zircon and monazite dating of selected samples were carried out to constrain the deformation and metamorphic events.

3.4.2.2. Lithology of PPP Corridor

The major lithologic units of the PPB corridor are charnockitized and non-charnockitized lithologic assemblages of leptynitic garnet-biotite gneiss, khondalite and cordierite-gneiss, with minor mafic granulite, calc-silicate, quartzite, and massive granite. All these lithologic units have undergone charnockitization to varying degree and intensity, resulting in extensive occurrence of various types of charnockites: unfoliated, gneissic and incipient charnockites are widely distributed throughout the PPP. Thus charnockites within various parts of the PPP corridor include charnockitized equivalents of khondalite, garnet biotite gneiss, cordierite gneiss and massive granite. All these rocks are cut by the granitic pegmatite.

3.4.2.2.1. Lithological descriptions

Garnetiferous quartz biotite gneiss: The most common rock type in the KKB is garnetiferous quartz biotite gneiss (GQBG). The rock contains irregular veins of quartz and feldspar (QFV) with variable amounts of biotite and garnet. Garnet has grown after the development of QFVs and is thus post-tectonic (Fig. 3.62). An earlier generation of garnet has been suggested by others (Sacks et al. 1997). Common accessory minerals in GQBG are graphite, zircon and apatite.

Khondalite: Khondalite is a name given by Walker (1902) after the Khond tribe which inhabited the state of Orissa, India, for a para-schist and para-gneiss sequence dominated by garnetiferous quartz-sillimanite rocks. In the KKB the mineralogy of khondalite is quartz-

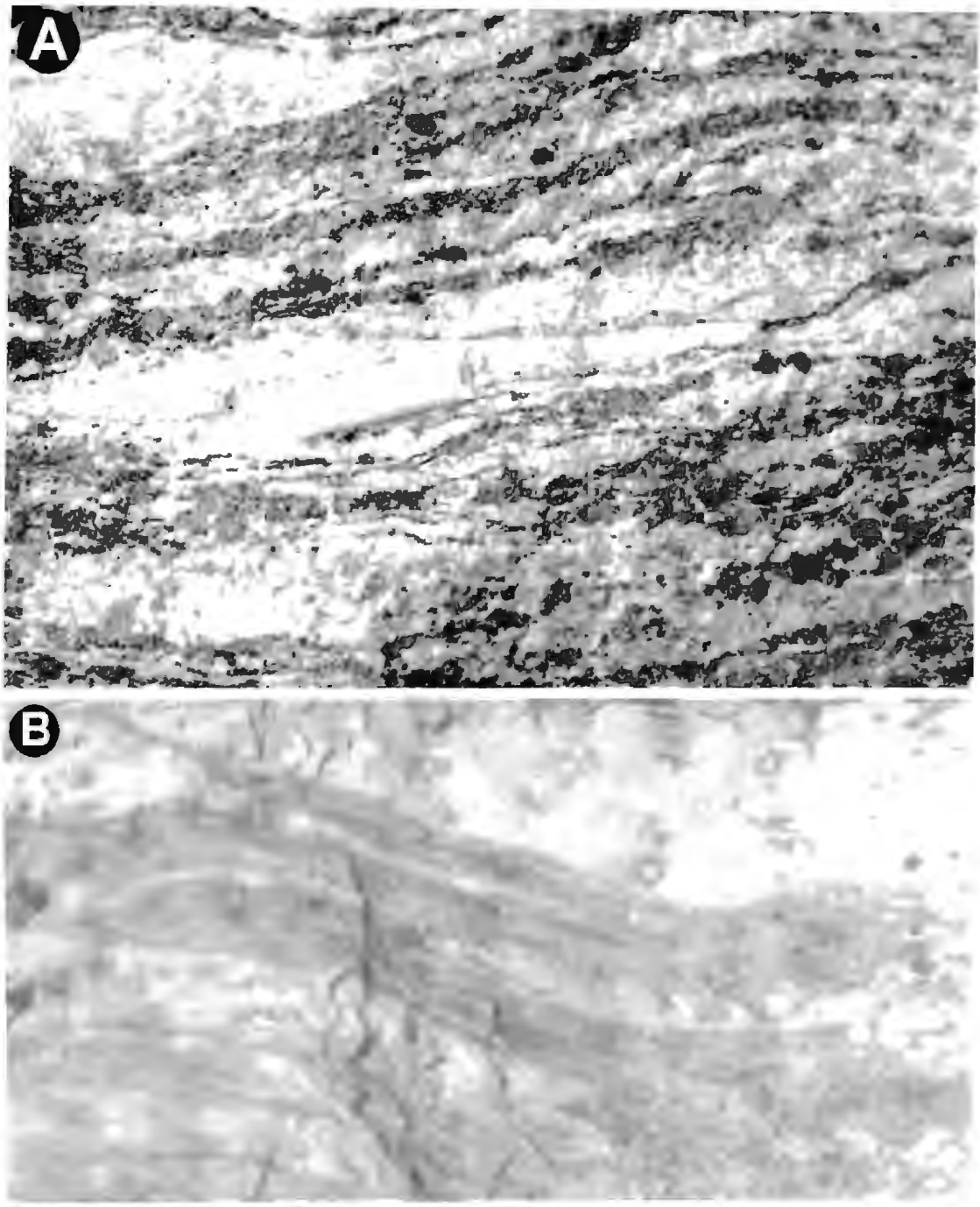

Fig. 3.62. Quartzo-feldspathic veins (QFVs) within garnet-biotite gneiss and khondalite in the KKB. Location numbers refer to Fig. 3.61
A. Dense subparallel intrusion of QFVs within garnet-biotite gneiss. Note that equant garnets cut across the margins of the QFVs and the gneissosity (location, 320, Fig., 3.61).
B. QFVs coaleses to form thick veins (upto several metres) alternating with khondalite (location 333)
C. QFVs both parallel and at high angle to the gneissosity in the garnet-biotite gneiss (location 319).

biotite-garnet-K-feldspar-graphite ± cordierite ± rutile.

Cordierite gneiss contains cordierite-garnet-plagioclase-quartz-biotite as the major mineral assemblage. In places, it may also contain hypersthene or sillimanite. Although cordierite is present in almost all rock types of KKB, there is a discontinuous and wide zone (~10 km) of cordierite gneiss spatially associated with the Achankovil Lineament (Sinha-Roy et al. 1984; Santosh, 1987) . It is believed that the cordierite-producing reaction was caused by isothermal decrease of pressure during uplift (Chacko et al. 1987; Santosh, 1987). The cordierite producing reactions are also believed to be dehydration reactions (Santosh, 1996) which are:

(i) Biotite + Garnet + Quartz = Orthopyroxene + Cordierite + K-feldspar + H_2O

(ii) Garnet + Quartz = Cordierite + Orthopyroxene

Cordierite development in charnockite is mainly controlled by bulk composition, where Mg/Fe ratio is high. Santosh et al. (1993) calculated P-T conditions of 4.2 ± 1.2 kbar and 753 ± 32°C for the cordierite-orthopyroxene reaction.

Leptynites are garnetiferous quartzo-felspathic gneisses with or without biotite (generally less than 10%). They occur as elongate (up to tens of metres in length) layers or lenses along the foliation of the gneisses. Leptynites may represent original arenite/arkose layers intercalated with pelites. They may also represent metamorphosed quartzo-felspathic veins (QFVs).

Granite: Other than the ubiquitous granitic gneisses and the charnockitized gneisses that occur throughout the region, there are a number of isolated massive, non-foliated granite bodies that have intruded gneisses. These bodies are mostly elongate in shape and are emplaced subparallel to the regional trend of the foliation. Two types of intrusive granitic rocks are present: (i) medium grained mesocratic biotite-bearing granite which occurs as long bodies up to several km in length; and (ii) coarse biotite-bearing pegmatitic-granite. While the massive granite bodies have been charnockitized in many places, the pegmatitic granitic veins have, in turn, bleached (retrograded) the charnockites (Fig. 2.12). This difference in their

relative emplacement ages has been corroborated by U-Pb zircon dating of these two types of rocks from Nirettipara quarry (location 318) where they occur close together. The massive granite is found to be ~550 Ma and the pegmatitic granite is ~530 Ma (see Chapter-4). The massive biotite- bearing granites are best exposed around Kalipara, ~6 km NE of Kalanjur (Fig. 3.61) Accordingly this granite is, hereafter, referred to as the Kalipara Granite. The Kalipara Granite is the youngest magmatic body that has been affected by charnockitization

3.4.2.2.2. Intrusion of Kalipara granite and later granites

In the central part of the PPP corridor, in a number of isolated areas, massive Kalipara-type biotite-granite has intruded the gneisses. It shows crosscutting relationships with the S_2 and is thus younger than D_2 deformation event. These granites do not have any planar penetrative fabric. In places, veins of Kalipara-type are tightly folded by D_3 folds (Fig. 3 63) suggesting that they could be pre- or syn-D_3. Intrusion of the Kalipara Granite was followed by widespread development of charnockitization in the area. Charnockitization in the Kalipara Granite is present in various stages of development. The Kalipara Granite is the youngest intrusive rock which is charnockitized. It is intruded by a number of bronze coloured, biotite-bearing granitic and pegmatitic veins. These veins are present only locally and are a few cm to a few metre thick. Wherever these veins have intruded charnockitized parts of the host rocks, there are a selvage of retrogressed charnockites around them (Fig. 2.12). Such retrogression might have caused by H_2O-rich fluids associated with such granitic veins (Srikantappa et al 1985; Ravindra Kumar and Chacko, 1986)

3.4.2.3. Charnockitization in PPP Corridor

Charnockitization is more pervasive and intense in the northern part of the area adjacent to the continuation of the Cardamom Hill Massif. Here, near complete transformation of metasediments and granitic gneisses to charnockites has given rise to vast expanses of massive

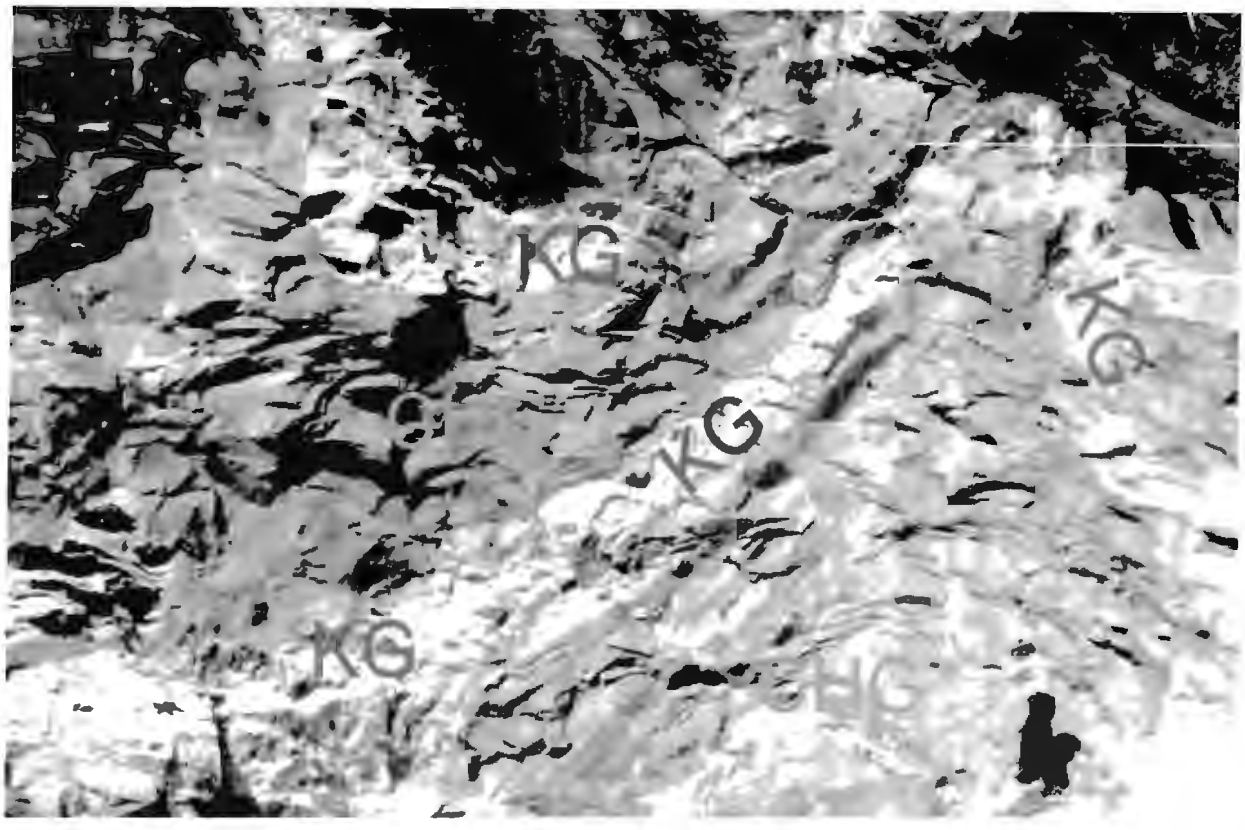

Fig. 3.63. Open F_3 folding of the Kalipara Granite (KG) dyke within charnockite gneiss (CHG). A man standing in the lower right part for scale (Location, 326 in Fig. 3.61)

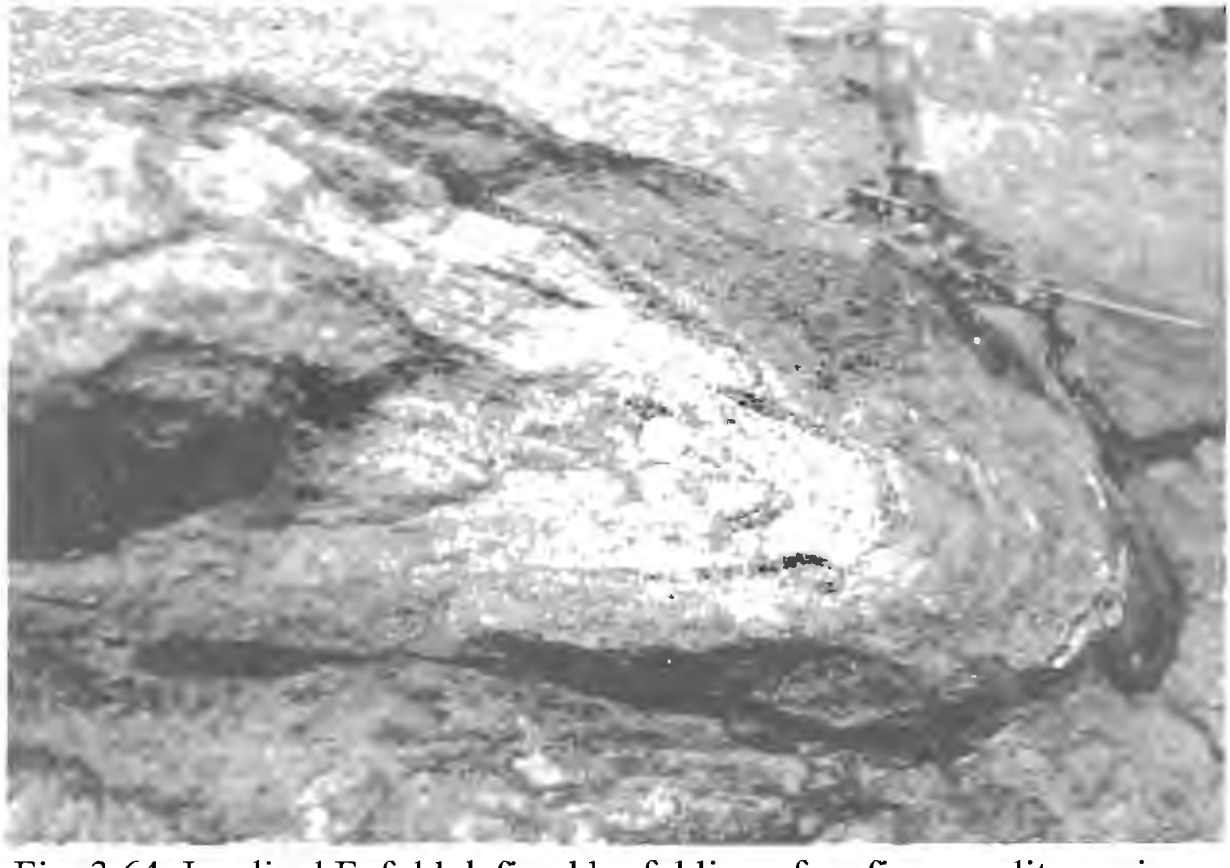

Fig. 3.64. Isoclinal F_1 fold defined by folding of mafic granulite gneiss. Plan view. Axis of the fold is subvertical. Coin for scale in the center is 2 cm in diameter. Location S-323 (Fig. 3.61).

charnockite. Charnockite of the Cardamom Hill Massif is often regarded as magmatic charnockite on the basis of its geochemical signature and high (~1000°C -1100°C) estimates of paleo-temperature using the Al-based geothermometry (Chacko et al. 1987; Chacko et al. 1996). In the southern part of the PPP corridor, charnockites occur as isolated bodies within khondalite metasediments (Fig. 3.61) and are regarded as the product of metasomatic alteration of pre-existing rock types (Srikantappa et al. 1985; Ravindra Kumar and Chacko, 1986; Harris and Bickle, 1989; and Santosh, 1992). In this area paleo-temperature estimates on charnockites of the KKB range between ~700°C and 950°C, with a very broad increase in temperature estimates towards the Achankovil lineament. The paleo-pressure estimates are between 4 and 6 kb.

During the present study, destruction of original planar fabric of the rock through recrystallization of pre-existing granites and gneisses during charnockitization was observed in both northern and southern part of the corridor. In gneisses, the gneissose layering can be recognised in the charnockitized part in continuity with the gneissose layering in the non-charnockitized gneisses (Fig. 2.9, 2.3). Although charnockite gneisses of the northern part of the area is generally regarded as magmatic charnockites (Chacko et al. 1997, Santosh, 1996), intrusive relationship between charnockite gneiss and non-charnockitized parts could not be observed. In places, however, original intrusive relationships between late Kalipara-type granites and paragneisses are preserved in the charnockitized parts also (Fig. 2.7). Thus presence of C-type (C denotes charnockite) magma as proposed for the Cardamom Hill charnockites (Chacko et al. 1996, Santosh, 1996) cannot be supported on the basis of field observations. The higher temperature estimates in the Cardamom Hill area than in the Trivandrum Block as recorded by Chacko et al. (1996) are likely to be the reflection of more pervasive charnockitization in the area.

3.4.2.4. Migmatization in the PPP Corridor

The most conspicuous feature of the PPP corridor is the extensive migmatisation of various lithologic units. Almost all the rock types have been densely intruded by pale grey colored quartzofelspathic veins (hereafter referred as QFV) containing quartz, alkali feldspar and biotite, with QFV, often comprising up to half of the rock volume. These veins are commonly a few cm in width, but locally they coalesce into pods and dyke upto a metre or two thick. They have intruded sub-parallel to the pre-existing fabric but locally cross-cut this fabric at high angle (Fig. 3.62; 3.65a). Whether the QFVs represent leucosome melts as a result of in situ melting or subparallel dense intrusion of allochthonous granitic melt is not clear. Biotite rich pods and layers are often interpreted as melanosome restites. In many places they are found to be alteration products of mafic granulite bands or pods (Fig. 3.65b). Subparallel impregnation of pre-existing rocks by QFV throughout KKB has given rise to prominent gneissic banding in almost all the rock types except the mafic granulites in which the QFV impregnation is less conspicuous.

The subparallel orientation of the mafic granulites and adjacent garnetiferous quartz-biotite gneiss (QBG), and the absence of clear-cut cross-cutting relationship between them are often cited as evidence of sedimentary origin of mafic granulite (original Fe-Mg rich sediments) and adjacent quartz-biotite gneiss (original arkosic sediments; e.g., Chacko et al. 1992). However, such subparallelism of the QBG and mafic granulites can also be explained by an early folding and flattening of the sequence. Subsequently subparallel impregnation of the whole sequence by QFVs resulted in the development of prominent gneissosity in the QBG and alteration of the mafic granulites along the margins into biotite-rich quartzofelspathic gneiss. Such marginal alteration of the mafic granulite bands has caused gradational contacts between mafic granulites and QBGs (Fig. 3.65b). The conspicuous gneissosity present in different rock types of the KKB may thus be the result of preferential emplacement of granitic veins subparallel to a preexisting anisotropy in various rock types; this could explain absence of any obvious

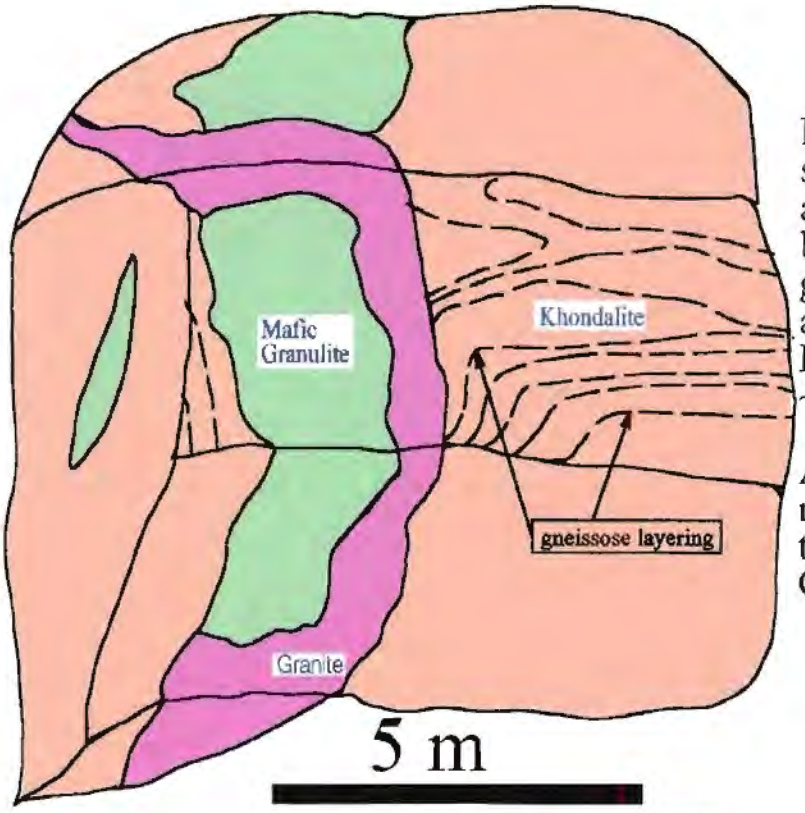

Fig. 3.65. Field sketches showing inter-relationships among khondalite, garnet biotite gniess, massive granite (Kalipara Granite) and mafic granulite. Location, Kanamukku quarry, ~8 km NW of Pattanammitta.

A. Khondalite is intruded by mafic granulite which in turn is intruded by Kalipara Granite (massive).

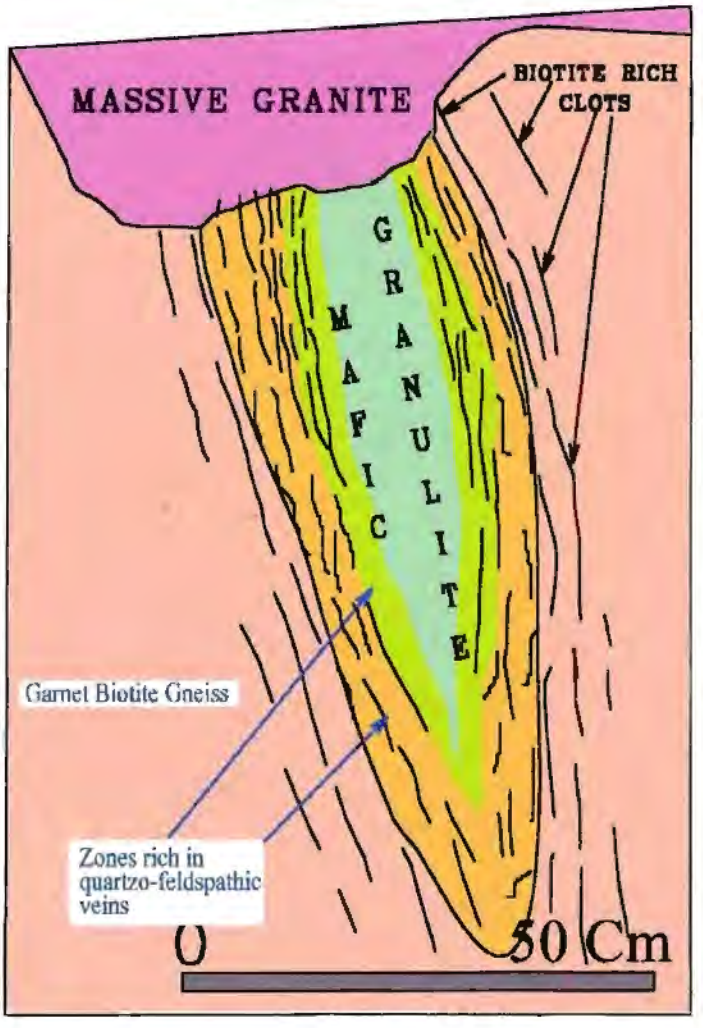

B. A patch of Mafic granulite emplaced sub-parallel to the gneissosity of garnet-biotite gneiss. Margins of mafic granulite are extensively densely intruded by quartzo-feldspathic veins. Along margins mafic granulites are altered to migmatitic rocks and have subparallell alignment of biotite clots in them. Such alteration along margins often make it difficult to study their contact relationships.

crosscutting relationship between QBG and mafic granulite bands.

Rocks unaffected by QFVs are uncommon. Where present, they allow identification of original rock types. Thus locations 319 and 320 in Fig. 3.61 expose weakly schistose granite. Because of the rarity of such exposures, however, it is difficult to identify the original protoliths of various quartzo-felspathic gneisses in most outcrops.

3.4.2.5. Stratigraphy and nature of the protolith of gneissic rocks of the KKB

The stratigraphic relationship and nature of the protolith of various gneissic rocks of the KKB are not well understood. Many workers (Srikantappa et al. 1985; Ravindra Kumar and Chacko, 1986; Chacko et al. 1987; Hansen et al. 1987) hold the view that the various lithologic units of the KKB are of sedimentary origin because they are interlayered and contacts between them show no obvious intrusive or tectonic relationships. Abundance of graphite (≈1%) in the leptynite-khondalite rocks is taken as an additional evidence of sedimentary origin. Whole rock or trace element geochemistry on various gneissic rocks of the KKB have been used to discriminate between various types sedimentary protoliths for different gneissic rocks of the KKB on the assumptions that they represent metasedimentary rocks (Srikantappa et al. 1985; Chacko et al. 1987, 1992). It is generally inferred on the basis of these geochemical analyses that the leptynitic rocks represent arkosic metasediments while khondalitic gneisses represent pelites (Chacko et al. 1987, 1992; Srikantappa et al. 1985). However, none of these analyses unequivocally discriminate between a magmatic or sedimentary protolith. Instead, relative consistency in K/Na ratio over wide area (Chacko et al. 1988) and very tight clustering of the analyses of leptynites (Srikantappa et al. 1985) may be suggestive of magmatic origin of majority of these gneissic rocks of KKB.

Carbon isotope ratios of the disseminated graphite in Khondalite and potassic garnet-biotite gneisses from southern Kerala ($\delta^{13}C$ -34‰ to -17‰) broadly corresponds to a sedimentary-

biogenic origin (Soman et al. 1986, Klatt et al. 1988; Jackson et al. 1988, Wada and Santosh, 1993), which generally varies between -32‰ and -25‰. It is argued that the positive shift in isotope ratios are very likely in part due to the higher grade of metamorphism (Valley, 1986) and in part due to participation of magmatic carbon in graphite genesis. The origin of graphite through reduction of carbonate phases and through recycling of the biogenic sediments through melting cannot be ruled out. $\delta^{13}C$ in graphites of pegmatite of Kerala is around -12.5‰ (Soman, 1986). Such graphite could have been formed during reduction of CO_2 by H_2.

Elevated $\delta^{18}O$ values (9.3-10.6‰) of the most dominant of the gneissic rocks, garnet biotite gneiss, is also cited as evidence for their sedimentary origin (Chacko et al. 1988). But these values are not unusual for magmatic rocks.

On the basis of the major and trace element data, Chacko et al. (1992) suggested that massif charnockite of the Cardamom Hill Massif constituted the main source of the metasediments of the KKB. However, this hypothesis is based on the assumption that the charnockites of CHM are magmatic, which is not proven. Since charnockites of the CHM are of metasomatic origin (Chapter 2), it is likely that protolith of these charnockites are continuous with the (para-)gneisses of the KKB.

3.4.2.6. Structure and metamorphism

There has been very little structural work in the Kerala Khondalite Belt. Yoshida and Santosh (1987) and Radhakrishna et al. (1990) have described local structural features while Sinha Roy et al. (1993) reviewed the regional structural geometry of KKB. Recently Sacks et al.(1997) recorded their observations on features of Tenmala Shear Zone.

All the rock types of the area, except the Kalipara Granite and younger granites, show pervasive development of schistosity and gneissosity. Schistosity is defined by subparallel

planar alignment of biotite flakes, hornblende and ellipsoidal quartzo-felspathic minerals. Two kinds of gneissosity are recognised in the area. The earlier one (Gn_1) is defined by regular alternation of mafic-rich and mafic-poor minerals layers (few mm to few cm thick). In mafic the granulites this gneissosity is represented by an alternation of garnet-rich and garnet-poor layers. The second kind of gneissosity (Gn2) comprises dense subparallel QFV layering in a variety of lithologic units of the area. This kind of gneissosity may be called migmatitic banding. However, whether they represent migmatitic banding, partial melt veins or impregnation by allochthonous melts is not clear. Distinction between the two types of gneissosity is often difficult. However, the later impregnated QFVs are generally of uneven thickness and also often merge into pod and lenses, which helps their distinction from earlier gneissosity, which is generally very regular.

The earliest deformational structure present in the area is the Gn1 gneissosity in the mafic granulites and in the garnetiferous quartz biotite-gneiss. These structures have been recorded as D_1 structures (Radhakrishna et al. 1990; Sinha Roy et al. 1984). Radhakrishna et al. (1990) inferred that this deformation event was accompanied by regional high grade metamorphism, resulting in the development of sillimanite gneisses and other high-grade rocks. Isoclinal and tight folds of Gn1 gneissosity have been ascribed to a second, D_2 deformation (Sinha Roy et al. 1984 and by Radhakrishna et al. 1990). Yoshida and Santosh (1987) mentioned two more deformation events, which they termed D_3a and D_3b. Although Radhakrishna et al. (1990) and Sinha Roy et al. (1984) mentioned the presence of sporadic development of intrafolial isoclinal folds in the garnet biotite gneiss in different parts of the Kerala Khondalite Belt, such folds were not observed in the present area. Possibly, traces of earlier mesoscopic folds have been obliterated by later pervasive QFVs and development of Gn2. Yoshida and Santosh (1987) mentioned cross-cutting relationships between folds associated with D_2 deformation and the Gn2. Isoclinal fold associated with D_2 deformation are, however, common in the mafic granulite bands, where they have folded Gn1 gneissosity. These folds have NW-SE trends with subvertical axial planes and steep but variable plunges. In some quarries (for example, the

Kunnanpara quarry reported by Yoshida and Santosh, 1987) mafic granulite bands outline mesoscopic folds. D_2 deformation was followed by pervasive intrusion of various lithologic units by QFVs. Subparallel dense intrusion of the lithologic units by QFVs following earlier deformation fabric of the rocks has given rise to Gn2 gneissosity. Sinha-Roy (1979) believes that migmatitic banding and mafic granulite have been subjected to isoclinal folding, which resulted in the dominant NW-SE trend of the gneissic foliation in KKB. Santosh (1996) also reports the presence of augen structure in garnet-biotite gneiss defined by subparallel alignment of large feldspar crystals in the QFVs. However QFVs lack development of any post-emplacement penetrative planar fabric. Subparalle alignment of feldspar megacrysts in the QFVs have been interpreted by some workers as augen structures. But they have sharp crystal boundaries, without any evidence of marginal granulation or recrystallization. As such there is no evidence to indicate that such subparallel alignment is the result of flattening in the rock; on the contrary this is probably an inherited feature.

In a few quarry sections the migmatitic gneissic rocks delineate broad large scale folds with N-S axial trends. These large scale broad folds have been designated by Sinha Roy et al. (1984) as D_3 folds and by Yoshida and Santosh (1987) as D_4 folds. Sinha Roy et al. (1987) regarded that this D_3 event is responsible for the regional NW-SE orientation of the various lithologic units of the area. In the PPP corridor it is observed that D_3 fold are only locally developed and have curvilinear axial traces. There is no axial planar penetrative fabric associated with D_3 folds. It appears more likely that D_3 folds have caused local variation in the trends of various lithologic units and that the regional NW-SE trend of the lithologic units of the Kerala Khondalite Belt are related to D_1 and D_2 deformation events.

3.4.3. Status of Achankovil or Tenmala shear zones

A major shear zone of about 10 km wide following the Achankovil lineament has been proposed by Drury et al. (1980). The main arguments in favour of existence of this shear zone

had been (i) the contrast in the trend of the lithologic units on northeastern and southwestern side of the lineament as observed in satellite imagery, the northern side shows a dominantly N-S trend while the southern side shows dominantly NW-SE trend. (ii) The contrast in the litho-assemblage, the northeastern side being dominated by massive charnockite, while the southwestern side is dominated by an assemblage of charnockite and metapelites. (iii) The contrast in attitude of various lithologic units. Lithologic units of the northern side were interpreted to have subvertical to steep dips while the southwestern side has shallow plunging beds.

In the present study none of the above criteria have been found to be ubiquitous. The lineaments as expressed in the satellite imageries are determined by the distribution charnockites (which form positive geomorphic features) and granitic gneisses (which generally form negative geomorphic features). Since charnockite-granite gneiss boundaries are metasomatic boundaries that may not have tectonic significance, such lineaments identified in satellite imageries may also not have tectonic significance, but merely enhance lithological boundaries. Geological maps of the area clearly show that in many places (e.g., in the area north of Rajampalayam, see geological map in the pouch) quartzite and other metasedimentary bands are at a high angle to the charnockite-granite gneiss contacts. Thus trends of lineaments interpreted from satellite imagery do not necessarily correspond with tectonic trends.

The contrast in the lithologic assemblagebetween the northeastern and southwestern sides of the lineaments is also proposed to be an artifact of the process of charnockitization rather than a difference in their original tectono-stratigraphic makeup. In the present work, similar lithologic assemblages have been noticed on either side of the lineament. The only difference between these two sides of the lineament is the difference in the degree of charnockitization. The extent of charnockitization in the northeastern part of the lineament is greater than that in the southeastern part. Fig.3.61 clearly shows that the boundary between the massive charnockite and the non-charnockitized areas is highly irregular, cutting across the structural

trends of the host lithologic units. Regional charnockitization is clearly a post-tectonic (post D_3) phenomenon superimposed on the regional structural trend of the rocks.

The present work shows (Fig. 3.61) that there is no perceptible variation in the dips of various lithologic units in the northeastern and southwestern sides of the lineament. The interpretation of Drury et al. (1984) that the southern part of the lineament is dominated by shallow dipping litho-units was not found to be true.

Sacks et al. (1997) have reported field features suggestive of dextral strike-slip movement along the Tenmala Shear Zone, (a shear zone lying about 15 km south of and subparallel to the Achankovil lineament). On the contrary, Rajesh et al. (1998), from the same area, reported field features indicating sinistral sense of shear movement. Kinematic indicators like stretched and asymmetric porphyroblast, shear bands, asymmetric folds, rolling structure (cf., Van Den Driessche, 1986) have been reported by both Sacks et al. (1997) and Rajesh et al. (1998).

My field observations in the PPP corridor, which includes areas studied by Sacks et al. (1997) and Rajesh et al. (1998) could not, however, confirm the presence of any consistent shear sense indicators in either the Achankovil or the Tenmala shear zones. Shear bands (Fig. 2.7) and asymmetric folds have been observed in some isolated exposures; but these could not be related to any consistent shearing movement along the Achankovil Lineament. Pervasive dense intrusion of the QFVs within pre-existing gneissic rocks have obliterated and modified the majority of the minor structural features that might have been present in the pre-existing rocks. Nowhere do QFVs show any penetrative planar fabric. The majority of the garnets present in the gneisses are post-tectonic and do not show any evidence of deformation (neither in field nor in thin section). Structures similar to the stretched and rotated garnet porphyroblasts were observed in many places. However, such structures are found to be aggregates of undeformed garnet crystals and the shapes of these aggregates vary from place to place. Structures similar

to the rolling structures described by Rajesh et al. (1998) as their principal argument for sinistral shearing movement along the ASZ are the result of irregular shapes of the QFVs within pre-existing gneisses (Fig. 3.62). In the northwestern part of the Tenmala Shear Zone (location 353, Fig.3.61) the rocks were found to be totally recrystallized, and kinematic indicators as reported by Sacks et al. (1997) could not be found. Thus, while isolated occurrence of shear sense indicators is suggestive of shearing movement, consistency of shear sense (either dextral or sinistral) could not be verified. Any shearing movement that might have been present is pre-Kalipara granite in age since the Kalipara Granite has not suffered any major deformation.

Study of regional structural fabric suggests that the Achankovil Lineament marks the southwestern limb of a regional NW-SE trending fold (Fig. 5.1; Chapter-5) which may explain the presence of localised dextral kinematic sense indicators as reported by Sacks et al. (1997). On the other hand, the presence of a major shear zone, running subparallel to the west coast of India, with sinistral sense of movement is proposed in the present work (Chapter 6). If true, this may explain the localised sinistral kinematic indicators as reported by Rajesh et al. (1998).

3.4.4. Geochronology

Barring some recent Rb-Sr, Sm-Nd whole and mineral isochron data and a few U-Pb zircon age data, geochronological data from the Kerala Khondalite Belt are scarce.

Protolith Ages: There is no reliable age information about the age of the basement or the age of the protolith of the metasediments of the KKB. Odom (1982) reported a U-Pb zircon age of ~2.9 Ga from a charnockite body near Trivandrum. However, the continuity of this rock, and whether the age represents that of the basement or of detritus is not known. Recent attempts to date zircons from khondalite (Soman et al. 1995) and from charnockite gneiss (Buhl, 1987) from the KKB have resulted in highly discordant U-Pb ages, with poorly-defined upper

intercept ages of ~2200 Ma and ~1970 Ma, respectively. Metasediments from the KKB also yielded a poorly defined Rb-Sr whole rock isochron at around 2100 Ma (Chacko et al. 1987). These ages have been interpreted to constrain the minimum age of deposition of the protolith of the paragneisses of KKB to < ~2.0 Ga..

From structural work, the oldest identified magmatic protolith identified is the mafic granulite. This and some granite gneiss xenoliths within the Kalipara granite were analysed for U-Pb zircon dating. Both these rock types have yielded highly discordant zircons and could not provide any meaningful upper intercept ages (Chapter 4). One of the possible reasons for zircon grains being highly discordance is recrystallization of zircons at a later stage, possibly related to Neoproterozoic thermal activity. This aspect has been dealt with in chapter- 4. A few zircon grains from massive charnockite from the Kottaram quarry of the Nagercoil Block yielded a core age, of ~2100 Ma and a rim age of 570 Ma by the SHRIMP method (Chapter 5). Since the protolith of the charnockite is paragneiss, the ~2100 Ma age represents the age of detrital zircon. Thus, with the presently available data it cannot be said whether or not the basement of the KKB is of Archaean age. In other words, it is not known whether Dharwar craton, which extends at least up to the north of the KKPT Shear Zone, includes the KKB.

3.4.5. Ages of metamorphism, charnockitization and other thermal events

The KKB has suffered more than one granulite facies metamorphism. Neoproterozoic granulite facies metamorphism is expressed in the form of extensive charnockitization of various protoliths of the area. An earlier granulite facies metamorphism is suggested by the presence of sillimanite facies khondalite, widespread within the KKB. These khondalite have been charnockitized during a Neoproterozoic event. The age of the earlier granulite facies metamorphism is not clear. A Mesoproterozoic age (~1.8 Ga) age of granulite facies metamorphism has been suggested by laser probe Ar-Ar analysis of the biotite included within garnet from KKB paragneiss, while biotite in the matrix of the same sample gave an ~455 Ma

age corresponding to a cooling age following Neoproterozoic granulite facies metamorphism (Kelly et al. 1997). Indication of ~1.8 Ga granulite facies metamorphism can also be found from one of the Sm-Nd whole rock-garnet age data of Choudhary et al. (1992) from charnockitized paragneiss of the Ponmudi quarry, which suggests ~1793 Ma age and from zircon evaporation age of 1803 ± 15 Ma from khondalite (Bartlett, 1995).

The Neoproterozoic charnockitization event is well documented by a number of recent determinations of Sm-Nd whole rock and mineral isochrons (Choudhary et al. 1992; Unnikrishnan-Warror et al. 1995, 1997; Santosh et al. 1992. These studies variously estimate that the timing of resetting of Sm-Nd systematics in various minerals of charnockites, khondalites and cordierite gneiss ranging between 520 Ma and 560 Ma. This range may indicate that Neoproterozoic charnockitization spanned for a long period, or that the region remained at an elevated temperatures for such a period indicating slow cooling. In the present work the age of Neoproterozoic charnockitization has been more precisely constrained by dating zircons from the Kalipara Granite, which yielded 548 ± 2 Ma, and from pristine pegmatitic granite, which has retrogressed charnockite and yielded 526 ± 2 Ma (Chapter 5). Monazite from a non-charnockitized khondalite enclave within charnockitized massif in the southern part of the Cardamom Hills yielded 524±2 Ma (sample S-355E, chapter 5). This age may reflect a cooling age immediately following charnockitization, since charnockites have been retrogressed by ~530 Ma old granite.

Rb-Sr plagioclase-biotite-whole rock mineral isochrons from two samples in Ponmudi quarry indicate 441 ± 16 Ma and 488 ± 96 Ma, respectively (Buhl, 1983). Khondalites of the KKB have yielded Rb-Sr mineral ages between 473 ± 9 Ma and 467 ± 9 Ma. Immediately north of the Achankovil lineament in the Ottapalam area, a Rb-Sr mineral isochron of charnockite indicates ~500 Ma (Unnikrishnan-Warrior et al. 1995). These ages have been interpreted as the time of cooling and isothermal uplift. Assuming the closure temperature for U-Pb of monazite to be ~750°C (Parrish, 1990) and closure temperature of biotite to be ~320°C

(Dodson, 1979), a cooling rate of ~8°C/Ma can be calculated.

3.5. Conclusion

This chapter dealt with my field observations within some corridors across previously-interpreted major crustal scale shear zones in the Southern Granulite Terrain. The regional structural pattern and role of major shear zones in the SGT are described in Chapter 5. On the basis of present field observations the following inferences can be drawn regarding major shear zones in the SGT.

(i) MSZ, BSZ and PCSZ are subvertical shear zones with predominantly subvertical movement. There is no evidence of significant strike-slip movement on these shear zones. This is corroborated by the fact that Archaean structural grains continue from the Dharwar craton across these major shear zones. Granites syntectonic with respect to movement along these shear zones have been dated at ~600 Ma. Also monazite from quartzite within the MSZ in the Bhavani area is ~610 Ma old. Thus these shear zones were active (either reactivated or were formed) at ~600 Ma.

(ii) A new shear zone, the KKPT Shear Zone, has been identified in the Madurai Block on the basis of study of regional structural pattern (discussed in detail in Chapter 5). The presence of this shear zone has been confirmed by field observation in a part of this shear zone, east of Kotamangalam.

(iii) The existance of the Achankovil Shear Zone along the southwestern margin of the Cardamom Hill Massif could not be confirmed by field observation across the shear zone. The Achankovil lineament marks the boundary between the Cardamom Hill charnockite massif and the khondalite-dominated gneisses of the Kerala Khondalite Belt. This boundary is a metasomatic boundary, younger than post-tectonic Paleozoic charnockitization in the area.

Chapter 4: Geochronology

4.1: Introduction

Modern geochronological techniques include a number of isotopic chronometers based on the decay of radioactive elements incorporated into a rock or its constituent minerals at the time of its crystallization. The radioactive element (known as the parent element) decays into a different element (known as the daughter element). By measuring the amounts of parent and daughter elements, the age of the mineral or rock can be calculated given a known rate of decay. Specific chronometric systems vary in their ability to retain parent and daughter elements in response to new physico-chemical environments that the system undergoes. The temperature below which parent and daughter elements are retained within a mineral or rock is called the closure temperature for that system.

The U-Pb decay system is particularly robust because two different isotopes of U (^{235}U and ^{238}U) decay into two different isotopes of Pb (^{207}Pb and ^{206}Pb, respectively). These two mutually independent decay schemes thus provide an internal check on their parent-daughter ratios. Two commonly used minerals for U-Pb geochronology, zircon and monazite, have the added advantage of high closure temperature with respect to both the parent and daughter elements. Once crystallized, zircon generally is little affected by even severe later thermal events, and retains its crystallization age, although a new generation of the mineral may be grown. On the other hand, monazite is reset at temperatures comparable to that of granulite facies metamorphism (~750°C) and it is also a common new mineral in high-grade metamorphic rocks. For this reason zircon and monazite are valuable minerals in unravelling the tectono-magmatic history in high-grade metamorphic terrains. In the present investigation, therefore, U-Pb dating of zircon and monazite, together with sphene and apatite was carried out on a number of samples from different parts of the SGT in the Peninsular India. A brief

overview of the principles of U-Pb dating of zircon and monazite, and their response to high grade metamorphism is given in Appendix- A.4-I.

4.2. Southern Indian Geochronology

Available geochronological data from the Southern Granulite Terrain (SGT) of India are meagre (Fig. 1.11; Table 1.3 in Chapter 1) but do provide a broad geochronological framework. The protolith ages of some charnockites in the SGT are now known from recent U-Pb zircon and Rb-Sr whole rock studies (Crawford, 1969; Spooner and Fairbairn, 1970; Bühl, 1983, 1987; Peucat et al, 1989, 1993; Jayananda and Peucat, 1995). The northern part of the SGT, from the Krishnagiri-Biligirirangan Hill in the north to as far south as the Nilgiri Hills (Fig. 1.4, 1.11), is mainly underlain by 2.52 Ga old granitic gneiss with some vestiges of > 2.9 Ga old granitic rocks in the Biligirirangan Hill area. High grade metamorphism, deformation and charnockitization in this part of the SGT immediately followed the 2.52 Ga granitic emplacement (Friend and Nutman, 1992, Peucat et al. 1993). South of the Palghat-Cauvery Lineament (PCL), protolith ages are not well established. Only zircon evaporation ages of ~2.11 Ga and ~2.43 Ga from the Kodaikanal area of the Madurai Block (Jayananda et al. 1995; Bartlett et al. 1995) are available. Because the evaporation method provides only a minimum age for simple zircon grains and often geologically meaningless mixed ages for zircons with more than one period of growth (Appendix- A-4-II), these data can not be taken as reliable indicators for the ~2.52 Ga old Dharwar-like granitic gneiss in the Madurai Block.

Further south, Nd-model ages from the Cardamom Hills in the Madurai Block (Brandon and Meen, 1995) and from the Kerala Khondalite Belt (Harris et al. 1994; Bartlett et al. 1995) range widely from ~2.6 Ga to 1.3 Ga. Odom (1982) obtained an U-Pb age of 2930 ± 50 Ma for a zircon fraction from charnockites in the Trivandrum area of the KKB, that gave the first possible evidence of Archaean basement rocks in the southern part of the Peninsula. However, they could just as well be inherited detrital zircons. Zircon analyses from the granitic gneisses

of the Kerala Khondalite Belt indicate extreme complexity due to Pb-loss and overgrowth. Soman et al. (1995) reported analyses of zircon fractions from the KKB that are ~50-80% discordant and have a poorly defined upper intercept age of 2144 ± 130 Ma, with a lower intercept age of 564 ± 77 Ma . Srikantappa et al. (1985) also reported similar upper and lower intercepts of ~1930 Ma and ~540 Ma for zircon fractions from charnockites. Such discordant ages from a polymetamorphic terrane may not be geologically meaningful and thus the antiquity of these rocks is not firmly established. However, a Rb-Sr whole rock age from the Kerala Khondalite Belt (KKB) also gives an age of ~2100 Ma (Chacko, 1987). Santosh et al. (1989) compiled Rb-Sr whole rock and K-Ar biotite ages of nine Neoproterozoic to Early Cambrian (765-550 Ma) granitic plutons widely spread over the SGT from west of Marcara, ~400 km north of the Moyar lineament, to near the southern tip of Peninsular India

Charnockitization and high-grade metamorphism in the KKB have been interpreted to have occurred between 550 Ma and 520 Ma on the basis of Sm-Nd whole rock and mineral isochrons (Choudhary, 1992, Unnikrishnan-Warrior, 1995, 1997). North of the KKB, in the Kodaikanal area of the Madurai Block, zircons from charnockite record low-temperature evaporation ages of ~550 Ma which have also been interpreted as the charnockitization age (Bartlett et al. 1995; Jayanada et al.1995). Thus, Neoproterozoic/Early Cambrian charnockitization has been suggested to extend from the southernmost tip of India to at least as far north as Kodaikanal over an area of over 150,000 km^2. Time of movement along the major shear zones (discussed in Chapter 3) has not been well constrained. Only recently, Deters-Umlauf et al. (1997) provided Rb-Sr and Sm-Nd whole rock and mineral isochron ages that indicate Neoproterozoic to Early Paleozoic (~624 Ma to ~472 Ma) activity along the Moyar and Bhavani Shear Zones.

4.3. U/Pb single zircon and monazite geochronometry

4.3.1. Analytical results

Zircon geochronometry has experienced rapid growth in last two decades. In the 1970s conventional isotope dilution thermal ionization mass spectrometry (IDTIMS) techniques required milligram quantities of zircon, mainly because of high laboratory Pb blanks (100s of picograms; 1 picogram = 10^{-12} gram). Age uncertainties were usually on the order of several % of the age. Today, the technology (chemistry and mass spectrometry) has improved: a few picogram to sub-picogram laboratory Pb blanks can be achieved. Age uncertainties of a few tenths of a percent are obtainable even on microgram-sized single zircon crystals (Krogh, 1982; Davis et al. 1997; Bowring et al. 1998). Such significant developments have spread the use of zircon geochronometry to high resolution stratigraphy and tectonic analyses (Bowring, 1993, 1998). Two other techniques, namely, the sensitive high resolution ion microprobe (SHRIMP, Compson et al. 1984) and direct TIMS zircon evaporation (Kober, 1986,1987) were developed in the 1980s. A discussion of these three different techniques and their relative advantages and disadvantages are given in Appendix IV-II. With these new developments, U-Pb geochronology has emerged as one of the most suitable techniques for high precision geochronological work.

For this project, two of the three U-Pb geochronological techniques, namely, the IDTIMS and SHRIMP, were used on single crystals of zircon, monazite, sphene and apatite. A number of samples with well constrained geological relationships were collected from various corridors of study across major lineaments in the SGT (Chapter 3).

Analyses were performed in three different laboratories. Table 4.1 summarizes number of samples analysed in different laboratories.

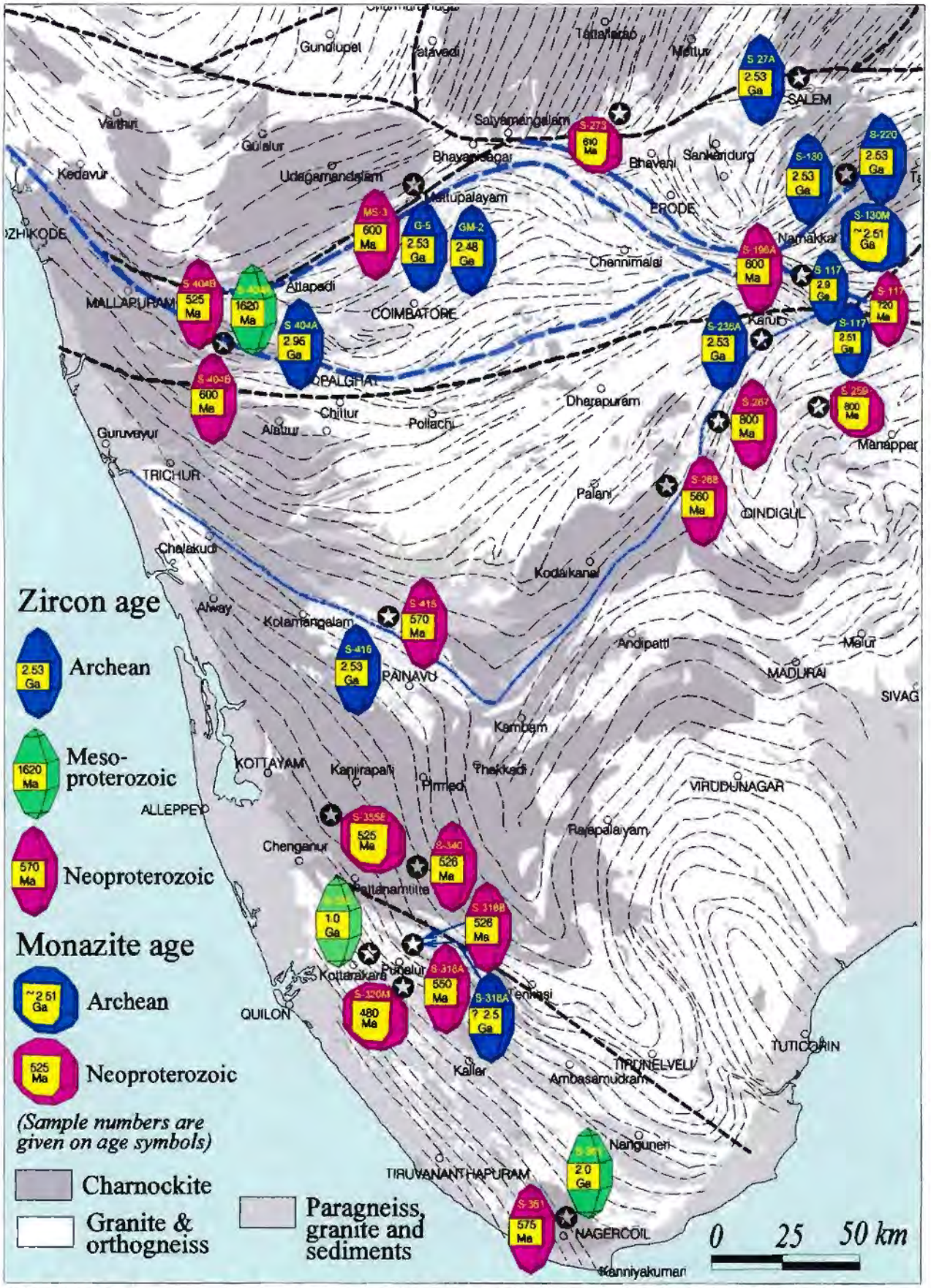

Fig.4.1. Summary of new U-Pb ages from the SGT determined during this study. Names of the shear zones are same as in Fig. 1.2

Table 4.1. Summary table of number of analyses carried out in different laboratories.

Laboratory	Number of samples analysed	Number of zircons(Z)/ Monazite (M)/ Apatite (A)/ Sphene (S) analysed
Massachusetts Institute of Technology, USA	8	27 (Z), 2(S) and 2(A)
University of Cape Town, South Africa	19	95(Z) / 17(M)
Curtin University, Australia	6	104 spots (Z), 20 spots (M)

Initial geochronological work was done in 1996 in the isotope laboratory of Prof. Sam Bowring at the Massachusetts Institute of Technology where I was introduced to the single crystal zircon, monazite, sphene and apatite geochronological techniques. Eight samples, one each from granite gneiss, granite mylonite, mafic granulite, granitic pegmatite and two charnockite samples collected from the Bhavani Shear Zone were analysed using IDTIMS (Table A.4.2, in Appendix).

Subsequently, during 1997 and 1998, the bulk of the analyses (19 samples) reported in this Chapter were carried out in the Radiogenic Isotope Facility at the University of Cape Town under the guidance of Prof. Robert Zartman (Table 4.3) These analyses yielded the first precise U-Pb zircon ages determined in this laboratory.

In 1998, I analysed six samples with complex (identified by initial IDTIMS analyses) zircons and monazite in the SHRIMP-II facility at Curtin University, Perth, Western Australia (Table 4.4, in Appendix), with the help of Dr. Pete Kinny.

A summary of the analytical data set is documented in Tables 4.2 to 4.4. Age data obtained and locations of various samples are given in Fig. 4.1. Detailed descriptions of the various samples analysed, and interpretation of results are provided in Table 4.5.

Table. 4.2. U-Pb geochronological data of different rock types in the Mettupalayam area of the BSZ, Corridor-III, carried out at the MIT, USA by IDTIMS method

	Sample no.	Wt (mg)	Conc (ppm)		Isotopic ratios			2-sigma err		2-sigma err		2-sigma err	Age (Ma)			Corr.	Common Pb (pg)	
			U	Pb	$^{206}Pb/^{204}Pb$	$^{208}Pb/^{206}Pb$	$^{206}Pb/^{238}U$	(%)	$^{207}Pb/^{235}U$	(%)	$^{207}Pb/^{206}Pb$	(%)	$^{206}Pb/^{238}U$	$^{207}Pb/^{235}U$	$^{207}Pb/^{206}Pb$	coef.	Total	Blank
Granite Gneiss	*Zircon*																	
	G5 Z15	0.0014	699.43	420.36	758.45	0.220	0.47673	(.41)	10.90163	(.41)	0.16585	(.07)	2513.0	2514.8	2516.2	0.986	35.1	3.5
	G5 Z13	0.0043	108.13	82.23	452.32	0.558	0.47580	(.15)	10.85753	(.17)	0.16550	(.08)	2508.9	2511.0	2512.7	0.884	28.1	3.5
	G5 Z16	0.0023	529.94	303.81	15040.72	0.248	0.47081	(.09)	10.79206	(.10)	0.16625	(.04)	2487.1	2505.4	2520.2	0.897	2.0	2.0
	G5 Z11	0.0033	297.46	159.62	11956.67	0.162	0.46933	(.13)	10.74958	(.14)	0.16612	(.05)	2480.6	2501.7	2518.9	0.946	2.5	2.5
	G5 Z17	0.0011	258.05	165.54	908.10	0.392	0.46523	(.21)	10.48368	(.22)	0.16344	(.07)	2462.6	2478.5	2491.5	0.943	8.7	3.5
	G5 14	0.0022	986.01	503.88	34087.18	0.144	0.45337	(.10)	10.37223	(.11)	0.16593	(.04)	2410.2	2468.6	2517.0	0.929	1.9	1.9
	G5-9,10	0.0011	91.09	60.10	173.07	0.199	0.45392	(.58)	10.11289	(.63)	0.16158	(.23)	2412.7	2445.1	2472.3	0.933	35.1	3.5
	G5 Z8	0.0059	960.58	404.50	20654.84	0.132	0.37694	(.06)	8.59031	(.07)	0.16529	(.04)	2062.0	2295.5	2510.5	0.826	16.4	3.5
	Sphene																	
	G5-S2	0.0597	5.87	2.45	29.60	0.436	0.08714	(.57)	0.94311	(3.25)	0.07850	(3.00)	538.6	674.5	1159.4		109.9	3.5
	G5-S1	0.0502	2.06	0.83	29.82	0.457	0.08767	(1.79)	0.90278	(3.64)	0.07468	(2.75)	541.8	653.2	1060.0	0.515	33.1	3.5
Granite Mylonite	*Zircon*																	
	GM-2 Z1	0.0017	518.14	267.23	6653.38	0.206	0.43838	(.15)	9.69436	-0.17	0.16039	(.07)	2343.4	2406.2	2459.7	0.899	3.7	3.5
	GM-2 Z2	0.0016	355.92	148.03	3260.91	0.155	0.37032	(.15)	7.51485	-0.16	0.14718	(.06)	2030.9	2174.8	2313.4	0.923	4.1	3.5
Amphibolite	*Zircon*																	
	2S Z4	0.0241	187.22	122.11	12956.39	0.433	0.47252	(.15)	10.80175	(.16)	0.16580	(.05)	2494.6	2506.2	2515.7	0.958	9.6	3.5
	2S Z6	0.0065	192.16	117.19	4513.88	0.338	0.46831	(.10)	10.64984	(.11)	0.16493	(.05)	2476.1	2493.1	2506.9	0.887	7.7	3.5
	2S Z1	0.0046	548.11	291.62	8321.20	0.162	0.46488	(.19)	10.42528	(.19)	0.16265	(.04)	2461.1	2473.3	2483.3	0.975	8.3	3.5
Mafic Granulite (I)	*Zircon*																	
	376/9 Z2	0.0058	109.94	76.61	204.42	0.214	0.47578	(.15)	10.65985	(.19)	0.16250	(.11)	2508.9	2493.9	2481.8	0.820	88.4	3.5
	376/9 Z4	0.0049	167.20	98.81	315.25	0.207	0.43660	(.22)	9.79835	(.38)	0.16277	(.28)	2335.4	2416.0	2484.6	0.678	66.0	3.5
	Apatite																	
	376/9 Aa	0.0457	7.25	7.82	20.75	0.746	0.10955	(.58)	1.60436	(3.04)	0.10621	(2.75)	670.1	971.9	1735.4	0.581	302.9	3.5
	376/9 Ab	0.0916	5.18	6.03	19.99	0.688	0.10696	(.55)	1.57935	(4.84)	0.10709	(4.37)	655.1	962.1	1750.4	0.861	476.9	3.5
Mafic Granulite (II)	*Zircon*																	
	MS-2 Z2	0.0009	124.52	60.14	1411.84	0.012	0.47549	-0.34	11.08065	-0.34	0.16901	-0.07	2507.6	2529.9	2547.9	0.981	2.5	2.5
	MS-2 Z5	0.0031	164.65	104.82	262.74	0.169	0.46988	-0.14	10.4624	-0.17	0.16149	-0.09	2483	2476.6	2471.3	0.856	53.7	3.5
	MS-2 Z8	0.0018	55.48	28.21	558.6	0.105	0.45135	-0.61	10.16106	-0.64	0.16328	-0.17	2401.2	2449.5	2489.9	0.961	5.1	3.5
	MS-2 Z7	0.0055	2392.2	1135.93	70881.49	0.106	0.43416	-0.07	9.89943	-0.08	0.16537	-0.04	2324.4	2425.5	2511.3	0.858	4.9	3.5
	MS-2 Z9	0.0021	68.39	29.56	526.54	0.161	0.36609	-0.55	7.66954	-0.56	0.15194	-0.1	2011	2193	2367.9	0.983	6.2	3.5
Tonalite gneiss	*Zircon*																	
	MS-4B Z1	0.0214	38.48	24.72	3243.79	0.401	0.47221	-0.1	10.85925	-0.11	0.16679	-0.05	2493.2	2511.2	2525.7	0.913	7.1	3.5
	MS-4B Z2	0.0197	87.2	56.03	1910.5	0.412	0.46432	-0.09	10.55302	-0.1	0.16484	-0.04	2458.6	2484.6	2505.9	0.902	23.7	3.5
Charnockite	*Zircon*																	
	GM 4 Z2	0.0025	1280.91	688.19	8122.06	0.134	0.47794	-0.08	10.97024	-0.09	0.16647	-0.04	2518.3	2520.6	2522.5	0.887	10.8	3.5
	GM 4 Z1	0.0057	718.92	401.78	884.68	0.127	0.47606	-0.14	10.90515	-0.15	0.16614	-0.05	2510.1	2515.1	2519.1	0.935	123	3.5
Pegmatite	*Zircon*																	
	MS-3 Z5	.01	1793.05	164.79	7342.04	.109	.09084	.10	.74798	.12	.05972	.05	560.5	567.1	593.4	.884	13.9	3.5
	MS-3 Z4	.01	903.25	80.97	9427.6	.02	.09620	.09	.79452	.1	.05990	.05	592.1	593.7	600.1	.875	5.9	3.5
	MS-3 Z3	.01	383	34.64	7712.18	.113	.08968	.07	.74002	.11	.05985	.08	553.7	562.4	598.0	.68	2.9	2.9

Table-4.3. U-Pb zircon and monazite geochronological data by IDTIMS method carried out at the UCT laboratory.

	Sample No.	Wt (µg)	Concentration (ppm)			Th/U ratio	Spiked Data			Isotopic Composition of Pb (unspiked)				Age, in million years				Isotopic ratios				
			U	Th	Pb		$^{206}Pb/^{204}Pb$	$^{208}Pb/^{207}Pb$	$^{206}Pb/^{208}Pb$	^{204}Pb	^{206}Pb	^{207}Pb	^{208}Pb	$^{206}Pb/^{238}U$	$^{207}Pb/^{235}U$	$^{207}Pb/^{206}Pb$	$^{208}Pb/^{232}Th$	207/235	Error (%)	206/238	Error (%)	Rho
Granite gneiss in Salem, Corridor-I	S-27A Z1	13	397	1134	206	2.86	1766.6	5.79619	8.99240	0.0353	78.0560	13.4567	8.4519	2479 ± 4	2504 ± 2	2525 ± 0.7		10.7781	0.212	0.468827	0.208	0.978181
	S-27A Z2	7	66	197	55	2.98	323.0	5.09395	1.34550	0.1233	50.9009	10.0300	38.9458	2506 ± 26	2516 ± 12	2525 ± 2	2086 ± 17	10.9205	1.29	0.475008	1.28	0.9956579
	S-27A Z3	5	85	666.7	63.2	7.84	126.5	3.88749	1.43745	0.2772	53.3441	12.2869	34.0919	2309 ± 62	2417 ± 30	2510 ± 10		9.81102	3.29	0.430712	3.19	0.982306
	S-27A ZA	24	48.2	30.4	26.8	0.63	2078.4	5.84047	5.05035	0.0137	73.6558	12.4143	13.9167	2505±7	2517±3	2527±1	2533±13	10.9288	0.352	0.474822	0.352	0.9921133
	S-27A Z-5	6	65.3	45	35.4	0.69	747.5	5.58960	3.97620	0.0306	71.6473	12.1862	16.1359	2388±19	2451±9	2504±2	2527±4	10.1788	0.982	0.448415	0.969	0.989739
Biotite gneiss, north of Namakkal, Corridor-I	S-220 ZA	8	222	351	164	1.58	285.2	4.82124	1.87128	0.1901	57.2566	11.8687	30.6847	2498 ± 8	2507 ± 4	2515 ± 2	2445 ± 7	10.8161	0.428	0.473374	0.405	0.958293
	S-220 ZB	15	133	1289	81	9.69	886.7	5.64526	2.79099	0.0280	66.1753	11.2584	22.5383	2478 ± 14	2493 ± 6	2506 ± 1	384 ± 3	10.6498	0.688	0.468619	0.681	0.9963309
	S-220 ZC	8	183	234	128	1.28	351.5	5.03360	2.22670	0.1584	60.6284	12.0142	27.1991	2510 ± 9	2511 ± 4	2512 ± 2	2553 ± 16	10.8574	0.47	0.476023	0.451	0.967207
Charnockite syntectonic with DI shearing in Namakkal, Corridor-I	S-130 Z1	21	137	234	94	1.71	910.9	5.65601	2.12355	0.0577	60.5802	10.7161	28.6460	2499 ± 9	2504 ± 4	2507 ± 1		10.7716	0.443	0.47365	0.437	0.989014
	S-130 Z2	12	224.7	278	146	1.24	1225.6	5.73460	2.18800	0.0369	61.4449	10.6156	27.9027	2436 ± 23	2475 ± 10	2507 ± 1		10.4458	1.12	0.459305	1.12	0.9987124
	S-130 Z3	26	346	180	186	0.52	13690.1	5.95184	8.49228	0.0071	77.7994	13.0927	9.1057	2538 ± 4	2538 ± 2	2537 ± 1	2021 ± 20	11.1715	0.2	0.482429	0.191	0.955902
	S-130 Z4	15	251	200	144	0.80	4015.9	5.93143	4.27610	0.0038	71.5875	11.9755	16.4331	2509 ± 8	2517 ± 4	2524 ± 1	2587 ± 66	10.932	0.416	0.475812	0.408	0.98342
	S-130 Z5	15	578	330	318	0.13	22660.0	5.97030	6.07940	0.0017	75.0485	12.5911	12.3588	2532 ± 5.5	2532 ± 2.5	2533 ± 1	2534 ± 4.5	11.09039	0.2	0.480406	0.189	0.944002
	S-130 Z6	27	268	121	143	0.45	23843.0	5.97860	7.71084	0.0012	77.0984	12.9144	9.9860	2523 ± 5.5	2527 ± 2	2531 ± 1	2519 ± 6	11.0499	0.266	0.47902	0.263	0.986924
Monazite from charnockite gneiss, Namakkal, Corridor-I	S-130 M-1	28	322.2	172	1.23%	0.53	2252.0	6.39130	0.00891	0.0003	0.8823	0.0231	99.0943	2107 ± 12	2241 ± 6	2367 ± 2	152 ± 71	8.08957	0.674	0.386442	0.665	0.988262
	S-130 M-2	47	152	690000	47580	4539.47	8582.0	6.80300	0.00854	0.0000	0.8378	0.1229	99.0393	1705 ± 16	1992 ± 10	2304 ± 6.6	1479 ± 313	6.10817	1.12	0.302674	1.04	0.937791
	S-130 M-3	26	514.3	243500	223000	473.46	3021.3	5.93620	0.00940	0.0002	0.9135	0.1538	98.9324	2418 ± 15	2465 ± 8	2507 ± 5.4	1943 ± 53	10.3477	0.823	0.454985	0.751	0.920955
	S-130 M-5	20	768	680000	27495	885.42	2284.0	7.26700	0.00734	0.0003	0.7247	0.0992	99.1759	1681 ± 61	1890 ± 35	2127 ± 6	883 ± 50	5.42856	4.13	0.297866	4.11	0.9965983
	S-130 M-6	44	74	25760	3475	348.11	152.2	4.32800	0.00940	0.0039	0.9256	0.2126	98.8558	2412 ± 10	2364 ± 5	2322 ± 5	2776 ± 21	9.25334	0.584	0.453626	0.502	0.86788
	S-130 M-8	20	54	8.5	1969	0.16	3337.0	6.94350	0.00807	0.0002	0.7997	0.1151	99.0849	1875 ± 3	2051 ± 1	2233 ± 1		6.53636	0.179	0.337433	0.169	0.943069
Neosome of migmatite, south of Namakkal, Corridor-I	S-196A ZA	10	295	6.1	45.2	0.02	848	4.38376	2.22637	0.6385	61.6812	12.9688	24.7115	553 ± 9	563 ± 8	607 ± 10	1238 ± 153	0.741584	1.81	0.0894942	1.75	0.970566
	S-196A ZC	5	658	23.9	69	0.04	172.9	7.03428	4.37727	0.3081	77.7981	9.1881	12.7057	548 ± 9	564 ± 8	629 ± 12	802 ± 75	0.742903	1.89	0.0887665	1.8	0.958931
	S-196 Z-4	24	596	18	48.2	0.03	20145	15.05566	36.15660	0.0263	92.2538	5.8695	1.8503	534 ± 1.5	545 ± 1	591 ± 5	511 ± 14	0.710418	0.371	0.0864102	0.289	0.79403
	S-196 Z-5	14	291.3	10	24.15	0.03	1125.4	13.93300	22.47030	0.0194	92.3390	5.8107	1.8309	548 ± 3	558 ± 3	597 ± 2.4	597 ± 17	0.731836	0.645	0.0887424	0.633	0.984608
	S-196 Z-6	4	358	10	29	0.03	652.0	12.63400	15.07900	0.0246	92.3957	5.7799	1.7998	543 ± 6	545 ± 5	556 ± 5	558 ± 48	0.710982	1.23	0.0878447	1.2	0.981605
	S-196 Z-7	4	669.3	19.48	54	0.03	1547.5	14.65700	28.97800	0.0068	93.0672	5.6759	1.2501	540 ± 2.9	552 ± 2.4	601 ± 2	619 ± 23	0.721811	0.367	0.0873565	0.356	0.982695
	S-196 Z-8	5	217	7.32	21.3	0.03	239.9	8.44805	6.04553	0.2254	82.1914	8.2374	9.3458	548 ± 5	562 ± 5.6	620 ± 18	580 ± 75	0.739213	1.31	0.0886804	0.954	0.76745
	S-196 Z-9	18	488	25.25	43	0.05	818.7	12.91348	17.28151	0.0948	88.5196	6.7090	4.6766	550 ± 1	563 ± 2	613 ± 2	430 ± 75	0.740329	0.235	0.0890898	0.213	0.90879
Granite gneiss south of PCSZ, Karur area, Corridor-I	S-236A Z1	13	167	319	159	1.91	1013.6	5.64080	5.67270	0.0593	74.1070	13.0770	12.7566	2460 ± 13	2499 ± 6	2530 ± 2	2400±8	10.2539	0.267	0.446833	0.263	0.98445
	S-236A Z2	8	196.7	100.2	105.34	0.51	931.9	5.57365	5.61651	0.0468	74.6136	13.0679	12.2717	2449 ± 8	2495 ± 3	2532 ± 1	2437 ± 14	10.6969	0.508	0.463451	0.504	0.994726
	S-236A Z2 NM	8	208	195	102	0.94	1731.4	5.77530	6.24419	0.0087	76.0780	12.8313	11.0870	2381 ± 5	2458 ± 2	2522 ± 1	2400 ± 8	10.7152	0.643	0.464617	0.628	0.980128
	S-236A Z-4	11	217	89	108	0.41	1426.3	5.78250	7.07005	0.0277	76.8441	13.0616	10.0666	2361 ± 7	2442 ± 3	2511 ± 1	2359 ± 14	10.0789	0.37	0.442204	0.362	0.979595
	S-236A Z-5	7	155	108	82	0.70	1237.1	5.70883	6.06176	0.0238	75.7085	12.9317	11.3360	2434 ± 10	2485 ± 4	2527 ± 1	1733 ± 14	10.5565	0.494	0.458816	0.487	0.987092
	S-236A Z-6	18	160	81	82	0.51	3306.6	5.91518	6.45485	0.0082	75.9268	12.7225	11.3425	2387 ± 5	2460 ± 2	2520 ± 1	2375 ± 9	10.2708	0.256	0.448144	0.25	0.979299

cond.

Table-4.3. U-Pb zircon and monazite geochronological data by IDTIMS method carried out at the UCT laboratory.

	Sample No.	Wt (µg)	Concentration (ppm)				Spiked Data			Isotopic Composition of Pb (unspiked)				Age, in million years				Isotopic ratios				
			U	Th	Pb	Th/U ratio	$^{206}Pb/^{204}Pb$	$^{206}Pb/^{207}Pb$	$^{206}Pb/^{208}Pb$	^{204}Pb	^{206}Pb	^{207}Pb	^{208}Pb	$^{206}Pb/^{238}U$	$^{207}Pb/^{235}U$	$^{207}Pb/^{206}Pb$	$^{208}Pb/^{232}Th$	207/235	Error (%)	206/238	Error (%)	Rho
Detrital zircons from Khondalite Vidiya Malai Hill, south of Palayam	S-259 Z-1	10			201		188.0	5.85210	4.51570	0.0637	71.7377	12.2852	15.9134			2452 ± 4						
	S-259 Z-11	12	99	84	47	0.85	5116.0	6.19930	5.16760	0.0007	73.8095	11.9064	14.2834	2201 ± 3	2346 ± 2	2468 ± 1	1729 ± 5	9.04426	0.194	0.406931	0.184	0.953803
	S-259 Z-12	8.5	170	96	69	0.56	3372.0	7.85380	5.80560	0.0096	76.6055	10.1853	13.1996	1990 ± 3	2014 ± 1	2039 ± 1	2006 ± 4	6.26736	0.187	0.361658	0.18	0.967479
	S-259 Z-14	10			216		115.0	3.69100	2.93620							2477 ± 5						
	S-259 Z-16	6	276	64	131	0.23	7402.0	6.47100	15.41600	0.0012	82.0065	12.6726	5.3197	2398 ± 20	2396 ± 9	2395 ± 1	2311 ± 23	9.58984	1.02	0.450614	1.02	0.99898 48
Granite syntectonic with D2(?) shearing along the Palghat Shear Zone, Palghat Corridor-IV	S-404B Z-1	5	188	213	29	1.13	151.9	6.56369	1.42600	0.2069	56.6866	6.4195	36.6870	563 ± 14	575 ± 12	626 ± 9	576 ± 14	0.758437	3.31	0.0911682	3.25	0.985379
	S-404B Z-2	20	2950	65	261	0.02	376.7	10.23550	8.92910	0.2141	82.6376	8.0283	9.1201	502 ± 1	518 ± 1	587 ± 3	969 ± 11	1.11843	5.21	0.120073	5.11	0.982782
	S-404B Z-3	32	4986	425	389	0.09	21098.0	17.15830	34.08297	0.0026	91.9757	5.3495	2.6722	517 ± 1	517 ± 1	520 ± 1	525 ± 1	0.664291	0.167	0.0834212	0.161	0.968311
	S-404B Z-4	1	430	328	89	0.76	94.6	4.67615	1.67791	0.4014	60.2057	9.8368	29.5562	731 ± 3	762 ± 27	867 ± 16	830 ± 42	0.664542	0.237	0.0809609	0.191	0.8145
	S-404B Z-6	2	413	230	59	0.56	198.1	7.51169	2.79151	0.2053	71.2529	7.5048	21.0370	687 ± 18	698 ± 14	728 ± 7	766 ± 23	0.989947	2.92	0.112932	2.9	0.9941681
	S-404B Z-7	1	3060	252	237	0.08	20043.0	17.13700	33.94438	0.0002	92.1024	5.3309	2.5665	514 ± 1	516 ± 1	524 ± 1	541 ± 1					
	S-404B Z-8	5	209	66	23	0.32	587.0	11.92301	5.59733	0.0768	81.1247	6.0970	12.7065	628 ± 4.2	633.5 ± 5.3	652.7 ± 18	763 ± 10	0.66204	0.178	0.0829997	0.171	0.960238
	S-404B Z-8(ii)	5	209	66	23	0.32	589.0	12.13790	5.60564	0.0874	80.7834	6.1025	13.0268	628 ± 3	622 ± 3	600 ± 4	761 ± 5	0.844461	0.61	0.102257	0.57	0.942436
	S-404B Z-11	3	431	191	49	0.44	1068.0	14.54700	5.32000	0.0238	79.5676	5.4645	14.9442	639 ± 2	665 ± 2	756 ± 2	803 ± 3	0.92535	0.339	0.104154	0.316	0.948006
	S-404B Z-13	9	2560	81	103	0.03	1056.0	16.50500	59.70400	0.0078	92.8129	5.6274	1.5518	273 ± 1	308 ± 1	580 ± 3	362 ± 11	0.354223	0.439	0.043277	0.4	0.935311
Granite gneiss from the KKPT Shear Zone, Kota mangalam	S-416 Z-1	7	617	341	269	0.55	511.6	5.49821	4.59120	0.1298	73.5426	12.9582	15.3693	1958 ± 3	2196 ± 2	2435 ± 1	1880 ± 5	7.69868	0.216	0.353225	0.208	0.965854
	S-416 Z-2	8	699	228	260	0.33	3552.0	6.34577	10.20780	0.0121	79.9704	12.5080	7.5099	1912 ± 3	2157 ± 2	2399 ± 1	1765 ± 7	7.36675	0.216	0.345301	0.212	0.978941
	S-416 Z-3	9	359	233	157	0.65	2150.0	6.14017	5.30400	0.0230	74.1498	12.0404	13.7868	2050 ± 4.5	2251 ± 1.8	2438 ± 1	1895 ± 4	8.17498	0.241	0.37446	0.238	0.86263
	S-416 Z-4	8	478	275	189	0.58	1929.0	6.01808	5.48543	0.0265	74.4342	12.2788	13.2605	2185 ± 4	2332 ± 2	2461 ± 2	2173 ± 6	8.94852	0.236	0.404419	0.231	0.980801
	S-416 Z-5	10	338.5	173.6	101	0.51	944.4	6.41400	5.28700	0.0582	74.9099	11.4807	13.5512	1471 ± 4	1831 ± 2	2268 ± 1	1476 ± 9	5.06816	0.315	0.256375	0.309	0.987999
	S-416 Z-6	11	301.5	125.5	131.5	0.42	2303.0	6.09050	7.47866	0.0186	77.4197	12.6510	9.9106	2129 ± 4	2298 ± 2	2451 ± 1	2098 ± 20	8.61373	0.244	0.391363	0.24	0.983419
Granite syntectonic along the KKPT Shear Zone, Kottamangalam Corridor-IV	S-415 Z-1	7	319	794	48	2.49	557.8	11.97000	4.22700	0.0336	53.2898	3.6417	43.0353	556 ± 15	564 ± 5	572 ± 3	559 ± 6	0.74137	1.12	0.0911101	1.11	0.991383
	S-415 Z-3	9	136	264	19.5	1.94	236.9	8.47400	1.38380	0.0955	56.5614	4.7437	38.5993	556 ± 14	561 ± 11	581 ± 7	571 ± 15	0.756386	1.29	0.0889689	0.186	0.989488
	S-415 Z-4	13	852.4	376.1	23	2.47	692.8	12.78275	1.28250	0.0255	54.2519	3.5692	42.1535	573 ± 6	572 ± 5	566 ± 2	557 ± 9	0.767207	1.22	0.0934421	1.21	0.9952606
	S-415 Z-5	9	122	304	19	2.49	343.8	8.77138	1.19527	0.0743	51.7038	4.9869	43.2351	563 ± 8	682 ± 14	1096 ± 44	568 ± 9	0.957188	2.84	0.0912905	1.55	0.63469
	S-415 Z-6	12	94	207	13	2.20	1203.9	14.49233	1.41828	0.0081	56.3574	3.4463	40.1881	560.4 ± 4	562 ± 3.4	569.5 ± 4	564 ± 7	0.739656	0.8	0.0908214	0.778	0.976473
	S-415 Z-7	22	85	172	12	2.03	1079.0	14.08206	1.52564	0.0299	57.9129	3.8479	38.2093	562 ± 2	562.6 ± 2	565 ± 4	560 ± 3	0.740308	0.438	0.0910971	0.386	0.89803
Charnockitized granite close to the KKPT shear Zone, north of Dindigul, south of the Corridor-I	S-267 Z-2	7	191.3	286	21	1.50	232.4	8.39300	2.47200	0.1296	70.0868	6.0359	23.7077	535 ± 5	546 ± 5	600 ± 10		0.712527	1.12	0.0862756	1.01	0.908098
	S-267 Z-3	8	205.3	68.2	25	0.33	741.5	12.13700	6.56700	0.0066	84.9604	5.6011	9.4320	716 ± 4	729 ± 3	770 ± 4	736 ± 4	1.05016	0.579	0.117351	0.541	0.9437688
	S-267 Z-4	5	943	400	127	0.42	1463.0	13.38600	7.15250	0.0229	83.5500	5.8147	10.6124	789 ± 3	790 ± 2	796 ± 1		1.17756	0.432	0.130079	0.426	0.985899
	S-267 Z-4a	5	218	89	26.62	0.41	321.5	9.41890	4.82490	0.1465	79.3814	7.1912	13.2810	669.4 ± 7	689 ± 6	728 ± 4	588 ± 8	0.959462	1.15	0.109422	1.15	0.985396
	S-267 Z-5	5	468	207	62	0.44	255.6	8.38162	4.19662	0.1420	79.5229	7.1713	13.1639	721 ± 13	730 ± 10	755 ± 5	530 ± 12	1.05143	1.98	0.118388	1.96	0.9932633
	S-267 Z-6	5	431	105	82	0.24	83.2	4.30500	2.05070	0.6764	58.1710	13.3252	27.8274	626 ± 3	624 ± 5	617 ± 20	471 ± 12	0.848778	1.14	0.101987	0.545	0.56706
	S-267 Z-7	6	202	46	26	0.23	291.0	9.13000	5.12900	0.2607	76.1190	8.5008	15.3195	641 ± 11	650 ± 9	682 ± 12	647 ± 14	0.896793	1.82	0.104518	1.72	0.949373
	S-267 Z-8,9	12	244	111	30.3	0.45	1084.4	12.98067	6.84295	0.0375	83.1242	5.9112	10.9271	724 ± 32	733 ± 25	762 ± 2		1.05851	3.85	0.118815	3.84	0.9997624
	S-267 Z-10	12	181	44	20	0.39	2429.9	14.63900	10.35700	0.0043	86.9962	5.5817	7.4178	711.4 ± 23	714 ± 17	723 ± 1.6		0.987719	0.422	0.112936	0.416	0.986392

Table-4.3. U-Pb zircon and monazite geochronological data by IDTIMS method carried out at the UCT laboratory.

	Sample No.	Wt (µg)	Concentration (ppm)			Th/U ratio	Spiked Data			Isotopic Composition of Pb (unspiked)				Age, in million years				Isotopic ratios				
			U	Th	Pb		$^{206}Pb/^{204}Pb$	$^{206}Pb/^{207}Pb$	$^{206}Pb/^{208}Pb$	^{204}Pb	^{206}Pb	^{207}Pb	^{208}Pb	$^{206}Pb/^{238}U$	$^{207}Pb/^{235}U$	$^{207}Pb/^{206}Pb$	$^{208}Pb/^{232}Th$	207/235	Error (%)	206/238	Error (%)	Rho
Youngest granite charnockitized, Nirettipara, PPP corridor	S-318A Z3	8	131	55	12	0.42	437.0	11.14665	4.74442	0.0410	81.6059	5.5305	12.8226	518 ± 8	537 ± 8	615 ± 21	539 ± 11	0.696757	1.04	0.0838488	0.691	0.71908
	S-318A Z5	14	124	94	14	0.76	235.2	8.44140	2.64560	0.1660	70.5511	6.5405	22.7424	543 ± 9	544 ± 8	549 ± 5	543 ± 10	0.708503	1.79	0.0878091	1.77	0.9910513
	S-318A Z-7	9	554	397	143	0.72	2959.3	6.73420	6.17160	0.0153	76.5409	11.3002	12.1435	1379 ± 2	1779 ± 2	2288 ± 1	1024 ± 3	3.64852	1.03	0.182528	1.03	0.9989558
	S-318A Z-8	11	203	151	100	0.74	546.0	5.68590	4.01280	0.1014	70.8566	12.1845	16.8576	1974 ± 8	2185 ± 4	2389 ± 1	1738 ± 9	7.599999	0.492	0.358312	0.482	0.987941
	S-318A Z15	6	106	63	10.4	0.60	446.3	14.20500	4.51720	0.0633	77.3529	5.4484	17.1354	542 ± 7	543 ± 6	549 ± 6	550 ± 7	0.707799	1.35	0.0877378	1.33	0.903333
	S-318A Z-8(I)	11	201	149.5	90	0.74	2669.0	6.17100	4.68990	0.0106	73.0884	11.7252	15.1757	1904 ± 11	2174 ± 7	2440 ± 5	1735 ± 19	7.50916	0.745	0.34353	0.675	0.906469
	S-318A Z-10	10	143	111	14	0.77	1051.5	14.18126	3.68432	0.0209	75.7946	4.7347	19.4498	542 ± 3	543 ± 3	547 ± 4	542 ± 4	0.707612	0.673	0.0877781	0.633	0.94977
	S-318A Z-12	3	92	72	23	0.79	248.2	8.82948	2.69590	0.1079	72.4524	5.8238	21.6159	539 ± 8	541 ± 6.8	547 ± 10	541 ± 9	0.703195	1.63	0.0872506	1.55	0.962491
Granite intruded and retrogressed charnockite, Nirettipara, PPP corridor	S-318B ZA	20	469	370	139	0.79	49.2	2.81400	1.11850	0.8846	44.1398	15.6126	39.3631	600 ± 10	627 ± 40	724 ± 170	492 ± 70	0.805697	5.14	0.0903994	0.904	0.3465
	S-318B ZB	20	199	104	18	0.52	435.6	11.07450	4.08580	0.0383	80.0307	5.2511	14.6800	519 ± 9	524 ± 8	549 ± 13	516 ± 12	0.680941	1.84	0.0839499	1.71	0.946288
	S-318 ZF	12	256	167	25	0.65	359.3	10.25348	3.94640	0.1443	76.0771	6.5671	17.2115	512 ± 4	520 ± 4	555 ± 7	397 ± 4	0.6686-48	0.93	0.0826706	0.858	0.93287
	S-318B ZE	16	305	202	31	0.66	430.3	11.04806	3.52160	0.1086	74.5085	5.9411	19.4417	517 ± 4	519 ± 3	526 ± 5	510 ± 7	0.666584	0.641	0.0835025	0.252	0.919179
	S-318B ZH	24	130	115	13	0.89	1460.0	14.91227	3.28536	0.0261	73.4028	4.6421	21.9290	524 ± 2	525 ± 2	532 ± 2	527 ± 2	0.677722	0.444	0.0846692	0.154	0.956399
	S-318B ZK	37	202	297	15	1.46	5940.9	16.71947	4.54050	0.0020	78.3563	4.5671	17.0745	430 ± 2	446 ± 2	526 ± 1		0.671927	0.27	0.0841639	0.265	0.981438
Granite retrogressing charnockite, Vadakkupuram, PPP corridor	S-340 Z-1	56	53	126	7	2.40	1256.0	14.62600	1.29080	0.0247	54.1955	3.5044	42.2754	528 ± 2	527 ± 1	524 ± 2	529 ± 7	0.681274	0.365	0.0854113	0.354	0.973907
	S-340 Z-3	50	69	151	9	2.20	1398.0	15.66600	1.41170	0.0236	56.4160	3.6011	39.9593	521 ± 3	521 ± 3	520 ± 2	519 ± 14	0.670667	0.718	0.0842478	0.713	0.993058
	S-340 Z-4	48	57	157	8	2.77	1289.0	15.67700	1.10800	0.0207	50.8475	3.2451	45.8867	526 ± 1	526 ± 1	525 ± 3	530 ± 2	0.67887	0.272	0.0850783	0.239	0.88513
Granite gneiss xenolith within the Kalipara Granite, Athuringal quarry, PPP corridor	S-325C Z1(F)	10	1147	660	106	0.58	622.0	13.59200	4.52480	0.0563	77.1959	5.6869	17.0608	506 ± 2	545 ± 2	714 ± 3	542 ± 3	0.71625	0.465	0.0816742	0.425	0.946824
	S-325C Z3	10	938	1045	163	1.11	830.0	12.80800	2.52900	0.0367	67.8395	5.2967	26.8271	820 ± 3	854 ± 2	941 ± 3	886 ± 3	1.3177	0.373	0.135702	0.335	0.926068
	S-325C Z4	12	1130	1129	137	1.00	733.0	13.02000	2.97200	0.0434	70.7211	5.4301	23.8054	607 ± 2	666 ± 2	872 ± 4	605 ± 3	0.925967	0.43	0.0986103	0.367	0.8886
	S-325C Z6	10	1187	454	155	0.38	886.0	12.89600	6.33780	0.0440	80.9040	6.2876	12.7644	742 ± 2	790 ± 2	925 ± 2	607 ± 2	1.17564	0.336	0.122044	0.306	0.935045
	S-325C Z7	48	234	90	34	0.38	1706.0	14.20200	7.58610	0.0013	83.1773	5.8568	10.9646	842 ± 3	868 ± 3	935 ± 1	912 ± 4	1.35064	0.493	0.13955	0.488	0.9905471
Monazite from Khondalite, Cardamom Hills, PPP corridor	S-355E M-2	14	1603	36111	819	22.3	4697.4	16.48149	0.15000	0.0018	14.3974	0.8580	84.7429	516 ± 1	518 ± 2	524 ± 8	427 ± 42	0.665263	0.49	0.083405	0.27	0.6178
	S-355E M-3	28	197	27700	667	140	1016.7	13.97794	0.02263	0.0003	2.1524	0.1285	97.7188	517 ± 4	519 ± 3	526 ± 5	523 ± 4	0.666214	0.853	0.083436	0.819	0.966657
	S-355E M-4	16	806	21140	560	26.24	3280.6	16.21450	0.12129	0.0024	10.6634	0.6477	88.6865	527 ± 1	525 ± 1	514 ± 1	523 ± 1	0.676492	0.181	0.0851985	0.173	0.953649
	S-355E M-5	19	1456	54980	1400	37.75	4026.0	16.34553	0.08452	0.0008	7.6983	0.4571	91.8438	527 ± 1	527 ± 1	523 ± 1	521 ± 2	0.67958	0.225	0.0852493	0.215	0.959436
	S-355E M-6	6	1874	46520	1251	24.83	2040.8	15.49679	0.12772	0.0035	11.1424	0.6968	88.1572	528 ± 1	527 ± 1	522 ± 1	527 ± 2	0.68013	0.237	0.0853445	0.228	0.964612
Charnockitized khondalite, Kottaram, Nagercoil Block	S-361A ZA	20	310	92	87	0.30	245.7	7.15813	4.28197	0.2698	73.5745	9.9347	16.2211	1300 ± 5	1291 ± 3	1278 ± 5	1264 ± 12	1.04285	1.2	0.0870602	0.973	0.83132
	S-361A ZB	20	311	92	38	0.30	164.1	5.86862	3.04895	0.3536	68.3944	10.9024	20.3496	538 ± 5	725 ± 6	1358 ± 13		2.5688	0.486	0.223505	0.401	0.85665
	S-361A ZD	20	696	169	17	0.24	81.3	3.80532	1.88297	0.1868	77.0756	10.0379	12.6997			1561 ± 100		1.53481	0.512	0.130805	0.5	0.978354
	S-361A ZE	15	318	109	44	0.34	1500.0	10.74481	6.66048	0.0095	81.9554	7.1083	10.9268	792 ± 4	944 ± 3	1318 ± 2	947 ± 7	1.53458	0.317	0.130683	0.301	0.954123
	S-361A ZF	15	224	119	55	0.53	1484.6	8.38780	6.62635	0.0342	79.2023	9.3039	11.4596	1308 ± 10	1519 ± 7	1826 ± 1	1054 ± 60	2.28805	0.344	0.167731	0.318	0.928949
	S-361A ZG	15	209	72	37	0.34	2065.0	9.63515	7.30465	0.0108	81.4285	8.2043	10.3564	1000 ± 3	1209 ± 2	1604 ± 2	1135 ± 6	3.46233	0.841	0.224962	0.838	0.9969125

Table-4.3. U-Pb zircon and monazite geochronological data by IDTIMS method carried out at the UCT laboratory.

	Sample No.	Wt (µg)	Concentration (ppm)			Th/U ratio	Spiked Data			Isotopic Composition of Pb (unspiked)				Age, in million years				Isotopic ratios				
			U	Th	Pb		$^{206}Pb/^{204}Pb$	$^{208}Pb/^{207}Pb$	$^{206}Pb/^{208}Pb$	^{204}Pb	^{206}Pb	^{207}Pb	^{208}Pb	$^{206}Pb/^{238}U$	$^{207}Pb/^{235}U$	$^{207}Pb/^{206}Pb$	$^{208}Pb/^{232}Th$	207/235	Error (%)	206/238	Error (%)	Rho
Mafic granulite, Trivandrum, Trivandrum Block	T-4 Z-1	8	172	500	29	2.91	343.2	9.86590	1.02990	0.0570	48.8221	3.8370	47.2839	575 ± 6	594 ± 5	664 ± 7	585 ± 7	0.788707	1.18	0.0933298	1.13	0.965097
	T-4 Z-2	9	291	648	41	2.23	737.4	12.10688	1.70335	0.0254	60.8232	4.2866	34.8649	603 ± 5	636 ± 4	577 ± 2	478 ± 4	0.869856	0.897	0.0980023	0.885	0.988498
	T-4 Z-3	22	203	554.6	32	2.73	1518.3	14.23097	1.12506	0.0044	51.2254	3.2191	45.5511	572 ± 3	590 ± 2.5	661 ± 2	580 ± 4	0.784678	0.56	0.0926191	0.551	0.985463
	T-4 Z-4	17	136.3	341.3	22	2.50	325.4	9.63070	1.17310	0.1052	51.5520	4.6687	43.6740	570 ± 6	585 ± 5	640 ± 8	567 ± 6	0.772477	1.09	0.0923548	1.07	0.947373
Monazite from garnet-biot. gneiss, Trivandrum Block	S-320 M-1	15	510	230	49	0.4513	343.9	9.94000	4.18400	0.2029	74.8631	7.3849	17.5492	489 ± 1	504 ± 3	575 ± 12	471 ± 2	0.64297	0.669	0.0787597	0.352	0.5359
	S-320 M-2	47	139	62	13	0.4486	322.9	9.94130	4.37440	0.2115	75.7207	7.3584	16.7093	475 ± 2	474 ± 3	468 ± 11	401 ± 3	0.711873	0.673	0.0825149	0.38	0.62201
	S-320 M-3	40	117	35	14	0.3016	148.3	6.30300	2.90900	0.4283	66.8094	10.3640	22.3983	511 ± 2	546 ± 3	694 ± 11	570 ± 5	0.594826	0.703	0.0765142	0.452	0.67734
	S-320 M-5	80	68	13	8	0.1851	131.3	5.83580	3.05900	0.4916	66.8633	11.3078	21.3373	503 ± 2	535 ± 2	678 ± 5	421 ± 4	0.694332	0.418	0.0810703	0.337	0.82571
	S-320 M-6	46	213	105	20.3	0.4949	332.0	10.03800	4.17700	0.2111	74.9478	7.2929	17.5481	483 ± 1	488 ± 1	462 ± 4	412 ± 1	0.603557	0.306	0.077818	0.247	0.82551
	S-320 M-7	103	66	37	8	0.5661	170.1	6.93700	2.65500	0.3717	65.7993	9.2937	24.5353	497 ± 1	514 ± 2	591 ± 6	485 ± 2	0.658984	0.403	0.0800978	0.298	0.76604

Table 4. 4. U-Pb geochronological data using SHRIMP-II at the Curtin University, Australia.

Spot	U/ppm	Th/ppm	Th/U	Pb/ppm	204 counts	4f206	207/206-4	+/-	206/238-4	+/-	207/235-4	+/-	208/232-4	+/-	%conc-4	Age6/38-4	+/-	Age7/35-4	Age7/6-4	+/-	Age8/32-4	+/-
S-404a; Biotite Gneiss, Palghat, Corridor-IV																						
S-404a.74.1	489	351	0.717569	161	12	0.000579	0.101594	0.000546	0.291398	0.002622	4.08182	0.045077	0.085515	0.000932	100	1649	13	1651	1653	10	1658	17
S-404a.58.1	632	413	0.653527	207	26	0.001225	0.10059	0.000487	0.293196	0.00258	4.06643	0.042958	0.084891	0.000896	101	1657	13	1648	1635	9	1647	17
S-404a.58.2	437	102	0.232751	119	26	0.002786	0.101409	0.000981	0.266297	0.002553	3.723436	0.053779	0.080887	0.002171	92	1522	13	1576	1650	18	1572	41
S-404a.57.1	506	91	0.179798	270	13	0.000571	0.198467	0.000668	0.493827	0.00446	13.513414	0.135456	0.148526	0.002147	92	2587	19	2716	2814	5	2799	38
S-404a.57.2	151	113	0.752224	99	18	0.001731	0.198364	0.001114	0.535885	0.005586	14.656689	0.182372	0.150057	0.002167	98	2766	23	2793	2813	9	2826	38
S-404a 48.1	514	74	0.143091	291	11	0.000226	0.200514	0.000531	0.530868	0.00314	14.676833	0.099435	0.140429	0.001679	97	2745	13	2795	2830	4	2656	30
S-404a 48.2	848	38	0.045357	516	22	0.000124	0.198077	0.000326	0.583932	0.003203	15.947701	0.09441	0.162103	0.002515	105	2965	13	2874	2810	3	3037	44
S-404a.54.1c	1220	110	0.09003	712	12	0.000042	0.193243	0.000275	0.557078	0.002979	14.842973	0.084657	0.15234	0.001266	103	2855	12	2805	2770	2	2866	22
S-404a 54.2r	663	150	0.226981	352	11	0.000086	0.164849	0.000359	0.503168	0.002837	11.43671	0.071988	0.136605	0.001096	105	2627	12	2559	2506	4	2588	19
S-404a.61.1	333	113	0.338761	192	25	0.000721	0.189289	0.000598	0.522739	0.00321	13.643046	0.098911	0.138533	0.001419	99	2711	14	2725	2736	5	2622	25
S-404a.61.2	714	131	0.182795	413	22	0.00024	0.193404	0.000371	0.540526	0.003023	14.413975	0.088425	0.144275	0.001228	101	2786	13	2717	2771	3	2724	22
S-404a.71.1c	99	59	0.597677	65	13	0.000624	0.204076	0.001119	0.550887	0.004464	15.500834	0.160218	0.151382	0.002092	99	2829	19	2847	2859	9	2849	37
S-404a.71.2r	742	143	0.19256	445	18	0.000171	0.196602	0.000369	0.557543	0.003104	15.113559	0.092109	0.151314	0.001231	102	2856	13	2822	2798	3	2848	22
S-404a 31.1	779	624	0.801548	276	54	0.001151	0.098912	0.000355	0.294148	0.001643	4.011594	0.028099	0.107735	0.00072	104	1662	8	1637	1604	7	2068	13
S-404a 31.2	445	342	0.767916	150	14	0.000227	0.101243	0.000467	0.294388	0.001773	4.10949	0.033001	0.086002	0.000685	101	1663	9	1656	1647	9	1668	13
S-404a.31.3	447	340	0.760588	147	15	0.000444	0.101225	0.000536	0.289501	0.001784	4.040552	0.034804	0.081672	0.000676	100	1639	9	1642	1647	10	1587	13
S-404a.23.1c	182	97	0.533491	56	14	0.001096	0.099131	0.000811	0.281602	0.002018	3.848999	0.044374	0.083579	0.001085	99	1599	10	1603	1608	15	1622	20
S-404a.23.2c	1512	450	0.297848	467	24	0.00019	0.099495	0.00021	0.303168	0.001609	4.158986	0.024756	0.086508	0.000558	106	1707	8	1666	1615	4	1677	10
S-404a.23.3r	389	258	0.663333	126	13	0.00052	0.100866	0.000542	0.28912	0.001793	4.02091	0.034958	0.085462	0.00076	100	1637	9	1638	1640	10	1658	14
S-404a.8.1	837	162	0.193595	480	14	0.000115	0.19524	0.000381	0.534298	0.002972	14.383118	0.08806	0.144485	0.00116	99	2760	12	2775	2787	3	2728	20
S-404a-2.1	511	413	0.808173	166	11	0.000007	0.099964	0.000462	0.282875	0.001686	3.898859	0.031135	0.082716	0.000645	99	1606	8	1613	1623	9	1606	12
S-404a-34.1	1377	1328	0.964222	881	85	0.000721	0.193958	0.000289	0.505703	0.002708	13.52401	0.077558	0.141987	0.00083	95	2638	12	2717	2776	2	2684	15
S-404a-34.2	632	564	0.893004	423	18	0.000242	0.197661	0.000432	0.539165	0.003076	14.694138	0.093455	0.148131	0.000994	99	2780	13	2796	2807	4	2792	17
S-404a.36.1	497	358	0.720702	162	7	0.000023	0.100798	0.000448	0.289332	0.001728	4.021158	0.031671	0.083768	0.000661	100	1638	9	1638	1639	8	1626	12
S-404a 13.1	85	51	0.603423	52	25	0.001651	0.193108	0.000882	0.514898	0.003403	13.709551	0.116431	0.149678	0.001595	97	2678	14	2730	2769	7	2819	28
S-259; Monazite, Moyar Shear Zone, Bhavani area, Corridor-II																						
S-259.1	0.06%	6.60%	0.21%	136	8		0.000336	32.722704	0.002193	1.160421	0.021327			100	781	13	782	782	11	0	0	
S-259 2	0.22%	6.20%	0.19%	138	3	0.000007	0.000166	7.182528	0.002244	1.2063	0.020768			104	812	13	803	803	5	0	0	
S-259.3	0.15%	7.10%	0.21%	183	6	0.000039	0.00021	12.37878	0.002069	1.096641	0.019156			99	750	12	752	752	7	0	0	
S-259.4	0.11%	7.80%	0.23%	185	9	0.000026	0.000236	17.448932	0.002228	1.195587	0.02107			102	802	13	799	799	8	0	0	
S-259 5	0.15%	6.20%	0.18%	143	7	0.000007	0.000206	10.462139	0.002123	1.153012	0.020091			95	769	12	779	779	7	0	0	
S-259.6	0.13%	7.90%	0.24%	139	10		0.000221	15.790321	0.0022	1.189481	0.020845			99	794	13	796	796	7	0	0	
S-273; Monazite from Khondalite, Valya Malai Hill, Corridor-I																						
S-273.10	0.09%	1.50%	0.05%	46	3	0.000064	0.000289	5.118686	0.001721	0.840326	0.015236			105	626	10	619	619	10	0	0	
S-273.11	0.29%	8%	0.19%	176	12		0.00016	7.1577	0.001684	0.842461	0.014511			99	620	10	621	621	6	0	0	
S-273.12	0.13%	7%	0.21%	150	4		0.000245	14.087907	0.001981	1.240539	0.021671			65	719	11	819	819	6	0	0	
S-273.13	0.24%	6.10%	0.15%	169	4	0.000044	0.000179	6.758451	0.001686	0.834373	0.014466			103	620	10	616	616	6	0	0	
S-273.4	0.68%	5%	0.20%	161	9	0.00002	0.000104	2.076718	0.001738	0.867307	0.0147			105	640	10	634	634	4	0	0	
S-273.5	0.19%	1.70%	0.05%	49	2	0.000036	0.000206	2.315268	0.001562	0.774813	0.013558			94	575	9	583	583	7	0	0	
S-273.5.2	0.11%	0.50%	0.02%	16	5	0.00001	0.000265	1.11813	0.001612	0.799	0.014315			95	590	9	596	596	9	0	0	
S-273 6	0.73%	4.90%	0.80%	100	8		0.000083	1.493177	0.007993	10.934716	0.182675			101	2529	35	2518	2518	1	0	0	
S-273.7	0.35%	2.90%	0.11%	86	6	0.000023	0.000147	2.426369	0.001673	0.828942	0.014226			102	616	10	613	613	5	0	0	
S-273.8	0.18%	3%	0.09%	63	9		0.000207	4.662223	0.001621	0.805835	0.014106			96	596	10	600	600	7	0	0	
S-273.9	0.30%	5.90%	0.18%	141	6	0.00001	0.000169	4.846787	0.001884	1.173289	0.020078			64	690	11	788	788	4	0	0	
S-273.1	0.74%	3.70%	0.62%	88	3	0.000001	0.000081	0.891573	0.008151	11.035518	0.184365			103	2570	35	2526	2526	1	0	0	
S-273.2	0.33%	2.20%	0.08%	55	4	0.000005	0.00015	1.820683	0.001651	0.822805	0.01413			99	608	10	610	610	5	0	0	
S-273.3	0.29%	1.90%	0.07%	60	8	0.000024	0.000162	1.834681	0.001662	0.826912	0.014257			100	612	10	612	612	6	0	0	

Table 4. 4. U-Pb geochronological data using SHRIMP-II at the Curtin University, Australia.

Spot	U/ppm	Th/ppm	Th/U	Pb/ppm	204 counts	4f206	207/206-4	+/-	206/238-4	+/-	207/235-4	+/-	208/232-4	+/-	%conc-4	Age6/38-4	+/-	Age7/35-4	Age7/6-4	+/-	Age8/32-4	+/-
S-320; Garnet-biotite gneiss, Trivandrum Block, PPP corridor																						
S-320/2.1	4150	63	0.015187	149	60	0.002588	0.058232	0.000494	0.039059	0.00046	0.313605	0.004816	0.008685	0.002379	46	247	3	277	538	19	175	48
S-320/2.2	6929	357	0.051564	337	2403	0.092434	0.06614	0.001908	0.038094	0.000453	0.347396	0.011308	0.003655	0.00332	30	241	3	303	811	60	74	67
S-320/6.1	2081	16	0.007738	151	46	0.001574	0.057262	0.000391	0.079088	0.00093	0.624423	0.008944	0.020915	0.006853	98	491	6	493	502	15	418	136
S-320-5.1a	4917	104	0.021109	211	2229	0.099826	0.063043	0.002159	0.032599	0.000391	0.283367	0.010673	0.02923	0.0079	29	207	2	253	710	73	582	155
S-320-5.2a	4370	106	0.024196	171	934	0.046636	0.066783	0.001516	0.035427	0.000421	0.326212	0.008776	0.032637	0.005213	27	224	3	287	831	47	649	103
S-320-12.1a	5529	79	0.014263	144	201	0.01678	0.064416	0.001262	0.025046	0.000298	0.222447	0.005375	0.135084	0.005374	21	159	2	204	755	41	2561	96
S-320-12.3a	5482	98	0.017841	128	38	0.002345	0.059166	0.000558	0.025361	0.0003	0.206894	0.003312	0.004766	0.001446	28	161	2	191	573	21	96	29
S-320-12.4a	5403	82	0.015176	126	72	0.004839	0.059783	0.000727	0.025004	0.000296	0.206105	0.00371	0.005255	0.002452	27	159	2	190	596	26	106	49
S-320-15.1b	2188	21	0.009479	236	499	0.014158	0.077538	0.000661	0.109825	0.00129	1.174137	0.01803	0.059049	0.016692	59	672	7	789	1135	17	1160	315
S-320-15.2b	1983	25	0.012588	154	31	0.000674	0.071837	0.000448	0.083942	0.000992	0.831442	0.011666	0.035726	0.004128	53	520	6	614	981	13	709	81
S-320-15.3b	1527	23	0.015057	117	22	0.001018	0.068655	0.000425	0.082637	0.000976	0.782257	0.010955	0.023196	0.003294	58	512	6	587	888	13	463	65
S-320-15.4b	1611	26	0.01621	123	26	0.000928	0.069239	0.000429	0.082427	0.000973	0.786899	0.011014	0.026751	0.003294	56	511	6	589	906	13	534	65
S-320-17.1a	5428	77	0.014256	131	218	0.014132	0.05978	0.000955	0.024938	0.000295	0.205549	0.004324	0.007132	0.003716	27	159	2	190	596	35	144	75
S-320-17.2a	4902	64	0.012967	127	61	0.003273	0.061044	0.000615	0.027974	0.000331	0.235454	0.003876	0.013018	0.002523	28	178	2	215	641	22	261	50
S-320-18.1b	1436	14	0.009652	132	33	0.001029	0.078791	0.000471	0.098543	0.001165	1.07054	0.01488	0.036684	0.007492	52	606	7	739	1167	12	728	146
S-320-2.b	1673	19	0.011268	136	166	0.009729	0.071837	0.000839	0.084317	0.000999	0.835142	0.014737	0.047186	0.013404	53	522	6	616	981	24	932	259
S-320-1.1b	1712	25	0.014556	98	84	0.005972	0.063179	0.00077	0.061079	0.000725	0.532065	0.009604	0.018039	0.006659	54	382	4	433	714	26	361	132
S-320-46.1a	8753	112	0.012763	540	4708	0.152341	0.098471	0.0024	0.038295	0.000459	0.519942	0.014804	0.134325	0.017096	15	242	3	425	1595	46	2548	305
S-320-45.1b	1976	54	0.027465	123	36	0.001585	0.061003	0.000492	0.067471	0.000797	0.567505	0.008577	0.018513	0.002146	66	421	5	456	639	17	371	43
S-320.8.1b	1662	26	0.015837	111	29	0.001442	0.064483	0.000469	0.072114	0.000852	0.641154	0.009381	0.020236	0.003451	59	449	5	503	758	15	405	68
S-320.8.2b	2034	24	0.011631	119	38	0.001766	0.059139	0.000498	0.063588	0.000752	0.518502	0.007959	0.021743	0.004872	69	397	5	424	572	18	435	96
S-320.8.3a	3786	85	0.022339	130	94	0.005222	0.061744	0.000672	0.03653	0.000432	0.31099	0.005297	0.010355	0.002259	35	231	3	275	665	23	208	45
S-320.3.1b	1922	33	0.016996	143	133	0.008356	0.070078	0.000792	0.077624	0.00092	0.750036	0.013029	0.057554	0.007646	52	482	6	568	931	23	1131	146
S-320.38.1b	2622	37	0.013982	200	1726	0.114255	0.020623	0.002813	0.064147	0.000784	0.182401	0.025256	-0.727098	-0.032		401	5	170		8		96
S-320-20.1a	3926	70	0.017893	136	158	0.009574	0.06118	0.000825	0.036316	0.00043	0.306339	0.005833	0.013318	0.003573	36	230	3	271	646	29	267	71
S-361; Charnockite gneiss, Kottaram quarry, Nagercoil Block																						
S-361a.23.1	571	157	0.274595	53	16	0.001588	0.059509	0.00079	0.093095	0.001138	0.763845	0.01462	0.028496	0.000667	98	574	7	576	586	29	568	13
S-361a.23.2	409	187	0.45703	36	31	0.00544	0.055959	0.001303	0.084937	0.001064	0.655347	0.018204	0.025256	0.000659	117	526	6	512	451	52	504	13
S-361a.24.1	713	243	0.340127	65	26	0.001966	0.060821	0.000754	0.090772	0.001099	0.761206	0.013988	0.02819	0.000564	88	560	6	575	633	27	562	11
S-361a.26.1	552	116	0.210613	248	22	0.000618	0.127985	0.000396	0.438437	0.005238	7.736916	0.098323	0.126415	0.001824	113	2344	23	2201	2070	5	2406	33
S-361a.25.1	594	175	0.295331	57	65	0.010375	0.05934	0.00152	0.093869	0.001162	0.768016	0.022896	0.029067	0.001176	100	578	7	579	580	56	579	23
S-361a.31.1	223	86	0.387383	111	8	0.002126	0.125453	0.001472	0.470026	0.007105	8.130285	0.164738	0.121718	0.003684	122	2484	31	2246	2035	21	2322	66
S-361a.31.2	319	54	0.17033	132	25	0.001156	0.126961	0.000612	0.406977	0.004975	7.124283	0.09753	0.116932	0.002518	107	2201	23	2127	2056	9	2235	46
S-361a.31.3	378	70	0.184249	32	16	0.002581	0.059067	0.001263	0.085789	0.001084	0.698679	0.018283	0.028001	0.001317	93	531	6	538	570	47	558	26
S-361a.33.1	503	367	0.729689	184	20	0.000715	0.121526	0.000524	0.315909	0.003805	5.293384	0.070352	0.096047	0.001269	89	1770	19	1868	1979	8	1854	23
S-361a.33.2	610	166	0.272575	55	19	0.001744	0.060244	0.000883	0.090454	0.001108	0.751349	0.015208	0.028161	0.000723	91	558	7	569	612	32	561	14
S-361a.28.1	333	167	0.501868	138	33	0.001454	0.120825	0.000682	0.38422	0.004728	6.400875	0.09066	0.096518	0.001521	106	2096	22	2032	1968	10	1862	28
S-361a-z28.2	401	103	0.256581	33	9	0.001605	0.05822	0.00108	0.082803	0.001047	0.664689	0.015772	0.025762	0.000809	95	513	6	517	538	41	514	16
S-268; Anorthosite, Oddhanchattram, Corridor-I																						
S-268.35.1	806	66	0.082187	69	13	0.001496	0.059714	0.000614	0.091507	0.001103	0.753403	0.01265	0.029805	0.001256	95	564	7	570	593	22	594	25
S-268.36.1	679	55	0.081334	57	35	0.003402	0.058744	0.000868	0.089483	0.001087	0.724784	0.014684	0.028113	0.001993	99	552	6	553	558	32	560	39
S-268.nm1.1	894	57	0.063858	76	55	0.004838	0.060141	0.000795	0.090114	0.001083	0.747257	0.014149	0.032204	0.00235	91	556	6	567	609	29	641	46
S-268.nm2.1	1091	50	0.045787	93	52	0.003528	0.057876	0.000641	0.091806	0.001095	0.732599	0.012652	0.02606	0.002565	108	566	6	558	525	24	520	51
S-268.nm-3.1	203	47	0.231748	18	18	0.006508	0.062331	0.00232	0.090116	0.001246	0.774473	0.031977	0.030877	0.002095	81	556	7	582	685	80	615	41
S-268.nm-4.1	366	129	0.351577	35	29	0.00564	0.057887	0.001397	0.09417	0.001198	0.751616	0.021532	0.028793	0.00094	110	580	7	569	526	53	574	18
S-268.nm-5.1	791	39	0.048677	68	23	0.001803	0.059154	0.000747	0.092626	0.001116	0.755471	0.013987	0.033017	0.00285	100	571	7	571	573	27	657	56
S-268.nm-6.1	1254	136	0.108685	107	28	0.00167	0.058976	0.00055	0.090526	0.001078	0.736119	0.011791	0.028641	0.000932	99	559	6	560	566	20	571	18
S-268-nm-7.1	148	34	0.231841	13	16	0.007386	0.062756	0.003194	0.085173	0.001221	0.73698	0.04022	0.032042	0.002768	75	527	7	561	700	109	637	54

Table 4. 4. U-Pb geochronological data using SHRIMP-II at the Curtin University, Australia.

Spot	U/ppm	Th/ppm	Th/U	Pb/ppm	204 counts	4f206	207/206-4	+/-	206/238-4	+/-	207/235-4	+/-	208/232-4	+/-	%conc-4	Age6/38-4	+/-	Age7/35-4	Age7/6-4	+/-	Age8/32-4	+/-
S-117; Mafic Granulite, Namakkal, Corridor-I																						
S-117-51-1c	82	20	0.242873	61	22	0.001784	0.203137	0.001344	0.66898	0.007693	18.737158	0.26169	0.202399	0.00591	116	3302	30	3028	2852	11	3725	99
S-117-51-2r	538	76	0.141519	252	17	0.000365	0.165871	0.000511	0.451328	0.003986	10.322002	0.100249	0.13188	0.002059	95	2401	18	2464	2516	5	2504	37
S-117-51-3r	576	72	0.125892	279	16	0.000392	0.165483	0.000492	0.46803	0.004159	10.678928	0.103758	0.131944	0.002287	99	2475	18	2496	2512	5	2505	41
S-117-51-4r	663	123	0.186001	298	21	0.000595	0.162935	0.000535	0.4286	0.003789	9.628704	0.094421	0.121738	0.00171	92	2299	17	2400	2486	6	2322	31
S-117-51-5r	413	48	0.117048	192	12	0.000152	0.165889	0.000626	0.451025	0.004088	10.316179	0.105679	0.127045	0.002615	95	2400	18	2464	2517	6	2417	47
S-117-51-6r	81	45	0.561645	25	9	0.002972	0.13813	0.002343	0.27269	0.003781	5.193479	0.120541	0.083593	0.002599	71	1554	19	1852	2204	29	1623	48
S-117-51-7c	109	23	0.20913	75	21	0.001863	0.226275	0.001193	0.621578	0.006627	19.392506	0.241835	0.174174	0.00464	103	3116	26	3062	3026	8	3245	80
S-117-51-8c	60	18	0.300391	41	15	0.002463	0.192949	0.002003	0.619216	0.008103	16.473521	0.291442	0.164927	0.006627	112	3107	32	2905	2767	17	3086	115
S-117-51-9c	70	5	0.074703	46	27	0.003663	0.211552	0.001761	0.619014	0.007411	18.055898	0.27829	0.146379	0.021503	106	3106	30	2993	2917	13	2761	379
S-117-51-10c	73	17	0.230842	45	15	0.00222	0.199244	0.001631	0.567448	0.006787	15.588757	0.238719	0.166452	0.006061	103	2897	28	2852	2820	13	3112	105
S-117-52-1c	343	413	1.205016	109	12	0.000601	0.120203	0.000725	0.252543	0.002338	4.185536	0.048822	0.071253	0.00079	74	1452	12	1671	1959	11	1391	15
S-117-52-2r	313	460	1.469403	155	32	0.001871	0.14972	0.000748	0.364656	0.003382	7.527756	0.083329	0.102792	0.001109	86	2004	16	2176	2343	9	1978	20
S-117-554-1	49	33	0.667862	7	23	0.020856	0.061708	0.006912	0.121976	0.002041	1.037813	0.119671	0.037936	0.003021	112	742	12	723	664	242	753	59
S-117-54-2	55	36	0.657444	8	24	0.021095	0.064976	0.006588	0.121203	0.001983	1.085846	0.113691	0.036688	0.002893	95	737	11	746	774	215	728	56
S-117-18-1	62	39	0.636296	92	19	0.001609	0.320414	0.001455	1.149606	0.01377	50.788138	0.676999	0.303362	0.005283	138	4933	41	4008	3572	7	5355	82
S-117-18-2	78	49	0.630074	79	17	0.00181	0.289387	0.001544	0.793594	0.009147	31.664945	0.420897	0.216075	0.003812	110	3766	33	3540	3414	8	3954	63
S-117-8-1	31	30	0.958859	22	20	0.00456	0.171847	0.002989	0.575142	0.008838	13.627612	0.335355	0.160038	0.004796	114	2929	36	2724	2576	29	3001	84
S-117-31-1	133	109	0.822833	33	14	0.001539	0.119878	0.00159	0.213696	0.00232	3.532139	0.064149	0.061249	0.001155	64	1248	12	1534	1954	24	1202	22
S-117-41.1	142	54	0.382724	44	14	0.001452	0.130958	0.001262	0.285742	0.003018	5.159493	0.078227	0.08383	0.001908	77	1620	15	1846	2111	17	1627	36
S-117-30.1	20	22	1.090662	21	15	0.004147	0.180729	0.003248	0.796908	0.01453	19.858071	0.539226	0.229351	0.007253	142	3778	52	3084	2660	30	4174	119
S-117-30.2	20	21	1.045628	13	19	0.007354	0.192866	0.005386	0.475814	0.009126	12.653021	0.452993	0.149418	0.00637	91	2509	40	2654	2767	46	2815	112
S-117-6.1	74	56	0.7564	10	24	0.017551	0.056916	0.004861	0.115776	0.00166	0.908567	0.080269	0.033288	0.00183	145	706	10	656	488	189	662	36
S-117-12.1	58	42	0.722711	40	17	0.002779	0.161444	0.001645	0.589953	0.007371	13.132263	0.224306	0.152061	0.003339	121	2989	30	2689	2471	17	2861	59
S-117.11.1	32	38	1.213335	44	21	0.003774	0.163362	0.001962	1.085755	0.016508	24.455921	0.501813	0.267188	0.006236	190	4739	51	3287	2491	20	4786	99
S-117.10.1	72	63	0.884956	25	28	0.008966	0.132036	0.002406	0.28677	0.003539	5.220683	0.12139	0.077745	0.002016	76	1625	18	1856	2125	32	1513	38
S-117.9.1	81	57	0.700791	26	10	0.001833	0.136161	0.001882	0.28319	0.00339	5.316549	0.103062	0.080683	0.001872	74	1607	17	1872	2179	24	1568	35
S-117.50.1	107	72	0.679317	22	20	0.005825	0.103976	0.002192	0.184735	0.00214	2.6484	0.066996	0.053646	0.001478	64	1093	12	1314	1696	39	1056	28
S-117.2.1	65	44	0.688088	9	24	0.018563	0.058595	0.005446	0.11719	0.001756	0.946782	0.090863	0.033548	0.002232	129	714	10	676	552	204	667	44
S-117.45.1	96	65	0.6752	60	27	0.002891	0.168878	0.001235	0.531599	0.004551	12.378249	0.147743	0.139764	0.002163	108	2748	19	2634	2547	12	2644	38
S-117.46.1	52	28	0.525977	8	57	0.055597	0.057922	0.008873	0.119872	0.001878	0.957328	0.149275	0.036889	0.004695	139	730	11	682	527	341	732	92
S-117.46.2	55	34	0.620883	7	17	0.002826	0.080416	0.005682	0.118862	0.001638	1.317913	0.097075	0.043509	0.00261	60	724	9	854	1207	140	861	51
S-117.46.3	48	25	0.520013	6	22	0.019271	0.061598	0.006274	0.117207	0.001737	0.99546	0.104269	0.035008	0.003299	108	714	10	702	660	220	695	64

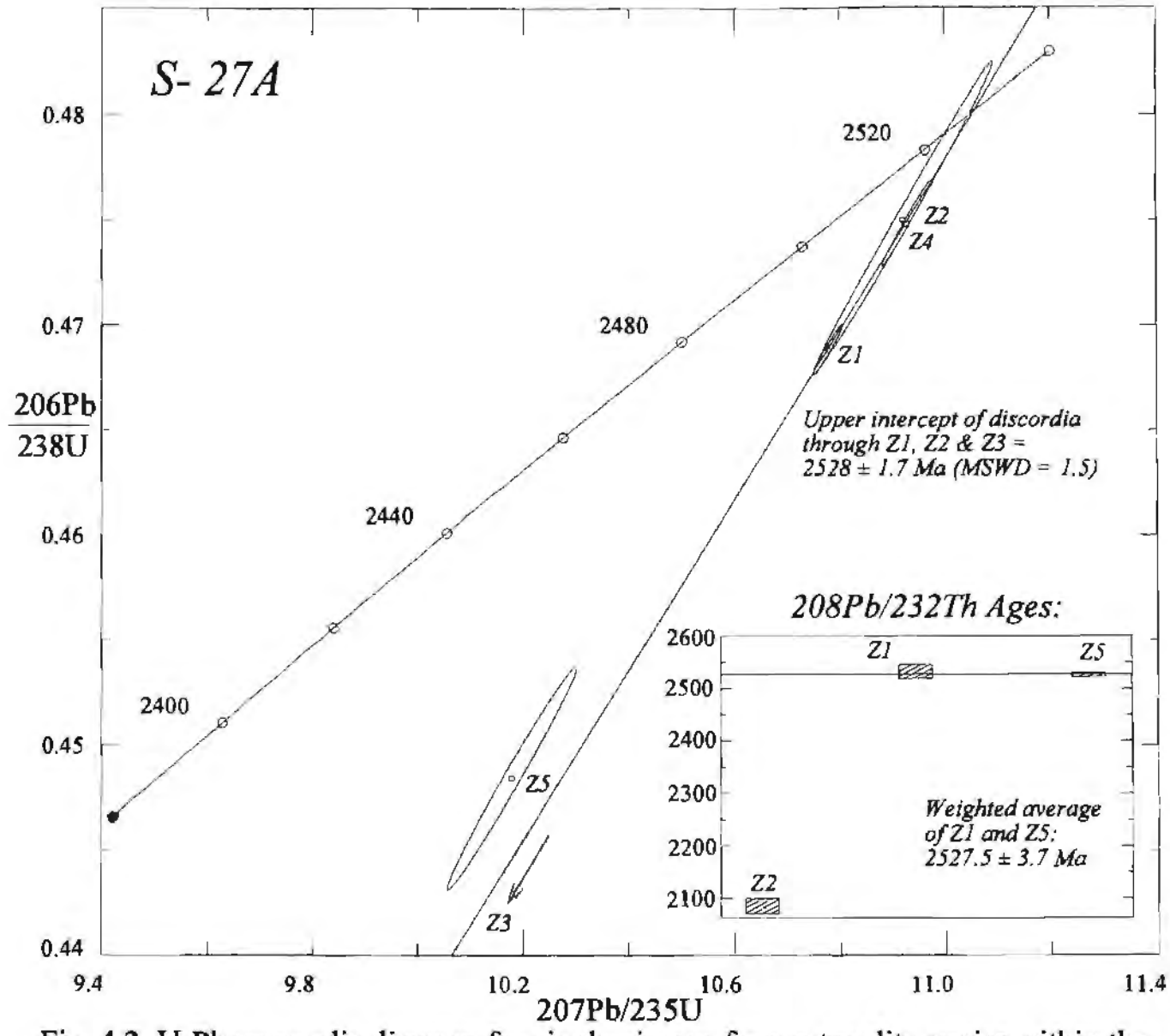

Fig. 4.2. U-Pb concordia diagram for single zircons from a tonalite gneiss within the Moyar Shear Zone, Salem area, Corridor-I.

Table: 4.5: Description of geochronological samples and their ages (includes both TIMS and SHRIMP analyses [Laboratory M= MIT; U= UCT; S=SHRIMP-II,CURTIN).

Sample no.	Laboratory	Location	Rock type and geological setting	Age	Interpretation	Comment
S-27A	U; 5 single crystals of zircons.	78°8'18"E ,11°37'32"N. A quarry section; ~200m north of Kattur village, ~ 2 km southwest of Salem	Tonalite gneiss from within the Moyar-Attur Shear Zone, Salem area. Enderbite gneiss occurs as patches within tonalite gneiss. Gneissosity in both enderbite gneiss and the tonalite gneiss are continuous (Fig. 3.2).	Zircons are colourless, prismatic and subhedral. Five single crystals were analysed. Upper intercept of discordia through four points (the most discordant point was ignored) gives 2528 ± 1.7 Ma age. Weighted average of $^{208}Pb/^{232}Th$ ages of two of three samples analysed is 2528 ± 3.7 Ma, which agrees with the best estimate of U-Pb age (Fig. 4.2).	Intrusive age of tonalite gneiss.	Tonalite gneiss in the area is intrusive into BIF and associated metasediments as well as mafic granulites. Thus, the BIF, its associated metasediments, and the mafic granulites are Archaean in age.

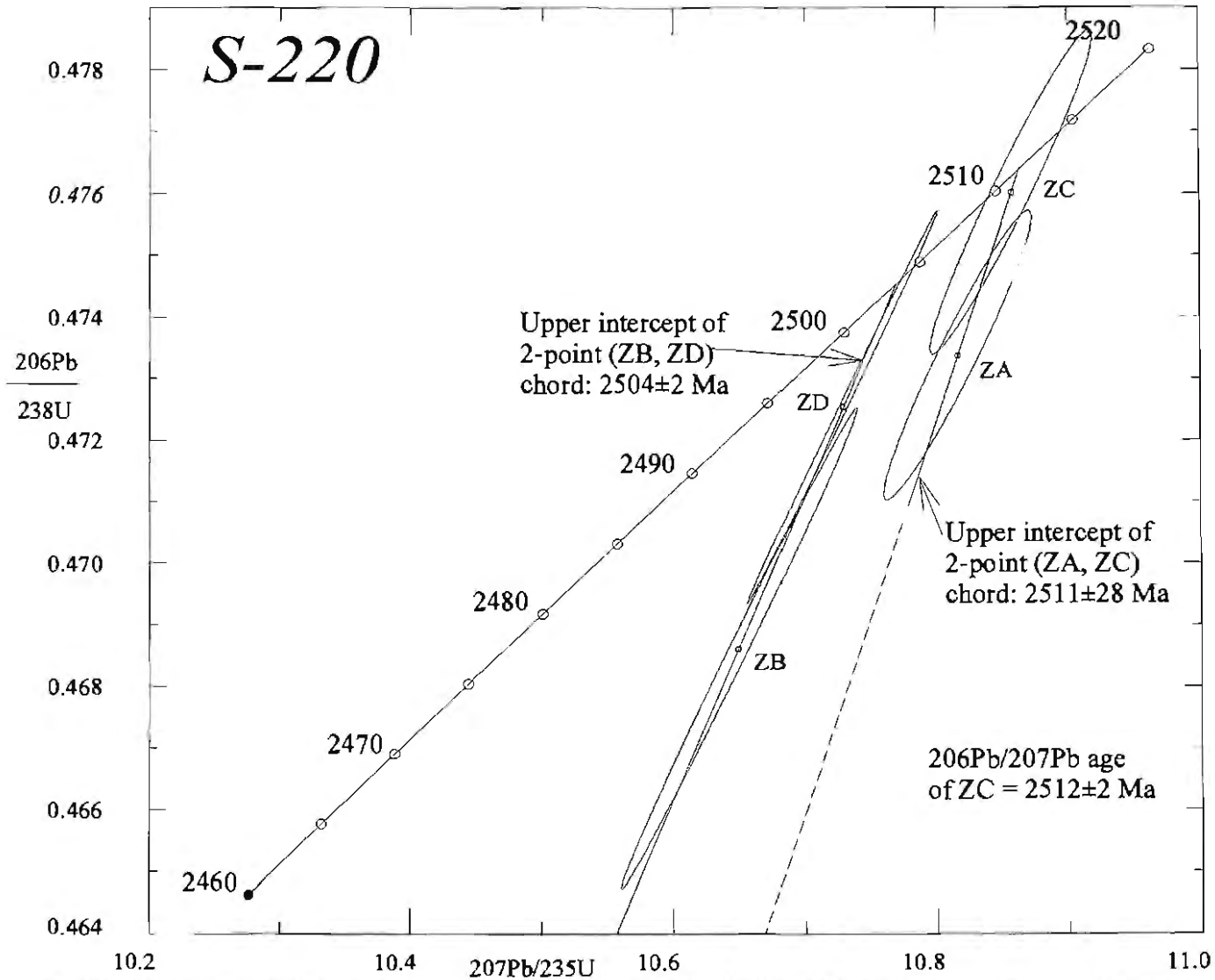

Fig. 4.3. U-Pb concordia diagram for single zircons from tonalite gneiss in the Namakkal area, Corridor-I. Only four crystals (ZA, ZB, ZC & ZD) were analyzed. The upper intercept of a discordia through the two of them (ZA and ZC) is at 2511 ± 28 Ma, which is possibly the best estimate of the age of the rock. Two other grains (ZB and ZD) give upper intercept date of 2504 ± 2 Ma. This date possibly represents a later thermal event. The older date is within error limit of the protolith date of enderbite gneiss from an adjacent (~10 km away) area. The near concordant point, ZC has a 207Pb/206Pb date of 2512 ± 2 Ma.

Sample no.	Laboratory	Location	Rock type and geological setting	Age	Interpretation	Comment
S-220	U; 3 single crystals of zircon.	78°14'33"E; 23°09'54"N; road cut ~2.5 km SE of Singalandapuram, ~20 km NNE of Namakkal.	Biotite gneiss intrusive into mafic granulite (Fig. 3.13).	Zircons are colourless and prismatic. Three single zircon crystals were analysed; all of them fall close to the concordia. The most concordant grain has $^{207}Pb/^{206}Pb$ age of 2512 ± 2 Ma (Fig. 4.3).	Intrusive age of the biotite gneiss.	This ~2.5 Ga granitic biotite gneiss is the most extensive rock type in the area.

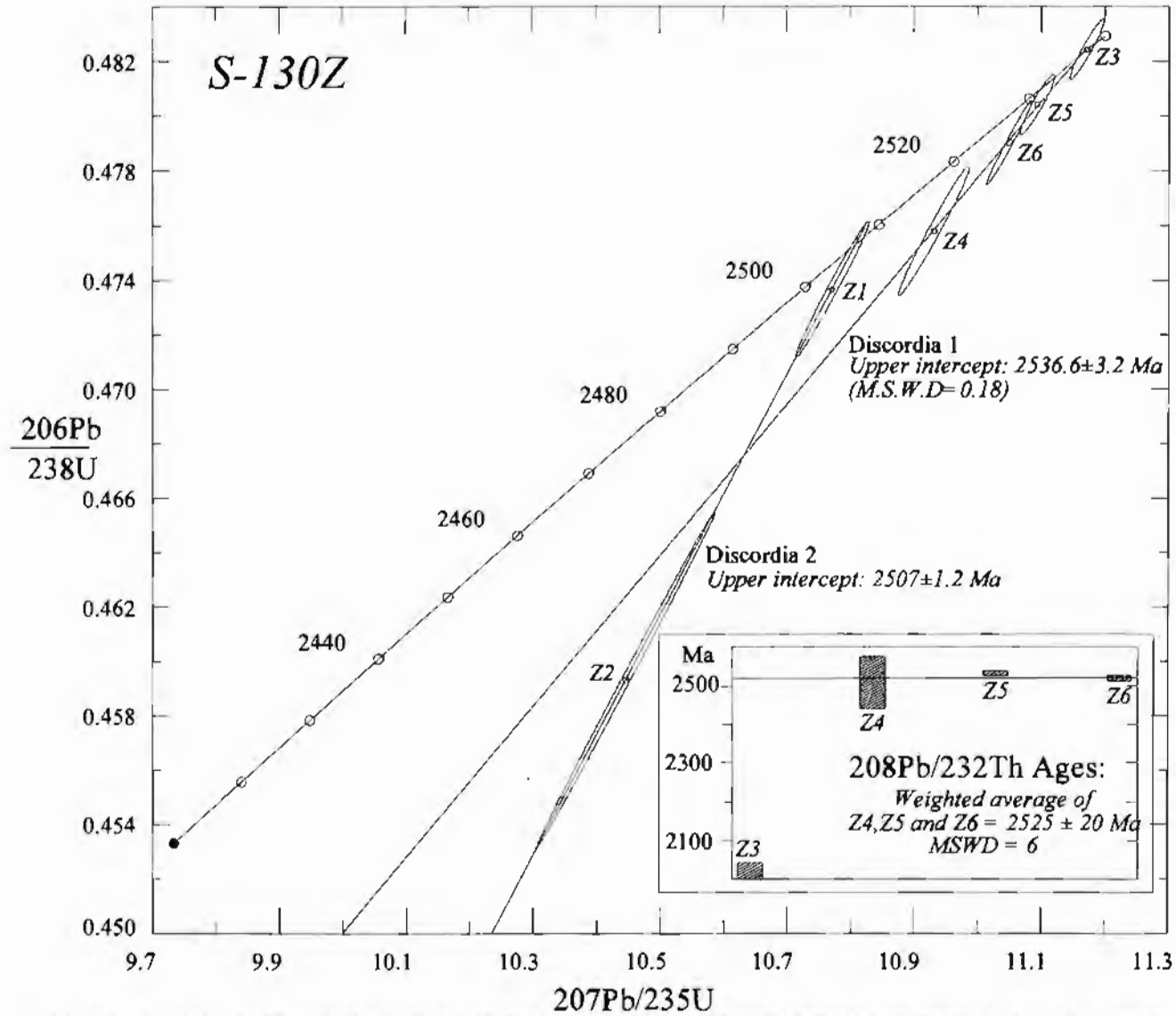

Fig. 4.4. U-Pb concordia diagram for single crystal zircons from a charnockite gneiss, syntectonic with D1 shearing in the Namakkal area, Corridor-I. Z3, Z4, Z5 and Z6 define a discordia with an upper intercept at 2537 ± 3 Ma. This is the best estimate of the protolith age. 208Pb/232Th ages (inset) are compatable with this age. Z1 and Z2 possibly form a different population with concordia upper intercept at 2507 ± 1.2 Ma. This age is similar to the reported U-Pb monazite ages from north of the MSZ and thus may represent zircon growth during Late Archean charnockitization. Monazites from the present rock also indicate similar age renge (Fig. 4.5).

Sample no.	Laboratory	Location	Rock type and geological setting	Age	Interpretation	Comment
S-130	U; 6 single crystals.	78°12'04"E; 11°19'40"N; hill top sample; ~1km NNW of Nainarmalai temple.	Charnockite gneiss from patches within granite gneiss. Gneissosity in both granite gneiss and charnockite gneiss are continuous. This granite gneiss body has intruded along the short limb of a mappable Z shaped fold (Fig. 3.13)	Zircons are light pink in colour, prismatic and subhedral. Four of the six grains with Th/U between 0.1 and 0.8 define a discordia with an upper intercept of 2536.6 ± 3.2 Ma. The most concordant grain has a $^{207}Pb/^{206}Pb$ age of 2537 ± 0.7 Ma. Two other grains with Th/U ratio of 1.24 and 1.71 define a discordia with a upper intercept of 2507 ± 1.2 Ma (Fig. 4.4).	The intrusive age of this body is 2537 ± 0.7 Ma. The 2507 ± 1.2 Ma age defined by a two point chord possibly indicates new zircon growth subsequent to its emplacement. This younger age tallies well with reported age of charnockitization from the Krishnagiri area, ~150 km north of Namakkal (Peucat et al. 1993).	This granite gneiss is interpreted as syn- or post-tectonic with the NE-SW trending D_1 shears present in the area possibly continuous with the Eastern Ghat trend. The younger age of ~2507 Ma may indicate an age of charnockitization.

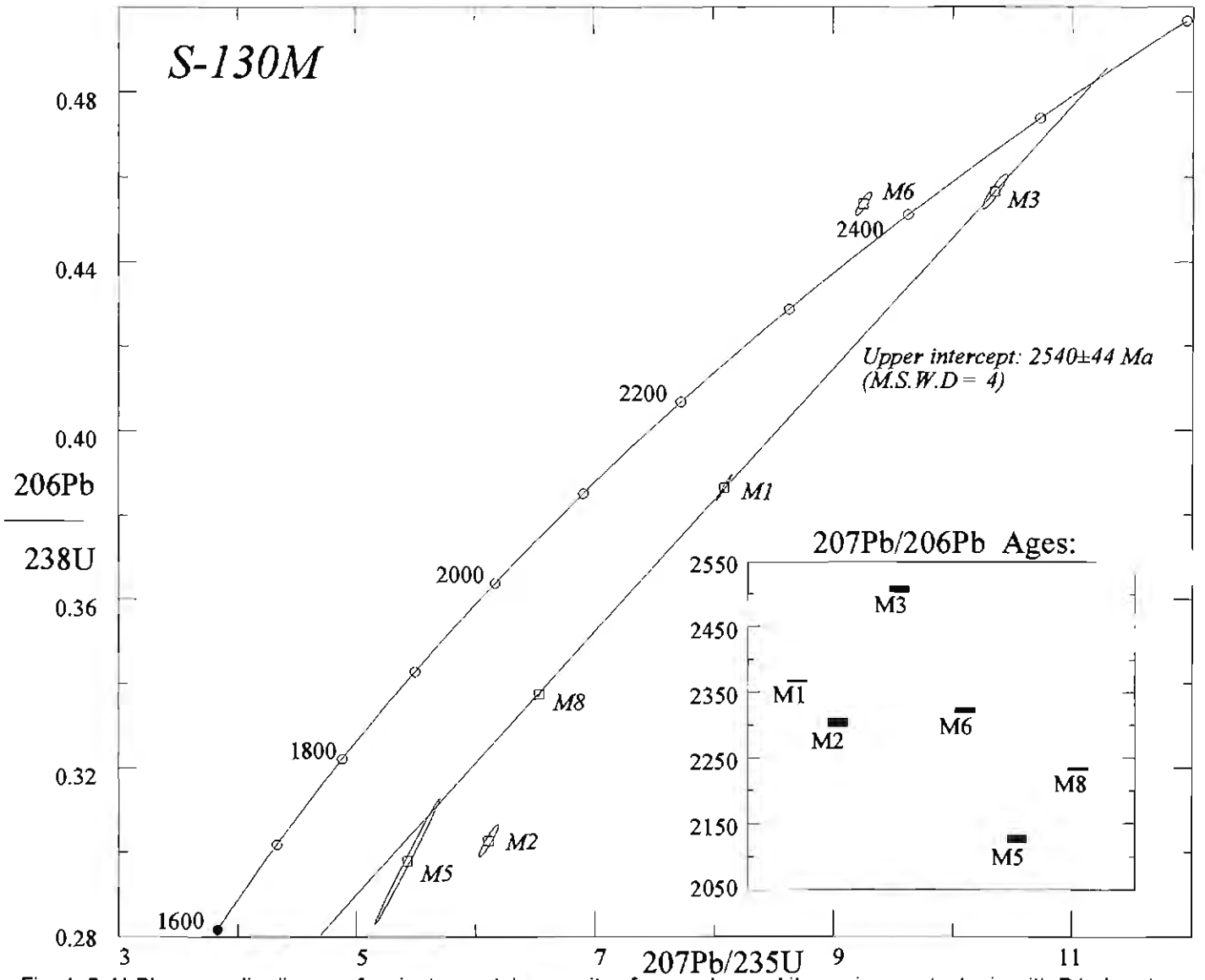

Fig. 4. 5. U-Pb concordia diagram for single crystal monazites from a charnockite gneiss, syntectonic with D1 shearing in the Namakkal area, Corridor-I. M1, M3, M5 and M8 define a discordia with upper intercept at 2540 ± 44 Ma. This large error in upper intercept age is because of large discordancy of the grains. The least discordant crystal (M3) has an 207Pb/206 Pb age of 2507 ± 5 Ma. This is the best estimate of the age of the monazite crystallization. This age may reflect the age of the high-grade metamorphism of the rock.

Sample no.	Laboratory	Location	Rock type and geological setting	Age	Interpretation	Comment
S-130M	U; 6 monazite crystals were analysed.	Same as S-130	Same as S-130	All the grains are discordant. They have very high Th (>3.5%) and consequently high ^{208}Pb content. This has affected precise estimation of ^{207}Pb content due to large tail effect of ^{208}Pb. The most concordant monazite crystals have a $^{207}Pb/^{206}Pb$ age of 2507 ± 5.4 Ma (Fig. 4.5). This age matches with the 2507 ± 1.2 Ma age defined by concordia upper intercept of two zircon crystals from the same rock (S-130Z, see Fig. 4.4)	The best estimate of the monazite age (2507 ± 5.4 Ma), probably reflects the age of Paleoproterozoic charnockitization in the area.	This age is similar to the monazite age obtained from the Krishnagiri area, north of the Moyar lineament (Fig. 1.11), which was interpreted as the age of the charnockitization (Peucat et al. 1993).

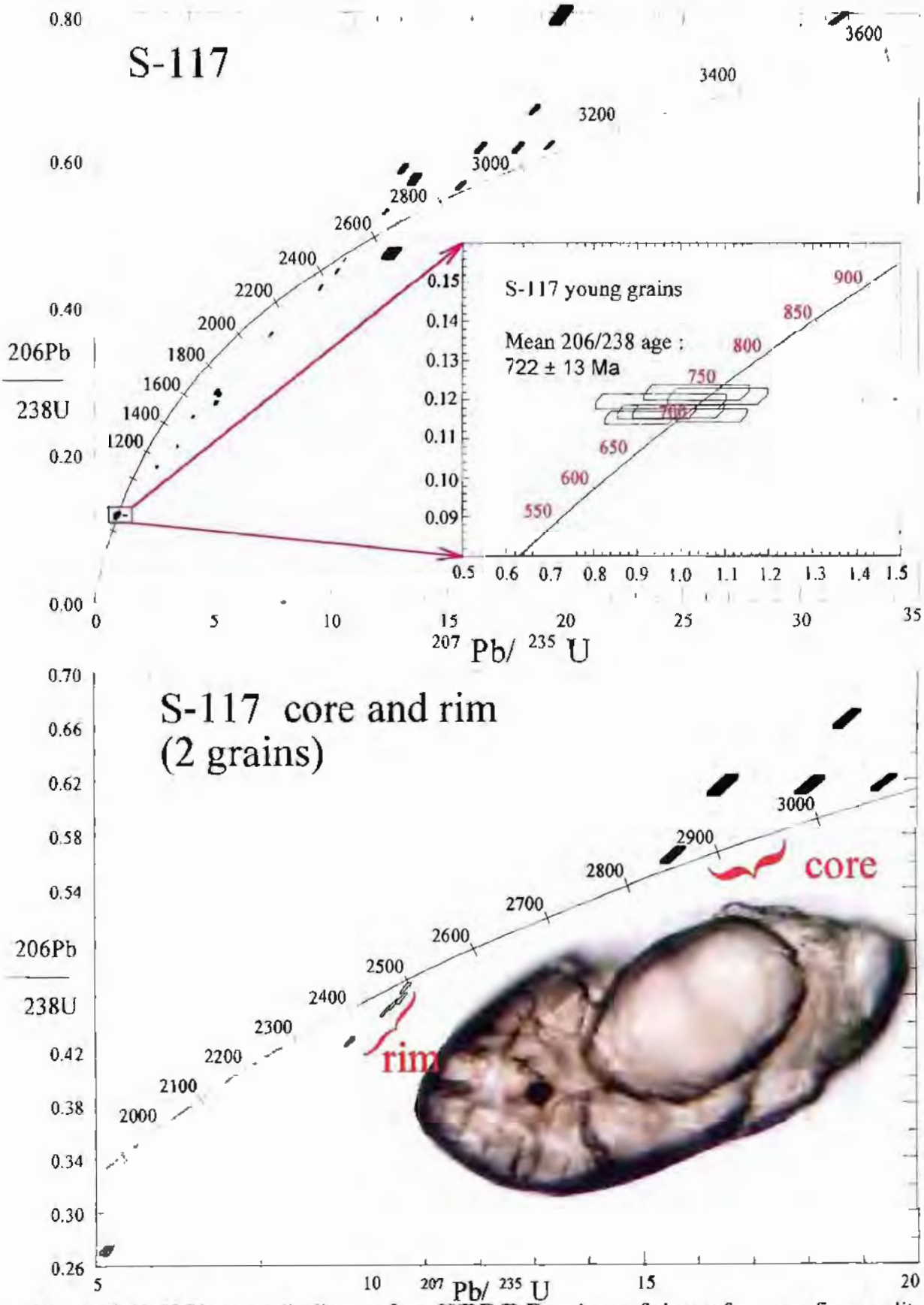

Fig. 4.6 (a,b) .U-Pb concordia diagram from SHRIMP-II analyses of zircons from a mafic granulite within a D2 shear zone in the Namakkal area, Corridor-I.
a. Three different age groups are present. (i) the oldest group have a mean age of ~2.86 Ma. This is mainly defined by age of cores of some complex zircons (B). A number of analyses align along a discordia joining ~2.5 Ga and ~720 Ma. Both these intercepts also have concordant analyses which confirm their geological significance.
b. Core and rim ages of two grains. The core shows points with an average 207Pb/206Pb age of ~2.96 Ga while the rim is near concordant at 2.5 Ga. Length of the inset grain is ~250 micron.

Sample no.	Laboratory	Location	Rock type and geological setting	Age	Interpretation	Comment
S-117	S; 33 spots from 19 grains were analysed.	78°11'57"E;11°07'56"N; hill top outcrop, ~3.5 km WNW of Valaiyappatti, ~10.5 km SSE of Namakkal, Corridor-I; within D_2 shear zone (Fig. 3.13)	Sample collected from anorthositic layer within mafic granulite. This band is affected by D_2 shearing. The mafic granulite has been intruded by ~2.53 Ma granite gneiss.	Zircons from this rock are colourless and equant in shape. Core and rim structure are common (Fig. 4.6). SHRIMP analyses of zircons yielded three different ages. (i) Core of some zircon grains have reversely discordant points with $^{207}Pb/^{206}Pb$ ages varying between ~2.9 Ga and ~3.0 Ga (ii) rims of some zircon grains define nearly concordant ages with $^{207}Pb/^{206}Pb$ ages of ~2.5 Ga (iii) concordant ages with $^{206}Pb/^{238}U$ age of 722 ± 13 Ma. There are a number of grains which fall on a well-defined discordia joining ~2.5 Ga and 722 Ma. These points reflect either Pb-loss from ~2.5 Ga zircons and/or overgrowth of 722 ± 13 Ma zircons on ~2.5 Ga zircons (Fig 4.6).	The Archaean age of ~2.9-3.0 Ga possibly represent intrusive age of the mafic granulite rather than inheritance because this body has been intruded by ~2.54 Ga old granite gneiss (S-130). The ~2.5 Ga rim age is probably related to thermal metamorphism during intrusion of granite gneiss (zircon age, S-130Z) or charnockitization which followed emplacement of granite gneiss (monazite age, S-130M). The new zircon grew at ~722 Ma which may be related metamorphism and/or deformation.	~2.9 Ga and ~730 Ma ages for mafic granulite has been reported recently by the Sm-Nd whole rock isochron and mineral isochron methods, respectively, from the Sittampudi area, ~50 km west of the present area (Bhaskar Rao et al. 1996). Present work confirms these Sm-Nd based ages.

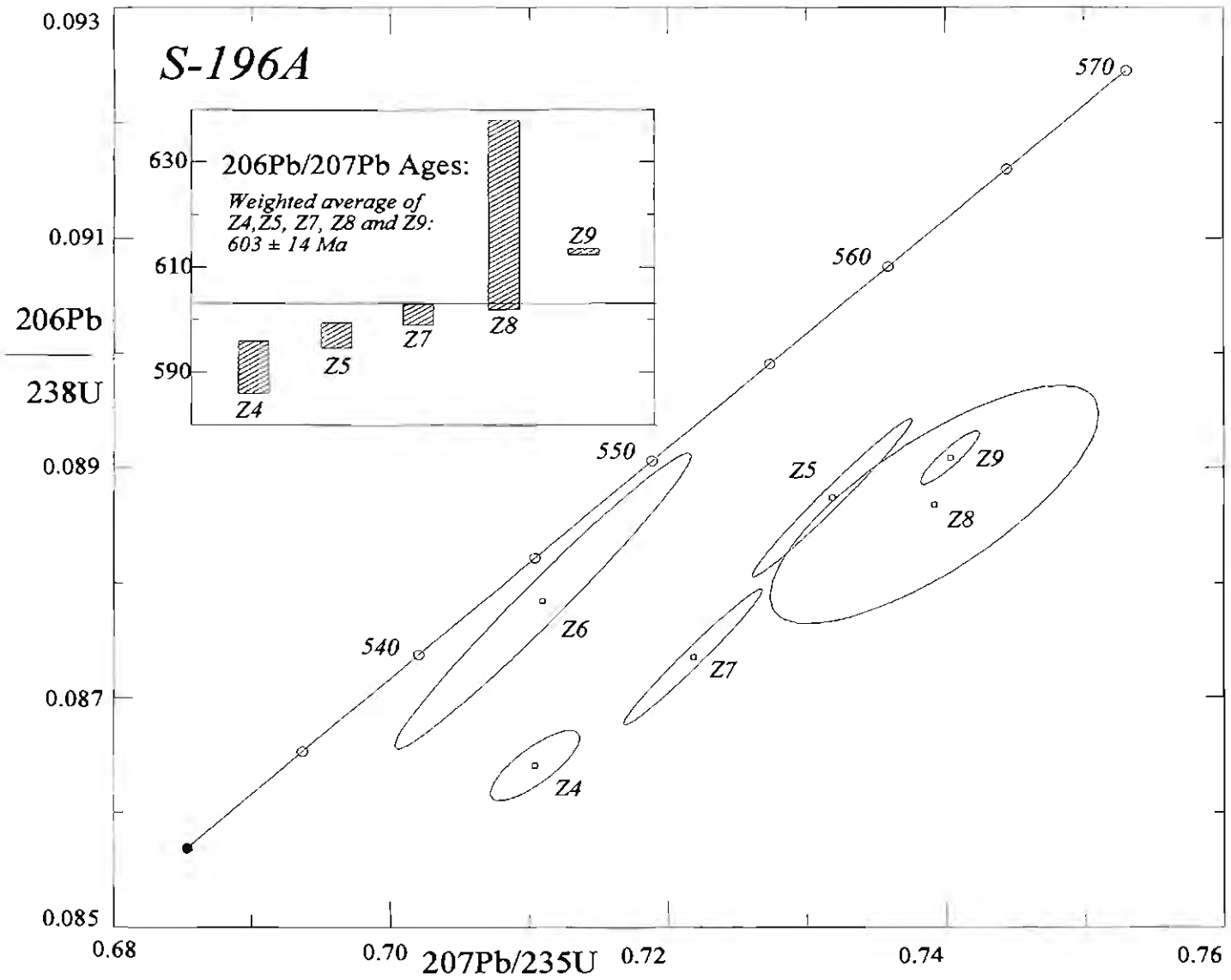

Fig. 4.7. U-Pb concordia diagram for single crystal zircons from a leucosome of a migmatite within a D2 shear zone, south of the Namakkal area, Corridor-I. Zircons crystals are all discordant. The most concordant crystal has a 206Pb/207Pb age of 556 ± 5 Ma.. However, all other crystals have moderately consistent 206Pb/207Pb ages with weighted average of 603 ± 13 Ma which is possibly the best estimate of the age of the emplacement of the neosome in the migmatite. The younger 206Pb/207Pb age of Z6 (556±7 Ma) is not well understood. It may represent a subsequent growth of zircon.

Sample no.	Laboratory	Location	Rock type and geological setting	Age	Interpretation	Comment
S-196A	U; 8 zircon crystals were analysed.	78°6'06"E, 11°7'45"N; the top of an isolated hill, ~1 km west of Ayyampalayam; ~ 12 km SSW of Namakkal (Fig. 3.13).	Sample from a ~1 metre thick leucosome within migmatitic gneiss within D_2/D_3 shear zones. Migmatitic veins are tightly folded.	Zircons are colourless, prismatic, subhedral. All zircon crystals analysed are discordant, The least discordant one (Z-6) has a $^{207}Pb/^{206}Pb$ age of 556 ± 5 Ma. All others have a weighted average $^{207}Pb/^{206}Pb$ age of 603 ± 14 Ma (Fig.4.7).	The best estimate of the age of the rock is 603 ± 14 Ma. This is interpreted as the age of migmatization in the area. Z-6, the least discordant grain, possibly represents new zircon growth at ~560 Ma. An alternative explanation is that these zircons nucleated at ~550 Ma on ~2.5 Ga cores.	Leucosome of migmatite have incipient charnockites at some places (Chapter-3). The 603 ± 14 Ma age constrain upper limit of latest Neoproterozoic tectono-thermal event. The ~560 Ma $^{207}Pb/^{206}Pb$ age of Z-6 may be related to charnockitization.

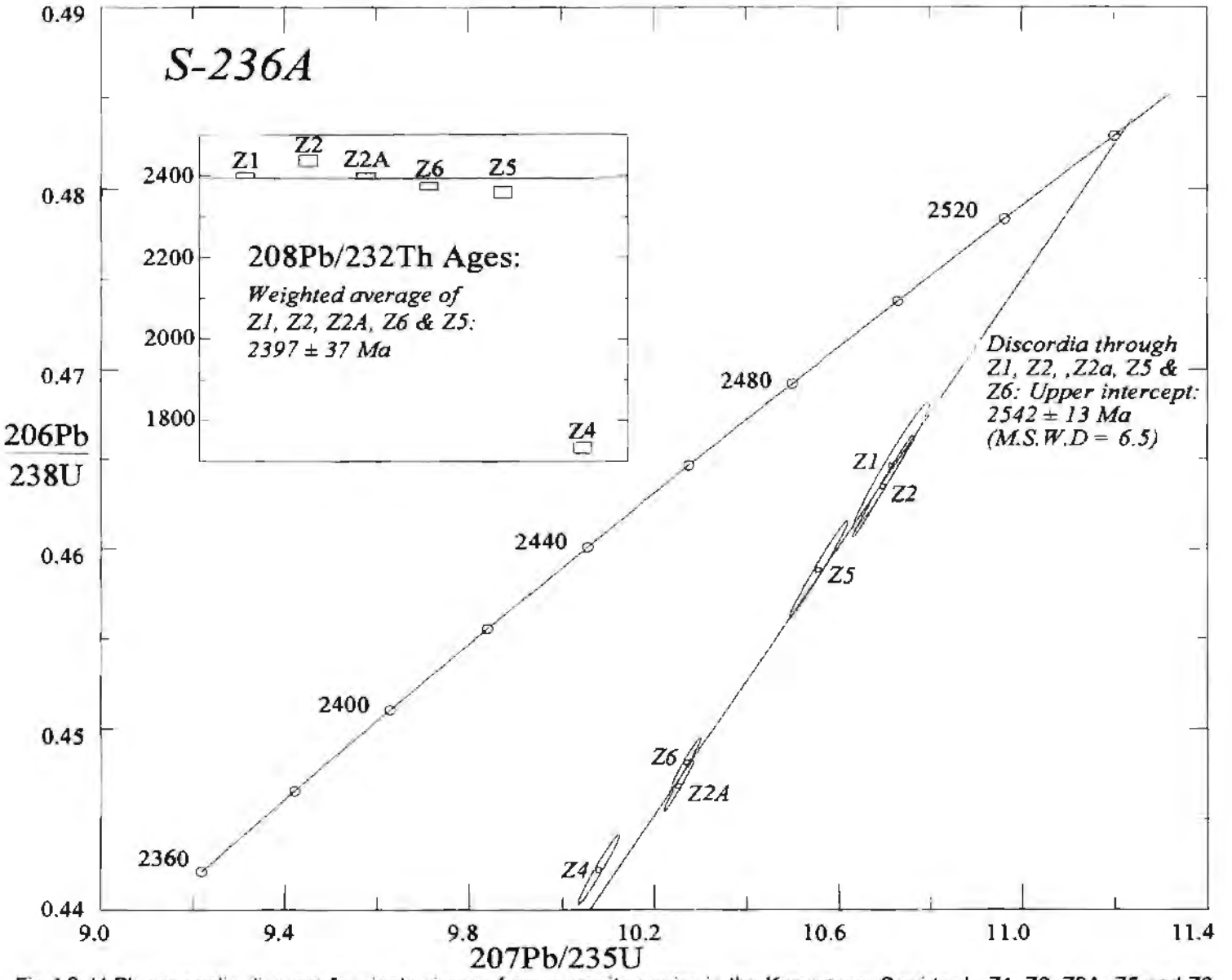

Fig.4.8. U-Pb concordia diagram for single zircons from a granite gneiss in the Karur area, Corridor-I. Z1, Z2, Z2A, Z5 and Z6 define a discordia with a upper intercept at 2542 ± 3 Ma. This is the best estimate of the protolith age. 208Pb/232Th ages (inset) are similar to the 207Pb/235U ages and give a weighted average of 2397 ± 37 Ma.

Sample no.	Laboratory	Location	Rock type and geological setting	Age	Interpretation	Comment
S-236	U, 6 zircon crystals were analysed (Fig. 4.8).	78°03'54"E, 10°54'27"N, a quarry section ~ 6 km SSW of Karur (Fig. 4.1).	Sample of a granite gneiss which has intruded mafic granulite and has been intruded by massive coarse grained granite. This granite gneiss body crops out to the south of the previously interpreted Cauvery Shear Zone (GSI, 1994).	Zircon are all subhedral and cylindrical, with numerous minute colourless lath-shaped inclusions. All the crystals are between 3 and 7% discordant. The upper intercept of discordia give an age of 2442 ± 13 Ma	Age of the granite gneiss.	Granite gneiss from Karur, Namakkal and from Salem all have ages between ~2.52 Ga and ~2.54 Ga. This suggests continuity of the granite gneiss of similar age across the Palghat-Cauvery Shear Zone (Fig. 4.1).

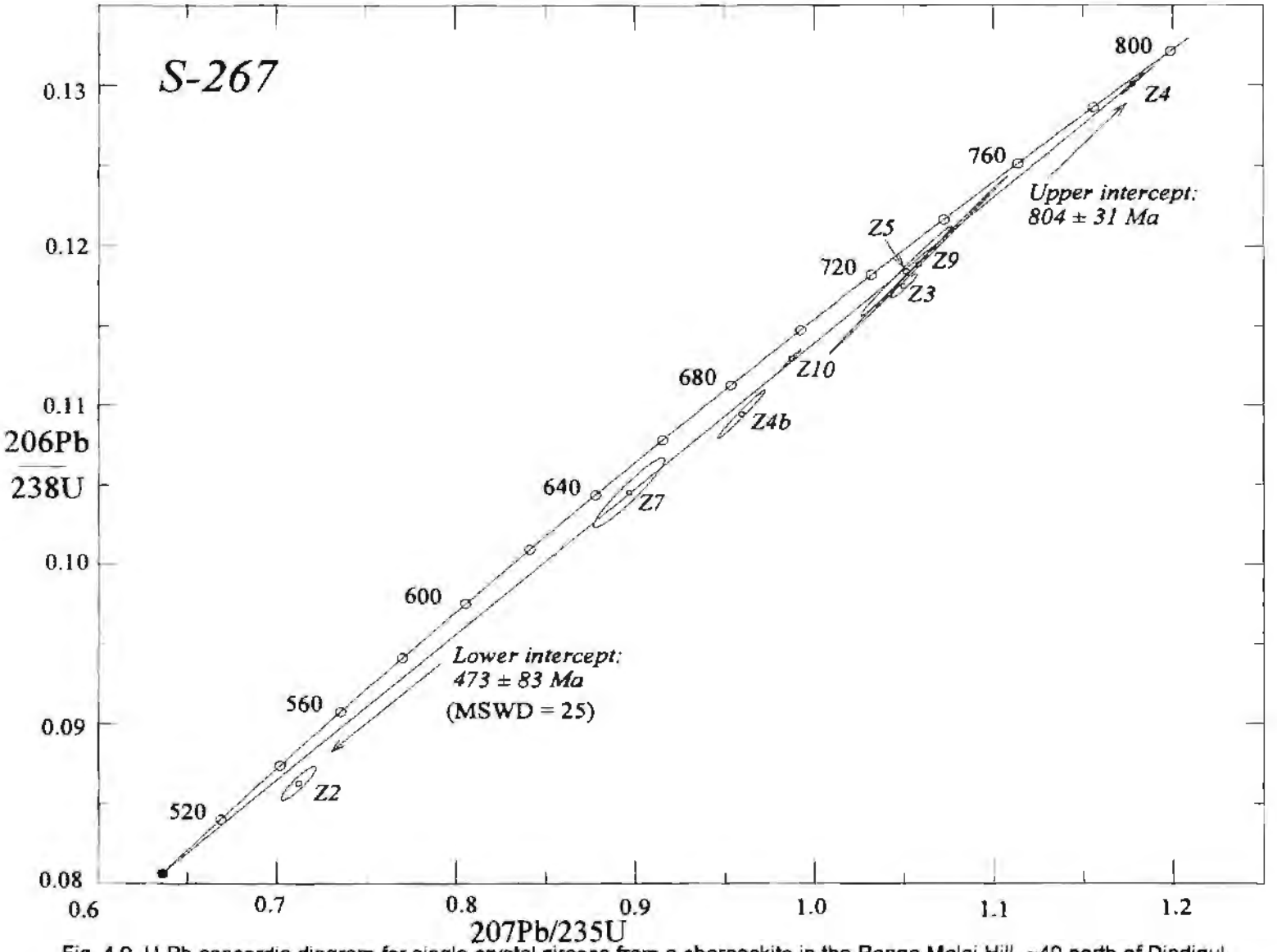

Fig. 4.9. U-Pb concordia diagram for single crystal zircons from a charnockite in the Ranga Malai Hill, ~40 north of Dindigul, (Fig. 4.1), south of Corridor-I. All the grains are discordant and define a discordia with upper intercept of 804 ± 31 Ma which is the best estimate of the intrusion age of the rock. The lower intercept at 473 ± 83 Ma is within error limit of the 550 Ma and 525 Ma charnockitization and granite activity reported in many parts of the SGT.

Sample no.	Laboratory	Location	Rock type and geological setting	Age	Interpretation	Comment
S-267	U; 8 zircon crystals were analysed.	77°56'48"E; 10°39'28"N; a quarry section on the eastern side of NH-7; ~13 km north of Vedasandur, ~40 km north of Dindigul (Fig. 4.1).	Charnockite. Fine 'ghost' layering in it represents early schistosity which is now recrystallized.	All 8 zircon crystals are within few percent discordant. The most concordant crystal (Z-4) has a $^{207}Pb/^{206}Pb$ age of 796 ± 1 Ma. A discordia through all the analysed points yield an upper intercept of 804 ± 4 Ma and a lower intercept of 473 ± 83 Ma (Fig. 4.9).	The best estimate of protolith age is given by the 796 ± 1 Ma $^{207}Pb/^{206}Pb$ age of the least discordant grain (Z-4). The lower intercept of 473 ± 83 Ma is within error limit of age of charnockitization recorded in the Madurai Block (Bartlett et al. 1995; Jayananda et al. 1995).	This ~800 Ma granitic activity is the first record of this age from the Madurai Block. In the present study the rocks of the Madurai Block, south of the KKPT Shear Zone, are believed to be in continuity with the Eastern Ghats where a ~800 Ma event is a commonly observed (Shaw et al. 1997). Discordancy of the most of the grains may be related to overgrowth/Pb-loss due to later charnockitization event.

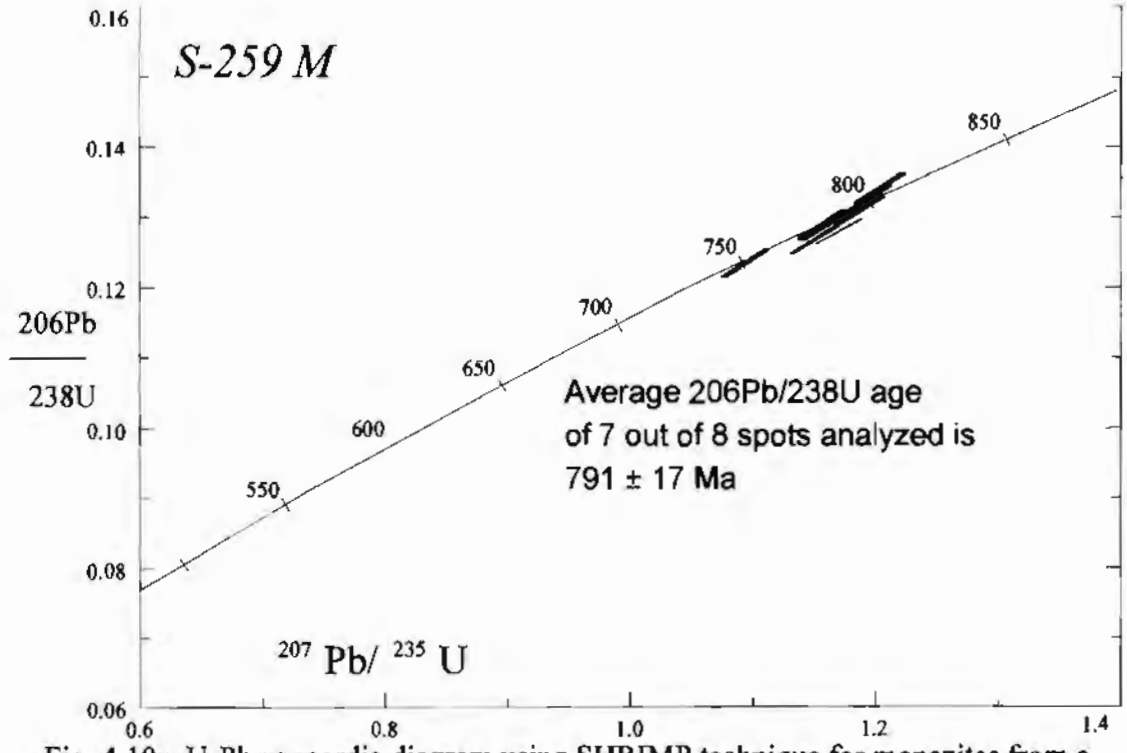

Fig. 4.10a. U-Pb concordia diagram using SHRIMP technique for monazites from a Khondalite sample in the Rangamalai Hill, southeast of the KKPT Shear Zone.

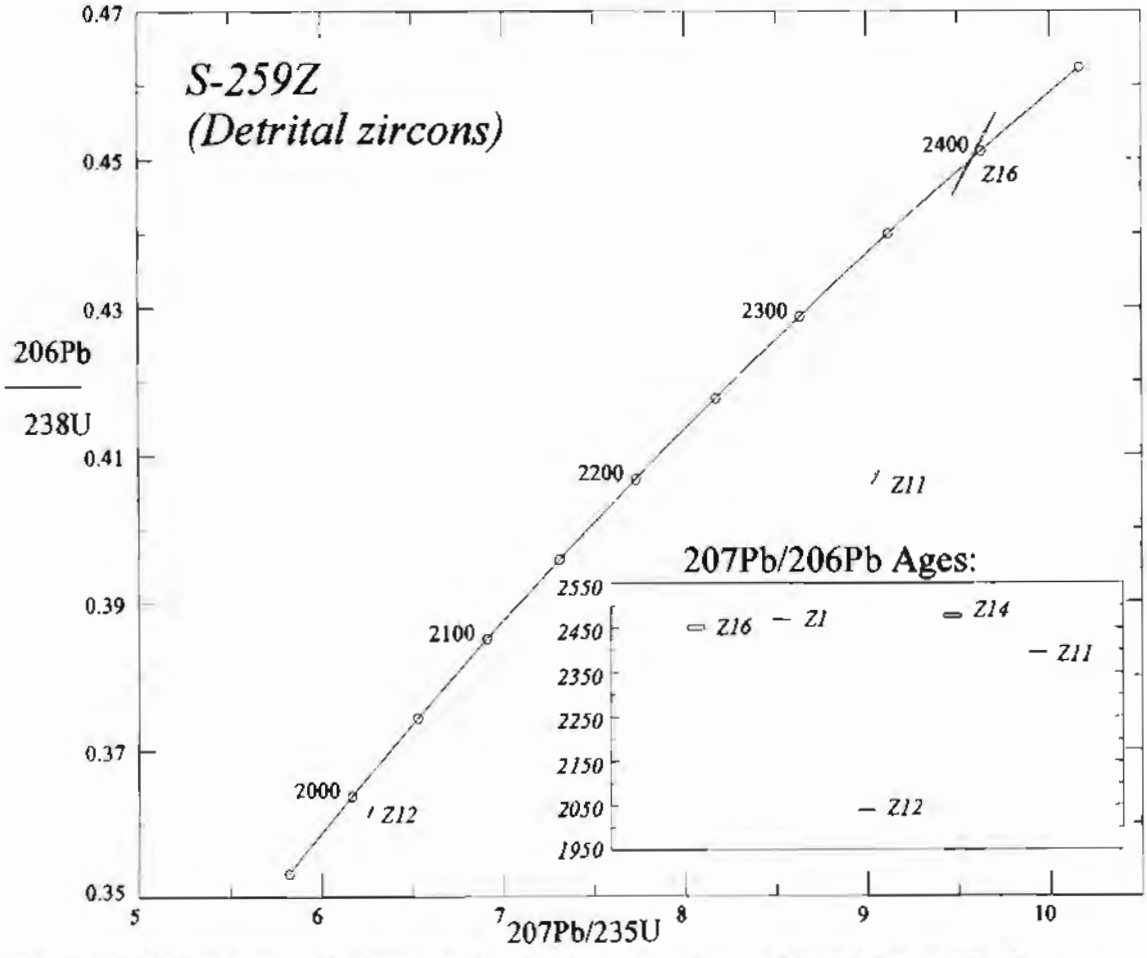

Fig. 4.10b. U-Pb concordia diagram for single zircons from a khondalite gneiss from the Vidhya Malai Hill, east of Palayam, Corridor-I. One of the three U-Pb ages is concordant at ~2.4 Ga while another is less than 2% discordant at ~2.0 Ga. 207Pb/206Pb ages are given in the inset. 4 out of 5 grains analyzed show 207Pb/206Pb ages between ~2.4 Ga and ~2.5 Ga. These ages suggest that the khondalitic metasediments are younger than ~2.5 Ga and probably younger than ~2.0 Ga, if Z12 is a detrital grain.

Sample no.	Laboratory	Location	Rock type and geological setting	Age	Interpretation	Comment
S-259M	S; 8 spots from 8 different monazite grains were analysed.	78°16'47"E; 10°41'06"N, southern slope of the Vaiya Malai Hill; ~6 km SSE of Maliampatti village; ~16 km ESE of Palaiyam (Fig. 4.1; 3.1).	Typical khondalite (paragneiss).	7 out of 8 analysed spots on different monazite crystals fall within a cluster on concordia and define an $^{206}Pb/^{238}U$ age of 791±17 Ma (Fig. 4.10a).	Latest high grade metamorphism in the area.	This age along with the similar age of charnockitized granite (S-267; 796 ± 1 Ma) from south of the Cauvery lineament indicate a regional tectono-thermal event at ~795 Ma.
S-259Z	U; 5 zircon crystals were analysed.	ditto	ditto	Zircons in this rock are all detrital. 4 out of 5 grains analysed have $^{207}Pb/^{206}Pb$ ages between ~2.4 Ga and ~2.5 Ga. The other one (Z12) is less than 2% discordant at ~2.0 Ga (Fig. 4.10b).	Detrital zircons include at least two age groups, viz., ~2.5 Ga and ~2.0 Ga.	Khondalites occurring south of the KKPT Shear Zone are younger than ~2.5 Ga and probably younger than ~2.0 Ga. This indicate that BIF associated metasediments (older than ~2.9 Ga) north of the KKPT Shear Zone and Khondalitic metasediments (younger than ~2.5 Ga) forms two distinct age groups.

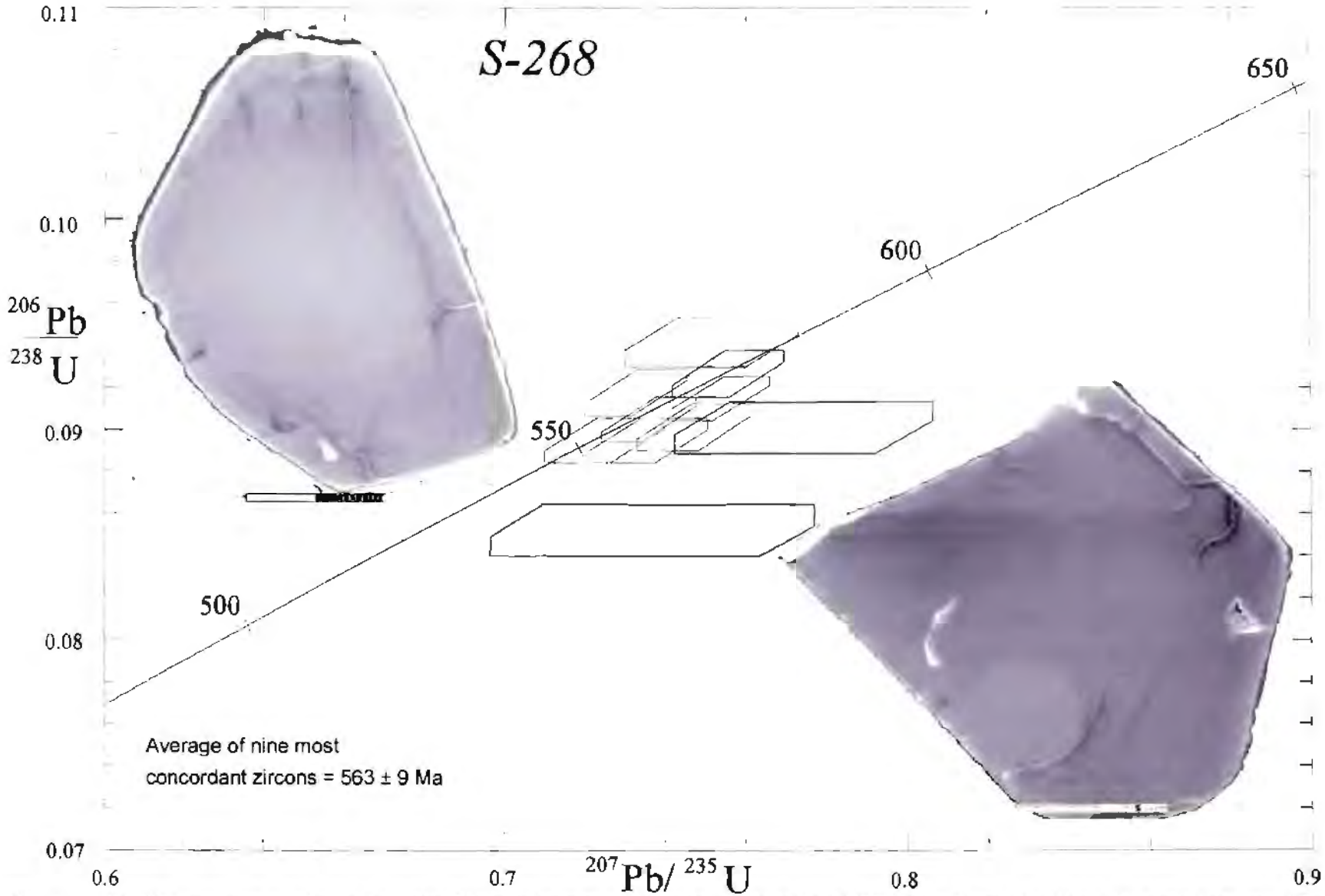

Fig. 4.11. SHRIMP analyses of zircons from the Oddhanchatram anorthosite, north of the KKPT Shear Zone, Corridor-I. 10 spots from ten different grains were analyzed. The average of nine most concordant spots yield an age of 563 ± 9 Ma which is taken as the intrusion age of the anorthosite body. Inset shows two zircon grains with fractures in the rim. Scale bars for upper and lower figures are 100 and 50 microns respectively.

Sample no.	Laboratory	Location	Rock type and geological setting	Age	Interpretation	Comment
S-268	S; 9 spots from 9 crystals were analysed.	77°46'E, 11°30'N, a dugwell quarry section, ~ 1 km NE of Oddanchatram, ~50 km WNW of Dindigul (Fig. 4.1)	Massive anorthosite Sample was collected from a quartz rich portion within the anorthosite. This body has suffered ductile deformation at the margins.	All the zircons are homogeneous (Fig. 4.11), spheroidal with fractures in the rim. In thin section, some plagioclase crystals carry zircon inclusions. 8 out of 9 zircon crystals analysed are concordant and yield best estimate of $^{206}Pb/^{238}U$ age as 563 ± 9 Ma (Fig. 4.11).	Age of crystallization of this anorthosite body.	This anorthosite body lie close to the KKPT Shear Zone and is elongated subparallel to the shear zone. It may be related to deformation along the KKPT Shear Zone.

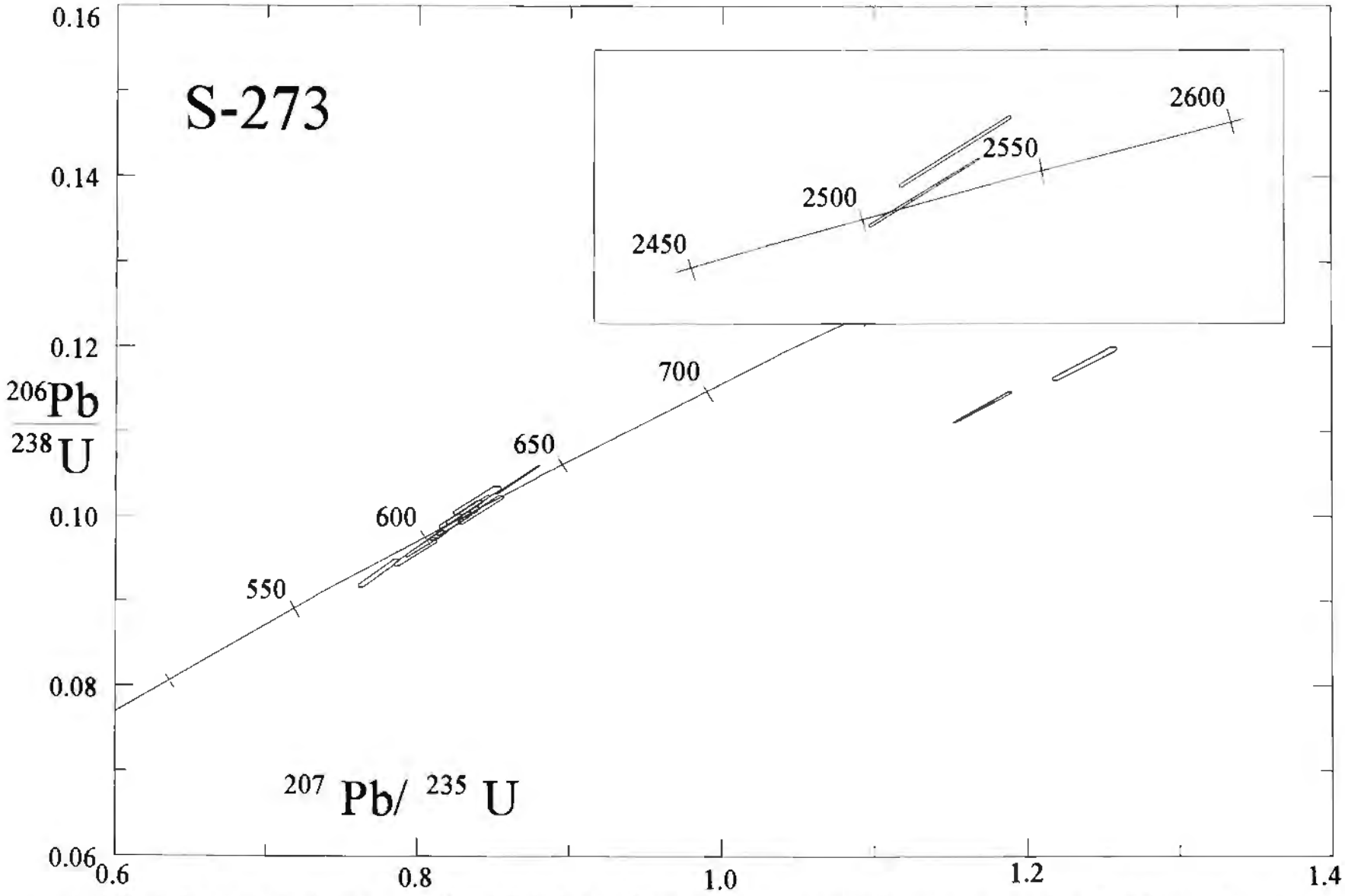

Fig. 4.12. U-Pb concordia diagram using SHRIMP technique for monazites from a fuchsite quartzite sample in the Moyar-Attur Shear Zone, Bhavani area. Two different age group could be identified; one at ~610 Ma and the other at ~2,5 Ga (see text for discussion)

Sample no.	Laboratory	Location	Rock type and geological setting	Age	Interpretation	Comment
S-273	S; 13 spots from 13 different monazite crystals were analysed.	77°36'47"E; 11°31'50"N; southern slope of a hillock ~2 km WNW of Puruvachchi village; ~15 km NNW of Bhavani (Fig. 4.1).	Fuchsite quartzite intruded by ~3.0 Ga old mafic granulite and sheared by the E-W trending Moyar Shear Zone.	Two concordant analyses have an average $^{207}Pb/^{235}U$ age of ~2522 ± 10 Ma age while others cluster near concordia with a $^{206}Pb/^{238}U$ age estimate of 612 ± 6 Ma (Fig. 4.12).	~2.5 Ga age gives either the protolith age or the age of initial high grade metamorphism. The 612 ± 6 Ma age indicates new monazite growth during a late Neoproterozoic tectonothermal event.	This age, along with the 603±14 Ma age of neosome of migmatite from the Namakkal area (S-196A) and the ~600 Ma (hydrothermal) zircon from pegmatite in Mettupalayam area (MS-3; discussed later) indicate that 600-610 Ma was a major period of thermal activity along Moyar, Cauvery and Bhavani Shear Zones.

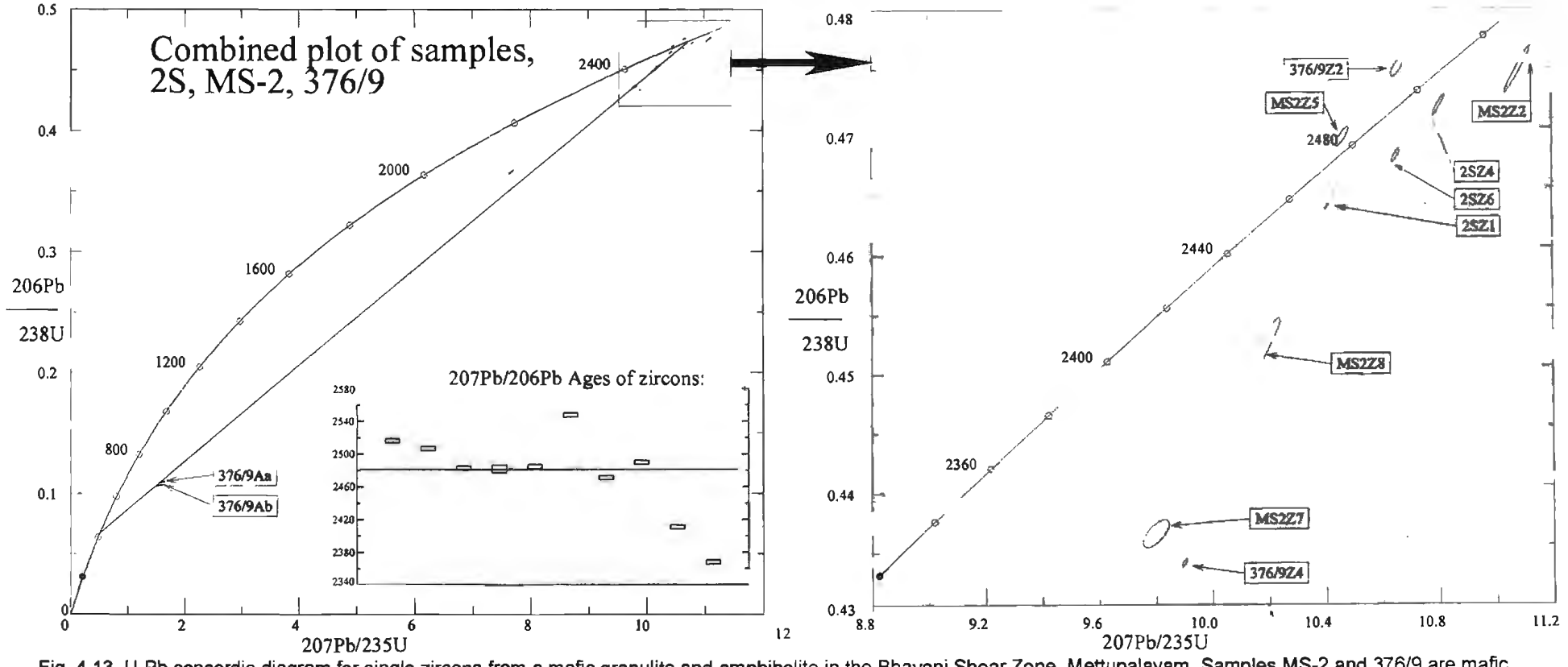

Fig. 4.13. U-Pb concordia diagram for single zircons from a mafic granulite and amphibolite in the Bhavani Shear Zone, Mettupalayam. Samples MS-2 and 376/9 are mafic granulites and the sample 2S is an amphibolite. Zircon crystals from these rocks show scatter which is likely to be due to inheritance and Pb-loss. Average 207Pb/206Pb ages of zircons is 2480 ± 30 Ma. Two apatite crystals (376/9Aa and 376/9Ab) from mafic granulite plot near the lower intercept of the concordia around ~420 Ma.

Sample no.	Laboratory	Location	Rock type and geological setting	Age	Interpretation	Comment
2S,MS-2,376/9	M; 2S, (3 grains); MS-2 (5 grains), 376/9 (2 zircon and 2 apatite crystals)	A quarry section ~1km east of Gudiyar; 4 km SE of Mettupalayam; 76°57'37";11°16'39" (Fig. 4.1)	MS-2 and 376/9 are mafic granulite; 2S is an amphibolite	Most grains scatter around the upper intercept of concordia have an average $^{207}Pb/^{206}Pb$ age of 2480±20 Ma concordia upper intercept. The scatter is due to inheritance and/or Pb-loss. 2 apatite samples were analysed. When these are regressed with zircons from 2S, the discordia define lower intercept age of ~410 Ma (Fig. 4.13)	The upper intercept at ~2.5 Ga possibly indicates either the protolith age or metamorphic growth of zircon. This mafic granulite is intruded by ~2.52 Ga granite gneiss (sample G5, see below) so zircon ages in mafic granulite may reflect a metamorphic ages.	Mafic granulites in this area has been dated by previous workers (Bhaskar Rao et al. 1996) at ~2.9 Ga by the Sm-Nd whole rock isochron method. This suggest that the ~2.5 Ga zircons are likely to be of metamorphic origin.

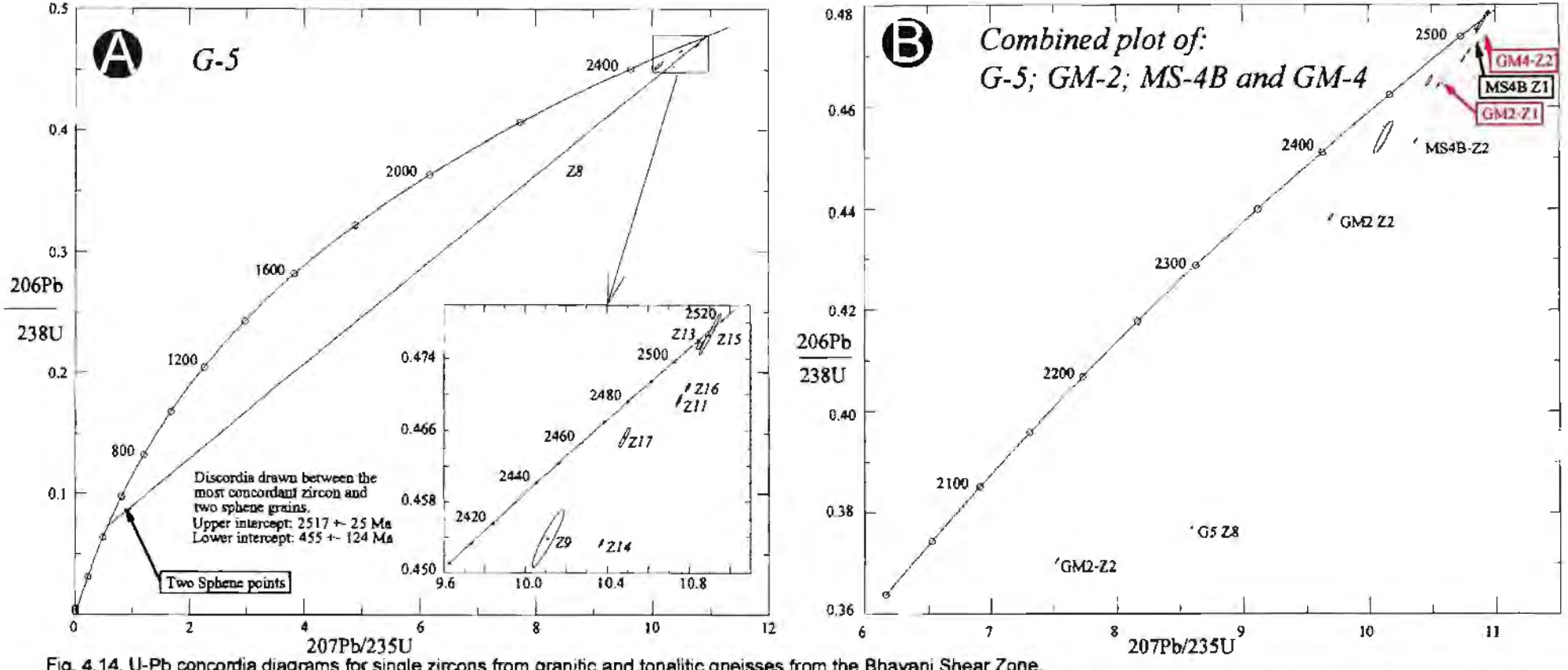

Fig. 4.14. U-Pb concordia diagrams for single zircons from granitic and tonalitic gneisses from the Bhavani Shear Zone.
A. Granite gneiss (G5). 8 zircon crystals and two sphene crystals were analyzed. The most concordant zircon (Z16) and two sphene grains were regressed together which yelld the upper and lower intercepts of 2517 ± 25 Ma and 455 ± 124 Ma respectively. The average of 206Pb/238U ages of two sphene grains is 540 ± 2 Ma

B. A combined concordia diagram for granite gneiss (G5), tonalite gneiss (MS-4B), granite mylonite (GM-2) and charnockite gneiss (GM-4).

Sample no.	Laboratory	Location	Rock type and geological setting	Age	Interpretation	Comment
GG-5, MS-4B	M;. GG-5, (8 grains); MS-4B (2 grains).	Same as in 2S and MS-2	G-5, granite gneiss; MS-4B, tonalite gneiss. Granitic gneisses are charnockitized in some places. They have intruded mafic granulite and BIF.	8 grains of granite gneiss (G5) were analysed; all fall close to concordia. The best age estimate is 2517 ± 2 Ma which is the average of the 4 most concordant zircons. Two sphene crystals from this rock were analysed and regressed along with the most concordant zircon grain. The lower intercept is at ~450 Ma. Two zircons of MS-4B (tonalite) also plot close to the upper intercept of the concordia and have 207Pb/206Pb ages of 2526 Ma and 2506 Ma (Fig. 4.14).	~2.52 Ma is the intrusive age of both granite gneiss and tonalite gneiss. Lower intercept of ~450 Ma may indicate thermal resetting or cooling.	
GM-4	M; 2 zircon crystals were analysed.	Same as in 2S and MS-2	Banded Charnockite	2 zircons were analysed; both are within 1% of concordant. The best estimate of the age is 2515 ± 9 Ma (Fig. 4.14).	The upper intercept at ~ 2.52 Ga gives the protolith age.	

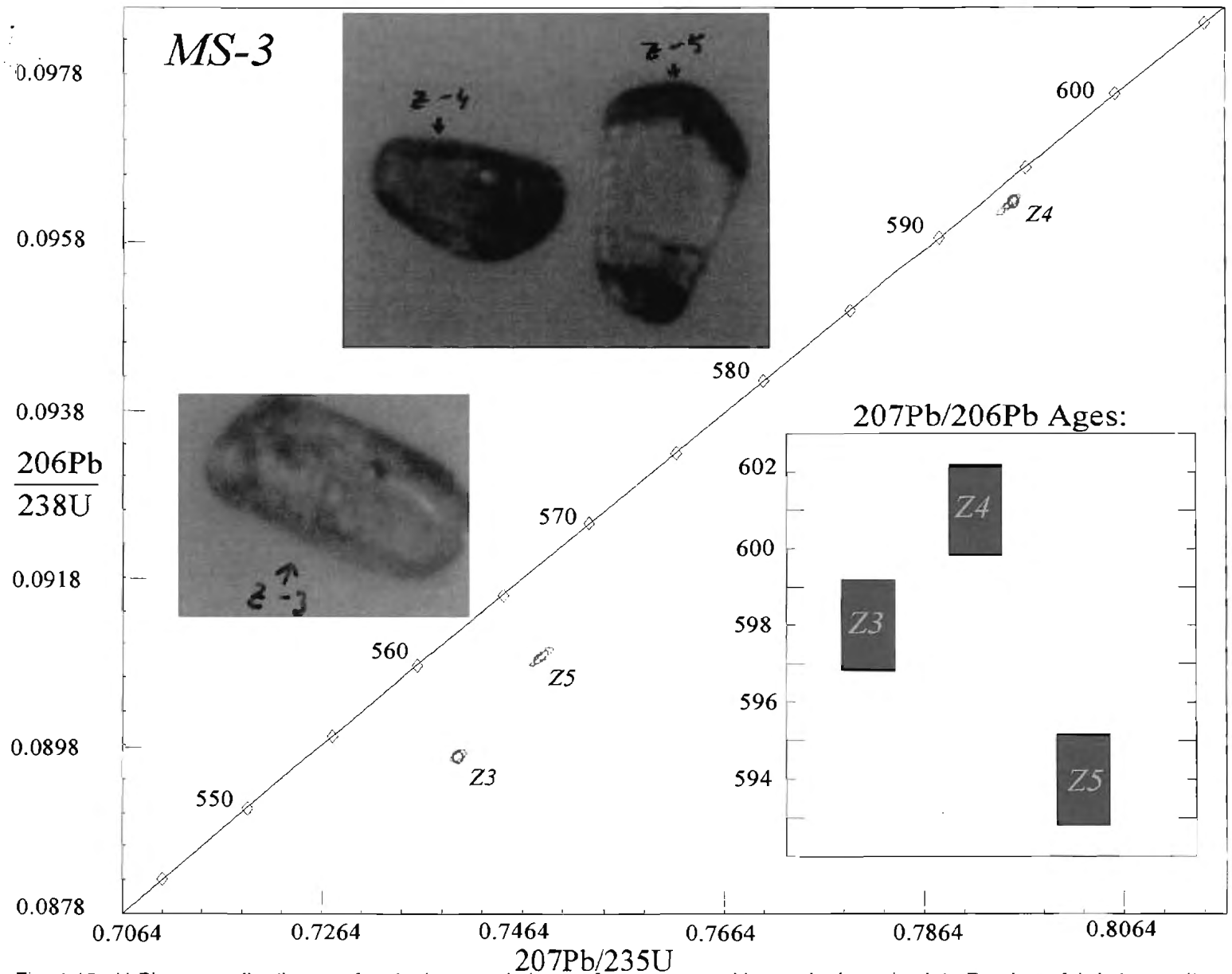

Fig. 4.15. U-Pb concordia diagram for single crystal zircons from a pegmatitic granite intrusive into D_2 shear fabric in granite gneiss in the Bhavani Shear Zone. Zircons from this rock are acicular or tabular in shape. The 207Pb/206Pb age of the most concordant grain is 601± 1 Ma which is the best estimate of the age of the pegmetitic granite. Z5 and Z3 are ~100 micron long.

Sample no.	Laboratory	Location	Rock type and geological setting	Age	Interpretation	Comment
MS-3	M; 3 zircon grains were analysed (Fig. 4.15).	Same as in 2S and MS-2	Pegmatite	All three analysed zircon grains were acicular and tabular in shapes and are probably of a primary (hydrothermal) crystallizing phase of pegmatite. The least discordant grain gives a $^{207}Pb/^{206}Pb$ age of 601±1 Ma (Fig. 4 15).	~600 Ma is the age of emplacement of the pegmatite body.	This age is in conformity with the sphene ages from charnockite. ~600 Ma age have also been reported from the Bhavani area in Corridor-II and the Namakkal area in Corridor-I

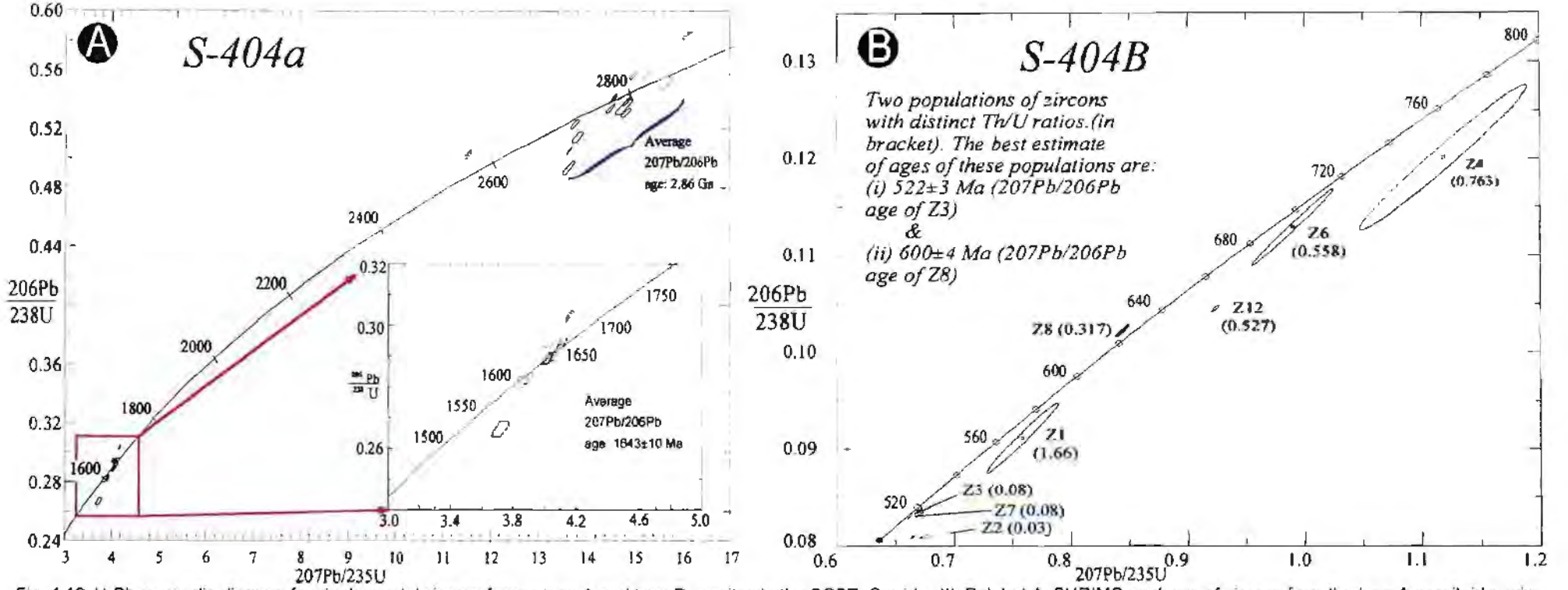

Fig. 4.16 U-Pb concordia diagram for single crystal zircons from a type A and type D granites in the PCSZ. Corridor-III, Palghat A. SHRIMP analyses of zircons from the type A granitoid gneiss. Two population of zircons are present. Both populations show magmatic zoning (Fig. 4.17, 4.18). The older population have average 207Pb/206Pb age of 2.86 Ga while the younger population have an average 207Pb/206Pb age of 1643±10 Ma.

B IDTIMS analyses of zircons from type D granitoid. Two populations of zircons are present. The older population is represented by colourless zircons with high (Th/U ratio). The best age estimate of this population is 600±4 Ma (207Pb/206Pb age of Z8). The younger population is represented by yellowish zircons with very low Th/U ratio. The best age estimate of this population is 520 ± 1 Ma (207Pb/207Pb age of Z3).

Sample no.	Laboratory	Location	Rock type and geological setting	Age	Interpretation	Comment
S-404B	U; 8 zircon crystals were analysed (Fig. 4.16b).	Same as in S-404A	Massive granite intrusive into granite gneiss (type A & B discussed above; Fig. 3 49). This variety is interpreted as syntectonic during a major shearing event in the area	Two populations of zircons are found in this rock. One of them, brownish-orange in colour with >3000 ppm U and very low Th/U ratio (0.08-0.02), yields an $^{207}Pb/^{206}Pb$ age of 522 ± 3 Ma. The other variety is colourless with a high Th/U ratio (1.3 - 0.3) and shows scatter possibly because of inheritance (these grains tend to fall on a line whose lower intercept with the concordia is closure to their $^{207}Pb/^{206}Pb$ ages but have quite high upper intercept age). The most concordant of these grains (Z8) has a $^{207}Pb/^{206}Pb$ age of 600 ± 4 Ma.	600 ± 4 Ma age is the age of the granite. The 522 ± 3 Ma age of a population with high U content possibly reflects hydrothermal growth. This hydrothermal activity may be related to uplift from high-grade metamorphic condition.	~600 Ma granitic magmatism has been recorded in the present investigation from the Cauvery, Moyar and Bhavani Shear Zones (discussed above). The presence of ~600 Ma syntectonic granite indicates that Palghat-Cauvery Shear Zone was also active at this time. ~525 Ma ages have also been recorded in monazite of charnockite from the Cardamom Hills (S-355E) and a pegmatitic vein (S-318B) which intruded the charnockites in the KKB, suggesting that the whole terrain from Palghat in the north to the southern tip of India was uplifted from high-grade metamorphic condition at ~522 Ma.

Sample no.	Laboratory	Location	Rock type and geological setting	Age	Interpretation	Comment
S-404A	S; 25 spots from 16 zircon crystals were analysed. (Fig. 4.16a)	76°33'13"E; 10°55'27"N; a quarry section within the Palghat Shear Zone, ~ 1 km NE of Maruthamkad village; ~20 km NNW of Palghat (Fig. 4.1).	Biotite rich granite gneiss with a few mm thick leucosomes alternating with biotite rich melanosomes (type A). This rock is interpreted to be the oldest granitic gneiss in the area. It is intruded by late granitic gneisses and granite (types B, C and D). The youngest one of which is dated at ~600 Ma (S-404B; Fig. 4.16b)	The majority of the crystals have well developed zoning indicating a magmatic origin (Pidgeon et al. 1992). Analysed points fall in two cluster around concordia (Fig. 4.16a). Both these clusters include well-developed zoned zircons (Figs. 4.17 and 4.18). One of the clusters of 13 spots scatters around a concordant age of ~2.86 Ga while the second cluster (12 spots) scatters around a concordant age of 1643 ± 10 Ma.	Since both concordant clusters include well-developed zoned crystals, it is possible that both population represents magmatic zircons. The ~2.86 Ga age is that of the biotite gneiss while the 1643 ± 10 Ma age possibly represents another granitic activity which may be represented by thin leucosomes in this rock (?Type B granite). Alternatively it could be a recrystallization event.	This sample is from within the Palghat Shear Zone where at least four different granitic phases have been identified (Fig. 3.49). The two population of zircons found in this rock may represent zircons from two different magmatic phases. The ~2.9 Ga age of biotite gneiss, which is common in the Dharwar craton to the north suggests continuation of this terrain as far south as the Palghat area. The ~1.6 Ga age of magmatic zircons is the first evidence for granitic activity or a metamorphic event of this age from the SGT.

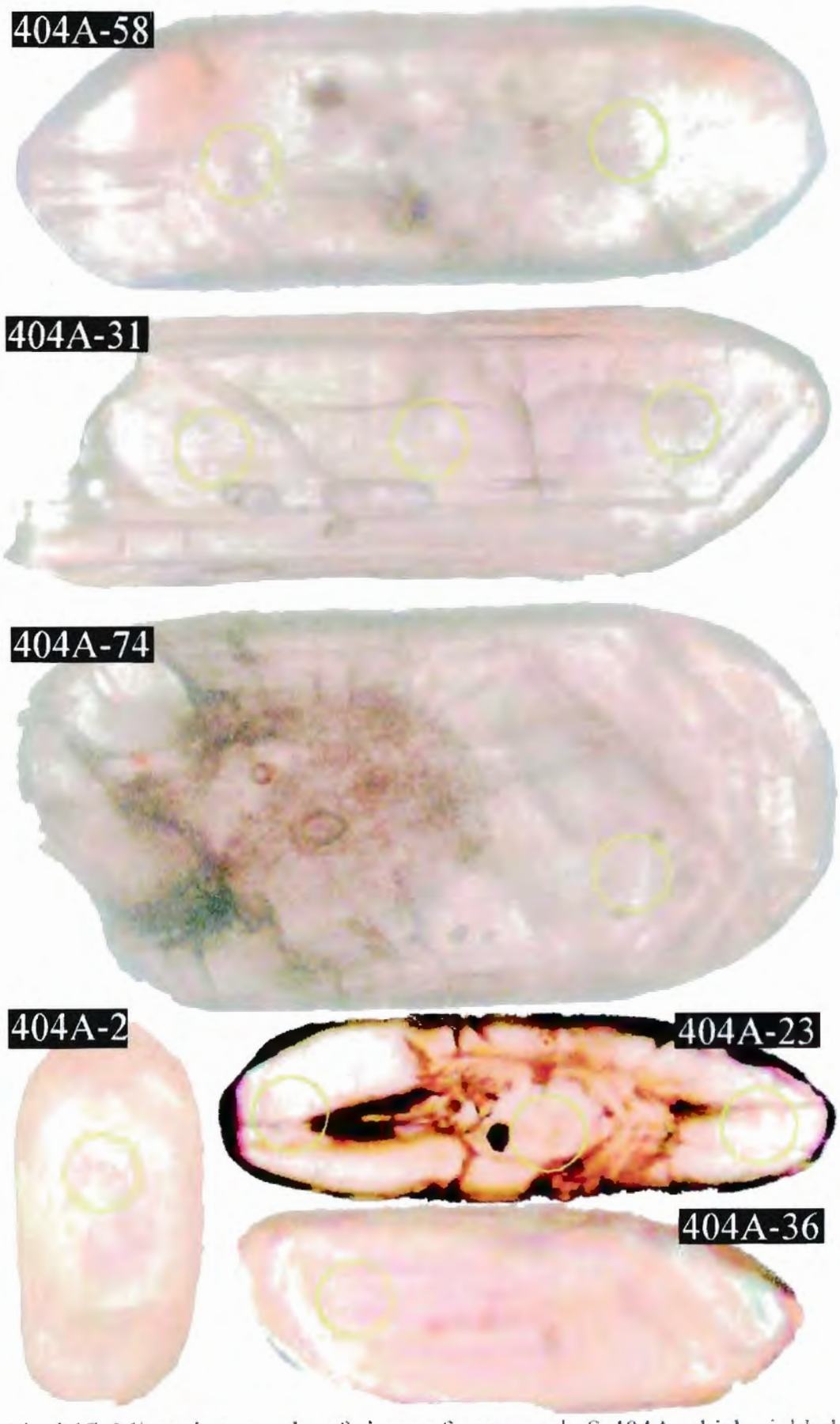

Fig.4.17. Microphotographs of zircons from sample S-404A which yielded ~1.60 Ga ages. Positions of SHRIMP spots (circled) are indicated. Note that both zoned and unzoned grains are present in this population.

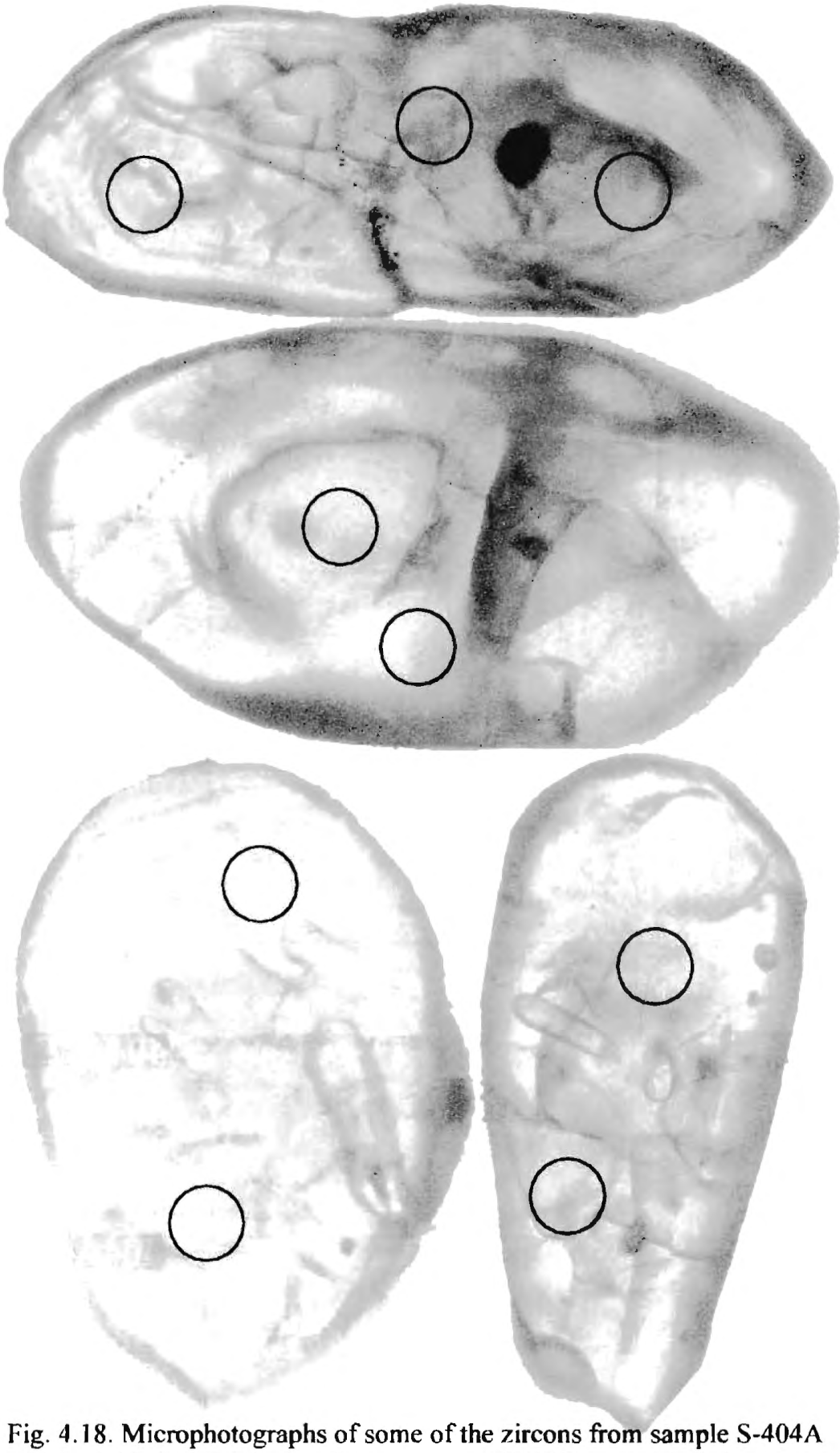

Fig. 4.18. Microphotographs of some of the zircons from sample S-404A which yielded ~2.9 Ga ages. Positions of SHRIMP spots (circled) are indicated. Note that both zoned and unzoned grains are present in this population.

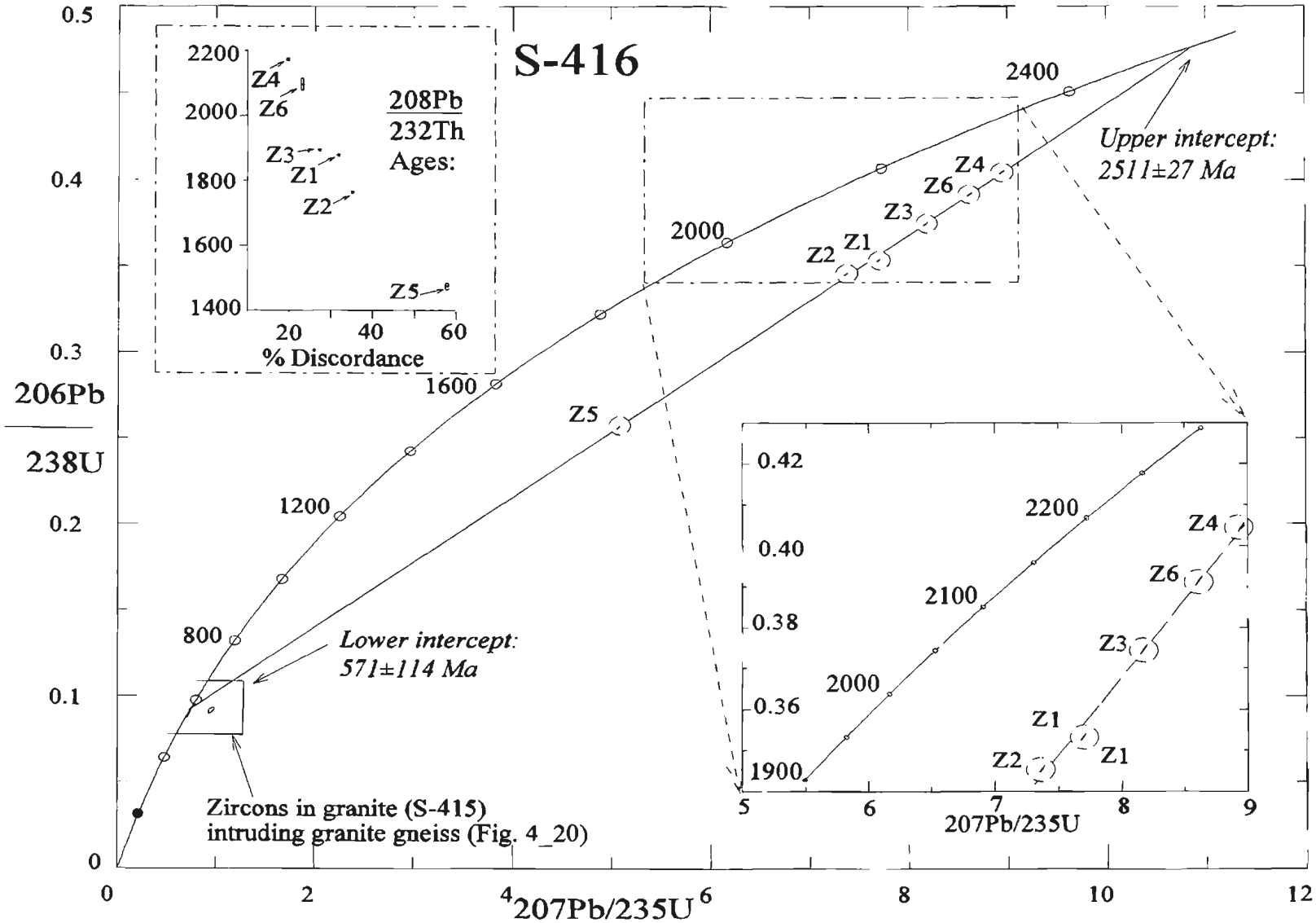

Fig. 4.19. U-Pb concordia diagram for single zircons from a granite gneiss in the Kotamangalam area on the western part of the KKPT shear zone. All six crystals analyzed are discordant and define a discordia with upper intercept at 2511±27 Ma. This is the best estimate of the protolith age. The lower intercept is at 571 Ma, which closely matches the U-Pb age obtained from a syntectonic granite (S-415) from the same area. The discordance of the zircons is interpreted to be due to Pb-loss during the ~571 Ma tectonothermal event rather than overgrowth of zircons from the ~571 Ma granite because of very different Th/U ratios of zircons from these two rock types. The 208Pb/232Th ages (inset) show moderately well defined coupling with the U-Pb ages as they form a linear array when plotted against % of their discordance (as defined in Appendix- A.4.1).

Sample no.	Laboratory	Location	Rock type and geological setting	Age	Interpretation	Comment
S-416	U; 6 zircon crystals were analysed (Fig. 4.19).	77°02'40"E; 9°44'20"N; ½ km south of Tallakod village; 28 km East of Kotamangalam. The area lies within few km of the KKPT Shear Zone.	Biotite gneiss, which is the dominant rock type of the area and has been intruded by a syntectonic granite (S-415; Fig. 3.57)	All 6 zircon crystals analysed fall on a well-defined discordia with an upper intercept of 2511 ± 27 Ma and a lower intercept of 571 ± 58 Ma.	~2.51 Ga is the intrusive age of the granite gneiss. The lower intercept age of ~571 Ma indicates a thermal reactivation associated with tectonism and magmatism. Age of a syntectonic granite which intruded the granite gneiss is 568 ± 2 Ma (S-415).	~2.5 Ga granite gneisses have been recorded in the present investigation from the SGT over a widely spread area, which includes Salem, Namakkal, Karur, Mettupalayam, and Kotamangalam. Similar ages of the most dominant rock type of the area across major shear zones suggests that no major crustal break occurs along the PCSZ.

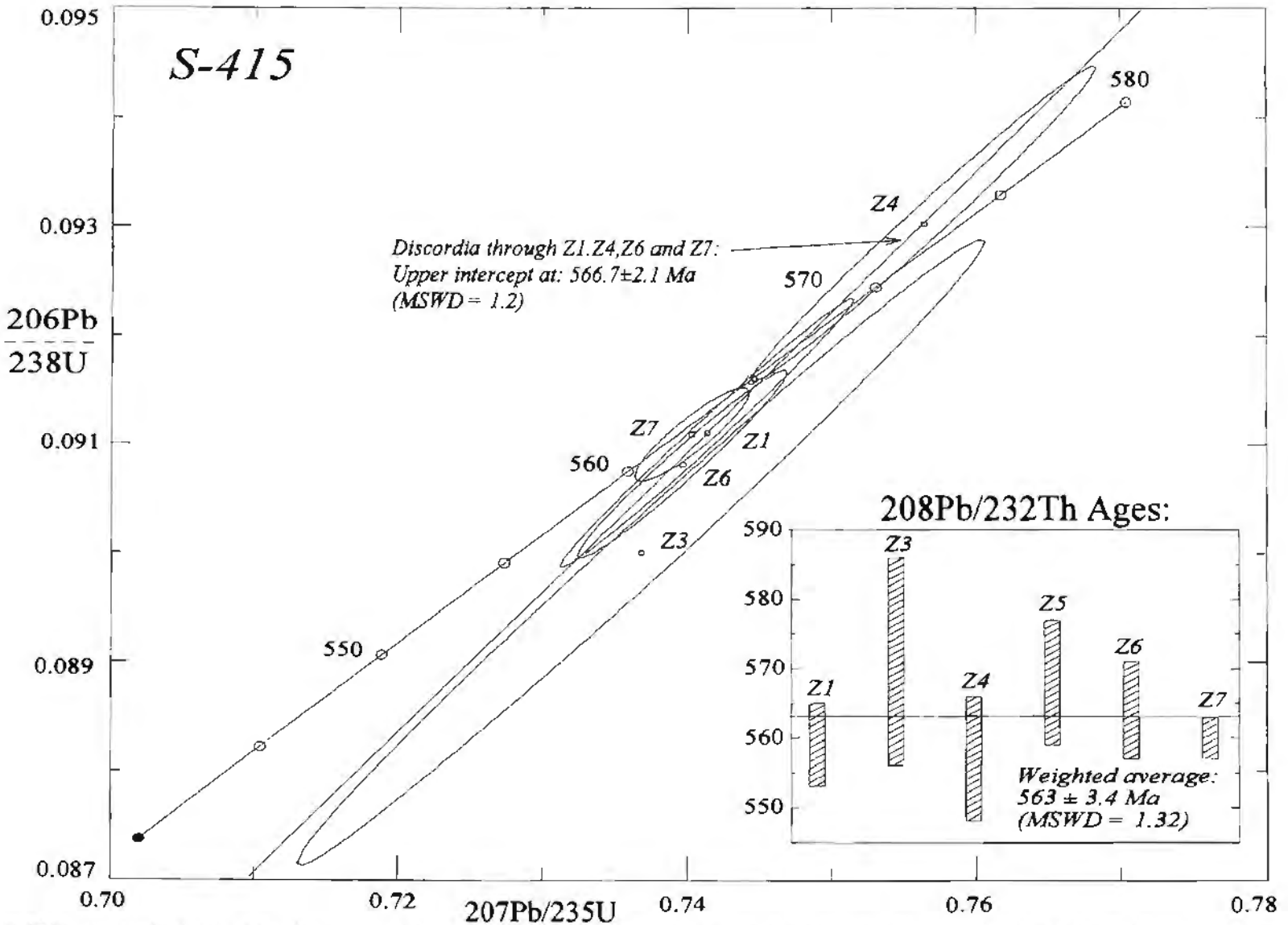

Fig. 4.20. U-Pb concordia diagram for single crystal zircons from a granite vein within granite gneiss, syntectonic with D_2(?) shearing in the Kotamangalam area, corridor - IV. Z1,Z4,Z6 and Z7 define a discordia with upper intercept at 566.7 ± 2.1 Ma. This is the best estimate of the protolith age of the rock. 208Pb/232Th ages (inset) are within error limit this age.

Sample no.	Laboratory	Location	Rock type and geological setting	Age	Interpretation	Comment
S-415	U; 6 zircon crystals were analysed.	Same as in S-416	A syntectonic granite which intruded the ~2.5 Ga biotite gneiss (S-416; Fig. 3.57b). This granite has been patchily charnockitized in places and thus constrains the upper age limit of charnockitization in the area.	Four of the six crystals analysed are concordant. Upper intercept of a discordia through these four crystals defines an age of 568±2 Ma. Weighted average of $^{208}Pb/^{232}Th$ ages of all six crystals is 563 ± 3.4 Ma (Fig. 4.20).	Age of the syntectonic granite is 568 ± 2 Ma, which may also be a time of shearing along the KKPT Shear Zone.	This age is within error limits of that for the Oddhanchattam anorthosite (S-268; 563 ± 9 Ma) which also lies close to the KKPT shear zone. Thus 568 ± 2 Ma may be a time thermal reactivation along the KKPT Shear Zone.

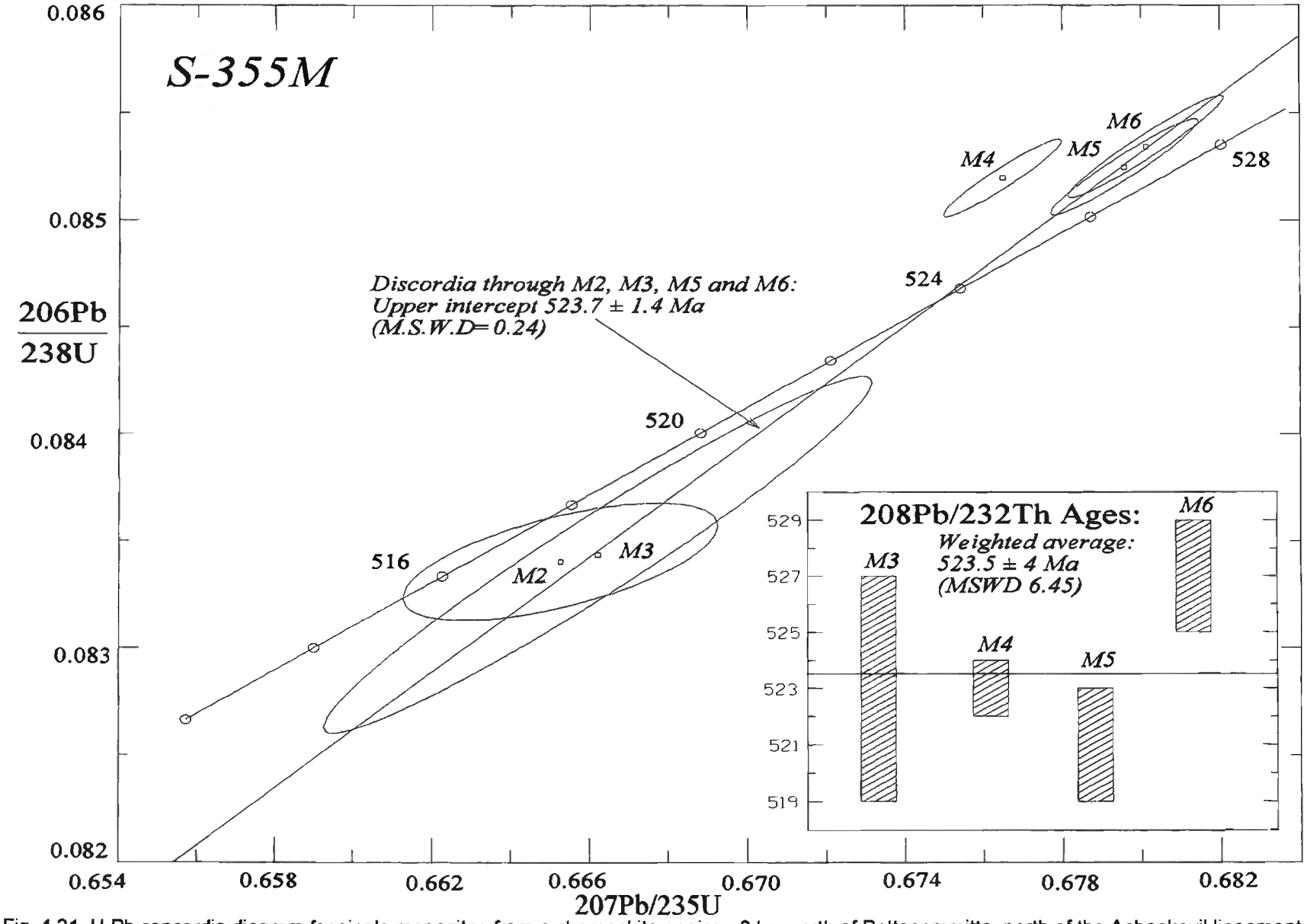

Fig. 4.21. U-Pb concordia diagram for single monazites from a charnockite gneiss ~8 km north of Pattanammitta, north of the Achankovil lineament. Concordia upper intercept is at 523.7 ± 1.4 Ma. 208Pb/232Th ages (inset) are within the error limits of this age.

Sample no.	Laboratory	Location	Rock type and geological setting	Age	Interpretation	Comment
S-355M	U; 5 monazite grains were analysed.	75°45'35"E; 9°19'30"; a quarry section, ~½ km east of Kanamukku village; ~8 km NNW of Patthanamthitta. (Fig. 3.61; 4.1)	Sample from a khondalite enclave (~2 m^2) within charnockitized khondalite.	All five monazite crystals are within 1% of concordant, three of them are reversely discordant while two others are normally discordant. The upper intercept of discordia through four most concordant crystals give the best estimate of the age of the monazite at 524 ± 2 Ma. Weighted average of four of the analysed $^{208}Pb/^{232}Th$ ages is 523.5 ± 4 Ma (Fig. 4.21).	The charnockite in the area has been retrogressed by a 526 ± 2 Ma granite (S-318B; S-340). The monazite age of 524 ± 2 Ma thus indicates a resetting age following charnockitization, may be related to uplift of the high-grade terrain.	~525 Ma age has also been recorded from the KKB and in the PCSZ in granitic veins which intrude and retrogressed charnockite. Together, these ages indicate the timing of cessation of high-grade metamorphic condition in the SGT.

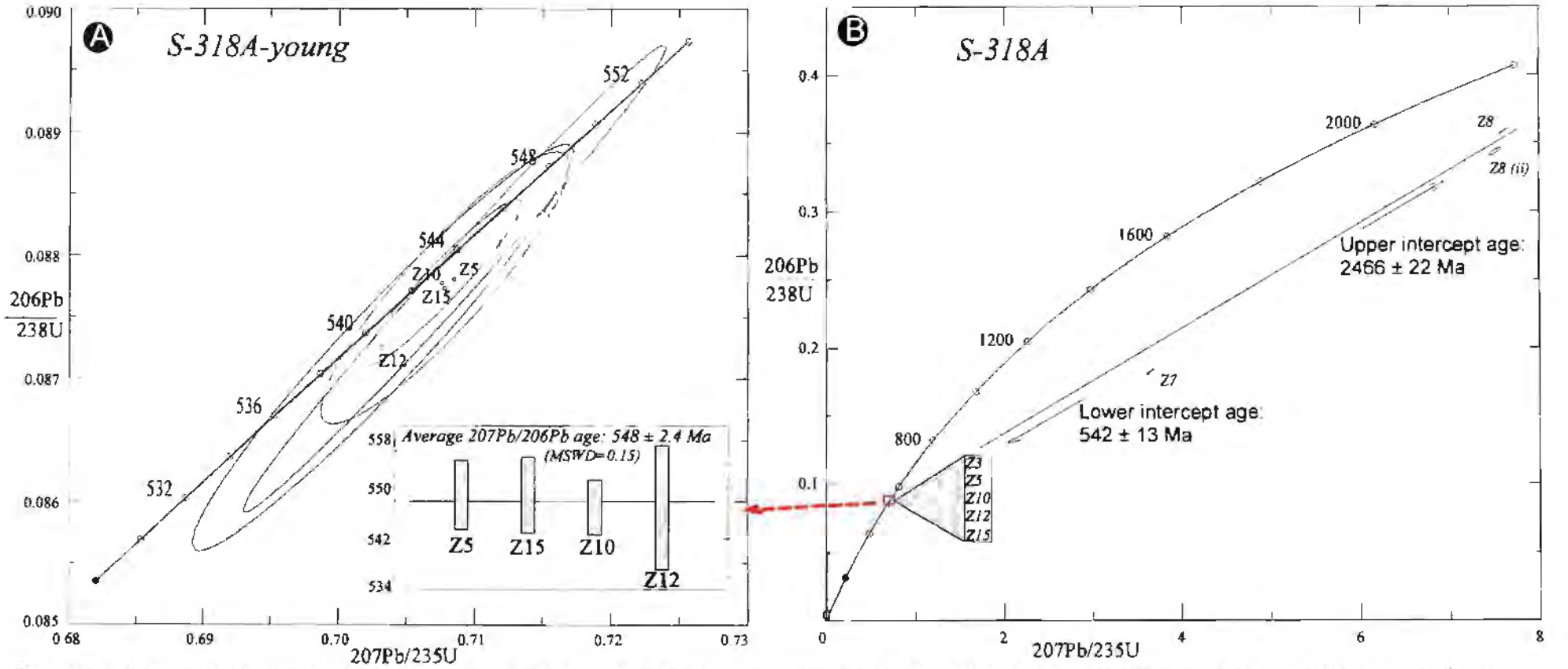

Fig. 4.22. U-Pb concordia diagram for single zircons from the Kalipara Granite, Nirettipara quarry, ~6 km NE of Kalanjur (Fig. 3.61). Four younger grains fall on concordia (A). Average 207Pb/206Pb age of these four grains is 548 ± 2.4 Ma. This is interpreted as the best estimate of the age of the Kalipara Granite. Some of the zircons have inheritence. These grains yeild 207Pb/206Pb ages >1.9 Ga (B). Regression of three most concordant grains (Z5, Z10 and Z15) with two grains with highest 207Pb/206Pb ages give a discordia with upper and lower intercept ages of 2466 ± 22 Ma and 542 ± 13 Ma respectively. This upper intercept age possibly represents age of inherited cores in those grains.

Sample no.	Laboratory	Location	Rock type and geological setting	Age	Interpretation	Comment
S318A	U; 8 zircon grains were analysed.	A quarry section ~½ km NNE of Nirettipara; ~6 km NE of Kalanjur; 76°53'56"E; 9°07'48" (Fig. 3.61)	Kalipara Granite with patchy charnockitization. This granite is the youngest granite charnockitized in the area.	5 of the 8 analysed zircons fall close to the concordia which gave best estimate of age of the rock as 548 ± 2 Ma. 3 other grains are highly discordant with $^{207}Pb/^{206}Pb$ ages more than 1.0 Ga (Fig. 4.22).	Intrusive age of the granite is 548 ± 2 Ma. Highly discordant zircons are the result of inheritance.	This is the youngest granite in the KKB which has suffered charnockitization. The Kalipara Granite bodies are emplaced along the Achankovil Lineament and are intrusive into main NW-SE trending fabric. In places they are also folded. Thus the main phase of deformation along the Lineament is pre- 548 Ma but deformation also continued after 548 Ma..

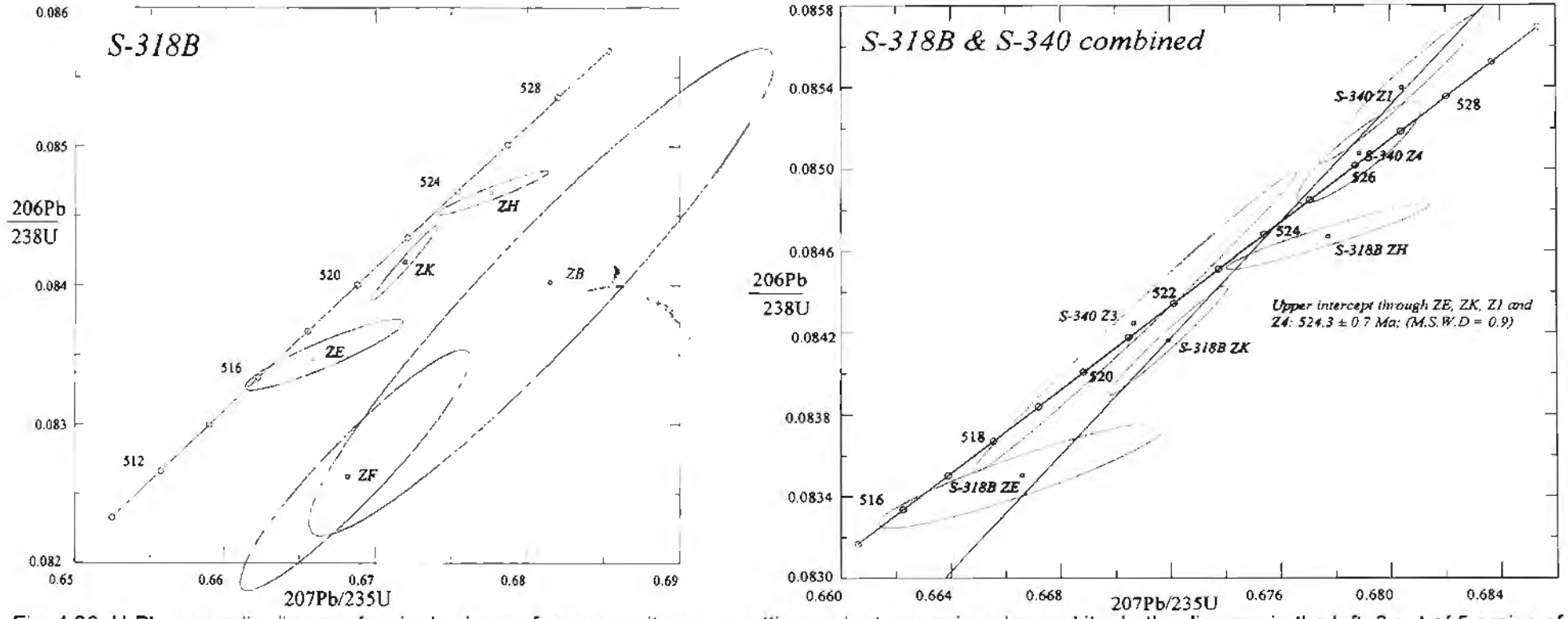

Fig. 4.23. U-Pb concordia diagram for single zircons from a granite cross-cutting and retrogressing charnockite. In the diagram in the left, 3 out of 5 grains of sample S-318B fall within 1% of the concordia, the other two being ~6-8% discordant. The diagram in the right includes 3 most concordant grains from S-318B and 3 other grains from a similar rock (S-340) from a adjacent locality. A combined isochron through 4 least discordant grains of these two samples yields an upper intercept age of 524.3 ± 0.7 Ma. This age is interpreted as the best estimate of the age of the granite.

Sample no.	Laboratory	Location	Rock type and geological setting	Age	Interpretation	Comment
S-318B	U; 6 zircon grains were analysed.	Same as in S-318A	A granite dyke within the charnockite (S-318A) which has bleached (retrogressed) the charnockite.	3 out of 5 analysed grains fall within 1% of concordant. The best estimate of the age of the dyke is obtained by taking the average $^{207}Pb/^{206}Pb$ age of these three grains, which is 526 ± 3 Ma (Fig. 4.23a) .	Intrusive age of the granite dyke is 526 ± 3 Ma	Since this granite has retrogressed the charnockite which constrains the minimum age for the charnockite formation.
S-340	U; 3 zircon grains were analysed.	A quarry section in Vadakkupuram, ~3 km SE of Pattanammitta; north of the Achankovil lineament (Fig. 3.61).	ditto	All three grains lies within 0.5% of concordance. The most concordant one (Z4) has a $^{207}Pb/^{206}Pb$ age of 526 ± 1 Ma. Since this sample and S-318B both have retrogressed charnockite, 4 least discordant grains from these two samples were regressed together which gives an U-Pb age of 524 ± 1 Ma (Fig. 4.23b)	The best estimate of the granite dyke is 526 ± 1 Ma	Sample S-318B & S-340 are both granite which has retrogressed charnockite. Both have the best estimated age of 526 ± 2 Ma. This is the minimum age of the charnockitization.

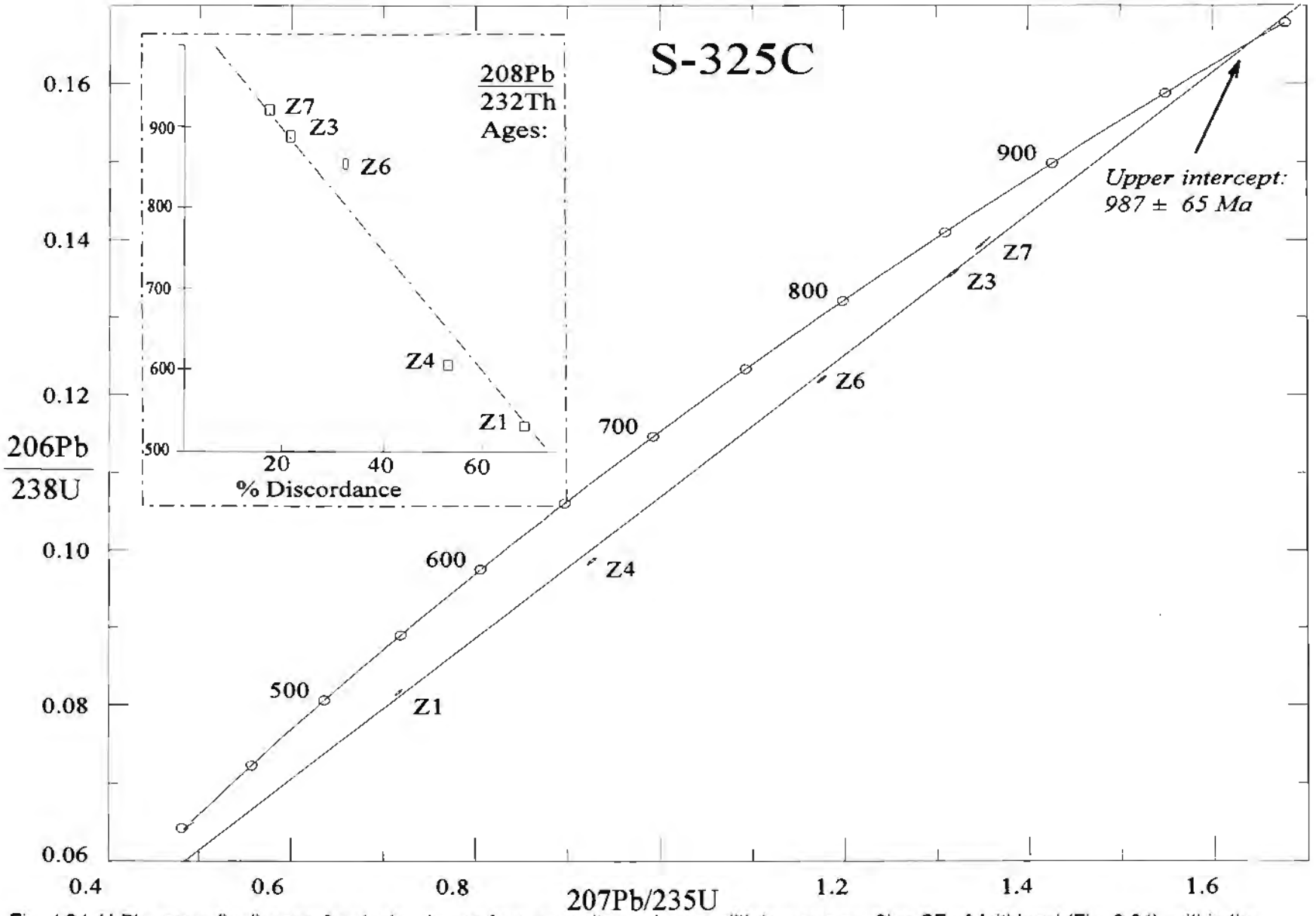

Fig. 4.24. U-Pb concordia diagram for single zircons from a granite gneiss xenolith in a quarry ~2km SE of Arithingal (Fig. 3.61), within the Achankovil Linament. Three out of four crystals analyzed define a discordia with upper intercept at 987 ± 65 Ma. The 208Pb/232Th ages (inset) show moderate coupling with the U-Pb ages forming a linear array when plotted against % of their discordance as defined in Appendix- A.4.1.

Sample no.	Laboratory	Location	Rock type and geological setting	Age	Interpretation	Comment
S-325C	U; 5 zircon grains were analysed	A quarry section ~2 km SE of Arithingal (Fig. 3.61).	Granite gneiss xenolith within partially charnockitized Kalipara Granite (Fig. 2.1).	All five zircons are long prismatic in shape. They yield highly discordant ages that fall on a moderately well defined discordia with upper intercept at 987 ± 65 Ma (Fig. 4.24).	The 987 ± 65 Ma age either reflects the intrusive age of the granite gneiss. The high degree of discordancy is likely to be Pb-loss and/or overgrowth during intrusion of host Kalipara Granite and subsequent charnockitization.	Although granitic gneisses (both para and ortho) are the most dominant rock in the KKB, zircons in them are highly discordant due to extensive recrystallization and Pb-loss as is evident from the analyses of T-4 and S-320 samples. Granite gneiss xenoliths within the Kalipara-Granite were perhaps shielded from later recrystallization and hence yielded more concordant ages. This rock gives the first indication that ~1.0 Ga granite may exist in the SGT

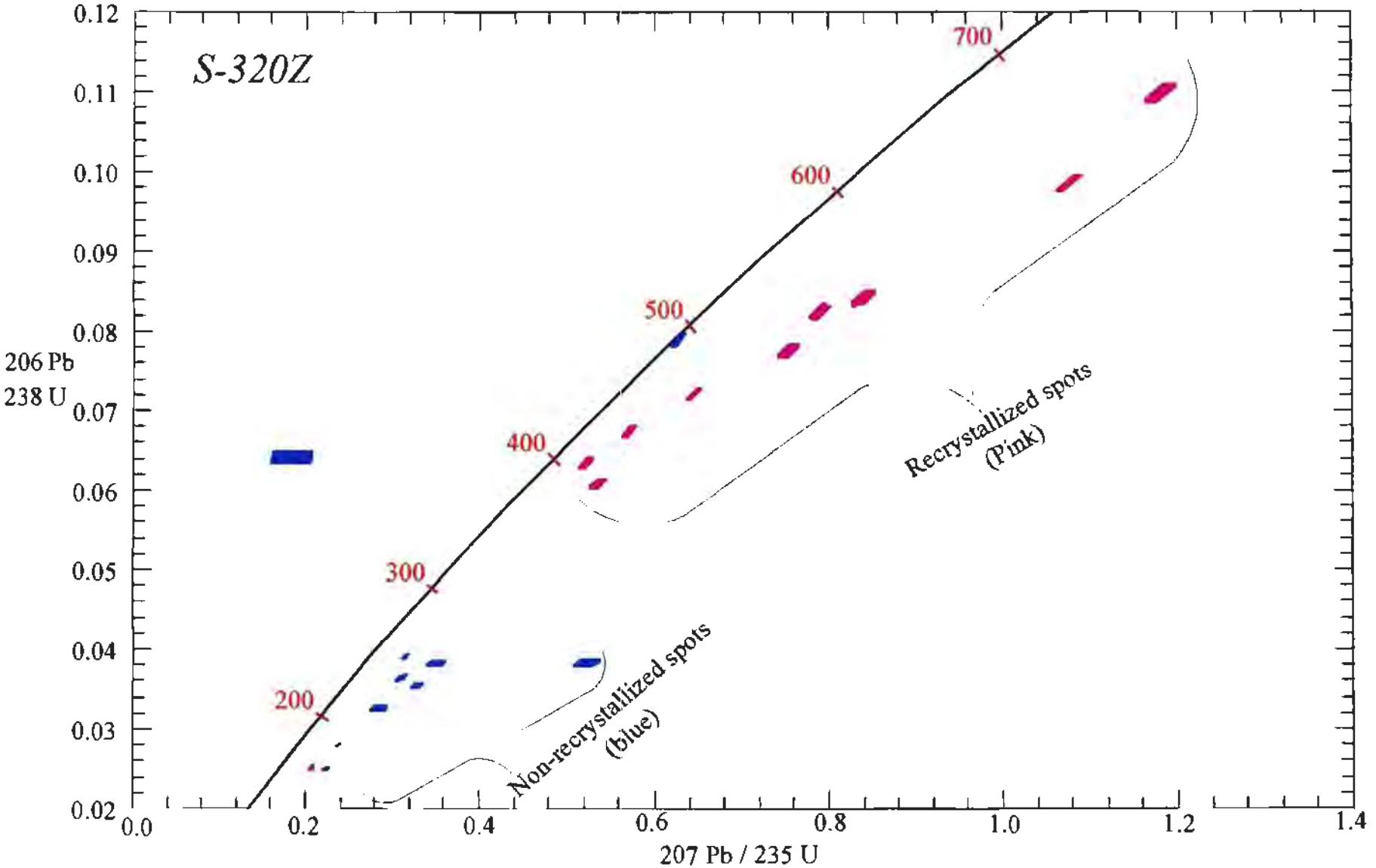

Fig. 4.25. U-Pb concordia diagrams for zircons from a sample of leucosome of a granite biotite gneiss (S-320) from the Kerala Khondalite Belt. Zircons in this rock are all partially to highly recrystallized (Fig. 4.26). Both the recrystallized and non-recrystallized spots plot at the lower end of a crudely defined discordia. The recrystallized spots plot towards upper end of such discordia

Sample no.	Laboratory	Location	Rock type and geological setting	Age	Interpretation	Comment
S-320Z	S+U; 2 zircon grains were analysed by IDTIMS followed by SHRIMP analyses of 25 spots in 15 crystals	A quarry section ~½ km SW of Punkulanji, ~5 km E of Kalanjur (Fig. 3.61).	Leucosome of garnet biotite gneiss.	Zircons in this rocks are pale greenish in colour and have lots of dusty opaque inclusions. IDTIMS analyses of two grains are highly discordant. The SHRIMP analysed spots are also highly discordant. 25 spots in 15 crystals were analysed. All the points are highly discordant and define a linear array mostly falling near a lower concordia intercept of ~400 Ma (Fig. 4.25). BSE images revealed highly irregular distribution of recrystallized domains (Fig. 4.26). The recrystallized domains fall towards the upper part of the array while the older zoned areas give analyses that fall in the lower part of the array.	These zircon have high U content and are thus susceptible to significant Pb-loss. No definite age of the protolith could be interpreted. The recrystallized patches which cut across the original magmatic zoning of these crystals are less discordant than the non-recrystallized areas (Fig. 4.25).	The recrystallized domains have annealed part of their crystal defects during recrystallization and so are less prone to Pb-loss following recrystallization while the non-recrystallized domains continued to lose Pb. This may explain why the analyses of recrystallized domains are less discordant than those from the non-recrystallized area

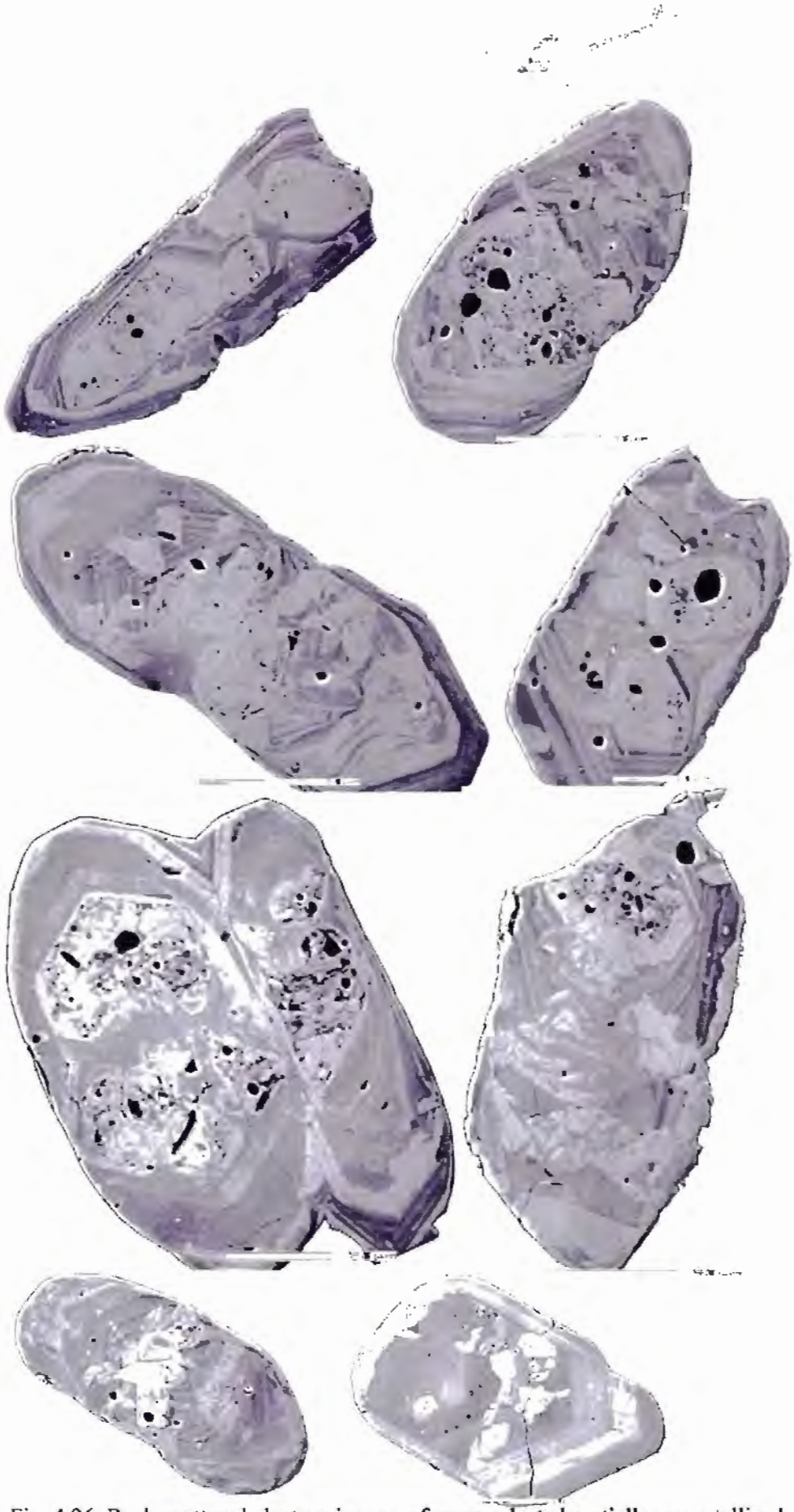

Fig. 4.26. Back-scattered electron images of some selected partially recrystallized igneous zircons in a sample of leucosome in garnet-biotite gneiss (S-320). Recrystallized domains (pale grey) cut across zoned areas (darker grey) and are less discordant than the later (Fig. 3.25). Length of each grains is ~150-250 microns.

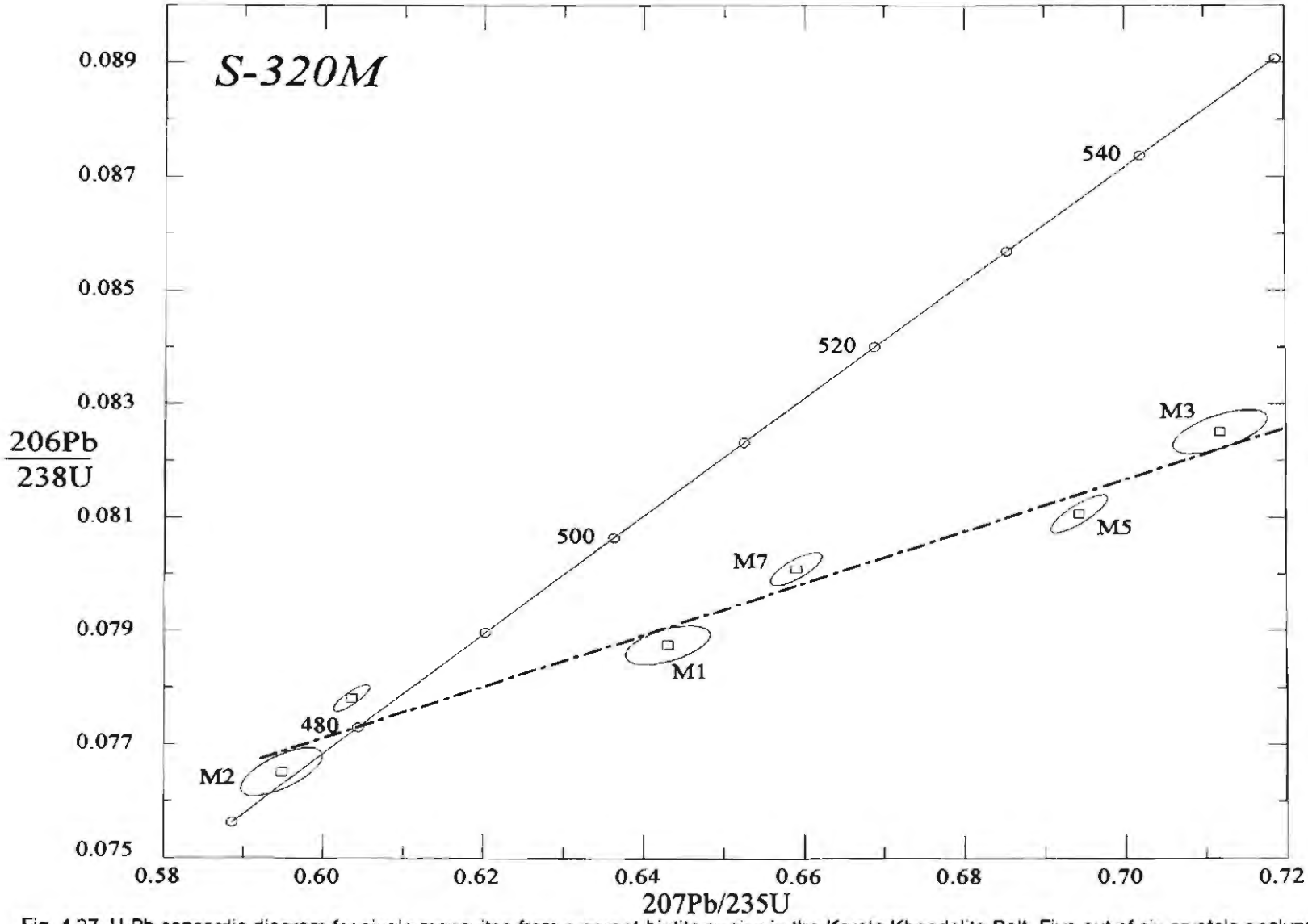

Fig. 4.27. U-Pb concordia diagram for single monazites from a garnet-biotite gneiss in the Kerala Khondalite Belt. Five out of six crystals analyzed are discordant and the other is concordant with a 207Pb/206Pb age of 468 ± 11Ma (M2). A best fit reference line through all six points has the lower intercept on the concordia at ~480 Ma. This age is similar to the Rb-Sr biotite-whole rock age reported from the area (Buhl., 1985; Unnikrishnan-Warrior, 1996). The ~480 Ma age may represent a thermal (or cooling) event in the area. The discordancy of most of the monazite grains could either be due to incomplete recrystallization, Pb-loss, or overgrowth on older cores. Zircons from the same rock are partially recrystallized (Fig. 4.26) and also highly discordant (Fig. 4.25) which has been interpreted as a result of partial recrystallization and Pb-loss.

Sample no.	Laboratory	Location	Rock type and geological setting	Age	Interpretation	Comment
S-320M	U; 6 monazite crystals were analysed.	ditto	ditto	Monazite crystals are pale greenish yellow in colour and are euhedral in shape. Two of the six grains are within 1% of concordant at ~480 Ma. The other grains are more discordant but align themselves along a line which cuts concordia at ~480 Ma (Fig. 4.27).	Age of the monazite crystals could not be ascertained due to high discordancy. Two crystals falling near concordia at ~480 Ma suggest a period of monazite growth during that time. The more discordant grains are, at least in part, older than ~480 Ma	Since the zircon analyses from this rock has indicated significant recrystallization and consequent Pb-loss (S-320Z), the monazite crystals may also have undergone recrystallization and Pb-loss, which may explain the high degree of discordancy of the majority of the monazite crystals.

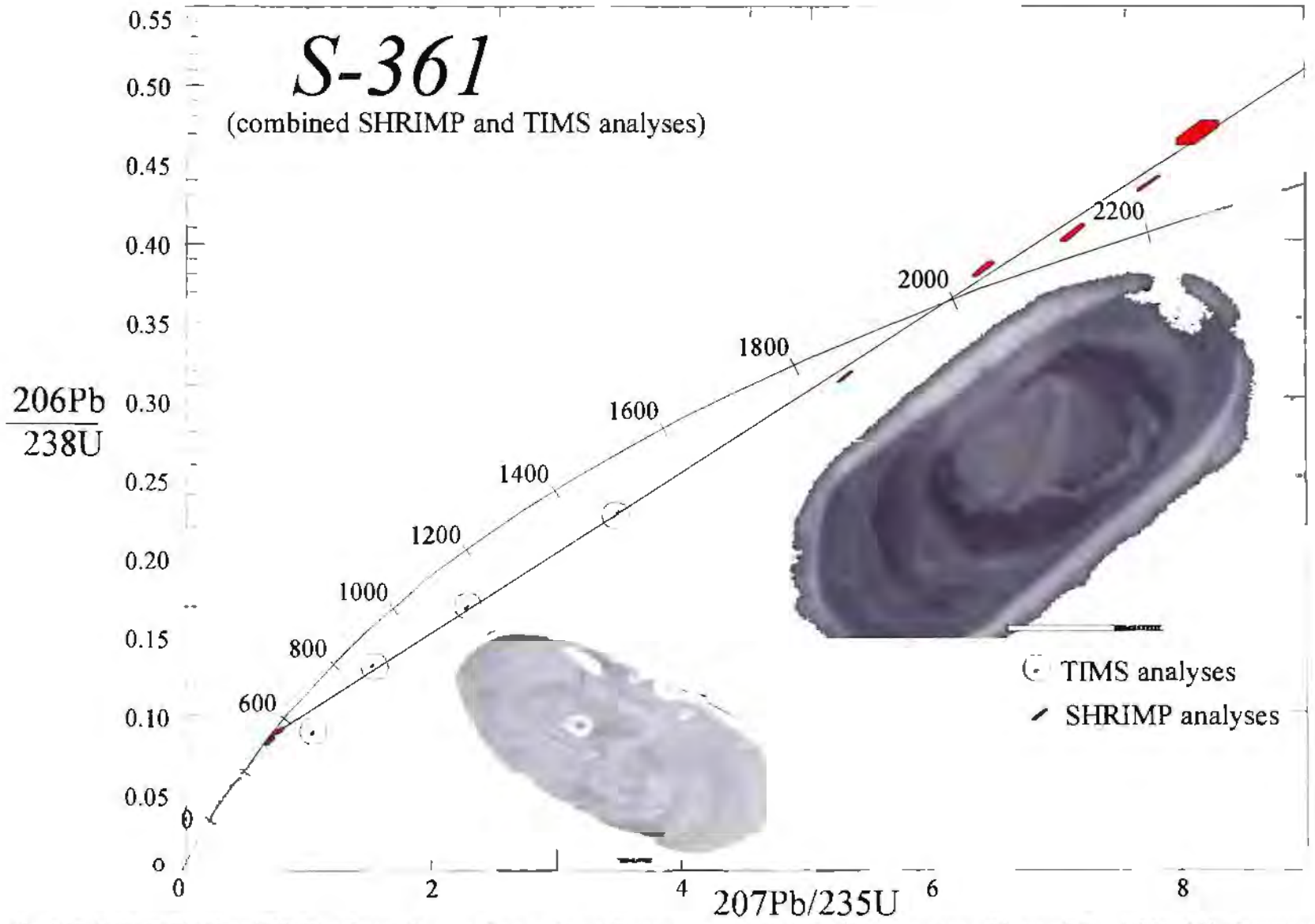

Fig. 4.28. U-Pb SHRIMP and TIMS analyses of zircons from a charnockitized granite dyke in the Kottaram quarry, Nagercoil Block (Fig. 2.1). Zircons in this rock have core and rim structures (inset). The SHRIMP analyses fall in two clusters. One of them has an average 207Pb/P06Pb age of ~2.0 Ga, while the other has an average 207Pb/235Pb age of ~575 Ma. The TIMS analyses fall on a moderately well-defined discordia connecting the two SHRIMP clusters. A best-fit reference chord connecting both SHRIMP and TIMS analyses have upper intercept on the concordia at ~2.0 Ga which is the best estimate of the cores.

Sample no.	Laboratory	Location	Rock type and geological setting	Age	Interpretation	Comment
S-361A	S+U;	A quarry section in the village of Kottaram, ~ 5 km north of Kanya Kumari; east of NH-7	A charnockitized granite dyke within charnockite gneiss	Zircons have core-rim structure (Fig.4.28). TIMS analyses of five grains all gave highly discordant ages. 12 spots from 7 grains were analysed by the SHRIMP technique with a resultant best estimate for the core age of ~2.0 Ga and the best estimate rim age of ~575 Ma.	The rim age of ~575 Ma is taken to be the age of the dyke intrusion while the core age of ~2.0 Ga is the age of inherited zircons.	The rim age puts constrain on the maximum age of charnockitization. The core age of ~2.0 Ga possibly reflect inherited zircon from the adjacent khondalite gneiss.

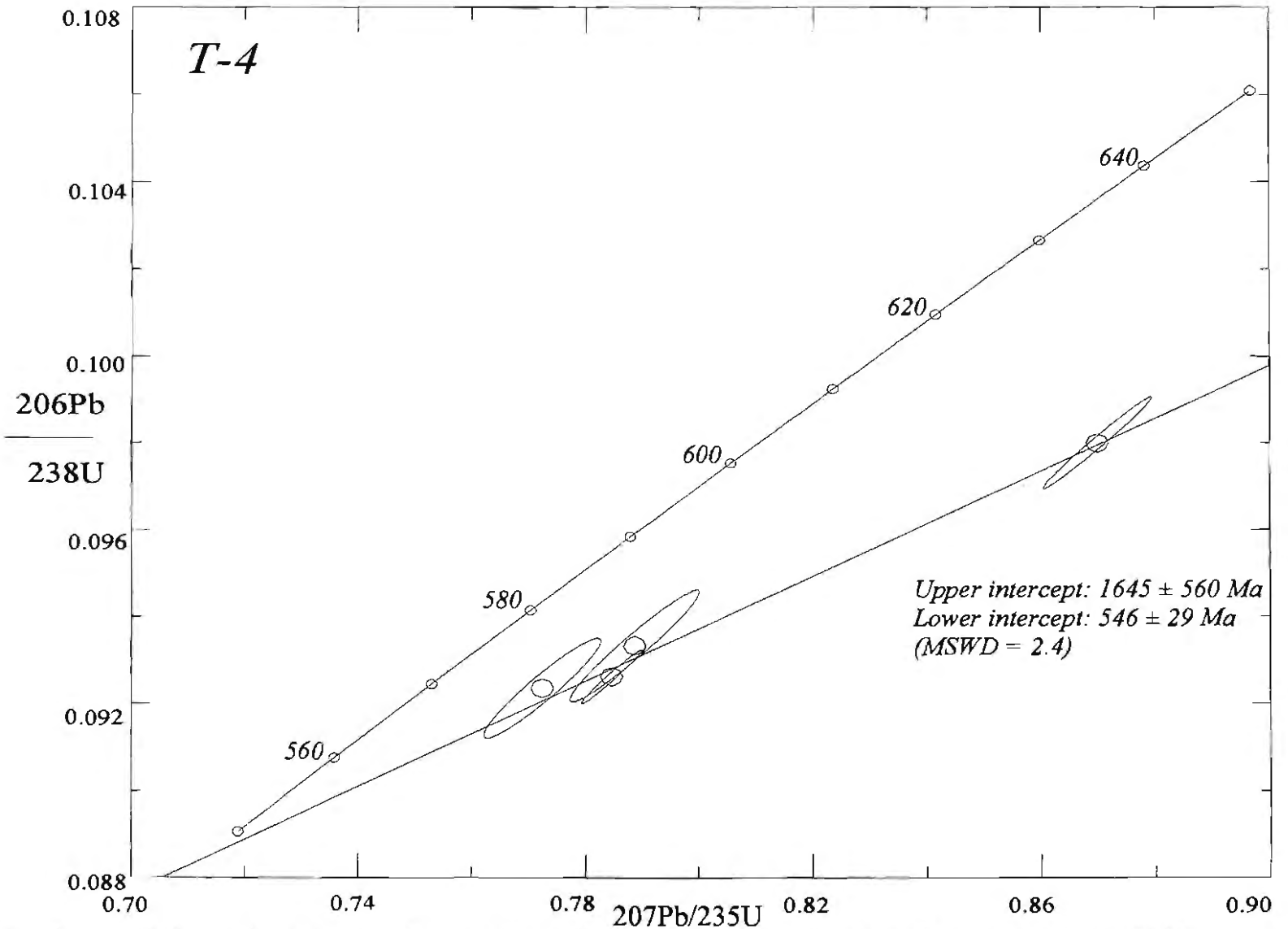

Fig. 4.29. U-Pb concordia diagram for single zircons from a mafic granulite in the Kerala Khondalite Belt. All four grains analyzed are highly discordant and plot near the lower intercept of a discordia with upper intercept at ~1.6 Ga and lower intercept at 546 ± 29 Ma. The large error in the upper intercept makes this age unusable, but the lower intercept age is similar to the age of the Kalipara Granite in the KKB. So the lower intercept age may be related to the tectono-magmatic events during this period.

Sample no.	Laboratory	Location	Rock type and geological setting	Age	Interpretation	Comment
T-4	U; 4 zircon grains were analysed.	A quarry section in Kunnanpuram, 13 km NNW of Trivandrum (Fig. 4.1).	Mafic granulite interlayered with charnockite gneiss.	Zircons are colourless and spheroidal in shape. All the crystals are discordant and cluster near the lower end of a discordia with a lower intercept of 546 ± 29 Ma and upper intercept of 1645 ± 560 Ma (Fig. 4.29).	The discordance of the zircon crystals are likely to be due to either inheritance or recrystallization. The lower intercept age agrees with the age of granulite metasomatism in the area. No protolith age can be interpreted from the analysed crystals.	Similar to the monazite and zircon analyses of sample S-320, zircons from this mafic granulite sample might also have suffered extensive recrystallization.

4.3.2. Discussion

4.3.2.1. Data from Corridor-I

The dominant rock types of this corridor include granitic and tonalitic gneiss and their charnockitized equivalents (Fig. 3.1). Mafic granulite, BIF and associated metasediments occur as enclaves within these gneisses. The central part of the corridor is dominated by extensive migmatite and granite intrusion. The southern part of the corridor at Palayam and further south is mostly underlain by metasediments intruded by granite and anorthosite.

Zircons from the granitic gneisses, their charnockitized equivalent, and mafic granulite from the Salem, Namakkal, Karur, and Palayam areas were analysed to determine the protolith ages across the Moyar and Palghat-Cauvery Shear Zones. Intrusive granites as well as anorthosite from Oddhanchatram at the southern end of the corridor provide insight into the age of later magmatic events. Monazite from charnockites and a khondalite from the central and southern part of the corridor, respectively, give ages of the high-grade metamorphism in the corridor.

4.3.2.1.1. Salem Area

The Salem area is dominated by granite and tonalite gneisses and their charnockitized equivalents. Previously, Spooner and Fairbairn (1970) dated the charnockites of the area at around 2476 ± 115 Ma using the Rb-Sr whole rock technique. Also, Peucat et al. (1993) dated charnockite and granite gneiss from the Krishnagiri area, ~150 km north of Salem, at 2.53 - 2.55 Ga by the U-Pb zircon technique.

Five zircon grains from a tonalite gneiss (S-27A) were analysed. The average of the four most concordant grains gives a U/Pb age of 2528 ± 1.7 Ma, and the $^{208}Pb/^{232}Th$ age of two analysed grains is 2528 ± 3.7 Ma (Fig. 4.2; Table 4.2). Circa 2.5 Ga gneisses have been reported from the Krishnagiri area of the Dharwar craton which is ~200 km north of Salem (Fig. 1.11)

These results provide support for the continuation of ~2.5 Ga granitic gneisses between the Krishnagiri and the Salem areas (Fig. 4.1).

4.3.2.1.2. Namakkal area

The ages of the biotite gneiss (S-220, Table 4.2) and the enderbite gneiss (S-130, Table 4.4) are 2512 ± 2 Ma and the 2537 ± 1 Ma, respectively, suggesting that they are broadly contemporaneous.

Monazite from the ~2.5 Ga old enderbitic gneiss (S-130) has a high a Th content (>3 wt%). The U-Pb ages of five analysed monazite crystals are somewhat discordant (Fig. 4 5, Table 4.2). The best estimate of the crystallization age of the monazite is given by the $^{207}Pb/^{206}Pb$ age of the most concordant grain, which is 2507 ± 5 Ma. This age is interpreted as the age of charnockitization which, therefore, closely followed emplacement of the tonalite gneiss (presently enderbite gneiss). Charnockitization has recrystallized the planar penetrative deformation fabric of the rock. Hence, the age of D_1 deformation is older than 2507 ± 5 Ma.

Younger massive granites and granitic veins have extensively intruded the older gneisses in some cases yielding migmatite. In places they crosscut shear planes related to D_2 deformation (Fig. 3.26). These migmatitic rocks have themselves been tightly folded (Fig. 3.33) in response to D_3 shearing. A sample (S-196A) from about a metre thick leucosome in the migmatite was collected for analyses. Six zircons from this rock are all a few percent discordant and yield a tight grouping of $^{206}Pb/^{238}U$ ages (534-550 Ma) but, in all but one case, significantly older $^{207}Pb/^{206}Pb$ ages (591-629 Ma). The causes of this discordancy are not well understood. If it is due to inheritance, then the age of the rock should be younger than the $^{206}Pb/^{238}U$ ages (i.e., younger than 550 Ma). On the other hand if it is due to Pb-loss, then the $^{207}Pb/^{206}Pb$ ages should approximate the age of the rock. The average of the five older $^{207}Pb/^{206}Pb$ ages is 603 ± 14 Ma (Fig. 4.7; Table 4.4). Because of this somewhat narrow range of $^{207}Pb/^{206}Pb$ ages, I

interpret this age as the best estimate of protolith age. This age is probably also the time of tectonic activity along the S_3 shears.

Mafic granulites in the Namakkal area are intrusive into the BIF and associated sediments, with which they are co-deformed and intruded by the ~2.53 Ga old tonalitic gneisses. The age of emplacement of the mafic granulites, therefore, must be older. Mafic granulite bodies commonly retain the igneous layering of felsic-rich and mafic-rich layers. Zircons from a felsic-rich layer (S-117) were analysed. The zircon crystals are colourless and show complex core and rim structure (Fig. 4.6b). SHRIMP analyses (Fig.4.6b; Table 4.3) reveal very complex geochronological information. Spots in the cores of zircon grains were all reversely discordant with $^{207}Pb/^{206}Pb$ ages varying from ~2.8 Ga to ~3.1 Ga, whilst the rim provided a number of concordant and slightly normally discordant points with $^{207}Pb/^{206}Pb$ ages of ~2.5 Ga (Fig. 4.6a). Because the rock has been intruded by ~2.5 Ga old tonalite, the rims might have grown during intrusion of the ~2.53 Ga granitoids in the area. Whether the cores represent zircon crystallized during emplacement of the mafic granulite, or are xenocrysts is not clear. Since field relations prove this body to be older than 2.53 Ga, the age of old zircon cores could represent age of crystallization of the mafic granulite.

A number of other zircon grains analysed from this sample define an array of 23 points along a discordia joining ~2.5 Ga and ~720 Ma (Fig.4.6a). Of these, 7 points cluster near the lower concordia intercept, with a mean $^{206}Pb/^{238}U$ age of 722 ± 13 Ma. The array may thus be interpreted as a mixing line between ~2.5 Ga zircons and new zircons grown at ~720 Ma, possibly in response to a tectonothermal event (D_2?). A similar age of 726 ± 6 Ma (Sm-Nd mineral isochron) has been reported from mafic granulite for an adjacent area, which was interpreted as the age of metamorphism in the area (Bhaskar Rao et al. 1996).

The Namakkal area thus records Mid- to Late-Archaean magmatic, metamorphic and tectonic activity. The ~2.9 Ga mafic granulite and older BIF and associated metasediments were

extensively invaded by tonalite at around ~2.5 Ga. Deformation (D_1) and subsequent charnockitization of the area closely followed this extensive granitoid activity. The area was later affected by a number of shear zones which were activated at different times between ~725 Ma (D_2) and ~600 Ma (D_3) south of Namakkal.

4.3.2.1.3. Karur

The Karur area is dominated by granite gneisses and their charnockitized equivalents. A granite gneiss sample (S-236A) from a quarry about 6 km southwest of Karur and south of the PCSZ (Drury et al. 1984 and GSI, 1994) was analysed. Six zircons from this rock are all normally discordant (3-7%) with an upper intercept age of 2545 ± 20 Ma. This age confirms the continuation of ~2.5 Ga old granite gneiss from the Salem area within the Mcyar-Attur Shear Zone to the Karur area across the PCSZ. The absence of obvious structural discontinuity across the PCSZ also supports the interpretation that this zone does not represent a major terrane boundary..

4.3.2.1.4. Charnockite of the Ranga Malai Hill area

The Ranga Malai Hill is located about 40 km north of Dindigul. Here charnockitized granite (S-267) has retained a ghost gneissosity defined by subparallel alignment of ellipsoidal mafic clots. The rock is, however, totally recrystallized and does not show any preserved penetrative planar fabric. The upper and lower concordia intercepts of 8 zircon grains are 804 ± 4 Ma and 473 ± 83 Ma, respectively (Fig. 4.9). The least discordant grain has a $^{207}Pb/^{206}Pb$ age of 796 ± 1 Ma, which is interpreted as the crystallization age of the precursor granite. The lower intercept age, poorly defined at 473 ± 83 Ma, possibly records cessation of high-grade metamorphism, but it could also represent an uplift/cooling age that might have caused Pb loss from the zircon grains resulting in their alignment along a discordia. The ~800 Ma protolith age of this rocks, along with the ~800 Ma monazite from Valya Malai, suggest that a thermal

event was regionally extensive at this time.

4.3.2.1.5. Khondalite of the Valya Malai Hill area

Valya Malai is located about 16 km ESE of Palayam. The area is occupied predominantly by khondalite and calc-silicate rocks. 14 monazite crystals from a sample of khondalite were dated at 791 ± 15 Ma by the SHRIMP (Fig. 4.10a; Table 4.1). The best interpretation is that this monazite age reflects the timing of latest granulite facies metamorphism (>750°C) in the area. It is important to note that in the Kodaikanal area (Fig. 4.1), ~250 km southwest of Valya Malai, the age of charnockitization has been interpreted to be ~550 Ma on the basis of Pb-isotopic ratios by low-temperature zircon evaporation analyses (Bartlett, 1995; Jayananda, 1995). This ~550 Ma event has apparently not affected the U-Pb systematics of monazite in the non-charnockitized rocks of the Valya Malai area. Thus the ~550 Ma charnockitization event was restricted to restricted areas of the SGT, rather than being present pervasively throughout the SGT.

4.3.2.1.6. The Oddanchatram Anorthosite

The Oddanchatram anorthosite occupies a ~35 km^2 elliptical massif, ~40 km to the south of the Palghat-Cauvery Lineament but close to the KKPT Shear Zone, which is here interpreted as a major decollement. The long axis of the body traces NNE-SSW, subparallel to the KKPT. This is a labradorite-type anorthositic massif (cf., Ashwal, 1993), with a central coarse-grained anorthosite facies and a marginal fine-grained gabbroic facies (Leelanandam, 1990). The pluton exhibits protoclastic granulation and flow differentiation (Narasimha Rao, 1977). The marginal rim of this massif bears evidences of metamorphism with development of garnet, biotite, quartz, K-feldspar and secondary high-calcic plagioclase (Leelanandam, 1990) however, the central part of the body is unmetamorphosed and preserves primary igneous textures (Janardhan and Wiebe, 1985).

Zircons from a sample (S-268) of the comparatively silica-rich central part of this massif were analysed by the SHRIMP (Fig. 4.11). Zircons from this rock are large (~300 μm^3) and equant and pale pink in colour. Cathodoluminiscence and back scattering electron imaging of these zircons show that they are homogeneous without zoning or recrystallization textures. Almost all of them show marginal granulation. Nine spots from nine different crystals were analysed which gave a tight clustering with an average $^{206}Pb/^{238}U$ age of 563 ± 9 Ma. This age overlaps with similar ages of syntectonic granite (S-415) along the KKPT Shear Zone. In Madagascar, Ashwal et al. (1999) have documented that many concordant zircons from a similar meta-anorthosite range in age between 631 Ma and 549 Ma. They attributed this age pattern to high temperature Pb-loss during one or more periods of granulite metamorphism from originally magmatic zircons. Clearly, caution should be applied in the interpretation of concordant zircon ages for these types of meta-igneous rocks.

4.3.2.2. Corridor-II

The northern part of Corridor-II is dominated by granite gneiss with enclaves of quartzite and mafic granulite. The central and southern parts of the area comprise migmatite similar to the Namakkal area of Corridor-I. Monazite from a quartzite sample in the northern part of the corridor, within the MSZ, has been dated by the U-Pb method.

4.3.2.2.1. Monazite from fuchsite quartzite in the Bhavani area

Monazite from fuchsitic quartzite (S-259) within the Moyar shear zone north of Bhavani (Fig. 4.1) was analysed by SHRIMP (Fig. 4.12). Two different ages were obtained: (i) ~2.56 Ga, represented by two concordant points and (ii) another concordant age, clustering around 612 ± 6 Ma. The ~2.56 Ga age closely matches the 2.52 Ga monazite and allanite ages reported from charnockites of Biligirirangan Hills (about 60-70 km northwest of this area), and may thus broadly represent the age of regional granulite facies metamorphism (Grew and Manton,

1984). The ~612 Ma cluster matches the zircon ages for migmatisation obtained in the Namakkal and Mettupalayam areas (Fig. 4.7, 4.16), and may represent the age of deformation and fluid activity in the shear zones of both areas.

4.3.2.3. Corridor-III

4.3.2.3.1. Granite gneiss, mafic granulite, and granitic pegmatite from the Mettupalayam area

The Mettupalayam area lies within the Bhavani Shear Zone. The predominant lithologies of the area include granite gneiss, mylonitized granite, mafic granulite, enderbite, and massive granite. Representative samples of each of these rock types were collected in a quarry in Gudiyar, about 5 km east of Mettupalayam. Zircons from these rocks were analysed by the IDTIMS method. Zircons from the granite gneiss, mylonitised granite, and enderbite are all nearly concordant with a best estimate of their intrusive age of ~2.53 Ga (Fig. 4.14). Zircons from the mafic granulite have a best estimated age ~2.5 Ga (Fig. 4.13). Field evidence suggests that the mafic granulites are intruded by the granitic gneiss. This similar age of the zircons from mafic granulite and from younger (~2.5 Ga) granitic gneisses is thus interpreted as growth of metamorphic zircons soon after emplacement of the granite gneiss. This age may also represent the time of general high-grade metamorphism and associated charnockitization.

Zircons from a granitic pegmatite vein (MS-3), which cuts across the main fabric of the Bhavani Shear Zone in the Gudiyar quarry, have very distinctive shapes ranging from platy to acicular (Fig. 4.15). The $^{207}Pb/^{206}Pb$ age of the most concordant of three such zircons analysed is 601 ± 1 Ma, which is taken as the emplacement age of the pegmatite body and, possibly, other massive granites present in the area. It may be noted that this age is similar to the age of a post-S_2 pegmatite (608 ± 1 Ma) reported from S. Madagascar (de Wit et al. MS in preparation).

4.3.2.4. Corridor-IV

The dominant rock type of the Palghat area is a biotite-rich granite gneiss (type A) that has been intruded by at least two phases of granitic veins (Fig. 3.49). One of these phases (type B) has densely intruded the type A rocks subparallel to their gneissosity; and both rocks have been co-folded into isoclinal folds (Fig. 3.49). The second phase of granitic vein (type C) is present as 10s of cm thick dikes that cut the gneissosity at high angle, and which are folded into broad shallow easterly plunging folds without axial planar fabric. Type B granite veins are possibly related to the D_2 deformation present in the area. The type C granitic veins are syntectonic with a late phase shearing event (D_3).

4.3.2.4.2. Granite gneiss

A sample of the biotite gneiss (S-404A, type A) was collected where it is least densely intruded by types B and C veins (Fig. 3.49). Zircons from this rock are colourless and transparent. They have well developed concentric zoning (Fig.4.17; 4.18), which is indicative of their magmatic origin (Pidgeon, 1992). Core and overgrowth rims are quite common in the zircons from this rock. SHRIMP analyses of the zircons yield two distinct clusters that plot close to concordia. One of the clusters (13 spots) scatters (~up to 5% normally and reversely discordant) around 2.86 Ga; the other (12 spots) is near concordant with a mean $^{207}Pb/^{206}Pb$ age of 1643 ± 10 Ma. The 2.86 Ga age is interpreted as the intrusive age of the type A granite gneiss while the 1643 ± 10 Ma age may be related to the intrusion of the type B granite because these zircons also display magmatic zoning.

4.3.2.4.3. Granite

Zircon from type C granite (S-404B) was analysed by IDTIMS. This rock has two distinct populations of zircons. One of them is colourless and the other is orange in colour. These two varieties have distinct geochemical signatures: the Th/U ratio of the colourless variety varies

from 0.5 to 1.5 while the Th/U ratio of the orange coloured variety lies between 0.02 and 0.05. The colourless variety is older than the orange coloured variety. The best age estimate of the colourless variety is 600 ± 4 Ma. The $^{207}Pb/^{206}Pb$ age of the most concordant zircon of the orange coloured variety is 522 ± 3 Ma. Thus the best estimate of the age of the type C granite is given by the colourless variety, i.e., 600 ± 4 Ma, while 522 ± 3 Ma age could represent younger (hydro)thermal activity (very low Th/U ratio in these zircons is suggestive of their hydrothermal origin), related to uplift following charnockitization. Circa 600 Ma ages have also been recorded along the Cauvery-Bhavani Shear Zone (CBSZ; S-196A, Namakkal area), and along the Bhavani Shear Zone (BSZ; S-273M; Bhavani area), which implies contemporaneity of tectono-thermal events along these shear zones. A 524 ± 2 Ma age has also been recorded in monazite from khondalite and in zircons in a late granite from the Pattanammitta area in the PPP corridor (Fig. 3.61) in the northern edge of the KKB.

4.3.2.5. Kottamongalam area (western part of the KKPT Shear Zone)

The Kottamangalam area lies close to the KKPT Shear Zone at the intersection of two different regional structural styles (Fig. 4.1). Lithologic units of the area are highly deformed. Samples (S-416 & S-415; Table 4.2) were collected from a quarry in which many syntectonic granitic veins have intruded the granite gneiss (Fig. 3.57). Both the granite gneiss (S-416) and a syntectonic granite (S-415) vein were sampled and analysed.

4.3.2.5.1. Granite Gneiss

Zircons from the granite gneiss were spheroidal and colourless. Six zircon grains were analysed. All of them fall on a discordia with upper and lower intercepts of 2511 ± 27 Ma and 571 ± 58 Ma respectively (Fig. 4.19). The upper intercept age is interpreted as the best estimate of the intrusive age of the granite gneiss. The lower intercept matches the age of the syntectonic granite from the same quarry, which yielded an age of 568 ± 2 Ma (Fig. 4.20). $^{208}Pb/^{232}Th$ ages for these analysed samples correlate moderately well with the U-Pb ages and

form a linear array when plotted against percent discordancy (Fig. 4.19) which is defined as the distance of a particular point on the discordia from its upper intercept expressed as percent of the length of the discordia (see Appendix- A.4.1.5).

The alignment of data points along a discordia is thus consistent with either overgrowth of the original 2511 Ma zircon by ~570 Ma old zircon, or a Pb-loss event at 570 Ma. The Th/U ratios of zircons from the granite gneiss ranges between 0.3 and 0.6, while in the granite the ratio varies between ~2.0 and ~2.5. Mixtures between these two types of zircon with contrasting Th/U ratios would thus be expected to give good correlation between the percent discordancy and the Th/U ratios of the mixed zircons. In this set of samples, however, there is no correlation between the Th/U ratios of the zircons and their percent discordancy (as defined in Appendix- A.4.1.5). This lack of correlation suggests that the more likely cause of discordancy is Pb-loss at 570 Ma rather than overgrowth by zircons from the younger granite.

4.3.2.5.2. Granite

Zircons from a syn-tectonic (syn-tectonic to a shearing event along the KKPT Shear Zone; D_2 or D_3) granite vein (S-415), which intruded granite gneiss (S-416), yield a concordant age of 567 ± 2 Ma. Also, $^{208}Pb/^{232}Th$ ages of these zircons have a weighted average age of 563 ± 3.4 Ma (Fig. 4.20). This age is similar to that of the zircon age from an ellipsoidal anorthosite body (563 ± 9 Ma; section 4.4.3.1.6), aligned subparallel and close to the KKPT Shear Zone, in the Oddahchattram area. This anorthosite body is deformed along its periphery. Together, these two ages suggest that shearing occurred along the KKPT shear zone between circa 560 and 570 Ma.

4.3.2.6. PPP corridor in the Kerala Khondalite Belt

The Kerala Khondalite Belt is dominated by various metasedimentary rocks and their

migmatized and charnockitized equivalents. These include khondalite, garnet-biotite gneiss, cordierite gneiss, quartzite, calc-silicate gneisses, etc. Mafic granulites are present as interlayered units within various paragneisses. All these lithologic units were intruded by later massive granite and pegmatite. Unequivocal orthogneisses were not observed during the present investigation in the PPP corridor. However, there are some enclaves of biotite gneiss and their charnockitized equivalents within younger massive granites, which may represent orthogneiss basement rocks to the metasediments. Charnockitization has affected all rock types present in the Kerala Khondalite Belt except a suite of pegmatitic granites which have intruded charnockites and have retrogressed the charnockitized patches in older rocks. The present investigation focussed on (i) dating the biotite gneiss and the mafic granulites, which may represent the basement of the metasediments, and (ii) to constrain the age of charnockitization.

4.3.2.6.1. Biotite gneiss

Granite gneisses in the KKB, mostly interpreted as paragneisses (Chacko et al. 1992), have suffered extensive migmatisation. Because unequivocal basement orthogneiss to the metasediments of the KKB could not be identified in the present work, zircon from a sample of neosome in a migmatitic garnet biotite gneiss (S-320; Fig. 4.24) and from a biotite gneiss enclave (S-325; Fig. 2.1a) within massive Kalipara Granite were analysed-- the former to obtain the age of the neosome and the latter to obtain the age of the possible basement of the metasediments of the KKB.

4.3.2.6.2. Neosome in the biotite gneiss (S-320)

Zircons from a neosome in the biotite gneiss are greenish in colour and are clouded with dusty opaque inclusions. Two grains were analysed by the TIMS method and 25 spots from 15 crystals were analysed by the SHRIMP. Analysed points scatter near the lower end of a

discordia whose lower intercept is ~200 Ma and upper intercept is older than ~2 Ga (Fig. 4.25). Zircons from this rock all have very high U content (2000 - 7000 ppm). BSE (Back Scattered Electon) images show the presence of recrystallized domains within each grain (Fig.4.26). The recrystallized domains have older $^{206}Pb/^{238}U$, $^{207}Pb/^{235}U$ and $^{207}Pb/^{206}Pb$ ages than the non-recrystallized domains (Fig. 4.25). This pattern suggests that the very high U-content of the zircon crystals have effected metamictization and consequent Pb-loss. At a subsequent stage parts of zircon crystals were recrystallized. Damage due to metamictization were annealed during recrystallization and the recrystallized domains were subsequently subjected to less Pb-loss than the non-recrystallized areas. This may explain why the analyses of recrystallized domains plot on the upper end of the discordia while those of the non-recrystallized areas plot towards the lower end. No meaningful age of the leucosome could be obtained from such highly discordant points.

4.3.2.6.3. Biotite gneiss enclave within the Kalipara Granite

A sample from a ~ 4-5 m long xenolith of biotite gneiss within the Kalipara Granite in the Arithingal quarry (Fig. 2.1a) was collected for zircon analyses. Since zircon analyses from mafic granulite (T-4) and from the leucosome of a biotite gneiss all were highly discordant due to Pb-loss and recrystallization, it was thought that a sample of a xenolith (S-325C) might have been protected from later fluid activity by the host granite and thus may yield its protolith age. Zircons from this biotite gneiss are of two different morphological varieties. One variety is globular in shape with indistinct core-rim structure and the second is transparent and long prismatic in shape. The latter variety was selected for analyses. Five crystals analysed are all discordant (between 20-60%) but they fall on a discordia defining an upper intercept age of 987 ± 65 Ma (Fig. 4.24). This age is likely to represent the protolith age of the granite gneiss xenolith. It may, however, represent zircon grown in the biotite gneiss during subsequent metamorphism/thermal event but prior to its incorporation in the host ~550 Ma Kalipara Granite.

4.3.2.6.4. Mafic Granulite

A mafic granulite sample (T-4) was collected from the Kunnampuram quarry, ~13 km NNW of Trivandrum, for zircon analyses. The zircons are all transparent, inclusion-free and globular. All four analyzed crystals fall towards the lower intercept of a discordia with lower intercept at 546 ± 29 Ma and upper intercept at ~1.6 Ga (Fig. 4.29). Discordant plots of these points could be due either to overgrowth or Pb-loss. The lower intercept age corresponds to the age of the Kalipara Granite (S-318a), which has intruded the mafic granulite. Thus, the lower intercept age may be due to zircon growth during the intrusion of the Kalipara Granite. The protolith age of the mafic granulite is poorly constrained by the upper discordia intercept, which gives only a suggestion of a considerably older age.

Analyses of zircons from a massive granite (S-318A) from the KKB have yielded 5 concordant to slightly discordant points (S-318A, Table 4.2) giving the best estimate of the age of the granite as 548 ± 2 Ma age. Zircons from this rock also include 3 discordant points with $^{207}Pb/^{206}Pb$ ages greater than 2.3 Ga. When two of these three (most discordant one was omitted) discordant analyses are regressed along with three most concordant analyses at ~550 Ma, they give an upper intercept age of 2466 ± 22 Ma age. Assuming that these three discordant points are the result of either Pb-loss or zircon overgrowth at ~550 Ma, the upper intercept age may represent a population of ~2.5 Ga old zircon, which may be the general age of the basement in this area.

4.3.2.7. Age of Charnockitization in the Kerala Khondalite Belt

There are many spectacular outcrops of incipient charnockitization in the Kerala Khondalite belt. Various lithotypes of the area have been affected by charnockitization (Srikantappa et al 1985). In the Nirettipara quarry, about 0.5 km NNE of Nirettipara; ~6 km NE of Kalanjur (Fig. 3.61), massive Kalipara Granite has intruded biotite gneiss. This massive granite displays

incipient charnockitization (Fig. 2.5), and these incipient charnockite patches, in turn, have been intruded by coarse granitic veins and dykes. Along their margins, these veins have bleached (retrogressed; i.,e., orthopyroxene has reacted to form quartz and biotite) the host incipient charnockite patches (Fig. 2.6). Numerous bodies of the Kalipara Granite occur within the Achankovil Lineament (Fig. 3.61), cutting across the prominent NW-SE trending fabric of the area. One of the largest such bodies, exposed in the Chenganoor area, yields a K-Ar hornblende age of 550 ± 25 Ma (Soman and Santosh, 1983). The Kalipara Granite is thus interpreted as post-tectonic in origin and the charnockitization in the Kerala Khondalite Belt is also post-tectonic. Zircons from a sample of the Kalipara Granite (S-318A) and of two late intrusive veins (S-318B and S-340) have been analysed to constrain the age of charnockitization. Zircons from the Kalipara Granite proved to be very complex. A number of the zircons plot discordantly with $^{207}Pb/^{206}Pb$ age varying from ~2.3 Ga and 2.5 Ga. Other zircons give a concordant to slightly discordant ages of ~548 ± 2 Ma (Fig. 4.22). The old discordant points are interpreted as inherited grains that have suffered younger Pb-loss or overgrowth. The grains plotting around 548 Ma are interpreted as the intrusive age of the Kalipara Granite. The coarse granitic veins (S-318B; S-340), which have intruded the incipient charnockite patches, have a well-defined age of 526 ± 1 Ma (Fig. 4.23). The age of Neoproterozoic charnockitization can thus be bracketed between 548 ± 2 and 526 ± 1 Ma.

Monazite from a non-charnockitized khondalite enclave (S-355M) within charnockite gneiss (charnockitized khondalite gneiss) from a quarry in Kanamukku village, ~8 km north of Pattanamitta (north of the Achankovil Lineament), yields a concordant U-Pb age of 524 ± 1 Ma (Fig. 4.21; Table 4.4) and a weighted average $^{208}Pb/^{232}Th$ age of 523.5 ± 4 Ma. Because the closure temperature of the U/Pb system in monazite is between 700°C and 750°C, the minimum age of the latest high-grade metamorphism can be taken as ~524 Ma. It is worth noting that the granite vein in the Nirettipara quarry (S-318B), which has bleached charnockite is dated at 526 ± 1 Ma. Thus the monazite age of 524 ± 1 Ma can be best interpreted as marking the cessation of high-grade metamorphic conditions or as uplift and cooling of the

terrain immediately following from high-grade metamorphic conditions.

Monazites from a leucosome of migmatised garnet biotite gneiss (S-320M) from a quarry ~5 km east of Kalanjur (Fig. 3.61) within the Kerala Khondalite Belt have yielded a number of highly discordant ages and two nearly concordant ages (~1% discordant). The most concordant monazite grain gives a $^{206}Pb/^{238}U$ age of 475 ± 2 Ma. In many places these leucosomes are charnockitized. Charnockitization is dated as having occurred between ~548 Ma and ~526 Ma. Therefore, this 475 Ma age can not be the formation age of leucosomes, but may indicate a period of uplift and cooling of the terrain. Similar ages have been reported by early workers in the area using Rb-Sr mineral isochrons (Santosh et al. 1992; Choudhary et al. 1992; Unnikrishnan-Warrior, 1997). It is interesting to note that monazites from a sample of khondalite enclave (S-355M) within massif charnockites in the southern slope of the Cardamom Hills have yielded 524 ± 1 Ma. This difference in the monazite ages between two samples seperated by ~60 km (Fig. 4.1) may mean either differential uplift between these two areas or the influence of host rock and and its environment with respect to fluid circulation. Geological evidence for substantial differential uplift between these two areas is lacking. Hence, later interpretation that the monazite in the migmatized garnet biotie gneiss have been affected by later fluid circulation is more likely the case. Rb-Sr mineral isochron ages from nearby area also have yielded similar ages (Santosh et al. 1992; Choudhary et al. 1992; Unnikrishnan, 1997). The closure temperature for the U/Pb system in monazite is generally taken to be between 700°C (Copeland et al. 1988) and 725°C (Parrish, 1990). On the other hand the closure temperature for Rb-Sr in biotite is less than 400°C (Verschure et al. 1980). Because in the KKB two different isotopic systems with very different closure temperatures yields similar ages, it likely that these isotopic systems were intensely affected and were reset by passage of fluids through them. Zircons from the same sample (S-320Z) have revealed extensive recrystallization and Pb-loss, which also suggests that fluids have affected the rock intensely. Thus ~475 Ma age for monazites from leucosome of granite gneiss (S-320M) is more likely to be the effect of fluid activity through the rock and may not represent the age of

the cessation of granulite metamorphismin the KKB.

4.4. Summary and conclusion

The present geochronological analyses have improved the geochronological database from the SGT of Peninsular India. Thirty-five rocks were precisely dated to bracket a number of tectonomagmatic events. A summary of new data obtained in this study is given in Fig. 4.30. The most important conclusions that can be made from these data are:

(i) Archaean and Paleoproterozoic events:

- Zircons from the mafic granulite of the Namakkal area (Corridor-I) and the biotite gneiss from the Palghat area (Corridor-IV) provide the southernmost Archaean single crystal zircon ages (~2.9 Ga) from Peninsular India, and indicate that the Dharwar craton may extend considerably further south than previously realized.

- Circa 2.5 Ga granites and tonalites are quite common in the Transition Zone (the area of transition from amphibolite facies rocks of the Dharwar craton and the granulite facies rocks of the SGT) and in the Eastern Dharwar Block (Peucat et al. 1993). During the present study, ~2.5 Ga single zircon ages have been obtained from the Salem, Namakkal, Karur, Mettupalayam and Kotamangalam areas (Fig. 4.1). These occurrences suggest that Late Archaean granitic activity was widely spread, covering a much larger area in the SGT than previously thought, and extending at least as far south as the KKPT Shear Zone. In the Namakkal area, field relationships indicate that these intrusions were coeval with NE-SW trending dextral shearing and were emplaced along shear zones, in the eastern part of the Dharwar craton.

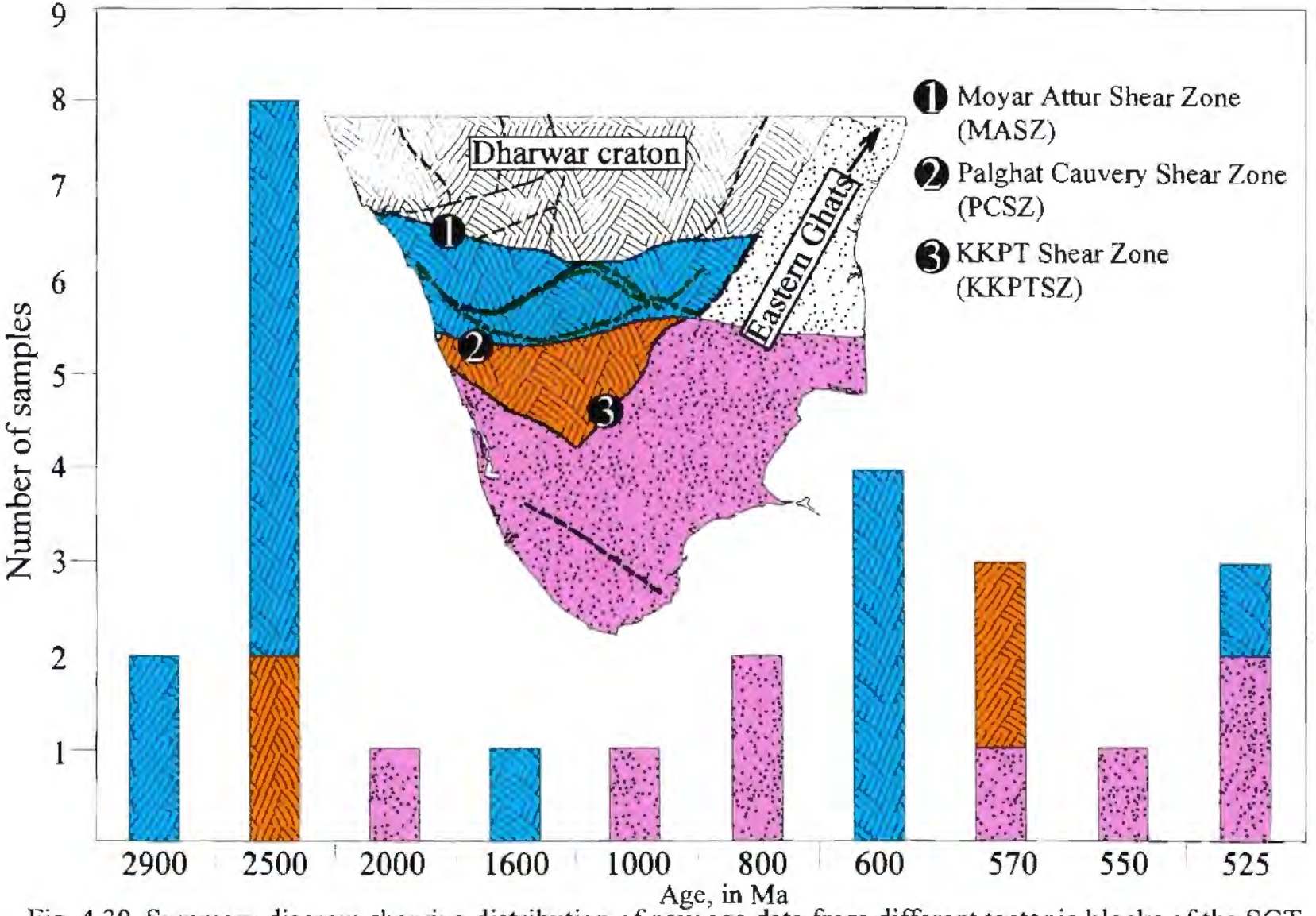

Fig. 4.30. Summary diagram showing distribution of new age data from different tectonic blocks of the SGT. Different colours indicate terrains bounded by major shear zones in the SGT. The new age data show that: (i) Neoproterozoic thermal events are present as far north as the MASZ and (ii) area south of the KKPTSZ have suffered at least six thermal events since ~2.0 Ga.

(ii) Mesoproterozoic events:

- A concordant ~1650 Ma age for zircon with concentric growth zoning (which is common in magmatic zircons) in granite gneiss from the Palghat area (sample S-404A) represents a new age for the SGT. The extent and significance of tectono-thermal activity at this time is not known. Kelly et al. (1997) reported an ~1.8 Ga Ar-Ar plateau age for biotite included within garnet from the Kerala Khondalite Belt, which was interpreted as a high-grade metamorphic event. It is also possible that Mesoproterozoic tectono-thermal events of unknown extent affected the SGT A ~1.0 Ga (987 ± 65 Ma) single zircon age has also been recorded for a granitic gneiss xenolith in the 548 Ma old Kalipara Granite. This ~1.0 Ga age is interpreted as the age of either intrusion or metamorphism prior to its incorporation in the Kalipara Granite. The ~1.0 Ga age is a commonly recorded thermal event in the Eastern Ghats (Shaw et al. 1997).

(iii) Neoproterozoic thermal events:

Santosh et al. (1989) has shown from existing age data that granitoids with ages ranging from ~765 Ma to 550 Ma are common from north of the Moyar Shear Zone to the southern tip of the Peninsula. This study records a number of Neoproterozoic events in the SGT with distinct zircon ages at ~800 Ma, ~720 Ma, ~600 Ma, ~570 Ma, ~550 Ma and ~525 Ma and monazite ages at ~800 Ma and at ~525 Ma. Thus, the SGT was episodically active in the Neoproterozoic over a 300 m.y. period of time, very similar to the Pan African events recorded in southern Madagascar (Paquette et al. 1994; Paquette and Nédélec, 1998; Kröner et al. 1996; Tucker et al. 1998 and de Wit et al. 1998) and East Africa (Pinna et al. 1993)

An 800 Ma event:

- Zircons from the charnockitized granite of Rangamalai (sample S-267; Table 4.2; Fig. 4.9) and monazites from khondalite of the Vidya Malai Hill area (sample S-259; Table 4.3; Fig. 4.10a) all give ~800 Ma ages. While the zircons from the Rangamalai Hill granite is affected by charnockitization at ~550 Ma (lower intercept on concordia), the Vidya Malai Hill monazite is not affected by this event. The ~800 Ma age is a common high grade metamorphism age in the classical Eastern Ghats terrain (Shaw et al. 1997). The present finding of ~800 Ma zircon and monazite ages from SGT suggests that there is a possible common ~800 Ma tectonothermal link between these two terrains.

A 720 Ma event:

- SHRIMP analyses of zircons from one mafic granulite from the Namakkal area (Sample S-117) gives a discordant array with upper and lower intercepts at ~2.5 Ga and ~720 Ma, respectively (Fig. 4.6). This mafic granulite body occurs within the sinistral NW-SE trending D_2 shear zone identified in the present work (Fig. 3.14). It is possible that the ~720 Ma age is related to a tectonothermal activity along the D_2 shear zone.

600 Ma, ~570 Ma, ~550 Ma and ~520 Ma events:

- The entirely of the SGT has experienced a number of Neoproterozoic events. Granites were emplaced as isolated batholiths and veins and charnockitization overlaps with the emplacement of these granitic bodies in the southern part of this terrain, as is evidenced by the ubiquitous patchy charnockitization of these granites and, in turn, the bleaching of these charnockites by younger granitic veins.

- A ~600 Ma age is recorded in four localities separated by 100s of kms. These localities

are, Namakkal (zircon age; Corridor-I), Bhavani (monazite age; Corridor-II), Mettupalayam (zircon age; Corridor-III) falling within the Cauvery-Bhavani (CB) and the Bhavani Shear Zones and in the Palghat area (zircon age; Corridor-IV) within the Palghat-Cauvery Shear Zone. Such widespread ages at around ~600 Ma suggests regional tectonothermal event of this period along these major shear zones.

- A ~570 Ma age is obtained for syntectonic granitic veins from the Kottamangalam area (Chapters 3 & 4; sample S-415) within the KKPT Shear Zone and for zircon rims age in the charnockites of the Nagercoil Block (sample S-361). Zircons from the Oddhanchatram anorthosite massif have been dated at 563 ± 9 Ma, which is interpreted as its age of intrusion subparallel to the KKPT Shear Zone. This massif is sheared along its margins. The ~570 Ma event may thus mark a period of major shear deformation in the area.

- Zircon ages of ~548 Ma were obtained from the patchily charnockitized Kalipara Granite from the Nirettipara quarry near Pattanamitta (Fig. 3.61) which are, in turn, retrogressed by an undeformed 526 ± 2 Ma granite vein. These ages thus constrain the age of charnockitization in the Kerala Khondalite Belt to have occurred between 548 Ma and 526 Ma. 523 Ma ages have also been determined for zircon from a syntectonic granite in the Palghat area (Corridor-IV) and pegmatitic granite veins in the Nirettipara area (PPP Corridor), and in monazite from charnockites of the Cardamom Hills north of Achankovil Lineament. These zircon ages together with the monazite age of ~525 Ma possibly signify a period of uplift and cooling, signifying the end of Neoproterozoic-Early Phanerozoic thermal activity in the area. These ages are similar to those found in East Africa and Madagascar, and will be discussed further in Chapter 5.

Chapter 5: Summary and conclusion

5.1. Introduction

The Southern Indian Granulite Terrain (SGT) is one of the largest and oldest granulite provinces on Earth. Together with its extensions in Antarctica, Sri Lanka and Madagascar in a pre-breakup Gondwana reconstruction, this granulite terrain forms an area of >700 000 km^2 of exposed deep continental crust. The vast expanse of granulite facies supracrustals in the SGT were once deposited/ emplaced at the surface of the Earth. This type of terrain is, therefore, of great interest to scientists studying the make-up and evolution of the middle crust of continents. Not surprisingly, then, the Southern Indian Shield (SIS) has been investigated by scores of Earth scientists for last two centuries. In these quests, understanding the transition between the high-grade terrain of the SGT and the low-grade terrain of the Dharwar craton to the north is of prime importance for several reasons. The Dharwar craton preserves a long Archaean history, part of which may also be inherited by the SGT. But the major questions as to how much of old Archaean craton might be preserved within parts of the SGT had not yet been satisfactorily answered. For nearly a century and a half, during which geological investigations were dominated by field investigations, this relationship was viewed mainly as one in which a mobile belt (the SGT) surrounds a stable craton (the Dharwar craton). In recent years, with inputs of modern techniques such as geophysics and high-precision isotopic works, there has been renewed interest in the SIS from Earth scientists from India and abroad. Principal contributions in recent years have been: (i) the identification of the processes of charnockitization whereby amphibolite facies rocks transform to granulite facies rocks through a combination of parameters such as pressure, temperature and in particular, fluid activity; (ii) the identification of major trans-continental shear zones in the SGT through study of satellite imagery; and (iii) the realisation that at least one of these shear zones marks a terrane boundary within the SGT.

The present study has generated more than 35 new high-precision U-Pb geochronological data

controlled within the framework of detailed filed observations in a number of critical areas within the SGT. These new data necessitate a re-evaluation of the tectonic framework of the SGT and in this Chapter a new model for the tectonic evolution of the SGT is explored. Since the SGT occupies a central part in the pre-fragmentation Eastern Gondwana, this new model has important bearing on the reconstruction of Gondwana. In view of the availability of recent data on the structure and geochronology of a similar high-grade terrain of Madagascar (de Wit et al. 1998; Tucker et al. 1998; Ashwal et al. 1998), time has also come for a re-evaluation of the correlation of geological structures and events, between India and Madagascar and to have these to evaluate the pre-fragmentation configurations of East Gondwana. This aspect will be dealt with in the later parts of this Chapter. First, I will summarize the regional tectonic framework of the SGT, using both the existing data and my own new observations and analyses.

5.2. Tectonic framework of the SGT

Major issues concerning the tectonic framework of the SGT are (i) the tectonic status of regional shear zones and folds in the SGT (ii) the relationship between the SGT and the Dharwar craton and (iii) the continuity of the Eastern Ghats into the SGT.

5.2.1. Major shears and folds in the SGT

The Southern Granulite Terrain (SGT) is a polymetamorphosed and polydeformed region dominated by granitic gneisses, high-grade metasedimentary rocks and charnockites. Contacts between protolith rocks and charnockites are transgressive and hence metasomatic in origin. Recrystallisation in charnockites has in many instances obliterated an early deformation fabric present in the protolith rocks. In many cases, metasomatic "fronts" can be seen to cross-cut the structural fabrics of the rocks and shear zones (Chapter 2). Within the charnockites, the early structural geometry may only be deciphered by "ghost" gneissic layering and/or by the

Quartzite

Calc-silic
gneiss

Mafic gr

Meta-ultı

Strike of
fabric

Shear Zo
(previous

Redefine
of shear

Regional

KKPT Sl

F_1 and F_2

F_3 fold a

F_4fold ax

alignment of lithologic remnants of quartzite, mafic granulite and calc-silicate layers. Trends of these various elements must be used to unravel the tectonic fabric of the SGT. Field studies reveal that the quartzite, calc-silicate and mafic granulites in different parts of the SGT are older than the granitic gneisses and have retained evidence of major deformation phases throughout area (Chapter 3 & 4). Structural trend lines defined by these lithological remnants records the geometry of all major regional folds and shear zones (Fig.5.1).

5.2.1.1. Major shear zones

Major shear zones identified by previous workers (Drury et al. 1984; GSI, 1994) are: (i) the Moyar-Attur Shear Zone (MAS); (ii) the Bhavani Shear Zone (BSZ); (iii) the Palghat-Cauvery Shear Zone (PCSZ) and (iv) the Achankovil Shear Zone (ASZ). These shear zones were interpreted to have significant strike-slip movement. In the present study, using compilation of existing maps and new fieldwork in critical areas across these shear zones in a number of corridors (Chapter 3 & 4), the existence of the first three of the above mentioned shear zones were confirmed. However, their location, geometry, orientation and movement direction have been redefined (Fig. 5.1). The Achankovil Shear Zone is a slide (flattend fold limb) rather than a simple shear zone. Two new shear zones have also been identified during the present study: (i) the Cauvery-Bhavani Shear Zone (CBSZ) and (ii) the Karur-Kambam-Painavu-Trichur Shear Zone (KKPTSZ), as discussed in Chapter 3.

(i) The Moyar-Attur Shear (MAS)

This shear zone has a E-W trend and can be traced from east of Attur in the eastern part to just south of Gundlupet in the west. This zone passes through Bhavani, Salem and Bhavanisagar (Fig. 5.1). In the west, this shear zone follows the course of the Moyar river and to the west of Gundlupet it is no longer discernable and have probably does not exist. The shear zone is ~5 km wide and within the shear zone, the NE-SW to NNE-SSW trending

lithologic units of the Dharwar craton have been transposed to an E-W orientation (Figs. 3.2, 3.34 and 3.39). Near Bhavanisagar, the Bhavani Shear Zone joins the MAS and further east, west of Bhavani, the Cauvery-Bhavani Shear Zone joins the MAS. Parts of this shear system have been studied in three areas: Salem, Bhavani and Bhavanisagar (Figs. 3.2, 3.36 and 3.39). No field evidence was found for dextral strike-slip movement along the MAS. In the Salem and the Bhavani area, field evidence reveals dominantly ductile flattening deformation with subvertical stretching lineations within the earliest planar fabrics. In the Bhavanisagar area, this early shear fabric is superimposed by late brittle to brittle-ductile shears with subvertical movement indicators.

(ii) The Bhavani Shear Zone (BSZ)

This shear zone is NE-SW trending. It extends from Bhavanisagar in the northeast to Attapadi in the southwest through Mettupalyam. Further south, it swings to NW-SE and continues beyond Kedavur sub-parallel to the west coast of India (Fig. 5.1). The trend of this shear zone is subparallel to the trend of the lithologic units on either sides of the shear zone. Brittle to brittle-ductile shear has been superposed on early highly flattened rocks. Kinematic indicators suggest that this late shearing was accompanied by subvertical movements.

(iii) The Cauvery-Bhavani Shear (CBS)

This is a newly defined NW-SE trending shear zone and is very conspicuous on the structural trend map (Fig. 5.1). It is ~15 km wide and extends from north of Tiruchirapally in the east, following the trend of the Cauvery River through north to just north of Karur and Erode. From there it continues along the course of the Bhavani River in the west; and merges with the MAS and the BSZ near Bhavanisagar. Parts of this shear zone have been studied in the Namakkal area where three distinct shearing events were identified: NE-SW trending D_1 dextral shears superposed by NW-SE trending D_2 sinistral shears and in turn by an E-W trending dextral shear (D_3) (Chapter 3). The pattern of regional variation in the trend lines of

the lithologic units across this shear zone reveals a dextral strike-slip movement along this shear (Fig. 5.1). This dextral shearing could be related to the dextral shears (D_3) identified in the Namakkal area.

(iv) The Palghat-Cauvery Shear Zone (PCSZ)

This shear zone was earlier interpreted as an E-W trending shear zone passing through Palghat in the west to the north of Karur in the east. However, the regional strike pattern suggests it is an arcuate shear zone, extending from Mallapuram in the west through Palghat and south of Chennimalai to north of Karur (Fig. 5.1). Part of this shear zone was studied in the area north of Palghat (Corridor-IV; Chapter 3). In the western extremity, this shear zone merges with the BSZ and in the eastern extremity it merges with the CBS. The PCSZ forms the southern boundary of a regional shear band whose northern boundary is defined by the CBS and BSZ. Trends of lithologic units adjacent to this shear band suggest a regional dextral sense of movement.

(v) The Karur-Kambam-Painavu-Trichur KKPT Shear Zone (KKPTSZ)

This is a newly recognized shear zone identified on the basis of presence of striking contrasts in structural style and lithological assemblage across it (Fig. 5.1). It is an arcuate shear zone extending from south of Karur in the east, with a NE-SW trend, to just south of Kodaikanal and from there just to the west of Kambam, where it bends towards the NW. From there, it can be traced to the west coast of India, just south of Trichur. The bend of this shear zone near Kambam appears to be in continuity with a regional fold axial trace that can be traced from the Dharwar craton in the north to the Tiruneveli area in the south across the KKPT Shear Zone (Fig. 5.1). Thus, the arcuate nature of the KKPT Shear Zone could be related to a late regional re-folding of the KKPTSZ. The structural and lithologic discontinuity across the KKPT Shear Zone is very pronounced in its eastern section. Here, the structural trend lines

adjacent to the northern part of this shear zone trend NE-SW, subparallel to the shear zone but south of the shear zone the trend lines define a complex structural pattern, resembling disharmonic folding, which has resulted from the superposition of more than one phase of folding. Axial traces of folds were interpreted on the basis of map patterns (GSI, 1995a,b). Early axial traces (interpreted as F_1 and F_2) in the southeastern part of the KKPT Shear Zone are transposed along the KKPT, while axial traces of late folds (F_3) abut against the KKPT Shear Zone and are not traceable north of it (Fig. 5.2). In the northwestern part, structural discontinuity across the KKPT Shear Zone is not distinct. There, the shear zone can be traced following the trend lines of the lithologic units parallel to the shear zone. A part of this shear zone in the northwestern part was studied in field (east of Kotamangalam) where granitic rocks are mylonitized and minor structures confirm the presence of a NW-SE trending shear zone (Chapter-3). The lithologies north and south of the KKPTSZ are also quite distinct. South of the KKPTSZ, the terrain is dominated by khondalite, paragneisses with abundant quartzite and calc-silicate bands, while to the north of the KKPTSZ, the terrain is dominated by granitic and tonalitic gneisses with mafic granulite, BIF and associated metasediments (Fig. 1.3). The khondalitic metasediments south of the KKPT Shear Zone have ~2.5 Ga and ~2.0 Ga old detrital zircons and so are Paleoproterozoic or younger. In contrast, the BIF and associated metasediments to the north are older than ~2.9 Ga (Chapter 4). The lithologic ensemble north of the shear zone is akin to the high-grade equivalents of the Dharwar craton, but the rocks in the south are more akin to those of the Eastern Ghats (Chapter 1). These structural and lithological differences across the KKPT Shear Zone suggest that it may represents a major terrane boundary. Large sections of the KKPTSZ are superposed by charnockite (Figs. 1.3, 5.1). Thus, the KKPTSZ pre-dates charnockitization (which is dated in the Kerala Khondalite Belt to have occurred between 526 Ma and 548 Ma, Chapter 4). Since charnockitization destroys the planar penetrative fabric of the rocks, it is unlikely that the original mylonites are preserved along large tract of this shear zone. A part of this shear zone was studied in detail in the area east of Kotamangalam (Fig. 5.1), where charnockitization is only patchily developed across the KKPTSZ. Here, granitic gneisses are highly deformed and

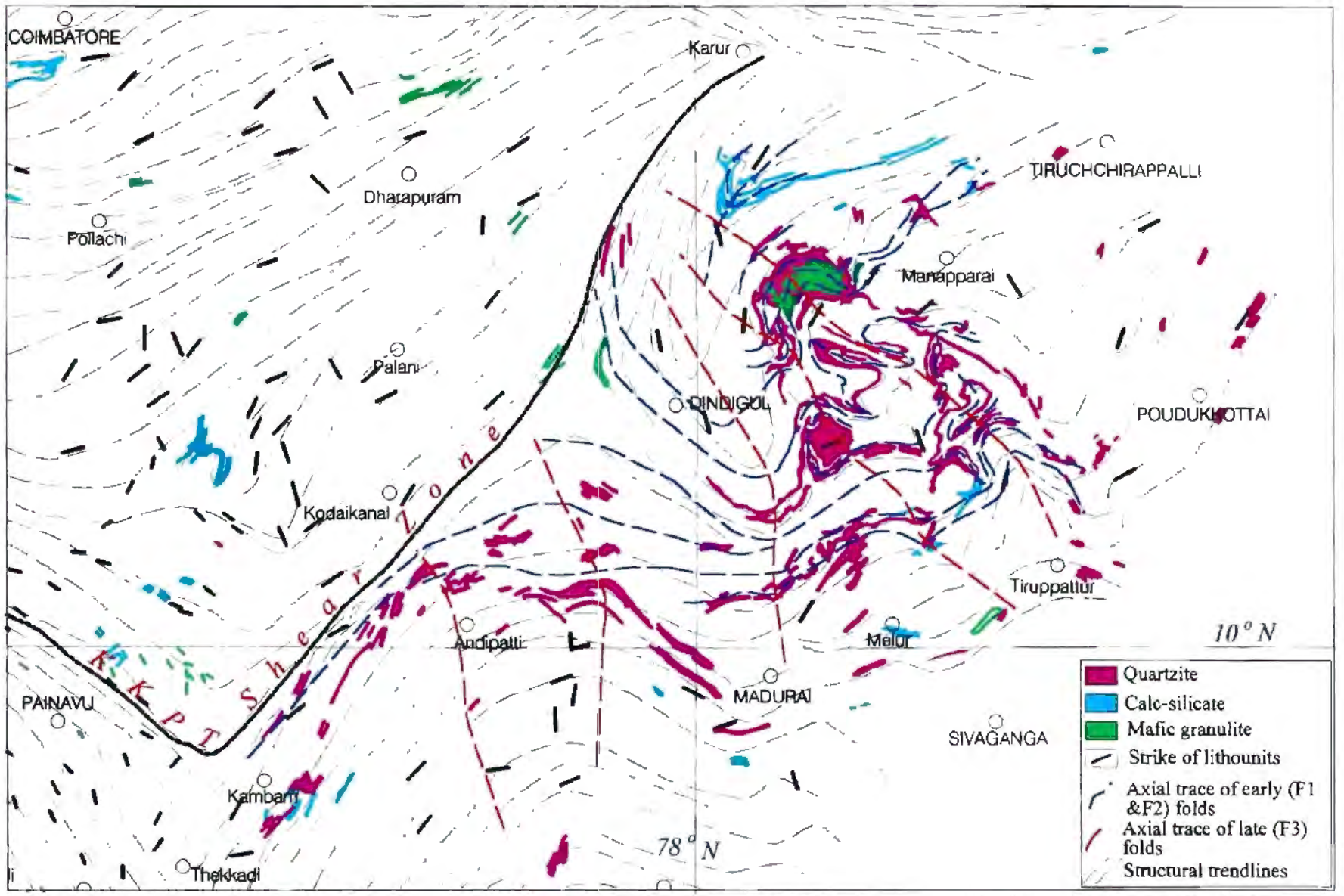

Fig. 5.2. Distribution of the quartzite, calc-silicate and mafic granulite layers around the Dindigul area, Corridor-I (modified from GSI, 1995). Also shown the interpretation of structural trendlines and fold interference patterns. Note the discordance of structural fabric across the KKPTSZ. Axial axial traces are drawn on the basis of map pattern (after GSI, 1995) without any field varification in the present work.

are mylonitized and display more than one phase of shearing (Fig. 3.55, 3.56). A granite vein, syntectonic with the latest phase of shearing, was dated as 568 ± 2 Ma in the present study using the U-Pb zircon technique (Chapter-4). A large NE-SW trending anorthosite massif (> ~35 km^2) was emplaced along this shear zone near Oddanchatram which has been dated as ~563 ± 9 Ma by SHRIMP U-Pb zircon technique (Chapter-4). The marginal part of this body is deformed, the inner parts are unmetamorphosed and undeformed. Thus, shearing along the KKPTSZ continued even after emplacement of this body at ~563 ± 9 Ma.

(vi) **West Coast Shear Zone (WCSZ)**

The orientation of the structural fabric of lithologic units of the western part of the SGT changes from E-W to NNW-SSE sub-parallel to the west coast of India. This realignment of the structural fabrics, including shear zones, suggest the presence of an off-shore dextral shear zone sub-parallel to the west coast (Fig. 5.1).

5.2.1.2. Ages and displacements of shear zones

There is little reliable direct age data from the major shear zones discussed above. Moreover, it is likely, as has been observed in the case of the CBSZ, that these shear zones were reactivated more than once, with variable senses of movements. These uncertainties are a major hindrance in reconstruction of the history of the shear zones. Some new ages obtained during this investigation, however, provide some first order constraints.

The BSZ and the western part of the MASZ bound the Nilgiri Hills Charnockite Massif in its southeastern and northern parts, respectively. Paleo-pressure estimates of the charnockites of the Nilgiri Hill Massif are ~10 kbar in its central part, and ~7-8 kbar at its peripheries (Raith et al.1990; Srikantappa, 1993). Further out, across the bounding shears of the massif, the paleo-pressures of the surrounding gneisses vary between 6 kbar and 5.5 kbar (Janardharn, 1982;

Srikantappa et al. 1992). Paleo-isobars of the Nilgiri Hills Massif are sharply truncated along the Bhavani Shear Zone suggesting relative uplift of the Nilgiri massif along these shears (Raith et al. 1990; Srikantappa, 1996). A U-Pb zircon age of a post-shearing granite from the Bhavani Shear Zone indicates a minimum age for brittle-ductile deformation at ~600 Ma (Chapter 4). In the Bhavani area of MASZ, U-Pb dating of monazite from the quartzite gives an age of ~600 Ma (Chapter 4). This indicates that latest thermal peak along both MASZ and BSZ was around 600 Ma. Rb-Sr biotite ages from western part of the MASZ in the Moyar area and from BSZ suggests that these shear zones were thermally active between 624 ± 37 Ma and 472 ± 12 Ma (Deters-Umlauf et al. 1997). It can be concluded, therefore, that the upliftment of the Nilgiri Hills Massif possibly occurred between circa 600 Ma and 500 Ma along both the BSZ and MASZ.

The brittle-ductile deformation along the BSZ and the western part of MASZ were superposed on an earlier ductile shearing fabric whose age is not known.

Structural studies in the CBSZ zone indicate that early sinistral D_2 shear is superimposed by later dextral D_3 shear (Chapter 3). Zircons from a mafic granulite along the northeastern margin of this shear zone, in the area south of Namakkal, gave a concordant age of 722 ± 13 Ma (Chapter 4). This mafic granulite has been intruded by ~2.5 Ga granitic gneiss. Thus the ~722 Ma age must represent a period of thermal activity or metamorphism. Within the D_2 shear zones, the mafic granulite has developed a schistose fabric and the rock has been mylonitized and transformed to amphibolite. Thus, the D_2 shear is likely to be younger than ~722 Ma. D_2 shears are cut by late granitic dykes (Fig. 3.26; 3.28) which are syn-tectonic with D_3 shears. These late granitic rocks have an age of 603 ± 14 Ma. Thus, the D_2 shears can be bracketed between ~722 Ma and ~ 603 Ma and the age of the D_3 shears is ~603 ± 14 Ma. Syntectonic granite from the Palghat area (Fig. 3.49) of the PCSZ is 600 ± 4 Ma old. These granites also have younger hydrothermal zircons of 520 ± 1 Ma old (Chapter 4). Thus, although it is likely that each of these shear zones had more than one period of shearing and

reactivation, the MSZ, the BSZ, the CBSZ and the PCSZ have either syntectonic granite emplacement or record a thermal high between ~600 Ma and 610 Ma. Thus, all these shear zones are likely to be part of a single shear system

The KKPTSZ in the Kotamangalam area has suffered more than one phase of shearing and granitic activity (Fig. 3.57). A late syntectonic granite (Fig. 3.55-3.57) within the KKPTSZ was dated at 568 ± 2 Ma. An anorthosite massif emplaced sub-parallel with the KKPTSZ but deformed within it has been dated at 563 ± 9 Ma (Chapter 4). Thus, it can be concluded that the late shearing in the KKPTSZ occurred between ~ 560 Ma and ~ 570 Ma old.

It is of interest to note that the hypothetical West Coast Shear Zone (WCSZ), off the western coast of India, has affected both Palghat-Cauvery and the KKPT shear zones. This shear zone is thus younger than both Palghat-Cauvery and KKPT shear zones.

The CBSZ, BSZ, and PCSZ together form a regional shear lens with an overall dextral sense of movement (Fig. 5.1). The amount of displacement along this shear system is not known because of the absence of obvious strain markers and lithologic tracers. A rough estimate of shear displacement however, can be made by assuming that the BIF layers of the Chennimalai Hill area were continuous with the southernmost BIF layers in the Kollimalai Hill south of Namakkal. These BIF layers are the southernmost mappable BIF bands on either side of the CBSZ. On the basis of this assumption, a maximum horizontal displacement of ~25 km is evident along the CBSZ.

Because major regional folds can be traced from the southwestern part of the Dharwar craton across the western part of MASZ, BSZ and the PCSZ (Fig. 5.1), none of these regional shears can have significant strike-slip movement post-dating this folding. These shear zones, north of the KKPTSZ are, therefore, intra-shield zones and do not represent major boundaries between allochthonous blocks (i.e., terrane boundaries).

The sense and amount of shear along the KKPT shear are not known. Folds and structural trend lines southeast of KKPT bend both clockwise and anticlockwise in the KKPT Shear Zone. Such variable style of bending of trend lines could not be used for shear sense determination on a regional scale.

5.2.1.3. Major folds in SGT

5.2.1.3.1 Folds north of KKPT shear zone

Marcara-Sargur-Gudalur Fold (MSGF)

In the northwestern part of the area (Fig. 5.1), the distribution of the metasedimentary and metavolcanic enclaves define a major mappable (λ>150 km) open-tight fold with a NNW trending axial trace. This fold closes towards south. The eastern limb of this fold can be traced from SE of Hassan through Mysore, Sargur and Gundlupet and then across the Moyar-Attur lineament to Gudalur and further south still. The western limb of the fold can be traced from Puttur in the northwest through Mercara, Iritti and Mattanur to Vaihathri across the Moyar lineament. The axial trace of this fold can be traced from east of Mercara in the north through west of Sargur then across the Moyar lineament to west of Gulalur (I refer to this as the MSG fold). This fold can be traced across a number of major shear zones identified in the present study, for example, the BSZ, the PCSZ and the KKPTSZ. All these shear zones are folded by the MSG fold. The bend in the KKPT Shear Zone near Kambam may also be related to this folding. If this is so then the MSG fold is younger than this shear zone i.e., younger than ~570 Ma and thus younger than the D_3 deformation present in the area.

The area to the east of the Chitradurga Boundary Shear Zone (CBSZ) has a near uniform NNE-SSW trend continuous with the eastern-limb of the MSG fold. These trend can be traced continuously across the Moyar-Attur Shear Zone where it takes on a NW-SE trend.

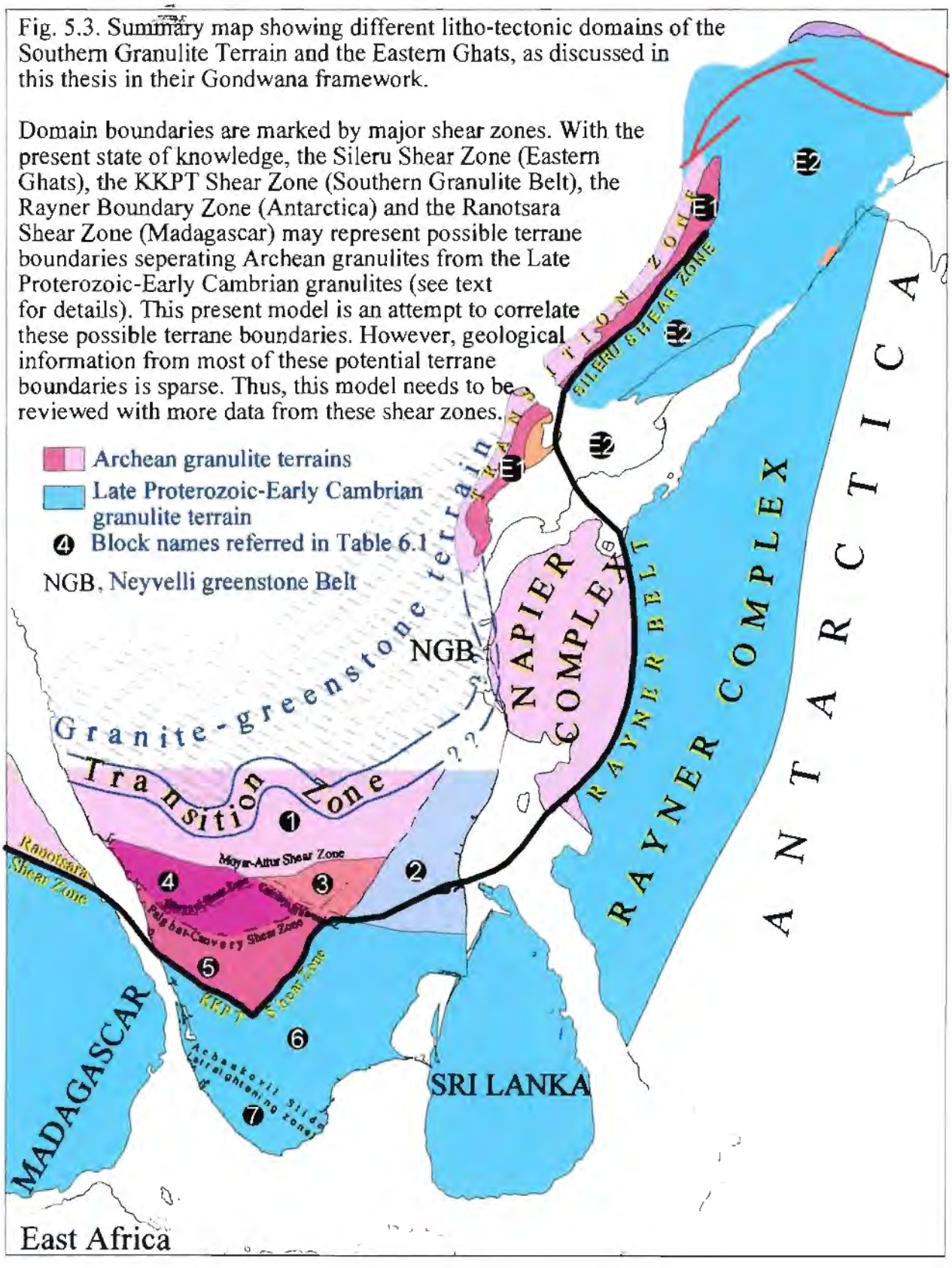

Fig. 5.3. Summary map showing different litho-tectonic domains of the Southern Granulite Terrain and the Eastern Ghats, as discussed in this thesis in their Gondwana framework.

Domain boundaries are marked by major shear zones. With the present state of knowledge, the Sileru Shear Zone (Eastern Ghats), the KKPT Shear Zone (Southern Granulite Belt), the Rayner Boundary Zone (Antarctica) and the Ranotsara Shear Zone (Madagascar) may represent possible terrane boundaries seperating Archean granulites from the Late Proterozoic-Early Cambrian granulites (see text for details). This present model is an attempt to correlate these possible terrane boundaries. However, geological information from most of these potential terrane boundaries is sparse. Thus, this model needs to be reviewed with more data from these shear zones.

5.2.1.3.2. Folds south of KKPT Shear Zone

South of the KKPT shear, the geometry of a number of fold structures is complex. Quartzite and the calc-gneiss bands around Dindigul display a number of hook-shaped refolded folds (Fig., 5.2; these represent type-II interference pattern of Ramsay, 1967). Axial traces of the early folds (F_1), which possibly include more than one generation of folds, are folded by later NW-SE trending folds (F_2). Extrapolation of the axial traces of both F_1 and F_2 from the Dindigul area to the west shows that both axial traces abut against the KKPTSZ and cannot be traced to the north of it.

Regional folds in the Tiruneveli area (Fig. 5.1) are well defined by various meta-sedimentary litho-units like calc-silicates, quartzite and khondalites. Axial traces of these major folds have trends varying from NW-SE to NNW-SSE. Two major fold closures are present in the area. First, around Tiruneveli, has a southwesterly closure. The other, to the east of Tiruneveli, has a NNW closure.

5.2.2. Relationship between the Dharwar craton and the SGT

For the purpose of discussion of the tectonic framework, the SGT can be subdivided into a number of domains bounded by a number of regional shear zones. These domains are numbered 1-7 and are marked on Fig. 5.3. A summary of characteristic lithology, structure and geochronology with each these different domains is given in Table 5.1. Differences in the lithological assemblages, structure and geochronology amongst different domains of the SGT suggest that, areas north of the KKPT Shear Zone (domains 1-5, as numbered in Fig. 5.3) have a similar geological history This is consistent with the observation that major shear zones and lineaments which define boundaries of these domains, do not have significant strike-slip movement. It is important to note that there is a general, gradual increase in the metamorphic grade of rocks in area from north to south. Thus, supracrustal rocks,

metasediments and greenstones present in the northern part of domain 1 are also present in the south but are at higher metamorphic grade. On the other hand, areas south of the KKPT Shear Zone, i.e., domains 6 and 7, have similar lithologies, structural patterns and geochronology which are distinct from those in domains 1-5. The KKPT Shear Zone is thus likely to mark a terrane boundary in the SGT, to the north part of which is the highly reconstituted and remobilized continuation of the Dharwar craton; to the south the paragneiss-dominated terrain could be the southern extension of the Eastern Ghats (Fig. 5.3).

The geology of the Domain 2 is not well constrained. Continuation with the Eastern Ghats (Ramakrishnan, 1993) and the Dharwar craton (Gopalakrishnan, 1995) have both been previously suggested. Considering that Cauvery-Bhavani Shear Zone has only a net dextral strike-slip movement of less than 25 km, it is likely that domain 5 continues into Domain 2. However, the eastern half of Domain 2 is largely covered by recent sediments. So it need not necessarily be continuous with the exposed high-grade terrain in the Domain 2. Future geophysical and geological studies in this domain may resolve this further

Table 5.1. Summary table showing lithology, structure and geochronology in different domains of the SGT (Domain numbers are shown in Fig. 5.3)

✓✓, common

✓, present

		Domain numbers →	Area north of the KKPT Shear Zone					Area south of the KKPT Shear Zone		Eastern Ghats	
			1	2	3	4	5	6	7	E1	E2
Lithology	Granitic orthogneiss (TTG and granite)		✓✓	✓✓	✓✓	✓✓	✓✓				
	Greenstone belt fragments		✓✓								
	BIF and associated metasediments (Archaean)		✓	✓	✓	✓	✓			✓	
	Charnockite, mafic granulite		✓	✓	✓	✓	✓	✓✓	✓	✓	✓
	Paragneiss (mainly khondalite and quartzite; Proterozoic)					✓		✓✓	✓✓	✓	✓✓
	Calc-silicates					✓	✓	✓✓	✓✓		✓
Structure			These domains are structurally coherent in which the dominantly NNW-SSE to NNE-SSW trending litho-units continue across domain boundaries.					These two domains are structurally coherent and have complex fold interference pattern. The NNW-SSE trending D3 folds do not continue into domains 1-5			
Geochronology	Ages of Granitic rocks	> 3.0 Ga	✓								
		~ 2.9 Ga	✓		✓	✓					
		~ 2.5 Ga	✓		✓	✓	✓				
		2.1-2.0 Ga							✓		
		1.6-1.7 Ga				✓			✓	✓	
		1.0 Ga							✓		✓
		800 Ma	✓					✓			✓
		600 Ma	✓		✓	✓					✓
		570-550Ma					✓	✓	✓		✓
		525 Ma					✓		✓		
	Age of charnockitization	~2.5 Ga	✓		✓						
		550--525 Ma			✓	✓	✓	✓	✓		✓
	Cooling age (Rb-Sr Biotite-WR age)	~2.0 Ga	✓								
		~480 Ma							✓		

5.2.3. Relationship between the Eastern Ghats and the SGT

Continuity between Eastern Ghats and the SGT has been suggested by some early workers on the basis of similarity of the lithological assemblages (Narayanaswamy and Laxmi, 1967) and structures (Sinha Roy, 1985). Continuity of the Bouguer gravity anomalies (>40 mgal) from the Eastern Ghats to the southern tip of SGT has also been recorded (Subrahmaniam, 1986). New age data from the SGT obtained in this study has brought out additional and more striking similarity with the Eastern Ghats (Table 5.4).

Table 5. 2. Comparison of age information from the Eastern Ghats and new age data from the Southern Granulite Terrain

Ages of magmatism/ high-grade metamorphism	**Eastern Ghats**	**SGT**	
		N. of KKPT	**S. of KKPT**
~2900 Ma	✔	✔	
~2500 Ma	✔	✔	
~1600 Ma	✔	✔	
~1000 Ma	✔		✔
~800 Ma	✔		✔
~550 Ma	✔		✔
~525 Ma			✔

The Eastern Ghats can be subdivided into two parts along the Sileru Shear Zone (Fig. 1.6), the western part (E1 in Table 5.1) contains charnockite with abundant BIF enclaves; and the eastern part (E2 in Table 5.1) is khondalite dominated. Lithological assemblages and geochronology of the E2 domain are similar to those of the domains 6 and 7 in the SGT Geochronological information from E1 is meagre. A ~1.6 Ga U-Pb zircon age (Mezger et al. 1996) and its lithological make-up suggest that this domain could be similar to the Domain 5 in the SGT. I, therefore, suggest that the KKPT Shear Zone may be continuous with East Ghats-Dharwar boundary.

5.2.4. Summary of new changes in the tectonic framework of SIS

Field and geochronological studies along several corridors in the SGT, and compilation of existing geological, geochronological and geophysical information on the SGT reveal that the Dharwar craton continues to the south into the SGT as far as the KKPT Shear Zone. The KKPT Shear Zone may mark a prominent structural discontinuity within the SGT. Continuity of the Dharwar craton south of the KKPT Shear Zone is not certain. The lithological assemblage south of the KKPT Shear Zone is more akin to the lithological assemblage of the Eastern Ghats. It is thus possible that the KKPT Shear Zone marks the boundary between the Dharwar craton and the continuation of the Eastern Ghats south in the SGT. It is not clear at present if this southernmost part of the SGT and the Eastern Ghats contain tectonic blocks of variable geologic histories. This will have to be resolved in the future.

5.3. India as a fragment in Gondwana

5.3.1. Introduction

The Southern Indian Shield occupies a central position in any Gondwana reconstruction (Lawver and Scotesse, 1987; de Wit et al. 1988; Powell et al. 1988). New data, both field and geochronological measurements, generated in this study necessitate a re-evaluation of the details of these existing reconstructions. There are two aspects of Gondwana reconstructions in which present work has an important bearing. One is the reconstruction of India with respect to Antarctica and Sri Lanka. The other is the correlation of India with Madagascar. The very striking unifying factor in the correlation of these dispersed Gondwana fragments (India, Antarctica, Sri Lanka and Madagascar) is that they all have been affected by high-grade metamorphism and charnockitization and/or granitic activity between ~650 Ma and ~525 Ma (Shiraishi et al. 1994 and references therein for Antarctica; Hölzl et al. 1994 and references

therein for Sri Lanka; Shaw et al 1997 and references therein and present study for the Eastern Ghats and SGT in India respectively; Tucker et al. 1998 and de Wit et al. 1998 for Madagascar). This, together with the lithological similarity amongst these fragments, geophysical data (Reeves, 1998; Sahu and Reeves, 1998) from these fragments and from the ocean floors separating them (Reeves and de Wit, 1998) have made it possible to achieve a broad consensus regarding relative positions of these dispersed fragments in a Gondwana reconstruction (Lawver and Scotese, 1987; de Wit et al. 1988; Yoshida et al. 1992; Shiraishi et al. 1994). Although a general fit is agreed upon, not all of these previous attempts were able to achieve reconstructions to a resolution better than a few hundred kilometres. Also, in detail, there are many of inconsistancies in these models. The main reasons for such discrepancy are the lack of high-quality geochronological data and field data that could serve as possible piercing points at the continental boundaries. Obtaining high-quality field and geochronological data for such a large area as Gondwana, is both time consuming and expensive. In these circumstances, the importance of using sub-vertical Precambrian lineaments/shear zones for a tighter reconstruction has been pointed out and used by some workers (Katz and Premoli, 1979, de Wit et al. 1995; Windley and Razakamanana, 1996; Kriegsman, 1995). This thesis is essentially directed at understanding the nature, kinematics and ages of various shear zones in the SGT. Data generated in this work can be used in constraining Gondwana reconstructions. In the following section I shall explore how these new data can be used to derive a tighter reconstruction of central Gondwana.

5.3.2. Reconstruction of India-Antarctica and Sri Lanka

Broad positioning of Antarctica and Sri Lanka against the eastern coast of India has been suggested by many workers on the basis of both geological and geophysical arguments and (Yoshida et al 1992; Harris et al. 1997 and references therein; Sahu and Reeves, 1998; Reeves, 1998 and references therein). Important for such correlation are (i) the Dharwar, Eastern Ghats and SGT in India (ii) the Rayner and Napier Complexes in the Antarctica and

the (iii) Wanni, Highland and Vijayan Complexes in Sri Lanka. Except for the Dharwar craton in India, all these areas have been affected by high-grade metamorphism and charnockitization. The most important factor guiding the fine-tuning of the reconstruction of these former Gondwana fragments is the status of major shear zones in these fragments, specially the ones which demarcate possible terrane boundaries. In Antarctica, the Napier complex represents an Archaean granulite terrain with protolith ages > 3. 9 Ga (Black et al. 1986). South of it is the Proterozoic granulite terrain, the Rayner complex which records 550-525 Ma old charnockitization and granitic activity (Shiraishi et al. 1994). The Napier and Rayner complexes have very contrasting Nd-model ages (the Napier Complex has Archaean Nd-model ages, while Rayner Complex has Paleoproterozoic to Mesoproterozoic Nd-model ages [Black et al. 1987]). The boundary between these two terrains, here termed as the Rayner Boundary Zone, is sharp but poorly exposed. It may represent a terrane boundary.

The Sileru Shear Zone (SSZ) in the Eastern Ghats may also represent a terrane boundary in that it separates two contrasting lithological associations (Ramakrishnan et al. 1998) similar to the KKPT Shear Zone in the SGT. It is thus possible that the KKPT Shear Zone in the SGT, the Rayner Boundary Zone in Antarctica and the Sileru Shear Zone form part of a single terrane boundary (Fig. 5.3) that separates an Archaean granulite terrane in the north and west dominated by charnockite, orthogneisses with mafic granulites and BIF enclaves, from a Proterozoic granulite terrain in the south and east dominated by khondalite, migmatite and their charnockitized equivalents. A possible correlation of different litho-tectonic blocks in the SGT, Eastern Ghats, Sri Lanka and Antarctica is shown in Table 5.3. The precise connection between the KKPT Shear Zone and the Rayner Boundary Zone across the Cauvery-Bhavani Shear Zone and Domain 2 in Fig. 5.3 is uncertain. Considering that the Cauvery-Bhavani Shear Zone does not have large strike slip component (≤25 kms), it is likely that the KKPT Shear Zone continues to the Rayner Boundary Zone through the Domain 2. Available geological information from Domain 2 is poor as the eastern part of the Domain 2 is covered

by alluvial sediments making it difficult to test a continuation of the KKPT Shear Zone through it.

Table 5.3. Tentative correlation of different litho-tectonic domains in the India, Antarctica and Sri Lanka.

	SGT	Eastern Ghats	Sri Lanka	Antarctica
Granite-Greenstone terrane	Domain 1 in Fig. 5.3	Dharwar craton, west of the Eastern Ghat, Neyvelli Greenstone Belt	absent	??
Transition Zone	Domain 1 in Fig. 5.3	Transition zone northwest of domain E1	absent	??
Archaean Granulite Terrain with ~2.5 Ga granulite metamorphism and protoliths older than ~2.9 Ga	Area north of the KKPTSZ, domains 1-5 in Fig. 5.3	Domain E1, west of the SSZ (Fig. 5.3)	absent	Napier Complex
Possible terrane boundary	The KKPT Shear Zone	The Sileru Shear Zone	??	Reyner Belt
Neoproterozoic granulite terrain dominated by metasediments with recorded high-grade metamorphism and/or granitic intrusion at ~1.0 Ga, ~800 Ma and ~600-520 Ma.	Area south of the KKPTSZ, domains 6 and 7 in Fig. 5.3	Area east of the SSZ, domain E2 in Fig. 5.3	West Vijayan and Highland complexes	Reyner complex

5.3.3. Reconstruction of India and Madagascar

Most reconstructions of Gondwana fragments, since the initial attempt by du Toit (1937) show eastern coast of Madagascar facing against the western coast of India, particularly the western Dharwar block (Katz and Premoli, 1979; Lawver, 1987; de Wit et al. 1988; Scotesse, 1988). Broad physiographic, lithologic, tectonic and geophysical similarities between these two fragments of the Gondwana has been pointed out by many workers (Narayanaswami and Laxmi, 1967, Sinha-Roy, 1987). Studies of the sea-floor gravity, magnetic anomaly and palaeomagnetic data also constrain the position of Madagascar close to the western coast of India (Norton and Sclater, 1979; Torsvik et al. 1998; Reeves, 1998 and references therein). The Ranotsara Lineament in southern Madagascar is a trans-island shear belt with NW-SE trend. This lineament has been interpreted by many as a shear zone (Bangolava-Ranotsara

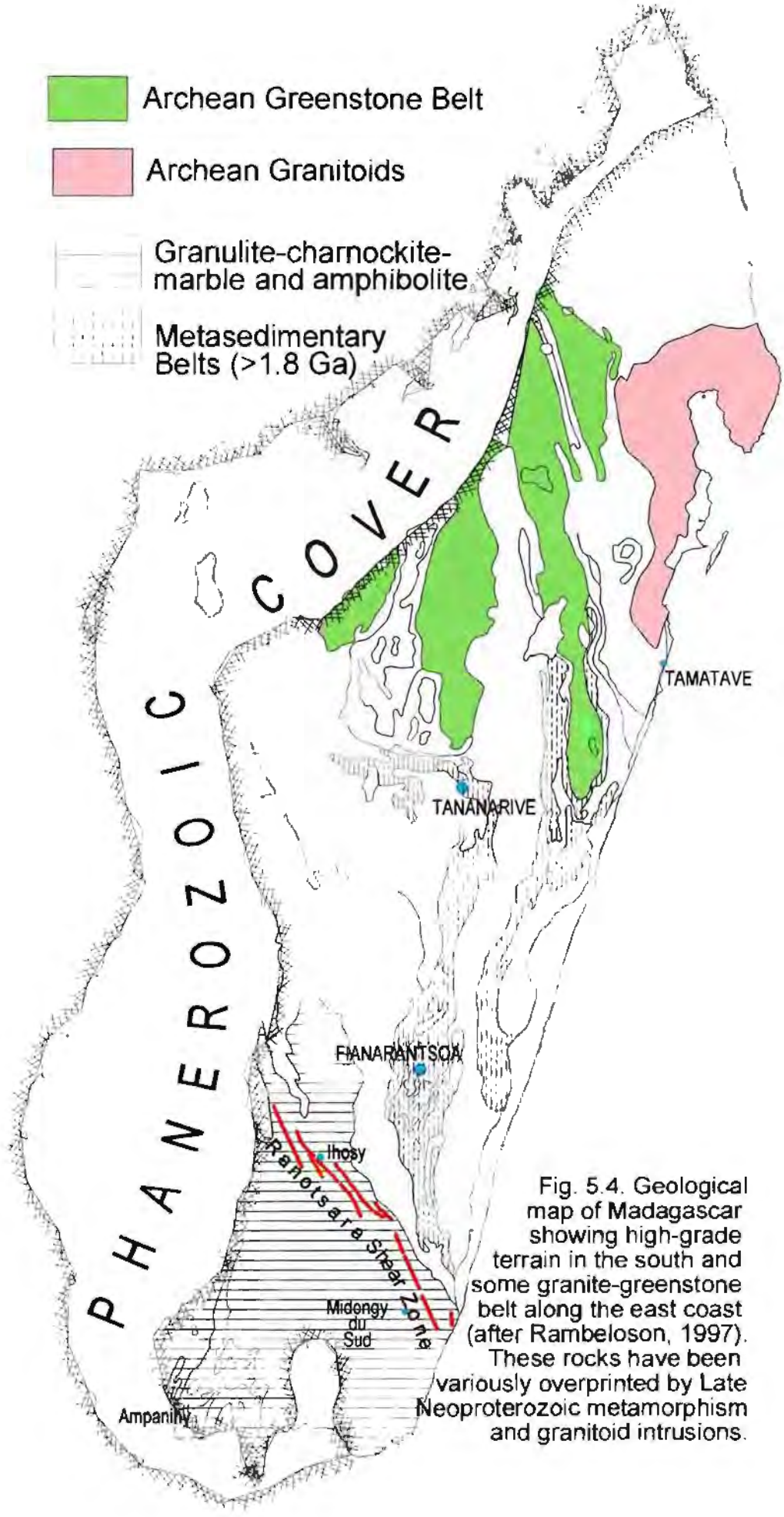

Fig. 5.4. Geological map of Madagascar showing high-grade terrain in the south and some granite-greenstone belt along the east coast (after Rambeloson, 1997). These rocks have been variously overprinted by Late Neoproterozoic metamorphism and granitoid intrusions.

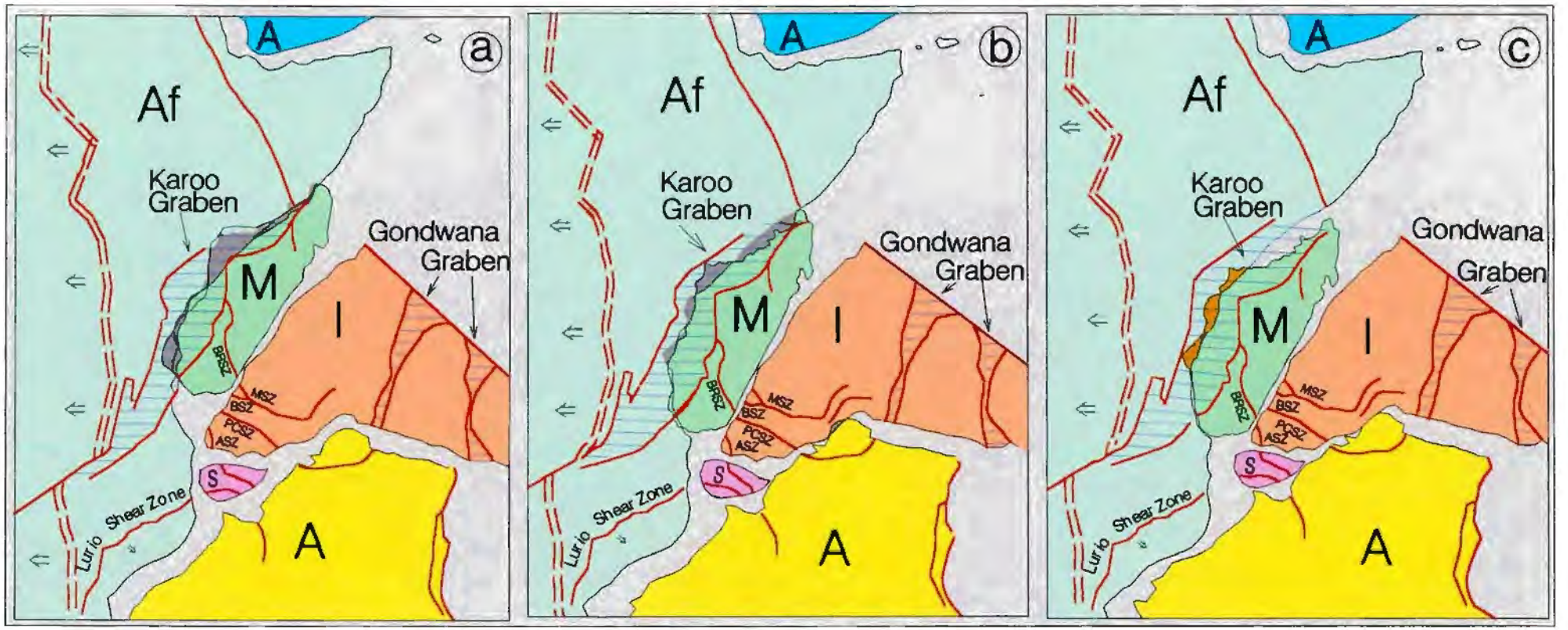

Fig. 5.5.Three examples of possible pre-break-up configurations involving India and Madagascar. BRSZ, Bangalova-Ranotsara Shear Zone; MSZ, Moyar Shear Zone; BSZ, Bhavni Shear Zone, PCSZ, Palghat-Cauvery Shear Zone; ASZ, Achankovil Shear Zone.

Shear Zone) having a sinistral strike-slip movement (Hottin, 1976; Windley et al. 1994; Müller et al. 1997; de Wit et al. 1998). A possible continuation of this lineament in southern India could be one of the three trans-peninsular lineaments, the Moyar-Attur Lineament, the Palghat-Cauvery Lineament, and the Achankovil Lineament (Fig. 5.5). All these lineaments were interpreted as shear zones having large strike-slip movement (Drury et al. 1984). However the basis of interpretation that these lineaments, both in Madagascar and in India, are shear zones with large strike-slip component are mainly satellite imagery-based studies. The problem of using these lineaments/shear zones as a tool for reconstruction without establishing their timing and kinematics have been pointed out by Naha and Srinasan. (1996) who pointed out that orogenic trends interpreted from satellite imageris could be very misleading. In fact, satellite imagery interpretation indicated a sinistral strike-slip movement along the ASZ while internal evidences collected by Sacks et al. (1997) showed a dextral strike-slip movement. This thesis also illustrates the need for re-defining and re-aligning the major shear zones of southern India. New field and geochronologic data presented in this thesis allow a first order approximation of the kinematics of major shear zones in southern India and timing of movement along them. Also, in southern Madagascar, though limited, some new data have been generated on the kinematics and timing of movement along major shear zones.

The western one-third of Madagascar is occupied by Phanerozoic cover rocks while the eastern two-third is occupied by Precambrian rocks (Fig. 5.4). Of these, the southern part is occupied by granulite facies rocks which include charnockite, khondalite, marble, and migmatite.

North of this high-grade rock association is an amphibolite facies association, which includes a number of greenstone belts (Rambeloson, 1997). In addition, the area contains a number of metasedimentary belts and Archaean granitic terrain (Fig. 5.5, Tucker et al. 1998). These Archaean granitic terranes and greenstone belts are important for correlation with the greenstone belts of the Dharwar craton in India. This shear zone is often interpreted as separating Archaean tectonite in the north from the Proterozoic tectonite in the south (de Wit

et al. 1995) . However, the metamorphic grade or lithological boundaries across this shear zone do not show abrupt discontinuity (Nicollet, 1990) and continue across the shear zone (Fig. 5.4), suggesting that the Ranotsara Shear Zone may not have large strike-slip component. The Ranotsara Lineament is best expressed in the south-central part of Madagascar around the town of Ihosy (Fig.5.4). Its continuation in the southeast up to the eastern coast of Madagascar is not certain. Satellite imagery does not show its continuation up to the eastern coast (Müller, personal communication). A field traverse taken in the present study across this lineament around Midongi did not reveal the presence of mylonites along the lineament. Compilation of available structural data from the southeastern part of Madagascar shows that in the southeastern continuation of the Ranotsara Lineament, the strike of the lithologic units changes from NW-SE to N-S i.e., it becomes sub-parallel to the coast. Therefore, it may be that in the southeastern part, the Ranotsara Shear Zone is subparallel with the eastern coast of Madagascar. This change in the strike of the shear zone may be due to the presence of West Coast Shear Zone, off the western coast of India, as proposed in this work.

The Ranotsara Shear Zone in Ihosy has affected ~ 620 Ma old D_2 fabrics related to the Amphanihy Shear Zone in southern Madagascar, and a post-tectonic granite from this shear zone has been dated at ~530 Ma old (personal communication, M. J. de Wit). Thus, movement along the Ranotsara Shear Zone is constrained to have occurred between ~620 Ma and ~530 Ma. It is important to note that movements along major shear zones in the SGT of India also fall within this time limit. However, in this study it has been possible to constrain the timing of movements along the PCSZ (~600 Ma) and the KKPTSZ (560 - 570Ma). Ongoing detailed geochronological work from the Ranotsara Shear Zone by Müller et al. (personal communication) may be able to further constrain the timing of movement along the Ranotsara Shear Zone which may allow identification of either the KKPTSZ or the PCSZ as a continuation of the Ranotsara Shear Zone in India.

Lithologically, the NW-SE trending RSZ of Madagascar broadly separates paragneiss-

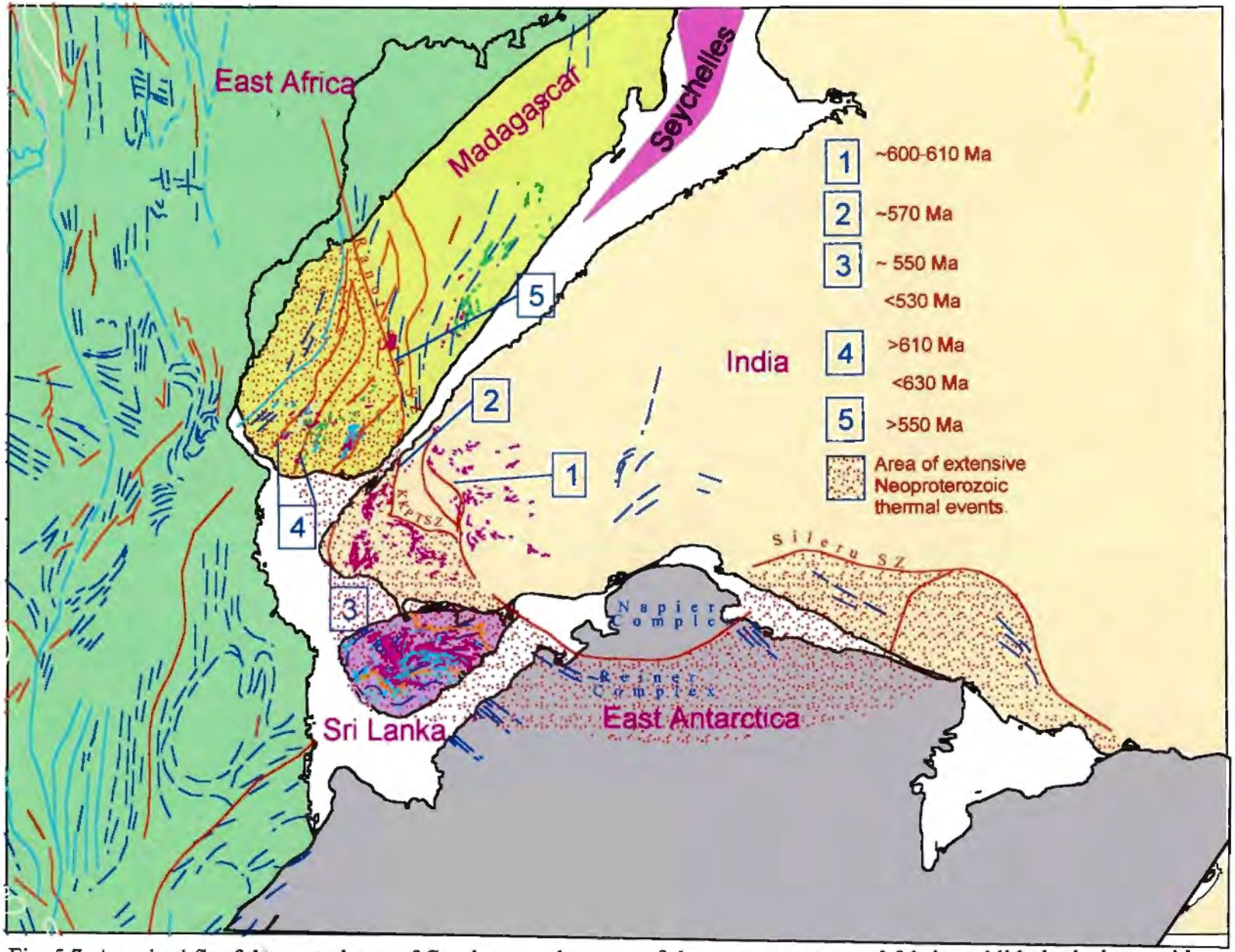

Fig. 5.7. A revised fit of the central part of Gondwana using ages of shear zones, structural fabric and lithological assemblages. Ages of shear zones in Madagascar are from de Wit et al. (in prep.)

khondalite-charnockite dominated lithologic assemblagein the southwest from the granite-greenstone dominated litho-assemblages in the northeast (Müller et al. 1997). The KKPTSZ in the SGT also separates similar litho-assemblages. Thus, it appears to me that the KKPTSZ could be the continuation of the RSZ in Madagascar; both separates Eastern Ghat-type of lithological assemblage from the Dharwar-type lithological assemblages. A reconstruction model in which the KKPTSZ and the RSZ are placed close to one another, reveals a broad correspondence between the structural trends of these two fragments (Fig. 5.6). NW-SE trend of lithologic units along the western coast of the SGT appears to continue in the eastern part of Madagascar between Fianarantsoa and Fort Dauphin. Geological information from the granite-greenstone belts of Madagascar is very scanty. Until such time when the geology and geochronology of these belts are worked out in some detail, a tighter reconstruction between India and Madagascar will remain uncertain.

With the present state of availability of information on the kinematics and ages of the major shear zones in India, Madagascar, Antarctica and East Africa, a model of reconstruction of East Gondwana is presented in Fig. 5.[illegible]. In this model an Archaean terrain, with metamorphic grade varying from greenschist to granulite grade, is separated from a Neoproterozoic-Early Paleozoic granulite terrain by a terrane boundary defined by the Sileru Shear Zone, the Rayner Boundary Zone, the KKPT Shear Zone and the Ranotsara Shear. Major drawback of this model is that field and geochronological data from the Ranotsara Shear Zone, and the Sileru Shear Zone are very meagre. Future works need to be directed in these areas to attain a realistic model of Gondwana reconstruction.

5.4. A summary of major conclusions on the structure, geochronology and tectonics of the SGT (based on new data presented in this thesis)

A. New U-Pb dates:

Age	Events	Tectonic Block/lineament	Evidence
~480 Ma	Thermal resetting	South of the KKPTSZ	Lower intercepts for zircons in charnockite (Fig. 4.9) and zircons and monazites from khondalites in the KKB (Figs. 4.27 & 4.29). Previous dates of ~480 Ma (Rb-Sr whole rock and mineral ages) from the KKB (Table 1 5) overlap with this date.
523 ± 2 Ma	Granite veins and dykes and high-grade metamorphism	SGT; Achankovil lineament and Cardamom Hills	(i) Zircon (with very high Th/U ratio, characteristic of hydrothermal zircons) dated in the PCSZ (Fig. 4.16B); (ii) Zircon from granite veins in the Achankovil Lineament (Fig. 4.23) cutting charnockites and (iii) monazite analyses from khondalite in the Cardamom Hills (Fig. 4.21).
525-550 Ma	Charnockitization	SGT; both north and south of the KKPTSZ	The youngest date of granite charnockitized along the CBSZ is ~600 Ma (Fig.4.7) and along the Achankovil Lineament it is 548 ± 2 Ma (Fig. 4.22A). Within the Achankovil lineament, charnockite is retrogressed by 523 ± 2 Ma granite dykes (Fig. 4.23).
548 ± 2 Ma	Deformation and granitic activity	SGT, Achankovil Lineament	Zircon dated from syntectonic granite emplaced along the Achankovil Lineament (Fig. 4.22A).
570-560 Ma	Shearing along the KKPTSZ; emplacement of anorthosite and granitic intrusion.	Along the KKPTSZ and south of the Achankovil Lineament	Zircon dated from syntectonic granite emplaced in the KKPTSZ (Fig. 4.20); zircon rims in charnockitized granite in the southern tip of the SGT (Fig. 4.28); zircon from the Oddhanchatram Anorthosite (Fig. 4.11).
~600 Ma	Granite emplacement and thermal activity	CBSZ, MASZ, BSZ and PCSZ	Zircon and monazites from the CBSZ (Fig. 4.7), MASZ (Fig. 4.12), BSZ (Fig. 4.15) and from the PCSZ (Fig. 4.16B)

Age	Events	Tectonic Block/lineament	Evidence
~720 Ma	Metamorphism	Along the CBSZ	Zircon dated from mafic granulite close to the CBSZ (Fig. 4.6).
~800 Ma	Granite emplacement and metamorphism	Area south of the KKPTSZ.	Zircon dated from a charnockite (Fig. 4.9) and monazite from a khondalite (Fig. 4.10a).
~1 Ga	Emplacement of biotite gneiss	KKB in the SGT	Zircon analyses from a granite gneiss enclave within ~548 Ma granite (Fig. 4.24).
~1.6 Ga	Thermal activity (metamorphism/ magmatism)	SGT (Palghat Gap area)	Zircon analyses from a granite gneiss within the PCSZ (Fig. 4.16A).
~2.0 Ga	Possible granitic activity	KKB in the SGT	Cores of zircons from the SGT (Fig. 4.28).
2.51-2.50 Ga	Charnockitization	Northeast of the CBSZ	Ca. 2.51 Ga zircon subsets from charnockite gneiss (Fig 4.9).
2.54-2.51 Ga	Extensive intrusion of granite/tonalite gneiss	Area north of the KKPTSZ	Numerous zircons dates for charnockite and granite gneisses from a number of places (Figs., 4.2, 4.3, 4.4, 4.6, 4.8, 4.13, 4.14 and 4.19).
~2.9 Ga	Emplacement of mafic granulite and biotite gneiss.	DC, as far south as the PCSZ.	Zircons from mafic granulite and biotite granite gneiss (Figs., 4.6 and 4.16).

B. Structural data:

1. Identification of two new regional shear zones; the CBSZ and the KKPTSZ (Fig. 5.1)
2. Re-alignment of the some of the previously identified shear zones (the MASZ, the BSZ and the PCSZ, see Fig. 1.3 and 5.1). The previously identified Achankovil Shear Zone is now interpreted as a flattened limb of a regional fold. It does not represent a fundamental (crustal-scale) shear zone.
3. Kinematic analysis of major shear zones in the SGT indicates that they all have sub-vertical movements accompanied by flattening and these are not large scale

strike-slip shear zones, as previously inferred.

4. Chronology of movements along the major regional shear zones have been constrained. The MASZ, BSZ, PCSZ and the KKPTSZ all have experienced a major deformation between ca. 600 Ma and ca. 570 Ma.

C. Summary of new tectonic interpretation:

1. The PCSZ does not represent a terrane boundary within the SGT.

2. The KKPTSZ may represent a possible terrane boundary within the SGT.

3. The area south of the KKPT possibly represent a continuation of the Eastern Ghats rocks.

4. A possible Gondwana terrane boundary may pass along Sileru Shear Zone in the Eastern Ghats, the boundary between the Reynar Complex and the Napier Complex, the KKPT Shear Zone and the Ranotsara Shear Zone in the Madagascar.

Chapter-6: Use of organic carbon isotope as stratigraphic markers in Gondwana stratigraphy

6.1. Introduction

The type locality of Gondwana stratigraphy[9] is in India. This is true for the other recognized type localities in South Africa, South America, Madagascar and other continents. Stratigraphic correlation between these sequences is important if we are to correctly reconstruct the paleoenvironmental history of this supercontinent. The present correlation schemes depend either on biostratigraphy or paleomagnetism. Neither of these have the resolution needed to resolve the climate change record which these sequences store, and that holds the key to unraveling the details of Gondwana events, such as the Permo-Carboniferous glaciation or the greatest of all mass extinction events across the Permo-Triassic boundary. In most instances, the latter, for example, is well-preserved in marine sequences in several places around the world. However, in order to gain a true global insight, the terrestrial sequences of Gondwana hold the key to understanding atmospheric chemical climate change. A precise terrestrial stratigraphic correlation tool is, therefore, needed to confidently compare and contrast terrestrial sequences as far apart as India and South Africa.

Changes in the isotopic composition of organic and inorganic carbon across major stratigraphic boundaries are well recognized (Baud et al. 1989; Thackeray et al. 1990; Jin-Shi et al. 1991; Koch et al. 1992; Meyer, 1992; Wang et al. 1993; Derry et al. 1994; Ripperdan, 1994). Such changes, whatever their cause,e are probably synchronous and of a global scale

[9] The name Gondwana 'System' was orginally introduced by Henry Medlicot in 1872 for a group of terrigenous sediments in the Satpura basin of Central India. Originally the Gondwana 'System' was meant to designate a continental sedimentary sequence ranging in age from late Carboniferous to early Cretaceous. Presently the term is used to designate a group of primarily terrigenous sediements, with minor marine inter-beds, ranging in age from earliest Permian to end Triassic.

because they are driven by atmospheric and oceanic global circulation patterns that mix carbon-bearing fluids efficiently over short periods of time relative to geological processes. In detail, however, such variations in the isotopic composition of organic and inorganic carbon are far from simple. Commonly there is more than one large spike in the variation of isotopic composition across major geological boundaries. Large variations (spikes) across geological boundaries are often explained in terms of catastrophic release of carbon from within Earth (endogenous) or by influx of extraterrestrial carbon.

Carbon isotope studies in carbonates and in organic carbon remains have also been used in high-resolution stratigraphic correlation (Underwood et al. 1997), as a tool for environmental tracers and for paleo-environmental reconstructions (Compton et al. 1990; Leavitt and Long, 1991; Hollander and McKenzie, 1991; Mora, et al. 1991; Des Marais et al. 1992; Isozaki. 1997; Hoffman, 1998; Bowring et al. 1998). The causes of variation in the carbon isotope ratios in the geologic records is far from understood, but continuously-changing carbon isotope compositions of Earth's fluid envelope makes it a potential powerful tool for stratigraphic correlation that cannot be neglected. To date, the use of carbon isotopes for stratigraphic correlation has primarily been restricted to marine carbonate rocks. In the marine environment the residence times for organic and inorganic carbons are greater than the mixing time for the oceanic water masses. This allow their stratigraphic use on a global scale. However, in the terrestrial environment mixing amongst sub-reservoirs of carbon may be difficult, which restricts its use as a stratigraphic marker. Available works on terrestrial organic carbon in geological samples (Morante et al. 1994 ; Faure et al. 1995) are few, but they highlight its usefulness as a potential stratigraphic tool for terrestrial deposits as well.

In the present study, more than 500 samples of terrestrial plant remains from different Gondwana basins in the Peninsular India, Madagascar and South Africa have been analysed to examine the possibility of using the variations in the carbon isotope ratio in plant remains as a tool for intra-basinal, inter-basinal and inter-continental correlation of Gondwana sequences. A

subsidiary aim of the present study has been to study the pattern of organic carbon isotope variation in terrestrial deposits. In course of this study, it became clear that organic carbon isotope in terrestrial deposits can also be used as a powerful tool for stratigraphic correlation though caution is needed to correctly interpret them.

6.2. Principles of carbon isotope analyses

6.2.1. Isotopes of carbon

Carbon has five radiogenic (^{10}C, ^{11}C, ^{14}C, ^{15}C and ^{16}C) and two non-radiogenic or stable (^{12}C and ^{13}C) isotopes. Of the radiogenic ones, ^{14}C has the highest half life (~5726 years) and is often used for environmental and geologic research. Of the two non-radiogenic isotopes, ^{13}C has an abundance of ~1% while ^{12}C constitute ~99% of total carbon present in the crust.

Variation in the different environmental parameters often influence variation in the relative abundances of ^{12}C and ^{13}C within and amongst different reservoirs of carbon. Thus the variations in their abundances are often used to monitor present day environment and to reconstruct paleo-environments. For most natural organic samples, the ratio $^{13}C/^{12}C$ is ~0.0112. Minor variation in this ratio are often present in geologic and present-day samples which is conventionally expressed with reference to a standard in the following way.

$$\delta^{13}C = \left[\frac{(^{13}C/^{12}C_{sample} - ^{13}C/^{12}C_{standard})}{(^{13}C/^{12}C_{standard})}\right] \times 10^3$$

The standard is a Cretaceous belemnite shell from Pee Dee Formation in South Carolina whose $^{13}C/^{12}C$ ratio is 0.0112372 (Holser et al. 1999). So the equation becomes, $\delta^{13}C = \left[\frac{(^{13}C/^{12}C_{sample})}{0.0112372} - 1\right] \times 10^3$

6.2.2. Major reservoirs of carbon and carbon cycle

Major reservoirs of carbon on Earth include 5 surficial reservoirs and 3 geologic reservoirs. The surficial reservoirs include (i) the atmosphere, (ii) terrestrial biota, (iii) surface ocean, (iv) deep ocean, and (v) litter, peat and soil carbon. The geologic reservoirs include (i) carbonate sediments (ii) sedimentary organic carbon and (iii) the mantle carbonate. Estimates of carbon stored in these reservoirs are illustrated in Fig. 6.1. There is large scale variation in the carbon content of these different reservoirs and their isotopic composition (Fig. 6.1a). The bulk of the surficial carbon is present in the deeper parts of ocean, which has ~7 times the carbon stored in terrestrial biota (Schlesinger, 1991; Heimann and maier-Reimaer, 1996). Living organisms encompass only a small fraction of the earth's carbon. So a mass extinction, even the one as severe as the one at Permian-Triassic boundary is unlikely to cause large changes in the $\delta^{13}C$ on a global scale. Fluxes of carbon among different surficial reservoirs can be quite high (Sandquist, 1985). For atmospheric CO_2, nearly 25% gets turned over every year. Thus any inequilibrium in the carbon cycle in involving surficial reservoirs can be expected to be very sharp and of short duration (few decades). For geologic reservoirs, precise estimation of their size of carbon storage is difficult. However, each of these reservoirs contain carbon many times more than all five surficial reservoirs put together. Isotopic composition of different geologic reservoirs also have large variation (Fig. 6.1b). However, equilibrium fluxes amongst geologic reservoirs are low. But a catastrophic change in the equilibrium amongst geologic reservoirs can swamp surficial carbon reservoirs and can easily cause large and detectable changes in the isotopic compositions of geologic samples. Observed isotopic changes in geologic past were thus more likely to have caused by release of (organic) carbon locked up in the solid Earth rather than in the fluid-enveloped Earth or by the influx of extra-terrestrial carbon.

Interactions amongst different reservoirs of carbon due to various bio-geochemical processes is accompanied by fractionation of carbon isotope amongst different reservoirs. Carbon from

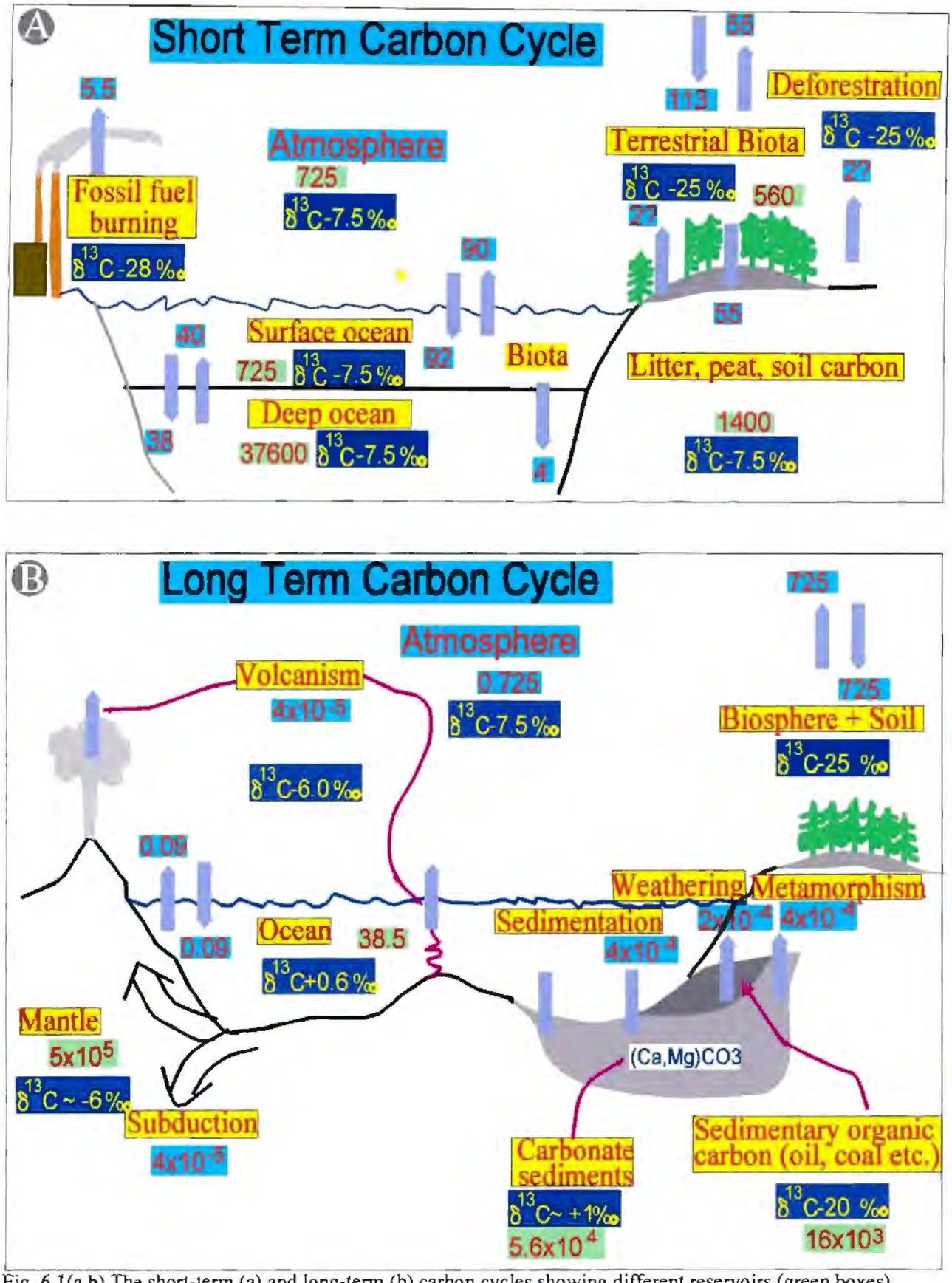

Fig. 6.1(a,b). The short-term (a) and long-term (b) carbon cycles showing different reservoirs (green boxes) and fluxes (pale blue boxes) amongst reservoirs. The numbers shown in (a) are in gigatons (10^{15} grams) and the numbers shown in (b) are in kilo-gitatons (10^{18} grams). Approximate isotopic composition of each reservoir is also shown. Source of data: Schlesinger, 1991 and Heimann and Maier-Reimer (1996).

inorganic reservoirs gets into the organic reservoirs mainly through photosynthesis, while carbon from organic reservoirs get into inorganic reservoirs mainly by oxidation. Photosynthesis is the prime cause of large scale fractionation of carbon isotope. Photosynthesizing organisms accumulate more of ^{12}C than ^{13}C during photosynthesis and on average the ratio of $^{12}C/^{13}C$ increases by about 25-28‰ $\delta^{13}C$ compared to the atmospheric ratio of ~7‰ (O'Leary, 1981). Short term and long term interactions amongst different reservoirs of carbon, their content and isotopic ratios are illustrated in Fig. 6.1.

6.2.3. Significance of carbon isotope stratigraphy

6.2.3.1. Identification of global events

Major era boundaries are typically marked by significant and often sharp fluctuations of carbon isotope ratios in both marine carbonates and organic carbons. For example, at the K-T boundary, shallow marine carbonates show a spike of ~ -3‰ which persisted for about 0.5 Ma. Hsü and Machans (1990) suggested this to be due to reduced photosynthesis at shallow oceans after a catastrophic event triggered by bolide impact or explosive volcanism. They also suggested such large variations seen at the P-T boundary and at the Precambrian-Cambrian boundary are due also to similar causes.

Schölle and Arthur (1980) have demonstrated some global excursions in the $\delta^{13}C$ values in the latest Jurassic to Early Tertiary oceanic pelagic sediments. They suggested the possible use of $\delta^{13}C$ excursions for fine scale stratigraphic subdivision of parts of Cretaceous time. A sharp negative spike (about 8-10‰ shift in $\delta^{13}C$ values of marine carbonate) exists at the Devonian-Carbonaceous boundary in the South China (Dao-Yi et al. 1986). This, they explained to be related to sudden decrease in the fertility of organisms in ancient ocean. The sharpness of spikes in $\delta^{13}C$ values indicates that the triggering factor was geologically of short duration. At the K-T boundary it has been shown while the planktonic forms were affected by

a $\delta^{13}C$ incursion, the deep water forms were not affected (Hsü et al. 1982) This possibly indicates that the duration of the incursion was not long enough to affect the $\delta^{13}C$ value of deeper water formation. At the Permian-Triassic boundary also, while the shallow water fauna suffered near total extinction, many of the deep water fauna were not much affected.

Similar incursions in the $\delta^{13}C$ values have also been shown from the Pleistocene pelagic sediments (Sommer and Matthews, 1975), and the Late Proterozoic sediments (Kaufman et al. 1991; Knoll et al 1986; Hoffman, 1996) and in many other global bio-events (Bowring and Erwin, 1998).

6.2.3.2. Paleoclimatic reconstruction

A positive shift in $\delta^{13}C$ value in organic carbons may reflect any of the following or combination of them:

(i) Shift in plant population from dominantly C_3 photosynthesis type[10] to C4 and /or CAM photosynthesis (which have very distinct isotopic compositions, see below). Although it is generally held that C4 and CAM photosynthesis are of recent origin, some authors held that CAM existed before breakup of Africa from South America (i.e., 140 Ma ago). A shift

---

[10] On the basis of type of photosynthesis used, plants are classified into three broad groups:
(i) C3 metabolism: Also called Calvin cycle photosynthesis. A metabolic pathway exhibited by autotrophs in which the three-carbon compound phosphoglyceric acid is the first identified product of carbon fixation. Almost all trees, most shrubs, herbs and forbs and cool season grasses and sedges use C3 metabolism.$\delta^{13}C$ varies from -23‰ to -35‰.
(ii) C4 metabolism: A metabolic pathway exhibited by autotrophs in which CO_2 initially combines with phosphophenol pyruvate, a four-carbon compound malate, or aspartic acid as the first identified product of carbon fixation. This is then translocated to bundle sheath cells where CO_2 is released and used in Calvin cycle reactions. Warm season grasses and sedges are most abundant C4 plants.$\delta^{13}C$ ranges from about -10‰ to -14‰ averaging about -13‰ (Cerling et al., 1993). Tropical savanas, temparate grassland and semiarid scrub lands are most common areas of such plants. C4 photosyntheric type is favoured when there is low concentration of CO_2 in the atmosphere. It is generally argued that C4 biomass originated and showed great expansion in both old world and New world starting forom 7 to 5 million years ago. This according to Cerling et al. (1993) was due to lower atomosphereic carbon dioxide level.
(iii) CAM metabolism: CAM is abbreviation for Crassulacean Arid Metabolism. This photosynthetic type combines features of both C_3 and C4 plants. Such plants are adapted to conditions of CO and water stress. They have intermediate $\delta^{13}C$ values.

towards C4 photosynthetic type is likely, under conditions of low atmospheric CO_2.

(ii) Low moisture availability (arid and semiarid lands) causes C_3 plants to be several ‰ enriched in $\delta^{13}C$ (Ehleringer and Monson, 1993).

A negative shift in $\delta^{13}C$ may be caused by any one or combination of the following factors. (i) Cooler temperature; (ii) Deficient light; (iii) wet condition; (iv) higher P_{CO2} in ambient atmosphere; (v) Plants richer in lipids than protein and carbohydrate and (vi) an anoxic or dys-aerobic depositional environment which favour preservation of hydrogenated compounds because of lack of oxic degradation.

Kaufman et al. (1991) observed deposition of $\delta^{13}C$-depleted carbonate during or immediately following three separate glacial events in the Late Proterozoic. Similarly, Knoll et al. (1986) observed that the area of enhanced burial of organic carbon (i.e., deposition of isotopically heavier carbonates) coincided with the major Eocambrian glaciations. According to Knoll et al. (1986), the occurrence of major glaciations implied the existence of a strong climatic gradient which, in turn, is very likely to have affected circulation within the ocean, possibly encouraging the development of deep circulation and reducing rates of burial of organic material. Significantly, we do not find any evidence of glaciation associated with the carbon isotope excursion across the Permo-Triassic boundary. The last phase of Permo-Carboniferous glaciation was in the mid-Permian (Erwin, 1993).

6.2.4. Carbon isotopes in terrestrial plant matters

Organic carbon isotope in terrestrial geologic samples is derived mostly from plant matter. Isotopic characteristics of plant-derived organic carbon are affected by a number of factors during the life time of plants. It is, thus, important to understand factors responsible for causing changes in the isotopic compositions of plants in order to correctly interpret isotopic records in geologic samples. The following section summarizes causes of variation in the

$\delta^{13}C_{org}$ in plant matters.

6.2.4.1 Photosynthesis and carbon isotope fractionation

During photosynthesis plants takes up CO_2 from the atmosphere with $\delta^{13}C$ of ~7.5‰ and implant this into various organic molecules, whose average $\delta^{13}C$ value is -25‰. Thus, photosynthesis is accompanied by large-scale fractionation of carbon isotopes. Each photosynthetic type generally occupies a particular ecological niche within each ecosystem. For example, in arid lands, the greatest fraction of non-succulent species are C_3 plants. The succulent species tend to be either stem or leaf succulent and mostly follow CAM photosynthesis. C_4 photosynthesis in arid lands are most frequent among perennial heliotypes and annuals. In arid lands, C_3 is the most common type in mesic sites, CAM occurs in the most driest locations and C_4 only on arid locations where there is significant summer precipitation and saline soil. In CAM plants, $\delta^{13}C$ varies from -10 to -22%. The range reflect different proportion of C_3 and CAM pathways in plants. Some CAM plants operate with C_3 photosynthesis during wet period whilst the photosynthetic tissues change to CAM under drought conditions. In some other plants, leaves operate on C_3 and stems on the CAM type photosynthesis. CAM plants which fix CO_2 during the nocturnal portion of their diurnal cycle shows more positive values of $\delta^{13}C$ than those fixing CO_2 during daytime.

The large range of $\delta^{13}C$ in C_3 plants reflect diffusional processes limited by leaf performance. In arid lands, twigs and stems also represent major photosynthetic surfaces (and which may include all three photosynthetic types C_3, C_4 and CAM). Photosynthetic twigs have na average of 1.5‰ higher $\delta^{13}C$ value than the leaves of the same plants. But in non-photosynthetic types, twigs show only an average of 0.1-0.2‰ higher $\delta^{13}C$ values than leaves.

Different isotopic composition among C_3 plants can be explained by differing proportions of stromal and mesophyll resistance to CO_2 uptake (O'Leary, 1988). If the stromal component is

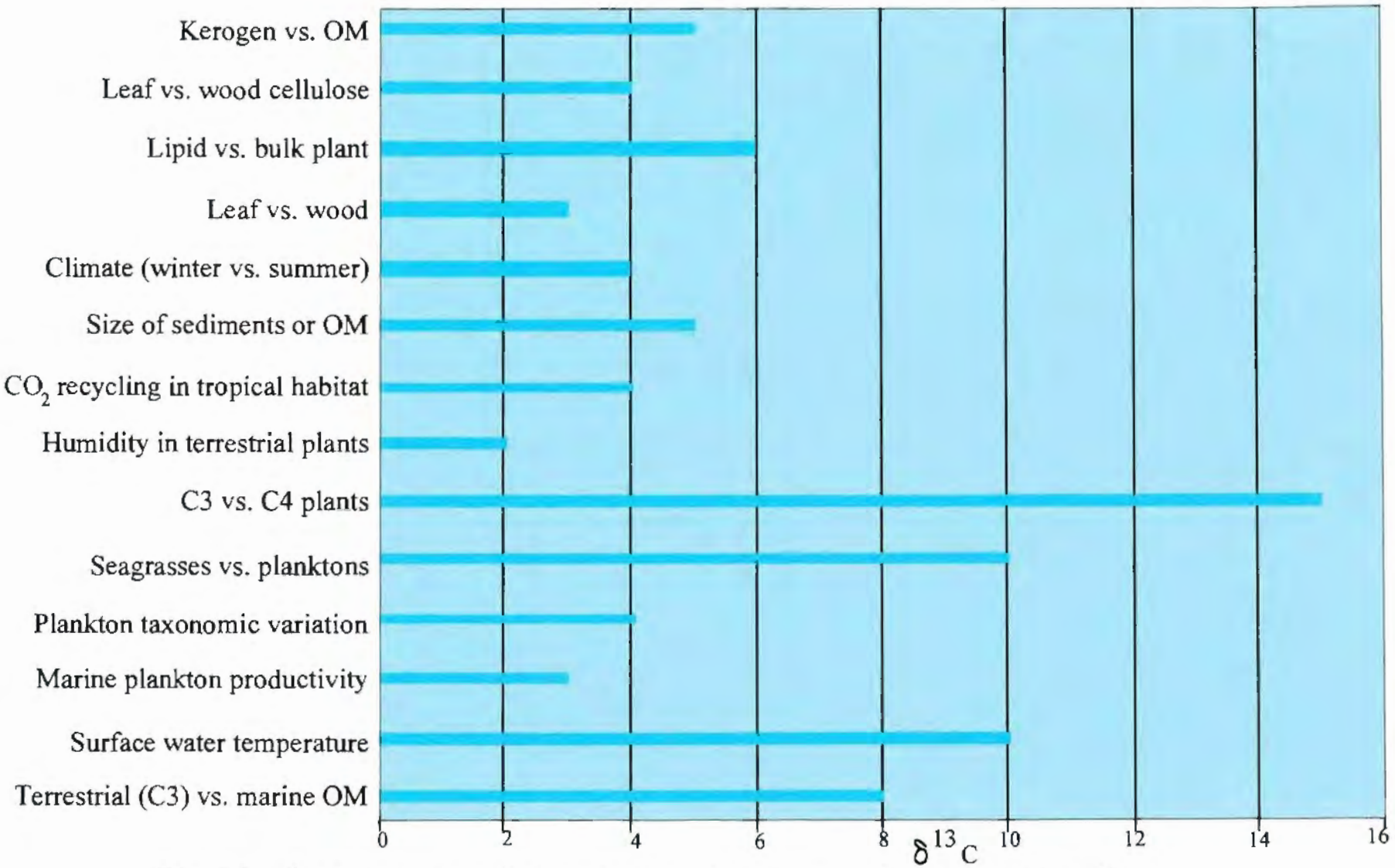

Fig.6.2. The range of variations in the $\delta^{13}C$ in recent Organic Matter (OM).

large, overall discrimination of ^{13}C is small, because the physical discrimination by slower diffusion of $^{13}CO_2$ as compared to $^{12}CO_2$ is very small. If the mesophyll component is very large, ^{13}C content of tissue will deviate greatly from ambient due to strong discrimination against $^{13}CO_2$ during carboxylation process. The variation in $\delta^{13}C$ in plants can be understood in terms of the C_i/C_a ratio which is the ratio of internal vs. ambient CO_2 partial pressure. Factors that increase the C_i/C_a ratio will reduce the $\delta^{13}C$ of a plant. Thus the C_i/C_a ratio should increase when carboxylation capacity is limiting, as might occur for example, under light- or nutrient- deficient conditions, or with low-temperature limitations. Conditions that mainly restrict CO_2 supply, for example water stress or saturating photon flux densities, will result in a low C_i/C_a ratio, and a higher value of the $\delta^{13}C$ for the plant.

6.2.4.2. Variation of $\delta^{13}C$ in plant matters

6.2.4.2.1. Variation in living plant matters

Variation among different plants

In living plant matters there is wide variation in $\delta^{13}C$ values. Such variations may exist between different parts of a plant and even in different bionuclides within a plant. Galimov (1980) showed that bionuclides within a single terrestrial plant could vary by as much as 4‰. Similarly $\delta^{13}C$ values are generally changed during carbonisation of non-living plant matters. Fig. 6.2. summarizes the principal sources and extent of variation in the $\delta^{13}C$ in plant matters. The principal causes of such variations are as below:

(a) **C_4 vs. C_3 plants**: Plants utilizing C_4 biosynthetic pathways utilize more of ^{13}C than ^{12}C . They are more effective in this aspect than plants utilizing C_3 biosynthetic pathways. Algae have intermediate $\delta^{13}C_{org}$ values. $\delta^{13}C_{org}$ values in C_3 plants in fresh and intermediate marshes range from -26.5 to -27.9‰ while C_4 plants growing in brackish and saline marshes of the

same depositional basins have $\delta^{13}C_{org}$ values around 13-14 ‰. Different species composition of the primary producers can cause isotopic variation. Terrestrial plants in the Permian, however, only used the C_3 photosynthetic pathway of fixing CO_2 (Thomasson et al. 1986).

(b) **Upper and Lower part of forest canopy**: In the tropical rain forests, a variation between the $\delta^{13}C_{org}$ values of the leaves of the upper part of the canopy and the leaves in the lower part of the canopy has been described: leaves in the upper part of the canopy have higher $\delta^{13}C_{org}$ values (as high as 7‰; Medina et al.1986). Medina et al. (1986) attributed such variation to the variation in the $\delta^{13}C$ values of the ambient CO_2 available to the plant. Shade flora assimilate CO_2 from soil respiration, which is depleted in $\delta^{13}C$.

(C) **Terrestrial vs. marine plants**: Terrestrial plants are enriched in ^{12}C by 5-8‰ when compared with the marine plants. This is possibly due to higher degree of utilization of the ambient CO_2 by water plants and partly due to differences between atmospheric sources ($\delta^{13}C$ ~ -7.8‰) and seawater bicarbonate ($\delta^{13}C$~-2‰). When preserved as fossil organic matter, this difference between terrestrial and marine plants (5-8‰) reduces to -3‰ to -5‰ only in their appropriate kerogen fractions. Transitional environments like continental reservoirs have intermediate values (Galimov, 1980)

Variations within different parts of plants

(a) There is some variation in the $\delta^{13}C_{org}$ values among different part of the same plant. Variation between the leaves and the stems of the same plant can be as high as 3.1‰ (Galimov, 1980). Organic compounds like carbohydrate and proteins are isotopically heavier than lipids. Variations in proportions of protein to lipids produced at different times by a group of algae causes differences in $\delta^{13}C$ values. Different components of lipid fractions like fatty acid, di- and tri-glycerides, chlorophyll etc. also shows large variation in carbon isotope (3-5‰; Galimov, 1980).

(b) Variation in tree rings in response to climate:

Carbon-isotope fractionation within different parts of plants depends on $\delta^{13}C$ of the atmosphere and also on any condition which affect the ratio of internal plant CO_2 to external CO_2 concentration (C_i/C_a). When this ratio is low, the plant does not discriminate as effectively against ^{13}C. This ratio is in turn, affected by the rates of CO_2 fixation and stromatal conductance. Draught, light, soil moisture, precipitation etc could affect this ratio. Combination of these environmental influences could affect $\delta^{13}C_{org}$ values of plants (Francey and Farquhar, 1982). Levitt and Long (1991) recorded variations as high as 3‰ amongst different tree rings of conifer and hardwood trees. They stated that soil moisture and radiation level have stronger correlation with the $\delta^{13}C$ of tree rings than change in the $\delta^{13}C$ of atmospheric CO_2. Increased soil moisture and low solar radiation reduces ^{13}C in the tree ring However, inter-species variation of $\delta^{13}C$ in tree ring in a site is not very significant.

Variation due to changes in climate

(a) Variation due to atmospheric CO_2:

High concentration of CO_2 favour enzymatic rate control over diffusional rate control in isotope fractionation, with the result that organic carbon synthesized under these conditions is isotopically more light.

(b) Variation due to temperature: Cooler temperatures generally result in greater fractionation of carbon isotope with the effect that ^{12}C uptake is increased. The theoratical temperature dependance of the thermodynamic carbon isotope effects for fossil organic matter is about 0.2-0.4‰ per °C (Galimov, 1980). However, this estimate varies. Emrich et al. 1970 (in Williams et al.1997) have shown that organic carbon isotopes are little affected by variation in temperature (0.035‰ per °C)

(C) Variation due to altitude: There is a pronounced altitudinal increase in the efficiency of

CO_2 uptake with respect to intercellular CO_2 levels This leads to a significantly reduced P_i/P_a (ratio of internal to external partial pressure) in plants. At High altitude there is a marked increase in $\delta^{13}C$ value (~ -26.15‰) than lowland average (-28.8‰) (Korner et al. 1988). For a single species altitudinal variation of 4.7‰) have been recorded (Korner et al. 1988).

6.2.4.2.2. Variation due to post-depositional processes

Variation during diagenesis

Isotopic changes due to processes involved during burial and diagenesis are illustrated in Fig. 6.3.

(a) *During early diagenesis:* After a organism or part of it is buried, the earliest diagenesis is microbial, initially aerobic but anaerobic after burial at moderate depth (<1.0m; Hayes et al. 1983). Bacterial oxidation may produce more negative $\delta^{13}C$ values. Also preferential degradation of carbohydrate and protein and selective preservation of lipids can cause a significant isotopic shift because lipids are much depleted in ^{13}C. Organic matter even in most recent sediments is systematically depleted in $\delta^{13}C$ by 2-4‰ relative to its biological source (Hayes et al.1983). Anoxic or dyaerobic depositional environments favour preservation of hydrogenated compounds because lack of oxic degradation.

(b) During *catagenesis*, mobile hydrogen rich organic matter is produced. The onset of the process sometimes occurs as low as at 60°C and continues up to 150°C. During *metagenesis*, (150°C to 250°C) hydrogen is lost in part by the elimination of methane. Catagenesis and metagenesis involve decreases in H/C ratio due to production of hydrocarbons. The amount of carbon lost depends on the amount of H available (which in turn depends on the source material) (Hayes et al.1983) and the environment of diagenesis (open system or closed system) (Scholle and Arthur, 1980). The transformation of organic matter to

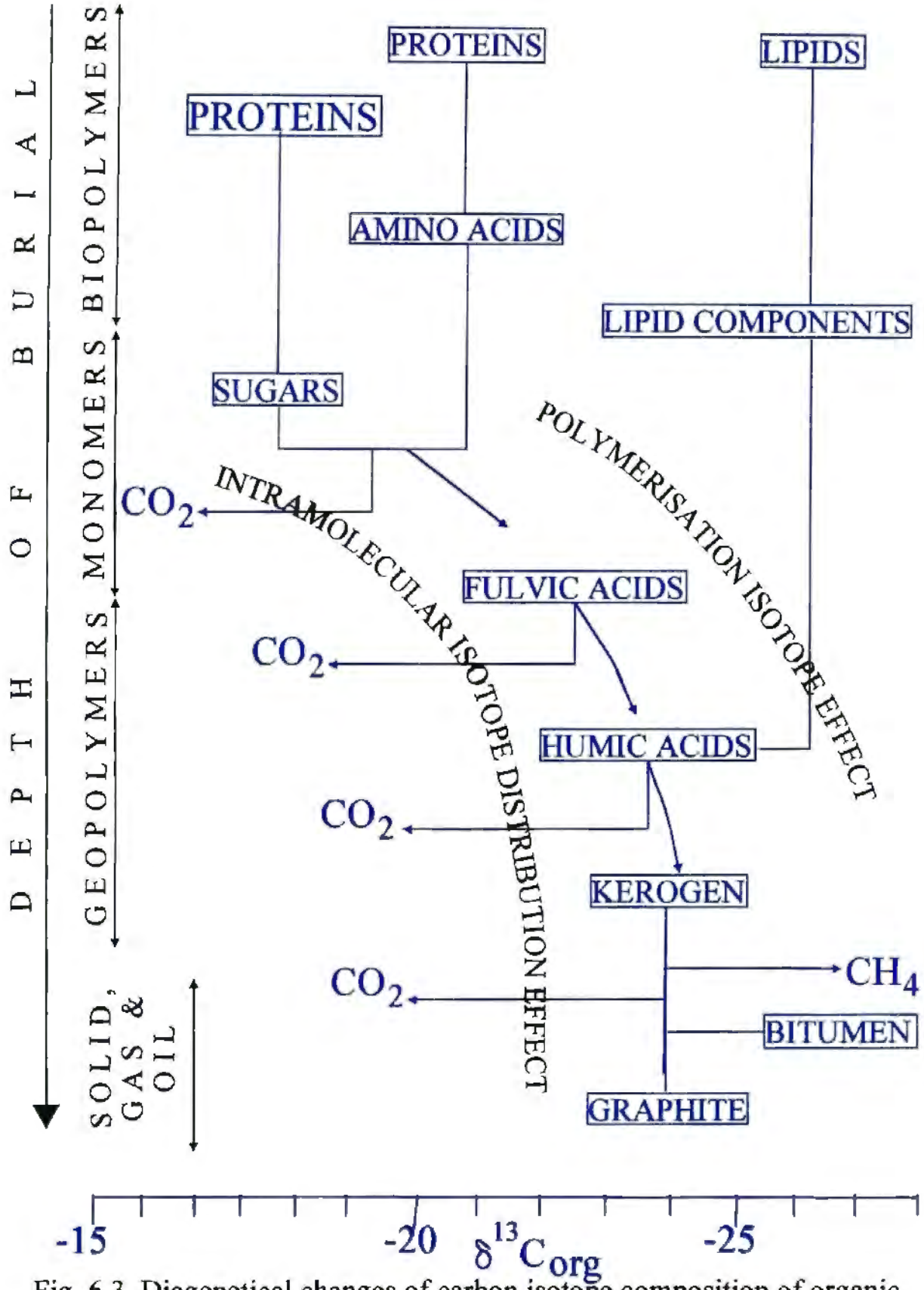

Fig. 6.3. Diagenetical changes of carbon isotope composition of organic matter (after Galimov, 1980).

lighter molecules is never complete. CH_4, CO_2, H_2O, H_2 co-exist with an insoluble residue (Durand, 1980). The isotopic consequences depend on the importance of these carbon-loss mechanisms. Gases generated during the coalification include principally methane and carbon dioxide. Relative to coal, methane is highly depleted in ^{13}C, in contrast to CO_2 which contains more ^{13}C (Degens, 1969). Diagenesis is generally held to cause very small shift in $\delta^{13}C_{org}$ value (Deines, 1980, Redding et al.1980, Scholle and Arthur, 1980, Hayes et al. 1983; Degens, 1969). However, there is no conclusive prove for this. Degens (1969) inferred this from near uniform value of $\delta^{13}C$ for different ranks of coal. But his data included samples from widely varying age and location. It is now known that these factors cause considerable variation in $\delta^{13}C$. So the uniform values shown by Degens (1969) could be due to coincidence

The effect of thermal alteration, and hence the carbon loss can be gleaned from a plot of atomic H/C vs. atomic O/C (van Krevelen plot). The overall composition of most organisms lie within a rather low range, with H/C values generally being within 10% of 1.54 and O/C values being within 20% of 0.5. Any significant departure from this will mean loss of carbon.

Post diagenetic alteration

(a) Differential thermal alteration of samples can cause variation in isotopic composition. The theoretical temperature dependance of the thermodynamic carbon isotope effects for fossil organic matter is about 0.2 -0.4‰ per 1°C (Galimov, 1980). The effect of thermal alteration can be gleaned from atomic H/C vs. N/C plots of kerogen.

(b) Character of the host rock: Imbus et al. (1992) found, in Precambrian shale, that kerogen that comprise < 0.15% of their host rock tend to be strongly enriched in ^{13}C. This they suggested to be due to relative ease of destruction of isotopically light organic carbon via oxidation and microbial activity. Scholle and Arthur (1980) have also made similar observation for marine organic limestone. Imbus et al.(1992) also observed that $\delta^{13}C_{ker}$ show a moderate depletion with increasing grain size of the sediments.

6.3. Permo-Triassic Extinction

Gondwana type sections include rocks formed across the Permian-Triassic extinction event. Thus, Gondwana sections provide an opportunity to look at the changes during the extinction event.

6.3.1. Pattern of Extinction

Erwin (1993, 1994) reviewed of the nature and the possible factors causing the Permo-Triassic extinction event. The pattern of extinction is not synchronous. Some organisms disappeared well below the boundary, some were very diverse well up to the boundary while others were not affected. This extinction event includes elimination of 90% of the species in the ocean and 70% of the vertebrate families on land.

The extinction was seen to be more severe among shallow water and planktonic fauna like epifaunal, suspension feeders, Paleozoic corals, articulate brachiopods, bryozoans echinoderms, trilobites etc. All of these, however, started declining from Middle Permian time on. While shallow water fuscilinid foraminifera suffered complete extinction, non-fuscilinid foraminifera experienced only slight extinction.

Many families like Nautiloids, Bivalvia, Bryozoa, Porifera were only slightly affected by the extinction event. Erwin (1994) noted that increased extinction among marine invertebrates with planktotrophic larval development may simply reflect the increased extinction in near-shore environments and in the tropics, both areas where planktotrophs dominate. The last appearance of shallow marine invertebrates had a close relationship with the extent of shallow marine sea over the time in question.

Among terrestrial fauna reptiles and amphibians suffered most. But the extinction was not restricted to the P-T boundary but was spread over a wide time interval from Lower Permian to Middle Triassic, with the heaviest loss at the Lower Triassic-Middle Triassic boundary (Olson, 1982) Insects also suffered considerably

Plant fossils showed little evidence of mass extinction. However, gymnosperm pollen was much reduced and a new arid-resistant pollen type appeared across the Permian-Triassic boundary. The timing of extinction for different living fauna, however, does not appear to be synchronous. But it must be remembered that the terrestrial fauna biostratigraphy is not well correlated beyond sub-regions.

Abrupt or gradual?

From the study of extinction of shallow marine invertebrates, it appears that P-T events had a very short time span (Erwin, 1992). In Alpine Austria, the sharp negative spike in $\delta^{13}C$ value has been estimated to have lasted for 1-3 m.y. (Margaritz, 1989 and Holser et al. 1991) on the basis of paleontological records. Radiometric dating of volcanic ash beds at the Permo-Triassic boundary in the Meishan section, South China yielded a $^{206}Pb/^{238}U$ age of 251.2 ± 3.4 Ma and the $^{207}Pb/^{235}U$ age of 250 ± 5.0 Ma (Claoue-Long et al. 1991) Although dated precisely, this work could not give the span of extinction event or carbon isotope spike. Recently, Bowring et al (1998), with the help of precise U/Pb zircon dating of number of volcanic ash beds across the P-T boundary estimated that in the same Southern China section, the span of $\delta^{13}C$ incursion to be less than 165,000 years. They dated the P-T boundary more precisely at 251.4 ± 0.3 Ma. However, the rarity of Late Permian marine deposits and associated volcanic ash beds do not allow to validate this record of short time span globally. The extinction pattern of terrestrial vertebrates does not appear to reflect such an abrupt change at P-T boundary (Olson, 1982). Thus, one of the ways to better understand the P-T extinction event is to examine the terrestrial records and examine how P-T extinction event is reflected in them.

Floral assemblage at the P/T boundary

After the ice age of Late Carbonaceous and Early Permian times, the climate warmed up There was rapid evolution of *glossopterid* flora (Chandra, 1998) Cool temperate swamps with thriving plant communities were extensive. The trees and shrubs of glossopterids had special aeration tissues in their roots suited to the boggy condition (White, 1986), which were adapted to their swampy habitats. It is likely that there had been a rapid change-over from cool-temperate climates of most of the Permian to a warm, moist interval near the Permo-Triassic boundary. Within this time interval the sudden appearance of new flora characterised by the first forked-fronted seed-ferns, conifers, Ferns, Ginkgos and Cycadophytes has been noted. Ferns and Lycopods foliage had a high content of lignin (30-50‰; average plants being between 10-25‰) So they had a better chance of preservation (Robinson, 1990)

All over Gondwana, the Glossopterids almost disappeared from the fossil record at the P-T boundary. Early Triassic flora show characteristics related to a warm moist climate without marked seasonal dry periods. They show large leaf foliose expressions and do not have the clear xerophile adaptation of those later in the Triassic.

6.3.2. Causes of Extinction

Various factors have been held responsible for P-T extinction, such as volcanism, extraterrestrial causes, oceanic anoxia, global warming and global cooling. Analysing the strengths of these factors, Erwin (1993) suggested that a complex web of factors may have been responsible for the mass extinction. Faure et al. (1995) related the extinction to the continental elevation due to final phases of consolidation of Pangea during the end of the Permian. However, with indications that Permian-Triassic extinction event and its associated spikes in carbon isotope record in marine carbonates are of very short duration (less than 0.2 Ma; Bowring et al. 1998), catastrophic causes like bolide (with hydrocarbons having highly

negative impact $\delta^{13}C$ values) impact have been proposed (Bowring et al. 1998). As noted above, there was no major effect on terrestrial fauna. There was also no major abrupt change in the physical environments. Expansion of habitats and colonisation of new environments for terrestrial fauna are evident from Middle Permian time. Changes of new environments might have caused elimination of certain families of terrestrial flora from Middle Permian onwards. There is a general increase in aridity in the circum equatorial regions of Gondwana from the Early Permian, which caused extinction of certain families of aquatic based terrestrial vertebrates. This also caused the appearance of the carnivore-herbivore food chain in the record.No large strictly terrestrial herbivorus existed while late in the Early Permian. A very rapid increase in body size took place among newly evolved terrestrial herbivores. Also large animal size tends to increase vulnerability to changes in environment. Thus, the extinction event that is recorded in shallow marine deposits as abrupt, does not appear to be so in terrestrial records. However, high-precision geochronology, along with carbon isotope stratigraphy from terrestrial sequences, are needed to resolve the question as to whether the short duration of the extinction and spikes in $\delta^{13}C$ values were global, and if they are global, whether they are synchronous.

Cooler or Warmer Temperature at the P-T boundary

Both cooler and warmer climates have been suggested as the cause of Permo-Triassic extinction. Stanley (1988) suggested that bipolar glaciation triggered the extinction. However Erwin (1993) and others observed that last phase of Permo-Carboniferous glaciation was in the mid-Permian. He held that cooler climate was possibly not the cause of extinction. But as in the K/T boundary (Holster and Margaritz, 1992), Wang et al. (1994) have held that there was a reduction in the primary productivity in the shallow marine environment. Also shallow water fusilinids suffered extinction at the P/T boundary, in contrast to the survival of deeper water, but more complex foraminifers. A cooler environment is consistent with this observation but may not be the cause.

6.3.3. Carbon isotope record at the Permo-Triassic boundary

6.3.3.1. In marine carbonates

The Permian-Triassic boundary in the marine section in Eurasia, particularly along the margins of the former Tethys Ocean, is characterized by a sharp drop in $\delta^{13}C_{carb}$ of ~3‰ (from +3 to 0‰; Holser and Magaritz, 1987; Baud et al. 1989) and a similar drop in $\delta^{13}C_{org}$ of ~3‰ (from mean values of -24.6 to -27.4‰) in shale and marl interbeded with carbonates in Alpine Austria (Magaritz et al. 1992). Along the former margin of the Panthalassan Ocean in Canada, in deep-water marine sediments, the drop in $\delta^{13}C_{org}$ also can be traced from marine (Tethyan sections in northwestern Australia to alluvial-paralic Panthalassan) sections in southeastern Australia (Morante, 1993; Morante et al.1994).

6.3.3.2. In terrestrial plants

A precipitous drop (3-5‰) in $\delta^{13}C_{org}$ in plant fossil remains across the Permian- Triassic boundary has been recorded in the Sydney and Bowen Basins of eastern Australia (Morante et al. 1994) and in the Karoo basin of South Africa (Faure et al. 1995).

6.3.3.3. In terrestrial animals

Thackeray et al. (1990) have recorded a decline of ≥6‰ in the $\delta^{13}C$ value of apatite in the fossil tooth enamel of therapsids, which were terrestrial herbivorous animals just below P/T boundary. This, they interpreted as reflecting biogenic variation associated with global changes in CO_2.

6.3.3.4. Changes in the $\delta^{13}C$ value at the P/T boundary: global or local

Although the general pattern of isotopic incursion is globally similar, in detail the isotopic patterns show variation, and similar isotopic spikes are also found in Upper Permian sediments (Faure et al.1995). One of the most detailed studies of isotopic incursions across the P-T boundary has been made in the GK-1 borehole in Austria (Holster et al. 1991). There, three distinct spikes are present spanning a sediment thickness of ~ 40m. In some other places, however, the variation in the $\delta^{13}C$ value appears to be sharp (for example, Wang et al.1994) Such differences could be due to variation in the local environment of deposition. It is important to note that in the GK-1 borehole cited above, all three $\delta^{13}C$ minima are associated with high concentration of pyrite, distinct negative $\delta^{34}S$ values, a peak in Ce^*/La^* value, high Ir concentration, high S/C ratios. This relationship indicates a correlation of $\delta^{13}C$ minima with a reducing environment. A global change in the atmospheric $\delta^{13}C$ value should be reflected in various types of sedimentary environment including reducing, open basin, marine and fresh water.

Based on available data, it is perhaps premature to say, for sure, that the isotopic excursion at the P/T boundary was a synchronous global event. However, the isotopic signatures at the Permian-Triassic boundary are so similar that global synchronous event seems likely.

6.3.4. Climate change and δ^{13} C spikes at the Permian-Triassic boundary

Regression

The traditional view holds that the Late Permian experienced a worldwide regression and that the transgression did not commence until the beginning of Triassic (Yang, Sheng and Yin, 1995). However, there are evidences that in South China, Italy, Arctic, Canada and at many other localities of Tethys that the transgression began not in the earliest Triassic but in the latest Permian (Sheng and Yin, 1995 and references therein). The Permian-Triassic boundary is regarded as the time of final consolidation of Gondwana (Faure et al. 1995). Amalgation of continental fragments is likely to have caused orogeny and uplift of landmass causing

widespread regression. Regression would cause exposure and oxidation of carbonates (in terrestrial and shallow marine environments) and carbon (oil/gas/gas hydrates) locked up in shale, sandstones and peat-coal. The average content of carbon locked up in carbonates is far in excess than that locked up in shale-sandstone and coal. Weathering of carbonate rock liberates carbon to the atmosphere-ocean system with a residence time far less than one m.y. With regression, the amount of carbonate carbon that is likely to be released in the ocean-atmosphere is far in excess than that from organic carbon released from sandstone-shale-coal together. The difference in $\delta^{13}C$ value of carbonates and atmosphere is ~7.5‰, cabonates being more positive but the difference between organic carbon and atmosphere is ~18‰. So if carbon released from carbonate is more that 3.5 times than the carbon released from organic carbon (which is more likely the case in the event of regression) a positive shift in the atmosphere is expected. But instead, in general, a sharp negative spike is observed in the marine carbonates across the Permo-Triassic boundary.

Organic carbon exposed during regression may get attached to atmospheric oxygen. Various estimates of atmospheric oxygen (Garrel and Lerman, 1984; Berner, 1989, 1990) show that atmospheric oxygen was rapidly decreasing from Carboniferous times giving one of the lowest concentration at the Permo-Triassic boundary. So the oxidative potential of organic carbon at Permo-Triassic boundary was much low at the Permo-Triassic boundary. On the contrary, red beds at the P-T boundary suggests an oxidative environment.

Arid Climate

A coal gap at the P-T boundary (Faure et al. 1995) may mean a decrease in primary productivity and/or non preservation of plant materials. A model with high CO_2 (due to release of locked CO_2) in the atmosphere should see higher productivity of land plants along with a shift towards negative values of $\delta^{13}C$ in organic matter. But then why were plants not preserved? Lignin is the most important constituent in plant matter that gets preserved as coal/peat. In modern environments, lignin is mainly destroyed by basidiomycetes organisms (like mushroom and allied algae) however, there lignolitic activity gets greatly reduced with decrease in oxygen in the atmosphere (Robinson, 1990), which was the case during P-T

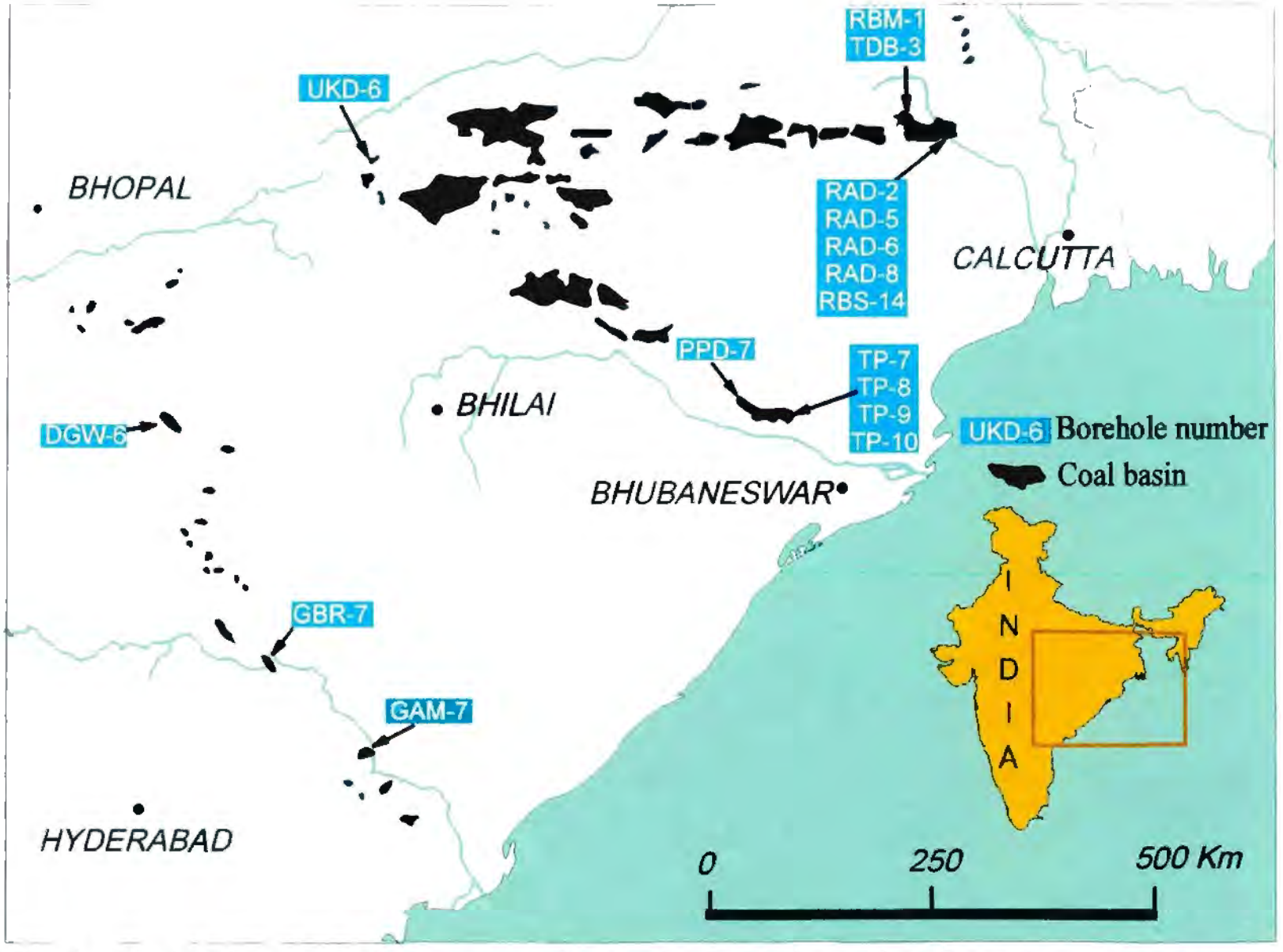

Fig. 6.4. Coal basins of part of Peninsular India showing borehole locations for carbon isotope study.

boundary. Lignin is also degraded abiotically by ultraviolet radiation, ozone, etc. Arid climate gets lot of ultraviolet radiation suitable for lignin degradation.

In Permian time most coals formed in temperate belts of high latitude (Rotallack et al. 1996); But by the end of the Permian, the first red beds occurred signifying the onset of climate change or prevailing oxidizing environments

6.4. Carbon isotope stratigraphy of some Gondwana sequences

In this study, a number samples from terrestrial Gondwana sections from Peninsular India, South Africa and Madagascar have been investigated for C-isotope stratigraphy. In the case of samples from India, in most cases, the same set of samples were also investigated for detailed palynology by collaborators from the Virbal Sahni Institute of Paleobotany, Lucknow, India. This allowed calibration of palyno-stratigraphy with C-isotope stratigraphy. Similarly, representative samples across the lower part of the Gondwana sequences from the Lingsburg basin in South Africa and from the Morondava basin in Madagascar have been analyzed for C-isotope stratigraphy. In the following section, analytical procedure and results of this study are summarized.

6.4.1 Sampling method

In general, samples were collected at small (2-4 m) intervals. In some cases, samples representing larger intervals were also collected. Samples from Peninsular India are all from 13 boreholes in different Gondwana basins within Peninsular India (Fig. 6.4). Two of these boreholes intersected almost the entire part of the Lower Gondwana sequence (i.e., from glaciogenic Talcher Formation at the lower part of Gondwana sequence to the reb-bed horizon of the Panchet Formation in the upper part of the Gondwana sequence). From other boreholes in Peninsular India only samples from across the Permian-Triassic boundary were sampled.

These sets of samples provided for comparative study of $\delta^{13}C_{org}$ signal across the Permian-Triassic boundary in different parts of a basin and among widely separated basins. Samples from the Morondava basin Madagascar and from the Laingsburg sub-basin of the Karoo basin of South Africa include samples across parts of the Upper Permian. These samples were collected from scarp sections. Samples from Madagascar were collected and processed by Mr. Nicolas Rakotosolomofo (M. Sc dissertation).

Samples with visible plant remains were preferrentially seperated for analysis. Where visible plant remains were not observed, dark grey or brown coloured samples were preferred over pale coloured ones. About 0.5 mg of organic matter were used for the analyses.

Sample preparation

All analyses were carried out at the University of Cape Town Stable Isotope Facility housed at the Archeology Department. Analyses carried out in this study constitute first set of analyses of coal and carbonaceous shales from geological samples using an automated CN analyzer attached to a mass spectrometer. Therefore, in the following section, sample preparation is discussed in some detail. Individual samples were cleaned with water to remove dirt adhered to the samples. Small chips of each sample were visually inspected for carbonaceous remains. Where present, the carbonaceous matter in samples were scooped with a knife and were kept in vials for further processing. Samples without visible carbonaceous matter were ground to coarse grain sizes (~60 mesh) and inspected under a binocular microscope for visible finer grained carbonaceous matter. Such carbonaceous matter was collected with a tweezer and were kept in vials for further processing. In samples where carbonaceous matters could not be separated in this way, a small (~1 gram) portion of the sample was finely ground for further processing.

Samples were immersed in dilute (1:6) HCl and kept in an oven at ~60°C for ~10 hours to

dissolve any carbonate that may have been present in the sample. It is essential to ensure that the sample is sufficiently fine ground so that HCl acid can permeate through the entire sample. This will ensure that carbonates and bicarbonates are dissolved. After all the samples were treated with HCl, they were washed a few times thoroughly with distilled water and then dried at ~60°C in an oven. Each dried sample was then inspected under a binocular microscope for final picking of the sample. For analyses in the automatic CN analyser attached to a mass spectrometer, it is essential that the sample size remains within a narrow limit so that CO_2 obtained by oxidizing the sample is similar in quantity to the reference gas used for analyses. Larger or smaller sized samples do not yield precise analyses. For the mass spectrometric set-up used for present analyses, coal or carbonaceous shale samples weighing ~0.06 mg gave good analyses. For samples in which carbonaceous matters could be seperated, physical description of each samples was noted. In samples where carbonaceous matter was not present a portion of the bulk sample was taken for analyses so that it contained ~ 0.06 mg of carbonaceous matter. Samples were packed within ~100 micro litre sized tin micro-capsules. Once packed samples are ready for analysis.

All samples in the present study were analysed in Finigan Mat® 252 mass spectrometer fitted with an automatic CN analyser with automatic sample loader. In this system the sample is loaded in a tin vial which is burnt in the CN analyser at ~1000°C. The resultant gas is passed through a dehydrant material and then through a gas chromatometer where CO_2 gas from the sample is separated from other gases. Separated CO_2 gas is then passed to the mass spectrometer for isotopic analyses. An internal standard was first calibrated using NBS-21 standard and one internal standard was analysed alternated almost with every 5 samples.

6.4.2. Analytical results

Analytical results for various borehole samples, recalculated with respect to PBD standard, are presented in Figs. 6.5-6.11. Table 6.1 summarizes isotopic results.

Table 6.1. Isotopic characteristics of samples analysed from different Gondwana basins of India, Madagascar and South Africa.

Gondwana basin	Bore-holes	Stratigraphic section	Isotopic characteristics	Discussion
Raniganj Coalfields, West Bengal, India	RBM-1;	13 samples from a 50m thick section across the Permian-Triassic boundary.	3 sharp negative excursions ($\delta^{13}C_{org}$ < -30) interspaced by positive excursions ($\delta^{13}C_{org}$ > -25) spanning a thickness of ~20m exist (Fig. 6.5).	The lowermost negative incursion is about 5m below palynologically defined Permian-Triassic boundary
	R-14 + TDB-3);	150 samples from a ~850m thick section from the top of glaciogenic Talcher Formation (Lower Gondwana) to the bottom of the Panchet Formation (Upper Gondwana)	There are at least two pronounced negative ($\delta^{13}C_{org}$ <-30 ‰) spikes near the palynogically defined Permian-Triassic boundary. One of them is just below the P-T boundary while the other is ~50m above the P-T boundary. In between these two negative spikes there is a zone of ~15m thickness with highly positive $\delta^{13}C_{org}$ value (~ -16 ‰). The total range of variation (from the most positive value to the most negative value) across the Permian-Triassic boundary is ~ 20 ‰). Below the P-T boundary there are a number of cyclic repetitions of $\delta^{13}C_{org}$ value of the order of ~3-4 ‰ which is superposed by a noise (random variation) of ~1-2‰ (Fig. 6.5, 6.6).	While the large negative incursion in the $\delta^{13}C_{org}$ (>5-6 ‰) is characteristic of the P-T boundary. A high positive value of ~ -16 ‰ in association of sharp negative spikes giving a total range of variation as high as ~20 ‰, is, however, not recorded yet from across the Permian-Triassic boundary is, however, unknown and the cyclic variation of 3-4 ‰ (Fig. 5.6) is possibly related to climatic changes. Random variation of 1-2 ‰ is probably due to natural variation in the organic matter and/or due to post-depositional changes.

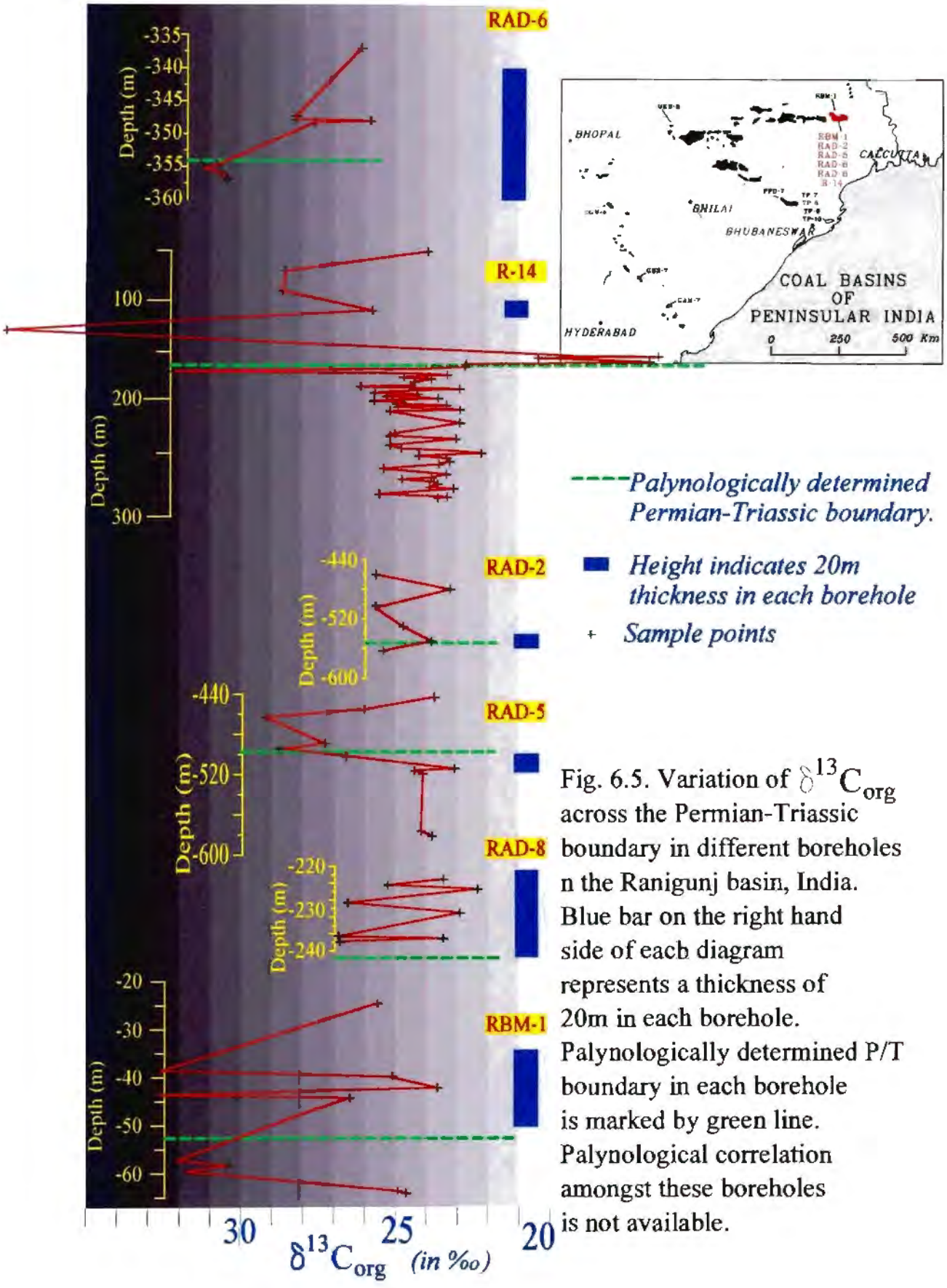

Fig. 6.5. Variation of $\delta^{13}C_{org}$ across the Permian-Triassic boundary in different boreholes n the Ranigunj basin, India. Blue bar on the right hand side of eacb diagram represents a thickness of 20m in each borehole. Palynologically determined P/T boundary in each borehole is marked by green line. Palynological correlation amongst these boreholes is not available.

Gondwana basin	Bore-holes	Stratigraphic section	Isotopic characteristics	Discussion
	RAD-2:	7 samples from a ~160m thick section across the Permian-Triassic boundary.	$\delta^{13}C_{org}$ value for 7 analysed samples vary randomly between -24 and -27 ‰. No definite pattern is evident is which is likely to be result of very sparse sampling density (Fig. 6.5).	
	RAD-5	11 samples across a 150m section from across the Permian-Triassic boundary.	There is a zone of pronounced -ve incursion ($\delta^{13}C_{org}$ value between -27 and -30) just above the palynologically defined P-T boundary. Below and above this zone $\delta^{13}C_{org}$ value is ~24 ‰ (Fig. 6.5).	The large -ve incursion at the P-T boundary is possibly related to some P-T event.
	RAD-6	10 samples across a~25 m thick section from across the P-T boundary	A large -ve excursion ($\delta^{13}C_{org}$ value <-30 ‰) spanning ~5-10m thickness exists around the palynologically defined Permian-Triassic boundary (Fig. 6.5).	The large -ve incursion at the P-T boundary is possibly related to some P-T event.
	RAD-8	10 samples across a~16 m thick section across the P-T boundary	$\delta^{13}C_{org}$ values of samples show 3 sharp negative spikes of ~4‰ interspaced by positive spikes (Fig. 6.5). However, negative excursion is much less pronounced in this section than in other sections.	Negative incursions in this section may be related to large negative excursions generally present across the P-T boundary.

Gondwana basin	Bore-holes	Stratigraphic section	Isotopic characteristics	Discussion
Talcher basin, India	TP-8:	178 samples from a 1000m section spanning from the top of the Talcher Formation (glaciogenic) in the lower part of the Gondwana sequence, up to the middle part of the Kamthi Formation in the upper part of the Gondwana sequence.	This set of samples covers almost the entire Lower Gondwana sequence in the peninsular India. The majority of the samples have $\delta^{13}C_{org}$ values between -26 and -23‰. There are three pronounced negative incursions ($\delta^{13}C_{org}$ value <-30‰) within a span of ~60m thickness across the P-T boundary. The lowermost one of these excursions peaks just below the palynologically defined P-T boundary. There are a number of cyclic variation in the $\delta^{13}C_{org}$ values in the Permian section. Positive and negative gradient in such cyclicity often coincide with distinct palynozones (Fig. 6.7, 6.8).	The presence of three large negative excursions across the P-T boundary spanning over a thickness of ~60m indicates that negative incursions at the P-T boundary are not a single short-lived event. Cyclic variation of 3-4‰ in the coal-bearing Permian section may be related to climatic variations since such variation also broadly coincide with palynozones. This needs much greater statistical analysis, beyond the scope of this thesis.
	TP-9:	9 samples from a 42m section across the palynologically determined Permian-Triassic boundary.	Two samples, one above the P-T boundary and the other below the P-T boundary have $\delta^{13}C_{org}$ values<-28‰. Other samples have $\delta^{13}C_{org}$ values between -20 and -26‰ (Fig. 6.7).	No definite pattern could be identified although very large negative values of two samples may be related to the P-T events.
	TP-10	11 samples spanning a 82m section across the palynologically identified P-T boundary	A large negative incursion of ~5‰ is present ~10m above palynologically determined P-T boundary (Fig. 6.7).	The negative incursion above the P-T boundary is probably related to the P-T event.

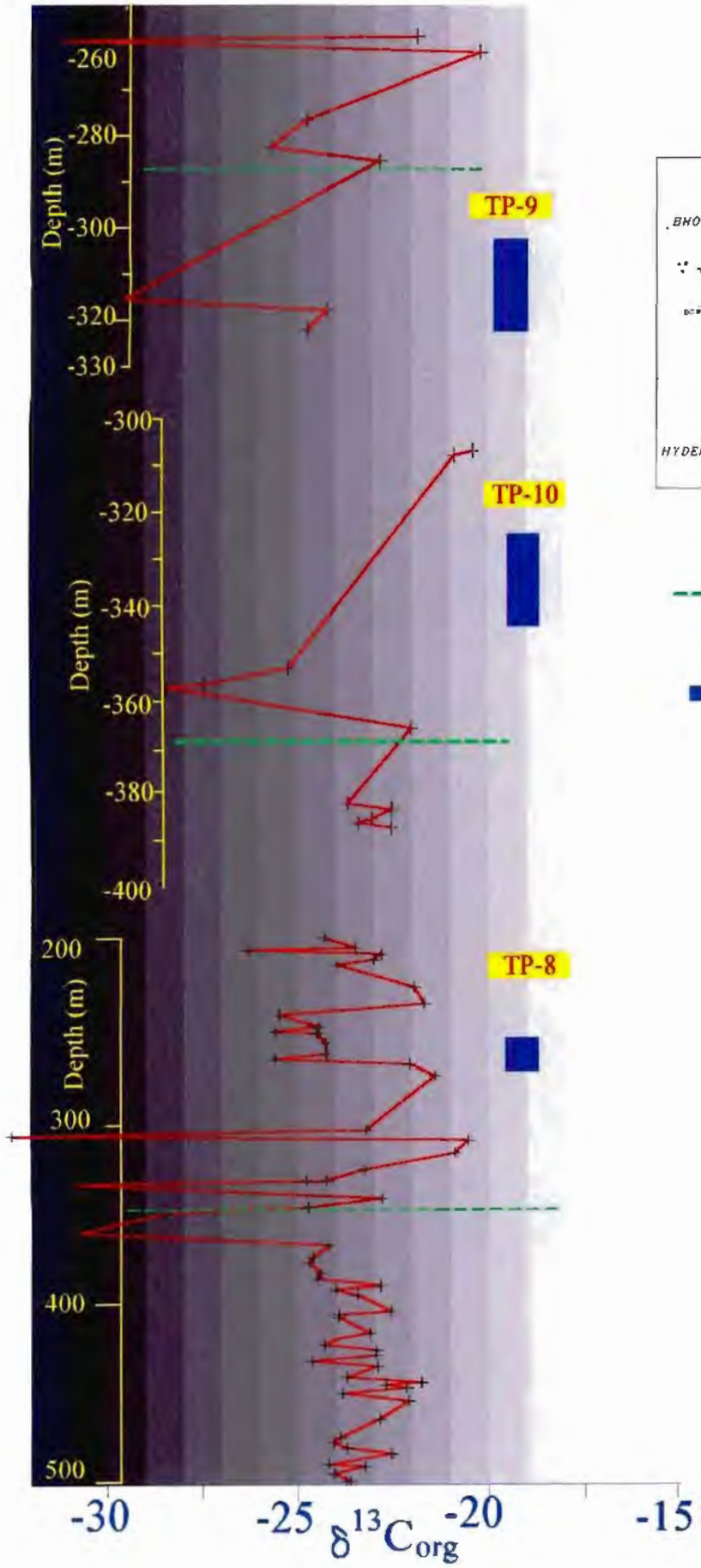

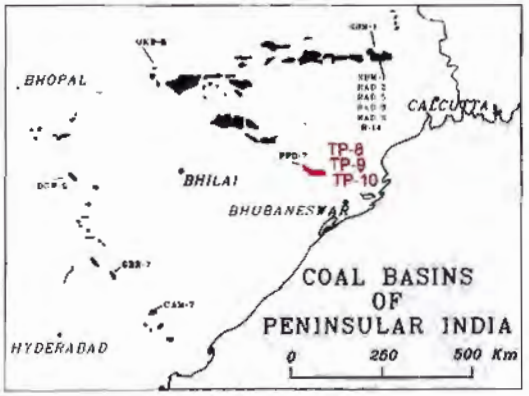

Palynologically determined Permian-Triassic boundary.

Height indicates 20m thickness in each borehole

Fig. 6.7. Variation in the organic carbon isotope ratio across the Permian-Triassic boundary in different bore-holes in the Talcher basin, India. Blue bar on the right hand side of each diagram represents a thickness of 20m in each borehole. Palynologically determined P/T boundary in each borehole is shown by green line. In the TP-9 borehole, the palynological boundary is uncertain. However, Upper Triassic palynoflora are present above 287m depth. Note the variation from one to three negative spikes in boreholes less than 30 km apart.

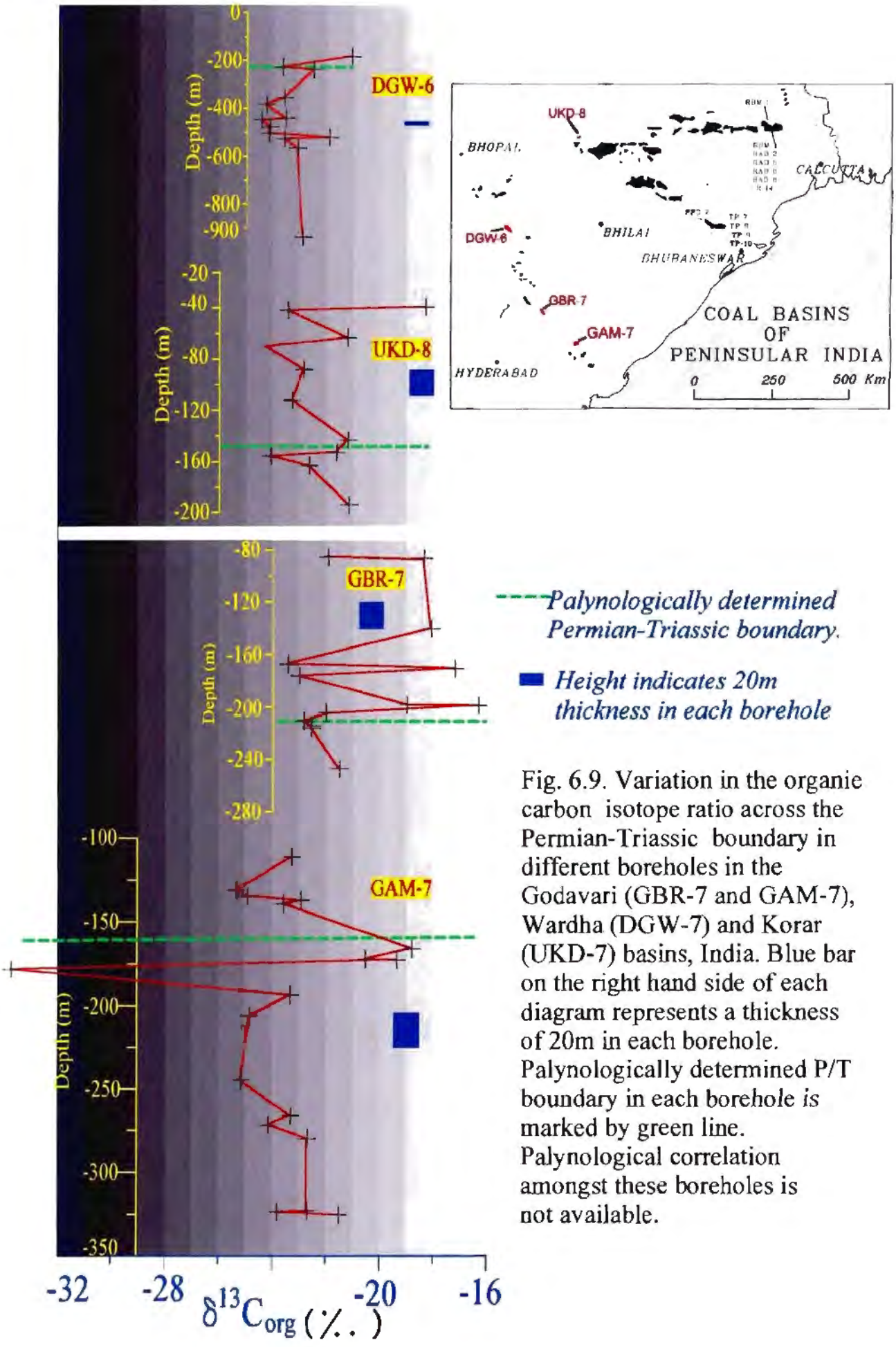

Fig. 6.9. Variation in the organic carbon isotope ratio across the Permian-Triassic boundary in different boreholes in the Godavari (GBR-7 and GAM-7), Wardha (DGW-7) and Korar (UKD-7) basins, India. Blue bar on the right hand side of each diagram represents a thickness of 20m in each borehole. Palynologically determined P/T boundary in each borehole *is* marked by green line. Palynological correlation amongst these boreholes is not available.

Gondwana basin	Bore-holes	Stratigraphic section	Isotopic characteristics	Discussion
Godavari Coalfield, Andhra Pradesh, India	GAM-7	**18** samples spanning a 224m section across the palynologically identified P-T boundary	A large (~8‰) negative incursion is present ~10 m below palynologically defined P-T boundary. This negative incursion is followed by a positive incursion (Fig. 6.9).	Both negative and positive incursions may be related to the P-T event.
	GBR-7	**14** samples spanning a section of 161m across the palynologically determined P-T boundary.	A 50m thick zone just above the P-T has three negative spikes interspaced by positive spikes. However the large negative spikes that are normally associated with P-T boundaries could not be detected in this section (Fig. 6.9).	It is not certain whether interspaced negative and positive excursions are related to the P-T event or not.
Wardha Basin, Madhya Pradesh, India	DGW-7	**12** samples spanning a depth of 754m across the palynologically determined P-T boundary	Samples are very widely spaced making it difficult to detect any negative incursion that might be present associated with the P-T boundary (Fig. 6.9).	A zone of ~150m thickness within the Permian section has $\delta^{13}C_{org}$ values which are ~2-3‰ more negative than the rest. It is not known, however, whether this zone of negative incursion is related to the P-T event.
	UKD-7	11 samples from a 160m thick section across the palynologically defined P-T boundary	There is no large negative spike associated with P-T boundary There is however ~3‰ variation within this section (Fig. 6.9).	

Gondwana basin	Bore-holes	Stratigraphic section	Isotopic characteristics	Discussion
Morondava basin, Madagascar		37 very widely spaced samples spanning a thickness of ~3km within Permian section.	The whole section is within the Permian. A very large (~6‰) negative incursion is present in the lower part of the section within the coal-bearing horizon (Fig. 6.10).	Such large negative incursion within the Permian coal-bearing horizons in India.
Laingsburg basin, South Africa		40 sample spanning from top of the glaciogenic Dwyka Formation to the Upper Permian Vischkuil Formation	The whole section is within Permian. There is sharp variation (of the order of ~4‰) in the $\delta^{13}C_{org}$ values across the lithostratigraphic boundaries (Fig 6.11)	Sharp break across lithostratigraphic boundaries highlights importance of using $\delta^{13}C_{org}$ values for high-resolution stratigraphy.

6.4.3. $\delta^{13}C_{org}$ variation across the P-T boundary

6.4.3.1. Raniganj coalfield, India

Samples from seven boreholes (RAD-2,5,6,8; R-14, TDB-3 and RBM-1, Table 6. ; Fig. 6.5) have been analysed. Of these, five boreholes have intersected the palynologically defined Permian-Triassic boundary (Fig. 6.5). Sharp negative spikes have been detected in four of these boreholes (RAD-5,6, RBM-1 and R-14). In these boreholes $\delta^{13}C_{org}$ values becomes more negative than -28‰. The zones of negative incursion (interspaced by positive incursions) span borehole thicknesses between ~200m (RBM-1) and ~40m (RAD-5). In RAD-2, sampling density is thin and any negative incursion that might be present has not been detected.

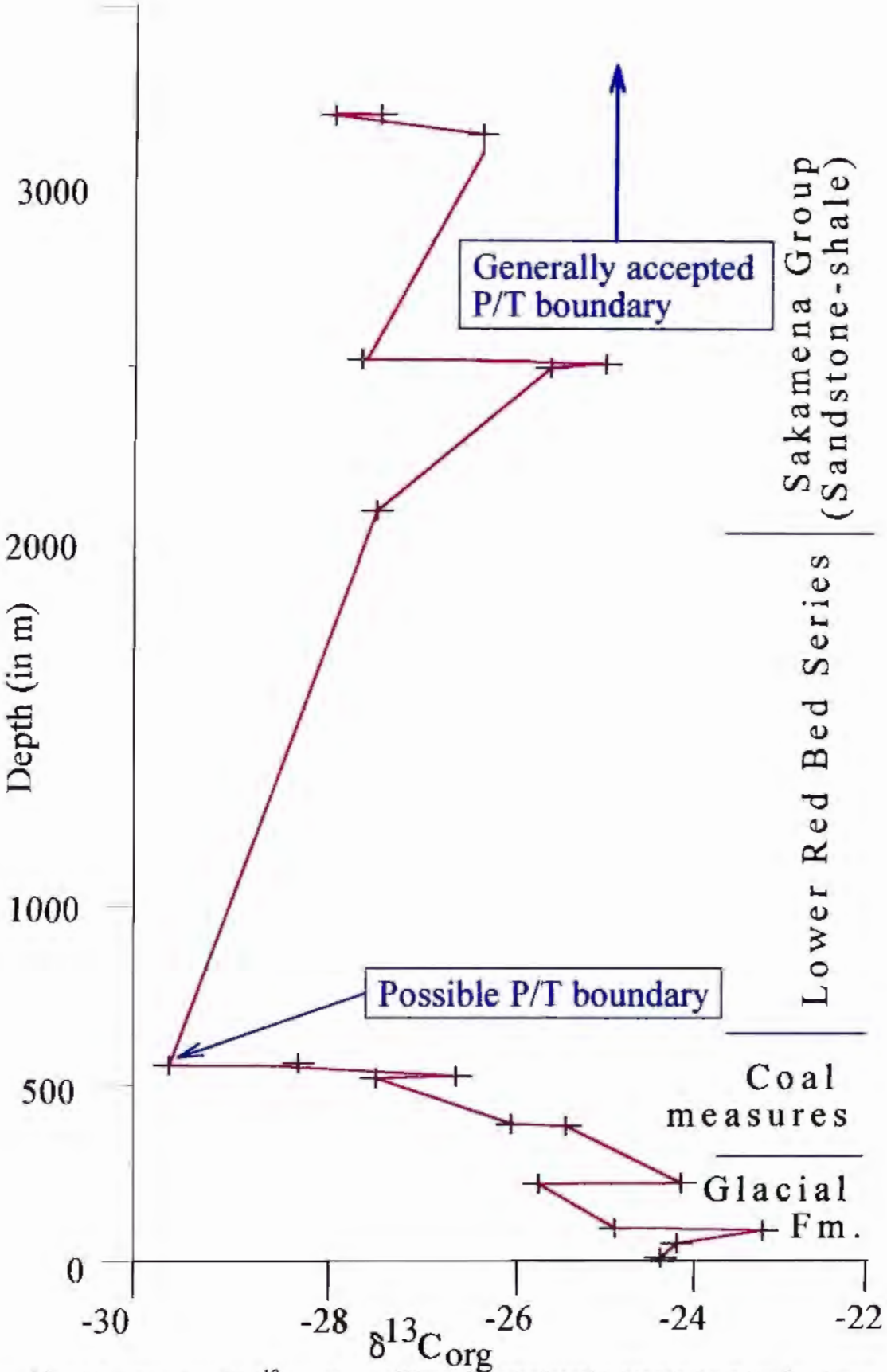

Fig.6.10 Variation in the $\delta^{13}C_{org}$ across different lithostratigraphic boundaries in the Gondwana sediments in the Morondava basin, Madagascar. Lithostratigraphy of the basin in also indicated. Permian-Triassic boundary is generally taken be within the Sakamena Group. However, a large (~6%) negative spike in the $\delta^{13}C_{org}$ in the upper part of the Coal Measures, and presence of red bed sequence above the Coal Measures points to the similarity with the P-T boundary sections in coal basins of India. Thus, the P-T boundary in the Morondava basin may as well be located near the upper part of the Coal Measures. Samples collected and processed by N. Rakotosolofo. For further detailed analyses see N. Rakotosolofo, M. Sc., in preparation)

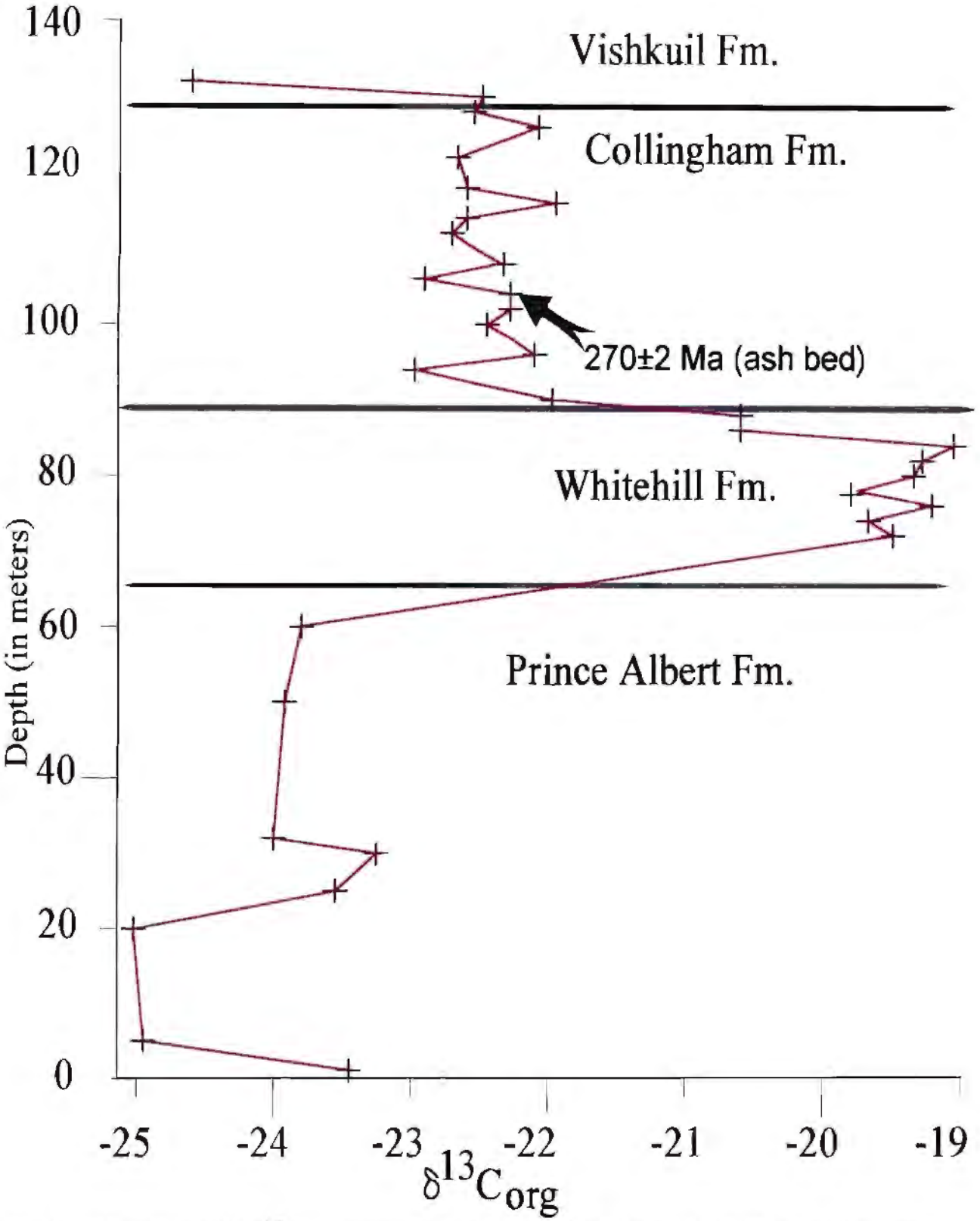

Fig.6.11 Variation in the $\delta^{13}C_{org}$ across different lithostratigraphic boundaries in the Gondwana sediments in the Laingsburg sub-basin of South Africa. Age shown in the arrow position is U-Pb age on zircon from intercalated ash bed (personal communication with Sam Bowring, MIT, USA). The Permian-Triassic boundary is not exposed in this section.

6.4.3.2. Talcher Coalfield, India

Samples from three boreholes (TP-8, 9 and 10) were analysed, all of which intersected the palynologically defined Permian-Triassic boundary (Fig. 6.7). TP-8 and TP-10 show sharp negative incursions associated with the Permian-Triassic boundary. In TP-9, the palynological P-T boundary is not welldefined. However Triassic palynoflora exists at least up to 288 m borehole depth. One sample having $\delta^{13}C_{org}$ value of -30‰ has been analysed at 315m depth, which may or may not be related to the P-T event. In TP-10, the sharp negative incursion is present within ~10 m above the palynologically defined P-T boundary. In the TP-8 borehole, three sharp negative incursions associated with the P-T boundary spans a borehole depth of ~60m.

6.4.3.3. Godavari, Wardha and Korar coalfields, India

Samples from two boreholes (GAM-7 and GBR-7) from the Godavari basin and one each from the Wardha basin (DGW-6) and the Korar basin (UKD-8) have been analysed. Of these, only GAM-7 shows a sharp negative incursion of ~8‰, followed by a positive incursion. In other boreholes, no regular pattern of variation across the P-T boundary is detected.

6.4.4. $\delta^{13}C_{org}$ stratigraphy in Gondwana sections

During the present study, a large number of samples were collected from two boreholes sections in Talcher (TP-8; 180 samples) and Ranigunj (TDB-3; 160 samples) Gondwana basins of India which intersected a substantial portion of the Gondwana succession in those basins, from the glacial deposits in the lower part to the Triassic red bed horizons in the upper part. Also ~40 representative samples covering a substantial portion of the Gondwana

successions from both the Laingsburg basin in South Africa and the Morondava basin in Madagascar were collected and analysed. These analyses show a similar variation patterns in the $\delta^{13}C_{org}$ values in the Gondwana successions across major lithostratigraphic boundaries (Fig. 6.10; 6.11) and also allow a comparative study of such variations across different continents (Fig. 6.12)

6.4.4.1. $\delta^{13}C_{org}$ stratigraphy in the Talcher basin, India

In this borehole 180 samples from the lower glaciogenic Talcher Formation to the Panchet Formation in the Upper Gondwana have been analysed (Fig. 6.8). Here, a number of cyclical changes, with an amplitude of ~3‰ in the $\delta^{13}C_{org}$ values, are present in the Permian section of this borehole. The overall positive gradient of these cyclical pattern often coincides with onset of a coal cycle, while negative gradients generally coincide with fluvial succession. Gradients in the cyclical changes also show moderately good correspondence with palynozones identified in this section. Near the P-T boundary within a zone of ~50m thickness, there are at least three large (~6‰) negative incursions interspaced by normal or positive incursions Above the P-T boundary, normal $\delta^{13}C_{org}$ values of ~25‰ are present.

6.4.4.2. $\delta^{13}C_{org}$ stratigraphy in the Raniganj basin, India

In this borehole 160 samples spanning from the glaciogenic Talcher Formation to the Panchet Formation in the Upper Gondwana have been analysed (Fig. 6.6) Similar to the TP-8 borehole, here too are a number of cyclical variations with an amplitude of ~3‰ in the $\delta^{13}C_{org}$ values of the Permian section. Detailed lithological logging and palynozones in this borehole are not yet available. At the P-T boundary, two large (>6‰) negative incursions are present within a span of ~40m thickness. Above the P-T boundary, normal values for $\delta^{13}C_{org}$ prevail.

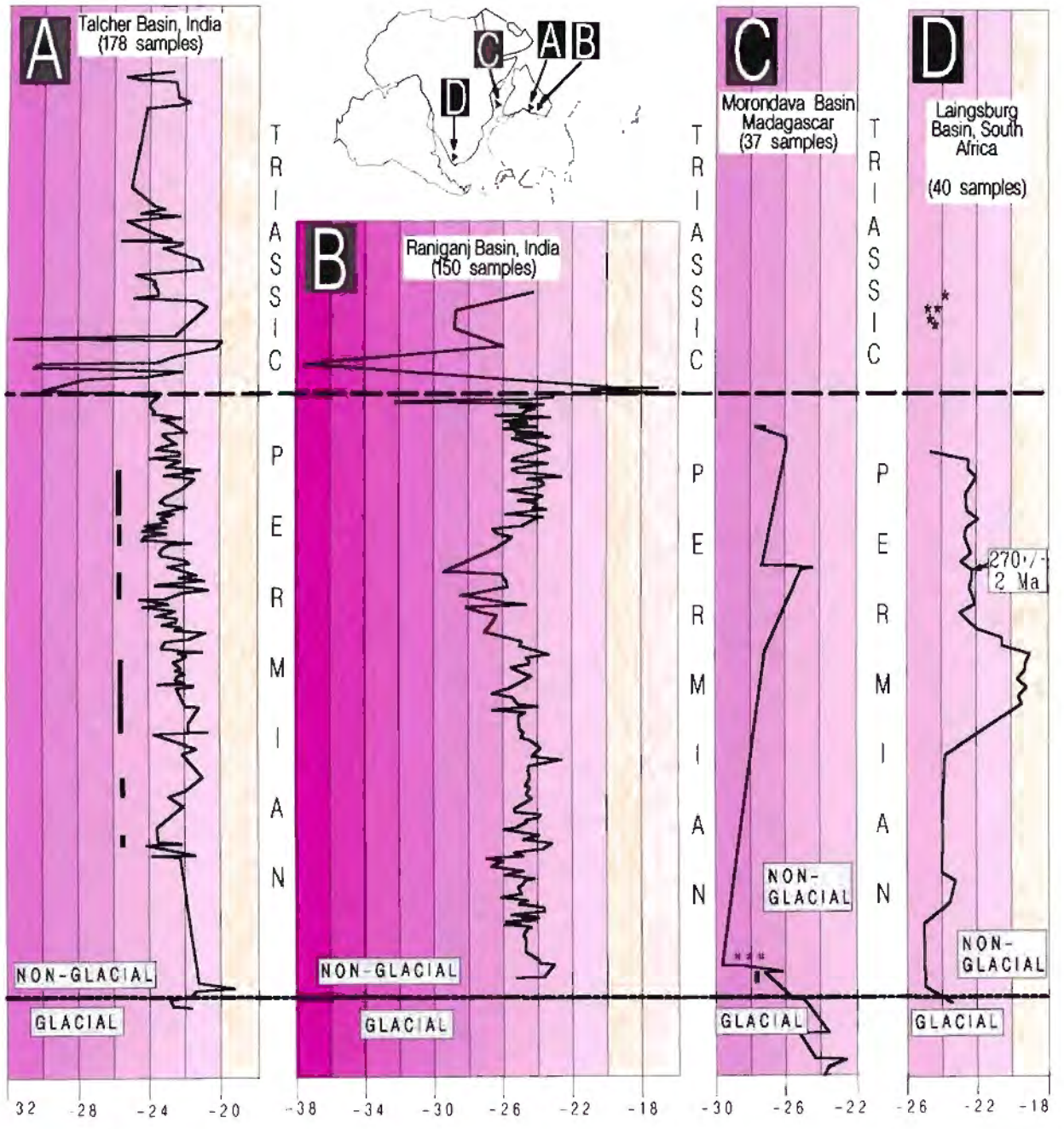

Fig 6.12 Variation in $\delta^{13}C$ of terrestrial plant remains in Gondwana sequences from different Gondwana fragments. A Talcher basin, India; B Raniganj basin, India; C Morondava basin Madagascar; D Laingsburg basin South Africa. Sequences of A and B are the best developed Gondwana sections and can be taken as chemostratigraphic references for terrestrial Gondwana sequences. Permian Triassic boundary in A and B are palynologically defined. Correlation between detailed palynostratigraphy and organic carbon isotope chemostratigraphy in these two sections are ongoing. Permian Triassic boundary in C and D are extrapolated from previous work on C it is palynologically defined and in D it is defined by vertebrate paleontology). Our C isotope work has not yet delineated the P T boundary in these two sections. Age constrains in section D is by U Pb single zircon age from an ash bed sample in this section (Som Bowring personal communication 1998). Analyses of Triassic samples in D (*) are from Faure et al., (1995). Glacial boundaries are defined lithostratigraphically. The Permo Triassic boundary in the Morondava basin of Madagascar may have been misplaced and may instead be represented lower in the lithostratigraphic sequence marked by (**) as suggested by sharp negative excursion at the lower part of the sequence (detailed work in progress V. Rakotosolofo M. Sc. thesis). ▮ Coal cycle Vertical scale is adjusted to align logs with lower and upper datum planes, i.e., the Permian Triassic boundary at the top and the glacial nonglacial boundary at bottom

6.4.4.3. $\delta^{13}C_{org}$ stratigraphy in the Morondava basin, Madagascar

In the Morondava basin of Madagascar, the coal-bearing horizon is condensed compared to the two basins described above. Here surface samples from a number places from the lower glaciogenic horizon in the lower part of the Gondwana succession to the Upper Gondwana, red bed succession, represented by the Sakamena Group have been sampled. Analyses of the samples show a large (~6‰) negative incursion towards the top of the Coal Measures. Whether this large negative incursion is related to the P-T event is not known. However, on the basis of similarity of the spikes at the P-T boundary and lithologic succession in India, I speculate this large negative spike in the Morondava basin may represent the P-T boundary. Above this spike, the $\delta^{13}C_{org}$ values become more positive. In the Morondava basin, the P-T boundary is generally taken to be present within the Sakamena Group which lies above Lower Red Bed Series although no paleontological work is definitive (N. Rakotosolofo, M.Sc.thesis).

6.4.4.4. $\delta^{13}C_{org}$ stratigraphy in the Laingsburg basin, South Africa

There are no coal beds in this part of the Karoo basin of South Africa. Here the glaciogenic Dwyka Formation at the bottom is succeeded by the Prince Albert Formation, the White Hill Formation, the Collingham formation and the Vischkuil Formation (Smith, R. M. H., 1990). The lower part of the Gondwana succession in this basin is very similar to those in the Madagascar and in India (M. de Wit., 1998, personal communication). Forty samples across four major lithostratigraphic horizons (the Prince Albert Formation, the White Hill Formation, the Collingham Formation and the Vischkuil Formation) have been analysed. There is a sharp variation of ~3-4‰ in the $\delta^{13}C_{org}$ values across lithostratigraphic boundaries (Fig. 6.11). The P-T boundary is known to occur above this sequnce. However, a few analyses from Triassic Gondwana sediments from an adjacent Gondwana basin are available (Faure et al. 1995). Those data have been plotted in Fig. 6.12 along with present analyses. Analyses of 40 samples across the P-T boundary are in progress (N. Rakotosolofo, M.Sc. thesis).

6.5. Discussion

A broad pattern of cyclical variation in the $\delta^{13}C_{org}$ values within the Permian sections of the Gondwana successions and 1 to 3 sharp negative incursions at the P-T boundary spanning ~50m thickness of sediments are present in both Ranigunj and the Talcher basins of India. In the Talcher basin, the cyclical variation in the Permian section is seen to broadly correspond with the palynological asseblages which suggests that cyclical variation in the $\delta^{13}C_{org}$ values may be used for high-resolution stratigraphic correlation. Because of non-availability of palynological data from the Ranigunj coalfield (TDB-3 borehole), it is not known now whether the cyclical variation in both the Talcher and the Ranigunj coalfields are stratigraphic equivalents. A random variation of ~2-2.5‰ is superposed on the cyclical variation patterns of both the Ranigunj and the Talcher coalfields. Assuming that the environment remained broadly similar, such variation could be explained by a number of ways. For example, there is always some variation in $\delta^{13}C_{org}$ value of different parts of plant both in arid land (Ehleringer, 1988) and in tropical wetland (Medina et. al., 1986). As a whole, leaves are more negative in $\delta^{13}C$ than stems and roots. And such variation could be as high as 3‰.

From visual observation of the trends in the $\delta^{13}C_{org}$ in Talcher Coalfield (TP-8; Fig. 6.8) borehole, Fig. from the Barakar Formation in the lower of the Gondwana sequence to the end of Permian there are some cyclic variation in the $\delta^{13}C_{org}$, having an amplitude of ~3‰ It appears that a coal cycle is broadly associated with increase in $\delta^{13}C_{org}$ while a clastic sediment cycle is associated with decrease in $\delta^{13}C_{org}$ value. The start of a coal cycle signifies greatly enhanced tree growth, which augments the biospheric removal of carbon dioxide from the atmosphere. CO_2 was generally present in considerably greater concentrations than it is today (Berner, 1990; Yapp and Poth, 1992). However, because of higher removal of atmospheric CO_2 due to higher photosynthetic rate, there is a limiting factor to which atmospheric CO_2 can rise. According to Idoso (1991) for current anthropogenic emission values and size of global forest, the CO_2 content of the atmosphere could only rise by only

another 170 ppmv. Continuation of increased photosynthesis depletes atmosphere of ^{12}C causing plants becoming more positive. An heavier atmospheric CO_2 should also cause carbonates deposited during that time to become enriched in ^{13}C. Gruszczynski et al. 1989 reports a positive spike in marine carbonate in Upper Permian time (Kazanian- Tartarian boundary). Similar positive spike of ~ 6-8‰ also precedes negative spike at the Permian-Triassic boundary in carbonate rocks of Delaware Basin of Western Texas (Magaritz et al. 1983). A positive spike also precede negative spike at the Ordovician - Silurian boundary at South China (Wang, 1993). Erwin (1993) calculated that if rapid oxidation of buried organic carbon is the sole cause of negative incursion at the Permian -Triassic boundary then oxidation of 6500 to 8400 gigatons of carbon are necessary compared to total volume of 800 gigatons in living biomass. This means a very large increase in CO_2 content of the atmosphere is necessary.

To summarize, this present study demonstrates that $\delta^{13}C_{org}$ analyses have great potential for use as a chemostratigraphic tool for intrabasinal and interbasinal correlation of Gondwana sequences. However, it is needed to calibrate this tool with other known methods of correlation such as lithostratigraphy, palynology. But the presently available database is too meagre for such an integrated apporoch. It is beyond the scope of this thesis at this stage, to analyze the data viz., a viz. other associated aspects like the origin of the P/T spike and cylcical variation of $\delta^{13}C_{org}$ within Gondwana sequence etc.

Appendix to Chapter 4

A.4.1. U-Pb dating of zircon and monazite and its application in high-grade metamorphic terrains.

A.4.2. Methodology of various zircon analytical techniques: their uses and limitations and a comparative study.

A.4.3. Pb-blank in U-Pb single crystal work- its sources and measures adopted at UCT to reduce it.

Appendix-A.4.1: U-Pb dating of zircon and monazite and its application in high-grade metamorphic terrains.

A.4.1.1 U-Th-Pb geochronology: Introduction

U-Th-Pb dating method uses three different decay systems: $^{238}U \rightarrow ^{206}Pb$; $^{235}U \rightarrow ^{207}Pb$ and $^{232}Th \rightarrow ^{208}Pb$. Coupling of these three decay systems provides internal checks on the age information obtained from their analyses. This unique feature of the U-Th-Pb dating method allows verification of one of the important assumptions in geochronology: that the isotopic system remained closed with respect to the parent and daughter isotopes. Thus, this technique is one of the most precise geochronological tool in polymetamorphic terrains where isotopic systems are prone to loss or gain in parent or daughter isotopes. In the present work, the U-Th-Pb method has been used extensively for precise geochronology. The principles of the U-Th-Pb technique are discussed below:

A.4.1.2. Principles of U-Th-Pb geochronology

There are four stable isotopes of lead. They are ^{204}Pb, ^{206}Pb, ^{207}Pb and ^{208}Pb. Except for ^{204}Pb, these are all radiogenic, being final decay products of ^{238}U, ^{235}U and ^{232}Th, respectively. For a system of age t, the equations for the nuclides involved in each decay scheme can be written as below:

$$^{206}Pb_P = ^{206}Pb_I + ^{238}U_P(e^{\lambda 238 t} - 1) \quad \text{.....(i)}$$

$$^{207}Pb_P = ^{207}Pb_i + ^{235}U_P(e^{\lambda 235 t} - 1) \quad \text{.....(ii)}$$

$$^{208}Pb_P = ^{208}Pb_I + ^{232}Th_P(e^{\lambda 232 t} - 1) \quad \text{.....(iii)}$$

where P indicates the abundance of a given nuclide at the present time and I indicates the initial abundance of that nuclide.

Half-lives ($t_{1/2}$) and the decay constants (λ) for these three decay series are as below:

Decay series	$t_{1/2}$, in Gyrs	Decay const., λyr^{-1}
$^{238}U \rightarrow ^{206}Pb$	4.47	1.55125×10^{-10}
$^{235}U \rightarrow ^{207}Pb$	0.704	9.8485×10^{-10}
$^{232}Th \rightarrow ^{208}Pb$	14.01	0.49475×10^{-10}

Some accessory minerals like zircon, baddyellite, monazite, allanite, sphene, rutile and apatite etc., preferentially incorporate uranium and exclude Pb. For the very little initial/common Pb that are present in these minerals, a correction can be made and then the equation (i) can be simplified as below:

$^{206}Pb^{*} = {}^{238}U(e^{\lambda 238t} - 1)$

where Pb^{*} represents radiogenic lead only. Taking ^{238}U to the other side yields the equation:

$^{206}Pb^{*}/^{238}U = (e^{\lambda 238t} - 1)$

Similarly, equation (ii) can be simplified to.

$^{207}Pb^{*}/^{235}U = (e^{\lambda 235t} - 1)$

Each of these two decay systems provide independent ages. Minerals which have remained closed with respect to U and Pb give concordant values of t from the above two equations. When $^{207}Pb^{*}/^{235}U$ and $^{206}Pb^{*}/^{238}U$ are plotted against each other, the locus of all points that represent the same age in both systems defines a curve known as concordia (Fig. A.4.1.1; Wetherill, 1956). Pb-loss and overgrowth in minerals cause the ^{235}U-^{207}Pb and ^{238}U-^{206}Pb ages to differ from each other and consequently the analyses plot off concordia. Very often, analyses of related samples lie on a straight line joining two points on concordia. Such straight

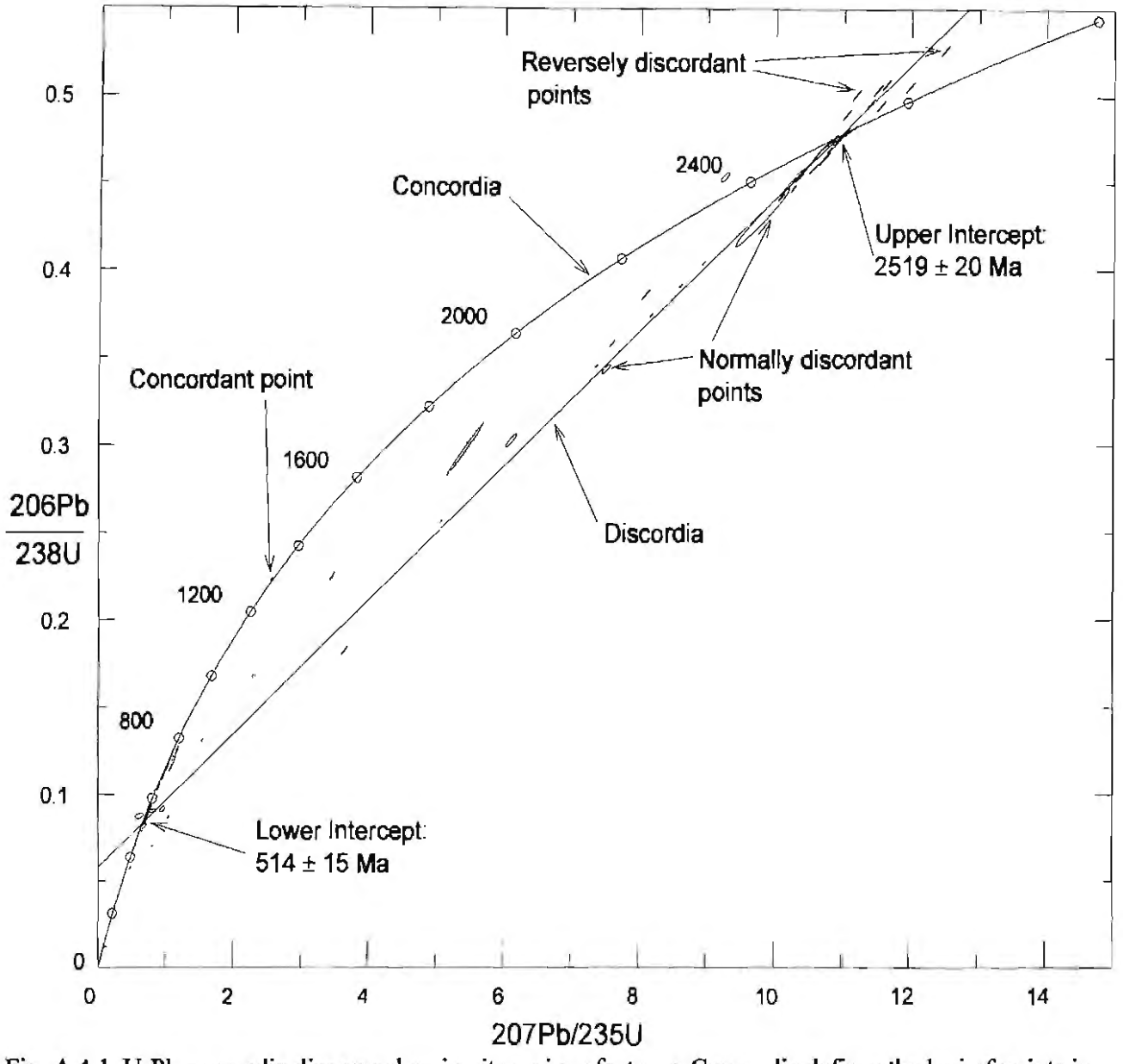

Fig. A.4.1. U-Pb concordia diagram showing its various features. Concordia defines the loci of points in a 206Pb/238U vs 207Pb/235U diagram having same 206Pb/238U and 207Pb/235U ages. A discordia is a chord joining any two points on the concodia. Sample points plotting on concordia are called concordant and provide a robust estimate of their crystallization age. Sample points which plot on the concave side of the concordia are called normally discordant and are usually caused by Pb-loss from the sample. Sample points which plot on the convex side of concordia are called reversely discordant and mayresult from U-loss or Pb-gain. The upper and lower intercepts of discordia on the concordia often approximates two different thermal events. However, caution is needed in such interpretation (see text).

lines are known as discordia. The present day ratio of ^{238}U to ^{235}U is 137.88. This ratio has changed over time because of the difference in the rate of decay of ^{238}U and ^{235}U. For example, when the Earth was accreted, this ratio was 3.17, it was 16 in late Archaean and 82 in late Proterozoic time. Since the rate of decay of ^{235}U is about six times faster than the ^{238}U, the relative rate of build up of radiogenic ^{206}Pb and radiogenic ^{207}Pb continuously changes and so the ratio $^{207}Pb/^{206}Pb$ varies systematically with age. Thus, the $^{207}Pb/^{206}Pb$ ratio in minerals gives their crystallization age if the system has remained closed with respect to the isotopes of Pb and U. This age is known as the $^{207}Pb/^{206}Pb$ age. In a concordia diagram the $^{207}Pb/^{206}Pb$ age is obtained by the intersection of concordia and a line joining the analysed point and the origin. The $^{232}Th \rightarrow ^{208}Pb$ decay series provides independent age information.

A.4.1.3. Geochemical behaviour of U, Th

In chemical environments typical of most magmas, uranium (atomic number 92) and thorium (atomic number 90) have comparable geochemical properties. They both form tetravalent ions with similar ionic radii (U^{+4}=0.1 nm; Th^{+4} =0.105 nm), and thus easily substitute for each other. Thorium has only one oxidation state, is insoluble in water and is one of the most inert element during exogenous processes. In contrast, U may takes on a hexavelant state, forming the uranyl ion UO^{+2}, which is highly soluble in water, and under oxidizing condition U may be significantly fractionated from Th.

A.4.1.4. Zircon geochronology

Zircon, a silicate of zirconium ($ZrSiO_4$), is one of the most useful minerals for high precision geochronometry mainly because of its resistance to thermal disturbances in respect to U and Pb (i.e., low diffusibility). U and Pb are strongly fractionated during the crystallization and growth of zircon because the ions of these two elements differ both in their charges (U is generally tetravalent U^{4+}, whereas Pb is generally divalent Pb^{2+}) and in their ionic radii (U^{4+}=1.00 Å; Pb^{2+}=1.29 Å, in VIII-coordination). In zircon, U^{4+} substitutes readily for Zr^{4+} which has an ionic radius of 0.84 Å. This explains the high U-content and high U/Pb ratios of zircon compared to other silicates, making zircon ideally suited for high precision geochronology.

A.4.1.5. Interpretation of U-Pb zircon ages

Zircons generally survive partial melting, entrapment in hot magmas and regional metamorphism without completely losing their age information. However, it is also known that in some cases, zircons tend to lose Pb during low grade metamorphism, fluid circulation, weathering or even without any apparently understood geological process (Mezger and Krogstad, 1997). Pb-loss, overgrowth and recrystallization often cause complications in zircon isotopic systematics. Pb-loss often occurs because Pb is much more incompatible in zircon crystal structure than U. Increase in temperature can cause preferential Pb-loss by diffusion or leads to recrystallization of damaged zircon.

Zircon grains that have remained closed with respect to U-Pb and Th-Pb isotopic systematics and do not have any younger overgrowth, should give consistent ages for all three decay systems ($^{235}U \rightarrow ^{207}Pb$, $^{238}U \rightarrow ^{206}Pb$ and $^{232}Th \rightarrow ^{208}Pb$). For the U-Pb decay systems, such grains should have concordant ages. Zircons with a single stage history of Pb-loss or overgrowth

should lie on a discordia line. In such cases, the upper intercept of discordia with concordia gives the age of the crystallization of the zircon grains while the lower intercept dates an event of Pb-loss and/or overgrowth. In general, discordant zircon grains fall on the concave side of concordia. Such discordant grains are called normally discordant zircons. Normally discordant zircon grains have $^{207}Pb/^{206}Pb$ age > $^{207}Pb/^{235}U$ age > $^{206}Pb/^{238}U$ age. In some instances, however, zircons fall on the convex side of concordia and are called reversely discordant grains. The cause of such reversely discordant ages is not well understood. Possible explanations for reversely discordant grains include Pb-gain or U-loss from the zircon grains. Reversely discordant grains have $^{206}Pb/^{238}U$ age > $^{207}Pb/^{235}U$ age > $^{207}Pb/^{206}Pb$ age. $^{208}Pb/^{232}Th$ ages often are more affected by both Pb-loss and Th-loss than the U-Pb ages. However, very often in young rocks $^{208}Pb/^{232}Th$ ages also approximates the age of the zircon grains and are concordant with U-Pb ages. Zircons having more than one episode of Pb-loss and/overgrowth often give a scattered plot on a concordia diagram. Any straight line passing through such grains that plot off concordia may not give any geologically meaningful age. The best estimate of the minimum age of such zircon grains is obtained from the $^{207}Pb/^{206}Pb$ age of the least discordant grain rather than from the upper intercept of discordia passing through some scattered points. Discordancy analyzed grains is generally expressed as the percent difference between the $^{207}Pb/^{206}Pb$ age and $^{206}Pb/^{238}U$ age expressed as percentage of the $^{207}Pb/^{206}Pb$ age (cf. Davis et al. 1997). In mathematical term this can be expressed as:

$$Discordancy(\%) = 100 \times \frac{(^{207}Pb/^{206}Pb\ age) - (^{206}Pb/^{238}U\ age)}{(^{207}Pb/^{206}Pb\ age)}$$

This definition of discordancy is good for analyses which plot near the upper end of the concordia and\or which have recent Pb-loss or overgrowth. In the present study many Archean rock samples have been affected by Neoproterozoic Pb-loss and/over growth which has caused many analyzed point spread over a discordia joining an Archean age and an Neoproterozoic age (Fig. 4.9; 4.19; 4.24). In such case, specially for analyses which plot far away from the upper intercept of discordia, the above definition of discorcancy do not reflect

the amount of Pb-loss or overgrowth. In this study, therefore, an alternative definition of discordancy has been used. In this new definition percent discordancy is distance of a particular analysis on the discordia from its upper intercept expressed as percent of the length of the discordia. Mathematically, percent discordancy can be expressed as:

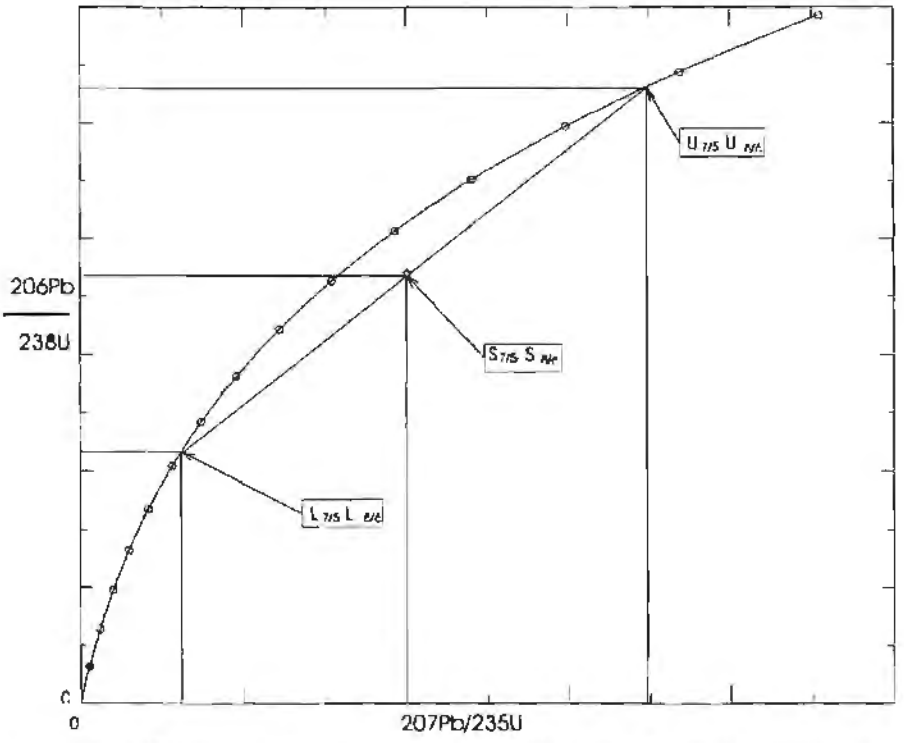

Fig. A.4.3. Diagram showing various parameters used for the new definition of discordancy

$$Discordancy\ (in\%) = 100 \times \frac{\sqrt{(U_{8/6}-S_{8/6})^2+(U_{7/5}-S_{7/5})^2}}{\sqrt{(U_{8/6}-L_{8/6})^2+(U_{7/5}-L_{7/5})^2}}$$

Where U, L and S denote isotopic ratios at the upper intercept, lower intercept and sample position respectively as shown in Fig. A. 4.3 and subscripts 8/6 and 7/5 stand for isotopic ratios of $^{238}U/^{206}Pb$ and $^{207}Pb/^{235}U$ respectively as shown in Fig. A.4.3.

It has been observed that zircon crystals sometimes tend to leak Pb continually and that this leakage is not strongly temperature dependent (Tilton, 1960). The most likely reason for low temperature loss must be related to the destruction of the zircon lattice by alpha-particles as a result of U-decay (=metamictization).

A.4.1.6. Zircon and monazite in the granulite facies metamorphism

Zircon:

Zircon ages are very difficult to reset completely, even by granulite grade metamorphism and partial melting (Pidgeon and Aftalion, 1978; Kröner et al. 1987a, 1987b). The closure temperature of zircon for U-Pb is around 800°C (Heaman and Parrish, 1991; Mezger et al. 1989). The response of U-Pb isotopes in zircon to CO_2 fluid-induced granulite-facies metamorphism has been studied in detail by Friend and Nutman (1992). These researchers analysed a number of samples across charnockitized patches (which were interpreted to have formed by CO_2 purging) within granitic gneiss in the famous Kabbal Durga quarry of the Dharwar craton (Fig.1.11). They concluded that the zircon U-Pb isotopic systematics are not disturbed by CO_2 fluid-induced granulite-facies metamorphism (charnockitization). In contrast, Paquette et al. (1994) working on rocks from SE Madagascar concluded from their U-Pb zircon studies that there is near total loss of Pb during granulite metamorphism and charnockitization. They concluded that the high temperature associated with CO_2-rich fluids during the granulitic facies event has possibly dissolved and recrystallized most pre-existing zircons.

In general, charnockitization involves LREE depletion and HREE enrichment (Touret, 1994). Depletion of Zr accompanies depletions in elements such as U, Th and Pb, which are particularly mobile. These chemical changes are principally related to the breakdown of biotite and amphibole and the production of pyroxenes and feldspars (Janardhan et al.1982; Glassley et al. 1989). Whether such changes in the trace element chemistry of major minerals are also

accompanied by U and Pb re-distribution in zircon is not known. Williams and Claesson (1987) have suggested that zircons grown under upper amphibolite and granulite grade of metamorphism generally have either very high or very low Th/U ratio.

SHRIMP analyses of zircons from the charnockite and granite gneisses of the KKB in the present work revealed significant recrystallization and new growth of zircon. An interpretation of zircon ages from high-grade terrains and charnockitized areas should, therefore, be treated with care. Recrystallization of zircon following Pb-loss often causes each analysed spot within a grain to be discordant because of incomplete loss of Pb from different parts of the grain. Thus, in the present work, SHRIMP analyses of both recrystallized and non-recrystallized spots in zircons from a biotite gneiss all plotted as a single discordant array, the non-recrystallized spots showing more Pb loss than the recrystallized spots.

Metamorphic reactions can lead to formation of metamorphic zircons. Zr can be derived from sphene, garnet, clinopyroxene and hornblende when they participate in metamorphic reactions (Heaman and Parrish, 1991). Although mafic igneous rocks are generally poor in zircon content, their metamorphosed equivalents often contain zircon which possibly may have been crystallized from zirconium released from clinopyroxene during alteration to amphibole (Heaman and Parrish, 1991). Thus zircons in many metamorphosed mafic rocks are metamorphic in origin.

Monazite:

Monazite is a La-Ce-rich light-rare-earth-element (LREE) phosphate. This is another suitable mineral for high temperature geochronometry because of its high (700 - 725°C, Copeland et al. 1988; Parrish, 1990) blocking temperature. Like zircon, monazite incorporates a small amount of initial Pb, but high Th and U. Ages can, therefore, be obtained with reasonable ease by analysis of single grains. However, there are two potential problems with U-Pb monazite dating. The first relates to the observation that many young monazite are reversely discordant. Many monazite crystals incorporate a high concentration of Th. Thus, during

crystallization, they may incorporate high amounts of ^{230}Th, which is a intermediate daughter product of the ^{238}U decay chain and has a half life of 75,200 years. The excess ^{230}Th decays to ^{206}Pb that is unaccounted for by the amount of ^{238}U present in the mineral, and, thereby, this can cause reverse discordance, specially if the Th/U ratio is very high. Another problem relating to U-Pb monazite analyses is that because of preferential high concentrations of ^{232}Th, monazite may contain very high ^{208}Pb. With a very high concentration of ^{208}Pb in the sample it is often difficult to resolve the ^{207}Pb peak in the tail of the ^{208}Pb during mass-spectrometric analyses. Normally, the concentration of Th is calculated from the ^{208}Pb present in the sample. However, in the present analyses a mixed tracer containing Th was used. This allowed measurement of Th contents and hence ^{232}Th-^{208}Pb ages.

Appendix- A.4.2. Methodology of various zircon analytical techniques: their uses and limitations and a comparative study

A.4.2.1. Introduction

There are now three well-established zircon chronometric techniques available. These are (i) Isotope Dilution Thermal Ionisation Mass Spectrometry (IDTIMS), (ii) Sensitive High Resolution Ion Micro Probe (SHRIMP) and (iii) Zircon Evaporation . Both the IDTIMS and SHRIMP dating techniques have been utilized in the present investigation. The IDTIMS technique was employed in the analyses carried out at the Massachusetts Institute of Technology and at the University of Cape Town. SHRIMP analyses were carried out at the Western Australia SHRIMP Facility housed at Curtin University, Perth. In the following section the methodology of these various techniques, their usefulness and limitations, and a comparison of these techniques are discussed.

A.4.2.2. IDTIMS (Isotope Dilution Thermal Ionisation Mass Spectrometry) technique

A.4.2.2.1. Analytical Procedure

The analytical procedure adopted for zircon and monazite analyses using conventional IDTIMS technique at the UCT laboratory includes the following steps.

(i) Separation of heavy minerals, (ii) abrasion of selected mineral fraction (for zircon only) (ii) selection of abraded grains, (iv) dissolution of grains, (v) separation of U and Pb from the dissolute, and (vi) isotopic analyses of U, Th and Pb.

(i) Separation of heavy minerals:

Zircon, monazite, apatite and sphene were analysed in the present study. These accessory minerals are liberated from the rock samples by conventional crushing and mineral separation techniques. Samples are pulverized using a jaw crusher and disk mill in two or three stages so that most of the rock sample is reduced to the -500μ to +80μ size range. The crushed sample is then passed over a Wilfley™ table to obtain a heavy mineral concentrate. This concentrate is dried using a heat lamp. A large hand magnet is passed over the thinly spread sample to remove iron filings and strongly magnetic minerals (like magnetite, ilmenite etc). The sample is then subjected to an initial magnetic separation in a Frantz™ isodynamic separator at ~0.35A current and side-tilt of 20° This process removes magnetic minerals like amphibole, pyroxene, and biotite from the concentrate. The concentrate is then passed through the heavy liquid, bromoform (ρ~2.86) to separate out quartz and feldspar. If the heavier fraction after this stage contains more than ~100 gram, the sample is passed through a second heavy liquid, methylene iodide (density, ρ~3.42), which removes most of the apatite. If the sample contains abundant pyrite, this is removed by a dilute HNO_3 wash. The concentrate at this stage consists mainly of zircon, monazite, some apatite, sphene, garnet and rutile. These minerals are separated by passing the concentrate through the magnetic separator repeatedly by varying current and side-tilt at each stage. Magnetic properties of accessory minerals depend on a variety of factors, such as contaminant, LREE content, etc. There is, therefore, no specific order in which the different accessory minerals are separated under increasing current in the isodynamic separator However, the general sequence of separation of accessory minerals with increasing current and decreasing tilt is: allanite, monazite, sphene, rutile, baddeleyite and zircon. Normally with a ~1.0 A current and a <6° side-tilt a pure zircon fraction is obtained as the non-magnetic fraction. The aim of such zircon selection is to obtain non-magnetic, inclusion-free, crack-free grains for analyses. This is facilitated by a procedure called magnetic splitting. First the zircon fraction is passed through the isodynamic separator at a 1.0 A current and a 1° or 2° negative side tilt in a so called diamagnetic setup. Normally the diamagnetic fractions of zircon are sufficiently clear and inclusion and fracture free to be suitable for

analyses. However, if the diamagnetic fraction does not yield sufficient number of suitable zircon grains, the zircon concentrate is split by using a paramagnetic setup with a ~1.5 A° current and positive side-tilt decreasing from 6° to 0° in steps of 1°. The less magnetic fraction is chosen for the next stage of processing.

(ii) Abrasion of grains (for zircon only): The least magnetic fraction of zircons are examined under a binocular microscope. Inclusion-free, crack-free, clear zircon grains are selected and are classified into different populations according to their physical properties like shape, colour, size etc. The reason for separating grains into different population is that zircons grown during different stages of crystallization/ recrystallization may have different physical properties. Each population of zircon grains is then abraded separately in an air-abrader along with pyrite grains of similar size following the technique described by Krogh (1982). Air abrasion removes altered rims and soft regions associated with excessive radiation damage and surface-correlated lead loss. Duration and air-pressure for abrasion vary according to the type of zircons. Normally ~48 hours of abrasion in ~2.5 psi. pressure abrades the grains sufficiently to thoroughly remove the outer rim of the grains. A periodic check at few hours interval is required to monitor abrasion

Each abraded grain is washed with dilute (~20%) HNO_3 to remove surface coating of pyrite. It is washed again with acetone. Abraded grains from each fraction are then studied under a binocular microscope for final selection of grains to be analysed.

(iii) Selection of grains: Abraded zircon grains or unabraded monazite, apatite, sphene grains are carefully selected under a binocular microscope for dissolution. Grains should be free of inclusion, fracture and overgrowth Selected grains are measured and photographed before being dissolved.

(iv) Dissolution of grains and separation of U-Th-Pb from the dissolute: Dissolution of

individual grains is carried out in 0.3 ml Savillex™ capsules after the addition of a mixed ^{235}U-^{230}Th-^{205}Pb tracer. Zircons were dissolved in ~120µl of 70% HF, while monazites were dissolved in 12N HCl. Apatites were dissolved in ~7N HNO_3 in 3ml Savillex™ beakeron a hotplate

For zircon and monazite grains, individual capsules were placed in a Paar™ acid dissolution bomb, in the presence of excess 50% HF in the reservoir of the bomb and heated at 210°C for 48 to 72 hours. The dissolute was then dried and an additional ~120µl of 6N HCl added. The capsules were heated again for an additional 24 hours at 180°C. Lead and Uranium were separated using HCl based ion chromatography following a procedure as outlined by Krogh (1973) using 0.05 ml columns. In this procedure, Pb is separated from the samples by elution with HCl (Catanzaro and Kulp, 1964) or with HBr (Chen and Wasserburg, 1981) on anion exchange resins. Pb has a high distribution coefficient onto the anion exchange resin in either 2-3 M HCl or 0.5-0.8 M HBr. Beyond these ranges of molarity of these acids, the distribution coefficient in resin falls sharply (Nelson and Kraus, 1954; Krogh, 1973).

In an anion exchange column using HCl, the dissolute is loaded in chloride form in 3M HCl. Except for Pb and U, all other elements (including Th) are eluted with 3M HCl which is collected in beakers for extraction of Th at a later stage. After that, Pb is eluted with 6.2M HCl and subsequently U is eluted with H_2O. For extraction of Th, the initial elutes in 3M HCl are converted into NO_3 form. The sample is then load in 7M HNO3 on the resin column. Except Th, all other elements are eluted with 7M HNO3. Th is extracted with H20 or with 0.5M HCl.

For samples with large quantities of Fe and Ti (for example whole rock samples, sphene, apatite etc), HCl chemistry is not efficient to separate Pb from Fe and Ti. However, HCl chemistry is more efficient in recovering Pb from samples with simpler chemistry (for example, zircon and monazite)

In the present work, both HBr chemistry and HCl chemistry were tried. HCl chemistry was found to be more efficient in recovering U, Pb and Th from zircons. Th is eluted along with zirconium and other elements (excepting U and Pb) during initial treatment of the dissolute by 3.1N HNO_3. This elute was collected in separate beakers for extraction of Th in HNO_3 medium at the end of elution of U. The total procedural steps are outlined in Table A..4.II.1 which includes a procedural checklist for U-Th-Pb column chemistry adopted in the University of Cape Town laboratory.

Table: A.4.II.1. Check-list for U-Pb column run using chloride chemistry.

UCT, Geological Sciences, Low-Pb isotope laboratory:

Name: Joy Gopal ghosh — **Checklist for zircon column run**

Date: — **With Chloride Chemistry**

Column No.	1	2	3	4	5	6	7
Sample number							
Fill the reservoir with 6N HCl							
~200 µl MQH_2O ~6 drops							
~200 µl 6N HCl ~6 drops							
~200 µl 6N HCl ~6 drops							
Precondition the Column:							
~200 µl 3N HCl ~6 drops							
Load sample (dissolved in 2 drops of 3N HCl)							
WASH the column drop wise (collect elute for thorium extraction):							
Beaker to collect WASH for Th extraction:							
~35 µl of 3N HCl ~1 drop							
~35 µl of 3N HCl ~1 drop							
~35 µl of 3N HCl ~1 drop							
Dry WASH in a hot plate inside bench							
Elute Pb:							
Beaker for collecting Pb elute (with +~5ml H_3PO_4)							
~60 µl 6N HCl ~2 drops							
~60 µl 6N HCl ~2 drops							
~60 µl 6N HCl ~2 drops							
Elute U:							
Beaker for collecting U elute (with +~5ml H_3PO_4)							
~60 µl MQH_2O ~2 drops							
~60 µl MQH_2O ~2 drops							
~60 µl MQH_2O ~2 drops							
Wash the column for Th extraction:							
~200 µl MQH_2O ~6 drops							
Precondition the column for Th extraction							
~60 µl HNO_3 ~2 drops							
~60 µl HNO_3 ~2 drops							
~60 µl HNO_3 ~2 drops							
Load sample: dried WASH in ~2 drops of 7N HNO_3							
~35 µl 7N HNO_3 ~1 drop							
~35 µl 7N HNO_3 ~1 drop							
~35 µl 7N HNO_3 ~1 drop							
Elute Th							
Place U beakers under the columns							
~60 µl MQH_2O ~2 drops							
~60 µl MQH_2O ~2 drops							
~60 µl MQH_2O ~2 drops							
Dry the sample with one small drop of H_3PO_4 on a hot plate (~150°C) inside bench.							

Jay Gopal Ghosh

(iv) Isotopic analyses of U and Pb:

Both U and Th were loaded on degassed Re filaments embedded into thin layers of colloidal graphite. Pb was loaded on separate degassed Re filaments using silica gel as a medium. Isotopic analyses of Pb were performed using a VG Sector (VG Sector 54 at MIT) thermal ionisation mass spectrometer fitted with six Faraday cups and a Daly detector . Two separate procedures were used for analyses of Pb isotopes: (i) Static mode multi collector procedure whereby all isotopes of Pb except ^{204}Pb was measured in Faraday cups. ^{204}Pb was measured using a Daly detector and was calibrated using frequently ran calibration factor (ii) Static mode using only the Daly detector in a peak jumping method. Multi-collector analyses were corrected for a 0.12% fractionation factor and single collector analyses were corrected for a 0.24% fractionation factor. Correspondence between these two methods of analyses was verified in selected samples and was found to be true within analytical error limit. U and Th were analysed using Daly detector only by the peak jumping mode.

A.4.2.3. A comparison between the analytical procedures adopted in MIT and UCT laboratories

The analytical procedure adopted in the UCT laboratory, as outlined above is similar to that in operation at the MIT laboratory. However, there are few differences:

(i) Spike

The MIT laboratory uses a mixed ^{205}Pb-^{235}U-^{233}U spike while the UCT laboratory uses mixed ^{205}Pb-^{235}U-^{230}Th spike. Use of double spike for U in the MIT laboratory helps in maintaining good control over fractionation of U isotopes during mass spectrometric run. This, in turn, helps in getting high precision in U concentration values.

In the UCT laboratory, use of spike mixed with ^{230}Th helps in getting precise $^{208}Pb/^{232}Th$ ages for samples analysed in addition to U-Pb ages. This also enables precise determination of Th/U ratios of analysed samples, which often helps in identifying different population of zircon/monazite within a rock and their varying chronologic information. Although Th/Pb systematics in high-grade metamorphic environments is not well-understood, a number of analyses in the present work point to a similarity in the Pb-loss behaviour between the U/Pb and Th/Pb systematics. To extract Th from the samples, a modification in the column chemistry procedure to that adopted at the MIT laboratory was introduced (see Table A.4.II.1).

(ii) Mass spectrometry:

The MIT laboratory uses a VG-54® mass spectrometer with 128 mm effective magnetic diameter and the UCT laboratory uses a VG Sector® mass spectrometer with an effective diameter of 64 mm. The MIT laboratory is thus capable of getting higher mass resolution.

(iii) Analytical blank:

Analytical Pb-blank during my analysis at the MIT was ~3 picogram. But the Pb-blank in my analyses at the UCT laboratory varied widely but improved with time (~1 year) from ~40 picogram to ~4 picogram. The initial analyses at the UCT laboratory thus lack the high precision generally obtainable in IDTIMS analyses.

A.4.2.4. A note on $^{208}Pb/^{232}Th$ ages obtained at the UCT laboratory

Conventional IDTIMS analyses generally do not include $^{208}Pb/^{232}Th$ ages mainly because (i) coupling between the $^{207}Pb/^{235}U$ and the $^{206}Pb/^{238}U$ ages gives precise age information of the analysed material and generally no better age information can be obtained from the $^{208}Pb/^{232}Th$ systematics (ii) unlike U/Pb systematics there is no independent method for validation of $^{208}Pb/^{232}Th$ ages and (iii) behaviour of the Th/Pb systematics in various geological environment

is not well understood.

In the present investigation, because of the availability of a mixed spike with ^{230}Th at the UCT laboratory, Th contents of zircon and monazite were also determined to obtain additional age information using $^{208}Pb/^{232}Th$ systematics. To recover Th from the zircon and monazite dissolutes, the standard chloride column chemistry (Krogh, 1973) was modified as outlined above (Table A.4.II 1). Th was analysed in the mass spectrometer along with U in a graphite medium.

For analyses with concordant zircon population, there is a fairly good correspondence between the U/Pb concordant ages and the Th/Pb ages, and weighted average of Th/Pb ages are often within error limits of U/Pb concordant ages (Fig. 4.2, 4.4, 4.19, 4.20, 4.21 and 4.24) For discordant U/Pb analyses, the Th/Pb ages also decrease along with $^{206}Pb/^{238}U$ and $^{207}Pb/^{235}U$ ages (Fig. 4.8, 4.19 and 4.23). Particularly, in the case of granite gneiss samples S-416 and S-325C, Th/Pb ages show a systematic increase with the increase in the concordancy in the U/Pb ages (Fig. 4.19 and 4.24). However, within this general coupling of the U/Pb ages and the Th/Pb ages, a number of aberrations in the Th/Pb ages were also noticed. For example, the most concordant zircon crystal in sample S-130 shows the least Th/Pb age (Fig. 4.4) and in samples S-27A and S-236A there is no correspondence between the discordancy of the analysed crystals and their Th/Pb ages. The cause of such aberrations in the Th/Pb ages in comparison to the U/Pb ages is not known but may be due to incomplete equilibration between sample and spike. Another possible explanation is that Th and U concentration within a crystal may vary either due to the presence of inclusions rich in Th (for example monazite) or due to original variation during crystallization. Such variation may cause differential Pb-loss pattern from the Th-rich sites and U-rich sites which in turn causes aberration in the Th/Pb ages in comparison to the U/Pb ages.

A.4.2.5. Detail instruction sheet followed in the UCT laboratory for zircon dissolution and column chemistry.

A. Bomb digestion

1. Put on a pair of clean latex gloves. Lay a Teflon (or a low-lint paper) mat on laminar flow bench top and remove blue tongs with curved tips and three Teflon watch glasses from the cleaning box. Also have available the Teflon cup from a Paar® bomb, ultra clean Teflon-coated tweezers, 1-10μL micro pipette with Teflon spaghetti, paper wipes, dispensing bottles of "best" reagents (H_2O, 70% HF, 7N HNO_3), ^{205}Pb-^{235}U-^{230}Th spike, and petri dishes containing zircon. Take cover off Teflon cup, and, with blue tongs, remove and take apart three-tier puck assembly. Set the three pucks, each containing 5 sample digestion capsules, each of 0.3 mL capacity, at back of mat. Put cover back on Teflon cup and set aside

2. Place one of the pucks on one of the Teflon watch glasses, remove caps from capsules with ultra clean tweezers, verify matching numbers, rinse capsules and caps with H_2O, and replace caps. Repeat for other two pucks.

3. View petri dish containing zircon under binocular microscope, decide which grain(s) is to constitute sample 1, and dispense a drop of H_2O into dish. Remove cap from first capsule, use micro pipette to deposit a 1μL droplet of H_2O on inside of capsule. Pick up grain(s) of zircon in a second 1μL droplet of water, and touch to first droplet. Grain(s) should now be transferred into capsules (multiple grains may require several transfers). Each grain should be weighed or measured before tranferring into capsule. Wash zircon grains inside capsules. Washing is done initially by adding few drops of 6N HCl in each capsule and warming (60°C-70°C for few hours and then by rinsing the grains by H_20. Dispense 1 drop (~25μL) of HNO_3 on H_2O droplet containing zircon; the acid should cause the entire drop to

slide down to bottom of the capsule. Then dispense 4 drops (~100μL) of HF into capsule and replace cap.

4. Repeat step 3 for all capsules in the three pucks, except that one or more of the capsules can be processed without sample as blank analyses. Finally, remove caps sequentially from each capsule, use micro pipette to deposit a measured amount (usually 2-5μL) of ^{205}Pb-^{235}U-^{230}Th spike into each capsule, and replace caps.

5. Put three-tier puck assembly back together, remove cover from Teflon cup, and fill reservoir at base of Teflon cup with about 1mL "secon best" 7N HNO_3 and 4mL "second best" 50% HF. Insert puck assembly into Teflon cup, and replace cover on cup. The assembled Teflon cup can now be carried into anteroom and reinserted into steel Paar bomb. After reassembling the bomb, it is put into a 210°C oven. Paleozoic and older single zircon grain samples usually dissolve in 2-3 days; younger or larger samples may take longer.

6. After appropriate number of days, remove bomb from oven using heavy towel, allow to cool on aluminum plate for 2 hours, and dissemble to remove Teflon cup. Clean outside of Teflon cup with paper wipes wetted with MQ H_2O and acetone before bringing into clean laboratory. Put on a pair of clean latex gloves. Lay a Teflon (or low-lint paper) mat on laminar flow bench top and remove blue tongs with curved tips and three Teflon watch glasses from the cleaning box. Also have available ultra clean Teflon-coated tweezers, paper wipes, and dispensing bottle of "best" reagent (6.2N HCl). Break seal between cup and cover by applying a twisting motion to cover, then, with blue tongs, remove and take apart three-tier puck assembly. Set the three pucks containing digestion capsules at back of mat.

7. Place the pucks on the Teflon watch glasses, remove caps from capsules with ultra

clean tweezers, and check for undissolved sample. The capsule quite likely will still contain fluid at this time, but, if dry, may reveal a tiny residue of dissolved sample. Place all three pucks on 80°C hotplate and evaporate any remaining fluid to dryness. Caps should be protected under Parafilm during the time they are removed from the capsules. Turn off hotplate, allow pucks to cool somewhat, return to their respective watch glass, dispense 4 drops (~100μL) 6 2N HCl into each capsule, and replace caps on capsules.

8. Put three-tier puck assembly back together, remove cover from Teflon cup, and fill reservoir at base of cup with about 5mL "second best" 6.2N HCl. Insert puck assembly into Teflon cup, and replace cover on cup. The assembled Teflon cup can now be carried into anteroom and reinserted into steel Paar bomb. After reassembling the bomb, it is put into a 210°C oven for one additional day.

9. The following day remove bomb from oven using heavy towel, allow to cool on aluminum plate for 2 hours, and dissemble to remove Teflon cup. Use paper wipes wetted with MQ H_2O and acetone before bringing into clean laboratory. Put on a pair of clean latex gloves. Lay a Teflon (or low-lint paper) mat on laminar flow bench top and remove blue tongs with curved tips and three Teflon watch glasses from the cleaning box. Also have available ultra clean Teflon-coated tweezers, paper wipes, and dispensing bottle of "best" reagent (3.1N HCl). Break seal between cup and cover by applying a twisting motion to cover, then, with blue tongs, remove and take apart three-tier puck assembly. Set the three pucks containing digestion capsules at back of mat.

10. Place the pucks on the Teflon watch glasses, remove caps from capsules with ultra clean tweezers, and place all three pucks on 80°C hotplate and evaporate any remaining fluid to dryness. Caps should be protected under Parafilm during the time they are removed from

the capsules. Turn off hotplate, allow pucks to cool somewhat, return to their respective watch glass, dispense 2 drops (~50μL) 3.1N HCl into each capsule, and replace caps on capsules. Capsules are not reheated, but at least several hours should pass before transferring contents to an ion exchange column so as to insure sample dissolution.

B. Column separation

i. Preparing the beakers

Construct a table in the notebook with headings: "sample number"; "column number"; "Th beaker"; "Pb beaker"; "box position"; "turret position"; "U beaker"; "box position"; "turret position" to record the information needed for identifying samples.

Choose 15 clean "M" or "K" beakers for collection of lead, 15 of any other clean beaker for Th and 15 for U. The numbers of all beakers should be recorded in the notebook. Into each of the Pb and U beakers, put 1 micro drop (~ 7-8μl) of H_3PO_4 from the 30mL bottle in the bench. Keep the beakers closed until use.

ii. Preparing the columns

The stands for the columns are found in cupboard IVA and the Teflon column holders (wrapped in Parafilm) in the vertically set air box to the left of the benches. Assemble holders in stands and set out from 1 to 15 across the back of the laminar flow bench. Also set out column waste collection beakers (available in wall cupboard) in the stands.

The Teflon columns used for U, Th and Pb separation have a stem volume of around 50μL. They are stored in dilute HCl, which is kept at 40°C in a Teflon jar on the bench hotplate. The columns can be removed from the HCl with the blue tongs, and placed on a clean Teflon square available on the bench. Once all columns have been collected, they must be cleaned and

filled with resin. This is done by picking the column up at its stem with the blue tongs, inverting it and squirting MQ water through the stem (this can be done over the sink), as well as filling and empting the reservoir a few times. At this point, observe the number inscribed on the base of the column reservoir.

To add the resin, invert the column and squirt water into the stem again. When a droplet inside the reservoir is formed and before it runs out, turn the column upright halfway and quickly squirt in water until the reservoir is about 1/3 full. (This should allow enough time to add the resin while preventing an air bubble from forming in the stem if the water runs out too fast.)

Shake up the resin bottle and add ten drops of resin into the water in the reservoir. Once this has been done, the column can be turned completely upright, as resin slows down flow. Check that there are no air bubbles in the stem. If there are, try to get rid of them by squirting with water from the top, or use resin pipette (on bench, next to tweezers). Otherwise, discard by following the cleaning steps and fill again.

Place each column in the stands as you go along, noting each time in your book the number of the column from position 1 through 15. (Do not reach over columns, as lint or dust from your coat or glove could fall in and contribute to the lead blank!)

Check which columns are filled, and add resin drop wise into those that are not. (A filled column has resin up the top of the stem. Do not overfill the columns. If this happens, remove excess resin with the resin pipette.)

Keep the columns 1/3 full during resin settling, to prevent air bubbles from forming.

The checklist for the zircon column run is available in drawer 1. Follow the procedure listed in the checklist.

Once the water has run through all columns[11], fill all reservoirs with **6.2N HCl** , and allow to run through (about 45 minutes-1 hour).

Then add the following, allowing the liquid to run through completely after each addition.

-- 6 drops *reagent* **MQH_2O** (cleanest water, from the 30mL reagent bottle)

-- 6 drops **6.2N HCl**

-- 6 drops **6.2N HCl**

where 1 drop = 25 - 30 μL.

(NB. Remember to check off each addition on the checklist as you go along!!)

The 6.2N HCl should flush out the lead contaminants, and the H_2O the Th and U contaminants, that may be in the resin.

Precondition the columns for lead separation by adding 6 drops of **3.1N HCl**. 3.1N HCl holds Pb and U in the resin. Allow it to run through the column completely. The columns are now ready for loading the samples.

iii. Loading the sample

[11] if this takes too long, use resin pipette to remove excess.

List the sample numbers in your notebook as well as on the checklist. (Remember to include the bomb capsule numbers in the table.)

The samples in the capsules may be loaded in two ways: either with a pipette, or directly into the column from the capsule, using the method described below.

I. Clear a big enough area on the bench for your arm to rest on during loading

II. Bring the first stand forward, and turn lengthways from you, to reduce disturbance of the two columns which are not being filled during each loading. (Remember that you should avoid reaching over a column, especially during loading.)

III Using the ultra clean tweezers, lift the first capsule from the puck. Ensure that it is secure in the tweezers.

IV. Carry the capsule over to the columns in the stand. Rest your arm on the bench, parallel to the stand, with hand (holding the tweezers) resting sideways and small finger extended on the bench for extra support

V. Once near the designated column, the capsule can be turned over until it is almost upside-down *inside the column.* Try not to touch the inside of the column with the bomb capsule Hold firmly with the tweezers!

VI. With your free hand, flick a finger against the tweezers. The sudden jolt should free the sample droplet without causing too much movement of the capsule, which could cause the droplet to overshoot the column.

Repeat the procedure for all samples, making sure that they are done in the correct order and checking off on the checklist each time.

iv. Thorium and zirconium elution

Replace the column waste beakers with the thorium beakers, in the order listed in the book. At all times, you should avoid touching the tips of the columns with the beakers! Note the beaker numbers on the checklist as you go along as a double-check.

The Th and Zr will be washed from the resin with **3.1N HCl** as on the checklist -- 1 drop of 3.1N HCl is added and allowed to run through. This is done 3 times. U and Pb are held by the resin. Once all the HCl has run through remove the Th beakers. If the beakers touch the column tips, squirt MQ water on them to rinse the tips off, as they may be contaminated. Place thorium beakers on a hotplate in an air bench (not in the laminar flow bench, as acid fumes will escape into the room!) at 100-125° C (with lids off, and set out in order in the air bench) to evaporate off the liquid droplet.

v. Lead and uranium elution

In each of the clean beakers marked for U and Pb collection, add a ~10µl drop of 1N H_3PO_4. This will concentrate collected U and Pb within a small droplet.

Place the Pb beakers under the columns, and elute Pb with three separate washes of 2 drops **6.2N HCl**. (Remember to record the beaker numbers on the checklist again.) Once the final drop has been collected, the Pb beakers can be removed, and replaced with U beakers. As with the Th beakers, the Pb beakers should be placed on a hotplate for acid evaporation at 100-125°C. The U is eluted with 3 separate washes of 2 drops reagent **MQ water**. After the U has been collected, the beakers can be removed and closed. Do not dry the U sample at this point, as U beakers will be used to collect the Th as well.

The U beakers should then be replaced with waste beakers, and the column washed with 6 drops reagent MQ water before the collection of the Th.

vi. Collecting the thorium

At this point, the Th beakers should be dried down, leaving a visible spot of residue in each beaker. Add 2 drops 7N HNO_3 to each beaker and allow the residue to dissolve. While this is happening, precondition the column for Th extraction with 3 separate washes of 2 drops 7N HNO_3. Once the residue has gone into solution, the sample droplets can be dropped directly from the beaker into their corresponding columns.

The sample must be washed with 7N HNO_3 (3 separate washes of 1 drop) to elute the Zr and other elements, leaving the Th on the resin. The U beakers can then be placed under the columns, and the Th extracted with 3 washes of 2 drops reagent **MQ water**.

The U beakers can then be dried down on a hotplate as above.

A discussion on the analytical blank in single crystal works and procedures taken at the UCT laboratory to improve analytical blank is given in Appendix A.4.3.

A.4.2.6. SHRIMP (*S*ensitive *H*igh *R*esolution *I*on *M*icro*p*robe) analyses

A.4.2.6.1. Methodology

Zircon and monazite from five rock samples were analysed in the present work using SHRIMP II located in the Curtin University, Perth, Australia. The basic design of SHRIMP-II is illustrated in Fig. A.4.2.

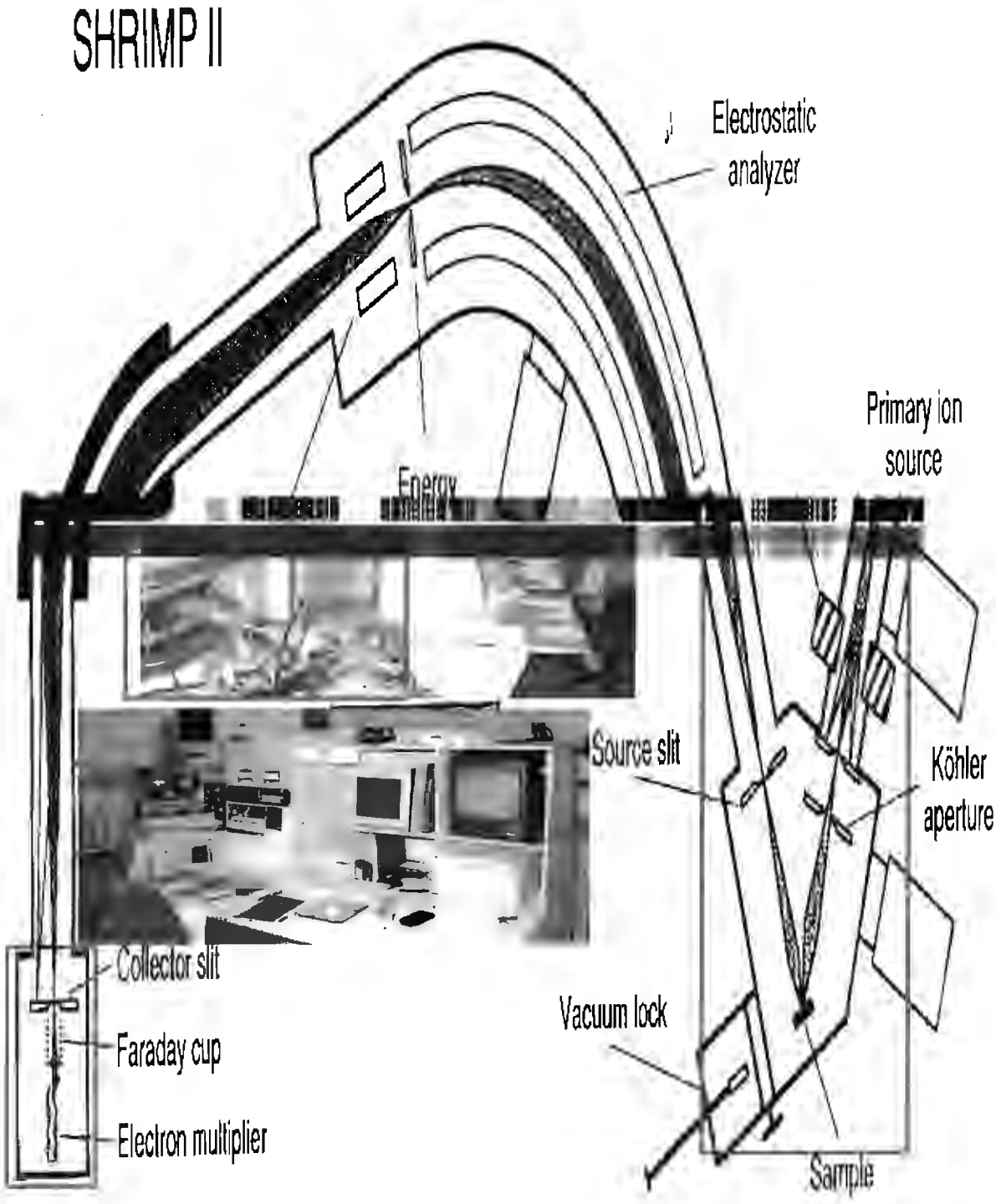

Fig. A.4.2. Design of SHRIMP-II at the Curtin University, Perth, Australia. Central inset photo shows side view of SHRIMP-II. Lower inset photo shows front view of the SHRIMP-II. Source unit is marked in blue box while the collector unit is marked in pink box.

Zircon or monazite are separated by the standard procedure of crushing, Wilfley® table, heavy liquid and magnetic separation techniques. Without any selection of grains the entire population of grains or representative fractions of different populations are mounted on a resin block for analyses. Selections of grains are avoided at this stage since SHRIMP allows analyses of small domains of grains with variable textures etc., thus facilitating analysis of complex zircons.

Mounting of grains

Double sided adhesive tape of about 2.5 cm wide is pasted on a ~3 cm wide glass slide. Grains are mounted within a ~2.5 cm diameter area on the upper side of the tape leaving an annular area of ~5 mm in the outer rim. It is desirable to mount grains of similar thickness on the same mount, so that, when subsequently polished, all grains can be easily abraded to almost half their thickness. Zircon or monazite grains from two or three samples can be mounted together in identifiable sub-areas within the circular area. Also mounted in the central part of the slide are 2-3 grains of standard zircon or monazite. Once all the grains are mounted, a Teflon mould is placed on the slide, encapsulating all the grains. A freshly prepared mixture of Epicompound® and Epi-hardener® (in 100:13 ratio) is poured slowly on to the mould along one of its sides. The liquid mixture of epoxy creeps slowly over the mounted grains avoiding any trapping of air bubbles. The sample is then allowed to stand for several hours. Once the resin hardens, the mould is taken out and the adhesive tape is slowly peeled off the glass slide. A fine sand paper is then applied on the hardened resin block to expose and section the zircon on its surface. The analytical surface is then polished using first 5-7 μm and then 1 μm diamond paste. The grains are then photographed with back-scattered electron microprobe (BSE) and then with Cathodoluminiscence (CL) to highlight the inhomogeneity in the internal structures of each grains. In general for high U grains and contrasts in the distribution of U are well highlighted by BSE at ~35K current. Inhomogeneity

in grains with low U content and those with contrasting Th distribution are better highlighted with Cathodoluminiscence. Study of BSE and CL images help identifying domains of different generations of zircon/ monazite growth or recrystallization within a single grain. Identification of such domains are important since during SHRIMP analyses specific domains of a grain can be analysed separately. The grains are photographically mapped at high magnification (~x200) to guide probing. The surface is then cleaned and a conductive coat of ultrapure gold is applied to the mount surface to induce the electrical potential of the mount as required for fixed and optimal extraction of secondary ions. The sample is now ready for loading in the SHRIMP.

Analyses of mounted grains:

The sample mount is placed in the sample holder in the SHRIMP where it is kept in high vacuum for several hours. High vacuum eliminates any hydrous phase that may come in contact with the sample, which may form undesirable hydride ions during ionisation.

During analyses, a primary beam of O^{-2} ions produced from a hollow cathode duoplasmatron, which is accelerated and focused, strikes the target grains at an angle of 45° with an ion current of about 4 nA. This primary beam creates a crater of 20-30 μm diameter. The sample surface is illuminated and its view is captured through an online CCT monitor. This helps in guiding the sample to specific areas of ionisation. The primary beam is subjected to a Wein filter to ensure isotopic purity of the beam so that OH^- ions are eliminated, and use is made of the Kohler illumination method so that the crater has sharply defined edges and a flat bottom. A proportion of the material sputtered from the crater becomes ionized and is extracted normally by 10 keV accelerating potential for transfer via matching lenses to the entrance slit of the mass spectrometer. The lens system constitutes a double focusing design comprising a cylindrical 85° electrostatic analyser with a turning radius of 1.27 m and a 72.5° magnet sector with turning radius of 1 m. The beam is measured by ion counting with a single electron

multiplier into which the masses of interest are directed by switching the field of the magnet. The source slit width is maintained to about 80 μm, which gives a mass resolution of approximately 6000. At this resolution all significant interferences with the masses of interest are removed (excepting for Pb hydrides which is reduced by maintaining very high vacuum).

Ion counting:

Before starting actual ion counting of the secondary beam, a defocussed primary beam is first used to clean the surface of the sample target for approximately 3 minutes with an aperture of about 100 μm. This removes any contaminant that might have adhered during polishing and gold coating. The secondary beam of ions is then collected while the magnet is cycled through field positions equivalent to nine masses of interest: $^{90}Zr^{16}O$, ^{204}Pb, ^{206}Pb, ^{207}Pb, ^{208}Pb, ^{238}U, $^{232}Th^{16}O$, $^{238}U^{16}O$, and a background reading (0.04 A.M.U heavier than ^{204}Pb). Seven scans over these field positions are made and a best fit track for each mass is taken to calculate the required isotopic ratios. $^{207}Pb/^{206}Pb$ ratios can be directly estimated from the ion counting statistics obtained from SHRIMP with small correction for any common lead present. The latter is monitored through ^{204}Pb ion counts in the case of zircon, and ^{207}Pb count in the case of monazite. The $^{206}Pb/^{238}U$ ratio of the grain is measured indirectly. This is because during ionisation, most of the Pb in zircon is yielded as Pb^+ ions, whilst most of the U is converted to UO^+ instead of U^+. Thus, the $^{206}Pb/^{238}U$ ratio observed by SHRIMP is much higher than the true ratio of $^{206}Pb/^{238}U$ in the target zircon. The bias is not constant, but at low sputtering rates of homogeneous zircons, there is a correlation between the emission of $^{206}Pb^+/^{238}U^+$ and $^{238}U^{16}O^+/^{238}U^+$ (Compston and others, 1984). It has been found through comparison with the TIMS analyses that the $^{206}Pb^+/^{238}U^+$ of the sample is related to the measured UO^+/U^+ by a simple power law (Claoue-Long et al. 1996):

$$^{206}Pb^+/^{238}U^+ = A(^{238}U^{16}O^+/^{238}U^+)^2$$

where A is a constant (~0.0069).

This forms the basis of comparative analysis which assumes only that the bias of observed $^{206}Pb^{+}/^{238}U^{+}$ relative to the real $^{206}Pb/^{238}U$ in the target is the same for the standard zircon as for the unknowns:

$$(^{206}Pb/^{238}U)_{unknown} / (^{206}Pb^{+}/^{238}U^{+})_{unknown} = (^{206}Pb/^{238}U)_{standard} / (^{206}Pb^{+}/^{238}U^{+})_{standard}$$

The reference zircon used in Western Australia SHRIMP-II at Curtin University is CZ-3 whose $^{206}Pb/^{238}U$ ratio is precisely known to be 0.0914 through repeated TIMS analyses. The reference monazite used is MAD whose $^{206}Pb/^{238}U$ ratio is 0.0830. The above equation then allows the $^{206}Pb/^{238}U$ of an unknown zircon to be measured from the difference between its observed $^{206}Pb^{+}/^{238}U^{+}$ and that measured for the standard at the same UO^{+}/U^{+}. The total uncertainty in the $^{206}Pb/^{238}U$ ratios is determined by combining counting statistics on the various masses, uncertainty introduced by correction for common Pb, and uncertainty in the factor that describes the position of the calibration curve. As the $^{206}Pb/^{238}U$ ratios are measured by difference from the determination of the position of the calibration curves, the uncertainty in calibration is the principal control on the accuracy obtained.

A.4.2.7. Kobar Evaporation Method

A single zircon evaporation technique was developed by Kober (1986, 1987) and by Kröner and Todt (1988). This method uses a double filament and thermal ion mass spectrometry. One of the filaments, called the evaporation filament, in which the zircon is embedded, is canoe shaped. This filament is placed in front of a second filament, known as the ionisation filament. At temperatures, typically between 1400°C and 1600°C, the evaporation filament emits Pb, which is then ionized by the ionisation filament held at a higher temperature. The ionized beam is then measured for Pb isotopic abundances. The evaporation technique is very fast and does not involve difficult chemical procedure associated with conventional zircon analyses.

However, because there is no capability for spiking during zircon evaporation, this method cannot measure Pb or U concentrations and is thus limited to $^{207}Pb/^{206}Pb$ model ages. Information on discordancy of the mineral grains cannot, therefore, be obtained.

The $^{207}Pb/^{206}Pb$ model ages approximate the crystallization ages of the minerals only if,

(I) the grains are simple and concordant grains, or

(ii) there has been only recent Pb-loss from the mineral.

In a high grade terrain, specially those suffering more than one thermal event, it is difficult to find grains that satisfy both of these two conditions. In multiply-deformed high-grade terrain, zircons often show one or more episodes of Pb-loss due to metamorphism, recrystallization and overgrowth. In such a case, $^{207}Pb/^{206}Pb$ model ages can only give a mixed (minimum) age of crystallization of the grain. Whether or not such minimum model ages approximate crystallization ages of zircons need to be validated by other independent analytical techniques like conventional dissolution method or SHRIMP.

It is often claimed that the evaporation technique can yield information on different stages of zircon growth (Cocherie et al.1992). The assumption behind such claim is that initial evaporation steps at lower temperatures emit Pb from the outer rims of the crystal, which is more susceptible to Pb-loss. $^{207}Pb/^{206}Pb$ ages obtained at this stage may thus approximate the thermal event causing Pb-loss. More strongly bound Pb within the $ZrSiO_4$ lattice is thermally stable and is emitted at higher evaporation temperatures. On the basis of these assumptions, different $^{207}Pb/^{206}Pb$ ages at different temperature steps are often interpreted as rim and core ages of grains. However, the behaviour of the zircon crystal at high evaporation temperature is not known. Thus the assumption that at lower evaporation temperatures Pb is emitted from the rim or weaker sites has not been validated. Observation on partially evaporated zircon has

indicated that Pb is preferentially lost from the metamict parts and the crystalline parts release their Pb during higher temperature steps (Chapman and Roddick, 1994). Thus, for metamict zircon early evaporation stages may yield geologically meaningless ages. The interpretation of zircon evaporation ages is more complicated if the metamict zircon is recrystallized in which case every parts of zircon may yield discordant ages.

A.4.2.8. A comparative study of different zircon and monazite geochronometric techniques

Each of the three zircon geochronometric techniques discussed above (the IDTIMS, the SHRIMP and the Evaporation techniques) has its own advantages and disadvantages. A comparative study of these techniques should focus on the following aspects.

(i) Cost and accessibility (ii) precision and accuracy and (iii) resolution.

A.4.2.8.1. (i) Cost and accessibility

The conventional IDTIMS technique demands maintenance of a high quality chemical laboratory, which, though not very expensive, necessitates highly skilled personnel. Both the evaporation technique and SHRIMP technique do not require maintenance of such a high-quality chemical laboratory. While the evaporation technique can run on a conventional mass spectrometer similar to IDTIMS, the SHRIMP technique demands a high resolution mass spectrometer which costs about 10 times that of a conventional mass spectrometer. This high cost of SHRIMP has limited its accessibility for many demanding geological problems.

The evaporation technique is least expensive of these three techniques. However, its serious inability in analysing Pb and U concentrations and, thus, the amount of concordance of the grains, has limited its use.

A.4.2.8.2. (ii) Precision and accuracy

While precision determines the reproducibility of the analysed grains, accuracy determines the nearness of the analyses to the true value. In IDTIMS, Pb and U are loaded in the mass spectrometer as PO_4^- and NO_3^- but ionized as Pb^+ and U^+, which are extracted from the mineral grain by chemical procedures. These metals are thus mostly free of numerous other metal and compounds that were originally associated with them. Separation of such metals ensures high signals for most of the isotopes and also, to a large extent, removes the possibility of isobaric interference from other possible interfering elements and compound. Purification of sample, good ion optics and stable ion beam are important for IDTIMS analyses. Individual analyses by the IDTIMS technique thus can achieve *very high* precision. In both the evaporation and SHRIMP techniques, Pb is ionized along with other elements present in the mineral grains. The possibility of isobaric interference in the Pb isotopes from other elements and compounds are thus high. While in SHRIMP a very high mass resolution (of the order of about ~6000) can remove most of the possible isobaric interferences, the evaporation technique is swamped by possible isobaric interference. Although in the SHRIMP technique, isobaric interference can be removed to a large extent, the amount of material sputtered from the target mineral for each analyses is quite small (typically ~0.2 ng), about 3 or 4 orders of magnitude less than the material used for IDTIMS or evaporation technique. Higher ion beam intensity in IDTIMS can yield stable and high precision counting statistics within individual analyses which cannot be achieved during SHRIMP or in evaporation analysis. The high precision of IDTIMS analyses for homogeneous grains can yield highly accurate measurements of the isotopic ratios of the grains. However, in cases of

inhomogeneous grains, such high precision ages gives an average value of the various inhomogenities present in the mineral. With the development of zircon abrasion technique developed by Krogh (1982), inhomogeneity in the outer rims of zircon grains are quite often successfully removed to yield a precise age of the core of zircon grain. In the case of SHRIMP analyses, the deficiency in the precision of individual analyses is partially overcome by increasing the number of analyses. Increased number of analyses in the case of homogeneous grains decreases errors in determination of crystallization age.

SHRIMP analysis is heavily dependent on standards for determining the abundances of U and Pb. A significant difference between the standard and the sample in terms of their U and or Pb content, metamictization, characteristics of the matrix, and even some undefined factors can cause significant differences ('matrix effect')in the sputtering of different ions from the standards and from the unknown minerals. Such differences can cause significant error in their age determination.

A.4.2.8.3. Resolution

While the evaporation technique and the IDTIMS techniques typically uses single grains of zircon which are normally between 50 and 200 μm in dimensions, the diameter of the sputtering area in the SHRIMP procedure is comparatively small (typically 25 μm to 30 μm diameter). The pit depth in each sputtering position is also very small (1-2 μm). Thus the SHRIMP method can analyze 10 to more than 50 spots within a single grain. This high resolution of analyses is able to detect inhomogeneity in the distribution of U and Pb and in the Pb isotopic composition within a single grain. Recent SHRIMP and IDTIMS analyses have shown that zircon grains in many rocks, specially peraluminus magmatic rocks and in multiply metamorphosed terrain are very heterogeneous. Often optically homogeneous zircons are

internally recrystallized (Fig. 4.26) and have inhomogeneous distribution of U and Pb. Such inhomogeneties are, in many cases, due to core and overgrowth relationship and/or due to irregular distribution of recrystallization patches within a single grain. While inhomogeneity in the distribution of U and Pb isotopes can easily be resolved using SHRIMP technique, the inhomogeneity due to recrystallization of zircon (which is a common feature in a polymetamorphic terrains) may not be resolvable even by the SHRIMP technique, because every parts of the recrystallized grains are potentially discordant. This is because recrystallization involves both Pb-loss as well as retention of Pb "memory".

Using the SHRIMP technique it is also possible to analyse U-Pb isotopic ratios of minerals from thin sections. The ability to analysé grains at such high resolution is one of the greatest advantages of the SHRIMP technique. The SHRIMP technique is ideally suited, therefore, for analyses of complex grains and can yield much information about the cryptic thermal, deformational and fluid history that the grain may have experienced.

Recent developments in achieving very low laboratory blanks in IDTIMS analyses have allowed many workers to analyse fractions of zircon and monazite crystals which are potentially inhomogeneous (Hawkins and Bowring, 1997). Inhomogenities identified by electron probe or Cathodoluminiscence are separated mechanically and analysed separately. This technique is, however, tedious and needs highly skilled personnel. But where this technique is applied successfully, it achieves high resolution with high precision.

A.4.2.8.4. Choice of zircon geochronological technique

In summary, the choice of the techniques for zircon geochronometry should depend on the nature of the material available and problems to be resolved. The evaporation technique is

cost-effective and can be employed where first order information on the age of a terrain is needed. Since this method can only yield $^{207}Pb/^{206}Pb$ model ages, it can only give minimum estimation of the age or, in some cases, grossly erroneous age of zircon grains. Although it is generally claimed that the evaporation method can yield information on multiple thermal events suffered by the grains, such claims remains unproven. The ability to analyse grains very quickly in SHRIMP makes this method useful for areas where many reconnaissance analyses are needed but this comes at significant costs. The greatest advantage of the SHRIMP is its ability to analyse sub-grain inhomogenities and *in situ* analyses in thin sections. This ability can extract a wealth of information on the chronology vis-a-vis paragenesis of minerals and multiple thermal events within a single grain. The SHRIMP method is heavily dependent on the analyses of standards. Any significant departure in the sputtering characteristic of the standards and the unknown can give aberrant results. The SHRIMP method is inferior in precision of data to that of IDTIMS method. The IDTIMS method is ideally suited for homogeneous population of zircons or where homogenous population can be isolated optically and/or by mechanically (abrasion, cutting, drilling etc). Very high quality data can be obtained at lower costs than similar SHRIMP analyses. However the IDTIMS method is unsuitable for complex zircons with cryptic sub-grain scale inhomogeneity unless such 'matrix effect' can be avoided. Also, maintenance of a good IDTIMS facility demands maintenance of a high-quality chemistry laboratory.

Appendix-A.4.3. Pb-blank in U-Pb single crystal work- its sources and measures adopted at UCT to reduce it.

A.4.3.1. Introduction

U-Pb single crystal work using the conventional IDTIMS method demands an ultra clean laboratory and maintenance of an extremely low Pb level. It is essential to ensure that various apparatus and chemicals used for the analyses do not contribute more than a specified amount of Pb (called Pb-blank). The quantity of an acceptable amount of Pb-blank in single crystal work varies according to the amount of radiogenic Pb present in the sample. As a rule of thumb, if the radiogenic Pb content of the sample is more than 50 times the Pb-blank (which is introduced during analytical procedures), then with good mass spectrometric runs, such analyses can accurately determine the isotopic ratios of the sample. In general, zircon crystals do not incorporate Pb during crystallization. Thus, the amount of Pb present in the zircon crystals is mainly derived from in-situ radioactive disintegration of U. Any Pb that is incorporated from the surrounding host during crystallization of the rock is called "common lead". Accumulation of Pb increases with time. Thus, the amount of radiogenic Pb in undisturbed zircon depends on the initial concentration U incorporated in the crystal and the age of the zircon.

The older the zircon the more likely that it will have more radiogenic Pb. For Archaean zircons, ~100 ppm of radiogenic Pb is fairly common. Given a prismatic zircon of 100 μm×100 μm×250 μm dimension, weighing about 10 microgram, the amount of radiogenic Pb would be ~1 ng. If a tolerable limit of the ratio of radiogenic Pb versus Pb blank is taken as 50, then for such crystal, up to 20 picogram of Pb blank will yield a reasonable determination of

the isotopic ratios of the sample. A higher Pb blank is acceptable only if the amount and isotopic ratios of such Pb blanks can be constrained by reproducible analyses of total procedural blanks. For larger grains, and grains with higher radiogenic Pb content, even higher Pb blank can be tolerated. Radiogenic Pb contents of younger zircons are generally less than older zircons. So precise analyses of younger zircons demands lower analytical Pb blanks.

A.4.3.2. Sources of Pb contamination in conventional Isotope Dilution Thermal Ionisation Mass spectrometry (IDTIMS) method and ways to reduce Pb-contamination

Conventional IDTIMS analyses of zircon and monazite broadly involves the following procedures: (i) Separation and selection of the grains (ii) complete dissolution of the grains by various acids, (iii) conversion of the dissolute into chloride or bromide salts, (iii) separation of U and Pb from these salts in anion exchange resin columns, (iv) loading of U and Pb onto Rhenium filaments and (v) mass spectrometric analyses of these metals. Each of these procedural steps are a potential source of Pb contamination.

A.4.3.2.1. Infrastructure

(a) Apparatus: One of the major steps to be completed in setting up a new low-Pb isotope laboratory, such as the laboratory at the University of Cape Town, is cleaning of various apparatus. Newly acquired apparatus may contain extraneous Pb and is thus prone to Pb-leaching for an extended period of time. During chemical procedures such leaching of Pb becomes a major source of contaminant of the sample. All newly acquired apparatus (for example, Teflon® beakers, digestion vessels, storage bottles, resin columns, pipette tips etc) were treated with various warm to hot strong acids (HNO_3, HCl, and HF) for an extended period of time (6-8 weeks). Various acids were alternated at 3-4 days intervals. This procedure was continued until the blank analyses from these different vessels gave an acceptably low level of Pb.

(b) Reagents: The main reagents used for separating U, Pb and Th from the samples are H_2O, HCl, HF, HNO_3, HBr, H_3PO_4 and anion exchange resin. Except for HBr, H_3PO_4 and resins, other reagents are cleaned by two cycles of two-bottle sub-boiling distillation. Water used for the distillation is provided by a Millepore® water purification system. Frequent replacement of filters and the placing of additional filters in this system help keep the Pb blank of H_2O to a low level. HBr and H_3PO_4 were cleaned by passing through an anion exchange resin in HBr medium. The anion exchange resin is cleaned by 6N HCl. Newly acquired resin is washed by clean H_2O and allowed to settle for some time. The finer fraction of the resin is then decanted off. This procedure is repeated several times until most of the finer fractions of the resin is removed. The resin is then washed alternately by 10-15 times by H_2O and 6N HCl over a 2 weeks period. Cleaned resin is then stored in H_2O.

A.4.3.2.2. Contamination during chemical procedure

Pre-dissolution contamination:

Surface defects and coatings on the selected zircon grain can become a major source of contamination. Before dissolution, zircons are abraded in an air-abrader to remove the outer surface of zircon grains. Surface adherence of pyrite and other contaminant are removed by treating the abraded grains in warm dilute (~30%) HNO_3[12] for about 15 minutes, decanting off the acid, and then washing with acetone. Selected crystals of zircon are transferred into 0.3ml Savillex® Teflon capsules for dissolution by 70% HF acid. Before acid dissolution, the zircons are again cleaned inside the Savillex® capsules with warm 6N HCl and MQH2O.

[12] Although Black (1987) states that this HNO_3 wash procedure leaches Pb out of zircon and is a major source of discordancy in the analytical results, a number of highly concordant analyses obtained in the present work in both old and young zircons does not support this interpretation. His interpretation was possibly influenced by the high Pb-blank (~200 picograms) in their analyses, which if not similar in all analyses can influence analytical results to a great extent.

Contamination during dissolution

Zircon grains are dissolved in ~150 µl of 70% HF acid in 0.3ml Savillex capsules. 15 such capsules are fit together in a Parr® acid dissolution bomb which is then kept in an oven at 210°C for 40-60 hours. After dissolution, the dissolutes are dried in a hot plate. The dried material are again mixed with ~150 µl of HCl for conversion of the sample to chloride and to ensure equilibration of the spike with the sample. A potential source of contamination in this stage is leaching of Pb from the Savillex® capsules. This is specially true for a newly acquired capsules. Before using these capsules for dissolution of samples, several blank dissolution procedures are carried out in these capsules and analysed to monitor Pb blank contributions of the capsules.

Contamination during separation of U, Th and Pb from the sample using column chemistry.

This is the most important step in zircon chemistry and is a major source of contamination because it involves several steps of handling of the samples by transferring from one container to the other.

Pb is normally separated from the samples by elution with HCl (Catanzaro and Kulp, 1964) or with HBr (Chen and Wasserburg, 1981) on anion exchange resins. If the reagents and the vessels for this procedure are clean, Pb-blank associated with this step can be improved by adhering to strict handling procedure. To keep handling of the samples to the minimum, the zircon dissolutes in chloride-form are directly transferred to the columns from the dissolution capsules.

Loading blank:

Pb and U+Th are loaded separately on Re filaments in silica gel and colloidal graphite medium, respectively. Re filaments are outgassed in high vacuum at 4-5 Amp current prior to loading samples on to them. Samples are transferred from the beaker to the Re filaments with clean Teflon® capillary tubing. Each Teflon® tubing is cleaned with warm 6N HCl prior to use--making sure that the inside of the tubes are also filled with 6N HCl.

Mass spectrometric run:

The first source plate of the mass spectrometer and hats covering the filament blocks are a source of common Pb inside the mass spectrometer. These items need to be cleaned and replaced prior to each set of analyses. During the mass spectrometric run, it is essential that data should be collected during a steady ion-beam. It is generally observed that at lower temperatures, the Pb ion-beam is generally affected by isobaric interferences. Such interferences at mass 204 can lead to apparent increases in common Pb estimation.

REFERENCES:

Aftalion, M., Bowes, D.R., Dash, B. and Demoster, T.J., 1988. Late Proterozoic charnockites in Orissa, India: A U-Pb and Rb-Sr isotopic study. Journal of Geology: **96**, 664-676.

Anand Mohan, 1996. The Madurai granulite block. In, M. Santosh and M. Yoshida (eds.) Archean and Proterozoic terrains in southern India within East Gondwana. 223-242

Anil Kumar, Sivaraman, T.V., Bhaskara Rao, Y.J. and Gopalan, K., 1989. Rb-Sr ages of two dyke swarms from the Dharwar craton, Karnataka (abstr.). Int. Symp, Structure and dynakics of the Indian Lithosphere, NGRI:3.

Anil Kumar, Gopalan K. 1992. Precise Rb-Sr age and enriched mantle source of the Sevathur carbonanites, Tamil Nadu . Curr Sci., **60**: 653-655.

Anil Kumar, Bhaskar Rao Y. J., Sivaraman T V, Gopalan K 1996 Sm- Nd ages of Archaean metavolcanics of the Dhawar craton, South India, Precambeian Res., **80**, 205-216.

Arndt, N. T. and Goldstein, S. L. 1987. Use and abuse of crust-formation ages. Geology, 15, 893-895.

Arogyaswamy, R, N, P, 1962 The Origin of the Palghat Gap, Rec Geol. Sur. Ind. **98**, 129-134.

Arthur, M.A., Dean, W.E. and Claypool, G.E. 1985. Anomalous ^{13}C enrichment in modern marine organic carbon: Nature, **315**, 216-218.

Ashwal LD, 1993. Anorthosites, Springer -Verlag, Berlin Heidelberg, New York.

Ashwal. L.D., de Wit, M.J., Cox, R. M., Tucker, R.D., Muller, B.G.J., Rambeloson, R.A. 1996. Geology of Madagascar: Overview and Perspectives, IGCP-368, Trivandrum, India.

Ashwal, L. D., Morel, V. P. I. and Hamilton, M. A. (1998). Geology,petrology and isotope geochemistry of massif-type anorthosites from southwest Madagascar: Contrib. Mineral. Petrol., **133**, 389-401

Ashwal, L. D., Tucker, R. D. and Zimmer, E. K. 1999. Slow cooling of deep crustal granulites and Pb-loss in zircon. Geochem. Coscochim. Acta. (submitted).

Aswathanarayana, U. 1964. Isotopic ages from the Eastern Ghats and Cuddapahs of India. Jour. Geophys. Res. **69**, 3479-3486

Balakrishnan, S. and Rajamani, V., 1985. Geochemistry and petrogenesis of granitoids around the Kolar schist belt, South India: contraints for the evolution of the crust in the Kolar area. Journal of Geology: **95**, 219-240.

Balakrishnan, S., Hanson, G. N. and Rajamani, V., 1990. Pb and Nd isotope constraints on the origin of high Mg- and tholeiite amphibolites, Kolar schist belt, southern India. Contrib. Mineral. Petrol., **107**, 272-292

Bartlett, J. M., Dougherty-Page, J. S., Harris, N. B. W., Hawkesworth, C. J. and Santosh, M. 1998. The application of single zircon evaporation and model Nd ages to the interpretation of polymetamorphic terrains: an example from the Proterozoic mobile belt of south India. Crontrib. Minreal Petrol., 131, 181-195

Bartlett, J. M; Harris, N. B. W; Hawesworth C. J. and Santosh, M. 1995. New Isotope constraints on the crustal evolution of south India and Pan-African granulite metamorphism. Mem. Geol. Soc. Ind. **34**. 391-397.

Baud, A., Margaritz, M., Rehovot, and Holser, W. T. 1989. Permian-Triassic of the Tethys: Carbon isotope studies. Geologische Rundschau, **78(2)**. 649-677.

Baur, N. , Kröner, A., Todt, W., Liew, T. C., Hofmann, A. W., 1991. U-Pb isotopic systematics of zircons from prograde and retrograde transition zones in high-grade orthogneisses, Sri Lanka. J. Geol., **99**, 527-545

Beckinsale, R.D., Drury, S. A. and Holt R.W., 1980. 3360-Myr old gneisses from the south Indian craton. Nature, **283**, 469-470

Ben Othman, D., Polve, M. and Allegre, C. J. 1984. Nd-Sr isotopic composition of granulite and constraints on the evolution of the lower continental crust. Nature, **307**, 510-515

Berner, R. A., 1989. A new model for atmospheric oxygen over phanerozoic time., Am. J. Sci., **289**, 333-361.

Berner, R. A., 1990. Atmospheric carbon dioxide levels over Phanerozoic time. Science, **249**, 1382-1386

Bernard-Griffiths, J., Jahn B-M., and Sen S.K., 1987. Sm-Nd isotopes and REE geochemistry of Madras granulites: an introdurtory statements. Precamb. Res. **37**, 343-355.

Bhaskar Rao, Y. J.; Chetty T. R. K.; Janardhan, A. S. and Gopalan, K. 1996. Sm-Nd and Rb-Sr ages and P-T history of the Archean Sittampundi and Bhavni layered meta-anorthosite complexes in Cauvery shear zone, South India: evidence for Neoproterozoic reworking of Archean crust. Contr. Minl. Petro., **125**, 237-250.

Bhaskar Rao, Y. J., Sivaraman, T. V., G. V. C. Pantulu, Gopalan, K. and Naqvi, S. M. 1992. Rb-Sr ages of Late Archean metavolcanics and granites, Dharwar craton, South India and evidence for Early Proterozoic thermotectonic event(s). Precambrian Research, **62**, 145-170.

Bhaskar Rao, Y. J., Naha, K., Srinivasan, R. and Gopalan, K., 1991. Geology, geochemistry and geochronology of Peninsular gneisses around Gorur, Hassan district, Karnataka, proc. Ind. Acad. Sci. (Proc. Earth Planet. Sci.), **100**, 399-412

Bhattacharyya, C., 1966. A reinterpretation of the colour of feldspars in charnockites from some parts of Srikakulam district, Andhra Pradesh. Q. Jr. Geol. Soc. India., 38, 61-62

Bhattacharyya, C., 1977. Present status of the charnockite problem with special reference to the progress of research on charnockite and orthopyroxene-bearing granolites of India., Indian Journal of Earth Sciences, S. Ray vol., 195-223

Bhattacharya, S., Sen, S. K., and Acharya, A., 1993. Structural evidence supporting a remnant origin of patchy charnockite in the Chilka Lake Area, Orissa. Geol. Mag., **130**, 363-368

Black, L. P., harley, s. L., Sun, S. S. and McCulloch, M. T., 1987. The Rayner Complex of East Antarctica: complex isotopic systematics within a Proterozoic mobile belt. J. Metamorph. Geol., **5**, 1-26

Black, L. P., Sheraton, J. W. And james, P. R., 1986. Late Archean granites of the Napier Complex, Enderby Land, Antarctica: a comparison of Rb-Sr, Sm-Nd and U-Pb isotopic systematics in a complex terrain. Precambrian Res., **32**, 343-368

Black, L. P. 1987. Recent Pb loss in zircon: a natural oLaboratory-induced phenomenon? Chemical Geology (Isotope Geoscience Section), **65**, 25-33.

Bohlender, F., van Reenen, D. D., Barton (jr) J. M., 1992. Evidence for metamorphic and igneous charnockites in the Southern Marginal Zone of the Limpopo Belt, southern Africa., Precambrian Research, **55(1-4)**, 429-450

Bowring, S. A., Grotzinger, J. P., Isachsen, C. E., Knoll, A. H., Pelechaty, S. M. and Kolosov, C. 1993. Calibrating Rates of Early Cambrina Evolution. Science. **261**, 1293-1298.

Bowring, S. A., Erwin, D. H., Jin, Y. G., Marti, M.W., Davidek, K., and Wang, W., 1998, Geochronology of the end-permian mass extinction: Science, 280, 1039-1045.

Bowring, S. A. and Erwin, D. H., 1998. A new look at evolutionary rates in deep time: uniting paleontology and high-precision geochronology, GSA Bull. (in press).

Brandon, A. D. and Meen, J. K. 1995. Isotopic evidence for the position of southernmost Indian terranes within East Gondwana. Precambrian Research, **70**, 269-280.

Bùhl, D. , Grauert, B., and Raith, M. 1983. U-Pb zircon dating of Archean rocks from the Southern Indian Craton: results from the amphibolite to granulite facies transition zone at Kabbal Quarry, southern Karnataka. Fortschritte der Mineralogie. **61(1)**, 43-45.

Bùhl, D. 1987. U-Pb and Rb-Sr Alterbestimmungen and undersuchungen zum stontium isotopenaustausch an granuliten sudiindiens, Thesis Ph. D., University of Munster, FRG (unpublished)

Buick, I. S. and Holland, T. J. B., 1991. The nature and distribution of Fluids during amphibolite facies metamorphism, Naxos (Greece). Jour. Metamorphic Geol. **9**, 301-314.

Burton, K. W. and O'Nions, R. K. 1990. The timescale and mechanism of granulite formation at Kurunegala, Sri Lanka. Contr. Minl. Petrol. **106**, 66-89.

Burton, K. W. and O'Nions, R. K. 1991. High-resolution garnet chronometry and the rates of metamorphic processes. Earth Planet. Sci. Lett. **107**, 649-71.

Catanzaro, E. J. and Kulp, J. L. 1964. Discordant zircons from the Little Butte (Montana), Beartooth (Montana) and Santa Catalinea (Arizona) Mountains. Geochim Coscochim. Acta. **28**, 87-124.

Chacko. T. 1987. Petrologic, geochemical and isotopic studies in the charnockite-khondalite terrain of southern Kerala, India: the deposition and granulite-facies metamorphism of a Precambrian sediemntary sequence. Thesis, Ph.D, University of North Caroline, U. S. A. (unpublished).

Chacko T., Kumar G.R.R. and Newton R. C., 1987. Metamorphic P-T conditions of the Kerala (south India) Khondalite Belt, a granulite-facies supracrustal terrain. Jr. Geol. **95**, 343-358.

Chacko, T., Ravindra Kumar, G. R. Meen, J.K. and Rogers, J.J.W., 1992. Geochemistry of high-grade supracrustal rocks from the Kerala Khondalite Belt and adjacent massif charnockites, South India. Precambrian Research. 55: 469-489.

Chacko, T., Lamb, M. and Farquhar, J., 1996. Ultra-high temperature metamorphism in the Kerala Khondalite Belt. In, M. Santosh and M. Yoshida (eds.) The Archean and Proterozoic terrains of southern India within East Gondwana., Gond. Res. Group Mem., 3, 157-165

Chacko, T.; Lamb, M. and Farquhar, J. 1996. P-T conditions in the Kerala Khondalite Belt revisited: evidence for ultra-high temperature metamorphism resulting from the intrusion of C-type magmas. In, M. Santosh and M. Yoshida (eds.) Proc. IGCP-368 International Field Workshop on Proterozoic Continental Crust of Southern India (August, 1996). Gond. Research Group Misl. Publ. (4).

Chapman, H. J. and Roddick, J. C. 1994. Kinetics of Pb release during the zircon evaporation technique. Earth Planet. Sci. Lett. 121: 601-611

Chandra, S. , 1998. Plant colonisation of Gondwana and sebsequent speciation/diversification on Gondwana fragments. Jr. of African Earth Sciences, 27(1A), 43

Chen, J. H. and Wasserburg, G. J. 1981. Isotopic determination fo uranium in picomole and sub-picomole quantities. Anal. Chem. **53**, 2060-7.

Chetty, T. R. K. and Bhaskar Rao, Y. K., 1996. The Cauvery shear zone in the Precambrian granulite terrain, South India: a case for westward thrusting. In., proc. Of the UNESCO-IUGS-IGCP-368

Int. Field Workshop on the Proterozoic Continental Crust of Southern India (August, 1996). Trivandrum (India). Gond. Res. Group. Miscell Pub. 4. , 17-19

Chetty, T. R. K. 1996. Proterozoic shear zones in Southern Granulite Terrain, India. *In*, M. Santosh and M. Yoshida (eds.) The Arhean and Proterozic terrains in Southern India within East Gondwana. Gondwana Research Group Memoir-3. 77-89.

Chetty, T. R. K. 1995. A correlation of Proterozic shear zones between Eastern Ghat, India and Enderby Land, East Antarctica, based on LANDSAT imagery. *In*, M. Yoshida and M. Santosh (eds.) India and Antarctica during the Precambrian. Geol. Soc. of Ind. Mem. **34**, 205-220

Choudhary, A. R., Harris, N.B.W., van Calsteren P. C., and Hawkesworth, C. J., 1992. Pan-African charnockite formation in kerala, South India, Geol. Mag. **129**, 257-267.

Claoué-Long, J. C., Zichao, Z., Guogan, M., and Shaohua, D., 1991. The age of the Permian-Triassic boundary: Earth and Planet. Science Lett., 105, 182-190

Clemens, J. D. 1990. The granulite-granite connexion. *In*, D. Vielzeuf and Ph. Vidal (eds.), Granulites and Crustal Evolution, Kluwer Academic Publishers. Netherlands. 25-36.

Cliff, R. A. 1985. Isotopic dating in metamorphic belts, Jour. Geol. Soc. London, **142**: 97-100.

Cliff, R. A.; Cahen, A. 1980. Uranium-lead isotope systematics in a regionally metamorphosed tonalite from the Eastern Alps, Earth Planet Sci. Lett. **50: 211-218.**

Cocherie, A., Guerrot, C., Rossi, P., 1992. Single zircon dating by step-wise Pb evaporation: comparison with other geochronological techniques applied to the Hercynian granites of France. Chem. Geol. Isot. Geosci., 25, 131-151

Compson, J. S., Snyder, S. W. And Hodell, D. A. 1990. Phosphogenesis and weathering of shelf sediments from the southeastern United States: Implications for Miocene $\delta^{13}C$ excursions and global cooling. Geology. **18**, 1227-1230.

Compson, W., Williams, I. S., Kirschvink, J. L., Zichao, Z. and Guogan, M. A. 1992. Zircon U-Pb ages for the Early Cambrian time-scale. Jr. Geol. Soc. of London, **149**, 171-184.

Compston, W., Williams, I. S. and Meyer, C. 1984. U-Pb geochronology of zircons from Lunar Breccia 73217 using a Sensitive High Mass-Resolution Ion Microprobe. Proceedings of the Fourteenth Lunar and Planetary Science Conference, Part 2: Journal of Geophysical Research, **89**, Supplement, B525-B534.

Condie, K. C. and Allen, P. 1984. Origin of Archean charnockites from southern India. *In*, A. Kroner et al. (eds.) Archean Geochemistry, Spiringer-Verlag, Berlin.

Copeland, P., Parrish, R. R. And Harrison, T. M., 1988. Identification of inherited radiogenic Pb in

monazite and its implication for the U-Pb system. Nature, **333**, 700-703

Craig, H., 1953. Geochemistry of the stable carbon isotopes., Geocheim, Coscochim. Acta, **3**, 53-92

Crawford, A.R., 1969. Reconnaissance Rb-Sr dating of the Precambrianrocks of southern Peninsular India: Geol. Soc. India Jour., **10**. p. 117-166.

Crawford, A. R., 1969. India, Ceylon and Pakistan: New age data and comparisons with Australia, Nature, **233**, 380-384.

Crookshank, H., 1938. The western margin of the Eastern Ghats in Southern Jeypore: Geol. Sur of India Records , **73**, 398-434.

Dao-Yi, Xu, Zheng, Y., Qin-Wen, Z., Zhi-Da, S., Yi-Yin, S., Lian-Fang, Y., 1986. Significance of a δ13C anomaly near the Devonian/Carboniferous boundary at the Muhua section, South China., Nature, 321, 854-856.

Dao-Yi, Xu and Zheng, Yan, 1993. Carbon isotope and iridium event markers near the Permian/Triassic boundary in the Meishan section, Zhejiang Province, China: Palaeogeography, Palaeoclimatoloty, Palaeoecology, **104**, 171-176.

Davidek, K., Landiing, E., Bowring, S. A., Westrop, S. R., Rushton, A. W. A., Fortey, R. A. and Adrian, J. M., 1998. New uppermost Cambrian U-Pb date from Avalonian Wales and age of the Cambrian-Ordovician boundary., Geol. Mag., 135 (3), 305-309.

Davis, D. W., Sewell, R. J. and Campbell, D. G. 1997. U-Pb dating of Mesozoic igneous rocks from Hong Kong, Jr. Geol. Soc. Lond., 154, 1067-1076

Degens, E. T., 1969., Biogeochemistry of stable isotope, In, G. Eglinton and M. T. J. Murphy (eds.), Organic Geochemistry: methods and results: New York, Springer-Verlag, 304-329.

de Paolo D. J., 1988. Neodymium isotope geochemistry. Springer, Berlin Heidelberg New York, 187p.

Derry, L. A., Brasier, M. D., Corfield, R. M., Rozanov, A. Y., Zhuravlev, A. Y., 1994. Sr and C isotopes in Lower Cambrian carbonates from the Siberian craton: A paleoenvironmental record during the Cambrian explosion., Earth and Planetary Science Letter, 128, 671-681

Deters-Umlauf, P., Srikantappa, C. and Köhler, H., 1997. Pan-African ages in the Moyar- and Bhavani shear zone (south India): First geochronological results. In, R. Cox and L. D. Ashwal (eds.), Proc. Of the UNESCO-IUGS-IGCP-348/368 Int. Field Workshop on Proterozoic geology of Madagascar., Antananarivo, Madagascar, 18-19

de Wit, M. J., Jeffrey, M., Bergh, H. and Nicolaysen, L. 1988. Geological map of Gondwana, scale 1:10,000,000 with explanations and references. Am. Assos. Petrol. Geol. Oklahoma.

de Wit, M. J, Vitali, E., and Ashwal, L. 1995. Gondwana Reconstruction of the East Africa - Madagascar - India - Sri Lanka - Antarctica fragments revisited. Centennial Geocongress, extended abstracts, vol. 1, Geological Society of South Africa, 218-221.

de Wit, M. J., Ghosh, J. G., Bowring, S. A. and Ashwal, L., 1998. Late Proterozoic shear zones in Madagascar and India: Gondwana "life lines". In, Special Abstract Issue, Gondwana-10, Jr. of African Earth Sciences, **27 (1A)**, 58

DeLaune, R.D., 1986. The use of $\delta^{13}C$ signature of C-3 and C-4 plants in determining past depositional environments in rapidly accreting marshes of the Mississipi river deltaic plain, Louisiana, U.S.A., Chemical Geology (Isotope Geoscience Section), **59**,315-320.

Des Marais, D. J., Straus, H., Summons, R. E. and Hayes, J. M., 1992. Carbon isotope evidence for the stepwise oxidation of the Proterozoic environment., Nature, 359, 605-609

Dickin, A. P., 1995. Radiogenic Isotope Geochemistry. Cambridge: Cambridge University Press. 452p.

Divakara Rao, V.; Subba Rao, M. V. and Murthy, N.N. 1989. Distribution of Th, U and K in the Eastern Ghat granulite belt-Evidence for post-metamorphic metasomatic activity. Y.J. Rao's 60th Birthday Volume, pp.85-90.

Dodson, M. H., 1979. The theory of colling ages. In, Lectures in Isotope Geology (eds. E. Jager and J.C. Hunziker), 194-202. Heidelber: Springer-Verlag.

Dodson, M. H., 1973. Closure temparatures in cooling geochronological and petrological systems. Contrib. Mineral. Petrol. **40**: 259-273.

Drury, S.A.,1983. The petrogenesis and setting of Archaean metavolcanics from Karnataka State, South India. Geochemica Coscochemica Acta: ,317-329.

Drury, S. A., and Holt, R.W. 1980. The tectonic framework of the south India craton: a reconnasissance involving LANDSAT imagery, Tectonophysics, **65**, T1-T15.

Drury , S. A., Harris NBW, Holt R. W., Reeves-Smith G.J and Wightman R. T., 1984. Precambrian tectonics and crustal evolution in south India., J. Geol., **9**. 277-287.

Drury, S. A., Holt, R. w. Van Clasteren, P. C. and Beckinsale, R.D., 1983. Sm- Nd and Rb - Sr ages for Archean rocks in western Karnataka, South India. J. Geol. Soc. India, **24**, 454 - 459.

Drury S.A. and Holt R.W., 1980. The tectonic framework of the South Indian Craton: a reconnaissance involving Landsat imagery, Tectonophysics. **65**, p. T1-T15

Du Toit, A. L., 1937. Our wandering continents. Oliver and Boyd, Edinburg. 366p.

Dunai, T. J. and Touret, J. L. R. 1993. A noble gas study of a granulite sample from the Nilgiri Hills,

southern India: implications for granulite formation. Earth and Planetary Sciences Letters, **119**, 271-281.

Dunai, T. J. and Touret, J. L. R. 1993. A noble gas study of agranulite sample from the Nilgiri Hills, southern India: implications for granulite formation. Earth and Planetary Sciences Letters, **119**, 271-281

Dunai, T. J.; Touret, J. R. L. & Villa, I. M. 1992. Mantle derived helium in fluid inclusions of a 2.5 Ga old granulite, Nilgiri Hills, Southern India. In, Water rock interaction, Kharaka & Maest (eds.). Balkema: Rotterdam.

Ehleringer, J. R., Sage, R. F., Flanagan, L. B. and Perarcy, R W., 1991. Climate change and the evolution photosynthesis., Tree., **6(3)**, 95-99

Ehleringer, J. R. and Monson, R. K., 1993. Evolutionary and ecological aspects of photosynthetic pathway variation., Annu. Rev. Ecol. Syst., 24, 411-39

Erwin, D.H., 1993. The great Paleozoic crisis., Columbis University Press, New York, Critical moments in paleobiology and earth history series, 327p.

Erwin, D. H., 1994. The Permo-Triassic extinction. Nature, 367, 231-236

Farquhar, J. and Chacko, T. 1991. Isotopic evidence for involvement of CO_2-bearing magmas in granulite formation. Nature. **354**. 60-62.

Faure, G., 1986. Principles of Isotope Geology, 2nd ed., New York: Wiley & Sons.

Faure, K., de Wit, M. and Willis, J.P. 1995. Late permian global coal hiatus linked to ^{13}C-depleted CO_2flux into the atmosphere during the final consolidation of Pangea: Geology, 23(6), 507-510.

Fermor, L. L., 1950. Pre-Cambrian formations of India. (Discussion). Geol. Mag. 87(2), 140-144.

Fermor, L. L., 1936. An attempt at the correlation of the ancient schistose formations of Peninsular India, Mem. Geol. Sur. Ind. v. 70.

Forsman J.P., 1963. Geochemistry of kerogen, In: Irving A. Berger (ed.) , Organic Geochemistry, Symposium Pubs. Divn., New York, Monogram 16.Earth Science Series.

Francey, R. J. and Farquhar, G. D., 1982. An explanation of $^{13}C/^{12}C$ variation in tree rings, Nature, **297**, 28-31

Friend, C. R. L. and Nutman, A. P. 1992. Response of U-Pb isotopes and whole rock geochemistry to CO_2 induced granulite facies metamorphism, Kabbaldurga, Karnataka, south India. Contrib. Mineral. Petrol. 111, 299-310.

Friend, C. R. L., 1981. Charnockite and granite formation and influx of CO2 at Kabbaldurga, Nature, **294**, p. 550-551.

Friend, C. R. L., 1985. Evidence for fluid pathways through Archean crust and the formation of the Closepet Granite, Karnataka, India. Precambrian Research, **27**, 239-250

Friend, C. R. L. and Nutman, A. P. 1991. SHRIMP U-Pb geochronology of Closepet Granite and Peninsular Gneiss, Karnataka, South India. J. Geol. Soc. India, **38**, p. 357-368

Fyfe, W. S. 1973. The granulite facies, partial melting and the Archean crust. Philos. Trans. R. Soc. London, Ser. A, **273**, 457-461.

Garrels, R. M., and Lerman, A., 1984. Coupling of the sedimentary sulfer and carbon cycles -- an improved model: American Journal of Science, 282, 474-511.

Ganguli, J; Singh, R. N. and Ramana, D. V. 1995. Thermal perturbation during charnockitization and granulite facies metamorphism in southern India. Jr. Metamorphic Geol., 1995, **13**. p. 419-430.

Galimov, E. M., 1980. C^{13}/C^{12} in Kerogen., In, B. Durand (ed.) Kerogen: insoluble organic matter from sedimentary rocks, Eclitus Technip, Technip, Paris. 271-299

GSI (Geological Survey of India). 1988. Isotopic age map of Peninsular India (with explanatory brochure. Scale 1:5 million).

GSI (Geological Survey of India). 1981. Geological and Mineral map of Karnataka and Goa (with explanatory brochure. Scale 1:0.5 million).

GSI (Geological Survey of India.) 1994. Project Vasundhara. Generalised Geological Map (scale 1:2 million).

GSI (Geological Survey of India). 1995a. Geological and Mineral map of Tamil Nadu and Pondichery (scale 1:0.5 million).

GSI (Geological Survey of India). 1995b. Geological and Mineral map of Kerala (scale 1:0.5 million).

Getty, S. R., Selverstone, J. Wernicke, B.P., Jacobson, S.B., Aliberti, E. and Lux, D.R. 1993. Sm-Nd dating of multiple garnet growth events in an arc-continent collision zone, northwestern U.S. Cordillera: Contrib. Mineral. Petro., **115**, pp. 45-57.

Ghosh, P.K. 1941. The charnockite series of Bastar state and western Jeypore. Records of the Geological Survey of India, **15**, 55

Gopalakrishna, D., Hansen, E.C., Janardhan, A.S. and Newton, R.C., 1986. The southern high-grade margin of the Dharwar craton. Journal of Geology: **94**, 247-260.

Gopalakrishnan, K., Venkata Rao, V. and Viswanathan, T. V. 1990. Role of Pleo-Sutures in the evolution of Southern Indian Granulite Terrain: Group discussion on Suture zones- young and Old (extended abstract), Wadia Institure of Himalyayan Geology, Dehra Dun, India., 55-60

Gopalakrishnan, K., 1981. Report on the traverses taken across Coimbatore and Nilgiri districts, Tamil Nadu. Geol. Sur. Ind. (Unpub. Report.)

Gopalakrishnan, K., 1995. An overview of Southern Granulite Terrain, India - constraints in Reconstructionof Precambrian Assembly of Gondwanaland. 9th International Gondwana Sym., Hyderabad, Ind.

Gopalakrishnan, K., 1998. Extensions of Eastern Ghats mobile belt, India - a geological enigma. Geol. Sur. Ind. Spl. pub. 44, 22-38

Grew, E. S.; and Manton, W. I., 1986. A new correlation of sapphirine granulites in the Indo-Antarctic metamorphic terrain: late Proterozoic dates from the Eastern Ghats Province of India. Precamb. Res. **33**, 123-137.

Grew, E. S. and Manton, W. I. 1984. Age of Allanite fromKabbaldurga quarry, Karnataka, J. Geol. Soc. India. **25**, 193-195.

Gruau, G.; Rosing, M.; Bridgwater, D. and Gill, R.C.O. 1996. Resetting of Sm-Nd systematics during metamorphism of > 3.7 Ga rocks: implications for isotopic models of early Earth differentiation. Chemical Geology v.133, 225-240.

Haggerty, S. G., 1990. Redox state of the continental lithosphere. *In*, Martin A. Menzies (ed.) Continental Mantle, Clarendon Press, Oxford. Oxford Monographs on Geology and Geophysics, **16**, 87-109.

Hansen, E. C.; Hickman, M.H.; Grant, N. K.; and Newton, R. C. 1985. Pan-African age of Peninsular Gneiss, near Madurai, South India. EOS, **66**, 419-420.

Hansen, E. C., Newton, R. C. and Janardhan, A. S. 1984. Fluid inclusions in rocks from the amphibolite-facies gneiss to charnockite progression in southern Karnataka, India: direct evideence concerning the fluids of granulite metamorphism. J. Metamorphic Geol. **2**, 249-64.

Hansen, E. C.; Stern, R. J.; Devaraju, T. C.; Mahabaleswar, B., and Kenny, P. J., 1997. Rubidium-strontium whole-rock ages of banded and incipient charnockites from southern Karnataka. Jour. Geol. Soc. Ind., **50**. P. 267-275.

Hansen, E. C., Janardhan, A. S., Newton, R. C., Prame, W. K. B. N. and Ravindra Kumar, G. R. 1987. Arrested charnockite formation in southern India and Sri Lanka. Contrib. Mineral. Petrol. **96**, 244-55.

Hari Narain and Subrahmanyam, 1986. Precambrian tectonics of the south Indian shield inferred from geophysical data. Jr. Geol., **94**. 187-198.

Harley, S. L. 1989. The origin of granulites: a metamorphic perspective. Geological Mag., 126, 215-247.

Harris, N. B. W., Holt, R. W. & Drury, S. A., 1982, Geobarometry, geothermometry and late Archaean geotherms from the granulite facies terrain of South India. J. Geol., 90, p. 509-527.

Harris, N. B. W. and Bickle, M. J., 1989. Advective fluid transport during charnockite formation; an example from southern India. Earth and Planetary Science Letters, **93**, 151-156.

Harris, N. B. W. and Santosh, M., 1993. Chronologic constraints on granulite formation in southern India and Sri Lanka. Mem. Geol. Soc. Ind. **25**, 361-379.

Harris, N. B. W.; Jackson, D. H.; Mattey, D. P.; Santosh, M and Bartlett, J; 1993. Carbon-isotope constraints on fluid advection during contrasting examples of incipient charnockite formation. Jr Metamorphic Geol., **11** p. 833-843.

Harris N.B.W.; Santosh M.; and Talor P.N., 1994. Crustal Evolution in South India: Constraints from Nd Isotopes. Jour. Geology, **102**, p. 139-150

Harris, N. B. W.; Bartlett, J. M. and Santosh, M. 1996. Neodymium isotope constraints on the tectonic evolution of East Gondwana. Jour. Southeast Asian Earth Sci. **14 (3/4)**, p. 119-125.

Harrison, T. M.l McDougall, I. 1982. The thermal significance of potassium feldspar K-Ar ages inferred from $^{40}Ar/^{39}Ar$ spectrum results, Geochem. Coscochim Acta, **46**: 1811-1820.

Hawkins, D. P. and Bowring, S. A., 1997. U-Pb systematics of monazite and xenotime: case studies from the Paleoproterozoic of hte Grand Canyon, Arizona., Contrib. Mineral. Petrol., **127**, 87-103.

Heaman, L. and Parrish, R., 1991. U-Pb geochronology of accessory minerals. *In*, Heaman, L., and Ludden, J.N. (Eds.), Application of radiogenic isotope systems to problems in geology- short course handbook, Min. Asson. Canada, **19**, 59-102

Heimann, M. And E. Maier-Reimer. 1996. On the realtions between the oceanic uptake of CO2 and its carbon isotopes. Global Biogeochem. Cycles., **10**, 89-110

Hoefs, J. & Touret. J. R. L. 1975. Fluid inclusion and carbonisotope study from Bamble grnulites (S. Norway). Contrb. Mineral. Petrol. **52**, 165-174.

Hoernes, S.; Fiorentini, E. and Hoeffbauer, R. 1994. The role of fluids in grnulite-facies metamorphism as deduced from oxygen and carbon isotope composition. Precambrian Research, **66**, 183-198.

Hoffman, P. F., Kaufman, A. J., Halverson, G. P. and Schrag, D. P., 1998. A Neoproterozoic snowball earth, Science, 281, 1342-1346

Holland, T. H., 1900. The charnockite series; A group of Archean hypersthenic rocks in peninsular India.

Geol. Sur. India Mem. 28(2), 192-249

Hollander, D.J., McKenzie, J.A. and Hsü K.J.,1993. Carbon isotope evidence for unusual plankton blooms and fluctuations of surface water CO_2 in "Strangelove Ocean" after terminal Cretaceous event. : Palaeogeography, Palaeoclimatoloty, Palaeoecology, v.104, 229-237.

Hollister, L. S., 1988. On the origin of CO2-rich fluid inclusions in migmatites. Jr. of Meta. Geol., **6**, 467-474

Hollister, L. S., 1990. Enrichment of CO2 in fluid inclusions in quartz by removal of H2O during crystal plastic deformation. Jour. Struc. Geol., **12**, p.895-901.

Holser, W. T.,Scidlowski, M., Mackenzie, F. T. and Maynar, J. B., 1988. Geochemical cycles of carbon and sulfer. *In*: C. B. Gregor, R. M. Garrels, F. T. Mackenzie and J.B. Maynar (eds.), Chemical cycles in the evolution of the Earth. Wiley Interscience Publication, New York, 105-173.

Holser, W. T., Schönlaub, H. P., Moses, A. Jr, Boeckelmann K., Klein P., Magaritz, M., Orth, C.J., Fenninger, A., Jenny, C., Kralik, M., Mauritsch, H., Pak E., Josef-Michael Schram., Stattergger, K. and Schmöller, R., 1989. A unique geochemical record at the Permian/Triassic boundary. Nature., 337(5), 39-44

Holser, W. T.,and Magaritz, M., 1987. Events near the Permian-Triassic boundary: Modern Geology, 11, 155-180.

Holt, R. W., and Wightman, R. T. 1983. The role of fluids in the development of a granulite facies transition zone in S. India. Geol. Soc. London Jour., **140**, 651-656.

Hottin, G. Présentation et essai d' interprétation du Précambrien de Madagascar- Bull. BRGM, **4**, 117-153.

Hölzl, S., Hofmann, A. W., Todt, W. and Köhler, H., 1994. U-Pb geochronology of the Sri Lankan basement. In: M. Raith and S. Hoernes (eds.), Tectonic, metamorphic and isotopic evolution of deep-crustal rocks- with emphasis on sri Lanka. Precambrian Res., **66**, 123-149

Howell, D. G. 1989. Tectonics of suspect terranes: mountain building and continental growth. 'Topics in Earth Science- 3'. Chapman and Hall. London. p.232.

Howie, R. A. 1954. The geochemistry of the charnockite series of Madras, India. Trans. R. Soc. Edinburgh, **62**, 725-68.

Howie, R. A, 1964. Cahrnockites. Science Progress, 52, **208**, 628-43

Howie, R. A., 1967. Charnockites and their colour. Jr. Geol. Soc. Ind., **8**, 1-7

Hsü, K. J., He, Q., McKenzie, J. A., Weissert, H., Perch-Bielsen, K., Oberhänsli, H., Kelts, K., LaBrecque, J., Tause, L., Krähenbühl, U., Percival, S. R. Jr., Wright, R., Karpoff, A. M., Peterson, N., Tucker, P., Poore, R. Z., Gombos, A. M., Pisciotto, K , Carman, M. F., Jr., and Schreiber, e., 1982., Mass mortality and it's environmental and evolutionary consequences. Science, **216** , 249-256

Ikramuddin, M. and Stueber, A.M. 1976. Rb-Sr ages of Precambrian dolerite and alkaline dykes, south-east Mysore State, India. Lithos, 9: 235-241.

Imbus, S.W., Macko, S.A., Douglas Elmore, R. and Engel, M.H., 1992. Stable isotope (C,S,N) and molucular studies on the Precambrian Nonesuch Shale (Wisconsis- Michigan, U.S.A.): Evidence for differential preservation rates, depositional environment and hydrothermal influence: Chemical Geology (Isotope Geoscience Section), **101**, 255-281.

Isozaki, Y., 1997. Permian-Triassic boundary supernoxia and stratified superocean: records from lost deep sea. Science, **276**. 235-238.

Jacab, K. and Narayanaswamy, S. 1954. The structural and drainage pattern of the Western Ghats in the vicinity of the Palghat gap. Proc. nat. Inst. Sci. India, **20(1)**, 101-118.

Jackson, D. H.; Mattey, D. P.; Harris, N.B.W. 1988. Stable isotope studies from charnockites of south India: the source and role of CO2 in granulite formation. Terra cognita., **8**, C3.

Jacob, K. and Narayanswami, S. 1954 The structural and drainage patterns of the Western Ghats in the vicinity of the Palghat Gap. Proc. Nat. Inst. of Sciences of India, **20**, 104-118.

Janardhan A. S.; Newton R.C. and Hansen E.C. 1982. The transformation of amphibolite facies gneiss to chrnockite in southern Karnataka and northern Tamilnadu, India. Contrib. Mineral. Petrol. **79**, 130-149.

Janardhan, A. S., Newton, R. C. and Smith, J. V. 1979. Ancient crustal metamorphism at low PH_2O: charnockite formation at Kabbaldurga, south India. Nature. **278**. 511-514

Janardhan A. S., Leake B. E. 1975. The origin of the metaanorthositic gabbros and garnetiferous granulites of the Sittampundi complex, Madras , India. J Geol Soc India, **6**:391-408.

Janardhan, A. S. and Wiebe, R. A., 1985. Petrology and geochemistry of the Oddanchatram anorthosite and associated basic granulites, Tamil Nadu, South India. Jour. Geol. Soc. India, 26, 163-176.

Janardhan A. S., Jayananda M, Shankara M. A. 1994. Formation and tectonic evolution of granulities from the Biligiri Rangan and Nilgiri Hills, S. India: geochemical and isotopic constraints. J Geol Soc India, **44**: 27-40.

Jayananda, M., Martin, H., Peucat, J-J and Mahabeswar, B. 1995b. The Late crust-mantle interaction: goechemistry of LRDD enriched mantle derived magmas. The Closepet batholith of southern India. Contrib. Mineral. Petrol. **119**, 314-329

Jayananda, M. and Peucat, J-J. (1995. Archaeancrust formation in southern India: geochronologic and isotopic constraints. In, M. Yoshida, M. Santosh and A. T. Rao (eds), India as a fragment of east Gondwana, Gond. Res. Group. Mem. 2, Field Science Pub., Osaka, Japan, 15-21

Jayananda, M.; and Peucat, J. J. 1996. Geochronological framework of southern India. *In*, M. Santosh and M. Yoshida (eds.) The Archean and Proterozoic terrains of Southern India within East Gondwana. Gondwana Research Group, Mem. 3. 53-75

Jayananda, M.; Janardhan, A. S.; Sivasubrahanian, P.; and Peucat, J. J. 1995. Geochronologic and isotopic constraints on Granulite formation in the Kodaikanal Area, Southern India. Mem. Geol. Soc. Ind., **34**. 373-390.

Jiang, J.; Clayton, R. N. and Newton, R. C. 1988. Fluids in granulite facies metamorphism: a comparative oxygen isotope study on the south India and Adirondack high-grade terrains. Jr. Geol. **96**, 517-533.

Jin-Shi, C., Xue-Lei, C. Mao-Rong, S. and Hua Zhong. 1991. Carbon isotope study of the Permian-Triassic boundary sequences in China. Chemical Geology. **89**, 239-251.

Katz, M. B. and Premoli, C., 1979. India and Madagascar in Gondwanaland based on matching Precambrian lineamnets: Nature, **279**, 312-315

Kaufman, A. J., Hayes, J. M., Knoll, A. H., and Germs, G. J. B., 1991. Isotopic compositions of carbonates and organic carbon from Upper Proterozoic successions in Namibia: stratigraphic variation and the effects of diagenesis and metamorphism., Precambrian Research, **49**, 301-327

Kalia, K. L. and Bhatia, S. C., 1981. Gravity study along Kavali-Udipideep seismic sounding profile in hte Indian peninsular shield. Some inferences about origin of Anorthosites and Eastern Ghat orogeny. Tectonophysics, **70**, 129-143

Kalia, K. L.; Roy Choudhary, K; Reddy, P. R.; Krishna, V. G.; Hari Narain; Subbotin, S. I.; Sollogub, V. B.; Chekunov, A. V.; Kharetchko, G. E.; Lazarenko, M. A. and Ilchenko, T. V., 1979. Crustal structure along Kavali-Udipi profile in the Indian Peninsular shield from deep seismic sounding. Jour. Geol. Soc. Ind. **20**, 303-333.

Katz, M. B. and Premoli, C. 1979. India and Madagascar in Gondwana based on matching Precambrian lineaments. Nature, 279, 312-315

Kaufman, A. J., Hayes, J. M.,Knoll, A. H. and Germs, J. B., 1991. Isotopic composition of carbonates and organic carbon from upper Proterozoic successions in Namibia: stratigraphic variation and the effects of diagenesis and metamorphism. Precam. Res., 49, 301-327.

Kelley, S. P.; Bartlett, J. M. and Harris, B. W. 1997. Pre-metamorphic Ar-Ar ages from biotite inclusions in garnet. Geochemia et Coscochemica Accta, **61(18)**, p. 3873-3878.

Khan, S. A. and Janardhan, A. S. 1989. Retrogression of charnockite to biotite gneiss/ carnbonated

gneiss in Attur Valley, Tamil Nadu. Jr. of Geol. Soc. Ind.: 385-392.

Kilpatrick, J.A. and Ellis, D. J., 1992 Transaction of the Royal Society of Edinburg, **83**, 155-164.

Kilpatrick, J. A. and Ellis D. J. 1992. C-type magmas: igneous charnockites and their extrusive equivalents. Transactions Royal Society of Edinburg: Earth Science, **83**, 155-164

Kinny, P. D., Black, L. P. and Sheraton, J. W. 1997. Zircon U-Pb ages and geochemistry of igneous and metamorphic rocks in the northern Prince Charles Mountains, Antarctica. AGSO Jour. of Australian Geology and Geophysics. **16(5)**, 637-654.

Klatt, E; Hoernes, S. and Raith, M. 1988. Characterization of fluids involved in the gneiss-charnockite transformation in Southern Kerala (India). Jr. Geol. Soc. Ind., **31** pp. 57-59.

Knoll, A. H., Hayes, J. M., Kaufman, A. J., Swett, K., and Lambert, I. B., Secular variation in carbon isotope ratios from Upper Proterozoic successions of Swalbard and East Greenland. Nature, **321**, 832-838

Kober, B. 1986. Whole grain evaporation for 207Pb/206Pb age investigations on single zircons using a double filament thermal ion source. Contrib. Minral. Petrol., **93**, 482-490

Kober, B. 1987. Single zircon evaporation combined with Pb+emitter beding for $^{206}Pb/^{207}Pb$-age investigations using thermal ion mass spectroscopy, and applications to zirconology. Contrb. Mineral. Petrol., **96**, pp. 63-71.

Koch, P. L., Zachos, J. C. And Gingerich, P. D., 1992. Correlation between isotope records in marine and continental carbon reservoirs near the Paleocene/Eocene boundary., Nature, **358**, 319-322

Körner, Ch., Farquhar, G. D. and Roksandic, Z., 1988. A global survey of carbon isotope discrimination in plants from high altitude. Oecologia, **74**, 623-632

Kriegsman, L.M., 1995, The Pan-African event in East Antarctica:A view from Sri Lanka and the Mozambique belt: Precamb. Res., **75**, 263-277.

Kriegsman, L. 1993. Geodynamic evolution of the Pan-African lower crust in Sri Lanka- structural and petrological investigations into a high-grade gneiss terrain. Ph.D thesis, Univ. Utrecht. p. 208.

Krogh T. E. 1982a. Improved acuracy of U-Pb zircon dating by selection of more concordant fractions using a high gradient magnetic separation technique. Geochim Cosmochim Acta, **46**, p. 485-94.

Krogh T. E. 1973. A low-contamination method for hydrothermal decomposition of zircon and extraction of U and Pb for Isotopic age determination. Geochemica et Cosmochimica Acta, **37**, 485-494.

Krogh T. E. 1982b. Improved accuracy of U-Pb zircon ages by the creation of more concordant systems using an air abrasion technique. Geochim. Cosmochim. Acta, **46**,. 631-5.

Krogstad, E. J., Hansen, G. N. and Rajamani, V., 1991. U-Pb ages of zircon and sphene for two gneiss terranes adjacent to the Kolar Schist Belt, South India: evidence for separate crustal evolution histories. Jr. Geol. **99**, 801-816.

Krogstad, E.J.; Balakrishnan, S.; Mukhopadhyay, D.K.; Rajamani, V. and Hanson, G.N. 1989. Plate Tectonics, 2.5 billion year ago: evidence at Kolar, south India. Science, **243**, pp. 1337-1340.

Kröner, A., Braun, I. and Jaeckel, P., 1996. Zircon geochronology of anatectic melts and residues from a high-grade pelitic assemblage at Ihosy, southern Madagascar: evidence for Pan-African granulite metamorphism. Geol. Mag., **133(3)**, 311-323

Kröner, A., William, I. S., Bar, N. Vintage, PW and Pereia, L.R.L. 1987. Zircon ion microprobe dating of high-grade rocks in Sri Lanka, Jour. Geol. **95**: 775-791.

Lamb, W., Valley, J.W. and Brown, P.E. 1987. Post-metamorphic CO2-rich fluid inclusions in granulites. Contrib. Mineral. Petrol., **96**, 485-495.

Lamb, W. and Valley, J.W. 1984. Metamorphism of reduced granulites in low-CO2 vapor-free environment, Nature, **312**, 56-58.

Lawver, L. A., and Scotese, C. R., 1987. A revised reconstruction of Gondwanaland. In: McKenzie, G. (Ed.), Gondwana Six: Structure, Tectonics and Geophysics, Geophys. Monograph 40, Amer. Geophys. Union, Washington, D. C., 17-24.

Leelanandam, C. 1990. The anorthosite complexes and Proterozoic mobile belt of Peninsular India: a review. in, S.M. Naqvi (ed.) Precambrian continental crust and its economic resources. Developments in Precambrian Geology. Elsevier, New York.

Levitt, S.V. and Long, A., 1991. Seasonal stable isotope variability in tree rings: possible paleoenvironmental signals, Chemical Geology (Isotope Geoscience Section), **87**, 59-70.

Mahabaleswar, B.; Jayananada, M.; Peucat, J. J. and Shadakshara Swamy N. 1995. Archaean high-grade gneiss comples from Satnur-Halagur-Sivasamudram areas, Karnataka, southern India: Petrogenesis and crustal evolution. Jour. Geol. Soc. Ind. **45**, 33-49.

Mahabaleswar, B. and Peucat, J.J. 1988. 2.9 b.y. Rb-Sr age of the granulite facies rocks of Satnur-Halagur and Sivasamudram areas, Karnataka, South India. Jr. Geol. Soc. Ind., **32**, P. 461-467.

Margaritz, M., Krishnamurthy, R. V., and Holser, W. T., 1992. Parallel trends in organic and inorganic carbon isotopes across the Permian/Triassic boundary: Am. Jour. Sci. 292, 727-737.

Medina, E.,Montes, G., Cuevas, E. and Rokzandic, Z. 1986. Profiles of CO_2 concentration and $\delta^{13}C$ values in tropical rain forests of the upper Rio Negro Basin, Venezuela: Jr. of Tropical Ecology, 2,207-217.

Meen, J. K., Rogers, J. W. and Paul, D. F. 1992. Lead isotope compositions of the Western Dharwar Craton, southern India: evidence for distinct Middle Archean terranes in a Late Archean craton. Geochimica et Cosmochimica Acta, **56**, 2455-2470

Meyers, P. A., 1992. Changes in organic carbon stable isotope ratios across the K/T boundary: global or local control? Chemical Geology (Isotope Geology section), **101**, 283-291

Mezger, K. Bohlen, S. R. and Hanson, G. N. 1988. U-Pb garnet, monazite and rutile ages: Implications for the duration of high-grade metamorphism and colling histories, Adirondack Mts., NY, GSA Abstract with Progr., A100.

Mezger, K.; Hanson, G. N. and Bohlen S. R. 1989. U-Pb systematics of garnet: dating the growth of garnet in the late Archean Pikwitonei granulite domain at Cauchon and Natawahunan Lakes, Manitoba, Canada, Contribution to Mineral. Petrol. **101**:136-148.

Mezger, K., 1990. Geochronology in granulites. In, D. Vielzeuf and Ph. Vida (eds.), Granulites and crustal evolution., Kluwer Academic Publishers. 451-470.

Mezger, K., 1992. Temporal evolution of regional granulte terranes; implications for the formation of lowermost continental crust. In, Continental Lower Crust. Developments in Tectonics (edited by Fountain D. M., Arculus R. and Ray R. W.) p. 447-478. Elsevier, Amsterdam.

Mezger, K., Cosca, M. A. and Raith, M., 1996. Thermal history of Eastern Ghats Belt (India) deduced from U-Pb and 40Ar-39Ar dating of the metamorphic minerals., In., Proc. Of the UNESCO-IUGS-IGCP-368 Int. Field Workshop on the Proterozoic Continental Crust of Southern India (August, 1996). Trivandrum (India). Gond. Res. Group. Miscell Pub. 4. , 98

Mezger K. and Krogstad E. J. 1997. Interpretation of discordant U-Pb zircon ages: An evaluation. Jr. Metamorphic Geology. **15**, p. 127-140

Misra, D. C. 1988. Geophical evidences for a thick crust south of the Palghat-Tiruchi Gap in the high grade terranins of South India. Jour. Geol. Soc. India, **31**, p. 79-81.

Mishra, D.C. 1990. Precambrian rifts and associated tectonics of Peninsular India. in S.M. Naqvi (ed.) Precambrian continental crust and its economic resources, developments in Precambrian Geology, Elsevier Pub. New York., 487-502

Mohan, A. and Windley. B. 1993. Crustal trajectory of sapphirine bearing granulites from Ganguvaripatti, South India: evidence for isothermal decompression path. Jour. Meta. Geol., **11**. pp. 867-878.

Mohan, A. 1985. Reaction textures in silica-deficient granulites of Ganguvarpatti, Madurai District,

Tamilnadu. Jour. Geol. Soc. Ind., **26**, 666-673.

Monrad, J. R. 1983. Evolution of sialic terrains in the vicinity of Holenarshipur belt, Hassan district, Karnataka, India. In, S. M. Naqvi and J. J. W. Rogers (eds.) The Precambrian of south India, Geol. Soc. India. Memoirs No. **4**, 343-364

Mora, C. I., Driese, S. G and Seager, P. G. 1991. Carbon dioxide in the Paleozoic atmosphere: Evidence from carbon-isotope compositions of pedogenic carbonate. Geology. **19**, 1017-1020.

Morante, R., 1993. Determing the Permian/Triassic boundary in Australia through C-isotope chemostratigraphy, in, P. G. Flood and J. C. Aitchison (eds.), New England orogen, eastern Australia: Armidale, Australia, University of New England, 293-298

Morante, R. Veevers, J. J., Andrew, A. S. And Hamilton, P. J. 1994. Determination of the Permian-Triassic in Australia from carbon isotope stratigraphy. APEA journal., 330-336

Mukhopadhyay, D., 1986. Structural pattern in the Dharwar craton. Journal of Geology: **94**, 167-186.

Müller, B. G. J., Ashwal, L. D., Tucker, R. D. And Rambeloson, R. A., 1997. The Ranotsara Shear Zone, Central Madagascar. In., Proterozoic Geology of Madagascar, R. Cox and L. D. Ashwal (eds.), Proceedings of the UNESCO-IUGS-IGCP International Field Workshop, GRG Miscell Pub., **5**, p. 60

N. G. R. I., 1978. Gravity map series of India (1:5,000,000), 1st edition with explanatory brochure, published by the National Geophysical Research Institute, Hyderabad, India.

Nagpaul, K. K. And mehta, P. P., 1975. Cooling history of south India as revealed by fission track studies. Am. J. Sci., **275**, 753-762

Naha, K., Srinivasan, R. and Naqvi, S. M. 1986. Structural unity in the early Precambrian Dharwar tectonic province, Peninsular India. Geol. Min. Met. Soc.Ind., **58**, 218-243

Naha, K and Srinivasan, R., 1996. Nature of the Moyar and Bhavani shear zones, with a note on its implication on the tectonics of the southern Indian Precambrian shield. Proc. Indian Acad. Sci., Earth and Planetary Science. **105(2)**. 173-189.

Nair P.K.R and Nair E. V. 1980. Superposed folding of Precambrian rocks around Ottapalam, Palghat district, Kerala; In: Geology and geomorphology of Kerala: Geol. Sur. Ind. spl. publ. **5**. 15-19.

Nair, M. M., 1990. Structural trendline patterns and lineaments ofthe western Ghats, south of 13° latitude: Jour. Geol. Soc. India, **35**, p. 99-105.

Nair, M. M., and Vidyadharan, K. T., 1982. Rapakivi granite of Ezhimala complex and its significance.

Geol. Soc. India Jour., **23**, 46-51

Nair, N. G. K., Soman, K., Santosh, M., Arakelyants, M. M. andgolubyev, V. N., 1985. K-Ar ages of three granite plutons from North Kerala., Jr. Geol. Soc. India, **26**, 676-686

Narayanaswami, S., 1975. Proposal for Charnockite-Khondalite system in the Archean shield of Peninsular India. In, Precambrian Geology of the Peninsular Shield, Misc. Pub. **23**, Geological Survey of India, 1-17.

Narayanaswamy, S. and Lakshmi, P. 1967. Charnockitic rocks of Tinnevelly District, Madras. Geological Soc. Ind. Jour., **8**, 35-50.

Nathan, N. P., Subramanian, N. and Raman, R. 1991. Granites and their environs in Sankaridurg area, Salem district, Tamil Nadu. Recs. Geol. Surv. India., **123**, 138-142

Nathan, N. P., Krishna Rao, A. V., Bhalla, J.K., Balasubramanian, E., Subramanian, N., Oberoi, L. K., Nararajan, V., Gopalakrishnan, K. And Raman, R. 1994. Geochemistry and geochronology of the pegmatoidal granite of Sankari-Tiruchengode area, Tamil Nadu. Indian Minerals, **48**, 113-122.

Nelson, F. and Kraus, K. A., 1954. Anion-exchange studies. XI. Lead (II) and Bismuth (iii) in choloride and nitrate solutions. Jour. of the American Chemical Society, **76**, 5916

Newton, R. C. and Hansen, E. C. 1983. The origin of Proterozoic and late Archean charnockite-evidence from field relations and experimental petrology. Geol. Soc. Am. mem. **161**, 167-78.

Newton, R. C., Aranovich, L. Ya., Hansen, E. C. and Vandenheuvel. 1998. Hypersaline fluids in Precambrian deep-crustal metamorphism. Precambrian Research, **91**, 41-63.

Newton, R. C. 1986. Fluids of granulite metamorphism. In: J. M. Walther and B. J. Wood (eds.) Fluid rock interaction during metamorphism. Advances in Physical Geochemitry **5**: 36-59. Berlin: Springer.

Newton, R. C.,Smith, J. V. and Windley, B.F. 1980. Carbonic metamorphism, granulites and crustal growth. Nature, **288** p. 45-50.

Newton, R. C. 1986. Fluids of granulite metamorphism. In: J. M. Walther and B. J. Wood (eds.) Fluid rock interaction during metamorphism. Advances in Physical Geochemitry 5: 36-59. Berlin: Springer.

Nicollet 1990. Crustal evolution of granulities of Madagascar. In: Vielzeuf D, Vidal Ph (eds) Granulites and crustal evolution (NATO ASI Series-C, 311) Kluwer Academic , Netherlands, pp 291-311.

Norshimha Rao, P. 1964. Anorthosites of Oddanhathram, Palni Taluk, Madras State. Indian Minerals., **5**, 99-104

Norton, I. O., and Sclater, J. G., 1979. A model for the evolution of the Indian ocean and the breakup of Gondwnaland., Jr. Geophy. Res., **84(B12)**, 6803-6830

Nutman, A.. P.; Chadwick, B.; Ramakrishnana, K.; and Viswanatha, M. N., 1992, SHRIMP U-Pb ages of detrital zircon in Sargur supracrustal rocks in western Karnataka, Southern India: Jour. Geol. Soc. India, 39, 367-374.

Nutman, A. P., Chadwick, B., Krishna Rao, B. and Vasudev, V. N., 1996. SHRIMP U/Pb zircon ages of acid volcanic rocks in the Chitradurga and Sandur Groups, and Granites adjacent to the Sandur Schist Belt, Karnataka., Jr. Geol. Soc. Ind., **47**, 153-164.

O'Leary, M. H., 1981. Carbon isotope fractionation in plants: Phytochemistry, 20(4),553-567.

O'Leary, M. H., 1988. Carbon Isotopes in Photosynthesis. Bioscience, 38(5), 328-337

Odom, A. L. 1982. Isotopic age determinations of rock and mineral samples from the Kerala district of India. Final report, U. N. case no. 81-10084 (unpublished).

Olson, E. C., 1982., Extinction of Permian and Triassic nonmarine vertebrates., Geol. Soc. Am. Spl. Pub., 190, 501-511

Palniswamy, V., Balasubramanian, E. and Balachandran, V. 1990. Geology of the area in and around the Gangavalli Shear Zone in parts of Salem, South Arcot and Tiruchirapalli district, Tamil Nadu, Recs. Geol. Surv. India, **123**, 138-142

Paquette, J. -L., Nédélec, A., Moine, B. and Rakotondrazafy, M. 1994. U-Pb, single zircon Pb-evaporation and Sm-Nd isotopic study of a granulitic domain in S. E. Madagascar., Jr. Geol., **102**, 523-38.

Paquette, J. -L. and Nédélec, A., 1998. A new insight into Pan-African tectonics in the East-West Gondwana collision zone by U-Pb zircon dating of granites from central Madagascar. Earth and Planet. Sci. Lett., **155**, 45-56.

Parrish R. R. 1990. U-Pb dating of monazite and its application to geological problems. Canadian Jour. of Earth Sci., **27**, 1431-1451.

Parsad, R., Lal, N. and Nagpaul, K. K., 1970. Tectonic uplift of the nellore Mica Belt, India, as revealed by fission track dating technique. Jour. Geol. Soc. Ind., **20**, 31-36

Pascoe, E. H., 1950. A manual of the Geology of India and Burma, 3rd ed., I, 1-483.

Paul, D.K., Ray Barman, T.K., Mcnaughton, N.J., Fletcher, I.R., Potts, P.J., Ramakrishnan M. and Augustine, P.F. 1990. Archaean-Proterozoic evolution of Indian charnockites. Isotopic and geochemical evidence from granulites of the Eastern Ghats blet. J. Geol. **98**, p. 253-296.

Peraraju, P.; Kovach, A.; and Svinger, E. 1979. Rubidium-Strontium ages of some rocks from parts of Eastern Ghats in Orissa and Andhra Pradesh. Jour. Geol. Soc. India. **20**, 290-296.

Percival, J. A., Roering, C., can Reenen, D. D., Smith, C. A. 1997. Tectonic evolution of associated greenstone belts and high-grade terrains. In: deWit, M. J., Ashwal, L. D. (eds.), Greenstone Belts. Oxford University Press, Osford, pp. 398-421.

Peucat J.J., Vidal P, Bernard-Griffiths J, Condie KC 1989. Sr, Nd, and Pb isotopic systematics in the Archean low-to high-grade transition zone of southern India: syn-accretion versus post-accretion granulites. J. Geol. 97:537-550.

Peucat, J.J.; Mahabaleswar R. and Jayananda M., 1993. Age of Younger tonaliteic magmatism and granulitic metamorphism in the South India transition zone (Krishnagiri area); comparison with older Peninsular gneisses from Gorur- Hassan area. Jr. Metamorphic Geology., **11**: p. 879-888

Peucat, J.J., Bouhallier, H., Fanning, C.M., Jayananda, M., 1995 Age of the Holenarsipur greenstone belt , relationships with the surrounding gnesis (Karnataka, South India). J. Geol. **103**, 701-710.

Pichamuthu, C. S. and Srinivasan, 1984. A billion year history of the Dharwar craton (3200-2100 m.y. ago), Mem. Geol. Soc. Ind., **4**, 121-142

Pichamuthu, C.S., and Srinivasan, R., 1984, The Dharwar craton. A Golden Jubilee publication: New Delhi, Ind . Nat. Sci. Acad., 34.

Pichamuthu, C. S. 1953. The charnockite problem. Mysore Geologists Association, Special Publication, 163p.

Pichamuthu, C. S., 1960. Charnockite in the making, Nature, **188**, 135-136.

Pichamuthu, C. S., 1961. Transformation of Peninsular Gneiss into charnockite in Mysore State, India. Jour. Geol Soc. India, **2** p. 46-49.

Pichamuthu, C. S., 1965. Regional metamorphism and charnockitization in Mysore State, India. Ind. Mineralogist, **6**, 119-126.

Pichamuthu, C. S., 1969. Nomenclature of charnockites, Ind. Mineral., 10, 23- 35

Pichamuthu, C. S., 1982. Schist-gneiss relation in Dharwar Craton. Current Science, **51**, 118-124

Pidgeon R.T.; Aftalion, M. 1978. Cogenetic and inherited zircon U-Pb systems in granites: Paleozoic granites of Scotland and England. In: Crustal evolution of northwestern Britain and adjacent regions, Bows R. D. and Leake B. E., eds., Geological Journal Special Issue, **10**: 183-220.

Pidgeon, R. T., 1992. Recrystallization of oscillatory zoned zircon: some geochronological and petrological implication. Contr. Mineral. Petro., **110**, 463-472

Pinna, P., Jourde, G., Calvez, J. Y., Mroz, J. P. and Marques, J. M., 1993. The Mozambique belt in northern Mozambique: Neoproterozoic (1100-850 ma) crustal growth and tectogenesis and superimposed Pan-African (800-550 ma) tectonism. Precamb. Res., **62**, 1-59.

Poitrasson, F.; Rin, C., Duthou J-L. 1995. Hydrothermal remobilization of rare earth elements and its effect on Nd isotopes in rhyolite and granite. Earth and Planetary Science Letters., **130**. 1-11.

Powell, C. Mac., Roots, S. R. and Veevers, J. J., 1988. Pre-breakup continental extension in East Gondwanaland and the early opening of the eastern Indian Ocean. Tectonophysics., **155**, 261-283

Prasad, C. V. R. K., Subba Reddy, N., and Windley, B. F., 1982. Iron formations in Archaean granulite-gneiss belts with special reference to southern India. Geol. Soc. Ind. Jour., **23**, 112-122

Purdy, J. W.; Jager E. 1976. K-Ar ages on rock forming minerals from the Central Alps, Mem 1st geol. Petrol Univ. Padova, **30**: 1-321.

Radhakrishna T., Pearson D.G. and Mathai J., 1995. Evolution of Archaean South Indian Lithospheric mantle: a geochemical study of Proterozoic Agali- Coimbatore dykes. Contr. Mineral. Petrol. **121**: p. 351-363

Radhakrishna, T. and Mathew, J. 1996. Late Precambrian (850-800 Ma) paleomagnetic pole for the south Indian shield from the Harohalli alkaline dykes: geotectonic implications for Gondwana reconstructions. Precambrian Research., **80**. p. 77-87.

Radhakrishna, T. and Joseph, M. 1993. Proterozoic paleomagnetism of South Indian Shield and Tectonic constraints. In, B.P. Radhakrishna (ed.), Continental crust of South India., Geol. Soc. Ind. Mem. **25**., 321-336

Radhakrishna, B. P. and Naqvi, S.M., 1986. Precambrian continental crust of India and its evolution. The Journal of Geology: **94**, 145-166.

Radhakrishna, B. P. and Vasudev, V. N., 1977. The Early Precambrian of the Southern Indian Shield. Jr. Geol. Soc. Ind., **18**, 439-456

Radhakrishna. B.P.1983, Archean granite greenstone terrain of the South Indian Shield, in Naqvi, S.M., and Rogers, J.J.W.. eds.. Precambrian of South India: Geol. Soc. India. Mem., **4**. 1-46.

Radhakrishna, T.; Mathai, J.; Yoshida, M. 1990. Geology and Structure of the high-grade rocks from Punalur-Achankovil sector, south India. Jour. Geol. Soc. India. 35, p. 263-272.

Rai, S. S., Ramesh, D. S., Srinagesh, D., Suryaprakasam, K., Mohan, G., Rajagopala, Sarma, P.V.S.S

and Satyanarayana, Y. 1992. Seismic tomography of the south Indian shield. In: Special issue: Seismology in India- an overview., Current Science., **62(5,6)**p. 213-226.

Rai, S. S.; Srinagesh, D. and Gaur, V. K., 1993. Granulite evolution in south India- a seismic tomographic perspective. Mem. Geol. Soc. India., **25**, p. 235-263.

Raith, M.; Stahle, H. J.; adn Hoernes, S. 1988. Kabbaldurga-type charnockitization: a local phonomenon in the granulite to amphibolite grade transition zone. Jr. Geol. Soc. Ind. **31**,116-117.

Raith, M.; Srikantappa, C.; Ashamanjari, K.G. and Spiering, B., 1990. The Granulite terrain of the Biligiri Hills (Southern India): Characterization of High grade metamorphism. In: Granulites and Crustal Evolution (eds. Vielzeuf, D. and Vidal P.), Nato ASI Series C., p. 339 -365. Kluwer Academic, Dordrecht.

Raith M, Rasse P, Ackermand D, Lal RK 1983. Regional geothermo-barometry in the granulite facies terrain of south India . Trans R Soc Edinburgh Earth Sci 73:221-244.

Raith, M.; Hoernes, S.; Stahle, H. J.; and Klatt, E. 1989. Contrasting mechanisms of charnockite formation in the amphibolite to granulite transition zones of Southern India. In: Bridgwater D. (ed.) Fluid movements, element trnsport, and the composition of the deep crust. NATO ASI series **C281**: 29-38, Kluwer Academic Publisher.

Rajesh, H.M.; Santosh, M. and Yoshida, M. 1998. Dextral Pan-Africanshearing along the southwestern edge of the Achankovil Shear Belt, South India: Constraints on Gondwana reconstruction: a discussion. Jour. Geol. 106, p. 105-114.

Rama Rao, B. 1945. The charnockite rocks of Mysore (southern India): their mode of occurrence, origin and distribution. Bull. Mysore Geological Department., **18** ,.163

Ramakrishnan, M., Viswanatha , M.N., 1987. Angular unconformity, structural unity argument and Sargur-Dhawrwar relations in Bababuban basin. J. Geol. Soc. India., **29**, 471-482.

Ramakrishnan, M. 1993. Tectonic evolution of the granulite terrains of southern India. Geol. Soc. India. Memoir, **25**, 35-44.

Ramakrishnan, M., Nanda, J. K. and Augustine, P. F., 1998. Geological evolution of the Proterozoic Eastern Ghats mobile belt., Geol. Sur. of Ind. Spl. Pub., **44**.,1-21

Ramesh, D. S.; Rai, S. S.; Srinagesh, D.; Gaur, V. K., 1990. Seismological evidence for a decoupled lithospheric segment in south Indian shield. Geophy. Jr. Int. **102**, p. 113-120

Ramesh D. S.; Srinagesh, D.; Rai S. S. and Prakasam, K. S., 1992. Anomalous granulite crust of South India- signatures from converted teleseismic waves. Proc. Indian Acad. Sci. (Earth Planet. Sci.), **101** 283-298.

Ramesh, D. S.; Rai, S. S.; Srinagesh, D.; Gaur, V. K., 1990. Seismological evidence for a decoupled lithospheric segment in south Indian shield. Geophy. Jr. Int. **102**, p. 113-120

Ramierngar, A. S., Ramakrishnan, M., and Viswanatha, M.N. 1978. Charnockite-Gneiss Complex relationship in southern Karnataka. Jr. Geol. Soc. Ind., **19**. p. 411-419.

Rao. A. T.; Divakara Rao, V.; Yoshida, M. and Arima, M. 1995. Geochemistry of charnockites from the Eastern Ghats granulite belt-evidence for possible linkage between India and Antarctica. Mem. Geol, Soc. Ind. **34**. P. 273-291.

Ramsay, J. G., 1967, Folding and fracturing of rocks., Mc-Graw Hill

Raval., U., 1995. Do the East Coast gravity high and Comorin ridge overlie the Marion plume trace between 120-85 Ma?, Extended abstract; 32nd Annual convention and seminar on marine geophysics. NGRI, India.

Ravindra Kumar, G. R. and Chacko, T. 1986. Mechanisms of charnockite formation and breakdown in southern Kerala: implications for the origin of the southern Indian Granulite Terrain. Jour. Geol. Soc. India. **28**. p. 277-288.

Ravindra Kumar, G. R. and Chacko, T. 1986. Mechanisms of charnockite formation and breakdown in southern Kerala: Implication for the origin of the southern Indian granulite terrain. Jr. Geol. Soc. Ind. **28**, 277-288.

Ravindra Kumar, G. R. and Chacko, T. 1994. Geothermobarometry of mafic granulites and metapelite from Palghat Gap, south India: petrological evidence for isothermal uplift and rapid cooling. Jour. Meta. Geol., **12**, pp. 479-492.

Ravindra Kumar, G.R., 1988. The Kerala Khondalite Belt. In: Workshop on the Deep Continental Crust of South India Guidebook. Geol. Soc. India, **28**: 277-288.

Ravindra Kumar, Gr. R. and Raghavan, V. 1992. The incipient charnockites of transition zone of south India: contrasting mechanisms and controlling factors. Jour. Geol. Soc. India. **39**, 293-302.

Ray, S. (Sr.) 1972. Charnockite of Kabbal, Mysore- a brief study. Q. J. Geol. Min. Met. Soc. Ind., 44, 163-166

Reddi, A.G.B.; Mathew, M.P.; Singh B.; and Naidu P.S., 1988, Aeromagnetic evidence of crustral structure in the granulite terrane of Tamil nadu-Kerala: Jour. Geol. Soc. India., **32**, 368-381.

Reeves, C. V., 1998. Aeromagnetic and gravity features of continental Gondwana and their relation to cotinental break-up: more pieces, less puzzle. Jr. of African Earth Sciences, **27**, 153-156

Retallack, G. J., Veevers, J. J. and Morante, R., 1996. Global coal gap between Permian-Triassic extinction and Middle Triassic recovery of peat-forming plants. GSA Bull., **108 (2)**, 195-207.

Ripperdan, R. L., 1994. Global variations in carbon isotope composition during the latest Neoproterozoic and earliest Cambrian., Annu. Rev. Earth Planet. Sci., 1994, **22**, 385-417

Robinson, J. M., 1990. Lignin, land plants, and fungi: Biological evolution affecting Phanerozoic oxygen balance., Geology., 15, 607-610

Rogers, J. J. W., Miller, J. S. and Clements, A. S., 1995. A Pan-African zone linking East and West Gondwana., In, M. Yoshida and M. Santosh (eds.), India and Antarctica during the Precambrian, Mem. Geol. Soc. Ind., 34, 11-23.

Rogers J. J. W. and Giral., 1997. The Indian Shild. In., M. de Wit and L. Ashwal (eds.), Greenstone Belts, Oxford monograph on geology and geophysics **(35)**, 620-635

Rogers, J. J. W.,1986. The Dharwar craton and the assembly of Peninsular India. Jr. Geol. **26**,129-143.

Sacks, P.E.; Nambiar, C. G.; and Walters, L. J. 1997. Dextral Pan-African shear along the southwestern edge of the Achankovil shearbelt, south India: constraints on Gondwana reconstructions: Jour. Geol., **105**, 275-284.

Sahu, B. K. and Reeves, C. V., 1998., Continental scale geophysical anomaly patterns: implications for Gondwana re-assembly.

Santosh, M., Jackson, D. H., Harris, N. B. W. & Mattey, M. P. 1991. Carbonic fluid inclusions in South Indian granulites: evidence for entrapment during charnockite formation. Crontrib. Mineral. Petrol. **108**, 318-330.

Santosh, M., Kagami, H., Yoshida, M., Nanda-kumar, V., 1992. Pan-african charnockite formation in East Gondawna: geochronologic (Sm-Nd and Rb-Sr) and petrogenitic constraints. Bull. Indian Geol. Assoc. **25**, 1-10.

Santosh, M., Iyer, S. S., Vasconcellos, M. B. A. and Ensweiler, J. 1989. Late Precambrian alkaline plutons in southwest India: geochronologic and rare earth element constraints on Pan-African magmatism. Lithos, **24**, 65-79.

Santosh, M., Jackson, D. H., Harris, N. B. W. & Mattey, M. P. 1991. Carbonic fluid inclusions in South Indian granulites: evidence for entrapment during charnockite formation. Crontrib. Mineral. Petrol. **108**, 318-330.

Santosh, M., Jackson, D. H., and Harris, N. B. W. 1993. The significance of channel and fluid inclusion CO_2 in cordierite: evidence from carbon isotope. J. Petrol., **34**, 233-258

Santosh, M., 1996. The Trivandrum and Nagercoil Granulite Blocks. In, M. Santosh and M Yoshida (eds.), The Archean and Proterozoic Terrains of southern India within East Gondwana. Gond. Res. Group, Mem. **3**, 243-277

Santosh, M. 1992. Carbonic fluids in granulites: cause or consequence? Jour. Geol. Soc. Ind. **39**, 375-399.

Santosh, M. 1987. Cordierite gneisses of southern Kerala, India: petrology, fluid inclusions and implications for crustal uplift history. Contrib. Mineral. Petrol., **96**, 343-356

Santosh, M., and Drury, S.A., 1988: Alkali granites with Pan-African affinites from Kerala, South India. Jr. Geol. **96**, 616-626.

Santosh, M., and Yoshida, M. 1986: Charnockite "in the breaking" :Evidences from the Trivandrum region, South kerala. J. Geol. Soc. India. **28**, 306-310.

Santosh, M. and Wada, H. 1993. Microscale isotopic zonation in granite crystals: Evidence for channelled CO influx in granulites. Earth and Planetary Science Letters, **119**, 19-26.

Santosh, M., Kagami, H., Yoshida, M. And Nanda-Kumar, V., 1992. Pan-African charnockite formaiton in East Gondwana: geochronology (Sm-Nd and Rb-Sr) and petrogenetic constraints. Bull. Ind. Geol. Ass., **25**, 1-10.

Santosh, M., Suzuki, K. And Msuda, H. 1994. Re-Os dating of molybdenites from southern India: implication for Pan-African metallogeny. J. Geol. Soc. India, **43**, 585-590.

Saravanan, S., and Ramanathan, S. 1973. Calc-granulites around Manalur, South and North Arcot Districts, Tamil Nadu, India. Geol. Soc. India Jour., **14**. 60-70.

Sarkar, A.N., Bhanumathi, L., and Balasubrahmanyan, M. N., 1981: Petrology, geochemistry and geochronology of the Chilka lake igneous complex, Orissa state, India. Lithos, **14**, 93-111.

Sawlowicz, Z., 1993. Iridium and other platinum-group elements as geochemical markers in sedimentaty environments. Palaeogeography, Palaeoclimatoloty, Palaeoecology: **104** ,253-270.

Scholle, P.A. and Arthur, M.A., 1980. Carbon isotope fluctuations in Cretaceous pelagic Limestones: potential stratigraphic and petroleum exploration tool. American Association of petroleum Geologist Bulletin, v.64(1), 67-87.

Schlesinger, W. H., 1991. Biogeochemistry. SanDiego: Academic Press.

Sen Gupta, P., Das Gupta, S.; Bhattacharya, P.K., Fukuoka, M., Chakraborthi, S. and Bowmick, S. 1990. Petrotectonic imprints in the sapphirine granulites from Ananthagiri, Eastern Ghats Mobile Belt, India. Jour. Petro., **31**, pp. 971-996.

Sen, S. K. and Bhattercharya, S., 1993. Patchy charnockites from south Kerala- nescent growths or modified relicts? Indian Minerals, **47(2)**, 103-112

Shaw, R. K.; Arima, M.; Fanning, C. M.; Shiraishi, K. and Motoyoshi, Y.; 1997. Proterozoic Events in the Eastern Ghats Granulite Belt, India: Evidence from Rb-Sr, Sm-Nd Systematics, and SHRIMP Dating: Jour. Geol., **105**, P.645-656.

Shiraishi, K., Ellis, D. J., Hiroi, Y., Fanning, C. M., Motoyoshi, Y. and Nakai, Y. (1994). Cambrian orogenic belt in east antarctica and Sri Lanka: Implications for Gondwana assembly. Jr. Geol., 102, 47-65

Sivasubramanian, P., Natarajan, R. and Janardhan, A. S., 1991. Sapphirine bearing assemblages from Perumal Malai, Palani Hills, Tamilnadu. Jour. Geol. Soc. Ind., 38, 164-171

Sinha Roy, S.; Mathai,J.; and Narayanaswamy, 1984. Structure and metamorphic characteristic of cordierite-bearing gnesis of South Kerala: Jour. Geol. Soc. India, **25**, 231-244.

Smith, R. M. H., 1990. A review of the stratigraphy and sedimentary environments fo the Karoo Basin of South Africa. J. Afr. Earth Sci., 10, 117-137

Snow J. Basu A. R 1986: The Sittampundi complex, S. India - Nd isotopic chronology of lower crustal granulites (abstract). EOS Trans Am Geophys Union, **67**: 400.

Soman, K.; Narayannaswamy and Van Schmus, W. R. 1995. Preliminary U-Pb zircon ages of High-Grade rocks in Southern Kerala, India. Jour. Geol. Soc. India., **45**., 127-136.

Soman, K.; Thara K. G.; Arakelyants, N. M.; and Golubyev, V. N. 1990. Mineral ages of Pegmatites from the Palghat Gap Region in Kerala and their Tectonic Significance. Jr. Geol. Soc. Ind., 35, 82-86.

Soman, K.; Santosh, M. and Golubyev, V. N., 1983. Early Paleozoic I-type granite from central Kerala and its bearing in possible mineralisation. Ind. J. Earth. Sci. **10**: 137-141.

Soman, K., Lobzova, R. V. and Sivada, K. M., 1986. Geology, genetic types, and origin of graphite in South Kerala, India. Economic Geology, **81**, 997-1..2

Spooner, C. M. and Fairbairn, H. W. 1970. Strontium 87/ Strontium 86 initial ratios in pyrosene granulite terranes. Jr. Geophy. Res., **75**, 6706-6713.

Spooner, C. M. and Fairbairn, H. W. 1970. Strontium 87/ Strontium 86 initial ratios in pyrosene granulite terranes. Jr. Geophy. Res., **75**, 6706-6713.

Srikantappa. C.Raith, M., and Touret, J. L.R., 1992. Sunmetamorphic high-density carbonicfluids in the lower crust: Evidence from the Nilgiri granulites, Southern India. Jr. Petrol. **33**, 733-760

Srikantappa, C., 1993: High pressure charnockites of the Nilgiri Hills, Southern India. In: Radhakrishna BP(ed) Continental crust of south India. Mem. Geol. Soc. India. **25**: 95-111.

Srikantappa, C., 1996. The Nilgiri Granulites. In, M. Santosh and M. Yoshida (eds.), The Archean and Proterozoic terrains of Southern India within East Gondwana., Gond. Res. Group Memoir-3. 185-222

Srinivasan B.V. and Ganesan, T. M., 1992. Synthesis of data of concept-oriented geological mapping and geochemical sampling along the Cauvery lineament project, Tamil Nadu. Rec. Geol. Sur. Ind., **125(5)**. 90-93

Srikantappa, C., Raith, M., and Spiering, B., 1985: Progressive charnockitization of a leptynite-khondalite suite in southern kerala, India evidence for formation of charnockites through decrease in fluid pressure?. J.Geol. Soc. India, **26**, 849-872.

Stacey, J. S. and Kramers, J.D. 1975. Approximation of terrestrial lead isotopic evolution by a two stage model. Earth Planet. Sci. Lett., **24**. pp. 277-288.

Stahle, H. J.; Raith, M.; Hoernes, S. and Delfs, A. 1987. Element mobility during incipient granulite formation at Kabbaldurga, Southern India. J. Petrology. **28**, 803-834.

Stattegger, K. and Schmöller. 1989: A Unique geochemical record at the Permo-Triassic boundary., Nature, **337** ,39-43.

Sterner, S. M. and Bondar, R. J. 1989. Sunthetic fluid inclusions- Vli. Re-equilibration of fluid inclusions in quartz during laboratory-simulated metamorphic burial and uplift. Jour. Metamorphic Geol., 7, 243-260.

Stillwell, F.L. 1918. The metamorphic rocks of Adelie land, Land Australina Antarctic Expedition, 1911-1914, Scientific Reports, Ser. A., III, pt.

Strauss, H., Des Marais D.J., Hayes, J.M. and Summons, R.E., 1992. The carbon isotope record. In: Schopf, J.W. and Klein, C. (eds.), The Proterozoic Biosphere: Cambridge, United Kindom, Cambridge University Press, pp.117-128.

Strauss, H., Des Marais D.J., Hayes, J.M. and Summons, R.E., 1992. Concentrations of organic carbon and Maturities and elemental Compositions of kerogens. In: Schopf, J.W. and Klein, C. (eds.), The Proterozoic Biosphere: Cambridge, United Kindom, Cambridge University Press, .95-100.

Stroh, P. T., Monrad, J. R., Fullagar, P. D., Naqvi, S. M. and Rogers, J. J. W . 1983. 3000 m.y. old Halekote trondhjemite: a record of stabilisation of Dharwar craton. In: Precambrian of south India., S. M. Naqvi and J. J. W. Rogers (eds.), Goel Soc. India. Memoirs, **4**, 365-376

Subramaniam, A. P. 1959. Charnockites of the type area near Madras- a reinterpretation. Am. Jour. Science. **257** p. 321-353.

Subrahmanyam, A. P. 1967. Charnockites and granulites of southern India - a review. Meddalelser fra Dansk Geologisk Forening Bd. 17 hefte4, p. 473-493.

Subrahmanyam, C. 1978. On the relation of gravity anomalies to geotectonics of the Precambrian terrains of the south Indian shield, J. Geol. Soc. Ind., **19**, 251-263.

Subrahmanyam, C. And Verma, R. K., 1982. A gravity interpretation of the Dharwar greenstone gneiss granite terrain in the southern Indian shield and its geological implication. Tectonophysics, **84**, 225-245

Subrahmanyam, C., 1983. An overview of gravity anomalies. Precambrian metamorphic terrains andtheir boundary relationships in the southern Indian shield. In: Precambrian of south India. Mem. Geol. Soc. India, **4**, p. 553-564.

Subramanian, K.S.; Muraleedharan, M. P., 1985. Origin of the PalghatGap in south India- a synthesis. Jr. Geol. Soc. Ind., **26(1)**. 28-37.

Sundquist, E. H., 1985. Geological perspectives on carbon dioxide and carbon cycle. *In*, E. T. Sundquist and W. S. Broecker (eds.), The carbon cycle and atomospheric CO2: natural variations Archean to present. Geophysical Monograph, **32**, 5-59.

Swami Nath, J., Ramakrishnan, M. and Viswanathan, M. N. 1976. Dharwar stratigraphic model and Karnataka craton evolution. Rec. Geol. Surv. India., **107**. p. 149-179

Taylor, P.N., Chadwick, B., Moorbath, S., Ramakrishnan, M. and Vishwanatha, M.N., 1984. Petrography, chemistry and isotopic ages of Peninsular Gneiss, Dharwar acid volcanic rocks and the Chitradurga Granite with special reference to the Late Archaean evolution of the Karnataka craton, South India. Precambrian research: **23**, 249-375.

Taylor, P. N., Chadwick, B., Friend, C. R. L., Ramakrishnan, M., Moorbath, S. and Viswanatha, M. N., 1988. New age data on the geological evolution of southern India. LPI Tech. Rep. 88-06, 181-186

Thackeray, J.F., cander Merwe, N.J., Lee-Thorp, J.A., Sillen, A., Lanham, J.L., Smith, T., Keyser A., Monteiro, P.M.S., 1990. Cnanges in carbon isotope ratios in the late permian recorded in therapsid tooth apatite. Nature, **347**, 751-753.

Thara, K. G.; Soman, K. 1993. Evidence for an isothermal depression path of granulites of the Palghat gap and its implications on the origin of the gap. Proceddings of the Fifth Kerala Science Congress. Kottaram. P. 288-292.

Thomasson, J. R., Nelson, M. E. and Zakrzewski, R. J., 1986. A fossil grass (Gramineae: Chloridoideae) from the Miocene with Kranz anatomy., Science, 233, 876-878

Torsvik, T., Tucker, R. D., Ashwal, L., Eide, E. A., Rakotosolofo, N. A. and de Wit, M. J., 1998. Madagascar: Cretaceous volcanism and the Marion Hot sopt., Jr. African Earth Sci., **27(1A)**, 197

Touret, J. L. R., 1995. The role and nature of fluids in the continental lower crust. In, M. Yoshida and M. Santosh (eds.), India and Antarctica during the Precambrian, Mem. Geol. Soc., Ind., 34, 143-160

Tucker, R. D., Handke, M. J., Hamilton, M. A., Ashwal, L. D., Le Grange, M. and Rambeloson, R. A. 1998. U-Pb ages and isotopic characteristics of the Archean greenstones and gneissic rocks of North Madagascar: Implications for the evolution of East Gondwana. Jour. Geol., in review.

Underwood, C. J., Crowley, S. F., marshall, J. D. and Brenchley, P. J., 1997. High-resolution carbon isotope stratigraphyof the basal Silurian stratotype (Dob's Linn, Scotland) and its global correlation., Jr. of Geol. Soc. Lond., **154**, 709-718

Unnikrishnan-Warrier, C. 1997. Isotopic Signature of Pan-African Rejuvenation in the Kerala Khondalite Belt, Southern India: Implications for East Gondwana reassembly. J. Geol. Soc. Ind., **50**, 179-190.

Unnikrishnan, C., Yoshida, M.,Kagami, H., and Santosh, M., 1992: Geochronological study of S. Indian granulites. 12th NIPR symposium on Antartic Geosciences. Tokyo. Abs. Vol. pp.9.

Unnikrishnan-Warrior, C.; Santosh, M. and Yoshida, M. 1995b. Sm-Nd mineral isochron ages of Madras charnockites and an evaluation of garnet geochronometry in granulites. In, M. Yoshida, and M. Santosh (eds.), India and Antarctica during the Precambrian. Mem. Geol. Soc. of Ind., **34**, 253-260

Unnikrishnan-Warrior, C.; Santosh, M. and Yoshida, M. 1995a. First report of Pan-African Sm-Nd and Rb-Sr mineral isochron ages from regional charnockites of southern India. Geol. Mag., **132**, p. 253-260.

Unnikrishnan-Warrior, C.; Yoshida, M.; and Santosh, M. 1993. Geochronologic constraints on granulite formation in southern India, Implications for East Gondwana reassembly., Jour. Geoscience, Osaka City Univ., **36**, 109-121.

Unrug, R. 1992. The supercontinent cycle and Gondwanaland assembly: Component cratons and the timing of suturing events. J. Geodynamics, **16** p. 215-240.

Vaidyanadhan, R., 1977. Recent advances in geomorphic studies of Peninsular India: A review. Indian Jr. Earth Sci. (Ray volume), 17-20

Valley, J. W., 1986. Stable isotope geochemictry of metamorphic rocks. In, Valley J. W., Taylor, H. P. And O'Neil, J. R. (Eds.) Stable isotopes in high temerature geological processes. Rev. in Mineralogy, Min. Soc. America, 16, 445-481

van Breemen, O. and Hawkesworth, C.J. 1980. Sm-Nd isotopic study of garnets and their metamorphic host rocks. Trans. R. Soc. Edinburg, **71**:97-102.

Vance, D. and O'Nions, R. K. 1990. Isotopic chronometry of zoned garnets: growth Kinetics and metamorphic histories: Earth Palnet. Sci. Lett., **97**, 227-240.

Venkata Dasu, S. P., Ramakrishnan, M. and Mahabaleswar, B. 1991. Sargur-Dharwar relationship around the komatite-rich Jayachamarajapura greenstone belt in Karnataka. Geol. Soc. of Ind. Jour. **38**, 577-592

Verma, R. K., 1985. Gravity field, seismicity and tectonics of Indian Peninsula and the Himalaya. D. Reidel Pub. Co., Dordrecht, also Allied Publishers, Madras, p.

Verschure, R. H., Andriessen, P. A., Boelrijk, N. A. I. M., Hebeda, E. H., Maijer, C., Priem, H. N. A. And Verdurmen, E. A. T. G., 1980. On the internal stability of Rb/Sr and K/Ar biotite systems: evidence from coexisting Sveconorwegian (ca. 870 Ma) and Caledonian (ca. 400 Ma) biotite in SW Norway. Contrib. Minreal. Petrol., **74**, 245-252.

Videl. Ph., Peucat J.J., Bernard - Griffiths, J., and Condie K. C., 1989: Sr, Nd, and Pb isotope systamatics of the Archean low to high grade transition zone of southern india. Terra Cognita, 8, 262.

Vielzeuf, D.; Clemens, J. D.; Pin, C. and Moinet, E. 1990. Granites, granulites, and crustal differentiation. *In*, D. Vielzeuf and Ph. Vidal (eds.), Granulties and Crustal Evolution, Kluwer Academic Publishers, Netherlands. 59-85.

Vinagradov, A.; Tugarinov, A.; Zhycov, C.; Stapnikova, N.; Bikinova, E. and Khorre, K. 1964. Geochronology of Indian Precambrian. 22nd Int. Geol. Cong. Rep. **10**, 553-557.

Viswanathan, T. V.; Gopalakrishnan, K., Ganesan, T.M. and Raman, R. 1990. Cauvery Suture Zone- its implications (extended abstract). Group Discussion on Suture Zones - Young and Old. Wadia Inst. of Himalayan Geology, Dehra Dun.

Vredenburg, E.W. 1919. Considerations regarding a possible relationship between the Charnockites and the Dharwars. Jour. Asiatic

Walker, T. S., 1902. Khondalites. Mem. Geol. Surv. India, **28**, 11

Wang, K., Orth, C.J., Attrep M. Jr., Cahatterton, B.D.E., Wang, X. and Li J. 1993. The great latest Ordovician extinction on the South China plate: chemostratigraphic studies of the Ordovician-Silurian boundary interval on the Yangtze platform., Palaeogeography, Palaeoclimatoloty, Palaeoecology, **104**, 61-79.

Wang, K., Geldsetzer, H. H.J. and Krouse, H. R., 1994. Permian-Triassic extinction: Organic $\delta^{13}C$ evidence from British Columbia, Canada., Geology, **22**, 580-584

Watson, G. A.; Reimer, G. M. and Jager, E. 1977. Cooling ages derived by apatite fission track, mica Rb-Sr and K-Ar dating: the uplift and cooling history of the Central Alps, Mem 1st geol Petrol Univ Padova, **30**: 1-28.

Watson, E. B.; Harrison, T. M., Ryerson, F. M. 1985. Diffusion of Sm, Sr and Pb in fluorapatite, Geochim. Coscochim Acta, **49**: 1813-1823.

Watson, G. A.; Reimer, G. M. and Jager, E. 1977. Cooling ages derived by apatite fission track, mica Rb-Sr and K-Ar dating: the uplift and cooling history of the Central Alps, Mem 1st geol Petrol Univ Padova, **30**: 1-28.

Watson, G. A.; Reimer, G. M. and Jager, E. 1977. Cooling ages derived by apatite fission track, mica Rb-Sr and K-Ar dating: the uplift and cooling history of the Central Alps, Mem 1st geol Petrol Univ Padova, **30**: 1-28.

Watson, E. B.; Harrison, T. M.l Ryerson, F. M. 1985. Diffusion of Sm, Sr and Pb in fluorapatite, Geochim. Coscochim Acta, **49**: 1813-1823.

Wefer, G. and Killingley J.S. 1986. Carbon isotopes in organic matter from a benthic alga halimeda incrassata (Bermuda): effects of light intensity: Chemical Geology (Isotope Geoscience Section), 59, 321-326.

Wetherill, G. W. 1956. An interpretation of the Rhodesia and Witwatersrand age patterns. Geochim. Coscochim. Acta, **9**, 290-2.

Wignall, P.B. and Hallam, A.,1992. Anoxia as a cause of the Permian/Triassic mass extinction: facies evidence from northern Italy and the western United States: Palaeogeography, Palaeoclimatoloty, Palaeoecology, **93**, 21-46.

Wiliams, I. S. and Claesson, S. 1987. Isotopic evidence for the Precambrian provenance and Caledonian metamorphism of high grade paragneisses from the Seve Nappes, Scandinavian Caledonides, II, Ion microprobe zircon U-Th-Pb. Contb. Minl. Petrol. **97**, 205-17.

Williams, I. S. 1998. Sensitive High Resolution Ion Microprobe. In, M. A. McKibben & W. C. Shanks (eds) Application of micro analytical techniques to understanding mineralizing processes. SEG Reviews in Economic Geology, **7**, in press.

Windley, B. F. and Razakamanana. 1996. The Madagascar-India connection in a Gondwana framework. In, M. Santosh and M. Yoshida (eds.) The Archean and Proterozoic terrains in Southern India within East Gondwana. Gondwana Research Group Mem. **3**., 25-37

Windley, B. F., Razafiniparany, A., Razakamana, R. and Ackermand, D., 1994. Tectonic framework of the Precambrian of Madagascar and its Gondwana connections. a review and reappraisal. Geol. Rundschau, **83**, 642-659

Yardley, B.W.D. 1977. An empirical study of diffusion in garnet. Am. Mineral., **62**: 793-780.

Yoshida, M. and Santosh, M. 1987. Charnockite 'in the breaking' and 'Making' in Kerala, South India: tectonic and micro-structural evidences. Jour. Geosciences. Osaka City Univ., **30**, 23-49.

Yoshida, M.; Funaki, M.; and Vitanage, P. W., 1992, Proterozoic to Mesozoic East Gondwana: the juxtaposition of India-Sri Lanka and Antarctica: Tectonics, **11**, 381-391.

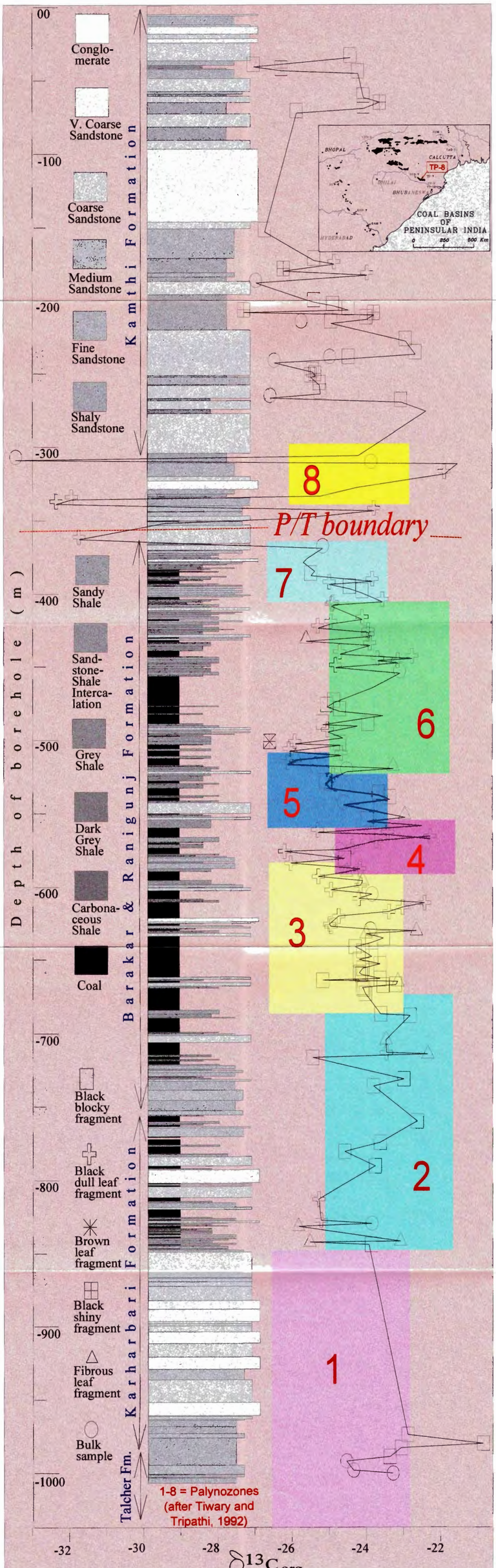

Fig. 6.8. Carbon isotope stratigraphy in the TP-8 borehole Talcher coalfield, India Coloured blocks (1-8) represent palynozones after Tiwari and Tripathi, 1992. These are; *1, Parasaccites Korbaensis; 2, Crucisaccites monoletus; 3, Scheuringipollennites barakarensis; 4, Faunipollenites varius; 5, Densipollenites indicus; 6, Gondisporites raniganjensis; 7, Densipollenites magnicorpus and; 8, Klausipollenites schaubergerii.*

Mafic Rocks

- Mafic Granulite
- Anorthosite Massif
- Gabbro, Diorite
- Amphibolite
- Meta–ultramafites, Anorthosite

Granitoids

- Granite Gneiss
- Granite Gneiss (sheared)
- Migmatitic Gneiss (foliated)
- Biotite Gneiss (garnetiferous)
- K–Granite (Closepet batholith)
- Foliated Granite (pink)
- Non–foliated Granite
- Alkaline Granites, Syenite

Metasediments

- Khondalite
- Quartzite
- Calc–granulite
- Leptynite
- Mica Schist

Charnockite

Sediments

- Paleozoic sediments
- Jurassic Sediments
- Cretaceous Sediments
- Tertiary Sediments
- Alluvial Sediments

Water bodies

- Rivers and Lakes

0 50 100 km

- Strike line of lithounits
- Structural Trend Lines
- Previously Interpreted Shear Zones (satellite imagery based; after GSI, 1994)
- Re–defined Alignment of Shear Zones (present work)
- Major Decollement in Southern Granulite Terrain of India (present work)

Geological Map of the Southern Granulite Terrain (SGT) of India (after GSI, 1995).

(Structural Interpretations: Present work) **Fig. 1.3**